Novel nitric oxide donors as antimicrobial agents

Author:
Kutty, Samuel

Publication Date:
2012

DOI:
https://doi.org/10.26190/unsworks/15842

NOVEL NITRIC OXIDE DONORS AS ANTIMICROBIAL AGENTS

This thesis is submitted in fulfilment of the degree of

Doctor of Philosophy

By

Samuel K. Kutty

Supervisors:

A/Prof. Naresh Kumar
Prof. David StC. Black

School of Chemistry
The University of New South Wales
Kensington, Australia

March 2012

This thesis is dedicated to my parents for
their unfailing love and years of sacrifices

Originality Statement

I hereby declare that this submission is my own work and to the best of my knowledge it contains no materials previously published or written by another person, or substantial proportions of material which have been accepted for the award of any other degree or diploma at UNSW or any other educational institution, except where due acknowledgement is made in the thesis. Any contribution made to the research by others, with whom I have worked at UNSW or elsewhere, is explicitly acknowledged in the thesis. I also declare that the intellectual content of this thesis is the product of my own work, except to the extent that assistance from others in the project's design and conception or in style, presentation and linguistic expression is acknowledged.‘

Signed …….....

Date …….....

Copyright Statement

Authenticity Statement

Abstract

The emergence of antibiotic resistance has highlighted the need to identify new antimicrobials that target bacterial pathogenicity without bactericidal effects. One such strategy exploits the inhibition of bacterial quorum sensing (QS) pathways, which are responsible for the expression of pathogenicity traits. Nitric oxide (NO) an endogenous cell mediator is also of major interest as an antimicrobial due to its ability to disperse and inhibit microbial biofilms *via* non-biocidal mechanism of action.

This project focuses on the design and synthesis of novel dual action NO donors based on quorum sensing inhibitors as antimicrobials.

Acylated homoserine lactone (AHL) based QS inhibitors mimicking the natural autoinducers were conjugated with NO donors such as nitrates, diazeniumdiolates and *S*-nitrosothiol to develop novel dual action NO donors.

Fimbrolides, a class of halogenated marine natural products isolated from *Delisea* species, are known for their potent bacterial QS inhibitory activity. A wide range of novel fimbrolide derivatives containing NO donor groups has been synthesized and evaluated for their antimicrobial properties. An unusual and hitherto-unknown conversion of the halogenated furanones to a thiophene skeleton was observed during preparation of thiol fimbrolides. A new class of fimbrolide disulfide compounds with no literature precedent was discovered.

Dihydropyrrolone based QS inhibitors were also conjugated with nitrates to develop novel hybrids. Novel indole based *C*-diazeniumdiolates and high load NO donors were also synthesized.

Crystal structure analyses of selected molecules revealed interesting intermolecular halogen bonding and carbonyl-carbonyl dipolar interactions. Molecular docking studies with LasR protein were also conducted to understand the influence of structural modification on the binding properties of the molecules. Docking studies also displayed possibilities of halogen bonding interactions in the ligand binding site.

The newly synthesized compounds were analyzed for their QS inhibitory efficacy and NO release properties in *in-vitro* assays. Their efficacy in biofilms inhibition and dispersion was also evaluated. The novel NO hybrid compounds showed significant biological activity which highlighted their potential for further development.

Acknowledgements

First of all, I would like to express my heartfelt gratitude to my supervisor, Associate Professor Naresh Kumar, for his immeasurable intellectual input, constant guidance, valuable suggestions, unparalleled encouragement and efficient support throughout my years of study. I am also genuinely grateful to my co-supervisor Professor David StC Black for very helpful discussions, ideas and motivation throughout this project.

I wish to express many thanks to Dr Scott Rice and Dr Nicolas Barraud for their guidance and technical assistance throughout this project at the biological end. I am also grateful to Amy Pham for her assistance in the biology laboratory and for carrying out the NO amperometric and biofilm assays. There would be no direction in this project without the biological testing performed at the Centre of Marine Biofouling and Bio-Innovation (CMBB).

I wish to thank Dr. Mohan Bhadbhade for performing the X-ray crystallography and for introducing me to this new subject. I would also like to thank A/Prof. Renate Griffith for her help with the docking studies.

I wish to thank all the faculty members in the School of Chemistry, especially Prof. Roger Bishop and A/Prof. Roger Read for their help during my thesis work. I am also thankful to the professional staff namely Ken McGuffin, Ian Aldred, Joseph Antoon, Toby Jackson, Barry Ward, Jodee Anning, Rick Chan, Nick Roberts and Anne Ayres for their timely help. I am also grateful for the help received from Berta, Thanh, Michael, Sharif, Peta, and Sveto in the teaching labs.

I am grateful for the help I received from the staff at the NMR facility and BMSF, particularly Jim Hook, Donald Thomas, Adelle Moore, Hilda Stender, Douglas and Lewis Adler. I would also like to thank Dr. Danmar Gloria for his help with the UV and IR analysis.

I am grateful to Dr George Iskander who has continuously mentored me on the experimental techniques which were crucial for my training as an organic chemist. I would like to thank all past and present members of A/Prof. Kumar‘s and Prof. Black‘s group for their friendship and help. It has been a really enjoyable experience to work in this friendly group. Most warmly, I want to mention Alam, Taj, Mandar, Ruth, Frank, Kasey, Kitty, Santosh, Megan, Daniel, Ren, Ray, Adeline, Chris, Mike, Hakan, Murat, Ibrahim, Venty, Nidup, Nick, Thanh, Eleanor, Marcin, Jo, Persefoni, Zahid and Dr. Abel Salek. Special thank goes to members of laboratory 336 for making it an enjoyable place to work, as well as Daniel Chan, Dr. Kasey Wood and Dr. Ruth Devakaram for proof reading my thesis. I would also like to specially thank Kitty for her help, support and friendship during my stay in Sydney.

I wish to thank all my teachers at various stages of my education and all my friends in India and in Sydney, especially Utpal, Karthik, Darwin, Punit, Hemant, Sagnik, Shreyans, Somendu, Abi, Anish, Twinkle, Nisha, Pridarshan, Deepti, Pooja, Rincy, Snehal, Sandeep, Suraj, and Somesh.

Lastly, I want to save my special thanks for my family. I am deeply grateful to my mother and father, not only for this life, but also for all their support, their selfless love

and encouragement. A special thanks also goes to my sister and brother for making my childhood memorable and for their love and support.

UIPA (University International Postgraduate Award) from UNSW during the three and half years is greatly acknowledged. I thank the School of Chemistry for the award of the supplementary Black Scholarship.

Thank You LORD for all your blessings.

Table of Content

Originality Statement i
Copyright Statement ii
Abstract iii
Acknowledgements v
Table of Content viii
Abbreviations xii
Publication and presentations xv
Chapter 1 ..... - 1 -
Introduction ..... - 1 -
1.1 Bacterial infectious diseases ..... - 1 -
1.2 Current treatments and drug resistance ..... - 1 -
1.3 Microbial biofilms ..... - 4 -
1.4 Quorum sensing: bacterial cell-cell communication ..... - 7 -
1.4.1 Quorum sensing signaling systems ..... - 8 -
1.4.2 AHL quorum sensing system ..... - 9 -
1.5 Quorum sensing inhibitors ..... - 12 -
1.5.1 AHL ligand-based inhibitors ..... - 12 -
1.5.2 Fimbrolides and their derivatives ..... - 16 -
1.6 Nitric oxide ..... - 20 -
1.6.1 Biosynthesis of nitric oxide ..... - 21 -
1.6.2 Nitric oxide inactivation ..... - 21 -
1.6.3 Biological effects of nitric oxide ..... - 22 -
1.7 Nitric oxide regulation in microbes ..... - 24 -
1.7.1 Nitric oxide as an antimicrobial and antibiofilm agent ..... - 26 -
1.8 Nitric oxide donors ..... - 28 -
1.8.1 Nitrates ..... - 30 -
1.8.2 Diazeniumdiolates ..... - 32 -
1.8.3 *S*-Nitrosothiols ..... - 36 -
1.8.4 Dual action drugs based on nitric oxide donors ..... - 36 -
1.9 Thesis aims ..... - 38 -

Chapter 2 ..... **- 40 -**
Acylated homoserine lactone-based nitric oxide donors ..... **- 40 -**
2.1 Introduction ..... - 40 -
2.2 Synthetic methodologies for AHL and 3-oxo AHL derivatives ..... - 42 -
2.3 Chapter aims ..... - 45 -
2.4 AHL and 3-oxo-AHL based nitric oxide donors ..... - 46 -
2.4.1 Preparation of AHL nitrate derivatives ..... - 46 -
2.4.2 Preparation of 3-oxo-AHL nitrate derivatives ..... - 49 -
2.4.3 Synthesis of AHL diazeniumdiolate derivatives ..... - 54 -
2.4.4 Synthesis of AHL *S*-nitrosothiol derivatives ..... - 61 -
2.5 Conclusion ..... - 63 -
Chapter 3 ..... **- 64 -**
Fimbrolide-based nitric oxide donors ..... **- 64 -**
3.1 Introduction ..... - 64 -
3.2 Synthesis of fimbrolides ..... - 66 -
3.3 Chapter aims ..... - 68 -
3.4 Synthesis of fimbrolide-based nitric oxide donors ..... - 69 -
3.4.1 Synthesis of fimbrolide-based nitrate derivatives *via* direct attachment ..... - 70 -
3.4.2 Synthesis of fimbrolide-based nitrate derivatives *via* linker region ..... - 73 -
3.4.3 Synthesis of fimbrolide-based diazeniumdiolate derivatives *via* O^2-attachment- 83 -
3.4.4 Synthesis of fimbrolide-based diazeniumdiolate derivatives *via* acid linkers ... - 88 -
3.4.5 Synthesis of fimbrolide-based *S*-nitrosothiol derivatives ..... - 90 -
3.4.6 Synthesis of fimbrolide-based S-nitrosothiol derivatives *via* *S*-nitroso-*N*-acetyl penicillamine ..... - 93 -
3.5 Conclusions ..... - 100 -
Chapter 4 ..... **- 101 -**
Dihydropyrrol-2-one-based nitric oxide donors ..... **- 101 -**
4.1 Introduction ..... - 101 -
4.2 Synthesis of dihydropyrrol-2-ones ..... - 104 -
4.3 Chapter aims ..... - 107 -
4.4 Synthesis of 1,5-dihydropyrrol-2-one nitrate derivatives ..... - 107 -
4.5 Synthesis of 1,5-dihydropyrrol-2-one-based diazeniumdiolate derivatives ..... - 114 -
4.6 Conclusion ..... - 117 -

Chapter 5 ..... **- 118 -**

Novel indole and high load nitric oxide donors ..... **- 118 -**

5.1 Introduction ..... - 118 -

5.2 Chapter aims ..... - 119 -

5.3 Indole-based nitric oxide donors ..... - 119 -

5.3.1 Indole and its biological significance ..... - 119 -

5.3.2 Reaction of indole with nitric oxide and its oxides ..... - 121 -

5.3.3 O^2-substituted indole *C*-diazeniumdiolates ..... - 128 -

5.4 Multiple high load nitric oxide donors ..... - 133 -

5.5 Conclusions ..... - 140 -

Chapter 6 ..... **- 142 -**

Molecular association via halogen bonding (C-halogen···O) and weak dipolar (C=O···C=O) contacts and their relevance in receptor binding: solid state and computational studies ..... **- 142 -**

6.1 Introduction ..... - 142 -

6.2 Non-covalent intermolecular interactions ..... - 143 -

6.2.1 Strong non-covalent interaction - hydrogen bonding ..... - 144 -

6.2.2 Weak non-covalent interactions ..... - 144 -

6.3 Chapter aims ..... - 147 -

6.4 Part A: Solid state X-ray crystallographic studies ..... - 147 -

6.4.1 Halogen bonding interactions ..... - 148 -

6.4.2 CO···CO interactions ..... - 149 -

6.4.3 Halogen bonding and CO··CO interactions ..... - 155 -

6.5 Conclusion ..... - 156 -

6.6 Part B: Computational protein-ligand docking studies ..... - 157 -

6.7 Protein-ligand docking ..... - 158 -

6.8 Quorum sensing in *Pseudomonas aeruginosa* ..... - 160 -

6.9 The *Pseudomonas aeruginosa* LasR protein ..... - 160 -

6.9.1 Analysis of the LasR-ligand complex ..... - 161 -

6.10 Protein-ligand docking protocol ..... - 162 -

6.11 Validation of protein-ligand docking ..... - 163 -

6.12 Protein-ligand docking results ..... - 164 -

6.12.1 Acylated homoserine lactone (AHL)-based nitric oxide donors ..... - 165 -

6.12.2 Fimbrolide and dihydropyrrolone-based nitric oxide donors ..... - 169 -

6.13 Halogen bonding interactions studies ..... - 172 -

6.14 Conclusions ..... - 175 -
Chapter 7 ..... - 177 -
Biological and chemical evaluation ..... - 177 -
7.1 Introduction ..... - 177 -
7.2 Quorum sensing inhibition assay ..... - 177 -
7.2.1 Assay method ..... - 177 -
7.2.2 Screening results ..... - 182 -
7.3 Nitric oxide release studies ..... - 193 -
7.3.1 Quantification of nitrate/nitrite by the Griess Reaction ..... - 194 -
7.3.2 Nitric oxide measurement by Apollo ..... - 198 -
7.4 Effect of nitric oxide on the bacterial *nirS* system ..... - 199 -
7.5 Studies on biofilm growth and dispersion ..... - 201 -
7.5.1 Biofilm inhibition assay ..... - 201 -
7.5.2 Biofilm dispersal assay ..... - 204 -
7.6 Discussion and conclusion ..... - 205 -
Chapter 8 ..... - 208 -
Experimental ..... - 208 -
8.1 General Information ..... - 208 -
8.2 Experimental Details ..... - 209 -
References ..... - 292 -
Appendix ..... - 313 -

Abbreviations

Ac_2O	acetic anhydride
AcONa	sodium acetate
AHL	*N*-acylated homoserine lactone
a.m.u.	atomic mass unit
Bn	benzyl
CF_3SO_3H	trifluoromethanesulfonic acid
CH_3COCl	acetyl chloride
CH_3I	methyl iodide
CH_3NH_2	methylamine
CH_2O	formaldehyde
CF_3COOH	trifluoroacetic acid
CoA	coactivators
COX	cyclooxygenase
COSY	correlation spectroscopy
DCC	*N,N*-dicyclohexylcarbodiimide
DCM	dichloromethane
DEPT	distortionless enhancement by polarization transfer
DMAP	*N,N*-dimethylaminopyridine
DMSO	dimethylsulfoxide
EDC	l-ethyl-3-(3-dimethylaminopropyl)carbodiimide hydrochloride
ESI	electrospray ionization
Et_3N	triethylamine
HCOOH	formic acid
HMBC	heteronuclear multiple bond correlation
HMQC	heteronuclear multiple quantum correlation
H_2O_2	hydrogen peroxide
HPLC	high-performance liquid chromatography
HRMS	high resolution mass spectrometry
HSL	homoserine lactone
IC	inhibitory concentration

IR	infrared spectroscopy
J	coupling constant
KBr	potassium bromide
K_2CO_3	potassium carbonate
KOAc	potassium acetate
KOH	potassium hydroxide
K_3PO_4	potassium phosphate
LAH	lithium aluminum hydride
lit.	literature
MeI	methyl iodide
mL	milliliter(s)
mmol	milli mol
m.p.	melting point
N	normal
$NaBH_4$	sodium borohydride
Na_2CO_3	sodium carbonate
$NaHCO_3$	sodium hydrogen carbonate
NaOH	sodium hydroxide
NaOMe	sodium methoxide
Na_2SO_4	sodium sulphate
$Na_2S_2O_3$	sodium thiosulphate
NBS	*N*-bromosuccinimide
NH_4Cl	ammonium chloride
nM	nanomolar
NMR	nuclear magnetic resonance
NOESY	nuclear overhauser enhancement spectroscopy
NO	nitric oxide
NSAID	non-steriodal anti-inflammatory agent
ORTEP	oak ridge thermal ellipsoid plot
OD	optical density
$POCl_3$	phosphorus oxychloride
P_2O_5	phosphorus pentoxide
PPA	polyphosphoric acid

pyBOP	benzotriazol-1-yl-oxytripyrrolidinophosphonium hexafluorophosphate
p-TSA	*p*-toluenesulfonic acid
QS	quorum sensing
RFU	relative fluorescence units
t-BuOK	potassium tertiary butoxide
TFA	trifluoroacetic acid
TFAA	trifluoroacetic anhydride
TLC	thin layer chromatography
TMS	tetramethylsilane
TMSCl	trimethylsilyl chloride
UV	ultraviolet spectroscopy
VS	virtual screening

Publication and presentations

A part of this research has been submitted for publication as well as presented at the following conferences:

Publications:

1. **Kutty, S. K**.; Bhadbhade, M. M.; Iskander, G.; Bishop, R.; Griffith, R.; Black, D. StC.; Kumar, N. Fimbrolide disulfanes: synthesis and crystal interactions, *Tetrahedron Lett.,* **2010**, 51, 4856-4858.

Presentations

1. **Samuel K. Kutty,** Nicolas Barraud, Amy Pham, Scott Rice, David StC Black, Naresh Kumar; Novel Nitric Oxide Donors Based on Fimbrolides. Poster presentation at 23rd International Congress on Heterocyclic Chemistry, Glasgow, Scotland, July 31-August 4, 2011

Chapter 1
Introduction

1.1 Bacterial infectious diseases

Infectious diseases are diseases caused by all kinds of pathogenic microbial agents, including bacteria, viruses, fungi and protozoa.[1] Despite the many advances and accomplishments in the development of antibiotics and vaccines, the steady outbreak of new infectious diseases and the re-emergence of old infectious diseases in the past decades have had a detrimental impact on human health and the global economy. Bacterial resistance, global climate change and population migration are factors that allow opportunistic infectious agents to multiply and spread among communities.[1-2] At present, infectious and parasitic diseases are the second major cause of death, accounting for 15 million deaths worldwide each year. Many of the diseases reported by WHO are associated with either viruses or bacteria, and the most frequently cited cases in hospital environments are due to bacterial infections.[3-4]

1.2 Current treatments and drug resistance

The introduction of antibiotics to combat infectious diseases is one of the most important medical interventions in reducing human morbidity and mortality. Since the discovery of natural antibiotics in the 19th century, antibiotics have been used extensively for the treatment of bacterial diseases worldwide.[5-6] The prototypical examples of antibiotics are penicillin **1**, the first natural antibiotic discovered by Sir Alexander Fleming in 1929 and sulfonamides such as Prontosil **2**, the first synthetic antibiotic reported by Gerhard J. P. Domagk in 1935. During subsequent years, many natural, semi-synthetic and synthetic antibiotics such as aminoglycosides (e.g.

streptomycin **3**), cephalosporins **4**, isoniazid **5** and glycopeptides (e.g. vancomycin **6**) have been developed and are routinely used in the treatment of bacterial infections.[7,6]

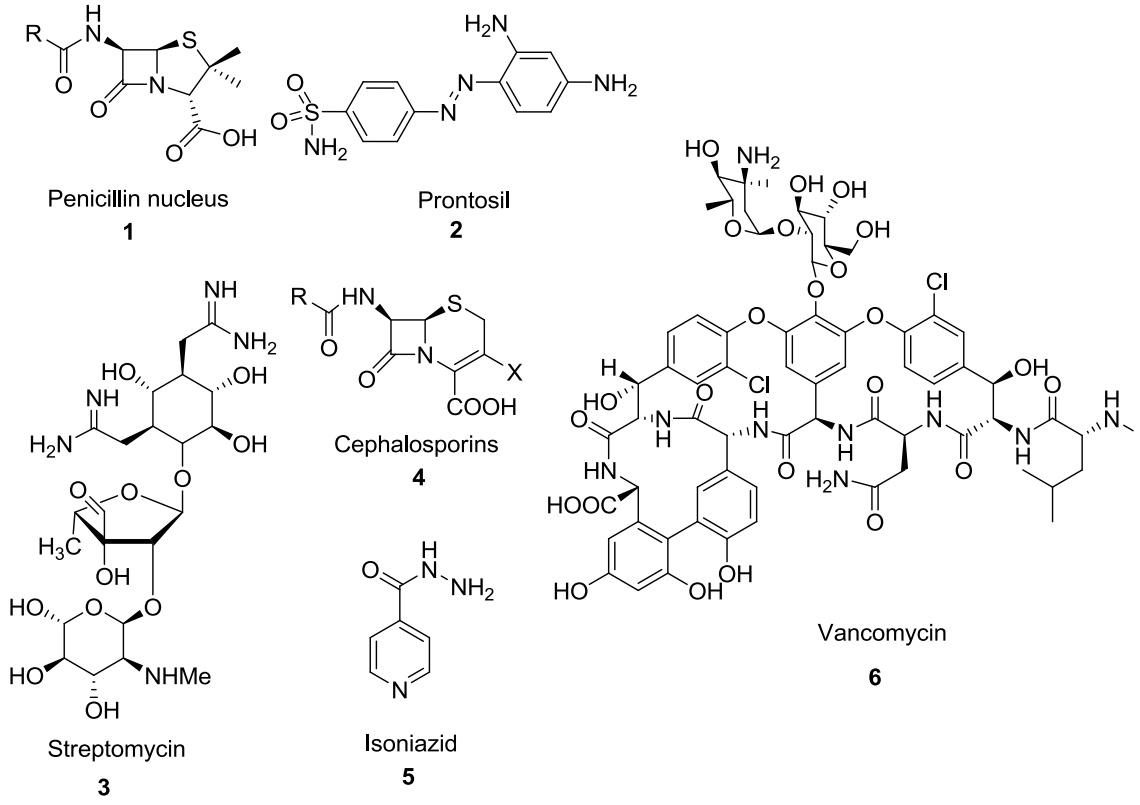

Figure 1.1: Structures of natural and semi-synthetic antibiotics.

Antibiotics are traditionally classified by their ability to kill bacteria (bacteriocidal) or inhibit growth (bacteriostatic). Antibiotics generally function by inhibiting various bacterial metabolic processes essential for bacterial survival. The mechanisms of action for traditional antibiotics can be grouped into the following categories:[8-12] inhibition of cell wall synthesis (e.g. inhibition of transpeptidase by β-lactams), inhibition of DNA or RNA synthesis (e.g. fluoroquinolones which inhibit gyrase), inhibition of protein synthesis (e.g. aminoglycosides that target ribosomes), inhibition of folate synthesis (e.g. dihydropteroate synthetase inhibition by sulfa drugs), or depolarization of membrane potential (e.g. daptomycin).

Since traditional antibiotics cause premature death of bacterial cells, this places bacteria under selective pressure to develop drug resistance in order to survive. Furthermore, the intensive and indiscriminate use of antibiotics over the years has accelerated the development of antibiotic resistance.[13] The first microbe to develop resistance to penicillin was *Staphylococcus aureus*, which developed the ability to produce β-lactamase.[14] It has been evident that the deployment of any novel antibiotic has been followed by the evolution of clinically significant resistance to that antibiotic in as little as several years. To date, most strains of bacteria have acquired resistance to at least one antibiotic.[15]

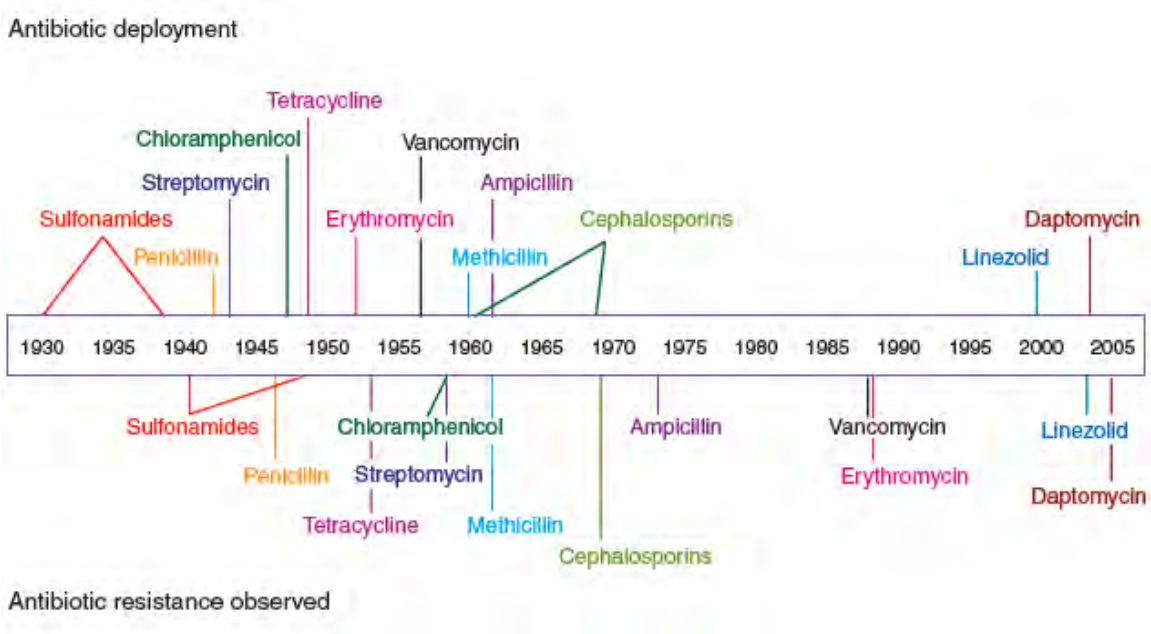

Figure 1.2: Timeline of antibiotic deployment and the evolution of antibiotic resistance. The year that each antibiotic was deployed is depicted above the timeline, and the year that resistance to each antibiotic was observed is depicted below the timeline.[15]

As we proceed further into the 21st century, the occurrence of bacterial infections in many hospital environments is continually increasing. The emergence of bacterial resistance and the lack of new antibacterial drugs have made microbial infections increasingly more difficult to treat. As a result, there is a great need to understand

bacterial virulence and survival mechanisms in order to discover novel drug targets in bacteria that may be less prone to selective pressure and resistance. One major virulence and survival mechanism adopted by bacteria is the formation of biofilms.

1.3 Microbial biofilms

Biofilms are highly-structured, sessile, surface-attached communities of cells enclosed in a self-produced matrix which acts as a barrier and protective membrane (Figure 1.5). Biofilm structures consist mainly of different bacterial communities held together by an extra-cellular polysaccharide (EPS) matrix materials, DNA and proteins.[16-18] Microbial biofilms vary in their modes of growth and in their complexity as different types of bacteria express different surface protein profiles. Despite this, the development cycle of microbial biofilms is the same for both Gram-positive and Gram-negative bacteria.[19]

The formation of the biofilm begins with the attachment of free-swimming planktonic bacterial cells to surfaces due to the amphiphilic nature of their outer membranes. When the conditions favour biofilm formation, the cells begin initiating the genes responsible for the production of exopolysaccharides (EPS) that irreversibly anchor the cells to the surface, providing both mechanical adhesiveness (to surface) and cohesiveness (between cells).[20] This instigates biofilm formation, transforming single cells to highly specialised micro-colonies covering larger surface areas.

In the second stage of the cycle, the biofilm matures into sophisticated communities with mushroom and pillar-like structures, held together by an extracellular matrix typically composed of polysaccharides, each with a definite role to support the biofilm‘s health.[21] In between the biofilm colonies are innervate amorphous networks of water channels which serve as a rudimentary circulatory system that promotes the flow of nutrients, prevents desiccation and carries waste products out of the biofilms. In the final

stage of cell death and dispersal, some single cells will detach from the biofilms and return to a planktonic mode of growth, in order to attract other microorganisms to form a new biofilm in another surface environment.

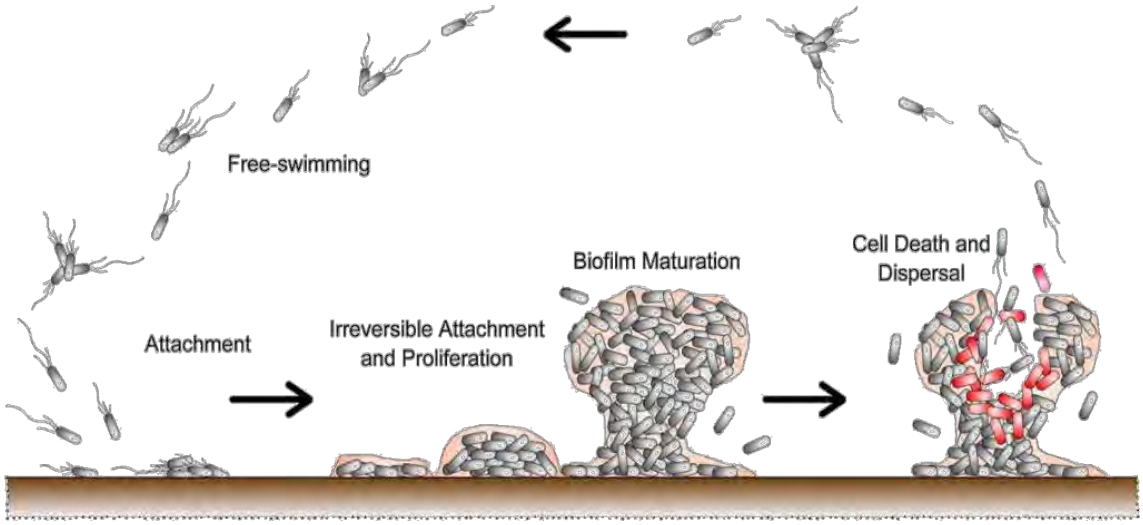

Figure 1.3: A schematic diagram of the biofilm formation cycle.

Bacteria embedded in biofilms are up to 10 to 1,000-fold more resistant to antimicrobial agents than their planktonic counterparts, and more importantly, they are also better able to withstand the host‘s immune responses, such as antibody-mediated phagocytosis.[22-25] Several factors have been suggested for the increased resistance of biofilm cells, including limited diffusion of antibiotics through the extracellular polymeric substances (EPS) matrix to the biofilm cells.[25-26] Secondly reduced metabolic activity and growth rate provides protection against antibiotics, such as the aminoglycoside tobramycin or β-lactam antibiotics such as penicillin, which are known to be more efficient against metabolically active cells.[27-28] Lastly, phenotypic diversification of biofilm cells within the biofilm community can lead to modulation of specific resistance genes, such as the over-expression of efflux pumps[20,22] and the decrease in the number of antibiotic key targets.[17,20] Biofilms thus promote adaptation of bacteria to harsh environments and are

particularly relevant to chronic infections, since the ability to withstand severe and fluctuating conditions inside a host is essential for bacterial persistence.[29]

The protection mechanism offered by biofilms makes biofilm-associated infections a major challenge for treatment and mitigation. In a medical context, it is estimated that 80% of clinical infections are biofilm-related.[26] Increased virulence of bacteria in biofilms and their intrinsic resistance to antibiotics often result in the establishment of chronic infections in humans, including otitis media (biofilms on surfaces of the ear),[30-31] bacterial endocarditis (biofilms on surfaces of the heart and heart valves),[32] cystic fibrosis (CF, biofilms on surfaces of the lungs)[33] and periodontal diseases.[34] Biofilms also readily form on clinical equipment and implant devices which have been increasingly used in hospitals for the treatment of patients.[35] Currently, more than 50% of hospital infections are associated with medical devices. The difficulty in treating such infections can lead to increased morbidity and mortality.

Biofilms can also have an economic impact in industrial settings, as their formation can lead to significant damage. For example, biofilms can cause fouling and corrosion in fluid processes such as water distribution and treatment systems (including filtration membranes), pulp and paper manufacturing systems, heat exchange systems and cooling towers,[36] and contribute to the souring of oil in pipelines and reservoirs.[37] From a public health perspective, biofilms are a common cause of food contamination. They are also receptacles of pathogens in water systems such as drinking water reservoirs and pipes,[38] and can also lead to undesirable taste and odour in drinking water.[39]

Thus, inhibition or dispersion of biofilms seems to be a key strategy in controlling and reducing microbial infectious diseases. Biofilm formation and dispersion is a complex process that involves diverse signaling/chemical networks such as quorum sensing and

c-di-GMP signaling, and physiological parameters including gradients of oxygen, nitric oxide, carbon monoxide and pH.[40] Quorum sensing (QS) plays a crucial role in the proper development of biofilms, in which bacteria utilize chemical autoinducers to communicate with their neighboring cells.[41-42] Nitric oxide (NO) has also been found to play a significant role in bacterial functioning along with biofilm formation and dispersion.[43-44] The roles of NO and other reactive oxygen and nitrogen intermediates (RONI) in biofilms is a subject of increasing interest.[45-46]

To develop novel antimicrobial agents, a better understanding of the roles of different intracellular process and chemical species in the formation and dispersion of microbial biofilms and the expression of other virulence traits in microbes is crucial. The ability to control or alter these intracellular species represents a key strategy in the fight against bacteria and its resistance. Thus, new approaches such as targeting bacterial virulence or disrupting the interaction between the host and the pathogen are attractive options. Such an approach aimed at inhibiting virulence rather than growth may impose weaker selective pressure for the development of antibiotic resistance relative to traditional antibiotics.[15]

1.4 Quorum sensing: bacterial cell-cell communication

Bacteria are consistently subjected to a myriad of environmental stimuli, and their growth and survival is dependent upon their ability to sense their environmental conditions and respond to external stimuli. Research has shown that bacteria utilize a rich lexicon of diffusible chemical molecules to communicate both between themselves and with other species.[47-48] These chemical cues are used in the downstream signal detection apparatus and signal transduction mechanisms of bacteria.[49]

The ability of bacteria to utilize extracellular signals to modify their behavior in a cell density-dependent manner was first described around 30 years ago by Nealson *et al.*,[50] who noticed that the bioluminescent bacterium *Vibrio fischeri* only produced light when bacterial cell numbers were high. Subsequent research characterized the signaling molecule, also known as an autoinducer, as well as the genes responsible for its synthesis and detection by the cell. It has been demonstrated that autoinducer sensing was dependent upon a critical number of cells in a defined volume. This threshold density of cells was first referred to as a quorum by Fuqua *et al.*,[51] and they proposed the term „quorum sensing (QS)" to describe this event. Thus, QS could be described as a generic regulatory cell-cell signaling mechanism that describes the ability of bacteria to generate and respond to small diffusible signal molecules known as autoinducers.[52-53]

1.4.1 Quorum sensing signaling systems

Three major classes of QS systems have been studied that possess a broad range of signal molecules as autoinducers (Figure **1.4**).[54-55] The most widely studied QS system is the autoinducer-1 (AI-1) system, which is mediated by *N*-acylated homoserine lactone (AHL) and is present in many typical Gram-negative human pathogens.[56]

The second type of quorum sensing system utilizes autoinducer polypeptide (AIP) as an autoinducer and is present in many Gram-positive opportunistic human pathogens such as *Staphylococcus aureus*, *Enterococcus faecalis* and *Streptococcus pneumoniae*. Such AIPs are post-translational oligopeptides that include both linear peptides and modified cyclic peptides with diverse structures.[57]

The third class of QS system is called the autoinducer-2 (AI-2) system, and is a combination of the standard Gram-negative and Gram-positive systems. The AI-2 system is regarded as a „universal" communication system proposed to be present in all

kinds of bacteria and is thought to play an essential role in the formation of mixed-species biofilms and virulence control. The AI-2 synthase, called LuxS, produces the molecule 4,5-dihydroxy-2,3-pentanedione (DPD), which undergoes a variety of spontaneous rearrangements and additional reactions to form distinct, biologically active AI-2 signaling molecules.[58-59]

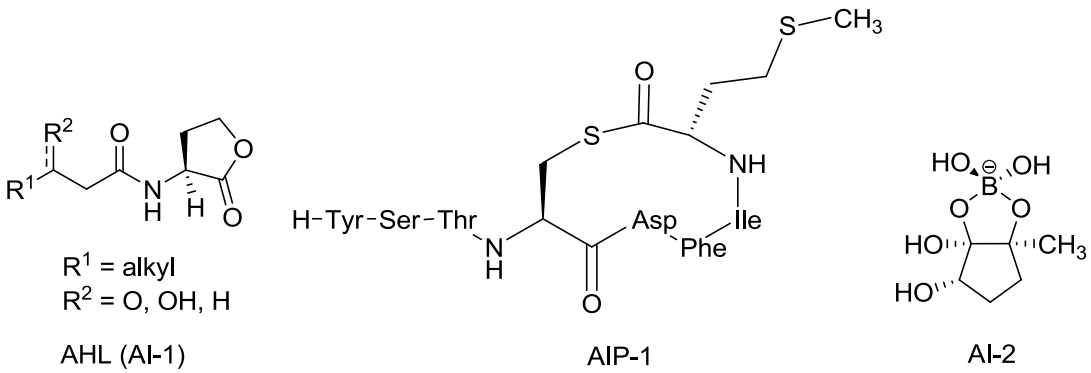

Figure 1.4: Major classes of autoinducers.

1.4.2 AHL quorum sensing system

Natural AHLs produced from different bacterial species share similar structural elements (Figure **1.5**). They consist of the same lactone group but vary in their alkyl chain length (from four to seventeen carbons) and they can be unsubstituted, 3-oxo- or 3-hydroxy substituted.[60,53] In addition, AHLs bearing double bonds have been identified, such as 8-*cis*-*N*-(3-hydroxytetradecenoyl)homoserine lactone from *Rhizobium leguminosarum*.[61-62] Furthermore, a new homoserine lactone signal, *p*C-HSL, derived from *p*-coumaric acid rather than cellular fatty acids, have been found in *Rhodopseudomonas palustri.* This reveals that natural AHLs are not limited to bearing straight chain acyl chains but may also contain aryl moieties.[63]

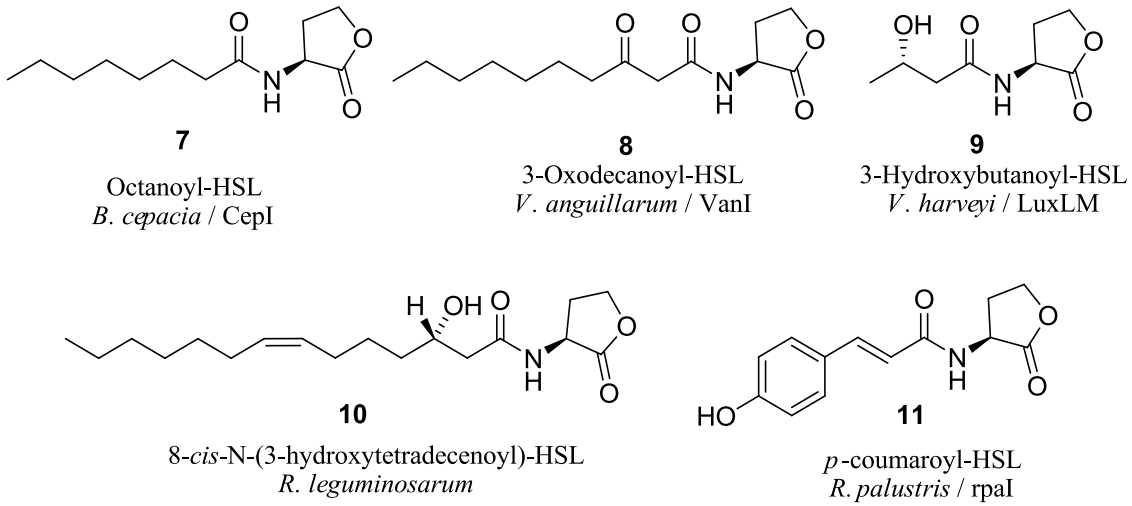

Figure 1.5: Natural signaling molecules and signaling synthases of Gram-negative bacteria

The mechanism of the AHL-meditated QS system (LuxI-LuxR system) begins with the generation of AHL signaling molecules by the LuxI-type protein. These autoinducers diffuse out of the cell and accumulate in the extracellular medium during the course of bacterial growth. When a critical threshold concentration of signal has accumulated, indicative of high cell density, diffusion into the cell overwhelms export. At this threshold concentration, AHL binds to its cognate cytoplasmic receptor LuxR-type protein to form the active dimer. The LuxR-AHL dimer complex unmasks the LuxR DNA-binding domain, allowing LuxR to interact with promoter sequences to alter the expression of target genes (Figure **1.6**).[54,64]

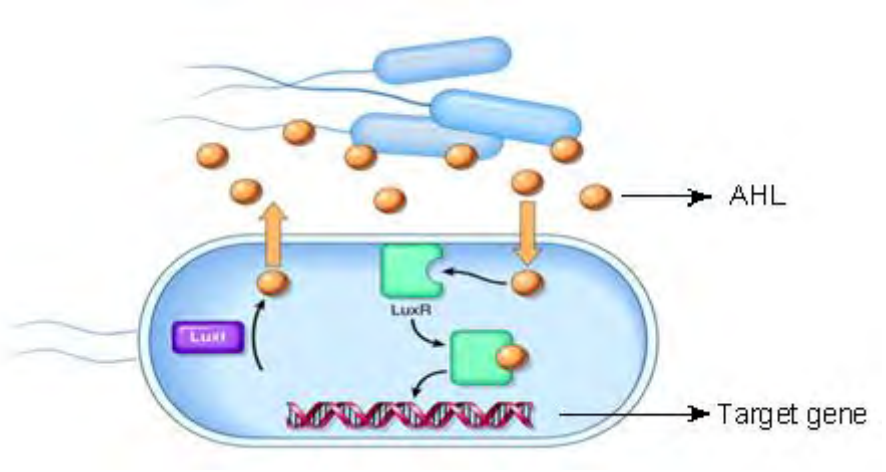

Figure 1.6: A schematic diagram of the QS system in Gram-negative bacteria. LuxI is responsible for production of AHL, and LuxR is the transcriptional regulator protein.[65]

QS signaling is involved in numerous processes, such as bioluminescence, activation of virulence factors, starvation responses, induction of competence, multicellularity, and biofilm formation.[56] The role of QS is significant in virulence, and has been shown to regulate the expression of several virulence factors, such as extracellular enzymes (elastase, protease, alkaline protease), secondary metabolites (pyocyanin, hydrogen cyanide, pyoverdin), and toxins (exotoxin A).[66-68]

QS circuits has also shown to regulate biofilms formation and dispersion and related studies have shown that *lasI* mutant strains that do not produce native AHL signal molecules form abnormal biofilms and terminate biofilm formation at the micro-colony stage, making them more susceptible to antibiotics when compared with the wild-type.[18] In another study, a mutant strain of *Y. pseudotuberculosis* lacking native AHL production showed dramatic differences in aggregation and motility compared to the wild-type.[69]

1.5 Quorum sensing inhibitors

Research on the QS phenomenon and bacterial biofilms have uncovered a new approach for the development of novel antimicrobial drugs. Blocking or interfering with the communication between bacteria to prevent the production of virulence factors or biofilm formation represents an attractive strategy to combat bacterial infections. Such a non-growth inhibition mechanism should not cause survival pressure on bacteria, and thus should not lead to development of drug resistance.[70-71]

One starting point for the development of new bioactive molecules is an understanding of the structure formed between an active receptor and its ligand. Modifying the cognate ligand of a receptor is one possible approach for finding new inhibitors of that particular receptor. Another approach is by exploring natural products that have similar structures to a ligand or that exhibit biological activity against the targeted receptor. These natural products could then be further modified to generate new derivatives with superior activity profiles. In the following sections, we describe examples of novel QS inhibitors, isolation of natural products as QS inhibitors, and the synthesis of their derivatives to provide an overview of previous research conducted in this field is described.[72-73]

1.5.1 AHL ligand-based inhibitors

Early research into the QS system of the Gram-negative bacteria focused on transforming a QS agonist (natural AHLs) into an antagonist (synthetic AHLs) by structural modification of the natural molecule. AHL inhibitors with similar structures to the natural AHL molecule can compete with its binding to the LuxR receptor. Binding of the ‗fake' signaling molecule to the LuxR receptor prevents signal transduction to its target genes, inhibiting the biofilm formation and virulence expression (Figure **1.7**).[74]

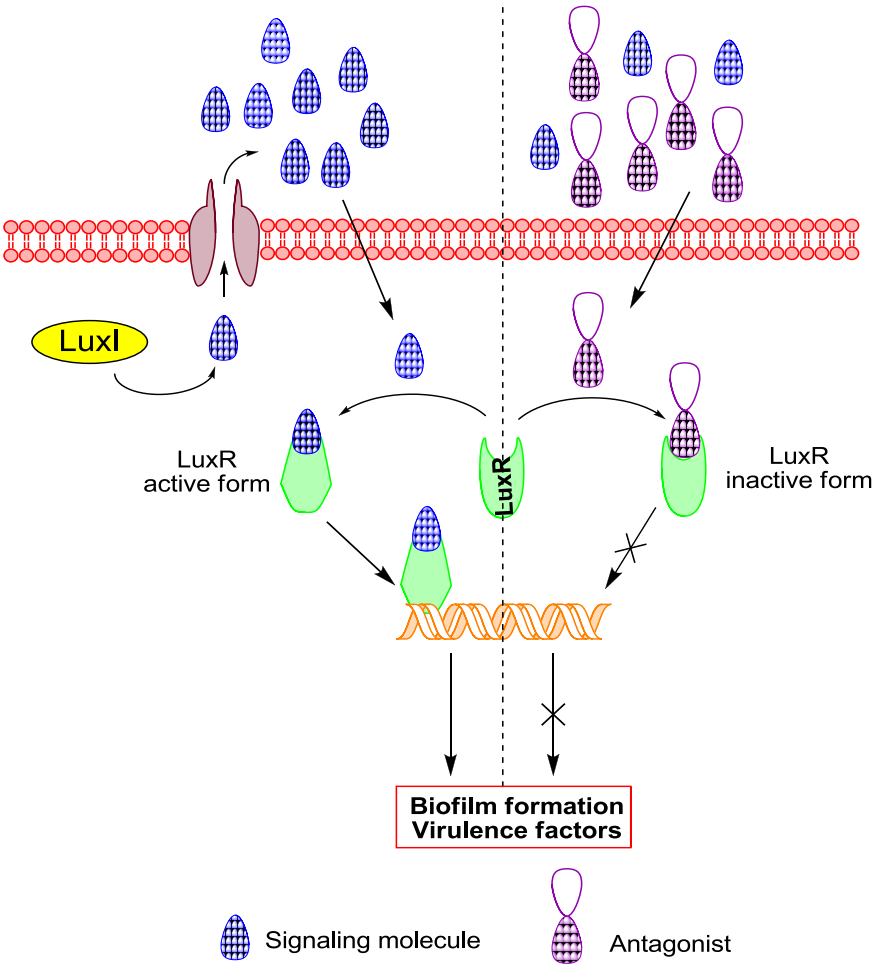

Figure 1.7: A schematic diagram of the AHL-mediated QS system (left) and disruption of the system by an antagonist (right).

Direct structural modification of AHL signal molecules is a straightforward approach for engineering an AHL antagonist[74]. Studies in this area have focused upon modification of (1) the acyl side chain, (2) the lactone ring, (3) both the acyl side chain and the lactone ring, or (4) the bond between the lactone ring and the side chain.

The effect of a particular AHL molecule on bacterial QS can vary from species to species, and differences in the acyl side chain of an AHL can greatly influence the functionality of the molecule. Research has shown that some natural AHL signaling molecules function as agonists in some bacterial species and as antagonists in others. For instance, compound **12** is an agonist of receptor AhyR, RhlR and SwrR, while

compound **13** is an agonist of CViR, but both act as antagonists of LuxR (Figure **1.8**).[75] Schaefer and co-workers studied more than 20 different AHL molecules and found that most receptors only respond to analogues which differed by less than two carbons from its cognate AHL molecules. Compounds that have decreased flexibility in the side chain or at lactone C2 position (near the amide bond) have no agonist activity. Hence, changes in the structure of AHLs can abolish their agonistic activities, while enhancing their inhibitory effects.[76]

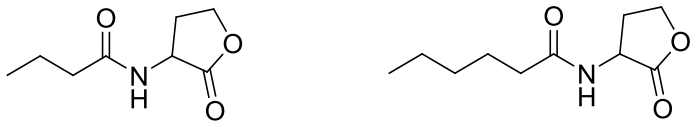

12 (AhyR, RhlR, SwrR) **13** (CviR)

Figure 1.8: Examples of natural AHL molecules and their corresponding receptors.[75]

Reverchon and co-workers synthesized a range of aryl and heteroaryl-substituted analogues (Figure **1.9**), and examined their effectiveness as AHL antagonists. Phenyl-substituted molecules **14** were found to possess antagonist activity, but the bulkier compounds **15-17** and the thiophenyl analogue **18** were inactive. The authors hypothesized that the aromatic phenyl group can enhance the interaction between the AHL molecules with one or several of the aromatic amino acids of the LuxR protein, but that bulkier aromatic systems may be subjected to steric hindrance.[77]

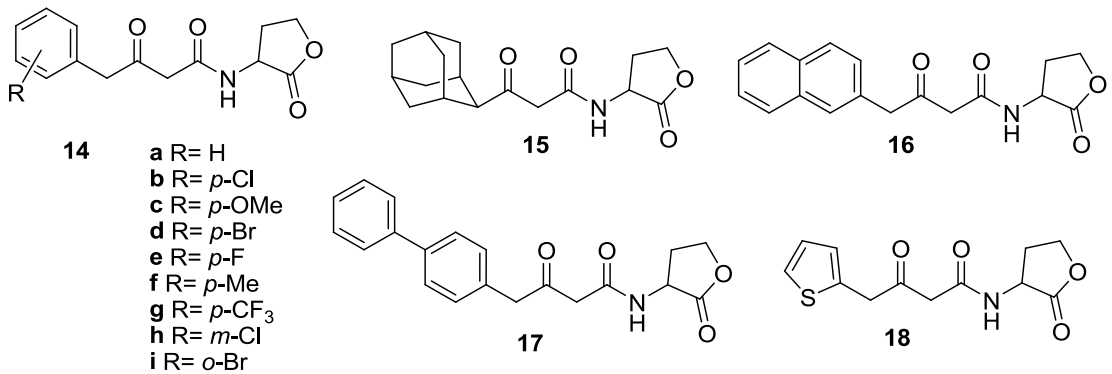

Figure 1.9: Aryl and heteroaryl-substituted AHL analogues.[77]

Passador *et al*. reported a series of antagonists through modification of the lactone ring to generate AHL analogues with thiolactone **20** or lactam rings **21** (Figure **1.10**).[78] Similarly, Smith *et al*. synthesized a library of analogues **22**-**29** derived from *P. aeruginosa* autoinducers 3-oxo-C12-HSL **19** and C4-HSL **12**, by altering the lactone ring while retaining their respective side chains (Figure **1.10**).[79-80]

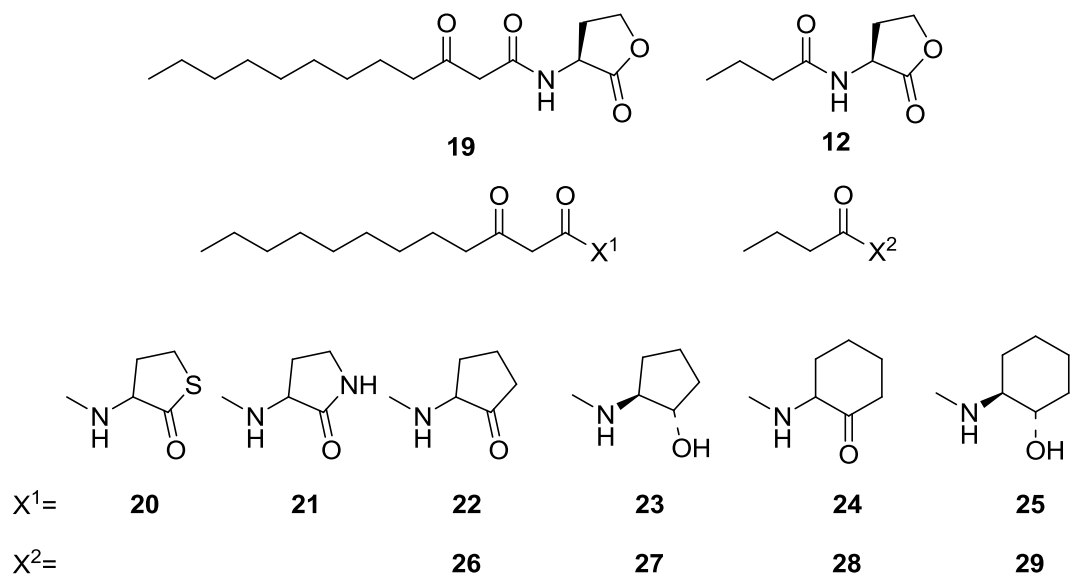

Figure 1.10: Structures of *P. aeruginosa* autoinducers and their analogues.

Castang *et al*. developed a new generation of AHL antagonists by replacing the carboxamide bond with a sulfonamide bond (Figure **1.11**). Compounds of type **30** exhibited antagonist activity, whereas the 3-oxo derivatives **31** were found to be inactive.[81]

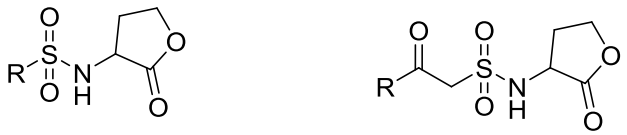

30 **a** R= C_4H_9
b R= C_5H_{11}
c R= $PhCH_2$
d R= PhC_2H_4

31 **a** R= C_3H_7
b R= $PhCH_2$

Figure 1.11: Racemic sulfonamide AHL analogues.

Geske *et al*. synthesized a range of compounds bearing some of the important antagonistic motifs described previously. The aryl-substituted *N*-phenylacetanoylhomoserine lactones (PHL) elicited remarkable QS responses in *V. fischeri*. PHLs displayed the characteristics of a ‗global' inhibitor of Gram-negative bacteria, as they strongly antagonize the signaling pathways of various bacterial strains. In general, sterically large lipophilic or halogen groups at the 4-position such as 4-phenyl **32a**, 4-trifluoromethyl **32b** or 4-iodo **32c** enhanced antagonistic effects. Interestingly, 3-nitrophenyl substitution generated a PHL analogue **33** with strong agonist activity.[82]

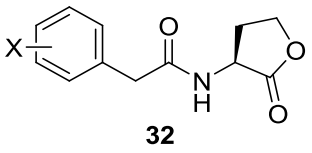

32

Entry	X	IC_{50} (μM)
a	4-Ph	1.1
b	4-CF_3	0.6
c	4-I	0.9

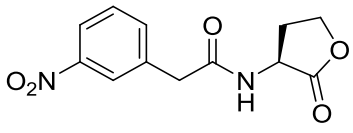

33

EC_{50} = 0.3 μM

Figure 1.12: *N*-phenylacetanoylhomoserine lactone (PHL)-based QS modulators.[82]

In summary, extensive research on AHL analogues have revealed that small structural changes to the parent signalling molecules can result in vastly different biological activities. Therefore, it is important to develop efficient synthetic routes to AHL analogues, so that the chemical space around these types of molecules can be effectively explored. This would facilitate the discovery of more novel and potent AHL-based QS modulators, which could in turn further our understanding of the relationships between AHL molecules and their biological activities.

1.5.2 Fimbrolides and their derivatives

Natural products have historically represented a major source of new chemical entities and pharmaceutically useful molecules.[83-84] Marine ecosystems have been shown to be a

rich source of diverse natural chemical species, particularly halogenated compounds.[85-86] Marine organisms produce these natural organohalogens for a specific purpose, usually the survival of the species.[87]

In the natural marine environment, the red marine alga *Delisea pulchra* (Figure **1.13**) has a unique ability to stave off colonization by common fouling organisms (epiphytes or bacteria) on their thallus surfaces.[88-89] This phenomenon has been attributed to the ability of *D. pulchra* to produce a range of halogenated furanones and enones.[90-92] These halogenated furanone derivatives, termed fimbrolides, share a common 4-halo-3-butyl-5-halomethylene-2(5*H*)-furanone skeleton. Fimbrolides are rarely-occurring metabolites residing in vesicles on the surface of the algae, and were first isolated in 1977.[93-94] In 1993, de Nys *et al*. isolated about twenty different halogenated furanones, including seven new halogenated furanones, from *D. pulchra*.[95,90] The structures of fimbrolides produced by *D. pulchra* (Figure **1.13**) vary primarily in their number and nature of the halogen substituents at C-6, and the presence or absence of oxygen functionality such as acetate or hydroxyl groups at the C-1′ position of the butyl side chain.[93,90]

Figure 1.13: a) Australia red seaweed, *D. pulchra*. b) Representative fimbrolides isolated from *D. pulchra.*

Natural fimbrolides have potent antimicrobial effects and are able to influence bacterial behaviour by interfering with the bacterial QS system. They possess the ability to alter

bacterial surface-dependent phenomena, such as swarming motility and biofilm formation.[88,96,92] The expression of virulence factors and bioluminescence has also been shown to be modulated by natural fimbrolides in different bacterial species.[91,97]

The ability of *D. pulchra* furanones and their synthetic analogues to disrupt QS in Gram-negative bacterial strains has been well documented. However, the molecular targets and precise mode of action of such compounds remain elusive, and this has been a topic of debate in the literature.[73] The structural similarities between AHL molecules and furanones has led some to hypothesize that these compounds bind to the AHL-binding site in the LuxR receptor protein, thereby displacing the cognate AHL autoinducers and interfering with the QS system.[91] Studies have also shown that halogenated furanones promote rapid turnover of the LuxR-type receptor protein, reducing the amount of active receptor able to interact with AHL and thus decreasing the concentration of the subsequently formed transcription regulator complex.[98] Therefore, inducing the degradation of the LuxR-type protein has also been hypothesized as a possible QS inhibitory mechanism by halogenated furanones. Defoirdt *et al.* have recently postulated that furanone **34d** blocks QS in the bacterium *V. harveyi* by decreasing the DNA-binding activity of the transcriptional regulator protein LuxR.[99]

Furanones have also been demonstrated to interfere with the autoinducer-2 (AI-2) bacterial system in some Gram-negative bacteria. Work by Ren *et al.* showed that (5*Z*)-4-bromo-5-bromomethylene-3-butyl-2(5*H*)-furanone **34a**, naturally produced by *D. pulchra*, inhibits AI-2-dependent QS in *E. coli*. It was shown that the furanone greatly inhibited swarming motility and biofilm formation in *E. coli*.[100] In summary, halogenated furanones may exert their QS inhibitory effects *via* a combination of different mechanisms or through a specific mechanism dependent on the furanone structure and the bacterial species involved.

Exploiting the fimbrolide scaffold for the development of novel antibacterial agents has received particular interest in the literature. Early work focused upon the development of furanone analogues retaining a high degree of structural similarity to the natural fimbrolide **34a** (Figure **1.14**).[101] For example, a series of unnatural dibromomethylene derivatives **35** with different alkyl chain length were synthesised. In addition, compounds **36-37** retaining the furanone skeleton without alkyl chain have also been developed. [102-104]

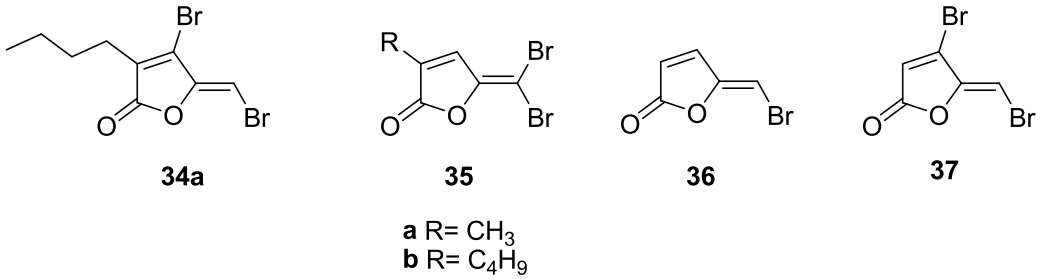

Figure 1.14: Synthetic furanone compounds derived from natural fimbrolide **34a**.

The inhibitory activity of furanone **36** was investigated on *P. aeruginosa* cultures in the presence of the native AHL signalling molecule, 3-oxo-C11-HSL (OdDHL). The results showed that furanone **36** is able to compete with OdDHL for binding to the receptor protein. Also, furanone **36** displayed no effects on bacterial growth and protein synthesis,[67] but was found to affect a wide range of genes including QS-associated virulence genes and other multidrug efflux genes in *P. aeruginosa*.[105] Interestingly, co-administration of furanone **37** and OdDHL showed significant inhibition of green fluorescent protein (GFP) production at a 10-fold lower dose than required for furanone **36** alone.

Investigation of furanone analogues was further extended to the synthesis of structurally similar dihydropyrrolone bioisosteres **38**–**41**, which showed similar biological activities with better hydrolytic stability (Figure **1.15**).[106] Among these compounds, pyrrolone **41a**

showed the best QS inhibition activity against *E. coli* AHL-monitor strain JB357, while compounds **38b, 38c** and **38e** also showed antagonist activity but were not as potent as their parent furanones.[107]

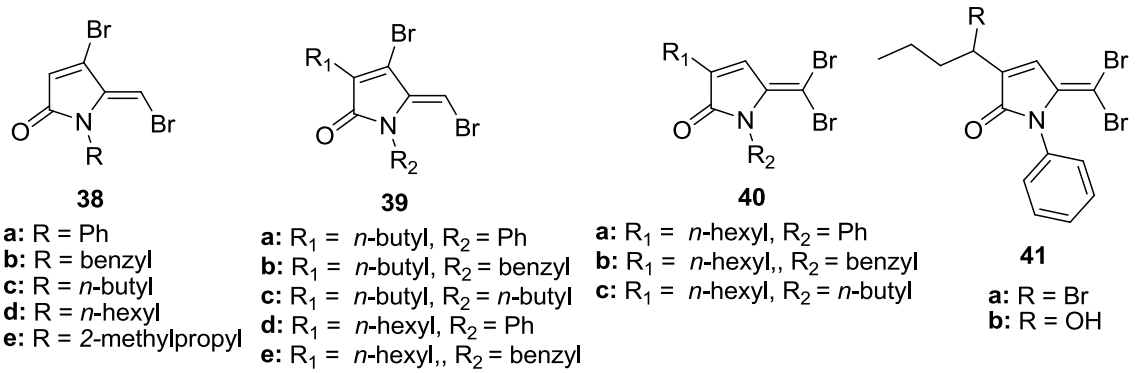

Figure 1.15: Synthetic dihydropyrrolones.[107]

1.6 Nitric oxide

Nitric oxide [nitrogen monoxide, •NO, IUPAC: oxidonitrogen(•)] is a colorless paramagnetic free radical gas formed in the troposphere during lightning or electrical storms. NO, initially suspected as a toxic, carcinogenic air pollutant produced from fuel burning, became the ‗molecule of the year' in 1992 on the cover story of *Science*[108] due to the discovery of its wide array of biological functions, including smooth muscle relaxation, inhibition of platelet aggregation, neurotransmission and host defense mechanisms. The 1998 Nobel Prize in Physiology and Medicine was awarded to Ferid Murad, Robert F. Furchgott and Louis Ignarro for their discovery of the signaling properties of NO.[109] Nitric oxide, with a molecular mass of only 30 g/mol, is the smallest, lightest and the first gas known to act as a biological messenger in mammals. Thus, over the past decades, the recognition of the multiple biological roles of NO has transformed this molecule from a menace into a wonder in various areas of biological research.

1.6.1 Biosynthesis of nitric oxide

Nitric oxide is biosynthesized by the enzyme nitric oxide synthase (NOS) through the stepwise oxidation of *L*-arginine, *via* an *N*-hydroxyarginine intermediate, into NO, citrulline and NADP (Figure **1.16**).[110]

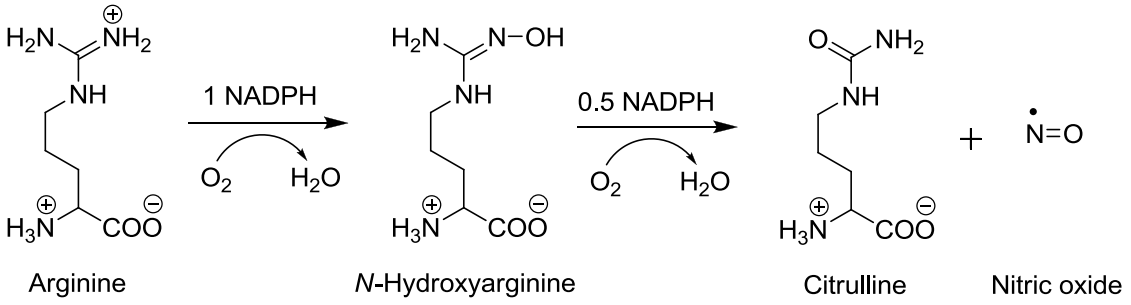

Figure 1.16: Biosynthesis of nitric oxide.

NOSs are dimeric flavoproteins containing tetrahydrobiopterin, FAD, FMN and iron protoporphyrin IX (heme), and have homology with cytochrome P450.[111] There are three major distinct isoforms of NOS, including two constitutive forms present under physiological conditions in endothelial cells (eNOS or NOS-III) and in neurons (nNOS or NOS-I), and an inducible form (iNOS or NOS-II) expressed in macrophages, fibroblasts, and Kupffer cells.[112-113] An additional isoform of NOS, mitochondrial NOS (mNOS), has been reported to help regulate mitochondrial energy production *via* NO signaling.[114] The constitutive enzymes are activated by calcium-calmodulin generate small amounts of NO, whereas iNOS produces much greater amounts of NO, especially during infection and inflammatory responses.[115-116]

1.6.2 Nitric oxide inactivation

Nitric oxide is an unstable gas, and reacts primarily with oxygen, superoxide or redox metals. NO reacts with oxygen to form N_2O_4, which combines with water to produce a mixture of nitric and nitrous acids, or can be oxidized into nitrite or nitrate which are

excreted through the urine.[117] NO readily forms complexes with transition metals, such as the heme group of hemeglobin, leading to inactivation of NO. Low concentrations of NO are relatively stable in air. However, NO reacts rapidly with even low concentrations of superoxide anion (O^{2-}) to produce the peroxynitrite anion ($ONOO^-$). The peroxynitrite anion is a strong oxidizing and nitrating species responsible for some of the toxic effects of NO, through free radical-mediated lipid peroxidation, sulfhydryl oxidation, tyrosine nitration and DNA deamination.[116-119]

1.6.3 Biological effects of nitric oxide

Nitric oxide mediates many diverse physiological processes in the body, and its effects are largely concentration-dependent (Figure **1.17**).[120-121] At low concentrations, NO exerts direct effects on cellular systems, which are broadly orchestrated by two major biochemical signaling pathways.

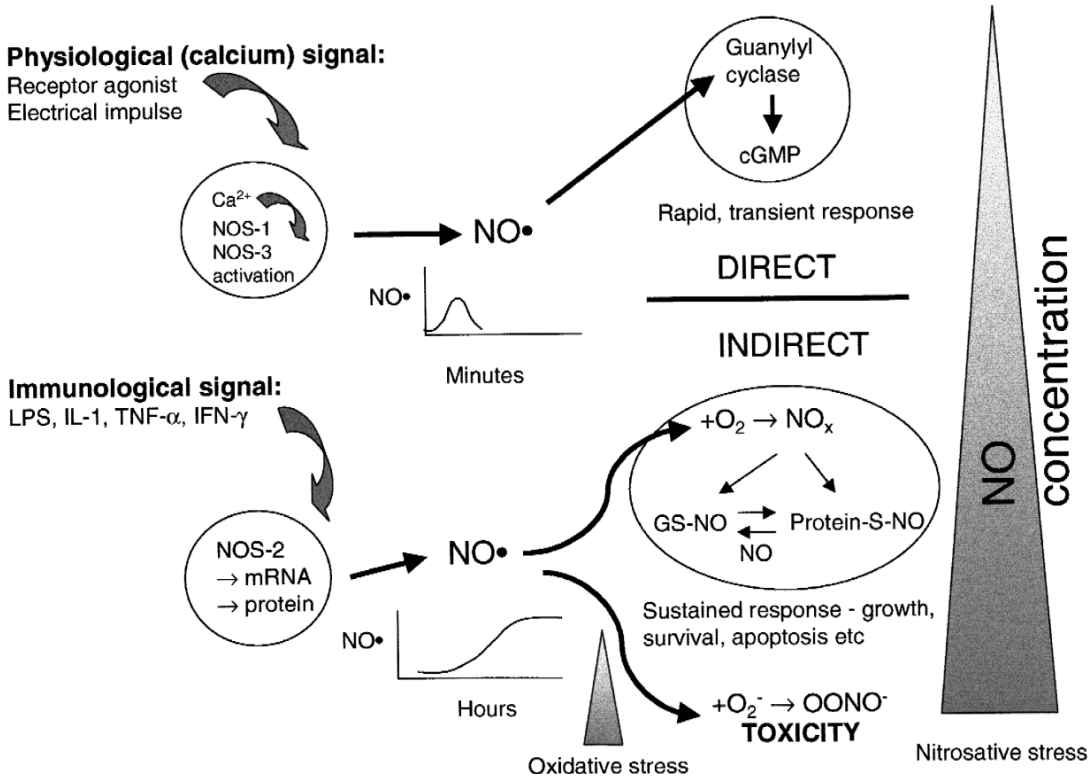

Figure 1.17: Summary of NO biochemistry and its associated effects.[120-121]

One of the most important biochemical effects of NO is the activation of soluble guanylate cyclase (sGC), a heterodimeric enzyme present as distinct isoenzymes in vascular and nervous tissue. NO activates sGC by combining with its heme group to form a nitrosyl-heme complex, which results in the production of the secondary messenger cGMP from GTP.[122] This, in turn, leads to the activation of cGMP-dependent protein kinases, cGMP-regulated phosphodiesterases, and cyclic-nucleotide-gated ion channels, which ultimately promote the main biological functions of NO, including vasodilation, neurotransmission, inhibition of platelet aggregation and smooth muscle relaxation.[123]

The second mechanism by which NO exerts its biological functions occurs through the reaction of NO with thiols and transition metals such as zinc. NO can also modify proteins, DNA and lipids directly, without requiring enzymes involved with nitration or nitrosylation. *S*-nitrosylation of cysteine thiol groups is a reversible modification which regulates the function of many intracellular proteins and thus controlling cellular signaling pathways and activities.[124]

By comparison, higher concentrations of NO have an indirect effect on biomolecules, which is possibly mediated *via* the formation of reactive nitrogen species (RNS) from molecular O_2 or superoxide (O_2^-).[117] Large amounts of NO released following induction of NOS or excessive stimulation of NMDA receptors in the brain cause cytotoxic effects *via* peroxynitrite anions.[125] NO contributes to inflammatory reactions and host defence against pathogens, but can also lead to tumour growth or neuronal destruction associated with overstimulation of NMDA receptors by glutamate.[121,126] Paradoxically, NO has also been reported to display cytoprotective effects under certain conditions.[127]

In summary, NO exerts a variety of regulatory effects *via* multiple biological pathways in the cell, and appears to play a vital role in the normal functioning and behavior of the human body.

1.7 Nitric oxide regulation in microbes

In bacteria, nitric oxide plays multiple roles in the bacterial life cycle, and thus the regulation of NO levels in bacteria has received particular interest. Overall, NO appears to be involved in the regulation of denitrification, iron acquisition and detoxification. The levels of NO can be controlled by the interactions between different regulators. To date, several NO-responsive regulatory networks have been identified in bacteria (Figure **1.18**).

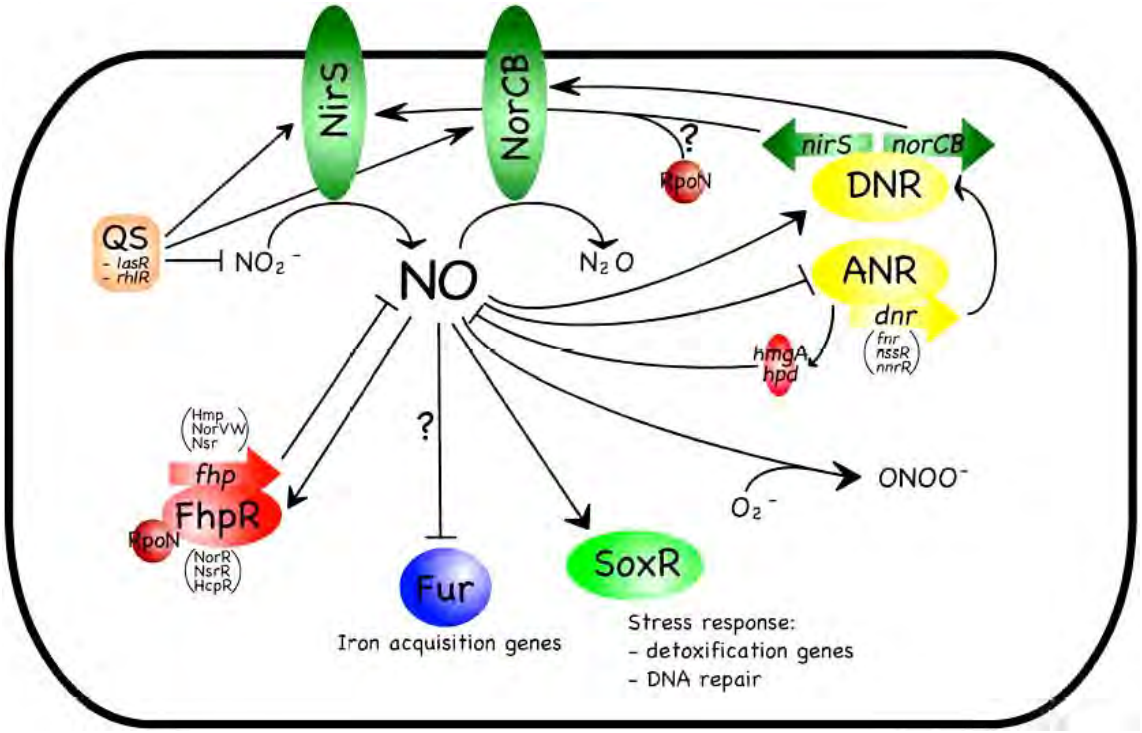

Figure 1.18: Hypothetical model of regulatory pathways controlling NO homeostasis in *P. aeruginosa*. Arrow-headed lines indicate activation and bar-headed lines indicate inhibition. Homologue genes or proteins, as indicated in parentheses, are also found in other microorganisms.[44]

NO is the reaction product and substrate of bacteria during the denitrification process, which involves dissimilatory reduction of different nitrogen oxide species such as nitrate to nitrite, and then further reduction to nitric oxide. Genes involved in denitrification are mainly regulated by two NO-responsive transcriptional activators: DNR (dissimilatory nitrate respiration regulator) and NNR (or NnrR; nitrite, nitric oxide reductase regulator).[128] These two factors are responsible for maintaining steady-state concentrations of NO below cytotoxic levels.[129-132] Another transcriptional activator in *P. aeruginosa*, termed ANR (anaerobic regulation of arginine deiminase and nitrate reduction), is involved in the regulation of the denitrification pathway. ANR appears to function in a hierarchical fashion with DNR, with the expression of DNR being under the control of ANR.[133-134] ANR activates different anaerobic pathways and induces the expression of DNR under low O_2 tension, and may also „shut down" the denitrification pathway in the presence of abnormal levels of NO.[135-136]

DNR controls the activities of different denitrification enzymes, including membrane-bound nitrate reductase or a periplasmic nitrate reductase (Nar), which brings about reduction of nitrate (NO_3^-) to nitrite (NO_2^-), and nitrite reductase (Nir), which is responsible for the conversion of nitrite (NO_2^-) to NO. Nir can be further classified into two categories: the cytochrome nitrite reductase (cd_1-dNir) and the copper-containing nitrite reductase (Cu-dNir).[137]Another denitrification enzyme is NO reductase (Nor), a member of the heme-copper oxidase family with a high affinity for NO usually found as part of the membrane-bound cytochrome *bc* complex.[138]

In *E. coli* and *B. subtilis*, NO was shown to inhibit DNA-binding by the ferric uptake regulator (Fur), leading to up-regulation of genes required for iron acquisition.[139-140] In *P. aeruginosa*, microarray studies have revealed a large overlap in genes up-regulated

upon exposure to NO, and those expressed under iron-limiting conditions, indicating correlation between NO and iron-limiting processes.[141-142]

Anaerobic growth of *P. aeruginosa* PAO1 has been shown to be affected by QS. Deletion of genes that produce autoinducer signals resulted in an increase in denitrification activity, which was repressed by exogenous signaling molecules.[143-144] Similarly, anaerobic processes and NO levels in biofilms have also been found to be regulated by QS. Microarray studies have revealed that both *nirS* (nitrite reductase) and *norCB* (NO reductase) are highly expressed in biofilms compared to planktonic cells, and that their over-expression is quorum sensing-dependent.[145-147]

Gene expression profiles in *P. aeruginosa* biofilms were shown to closely resemble those of bacteria in stationary phase (nutrient-limited), anaerobic and iron-limited modes of growth, or under QS regulatory control.[148,145,149] As described above, NO is intimately associated with each of these biofilm-relevant processes. Thus, NO appears to be involved in many processes known to be crucial for biofilm formation.

1.7.1 Nitric oxide as an antimicrobial and antibiofilm agent

Nitric oxide production from iNOS in mammals is stimulated by proinflammatory cytokines, and is a critical component of the mammalian innate immune response. The cytotoxic and/or cytostatic effects of NO have been associated with primitive non-specific host defence mechanisms against numerous pathogens, including viruses, bacteria, fungi, protozoa and parasites. The importance of this is evidenced by the susceptibility of mice lacking the iNOS gene to infections as diverse as leishmaniasis, malaria and tuberculosis.[121,150]

The antimicrobial mechanisms of NO are still poorly understood. NO may exert its effects through complexation with thiols, heme groups or the iron-sulphur centres of

enzymes essential for cell functioning, or may cause nitrosylation of nucleic acids, thereby interfering with DNA replication of bacteria. At higher concentrations, NO reacts to form reactive nitrogen and oxygen intermediates such as peroxynitrite or the hydroxyl radical, which are toxic due to its ability to induce nitrosation, deamination or oxidation reactions with DNA, enzymes, proteins and other macromolecules in microbial systems.[151-154]

Cell death and dispersal events in *P. aeruginosa* biofilms are related to oxidative and/or nitrosative stress.[45] In particular, NO or reactive species produced from NO can cause dispersion of the biofilm. For example, enhanced levels of $ONOO^-$ (peroxynitrite, produced from the reaction of NO and O_2) were found in microcolonies of mature 7-day-old biofilms, and were proposed to be responsible for cell death and dispersal. Moreover, a *ΔnirS* mutant strain (lacking nitrite reductase) without the ability to produce NO forms biofilms that fail to disperse, whereas a *ΔnorCB* mutant (lacking NO reductase), produces large amounts of NO and shows enhanced biofilm dispersal (Figure **1.19**).[155]

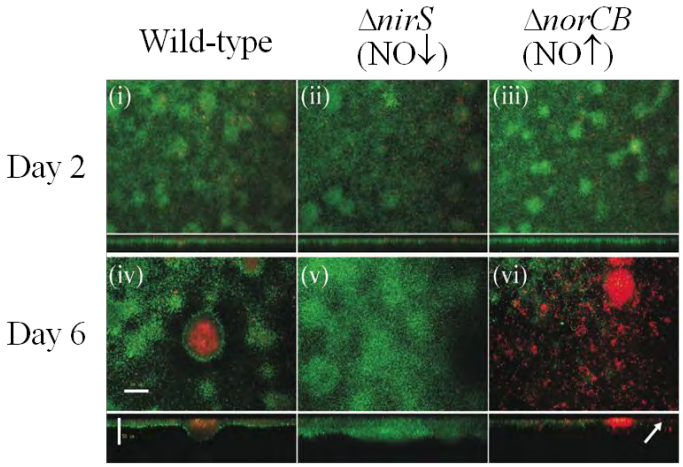

Figure 1.19: Biofilm development and dispersal of *P. aeruginosa* wildtype, nitrite reductase-deficient mutant (Δ*nirS*, unable to produce NO), and NO reductase-deficient

mutant (Δ*norCB*) strains. Biofilms grown and stained with LIVE/DEAD staining. Live cells are green, and dead cells are red.[155]

NO at low, non-toxic concentrations have also been shown to induce biofilm dispersal of *P. aeruginosa*, as well as a broad range of environmentally and clinically relevant bacterial species. The molecular mechanism involved in biofilm dispersal at low NO concentrations involves the secondary messenger c-di-GMP.[156] Exogenous NO, at sub-lethal concentrations, is able to induce the transition of bacteria in biofilms from a sessile mode of growth to a free-swimming, planktonic mode. NO at non-lethal concentrations has also been shown to increase the sensitivity of various biofilms to antimicrobial treatments (Figure **1.20**).[157]

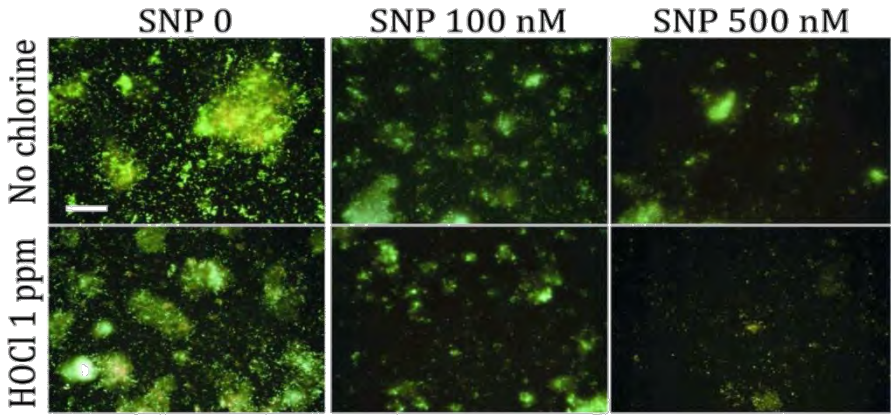

Figure 1.20: The images show microscopic pictures of recycled water biofilms after exposed to SNP for 18 h and treated with 1 ppm HOCl (lower panels) or no chlorine controls (upper panels) and stained with the LIVE/DEAD reagents. Live cells appear green, dead cells appear red.[157]

1.8 Nitric oxide donors

The discovery of the ever-increasing biological functions of NO has led to the development of a wide array of novel NO donors as research tools and as

pharmaceuticals. Most of the NO donors known today were discovered or synthesized before their role as NO donors were fully understood, or were rediscovered over the past few decades. In addition, a wide range of novel molecules with NO-releasing properties have also been reported in literature.[158-159]

NO donors can be classified into different types, based on either their chemical natures (Table **1.1**) or their mechanisms of NO generation. The wide variety of structural motifs among NO-donating compounds results in remarkably varied chemical reactivities and NO-releasing mechanisms. One such mechanism is the spontaneous release of NO through hydrolytic, thermal or photochemical self-decomposition, as exemplified by the diazeniumdiolates, *S*-nitrosothiols, or oximes. The second NO-releasing mechanism, exhibited by organic nitrates, nitrites and sydnonimines, is *via* reaction with acids, alkalis, metals, or thiols. The third NO-releasing mechanism is through oxidation by enzymes such as cytochrome P450, xanthine oxidase or NO synthases. For example, *N*-hydroxyguanidines, require metabolic activation by NO synthases to release NO. Some NO donors may release NO by more than one route, such as the organic nitrates which can generate NO by chemical reaction or by enzymatic catalysis.[109,160]

Table 1.1: Examples of NO donors.[160-161]

Entry	Name	Examples
1.	Organic nitrates (e.g. glyceryl trinitrate)	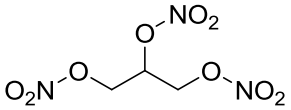
2.	Organic nitrites (e.g. *tert*- pentyl nitrite)	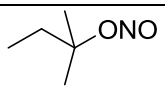
3.	Metal-NO complexes (e.g. sodium nitroprusside)	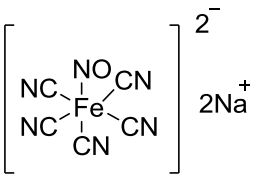

4.	*N*-Nitrosoamines (e.g. *N*-(2,5-dihydroxyphenyl)-*N*-methylnitrous amine)	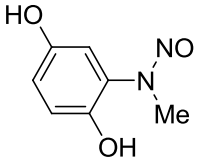
5.	*C*-Nitrosoamines (e.g. 2-nitro-2-nitrosopropane)	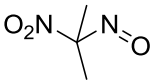
6.	*S*-Nitrosoamines (e.g. *S*-nitroso-*N*-valerylpenicillamine)	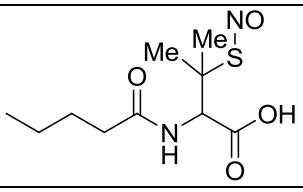
7.	Diazeniumdiolates (e.g. sodium 1-(pyrrolidin-1-yl)diazen-1-ium-1,2-diolate)	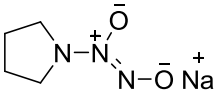
8.	Furoxans and benzofuroxans (e.g. 4-phenyl-3-furoxancarbonitrile)	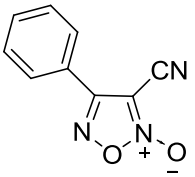
9.	Sydnonimines (e.g. molsidomine)	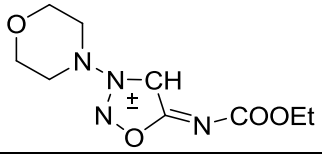
10.	Oximes (e.g. FK409)	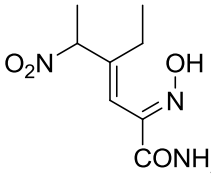
11.	Hydroxylamines (e.g. hydroxylamine)	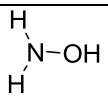
12.	*N*-Hydroxyguanidines (e.g. (*S*)-2-amino-5-(3-hydroxyguanidino)pentanoic acid)	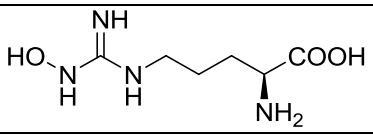

Of the NO donors described, nitrates, diazeniumdiolates and *S*-nitrothiols are of particular interest due to their distinct advantages, and these three NO donors are discussed in greater detail below.

1.8.1 Nitrates

Nitrates (nitroesters) have historically been more renowned for their explosive properties, rather than for their therapeutic effects. The first therapeutic use of organic

nitrates was discovered in 1867 by physician Launder Brunton, who used the inhalation of amyl nitrate vapors to relieve anginal pain.[162] This led to development of nitrates such as glyceryl trinitrate (GTN) **42**, isosorbide dinitrate (ISDN) **43** and isosorbide mononitrate (ISMN) **44**, which have been used as the main treatment of angina and other vasodilation-related cardiovascular diseases for over a century. Nitrates exert their effects *via* their metabolite NO, which activates guanylate cyclase leading to the formation of the secondary messenger cGMP, which in turn activates cGMP-dependent kinase to induce relaxation of vascular smooth muscle.[163-164]

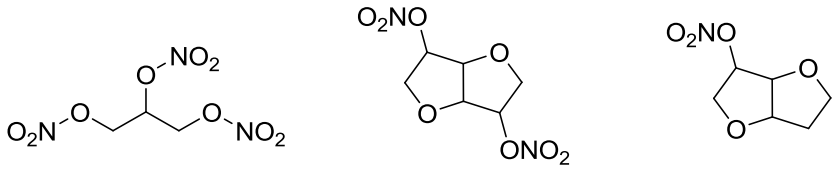

42 **43** **44**

Figure 1.21: Structure of clinically relevant organic nitrates.

The mechanism of NO release from nitrates under physiological conditions is still a matter of considerable debate, but can be broadly classified into two major endogenous mechanisms, the enzymatic and non-enzymatic pathways. The enzymatic mechanism proceeds through activation of the nitrate by glutathione *S*-transferase, cytochrome P450, and/or xanthine oxidoreductase, or alternatively through catalytic activity mediated by mitochondrial aldehyde dehydrogenase (ALDH-2).[165-167] On the other hand, the non-enzymatic mechanism involves denitration by reaction with thiol (SH) groups to generate an *S*-nitrosothiol, which discharges NO upon decomposition.[168] Dysfunction of these endogenous pathways may lead to nitrate tolerance, which is a major problem associated with the long term usage of nitrates such as GTN and ISDN.[169-172]

In order to overcome thiol depletion and tolerance, nitrates based on cysteine and 2-oxothiazolidine **45** have been developed.[173] Pentaerythrityl tetranitrate (PETN) **46** is also a tolerance-devoid nitrate.[174] Aminoalkylnitrate derivatives such as 2-nitrooxyethylammonium nitrate (AEN) **47** represent a new class of organic nitrates that do not cause oxidative stress or induce tachyphylaxis *in vitro*, and which possess impressively high potencies compared to the other mononitrates tested.[175-177]

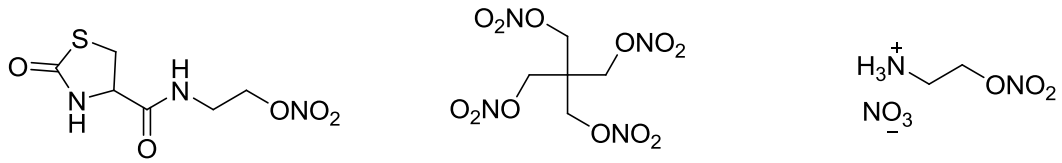

45 **46** **47**

Figure 1.22: Examples of organic nitrate derivatives less prone to nitrate tolerance.

1.8.2 Diazeniumdiolates

Diazeniumdiolates are anions containing the $[N(O)NO]^-$ functional group. The first report of diazeniumdiolates (NONOates) dates back to 1802, which described a sulfur-based diazeniumdiolate known as Pelouze's salt **48**. Over the last two centuries, a wide range of diazeniumdiolates bound to oxygen (*e.g.* Angeli's salt **49**), carbon (*e.g.* Traube product **50** and cupferron) or nitrogen (*e.g.* Drago complexes (DEA/NO, **51**)) have been prepared. Thus, diazeniumdiolates can be classified into different types based on the atom the $[N(O)NO]^-$ functional group is attached to, namely, the *S*-diazeniumdiolates, *O*-diazeniumdiolates, *C*-diazeniumdiolates and *N*-diazeniumdiolates.[161,178]

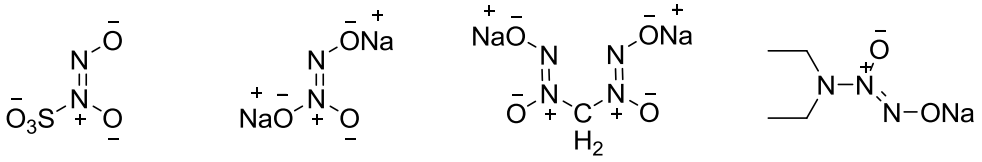

48 **49** **50** **51**

Figure 1.23: Examples of diazeniumdiolates.

Of special interest to this work are the *N*- and *C*-bound diazeniumdiolates, which can release biologically significant amounts of NO (Figure **1.24**). A wide array of *N*-diazeniumdiolates have been synthesized based on amines, particularly secondary amines.[179,180] Each molecule of *N*-diazeniumdiolate can release two molecules of NO under normal physiological conditions and the half-life of a *N*-diazeniumdiolate molecule is structure-dependent. The different rates of NO release of diazeniumdiolates could be leveraged to develop NO donors for very specific needs. For example, ultrafast short-burst NO donors such as proline-based *N*-diazeniumdiolate **52** with half life of 2 **s** could be used to generate highly localized anti-platelet and vasodilatory effects, or longer NO-releasing donors such as the diethylenetriamine/NO (DETA/NONO) **53** and spermate derivatives **54** could be utilized for implantable biomedical devices and lung inhalation therapy.[181,182,183]

C-Diazeniumdiolates, as the earlier-discovered counterparts of the *N*-diazeniumdiolates, have a rich chemistry and are in general more stable than their nitrogen analogues. However, C-diazeniumdiolates are not known for NO release as their general degradation product is nitrous oxide (N_2O).[178] Exceptions are the NO-releasing cupferron type *C*-diazeniumdiolates, as well as the recently-discovered enamines **55**, amidines **56**, enolate and nitrile-based *C*-diazeniumdiolates that have also been shown to release low amounts of NO along with N_2O under physiological conditions. *C*-diazeniumdiolate **57** is the only example of its class currently reported to release two molecules of NO under physiological conditions.[184-187]

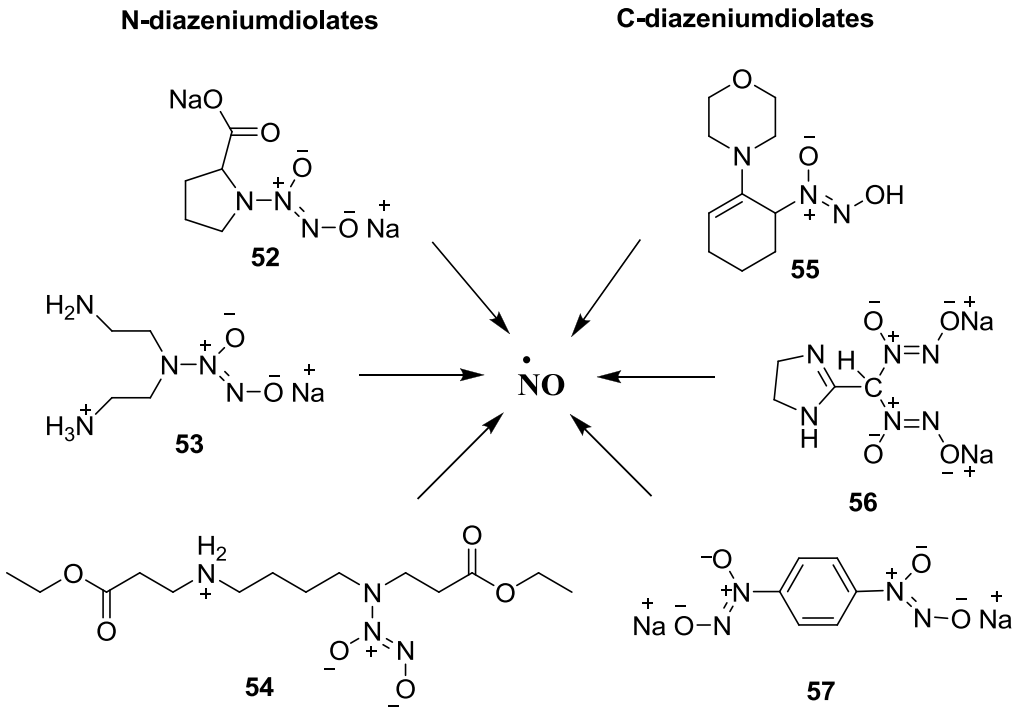

Figure 1.24: *N*- and *C*-diazeniumdiolates.

The NO release mechanism from *N*-diazeniumdiolates is commonly considered to follow a pseudo first order rate law, and is pH dependent. It generally involves protonation of the amine nitrogen attached to the diazeniumdiolate, followed by release of the parent amine and two molecules of NO (Scheme **1.25a**).[188-189] In the case of *C*-diazeniumdiolates, the NO release mechanism is considered to be more complex and depends on the nature of the tautomeric structure. The literature to date suggests that if **60a** is favoured over **60b,** dissociation to NO is inhibited and the production of N_2O is favoured. Additionally, the conjugated double-bond system shown in **61** is considered to be an intermediate for *C*-diazeniumdiolate derivatives having spontaneous NO-releasing properties (Scheme **1.25b**).[184]

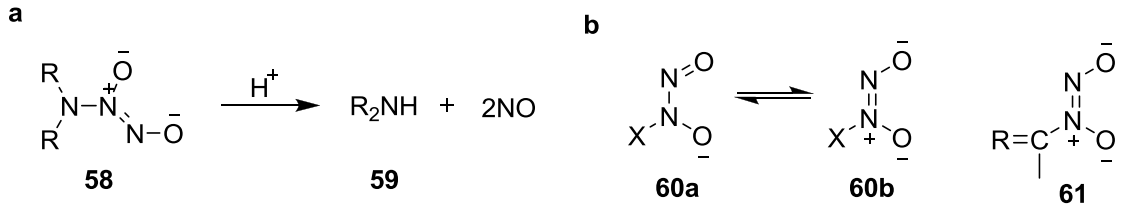

Scheme 1.25: **a)** NO release mechanism of *N*-diazeniumdiolates. **b)** Tautomeric and intermediate structures involved with NO release in *C*-diazeniumdiolates.

In general, a diazeniumdiolate can be synthesised by the reaction of appropriate nucleophiles with NO (Scheme 2.4). The synthesis of *N*-diazeniumdiolates was first reported by Drago *et al.* in the 1960s, and involved the reaction of an amine in a non-polar solvent under a high pressure of NO.[190-192] Similarly, *C*-diazeniumdiolates have been synthesised from suitable enolates, enamines, amidines and nitriles bearing a *C*-nucleophilic centre.[184-185,193]

Diazeniumdiolates can be synthetically modified through substitution reactions at second oxygen (O^2) of the diazeniumdiolate group. Many O^2-protected diazeniumdiolates have been synthesized to modulate the stability or NO-releasing properties of the parent diazeniumdiolates. For example, the MOM-protected diazeniumdiolate **62** has an extended half-life of NO release (~17 days in pH 7.4 phosphate buffer) due to the need of the protecting group to be hydrolyzed prior to NO release.[194] Similarly, O^2-substituted diazeniumdiolate **63**, which requires activation by enzymes such as esterase, and O^2-arylated diazeniumdiolate **64**, prepared by nucleophilic aromatic substitution reactions, have been developed.[195,196]

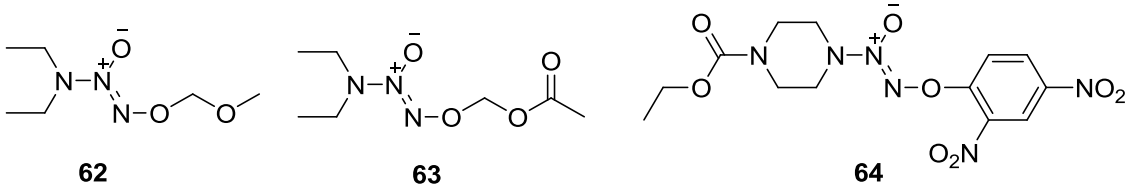

Figure 1.26: Examples of O^2- protected diazeniumdiolates.

1.8.3 *S*-Nitrosothiols

The *S*-nitrosothiol (S-NO)-based compounds are an important class of NO donor. *S*-Nitrosothiols such as *S*-nitrosoglutathione (GSNO) **65**[197] have been discovered as naturally occurring molecules in animal and human airways (leading to bronchodilation), and also as *S*-nitroso proteins (in cysteine-containing proteins) in blood plasma. Thus, S-NO has been considered a storage and transportation form of NO in plasma *via* the *S*-nitrosylation of serum albumin.[198-199] Various S-NO derivatives have been synthesized and reported in the literature. Studies have indicated that an S-NO group attached to a tertiary carbon or a peptide thiol (SH), as in the tripeptide GSNO, is more stable compared to other types of S-NO compounds.[200-202] The S-NO derivative *S*-nitroso-*N*-acetyl-*D,L*-penicillamine (SNAP) **66**, obtained from *D,L*-penicillamine, is one of the most stable non-peptide S-NOs reported.[203-204]

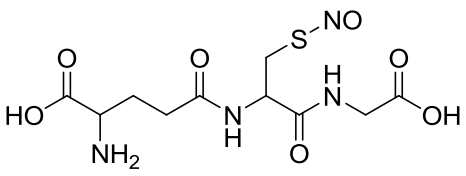

GSNO

65

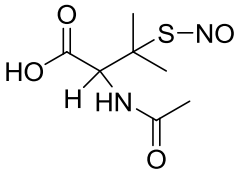

SNAP

66

Figure 1.27: Examples of some S-NO donors.

1.8.4 Dual action drugs based on nitric oxide donors

As discussed above, NO is associated with controlling a wide range of activities through the modulation of multiple targets in different biological systems. This property of NO makes it a useful functionality to conjugate with existing drugs to increase the therapeutic efficacy of the drug, and/or to overcome an adverse side effect. Such hybrids have the potential to broaden the application of existing drugs for the treatment of other pathological conditions.

This strategy has been employed to develop important multi-target hybrid drugs that combine the _native' or existing mechanism of action of a drug with NO-releasing activities, in order to improve the therapeutic efficiency and/or the reduce side effects of a particular drug. For example, the gastric toxicity of aspirin was alleviated by conjugation of aspirin with NO donors such as nitrate (e.g. NX0416 **67**). Similar results have been obtained by conjugating other non-steroidal anti-inflammatory drugs (NSAID) **68**, Ca^{2+} channel blockers **69-70**, 3-hydroxy-3-methyl-glutaryl-CoA (HMGCoA) reductase **71**, or anticancer drugs **72** with different NO donors such as nitrates, diazeniumdiolates, S-NO and furoxans.[205] These hybrids were shown to display improved therapeutic effects, such as an increase in the antiplatelet activity of aspirin, or more potent antihypertensive activity of angiotensin receptor antagonists. Such hybrids have also broadened the application of existing drugs for new pathological conditions, such as the use of an aspirin-based hybrid for the treatment of cancer.[109,206]

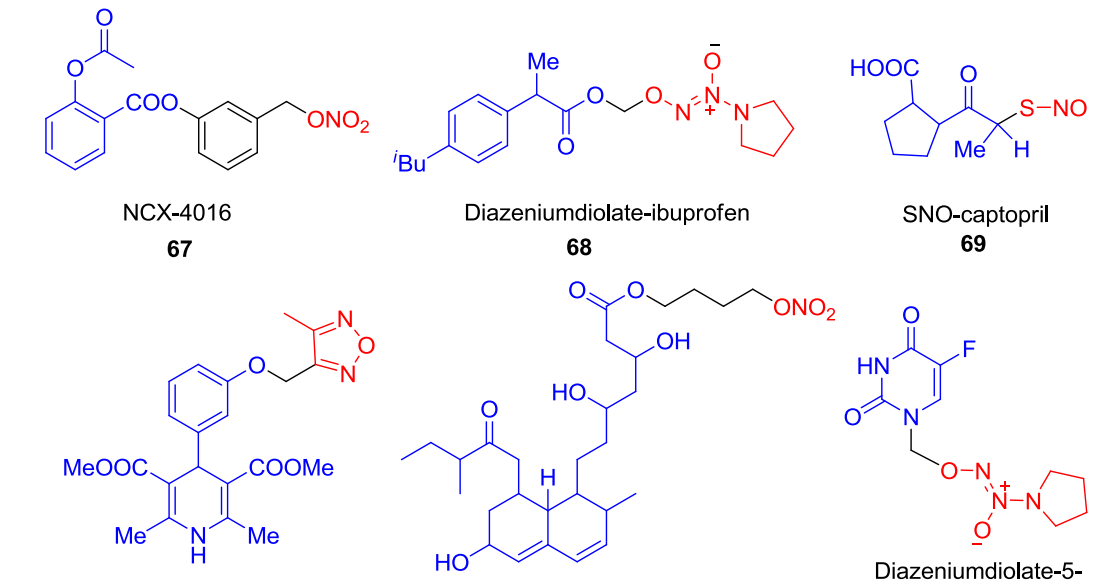

Figure 1.28: Examples of NO hybrid drugs.

While an increasing number of NO hybrid drugs for the treatment of inflammatory or cardiovascular diseases have been discovered, the application of such hybrids for

treating infectious diseases has received less attention.[207-209] Examples of promising anti-infectives reported thus far includes hybrids consisting of NO donors such as nitrates, diazeniumdiolates and furoxans combined with antibacterial agents such as cephalosporin **73** or antifungal agents such as ketakonazole **74**.

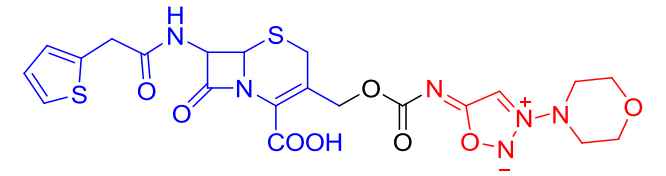

Furoxan-cephalosporin
73

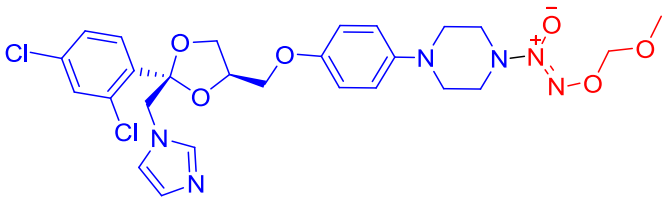

Diazeniumdiolate-ketaconazole
74

Figure 1.29: Examples of antimicrobial and antifungal NO hybrids.

The success of antimicrobial NO hybrids and NO hybrids in general, uncovers the possibility to explore and create new NO hybrids as antimicrobial agents.

1.9 Thesis aims

Due to the increasing frequency of antibiotic resistance among human pathogens, threatening the exhaustion of therapeutic options in the post-antibiotic era, there is a need for newer antimicrobial (and antivirulence) agents with novel mechanisms of action. A combination of quorum sensing inhibitors and nitric oxide donors could play very important roles in this scenario, as they are less prone to resistance and have the potential to control virulence and biofilm formation without exerting selective pressure on bacteria.

Considering the scope and importance of developing future anti-infective agents as described above, the aim of the work in this thesis is to develop novel antimicrobial (antivirulent) agents based on quorum sensing inhibitors and nitric oxide donors.

Chapter 2 covers the design and synthesis of novel dual action compounds based on AHL signaling molecules and nitric oxide donors as anti-microbial (anti-virulence) agents.

Chapter 3 covers the design and synthesis of novel dual action compounds based on the fimbrolide class of quorum sensing inhibitors and nitric oxide donors as anti-microbial (anti-virulence) agents.

Chapter 4 covers the design and synthesis of novel dual action compounds based on the dihydropyrrolone-derived quorum sensing inhibitors and nitric oxide donors as anti-microbial (anti-virulence) agents.

Chapter 5 of this thesis describes the synthesis of novel nitric oxide donors based on indole and also explores the possibility of multiple high-dose nitric oxide donors.

Chapter 6 covers the crystal structure interactions of novel compounds designed during the course of this work, and preliminary bio-molecular modelling studies to explore the interactions of novel hybrids with the AHL receptor protein. This method will offer information on the structure/conformation-activity relationships of the ligand-receptor complexes, and should assist in the design of new chemical scaffolds targeting the Lux-type Gram-negative bacterial signaling pathways.

Chapter 7 evaluates the nitric oxide release, QS inhibitory properties and antibiofilm effects of the novel hybrid molecules against the Gram negative bacteria *P. aeruginosa*.

Chapter 2

Acylated homoserine lactone-based nitric oxide donors

2.1 Introduction

Quorum sensing (QS) is one of the global regulatory processes found in bacteria, and has recently emerged as an important target for antimicrobial compounds. As discussed in Chapter 1, QS involves the conscription of different key chemical mediators that control the transcription of target regulatory genes, in order to produce a range of physiological effects. These chemical mediators vary from species to species, and include a diverse array of chemical scaffolds each mediating a particular regulatory system. One of the well-studied QS systems is the acylated homoserine lactone (AHL) system, which controls a wide range of bacterial responses, including biofilm formation and the expression of virulence factors. The AHL system is commonly found in Gram-negative bacteria, and its signaling molecules are exemplified by the autoinducers in Figure **2.1**.

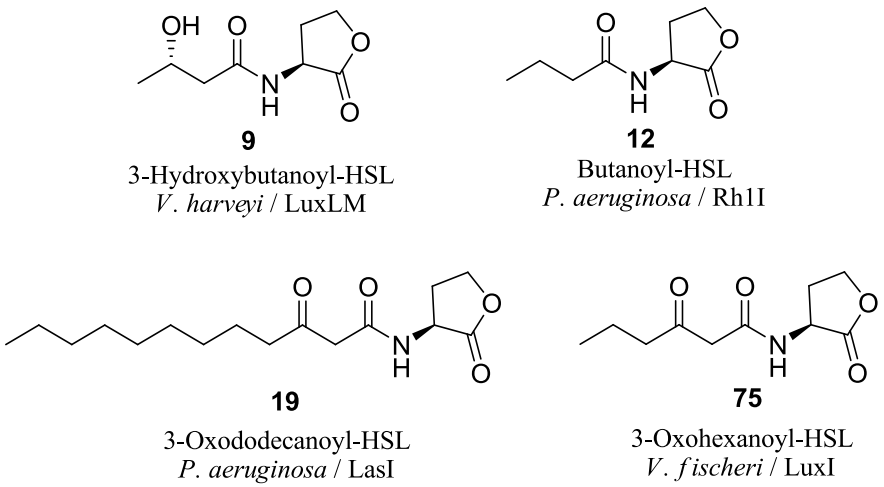

Figure 2.1: Acylated homoserine lactone (AHL) autoinducers in Gram-negative bacteria.

The natural signaling molecules of AHL systems across different species of Gram-negative bacteria share common structural motifs, including a common lactone ―head" and an acylated chain ―tail". The acylated tail can be unsubstituted, 3-oxo- or 3-hydroxy substituted. However, subtle differences in the natural signaling molecules of one species could promote antagonism in another species of bacteria.

In the QS systems of the Gram-negative bacteria, most research has focused on transforming an agonist (natural AHLs) into an antagonist (synthetic AHLs) by modification of the AHL structural motif. Many different approaches have been explored, including alteration of the acyl side chain and/or replacement of the homoserine lactone scaffold by other heterocyclic lactones. A wide variety of AHL-based analogues have been reported in the literature for their QS activities (Chapter 1, Section 1.5.1). Studies so far have indicated that the agonist or the antagonist activity of AHL analogues is very sensitive to the chain length, and that incorporation of an aryl functionality into AHLs, generally yields to analogs having the capability to act as universal inhibitors of the AHL QS system (Figure **2.2**).[210]

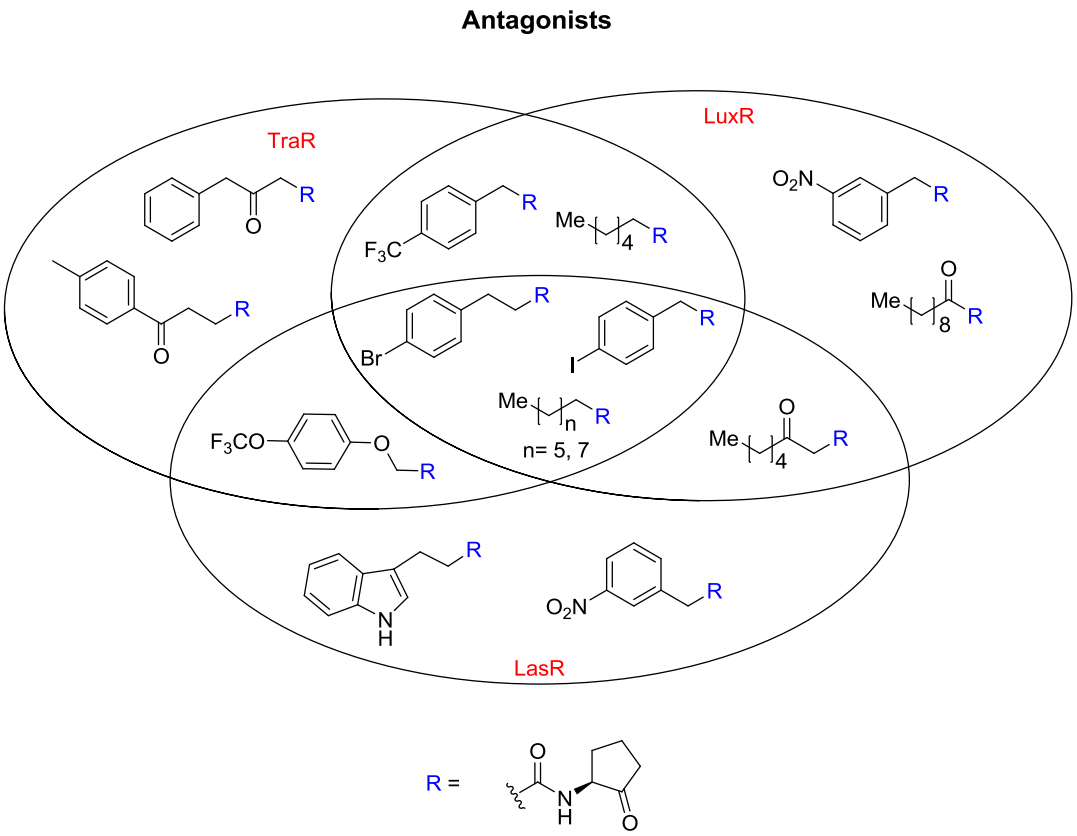

Figure 2.2: Venn diagram of synthetic AHL antagonists against QS receptors.

A range of synthetic strategies have been employed to synthesize these natural and non-natural AHLs and the 3-oxo AHLs.

2.2 Synthetic methodologies for AHL and 3-oxo AHL derivatives

Synthesis of AHLs generally involves the coupling of *L*-homoserine lactone (*L*-HSL) hydrochloride **76** (α-amino-γ-butyrolactone) with alkanoic acids using a peptide coupling agent such as l-ethyl-3-(3-dimethylaminopropyl)carbodiimide hydrochloride (EDC) or *N*,*N*-dicyclohexylcarbodiimide (DCC). Chhabra *et al.* reported the synthesis of AHL analogues by the addition of triethylamine to a stirred solution of *L*-homoserine lactone hydrochloride **76** in water followed by the addition of either an acid anhydride or an acid **77** and EDC. The mixture was stirred at room temperature overnight to obtain the desired AHL derivative **78** (Scheme **2.1**).[211]

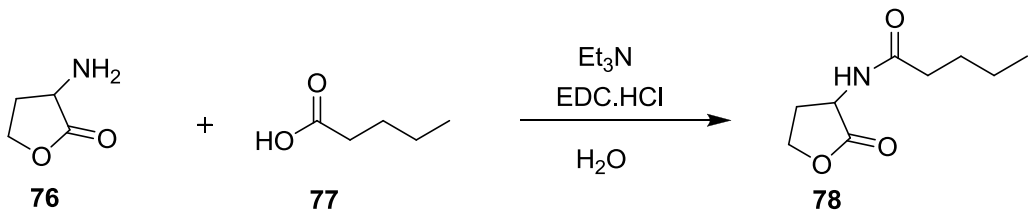

Scheme 2.1: Synthesis of AHL derivative **78**.

Chhabra *et al.* reported the DCC and *N,N*-dimethylaminopyridine (DMAP) catalyzed acylation of Meldrum's acid (2,2-dimethyl-1,3-dioxane-4,6-dione) **80** with carboxylic acids **79** to obtain the 5-acyl Meldrum's acid derivatives **81**. Amidation of **81** with *L*-HSL **76** in the presence of triethylamine in acetonitrile (CH_3CN) afforded the desired *N*-(3-oxoalkanoyl) analogues **83** (Scheme 2.2).[212] Similarly, Amara *et al.* utilized Meldrum's acid **80** for synthesis of the 5-acyl derivative **81**, but utilized dimethylformamide (DMF) as a solvent for the amidation reaction with **76** in order to obtain the desired 3-oxo-AHL derivative **83** (Scheme **2.2**).[213] This strategy, utilizing Meldrum's acid as a means of 3-oxo protection and alkanoic acid activation, represents a common method for the preparation of 3-oxo-AHL derivatives.

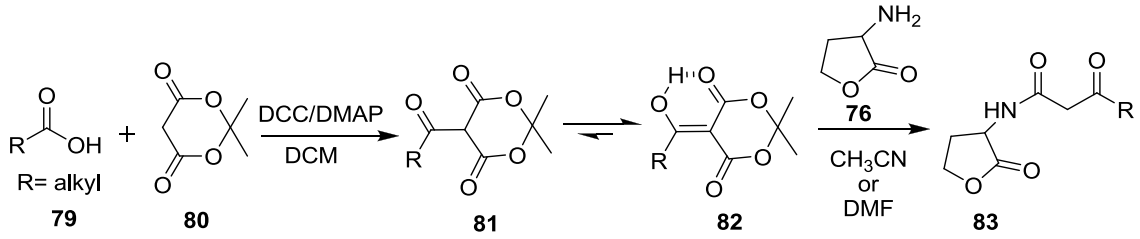

Scheme 2.2: Synthesis of 3-oxo-AHL derivatives *via* Meldrum's acid.

Other 3-oxo protected derivatives could also be used for the amidation reaction. For example, Chhabra *et al.* synthesized 3-oxo-AHL derivatives by coupling 3,3-(ethylenedioxy)alkanoic acid **84** and HSL **76** in aqueous solution using EDC, to generate intermediate **85**. Subsequent acid-catalysed removal of the ketal protecting group in **85**

by perchloric acid in methylene chloride (DCM) afforded the 3-oxo analogues **83** (Scheme **2.3**).[211]

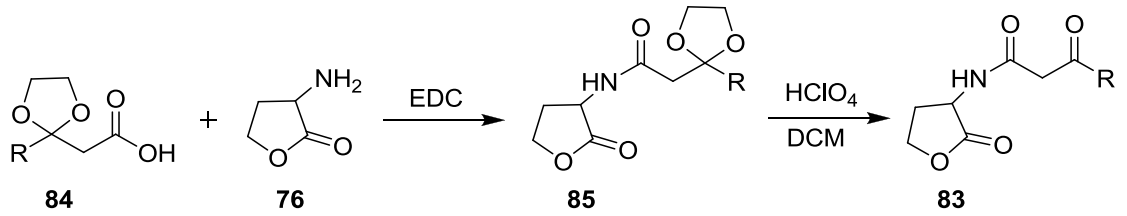

Scheme 2.3: Synthesis of 3-oxo-AHL derivatives *via* ketal protection.

Horikawa *et al.* treated a dianion of *tert*-butyl acetoacetate **86** with 1-bromo-3-butene **87** in the presence of sodium hydride (NaH) to generate the corresponding β-ketoester **88**. Removal of the *tert*-butyl group followed by coupling with *L*-HSL using EDC gave the 3-oxo-AHL derivative **89** (Scheme **2.4**).[214] Later on, Dubinsky *et al.* employed the homologation of a mono-*tert*-butyl malonate magnesium adduct **91** and a diazirine alkynyl acid derivative **90** to form the desired 3-oxo acid intermediate. Deprotection and coupling with HSL **76** using EDC yielded the diazirine alkynyl AHL derivative **92** (Scheme **2.5**).[215]

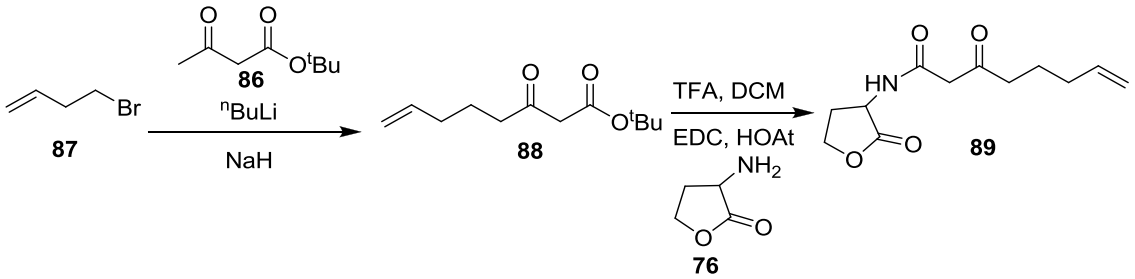

Scheme 2.4: Synthesis of 3-oxo-AHL derivative *via tert*-butyl acetoacetate.

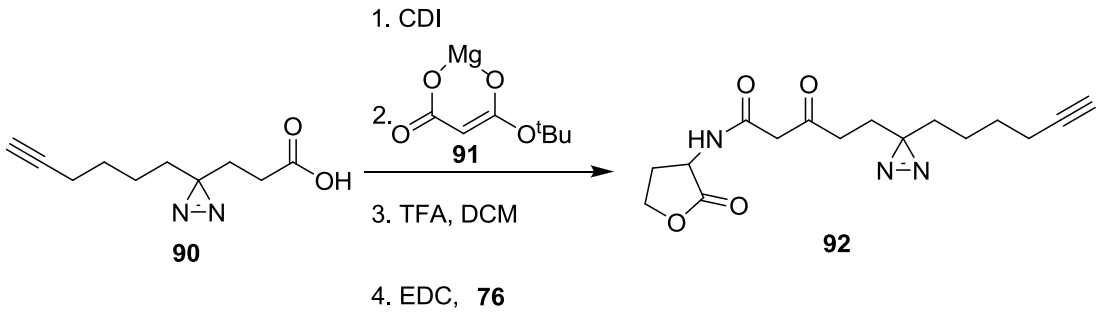

Scheme 2.5: Synthesis of 3-oxo-AHL derivative *via tert*-butyl malonate.

Gseke *et al.* employed solid phase synthesis for construction of *L*- and *D*-lactones through the use of either *N*-Fmoc-*L*- or *D*-methionine in the initial acylation step and the introduction of a wide variety of acyl groups, including alkyl or 3-oxoalkyl, to generate the corresponding AHL or 3-oxo-AHL analogues.[210] Oliver *et al.* used microwave irradiation and PS-carbodiimide resin to synthesize AHL and 3-oxo-AHL derivatives.[216] Recently, Praneenararat *et al.* utilized a small molecule macroarray platform for the synthesis and screening of non-native *N*-acylated *L*-homoserine lactones (AHLs) as QS modulators. A macroarray of AHLs was constructed using an efficient cyclization-cleavage strategy and was demonstrated to be compatible with QS reporter gene assays.[217]

2.3 Chapter aims

A wide range of AHL derivatives have been synthesized in the literature through simple chemical modifications, offering possibilities to modulate QS-related virulence in bacteria. As discussed in Chapter 1, NO exhibits multifunctional effects on bacterial systems and could be utilized to control bacterial pathogenesis. Consequently, hybrids based on AHL and NO donors could be expected to display synergetic anti-virulence effects against bacteria.

Therefore, the aim of this research was to develop novel AHL and 3-oxo-AHL based NO donors. These novel NO hybrids have two primary cores, the AHL scaffold and the NO donor moiety, attached *via* a linker region (Figure **2.3**). The NO donors utilized in this research are the nitrates (ONO_2), diazeniumdiolates (NONOate) and the *S*-nitroso (S-NO) derivatives.

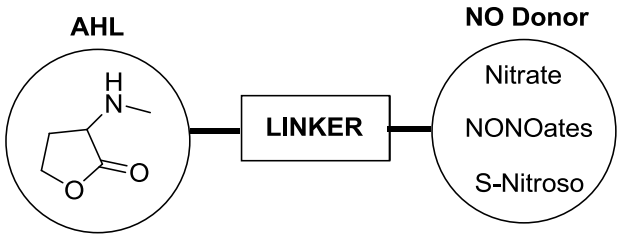

Figure 2.3: Schematic representation of AHL-NO donor hybrids.

2.4 AHL and 3-oxo-AHL based nitric oxide donors

In this work, the AHL scaffold was generated using HSL and different classes of nitric oxide donors such as the nitrates, diazeniumdiolates and the *S*-nitrosothiols, discussed in Chapter 1, Section 1.8.

2.4.1 Preparation of AHL nitrate derivatives

The primary strategy for the syntheses of AHL nitrate NO donors involved EDC coupling of homoserine lactone with the nitroester carboxylic acid derivatives. Therefore, the required alkyl nitrate (nitroester carboxylic acid) derivatives **94a-e** were initially synthesized from the desired starting bromo-alkanoic acids **93a-e** by reaction with silver nitrate (Scheme **2.6**). A typical ^{1}H-NMR spectrum for the nitrate derivative **94a** showed the downfield shift of the CH_2 protons from δ 4.21 to δ 4.96 due to the increased electronegativity of the newly formed nitroester group. The IR spectrum value of 1620 and 1280 cm^{-1} also confirmed the presence of the nitrate groups.

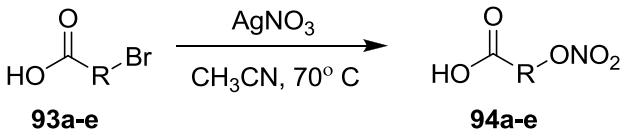

93a-e **94a-e**

Entry	R	% yield of **94**
a		86
b		94
c		93
d		96
e		94

Scheme 2.6: Synthesis of alkyl nitrates.

Following the synthesis of the alkyl nitrates, the desired AHL nitrate derivatives were prepared as discussed below.

The acetic acid 2-nitrate **94a** and EDC were added to a solution of *L*-homoserine lactone **76** containing triethylamine in water. The resulting reaction mixture was stirred for 40 h at r.t. followed by workup to remove the urea by-product, unreacted acid and HSL, to generate the desired product **95a** in 54% yield (Scheme **2.7**).

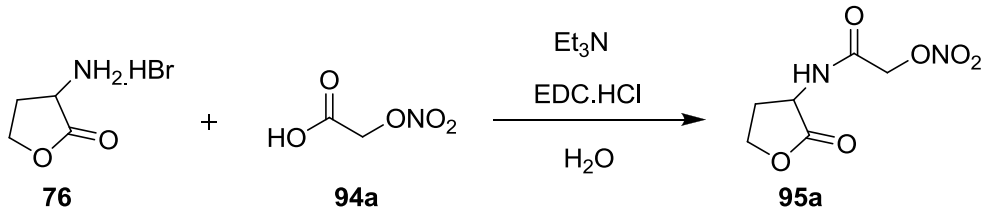

76 **94a** **95a**

Scheme 2.7: Preparation of AHL nitrate analog **95a**.

The identity of the product was elucidated using ^{1}H and ^{13}C NMR spectroscopic analysis. The ^{1}H NMR spectrum of **95a** showed the characteristic signals for HSL with multiplets at δ 2.20, 2.85, 4.32 and 4.56 and a triplet of a doublet at δ 4.47 all of which

integrated for one proton each. The NH of the amide bond appeared at δ 6.06 as a broad singlet. In addition, the CH_2 adjacent to the nitrate group appeared at δ 4.96 as a singlet. The IR spectrum value of 1764, 1688 and 1646 cm^{-1} also confirmed the presence of the carbonyl and the nitrate groups.

The structure of **95a** was additionally confirmed by X-ray crystallography, which showed the presence of the desired nitrate group (Figure **2.4**).

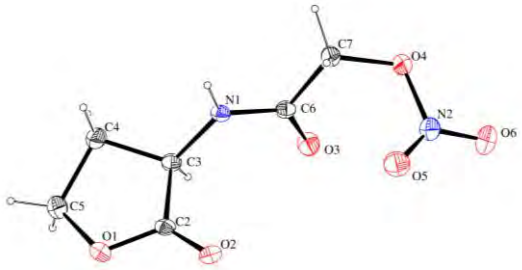

Figure 2.4: The ORTEP diagram for **95a**.

Similarly, the treatment of HSL with different nitrate acids **94b–e** by EDC coupling afforded the corresponding AHL nitrate derivatives **95b–e** (Scheme **2.8**). The compounds were purified by washing with ether or by column chromatography, and were characterized using NMR and other spectroscopic techniques.

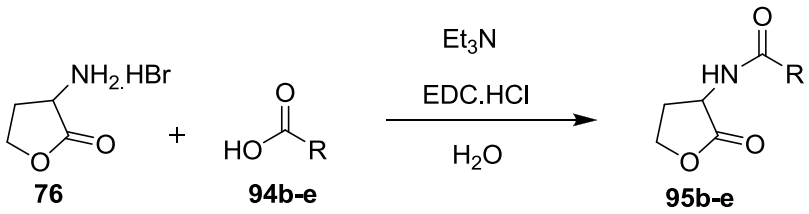

Entry	R	% yield of **95**
b	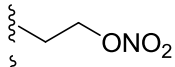	49
c	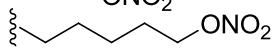	48
d	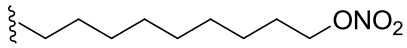	36
e	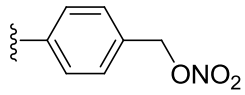	46

Scheme 2.8: Preparation of AHL nitrate analogues.

2.4.2 Preparation of 3-oxo-AHL nitrate derivatives

The next objective was the preparation of 3-oxo-AHL nitrate analogues using Meldrum‘s acid. We focused on the 3-oxo analogues bearing longer alkyl and phenyl linkers, as compounds **95d** and **95e** of the AHL nitrate series showed promising results in a preliminary QS inhibitory assay (discussed in Chapter 7).

The preparation of the Meldrum‘s acid conjugate initially involved DCC/DMAP-catalyzed coupling of 11-nitrate undecanoic acid **94d** with Meldrum‘s acid **80** in anhydrous DCM. The crude intermediate **96a** was then treated with HSL **76** in acetonitrile in the presence of Et_3N at r.t. for 2 h, followed by heating at reflux for 4 h (Scheme **2.9**). The TLC analysis of the reaction mixture indicated formation of multiple products, and subsequent purification with flash column chromatography was required to furnish the desired product **97a** in a very low yield of 4%. Analysis of the other products obtained from chromatography indicated the presence of unreacted starting material and a side-product **98** formed from an alternative coupling reaction between

HSL **76** with conjugate **96a**. A similar side reaction has also been reported in the literature during 3-oxo-AHL preparation using Meldrum's acid.[212]

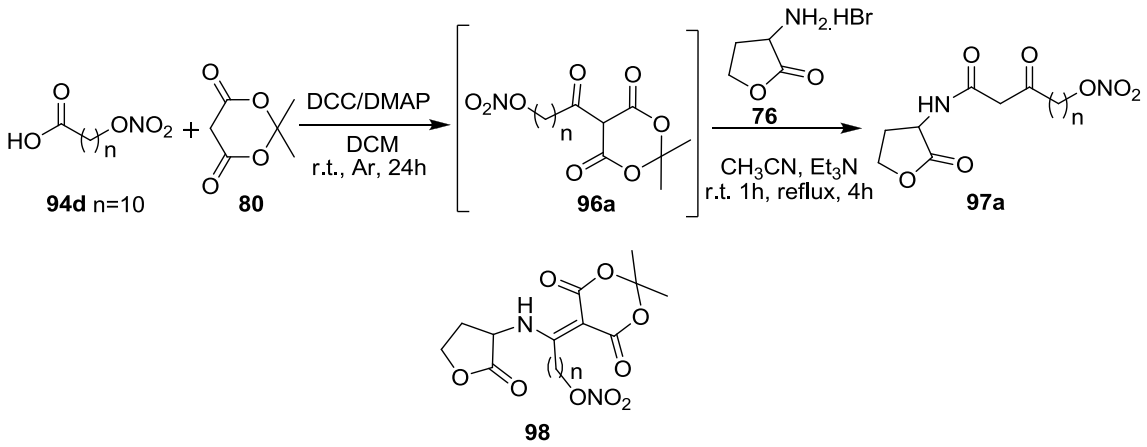

Scheme 2.9: Attempted synthesis of 3-oxo-AHL nitrate derivative.

The low yields of this synthesis prompted a reinvestigation of the reaction conditions to improve the yields. Parameters such as the solvent, the coupling conditions, duration and temperature of reaction were taken into consideration.

During this investigation another unexpected result was noted when, nitrate acyl chloride derivative **99d** (obtained by reaction of acid derivative **94d** with thionyl chloride, and a catalytic amount of DMF) was reacted with Meldrum's acid **80**, and the crude reaction product was subjected to subsequent amidation with HSL in pyridine under reflux (Scheme **2.10**).

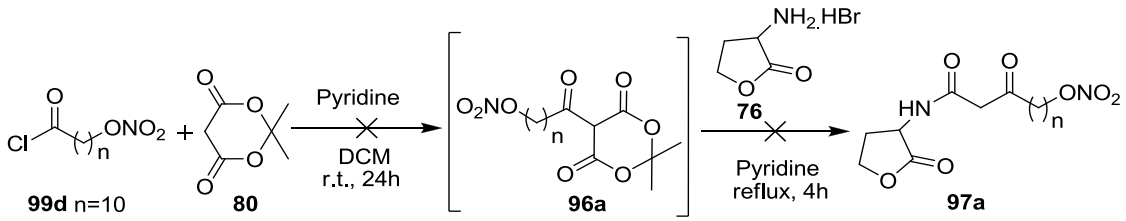

Scheme 2.10: Attempted synthesis of 3-oxo-AHL nitrate derivative.

The TLC of the crude product mixture indicated the formation of multiple products, which were isolated by chromatography. Interestingly, ^{1}H NMR spectrum analysis of the major product revealed the characteristic HSL peaks and two additional peaks, a doublet at δ 8.11 ppm (J = 14.6 Hz, 1H) and a singlet at δ 2.00 ppm (6H). However, the proton peaks belonging to the alkyl nitrate chain were absent. Thus, the compound was postulated to be the side-product **100** formed from the reaction between HSL **76** and Meldrum's acid **80**. This was confirmed by X-ray crystallography, showing the presence of an alkene linkage joining the HSL and Meldrum's acid (Figure **2.5**).53

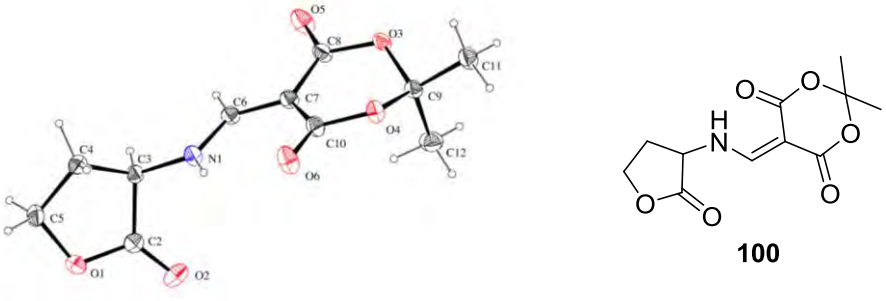

Figure 2.5: ORTEP diagram of side-product **100**.

The formation of side-product **100** could possibly be due to the reaction between the HSL and the formylated Meldrum's acid **80a** formed by the reaction of Meldrum's acid with DMF and thionyl chloride left over from the initial acyl chloride preparation step (Scheme **2.11**). However, the desired product could not be isolated from the reaction mixture.

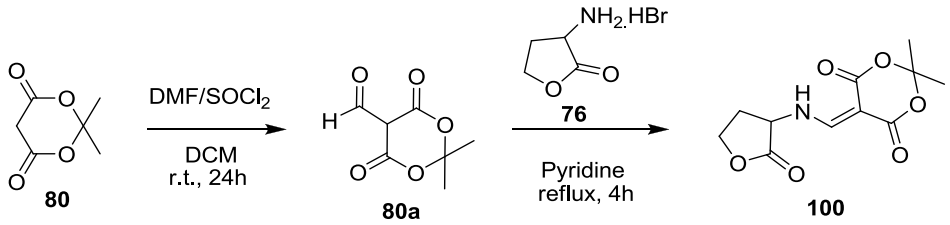

Scheme 2.11: Proposed formation of side-product **100.**

Eventually, after several attempts, the use of DMF as a solvent in the amidation step successfully gave the desired product in good yield. Thus, the acylation of Meldrum's acid **80** with nitrate acid **94d** or **94f** in anhydrous DCM with DCC/DMAP furnished the intermediate conjugates **96a** and **96b**, respectively. The crude reaction mixture was dissolved in DMF and HSL **76** was added, and the resulting mixture was stirred at r.t. for 2 h followed by heating at 60 °C for 4 h. After workup, the desired products **97a–b** were isolated by column chromatography in 54–57 % yields (Scheme **2.12**).

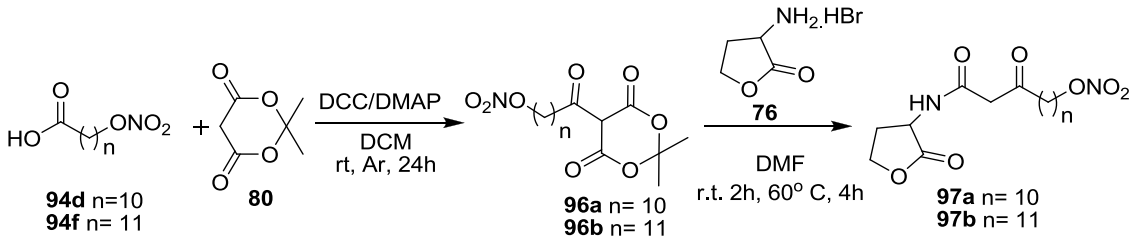

Scheme 2.12: Synthesis of 3-oxo-AHL nitrate derivatives.

The ^{1}H NMR spectrum of a typical 3-oxo AHL nitrate derivative such as **97b** exhibited the HSL peaks and two additional triplets at δ 4.42 (J = 6.7 Hz, 2H) and δ 2.51 (J = 7.3 Hz, 2H) corresponding to the CH_2 groups adjacent to the nitrate group and the C-3 carbonyl group, respectively. A singlet at δ 3.48 integrating for two protons was identified as the CH_2 group between the two carbonyl groups. Furthermore, the broadband decoupled ^{13}C NMR spectrum of **97b** indicated the presence of three carbonyl groups, while the DEPT-135 spectrum revealed the presence of the fourteen

characteristic methylene (CH_2) groups, confirming the formation of the 3-oxo-AHL analogue.

However, the same strategy when applied to the benzoic acid nitrate derivative **94e** furnished **101** as the major product, instead of the desired product **102**. This could be attributed to the lower stability of the benzyl nitrate compared to the alkyl nitrates, which could possibly lead to the hydrolysis of nitrate group under the reaction conditions utilized.

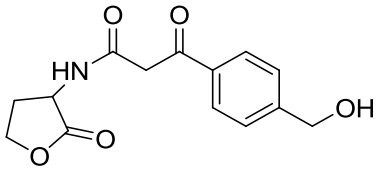

101

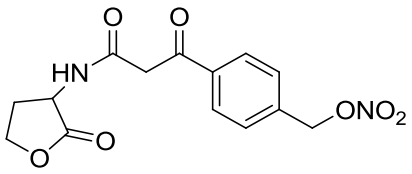

102

Additionally, an AHL nitrate derivative with a glycine molecule between the HSL **76** and the nitrate acid linker **94d** was synthesized as illustrated in the Scheme **2.13**. At first the Boc-glycine **103** was coupled to the HSL **76** *via* EDC coupling followed by deprotection of the Boc-group by trifluoroacetic acid. The HSL-glycine derivative **104** so obtained was then coupled with the alkanoic nitrate derivative **94d** using PyBOP coupling conditions to yield the desired product **105**.

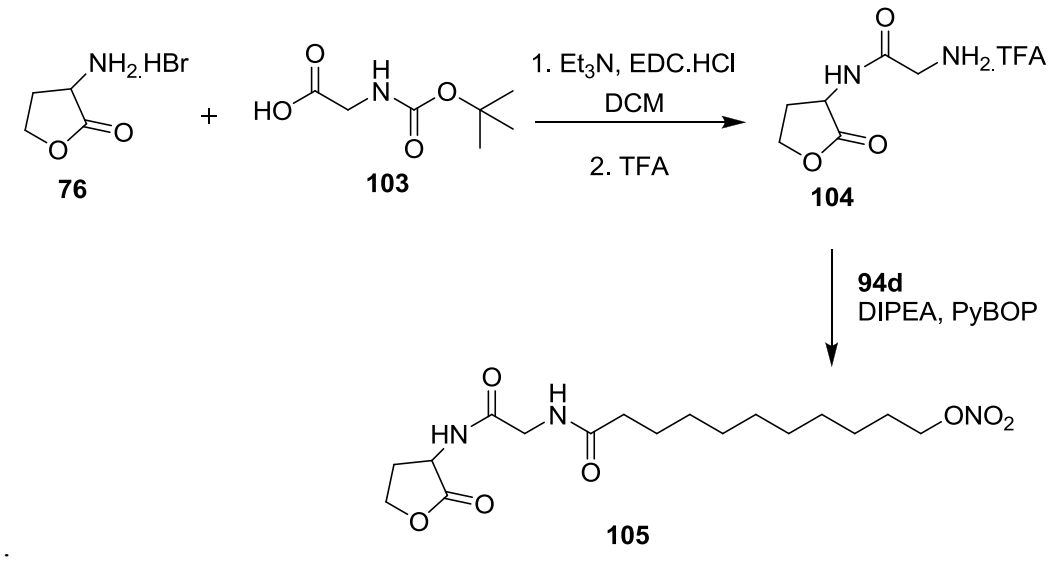

Scheme 2.13: Synthesis of AHL derivative

The ^{1}H NMR spectrum of the AHL nitrate derivative **105** exhibited the HSL peaks and two triplets at δ 4.52 (J = 6.6 Hz, 2H) and δ 2.12 (J = 7.3 Hz, 2H) corresponding to the CH_2 groups adjacent to the nitrate group and the carbonyl group of the alkyl chain respectively. A doublet at δ 3.48 (J = 5.9 Hz) integrating for two protons was identified as the CH_2 group between the carbonyl group and the NH, confirming the formation of desired product.

2.4.3 Synthesis of AHL diazeniumdiolate derivatives

Diazeniumdiolate-based hybrids can be synthesised by different approaches. One method is through coupling of easily accessible HSL acid derivatives with O^2-stabilized piperazine diazeniumdiolates. Thus, retrosynthetically, the desired AHL diazeniumdiolate **106** can be obtained by coupling the piperazine diazeniumdiolate to the AHL acid derivative **107**, which in turn can be synthesized by the reaction of a diacid derivative with *L*-HSL **76** (Scheme **2.14**).

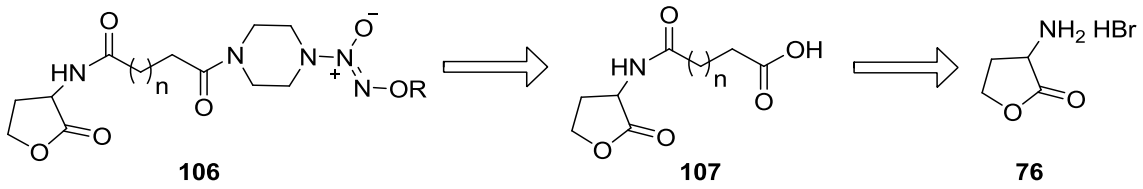

Scheme 2.14: Retrosynthesis of AHL diazeniumdiolates.

Following the retrosynthetic scheme, the first aim was to synthesize the desired *L*-HSL acid derivatives **107**. In the literature, various approaches have been reported for the synthesis of amides, including treatment of an amine with an acid anhydride, diacid chloride or diacid under basic conditions. A protecting group is typically required when using a diacid, with the benzyl ester derivative being the most commonly used.

Initial attempts to prepare amide **107a** involved the reaction of succinic anhydride **108a** with HSL **76** in ethyl acetate in the presence of triethylamine at 60 °C. The reaction was followed by ^{1}H NMR spectroscopy, but only a very low yield of the desired product was produced even after 40 h. The reaction was therefore repeated under different conditions, such as using DMAP as a base with different solvent such as DCM and THF but similar low yields were obtained (Scheme **2.15**).

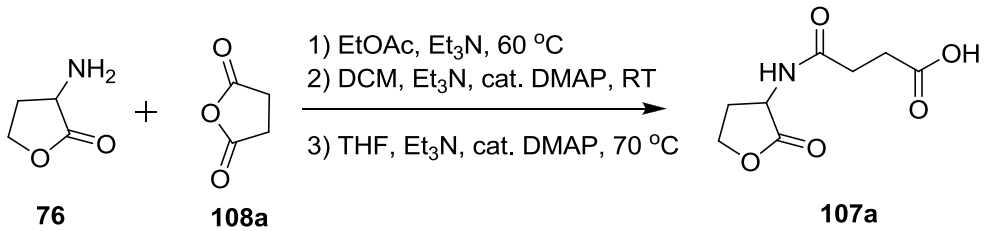

Scheme 2.15: Attemped synthesis of AHL acid derivative *via* succinic anhydride.

The synthesis of AHL acid derivatives **107a** *via* a diacid chloride was investigated next (Scheme **2.16**). HSL **76** in a solution of pyridine and DCM was slowly added over a

period of 30 minutes to a solution of succinyl chloride **109a** at 0 °C. The reaction mixture was stirred further at r.t. for 4 h followed by the addition of water and extraction of the organic layer. The ^{1}H NMR spectrum of the product showed the characteristic peaks of the HSL motif, but with the two CH_2 group of the diacid appeared as a singlet at δ 2.79, which suggested the formation of the salt of HSL and the diacid rather than the formation of the amide derivative **107a**.

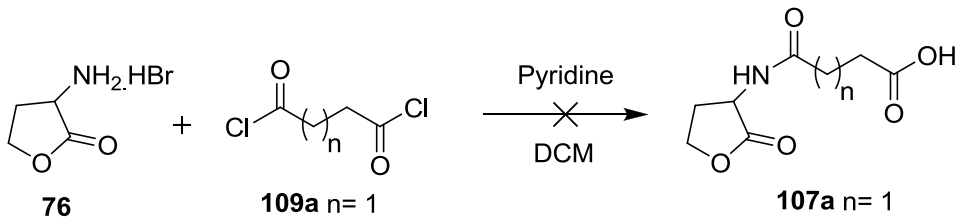

Scheme 2.16: Attemped synthesis of AHL acid derivative *via* succinyl chloride.

Finally, the protection and deprotection strategy for the synthesis of the AHL acid derivative was investigated (Scheme **2.17**). Succinic anhydride **108a** or adipic anhydride **108b** was first ring-opened with benzyl alcohol **110** to give a mono-protected acid derivative.[218-219] These protected acids **111a**–**b** were then coupled with HSL **76** using EDC to afford the HSL amide derivatives **112a**–**b**. In the ^{1}H NMR spectrum, the CH_2 protons from the benzyl group appeared as a singlet at δ 5.04, and the aromatic region appeared as a multiplet at δ 7.25. The deprotection of the benzyl group was carried out using hydrogenation conditions (Pd/C, H_2, r.t.) to furnish the desired products **107a–b** in 64–69% overall yields. The characterization of the products was performed by NMR spectroscopy. In general, the ^{1}H-NMR spectra of the AHL acid derivatives such as **107a** exhibited the characteristic HSL peaks as well as a multiplet at δ 2.36 corresponding to the two CH_2 groups that are adjacent to the carbonyl groups.

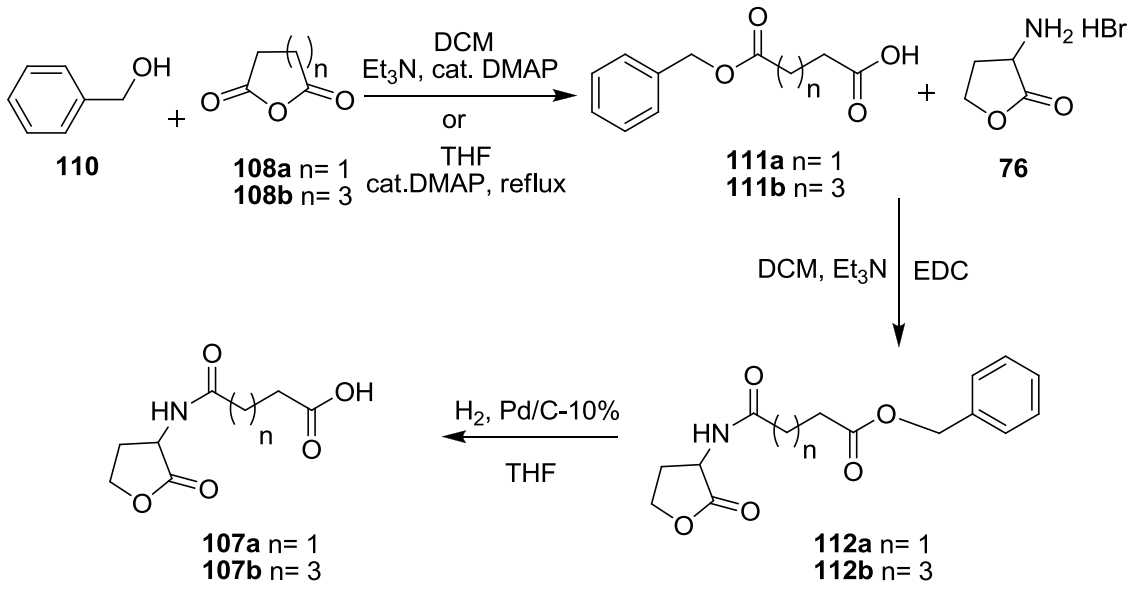

Scheme 2.17: Synthesis of AHL acid derivatives **107**.

The desired O^2-diazeniumdiolate derivatives **116** and **120** required for the coupling to AHL acids were prepared from the protected piperazines **113** and **117** respectively, by initially reacting the piperazines with NO in the presence of sodium methoxide (Schemes **2.18** and **2.19**).

The O^2-protection of the diazeniumdiolate derivative **114** was then carried out with dimethyl sulfate followed by deprotection of the carbamate group to yield the desired piperazine diazeniumdiolate derivative **116** (Schemes **2.18**).[220] The ^{1}H-NMR spectrum of product **116** showed two triplets at δ 3.02 and 3.36 ppm corresponding to the piperazine unit and the O^2-methyl appearing as a singlet at δ 4.00 confirmed the formation of the desired product. The IR spectrum value of 1380, 1290 and 947 cm^{-1} also confirmed the presence of the diazeniumdiolate group.

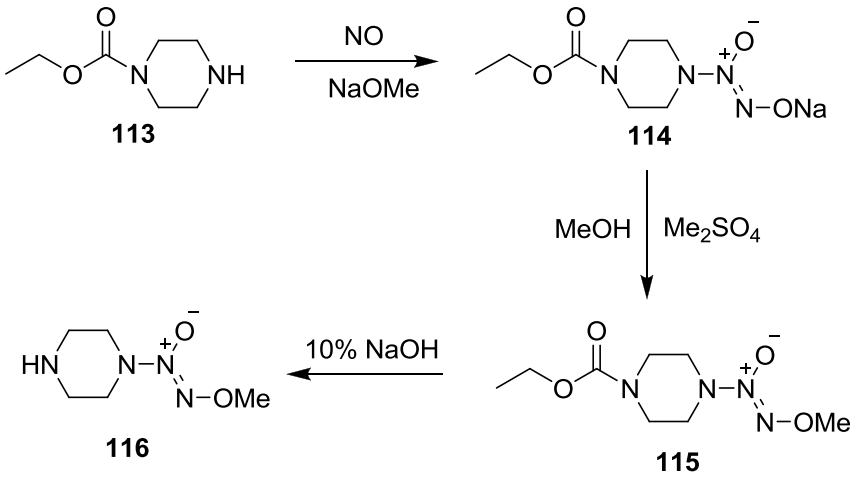

Scheme 2.18: Synthesis of O^2-Me piperazine diazeniumdiolate.

The diazeniumdiolate derivative **118** was O^2-protected with 4-fluoro-1,3-dinitrobenzene followed by *N*-deprotection of the *tert*-butyl carbamate group to yield the piperazine diazeniumdiolate derivative **120** (Schemes **2.19**).[221]

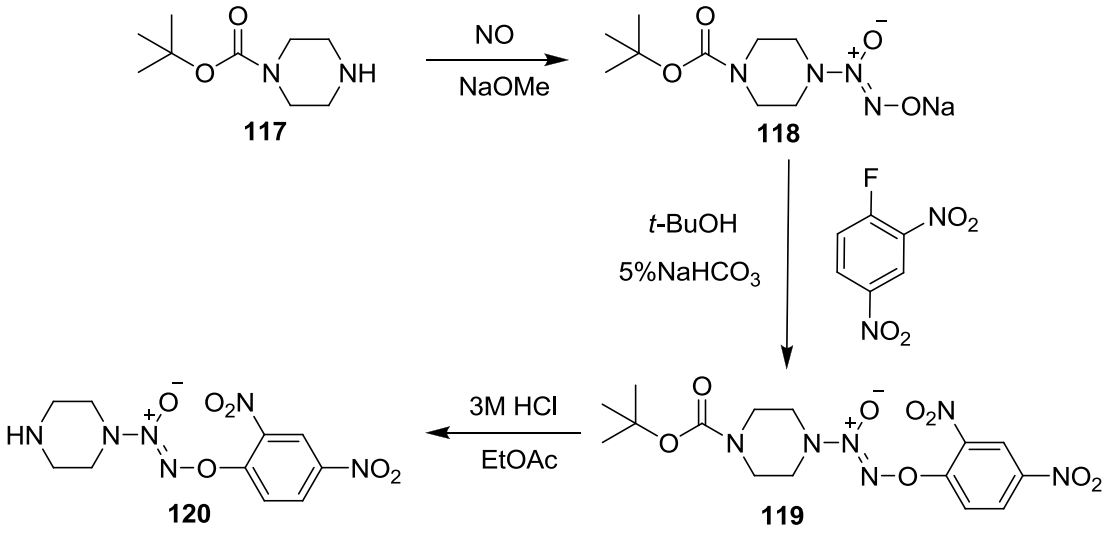

Scheme 2.19: Synthesis of O^2-dinitrobenzene piperazine diazeniumdiolate.

The ^{1}H-NMR spectrum of product **120**, showed two triplets at δ 3.38 and 3.89 corresponding to the piperazine unit while the O^2-dinitrobenzene aromatic peaks appeared as a doublet at δ 7.95 (J = 9.3 Hz), a doublet of doublets at δ 8.56 (J = 9.3 and

2.7 Hz) and a doublet at δ 8.89 (J = 2.7 Hz), all of which integrated to one proton thus confirming the formation of the desired product.

In the final step, the desired AHL acids **107a–b** were reacted with piperazine derivatives **116** and **120** using EDC coupling in a water/acetonitrile mixture at r.t. for 40 h. Work-up followed by chromatography gave the desired products **121a–b** and **122a–b** in 35–79% yield (Scheme **2.20**).

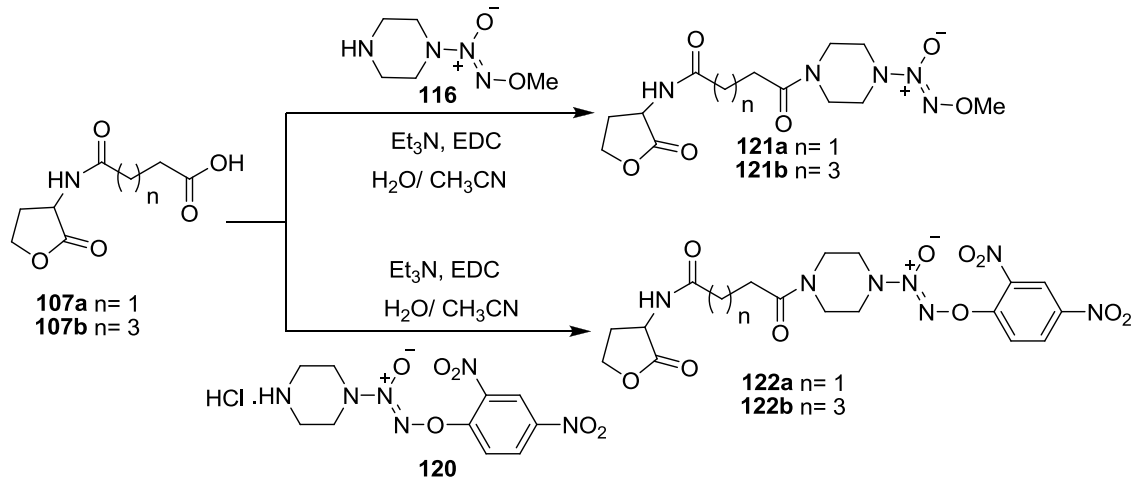

Scheme 2.20: Synthesis of AHL diazeniumdiolate derivatives.

The ^{1}H NMR spectrum of the a AHL diazeniumdiolate derivative such as **121b** exhibited the desired HSL ring pattern with multiplets at δ 2.17 and 2.68 corresponding to H4a and H4b respectively, along with multiplets at δ 4.24 and 4.56 for H5a and H3. The H5b proton appeared as a triplet of doublets at δ 4.43 ppm. The NH proton appeared as a broad doublet at δ 6.96 ppm. In addition, a quintet at δ 3.37 (J = 5.2 Hz, 4H) and two triplets at δ 3.62 and δ 3.75 (J = 5.2 Hz, each 2H) corresponded to the piperazine unit, while a singlet at δ 4.00 corresponded to the O^2-methyl group (Figure **2.6**). Furthermore, the ^{13}C broadband decoupled and DEPT-135 spectra of **121b** indicated the

presence of ten methylene (CH_2) groups and three carbonyl groups, confirming the formation of the piperazine diazeniumdiolate AHL hybrid linked *via* adipic acid.

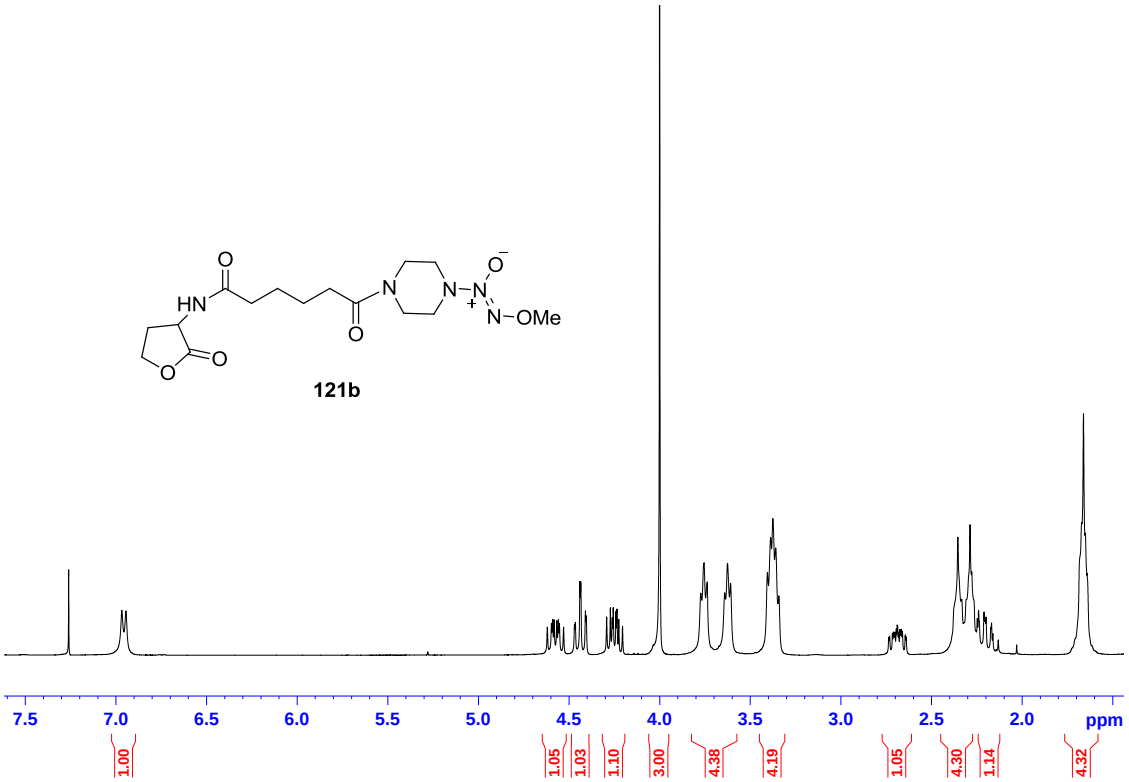

Figure 2.6: ^{1}H-NMR spectrum of **121b**.

The ^{1}H NMR spectrum of piperazine diazeniumdiolate **122a** exhibited similar HSL proton peaks as compound **121**. However, instead of the O^2-methyl peak, the spectrum contained characteristic peaks for the 2,4-dinitrophenyl functionality, including a doublet at δ 7.66 ppm (J = 9.2 Hz, 1H), a doublet of doublets at δ 8.45 ppm (J = 2.7 and 9.2 Hz, 1H) and a doublet at δ 8.87 ppm (J = 2.7 Hz, 1H). Furthermore, the ^{13}C broadband decoupled and DEPT-135 spectra of **122a** indicated the presence of the appropriate number of methylene (CH_2) groups, confirming the formation of the desired piperazine diazeniumdiolate AHL conjugate.

The structure of **122a** was further confirmed by X-ray crystallography (Figure **2.7**), which showed the presence of the AHL, piperazine and 2,4-dinitrophenyl motifs. The cisoid (*Z*)-type structural orientation of the diazeniumdiolate was also confirmed by X-ray crystallography.

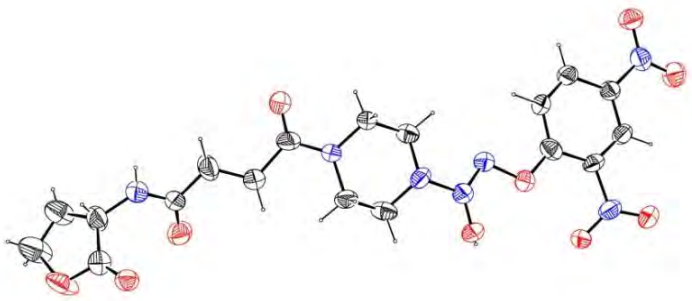

Figure 2.7: The ORTEP diagram for **122a**.

2.4.4 Synthesis of AHL *S*-nitrosothiol derivatives

The synthesis of the AHL *S*-nitroso (S-NO) derivatives was envisaged to proceed through a *D*-penicillamine amide derivative such as **125**, which contains the desired thiol (SH) functionality. In the literature, compound **125** has been obtained from thietanone intermediate **124** *via* the ring opening reaction with amine **123**. The thiol group can be subsequently converted to the S-NO derivative **126** by nitrosation using reagents such as acidic $NaNO_2$ or *t*-butyl nitrite (Scheme **2.21**).[222-223]

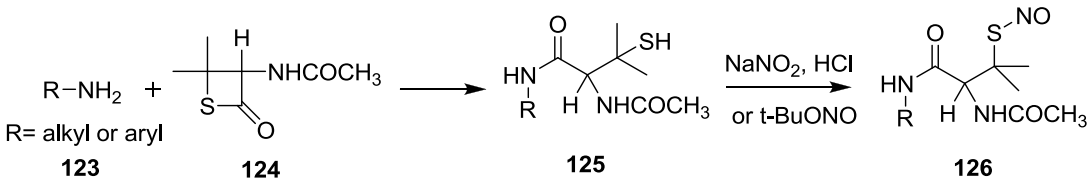

Scheme 2.21: General synthesis of SNAP analogues.

To generate the desired AHL S-NO derivative, the thietanone derivative **124** was synthesized by stirring *D*-penicillamine **127** with acetic anhydride and K_2CO_3 for 16 h (Scheme **2.21**). The resulting thietanone derivative **124** was then reacted with *L*-HSL **76** in a solution of chloroform (or DMF) containing triethylamine to furnish the desired thiol-containing product **128**. The ^{1}H NMR spectrum of **128** confirmed the presence of the HSL peaks, and revealed additional doublets at δ 1.42 and 1.48 (J = 4 Hz, each 3H) due to the two methyl groups, and a singlet at δ 2.06 ppm (3H) corresponding to the *N*-acetyl methyl group. The proton adjacent to the carbonyl group in penicillamine appeared as singlet at δ 4.51 ppm. The SH functionality was subsequently converted into a *S*-nitroso (S-NO) group by reacting compound **128** with *t*-butyl nitrite in chloroform for 45 min to afford the desired S-NO product **129** in 45% yield (Scheme **2.22**).

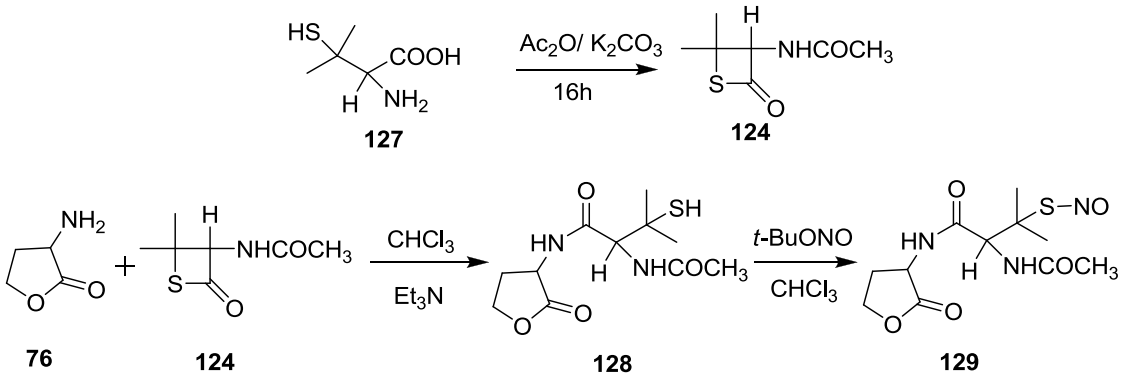

Scheme 2.22: Synthesis of HSL-SNAP derivative **129**.

The ^{1}H NMR spectrum of **129** exhibited similar peaks to **128** for the HSL protons. However, the proton adjacent to carbonyl carbon in penicillamine was shifted downfield to δ 5.25 ppm in compound **129**, compared to δ 4.51 ppm for compound **128**, due to the formation of the new S-NO bond. In addition, the ^{13}C NMR spectrum of **129** indicated the presence of three carbonyl (C=O) groups, consistent with the desired product.

2.5 Conclusion

A series of AHL-based NO hybrids comprising different NO donor groups, such as nitrates, diazeniumdiolates and *S*-nitrosothiols, have been successfully synthesized. These compounds have the potential to be further developed as dual-mechanism therapeutics against bacterial infection based on their QS-inhibitory and NO releasing properties which are discussed in Chapter 7.

Chapter 3
Fimbrolide-based nitric oxide donors

3.1 Introduction

As discussed in Chapter 1, quorum sensing (QS) inhibition is a key strategy for the development of novel antibacterial agents. As with other classes of pharmaceuticals, natural products have featured heavily in the search of new structural motifs for QS inhibitors. Terrestrial and marine flora and fauna produces chemical species that play vital roles in their interactions with the environment, including chemical defense mechanisms.[224] Defensive functions attributed to the production of secondary metabolites include predator deterrence,[225] antifouling,[226] inhibition of overgrowth[227] and UV radiation protection.[228] Organisms susceptible to bacterial infection have evolved natural strategies to counter this threat by targeting the different mechanisms involved in pathogenesis. In regards to the QS system, this could be carried out *via* the destruction of the signaling molecules or by the production of antagonists mimicking the natural signaling molecules. Nature has been observed to utilize both strategies to impede the QS system that ultimately controls the virulence of bacteria.

A variety of QS inhibitors containing a wide range of structural scaffolds based on natural products have been discovered (Figure **3.1**). De Nys *et al*. reported more than 20 halogenated furanones, including fimbrolide **34a**, from *Delisa pulchra*.[90] Analysis of the secondary metabolites of the North Sea bryozoan *Flustra foliacea* led to the isolation of a variety of brominated alkaloids, of which compound **130** was found to specifically block AHL-regulated gene expression. Alkaloid **130** was also able to suppress the production of extracellular proteases in *P. aeruginosa*, a phenotype under the stringent

control of AHL-dependent QS systems. In 2005, Rasmussen *et al.* identified the naturally occurring compounds penicillic acid **131** and patulin **132**, produced by *Penicillium coprobium* and *Penicillium radicicola*, respectively, as inhibitors of QS in *P. aeruginosa*. Girennavar *et al*. isolated the furocoumarin QS inhibitors bergamottin **133** and dihydroxybergamottin **134** from grapefruit juice. Solenopsin A **135**, a venom alkaloid from the fire ant *Solenopsis invicta,* bears structural similarity to the natural autoinducer AHL, and was shown to be a potent QS inhibitor against *P. aeruginosa*.[73,72]

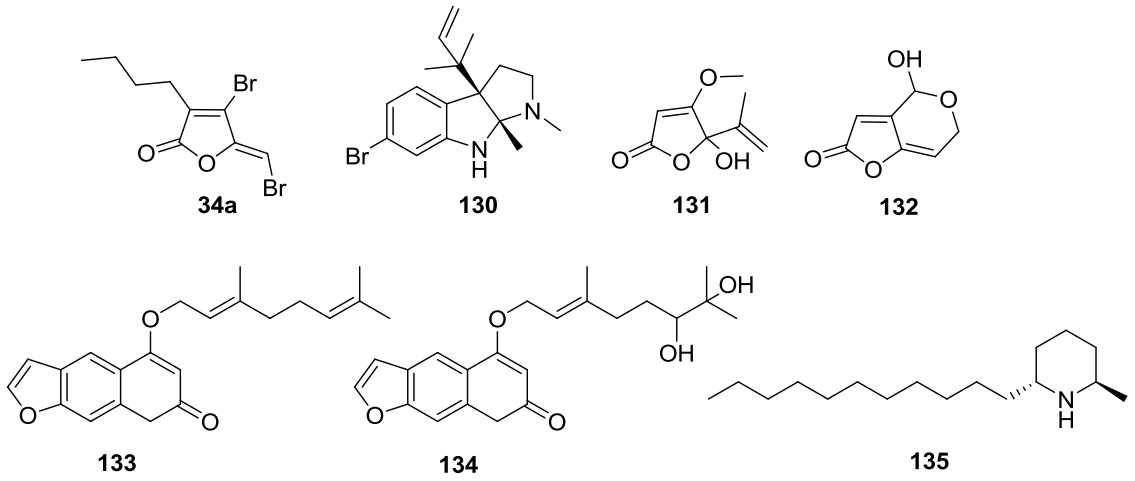

Figure 3.1: Natural products QS inhibitors.

Of these natural products, fimbrolide (described in Chapter 1) has been one of the most well-studied class of QS inhibitors. Fimbrolides are halogenated lactone marine natural products. They reside in the vesicles on the surface of algae such as *D. Pulchra*, and provide a defense against fouling of algae surfaces by marine organisms. It has been shown that fimbrolides or halogenated furanones act as antagonists of bacterial QS pathways, particularly by inhibiting AHL-dependent processes such as virulence and biofilm formation.

3.2 Synthesis of fimbrolides

Since the discovery of fimbrolides and their antibacterial properties, the synthesis of halogenated furanones has aroused keen interest. Beecham and Sims reported the first successful synthesis of the parent fimbrolide **137** through the acid-catalyzed cyclization of bromo-substituted levulinic acid **136** (Scheme **3.1**).[229]

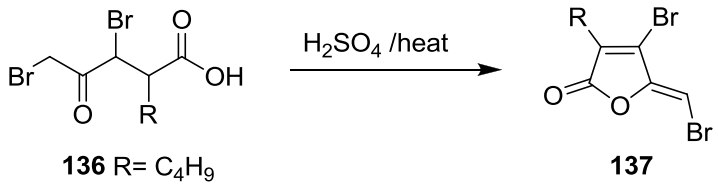

Scheme 3.1: Acid-catalyzed cyclization of levulinic acid by Beecham and Sims.

Following this, Caine *et al*. reported an alternative method for the preparation of the fimbrolides *via* cyclization of (*E*)-β-bromo-β-lithioacrylates **138** in the presence of acetic anhydride to form 5-hydroxy-5-methyl-4-bromo-3-alkyl-2-(5*H*)-furanone **139**. Sequential dehydration, bromination and dehydrobromination steps were then performed to give the desired furanones **137** (Scheme **3.2**).[230]

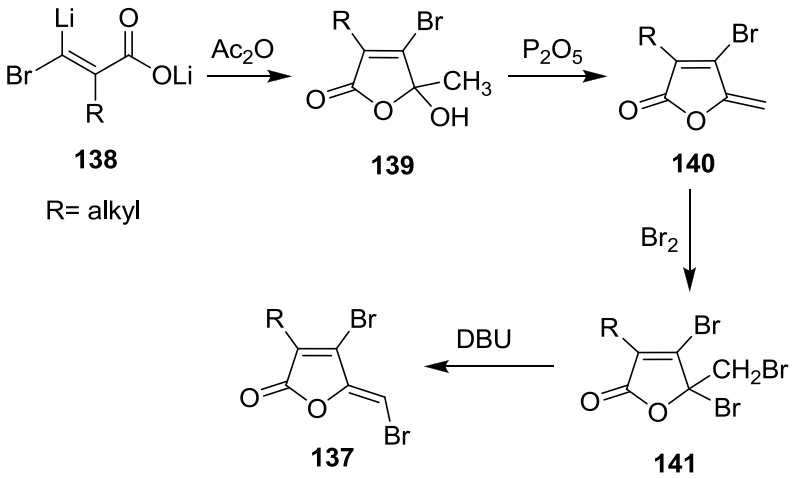

Scheme 3.2: Fimbrolide synthesis developed by Caine *et al*.

A decade later, new synthetic strategies were developed that could generate fimbrolide derivatives with an oxygen functionality at the α-carbon of the C3-alkyl chain. De March *et al*. have described the synthesis of the parent fimbrolide **34a** *via* the *N*-bromosuccinimide (NBS)-catalyzed bromolactonization of γ-monosubstituted allenic ester **142** to generate 4-bromo-3-butyl-5-methyl-2(5*H*)-furanone **143**. This intermediate was treated again with NBS and silver acetate to give 3-(1-acetoxybutyl)-5-hydroxy-5-methyl-2(5*H*)-furanone **144**, followed by the standard dehydration-bromination-dehydrobromination sequence to yield the desired C-1′-acetoxyfimbrolide **34b** (Scheme **3.3**).[231,101]

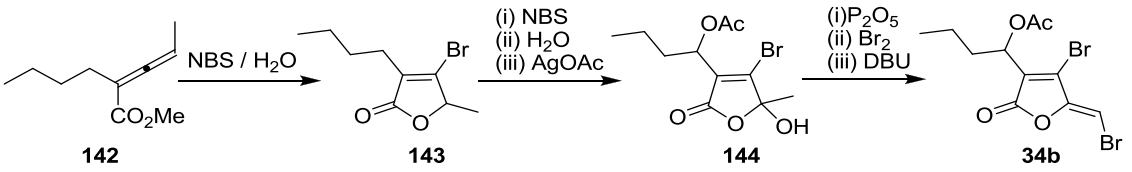

Scheme 3.3: Fimbrolide synthesis developed by De March *et al*.

However, most of these early fimbrolide syntheses are either inefficient or required extreme conditions or expensive reagents, and consequently were impractical for the large scale synthesis of furanone derivatives.

The sulfuric acid-catalyzed cyclization of brominated 2-alkyllevulinic acids reported by Beecham and Sims was reinvestigated by our group, and a more efficient and reliable synthesis of the parent 3-alkyl-5-bromomethylene- and 3-alkyl-5-dibromomethylene-2(5*H*)-furanones **151a-c** was developed (Scheme **3.4**).[232] The synthetic sequence begins with the alkylation of bromoalkanoate **145** with ethyl acetoacetate **146**, resulting in the formation of the diester **147**. Hydrolysis of the diester with aqueous NaOH afforded the intermediate diacid **148**, which undergoes decarboxylation upon heating to yield the keto-acid **149**. Bromination of the keto-acid gives the desired dibromo acids **150a**, in

addition to the mono-bromo (**150b**) and tri-bromo (**150c**) acids. Finally, sulfuric acid-catalyzed cyclization causes ring closure and concomitant oxidation to generate the lactone nucleus of the fimbrolide **151a**, 3-alkyl-5-dibromomethylene-2(5*H*)-furanone **151b** and 4-bromo-3-alkyl-5-dibromomethylene-2(5*H*)-furanone **151c**. Recrystallization of the crude mixture from light petroleum afforded the major product **151b** quite readily, while the remaining mixture of **151a** and **151c** could be separated by column chromatography.

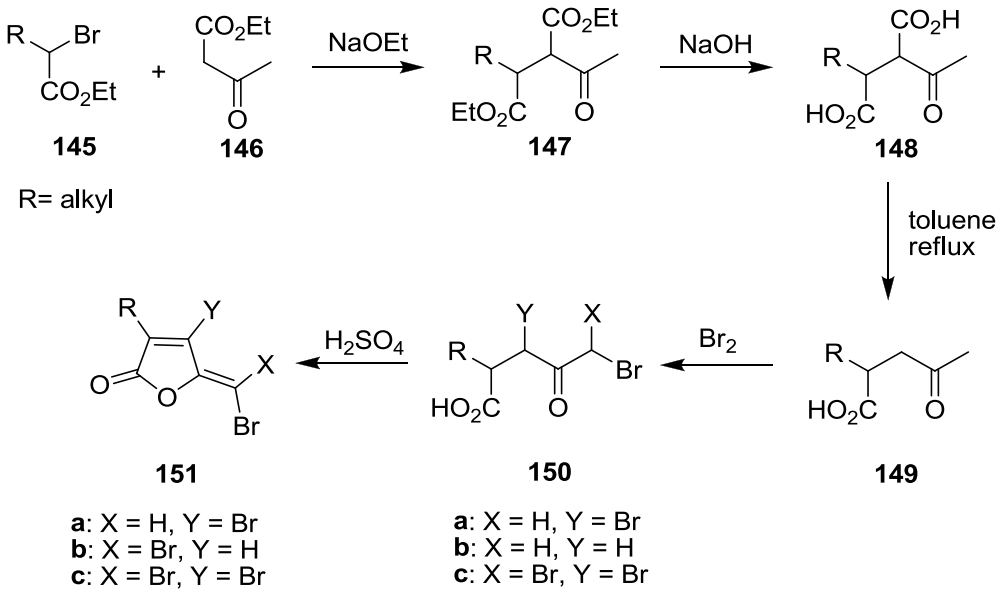

Scheme 3.4: Synthesis of fimbrolides from bromoesters **19** and ethyl-3-oxo butanoate **20**.

3.3 Chapter aims

A wide range of fimbrolide derivatives have been synthesized in our group using the above method, and have been found to be useful QS inhibitors. Given the key role nitric oxide plays in bacterial functioning, including biofilm formation and dispersion, it was anticipated that the synthesis of hybrids based on fimbrolides and nitric oxide donors

could serve as a valuable class of dual-action compounds exerting antibacterial action *via* multiple mechanisms.

Consequently, the aim of this research was to develop novel fimbrolide-based nitric oxide donors. These novel nitric oxide hybrids have a fimbrolide scaffold and a nitric oxide donor moiety attached either directly as in structure **152** or *via* different linkers as in structure **154** (Figure **3.2**). The α-carbon (C1') of the fimbrolide side chain was selected for NO donor attachment due the chemical reactivity of the position and also as the natural fimbrolides are in general functionalized at the α-carbon position. In addition, the C1' substituted natural fimbrolides are biologically more active than the parent unsubstituted compound.[91] The different nitric oxide donors utilized were the nitrates (ONO_2), diazeniumdiolates (NONOate) and *S*-nitroso (S-NO) derivatives.

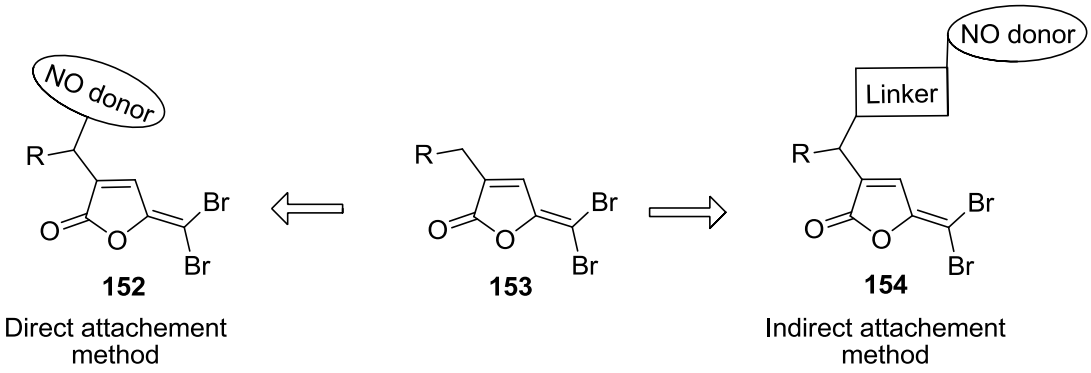

Figure 3.2: Modes of fimbrolide and NO donor attachment.

3.4 Synthesis of fimbrolide-based nitric oxide donors

In order to investigate the proposed fimbrolide-based NO donors, the corresponding fimbrolide derivatives **153** were initially synthesized *via* the sulfuric acid-catalyzed cyclization of brominated 2-alkyllevulinic acids.[232] This improved synthetic

methodology has enabled an easier access to a wider range of novel fimbrolides serving as precursors to the novel fimbrolide-based NO donors.

3.4.1 Synthesis of fimbrolide-based nitrate derivatives *via* direct attachment

The first objective was to synthesize fimbrolide-based nitrate derivatives *via* the direct attachment of the nitrates to the fimbrolide skeleton. Retrosynthetic analysis showed that the desired fimbrolide nitrate **155** can be synthesized from a fimbrolide halogen derivative **156**, which in turn can be obtained from the reaction of **153** with a suitable halogenating reagent under free radical halogenation condition (Scheme **3.5**).

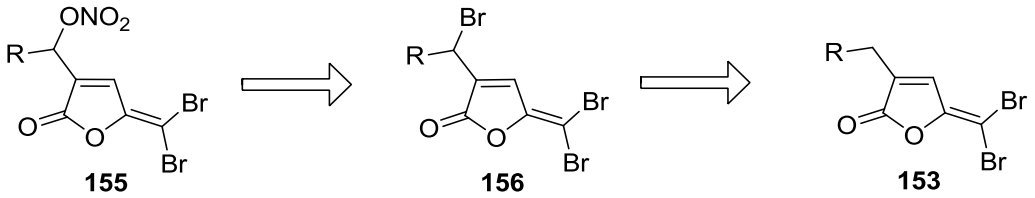

Scheme 3.5: Retrosynthetic scheme for fimbrolide nitroester

To investigate this strategy, the model fimbrolide **153a** was first converted to the α-bromo-substituted fimbrolide **156a** through photochemical allylic halogenation with *N*-bromosuccinimide (NBS) as the brominating agent (Scheme **3.6**). The radical bromination step was monitored by ^{1}H NMR spectroscopy, as the R_f values of the starting fimbrolide **153a** and the α-brominated compound **156a** were very similar. The completion of the reaction was confirmed through the ^{1}H NMR spectrum, as indicated by the downfield shift of the α-proton to δ 4.95, which also integrated for only one proton, upon substitution with the bromine functionality.

The C1'-bromobutyl fimbrolide **156a** was further reacted with silver nitrate in acetonitrile at 70 °C to generate the nitrate product **155a**. As before, the reaction was

monitored *via* ^{1}H NMR spectroscopy due to the similar R_f values of the starting material **156a** and the product **155a**. The reaction was observed to attain completion at 18 h, and the reaction mixture was filtered through a bed of Celite and silica to remove the silver salts. The resulting filtrate was evaporated to dryness. Purification of the crude product was performed using flash chromatography to give the desired nitroester derivative **155a** in 80% yield (Scheme **3.6**).

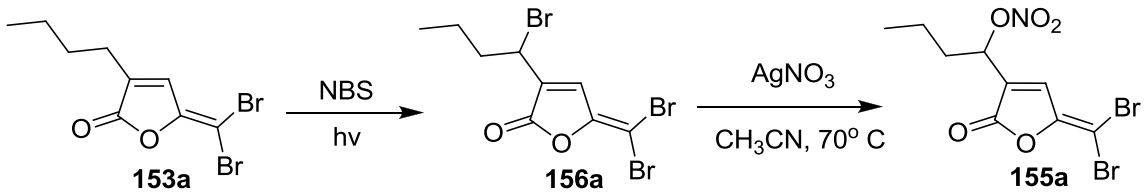

Scheme 3.6: Synthesis of fimbrolide nitrate derivative **155a**.

The ^{1}H NMR spectrum of the product **155a** exhibited a triplet with a downfield chemical shift of δ 5.70 (J = 7.5 Hz, 1H) assigned to the α-proton, due to the effect of the adjacent electron-negative ONO_2 group. The H4 proton of the furanone core appeared as a singlet at δ 7.54, while the aliphatic protons of the side chain appeared at δ 1.89 (q, J = 7.5 Hz, 2H), 1.46 (m, J = 7.5 Hz, 2H) and 0.97 (t, J = 7.5 Hz, 3H). Further characterization to confirm the presence of the nitrate group was achieved by ^{1}H-^{15}N-HMBC spectroscopy, which showed a nitrogen peak at δ 334 correlating with the α-proton of the product (Figure **3.3**). A peak at 1639 cm^{-1} in the IR spectrum also supported the presence of a nitrate group.

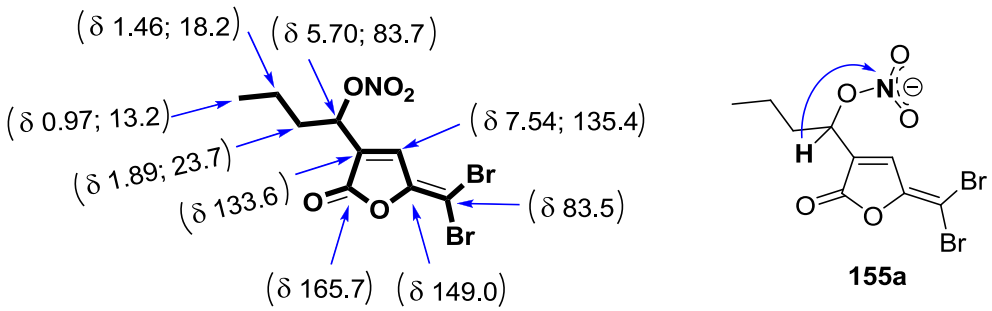

Figure 3.3: Characteristic ^{1}H and ^{13}C NMR signals (δ_H, δ_C) and ^{1}H-^{15}N-HMBC correlations for compound **155a**.

Following a similar synthetic strategy, fimbrolide nitrate derivatives **155b–f** were obtained from the starting materials **153b–f** (Scheme **3.7**). The product **155c** was successfully crystallized into a single crystal suitable for the X-ray crystallography, which further indicated the presence of the desired nitroester group in the product (Figure **3.4**).

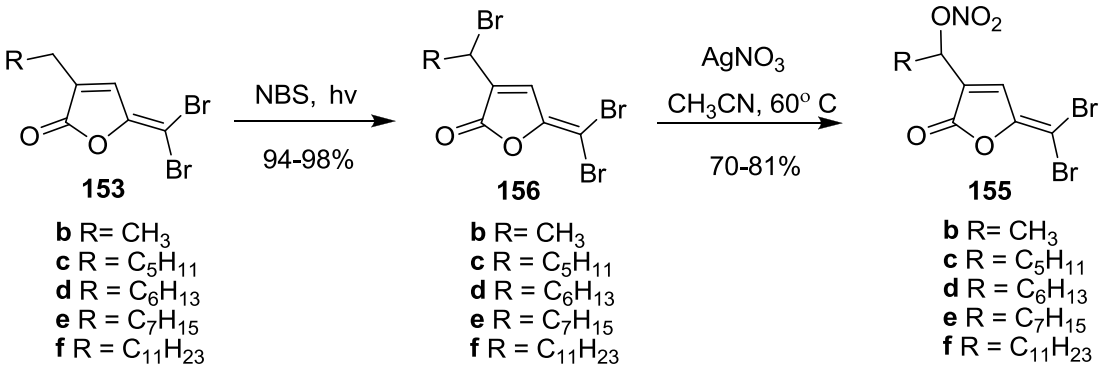

Scheme 3.7: Synthesis of fimbrolide nitrate derivatives

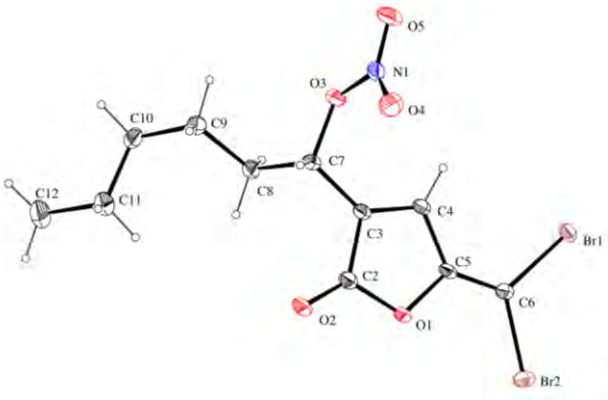

Figure 3.4: ORTEP diagram for **155c**.

3.4.2 Synthesis of fimbrolide-based nitrate derivatives *via* linker region

In the literature, a common strategy for the attachment of nitrate to biologically active molecules is through metabolically cleavable linkers such as esters. Thus, this strategy was also investigated as an alternative to the direct attachment strategy for the preparation of fimbrolide nitrate derivatives. To achieve this, two approaches involving the use of ester linkages or thioester linkages were explored. Both linkers can be enzymatically cleaved from the fimbrolide skeleton, to release the fimbrolide and the NO donor as separate entities.

For the preparation of fimbrolides with ester linkages, the precursor hydroxy fimbrolide **157a** was prepared in 59% yield from bromo-fimbrolide **156a** by stirring at r.t. for 72 h in DMSO with a few drops of water (Scheme **3.8**). This reaction is quite unusual as in general, vigorous conditions are required for the conversion of an alkyl halides to alcohols.

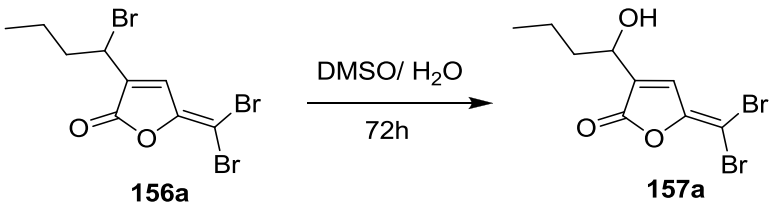

Scheme 3.8: Preparation of hydroxy fimbrolide **157a**.

The ^{1}H NMR spectrum of product **157a** exhibited a similar peak pattern to starting material **156a**, with the exception of the alkyl CH and CH_2 protons which gained additional coupling interactions with the hydroxyl group. Furthermore, a broad singlet at δ 2.00 for the hydroxyl group was observed in the spectrum of **157a**.

The hydroxy analogue **157a** can be converted into the desired ester derivatives *via* two different strategies. The first strategy (method A) involved the preparation of acyl chloride intermediates **159** by the reaction of bromo alkanoic acids **158** with thionyl chloride. The acyl chlorides **159** were then reacted with fimbrolide **157a** to give the bromo ester products **160** after column purification in 89-95% yield. The alkyl bromide substituent was converted into a nitrate group by nucleophilic substitution with silver nitrate in acetonitrile at 60 °C to afford the nitrate ester fimbrolides **161** in 72–76% yield (Scheme **3.9**). This functional group conversion was confirmed by the ^{1}H NMR spectrum, where the alkyl proton adjacent to the nitrate group shifted downfield to δ 4.5 from its initial value of δ 3.4.

In the second strategy (method B), the alkanoic acid nitrates **94** were first prepared from alkyl acids **158**. Treatment of **94** with thionyl chloride furnished the acyl chloride nitrates **39**, which were reacted with the hydroxy fimbrolide **34** to give the nitrate ester fimbrolide derivatives **40**, which were obtained in 68–75% yields after the workup and purification by column chromatography (Scheme **3.9**). Method B was found to be more

efficient as it required only one chromatographic purification step compared to two in the case of method A, the overall yield from both the methods was similar.

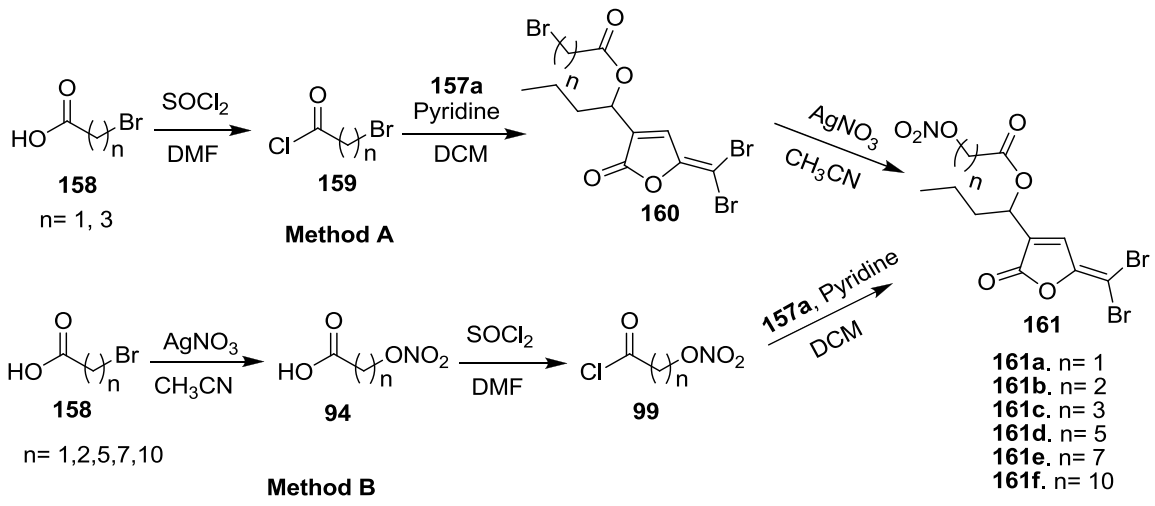

Scheme 3.9: Two strategies for the synthesis of fimbrolide derivatives with ester-linked nitrates.

The ^{1}H NMR spectrum of a typical ester-linked fimbrolide nitrate such as **161c** exhibited three characteristic triplets. Two triplets at δ 4.52 (J = 6.2 Hz, 2H) and 2.52 (J = 7.1 Hz, 2H) were assigned to the aliphatic protons adjacent to the nitrate and carbonyl functionalities, respectively. The final triplet at δ 0.94 (J = 7.2 Hz, 3H) was characteristic for the terminal CH_3 group of the alkyl side chain. The double triplet at δ 5.63 (J = 7.2 Hz, 1H) corresponded to the α-proton of the fimbrolide alkyl system. (Figure **3.5**). Furthermore, the ^{13}C broadband decoupled and DEPT-135 NMR spectra of **161c** indicated the presence of the desired number of methylene (CH_2) groups, in addition to the two carbonyl carbons at δ 166.0 and 171.3, confirmed the formation of the desired product. The NMR spectra of the other ester-linked fimbrolide nitrate derivatives **161** were found to exhibit similar patterns, differing only in the number of aliphatic protons from the linker region.

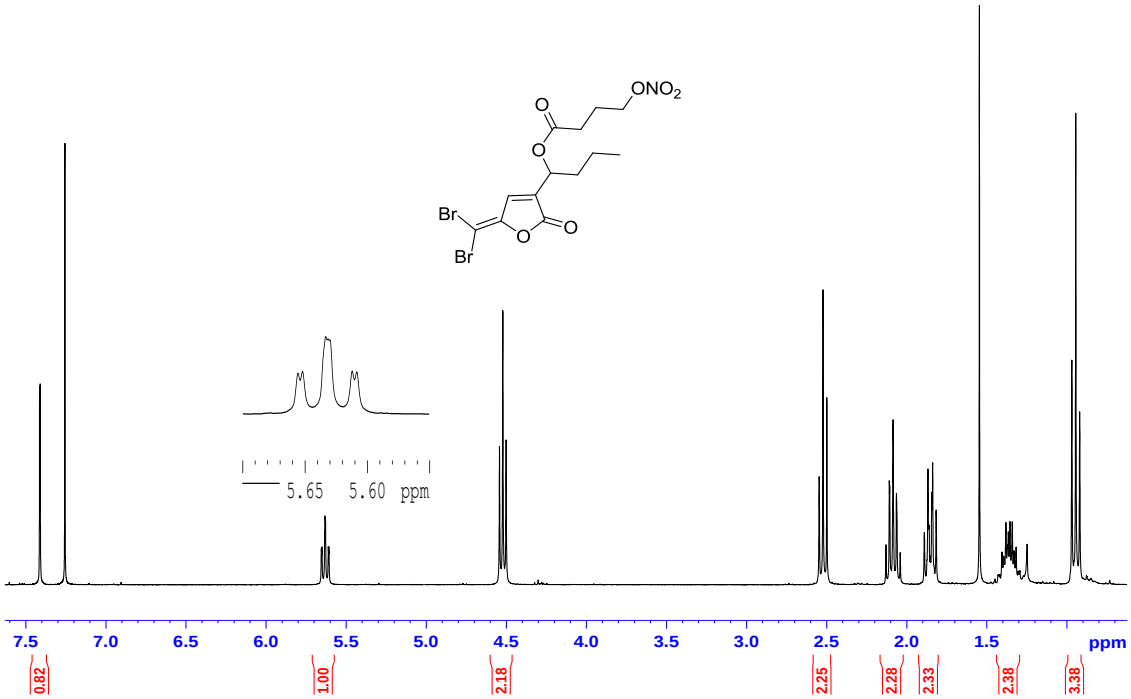

Figure 3.5: ^{1}H NMR spectrum of product **161c**.

It was interesting to note that in the case of **161b**, adsorption of the compound onto silica for an extended period of time (approx. 2 h) before column chromatography resulted in the formation of an additional product **162**. This could be due to the elimination of HNO_3 from **161b** in the presence of silica over a period of time, indicating the high sensitivity of the nitrate functionality in the alkyl ester system.

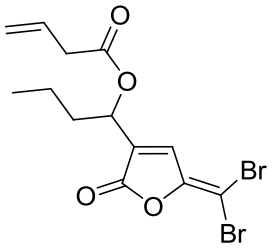

162

The second approach used to conjugate the nitrate group to the fimbrolide scaffold was through a thioester linkage. To achieve this, a thiol (SH) functionality first has to be introduced into the fimbrolide skeleton. It was hypothesized that the fimbrolide thiol

derivative **163** can be obtained from the hydrolysis of fimbrolide thioacetate **164**, which in turn can be synthesized by a nucleophilic substitution reaction on bromo fimbrolide **156a**.

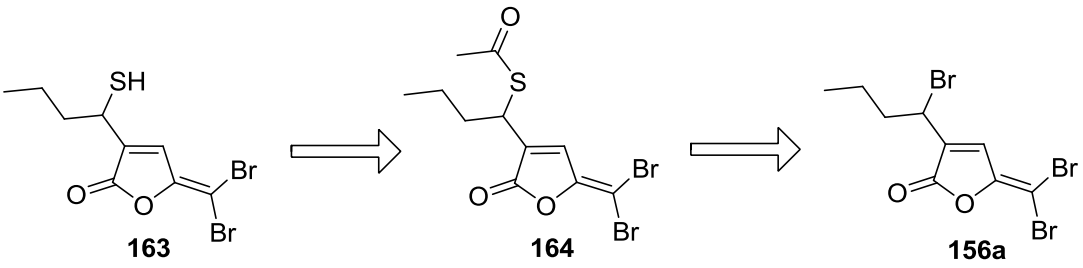

Scheme 3.10: Retrosynthesis of fimbrolide thiol derivative **163**.

To introduce the thioacetate functionality to the fimbrolide skeleton, fimbrolide **156a** was treated with potassium thioacetate in acetone at r.t. for 1 h, which afforded the desired nucleophilic substitution product **164** in 78% yield (Scheme **3.11**). The ^{1}H NMR spectrum of the crude product confirmed the substitution of the thioacetate functionality as indicated by the presence of an additional methyl peak at δ 2.33.

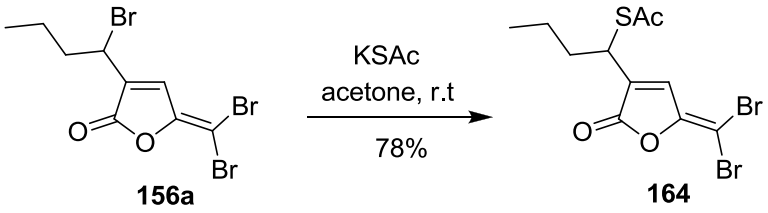

Scheme 3.11: Preparation of fimbrolide thioacetate **164**.

Acidic hydrolysis of the crude thioacetate-substituted fimbrolide **164** was first attempted by treatment with 0.1 M methanolic HCl at r.t., but the reaction did not proceed (Scheme **3.12**). At 60 °C, only a small amount of the desired product was formed (less than 5%) after 72 h, and degradation of starting material was observed as indicated by ^{1}H NMR spectroscopy.

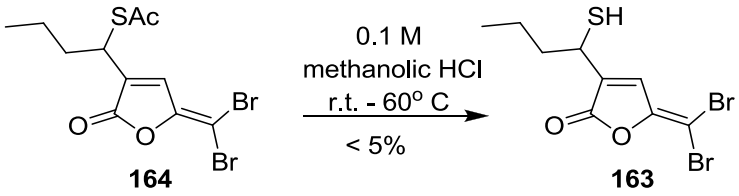

Scheme 3.12: Attempted acidic hydrolysis of **164** to obtain thiol **163**.

Therefore, the acid hydrolysis was performed using a higher concentration of acid (0.8 M HCl), and the reaction was heated at 80 °C overnight. TLC indicated formation of one major product, which was purified using column chromatography.

Interestingly, the ^{1}H NMR spectrum (Figure **3.6**) of the isolated compound was not consistent with the expected structure of fimbrolide **163**. The peak at δ 4.39 in the starting material had disappeared, corresponding to the loss of the α-proton of the fimbrolide system, while two atypical peaks appeared. The down-field singlet at δ 9.80 ppm (1H) suggested the presence of a deshielded proton such as an aldehyde or enol. The proton peak at δ 8.06 ppm indicated possibly towards an aromatic or methylene type proton, while the singlet at δ 3.86 (3H) indicated a methoxy group. A consistant structure could not be elucidated from the ^{1}H-NMR spectrum, therefore further analysis was required.

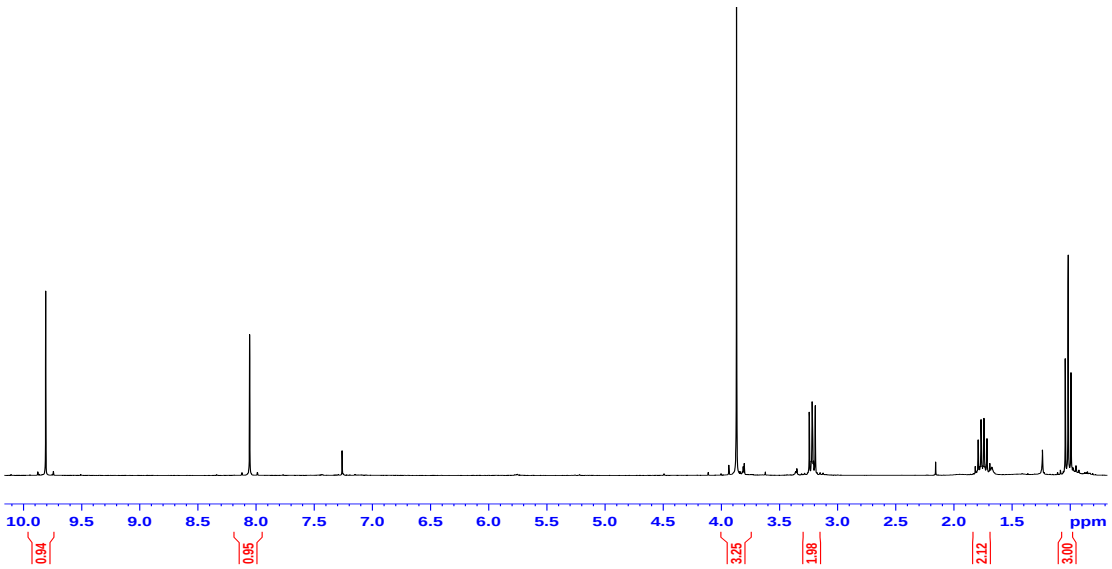

Figure 3.6: ^{1}H NMR spectrum of product from acid hydrolysis of **164**.

The ^{13}C broadband decoupled and DEPT-135 NMR spectra indicated the presence of two carbonyl groups, one CH_3, two CH_2, one CH groups and three quaternary carbons. Further analysis using 2D NMR was performed to elucidate the structure of the product. The COSY correlation peaks between the protons at δ 1.01 and 1.79, and δ 1.79 and 3.25 indicated the presence of a $CH_2CH_2CH_3$ alkyl chain system which is notably one carbon shorter than the alkyl chain in **164**. The HMBC correlations exhibited between the proton and carbon peaks also gave important information about the structure. The CH_2 protons at δ 3.25 correlated with the aliphatic chain carbons and with the carbonyl carbon at δ 165.3 which also correlated with the OCH_3 group indicated the presence of an alkyl chain adjacent to the ester group. The proton at δ 8.06 ppm correlated with the two carbonyl carbons; ester (C=O) at δ 165.3 and possibly a CHO δ 182.9 indicating its presence between these two carbonyl groups. The high resolution mass spectrometric analysis of the product revealed a molecular ion at 213.0577 $(M + 1)^+$, corresponding to molecular formula of $C_{10}H_{12}O_3S$ indicating the presence of a sulfur in the compound. The combined results of the analytical techniques suggested the presence of the

thiophene **165**. Thus, it is proposed that the fimbrolide thioacetate derivative **164** undergoes an unusual transformation to a thiophene derivative **165** under acidic conditions (Scheme **3.13**).

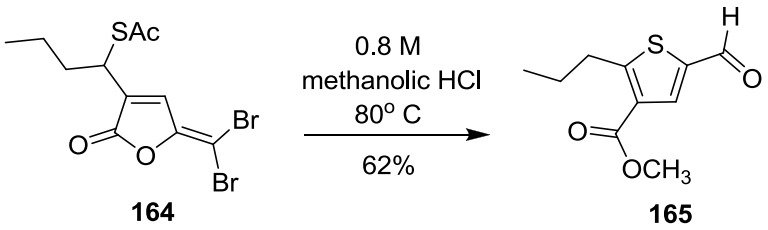

Scheme 3.13: Proposed conversion of fimbrolide thioacetate **164** to thiophene **165** under acidic conditions.

Finally, the thiophene structure **165** was confirmed by X-ray crystallographic analysis (Figure **3.7**).

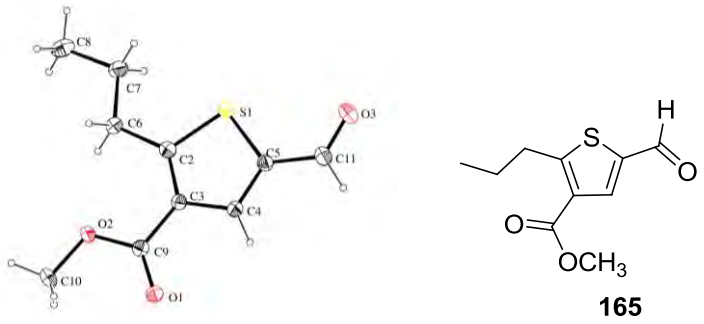

Figure 3.7: ORTEP diagram for **165**.

The mechanism for this unusual and hitherto-unknown conversion from the furanone to a thiophene skeleton was postulated to occur *via* the series of steps depicted in Scheme **3.14**. The *S*-acetate derivative **164** could undergo methanolysis, affording the ring-opened structure **166**. The structure **166** could subsequently cyclise to compound **167**, followed by a series of dehydration, hydrolysis and elimination reactions to give the thiophene compound **165**.

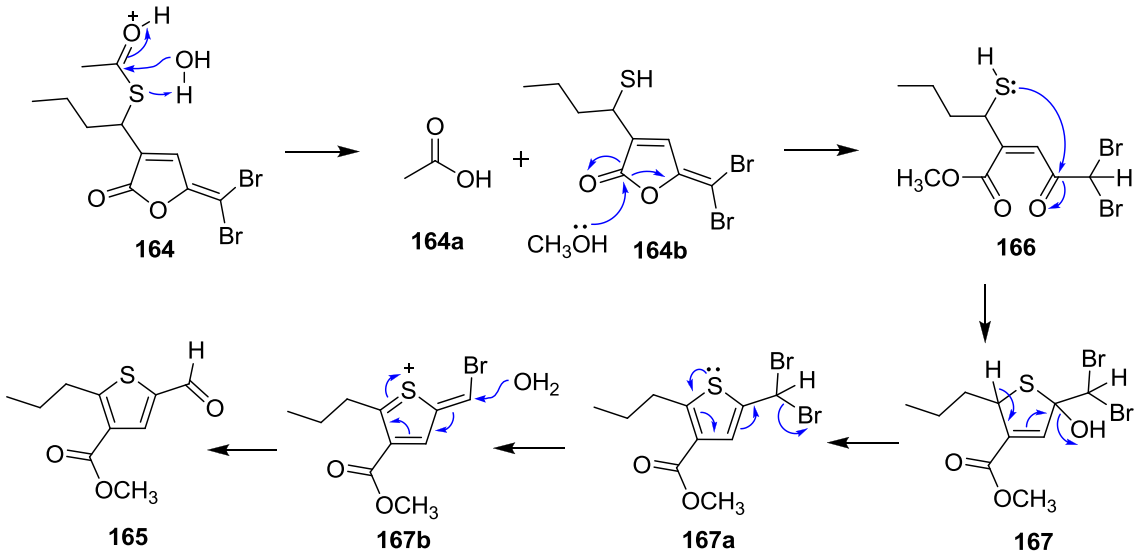

Scheme 3.14: Proposed mechanism for conversion from **164** to **165**.

This result indicated that the use of 0.8 M HCl was too harsh for the hydrolysis step. The final attempt for the synthesis of thiol **163** was performed by hydrolysis of thioacetate **164** with methanolic 0.3 M HCl solution at a temperature of 50 °C, and the reaction was monitored by TLC. It was observed that the starting material was reduced by about 90–95% after about 3 h with the formation of a single major product, but additional products were formed if the reaction continued after 3 h. Thus, the reaction was stopped after 3 h and the product was purified by column chromatography to provide the desired product **163** in 48% yield.

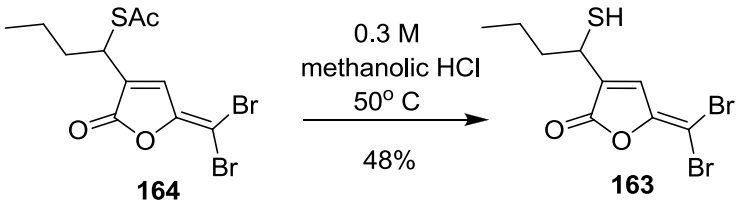

Scheme 3.15: Synthesis of fimbrolide thiol **163**.

The ^{1}H NMR analysis of **163** showed the disappearance of the acetate peak, and the appearance of a doublet at δ 2.4 (J = 7.5 Hz) corresponding to the SH group. In addition, the α-proton shifted upfield from δ 4.39 in the starting material **164** to δ 3.71 in the product **163**, indicating the successful hydrolysis of the thioacetate functionality.

The thiol derivative **163** was further used for the synthesis of desired thioester nitrate derivatives. The procedures used for the preparation of the thioester nitrate derivatives were similar to those employed for the nitrate ester derivatives described previously. In the first strategy (method A), the fimbrolide thiol **163** was first reacted with the acyl bromo derivative **159**, and the resulting bromo thioester **168** was subjected to nucleophilic substitution to furnish the thioester nitrate derivative **169b**. In the second strategy (method B), the acyl acid nitrate **99** was reacted with fimbrolide thiol **163** in DCM with pyridine to give the thioester nitrate product **169** (Scheme **3.16**). The structures of the intermediates and the products were successfully confirmed by ^{1}H NMR spectroscopy data.

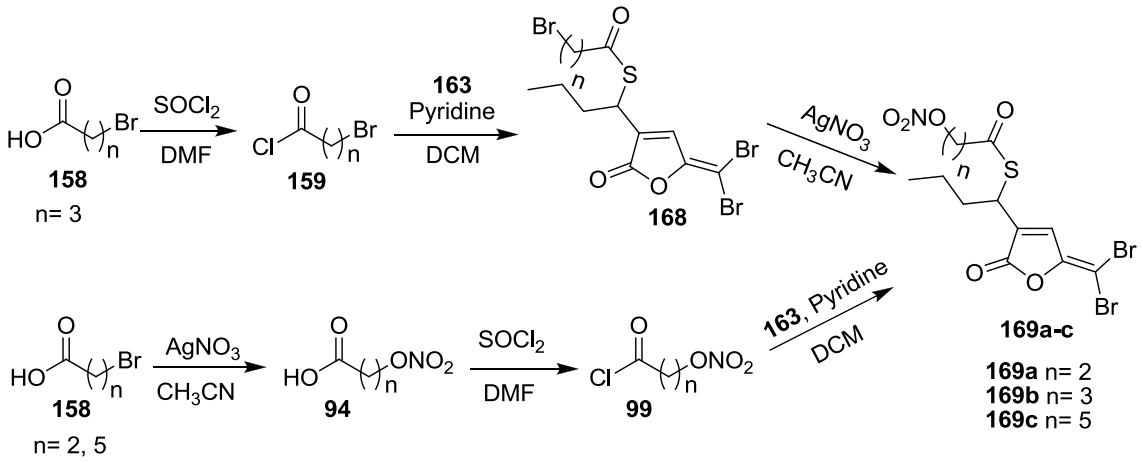

Scheme 3.16: Synthesis of fimbrolide thioester nitrate derivatives **169**.

Interestingly, an unexpected result was observed during the synthesis of thioester nitrate derivative **169d** (n = 1). The synthesis of **169d** was attempted with both strategies (methods A and B), but multiple products were formed in both cases (Scheme **3.17**).

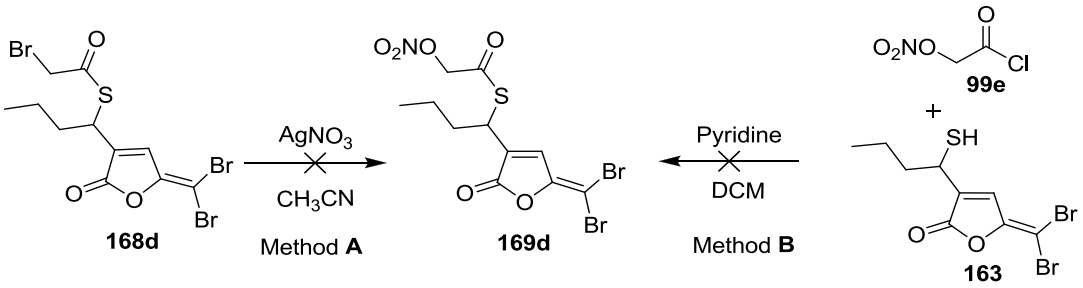

Scheme 3.17: Attempted synthesis of **169d**.

The major product isolated in the case of method A was found to be fimbrolide nitrate derivative **155a** (Scheme 3.6), as indicated by ^{1}H NMR spectroscopy. On the other hand, the major product isolated from method B reaction was found to be a disulphide-type product (discussed in Section 3.4.5). These results indicate the lower stability of the fimbrolide thiol derivatives, and their reactive nature under the reaction conditions utilized.

3.4.3 Synthesis of fimbrolide-based diazeniumdiolate derivatives *via* O^2-attachment

As discussed in Chapter 1, diazeniumdiolates are spontaneous NO donors. O^2-substituted diazeniumdiolates are comparatively more stable than unsubstituted diazeniumdiolates, and require metabolic activation to release NO. Thus, the attachment of the diazeniumdiolate functionality to the fimbrolide skeleton *via* O^2-substitution was first investigated. In the literature, there is strong precedence for the synthesis of O^2-substituted diazeniumdiolates through the use of alkylating agents such as alkyl or aryl

halides. Alkylation can take place between the salt of a diazeniumdiolate and the appropriate alkylating agent in the presence of a base such as $NaHCO_3$. Polar solvents commonly utilized for this reaction include acetone, DMSO, THF and alcohols.[194-196]

To achieve this direct attachement *via* O^2-substitution, fimbrolide **156a** was reacted with the diazeniumdiolate **160** under basic conditions at r.t. in acetone. The reaction was monitored at various intervals however no reaction was observed even after 48 h (Scheme **3.18**).

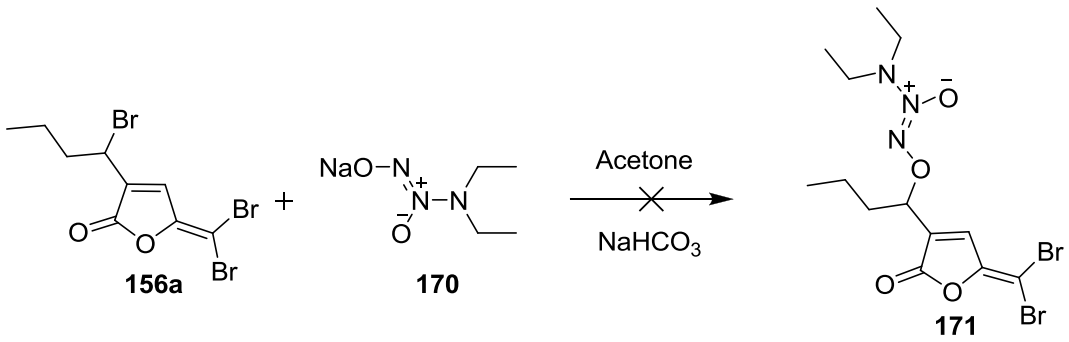

Scheme 3.18: Attempted synthesis of O^2-substituted diazeniumdiolate fimbrolide derivative **171**.

Therefore, the reaction was carried out in different solvents and various reaction times at r.t. to optimize the conditions for the synthesis of O^2-substituted diazeniumdiolate fimbrolide derivative **171** (Table **3.1**). Unfortunately, all attempts led to either no reaction or the formation of multiple products, which were found to include the 1-hydroxybutyl fimbrolide **157a** and other degraded fimbrolide products.

Table 3.1: Reaction conditions investigated for the synthesis of O^2-substituted diazeniumdiolate fimbrolide derivative **50**.

Entry	Reaction solvent	Time	Result
1	Acetone	24-48 h	No reaction
2	DMSO	24 h	Multiple products
3	THF	24–72 h	Multiple products
4	t-BuOH	72 h	Multiple products
5	Acetone/ H_2O	24 h	Multiple products

The failure to synthesize the desired O^2-substituted fimbrolide derivative **171** may be attributed to the low reactivity of α-bromo fimbrolide **156a** towards the O^2-alkylation reaction of the diazeniumdiolate and also to the low stability of starting diazeniumdiolates and the possible products. Hence, a more reactive halogen group was investigated to achieve the O^2-alkylation of the diazeniumdiolate. Acetyl bromide was introduced into the C1′-position by the reaction of hydroxy fimbrolide **157a** with 2-bromoacetyl bromide using the conditions for ester preparation (Section 3.4.2) to furnish the desired bromoacetyl-substituted product **160a** in 88% yield. The ^{1}H NMR spectrum indicated the substitution of the acetyl bromide group as revealed by the appearance of a new singlet at δ 5.2 ppm (2H) and the downfield shift of the α-proton to δ 5.6 ppm.

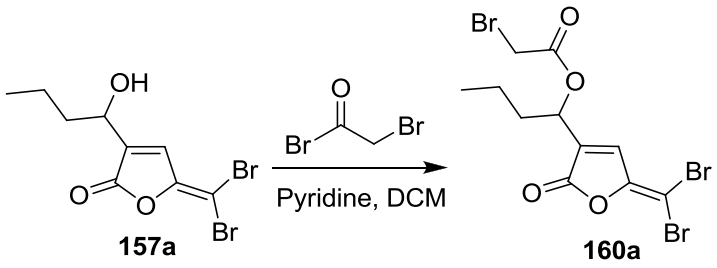

Scheme 3.19: Synthesis of bromoacetyl-substituted fimbrolide **160a**.

Once the desired bromoacetyl-substituted fimbrolide derivative **160a** was obtained, it was reacted with the sodium diazeniumdiolate **170** at 0 °C using DMSO as solvent and $NaHCO_3$ as base. $NaHCO_3$ is used to maintain a basic environment, as diazeniumdiolate are known to be more stable under basic conditions. The reaction was monitored by TLC, which revealed the disappearance of starting fimbrolide **160a** after 20 min. DCM was added to the reaction mixture and the resulting mixture was washed with water and brine. The organic layer was dried and evaporated to obtain a crude product, which was purified by preparative TLC to provide the desired O^2-substituted diazeniumdiolate fimbrolide derivative **172** in 46% yield. The product could also be obtained using DMF as the solvent, but this required a longer reaction time of 1 h with little alteration in the overall yield of the reaction.

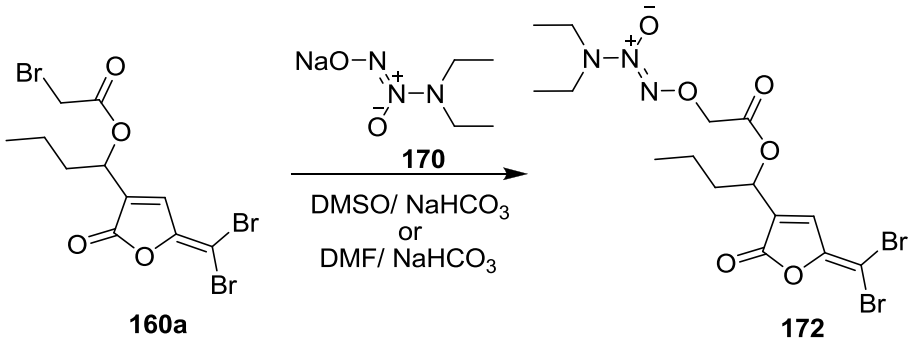

Scheme 3.20: Preparation of fimbrolide diazeniumdiolate **172** *via* O^2-substitution.

Using the same procedure with DMSO as the reaction solvent, O^2-substituted diazeniumdiolate fimbrolide derivatives **174** and **175** were synthesized from fimbrolide **160a** and the corresponding diazeniumdiolates **114** and **173** respectively (Scheme **3.21**).

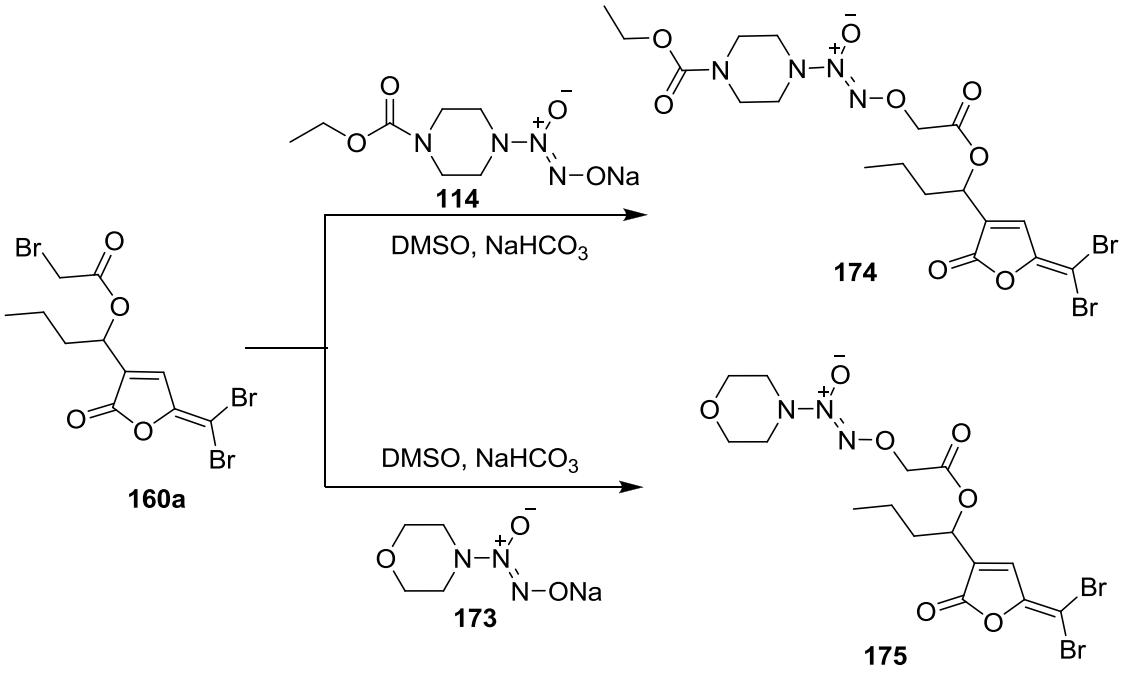

Scheme 3.21: Preparation of O^2-substituted diazeniumdiolate fimbrolide derivatives **174** and **175**.

In addition to the desired product all the reactions resulted in the formation of a side-product **176.** This could be a result of the hydrolysis of either the starting material **160a** or the products.

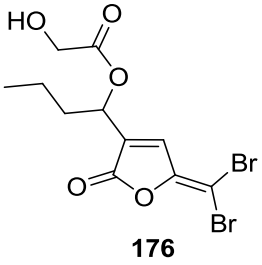

The ^{1}H NMR spectra for products **172**, **174** and **175** exhibited similar peak patterns for the aliphatic protons of the fimbrolide side chain. However, a shift was observed in the OCH_2CO protons to δ 4.82 (for **172**) and 4.78 (for **174** and **175**) after diazeniumdiolate substitution. The derivatives **172**, **174** and **175** can be easily differentiated by variation

in the pattern of the ^{1}H NMR signals depending on the type of diazeniumdiolate derivative attached (Table **3.2**).

Table 3.2: Characteristic ^{1}H NMR signals due to diazeniumdiolate secondary amine groups.

Product	Diazeniumdiolate	^{1}H NMR (δ)
172	Diethylamine	3.12 (q, 4H, 2×CH_2) and 1.10 (t, 6H, 2×CH_3)
174	*N*-ethylcarbamate piperazine	4.13 (q, 2H, OCH_2), 3.64 (t, 4H, 2×CH_2), 3.40 (t, 4H, 2×CH_2), 1.25 (t, 3H, CH_3)
175	Morpholine	3.76 (t, 4H, 2×CH_2) and 3.37 (t, 4H, 2×CH_2)

3.4.4 Synthesis of fimbrolide-based diazeniumdiolate derivatives *via* acid linkers

In addition to O^2-substitution reactions of the diazeniumdiolate, an alternative strategy was pursued *via* an amide bond linkage using piperazine diazeniumdiolate derivative **116**. To achieve this, the fimbrolide acid derivatives **177** were prepared by the reaction of hydroxy fimbrolide **157a-c** with diacid chloride derivatives **109a**–**b**. In general, the reaction involved the slow addition of hydroxy fimbrolide **157** with pyridine in DCM over a period of 30 minute to the corresponding diacid chlorides **109** at 0 °C. After complete addition, the reaction mixture was stirred for another 15 minutes at 0 °C and then at r.t. for 2 h to obtain the crude product. Workup followed by column chromatography gave the desired mono acid products **177** in 75–86 % yields (Scheme **3.22**).

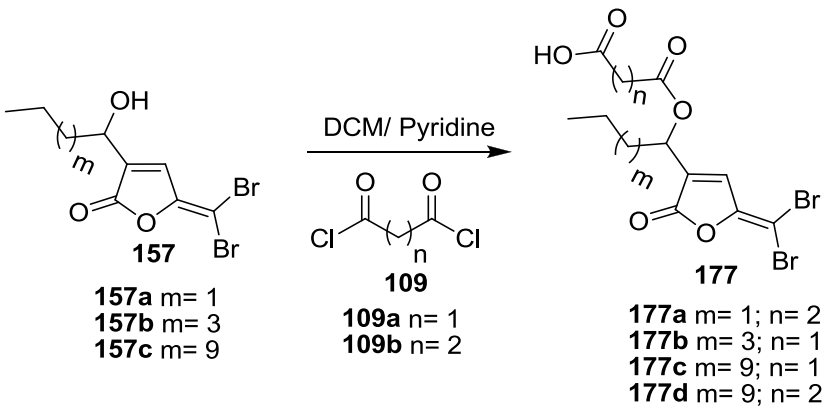

Scheme 3.22: Synthesis of fimbrolide diacid derivatives **177**.

Once the fimbrolide acid derivatives **177** were obtained, they were reacted with the piperazine diazeniumdiolate **116** using EDC coupling in DCM at r.t. to afford the desired diacid-linked piperazine diazeniumdiolate fimbrolide derivatives **178a**–**d** in 54–66% yields (Scheme **3.23**).

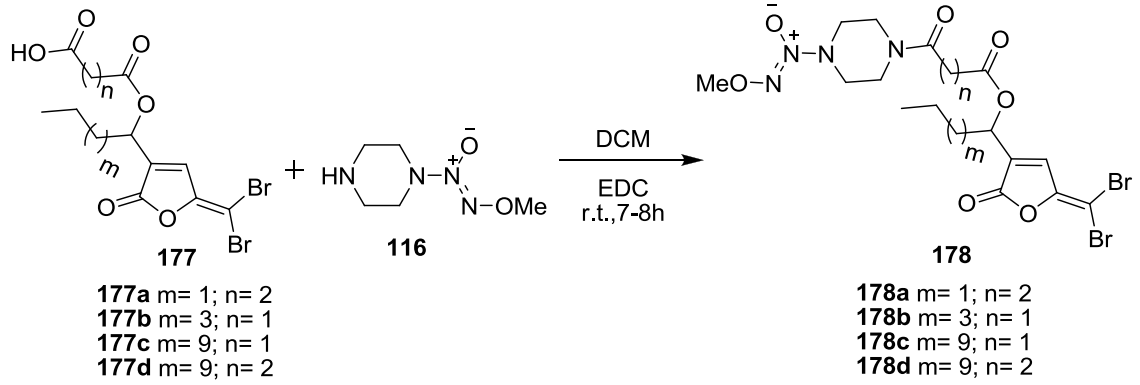

Scheme 3.23: Coupling of fimbrolide acid **177** and diazeniumdiolate **116** to furnish diazeniumdiolate fimbrolide hybrids **178**.

The ^{1}H NMR spectrum of the diacid-linked piperazine diazeniumdiolate fimbrolide derivatives **178a** exhibited a triplet at δ 5.53 assigned to the α-proton of the fimbrolide side chain, while the CH_2 protons of the acid linker appeared as a multiplet at δ 2.67. The ^{1}H NMR spectrum also revealed the protons of the piperazine group as two triplets

at δ 3.76 and 3.65 and a multiplet at δ 3.38. The O^2-methyl proton of the diazeniumdiolate was observed at δ 4.00 as a singlet. The ^{13}C broadband decoupled and DEPT 135 spectra indicated the presence of three carbonyl carbons at δ 166.2, 169.5, and 172.0 ppm and the appropriate number of CH_2 groups, indicating the formation of the desired diacid linked fimbrolide diazeniumdiolate products **178a** (Figure **3.8**).

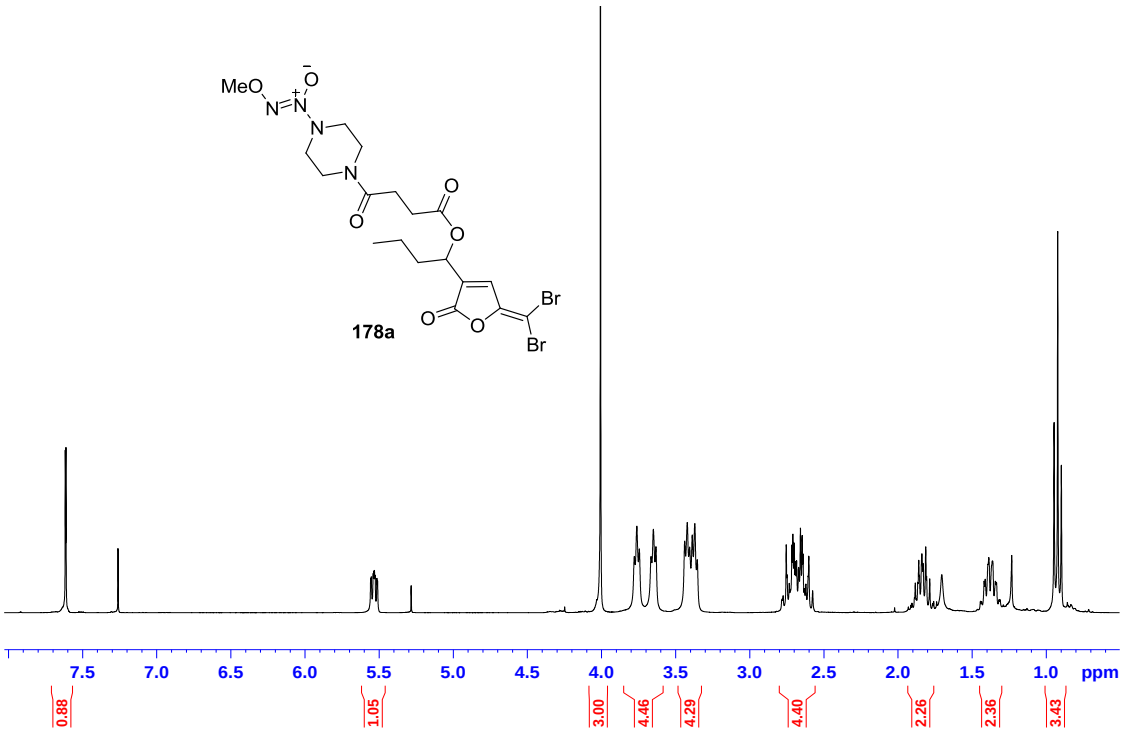

Figure 3.8: ^1H NMR spectra of piperazine diazeniumdiolate fimbrolide derivative with diacid linker **178a**.

3.4.5 Synthesis of fimbrolide-based *S*-nitrosothiol derivatives

The third kind of NO donors investigated were the *S*-nitrosothiols (S-NO), which were initially pursued by two different approaches. The first involved the direct attachment of S-NO to the fimbrolide skeleton, while the second approach involved the use of the well-studied S-NO derivative, *S*-nitroso-*N*-acetyl penicillamine (SNAP) to form a conjugate with the fimbrolide (Scheme **3.24**).

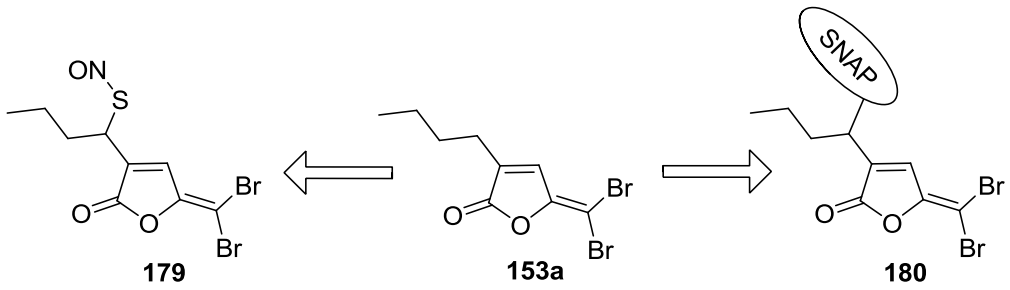

Scheme 3.24: Strategies towards the preparation of fimbrolide *S*-nitrosothiol derivatives.

The first strategy involved the preparation of the fimbrolide *S*-nitrosothiol derivative by direct attachment of S-NO to the fimbrolide skeleton. To achieve this transformation, the thiol derivative **163** was treated with the nitrosating agent *t*-butyl nitrite. The reaction was carried at r.t. and stirred for 1 h. ^{1}H NMR spectroscopic analysis of the obtained product indicated a change in the signal pattern of the fimbrolide, particularly the α-proton which changed from a quartet at δ 3.71 ppm in the starting thiol **163** to a multiplet (two triplets merged) at δ 3.59 ppm. However, it could not be determined whether the desired S-NO product was formed.

A study of the literature NMR values for S-NO products indicated that the signal of the proton adjacent to the thiol shifts downfield upon conversion to S-NO. However, the product obtained from reaction of thiol **163** produced an upfield shift in the α-proton, suggesting the formation of a product different to S-NO. It has been reported in the literature that S-NO derivatives can dimerize with the release of NO. Alternatively, thiols can undergo oxidation to form disulfides. Thus, one of the possible explanations for the unexpected result from the reaction of **163** with *t*-butyl nitrite could be the formation of a dimer compound *via* a disulfide bridge. The HRMS analysis of the product indicated a *m/z* value of 700.7283 (M+Na), consistent with the formation of the dimer product **181** with formula $C_{18}H_{18}Br_4O_4S_2$ (Scheme **3.25**).

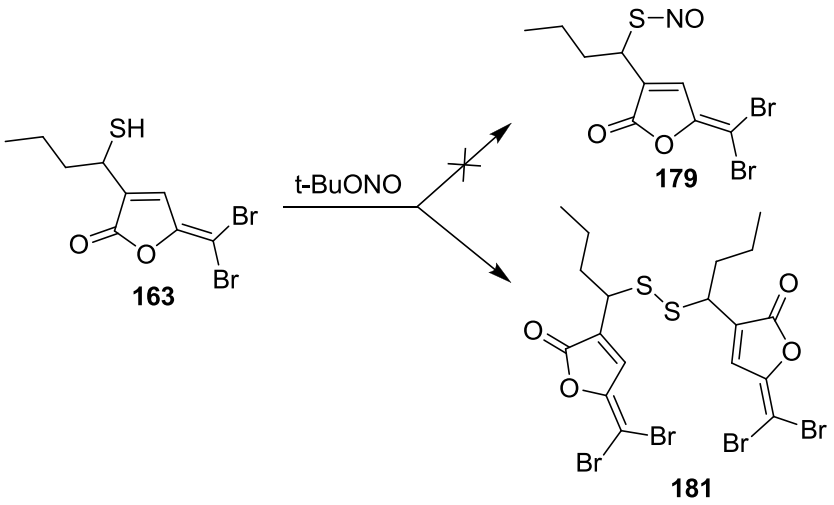

Scheme 3.25: Reaction of thiol **163** with *t*-butyl nitrite to form dimer **181**.

The structure of the product **181** was further confirmed by the X-ray crystal structure, which revealed the dimeric product with two fimbrolides attached *via* a disulfide bridge (Figure **3.9**). The crystal structure of **181** showed an equal ratio of *R,R* and *S,S* enantiomers. It appears that the reaction produces both the meso and racemic diastereomers but only the racemic diastereomer crystallises from solution. The crystal interactions relating to **181** are further discussed in Chapter 6.

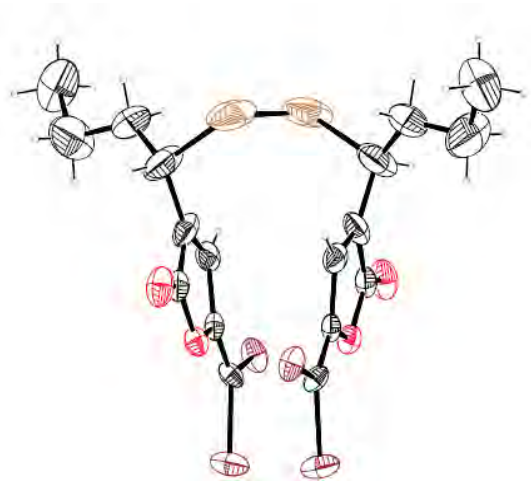

Figure 3.9: ORTEP diagram for **181**.

We were interested to determine whether the dimer structure was due to dimerization of the proposed S-NO derivative **179** or *via* oxidation reaction of the thiol **163**. To study this, a ^{1}H NMR kinetic study was performed at 0 °C to follow the reaction. The kinetics revealed that the formation of the dimeric product started within 5 min after the addition of *t*-butyl nitrite, but with no additional downfield peak indicating the formation of S-NO. Thus, the dimeric product **181** is postulated to be formed *via* an oxidative reaction mechanism rather than through a S-NO intermediate.

3.4.6 Synthesis of fimbrolide-based S-nitrosothiol derivatives *via S*-nitroso-*N*-acetyl penicillamine

The second strategy was to introduce S-NO into the fimbrolide skeleton as a *S*-nitroso-*N*-acetyl penicillamine (SNAP) **66** derivative. The usual method to introduce SNAP is through the ring-opening of the corresponding thietanone to form the SNAP derivative *via* an amide bond. A possible alternative approach for the preparation of the SNAP derivative is *via* an ester linkage, utilizing the acid functionality of SNAP. However, there are no reports of SNAP attachment by an ester linkage in the literature, possibly due to the reactive chemical nature of starting material *D*-penicillamine **182**, which has three possible nucleophilic sites complicating the preparation of an ester-linked derivative.

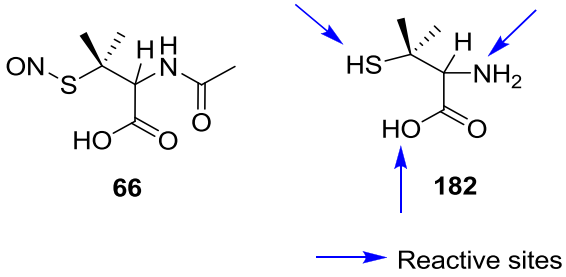

Figure 3.10: SNAP **66** and D-penicillamine **182**.

A wide range of protection strategies can be performed on *D*-penicillamine **182** in order to reduce the number of reactive sites. The initial attempts for the preparation of the fimbrolide SNAP conjugate aimed at synthesizing the product in the least number of steps. SNAP **66** was first synthesized from *D*-penicillamine **182** by *N*-acetylation followed by reaction with sodium nitrite under acidic conditions.

In the literature, the reaction of SNAP with amines using DCC coupling has been reported. Therefore, the first attempt involved the reaction of SNAP **66** with the hydroxybutyl fimbrolide derivative **157a** to form the ester-linked product **183** (Scheme **3.26**). The second attempt utilized the nucleophilic substitution reaction of *N*-acetyl penicillamine **184** with the bromobutyl fimbrolide **156a** according to a literature procedure for ester preparation using DBU as a base (Scheme **3.27**). Both the reactions when analyzed by TLC gave multiple spots with no sign of the desired product by ^{1}H NMR spectroscopy. The products isolated after column chromatography included the starting fimbrolide as well as compounds **186** and **124**. This outcome suggests that the *S*-nitrosothiol or thiol derivatives were not stable under the reaction conditions explored, and may require protection to avoid side reactions.

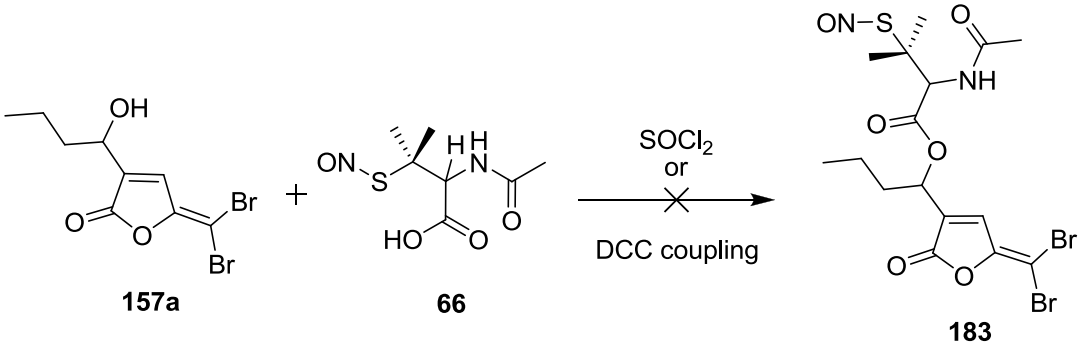

Scheme 3.26: Attempted synthesis of SNAP S-NO fimbrolide derivative **183** using DCC.

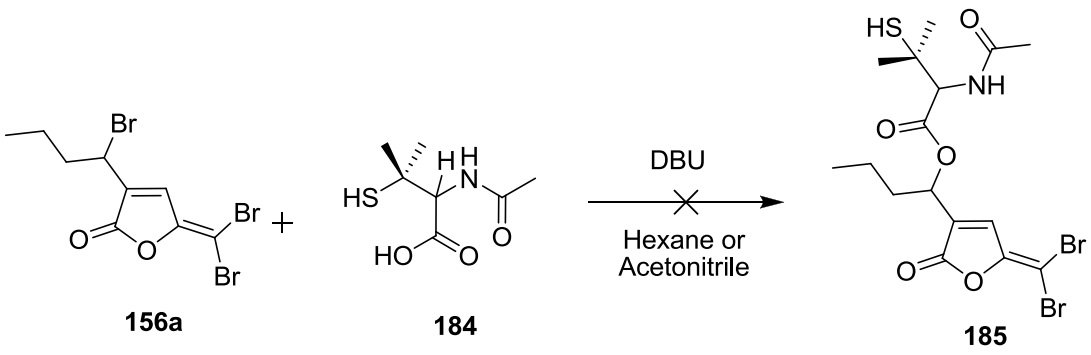

Scheme 3.27: Attempted synthesis of SNAP fimbrolide derivative **185** using DBU.

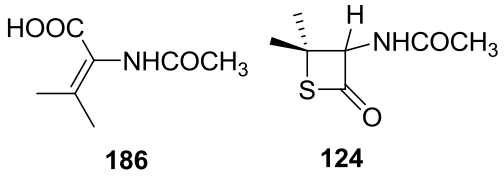

Hence, attempts were directed towards the attachment of *N*- and *S*-protected *D*-penicillamine to the fimbrolide. Protection of the NH and SH was initially attempted using an acetyl group. The *N*-acetyl derivative **184** was obtained from *D*-penicillamine **182** by treatment with acetic anhydride. Different approaches were attempted to protect the SH functionality, including acetyl chloride, acetic acid or acetic anhydride. However, all methods failed to give the desired *S*-acetyl protected derivative **187** (Scheme **3.28**).

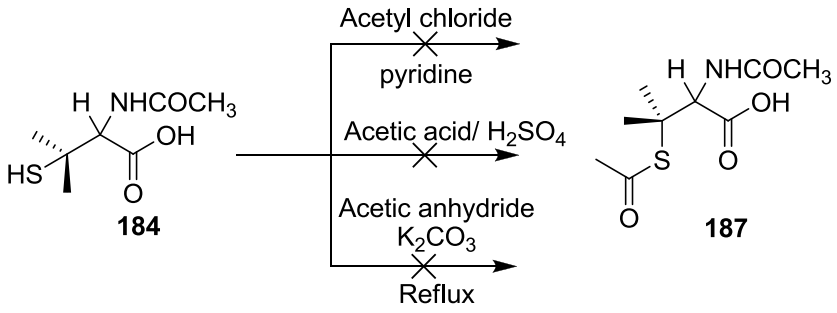

Scheme 3.28: Attempted *S*-acetylation reaction.

Thus, different thiol protection approaches reported in the literature were investigated and one protection strategy that looked quite promising was the protection of cysteine SH by thiazolidine formation. Therefore, *D*-penicillamine **182** was reacted with acetone at reflux for 6 h, followed by striring at r.t. for 18 h to furnish the desired thiazolidine derivative **188**. This compound was further *N*-protected with the acetyl group using acetic anhydride to obtain the *N*- and *S*- protected product **189**. The product **189** was then reacted with bromo fimbrolide derivative **156a** in DMF for 72 h to obtain fimbrolide thiazolidine ester derivative **190** as a diastereomeric mixture, which was submitted to column chromatography to isolate the two isomers (Scheme **3.29**).

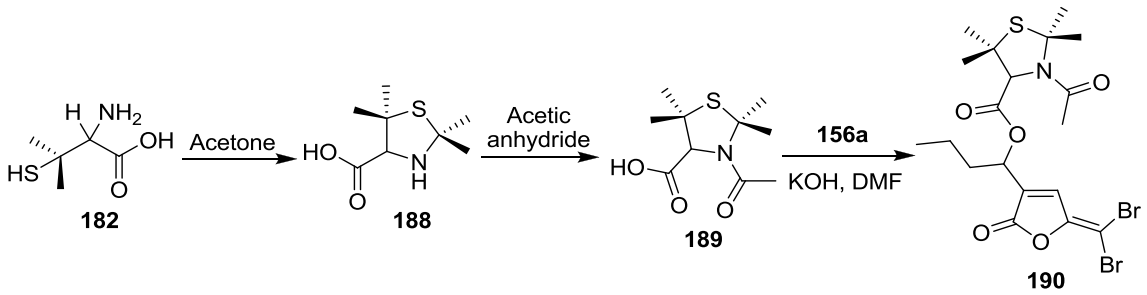

Scheme 3.29: Synthesis of fimbrolide thiazolidine derivative **190**.

The first product separated by chromatography (isomer 1), when analyzed by ^{1}H NMR spectroscopy revealed the H4 peak at δ 7.40, while the C-α-proton appeared at δ 5.65 from the fimbrolide motif. The thiazolidine motif was confirmed by signals at δ 1.66 and 1.33 ppm corresponding to the four methyl groups. The *N*-acetyl protons appeared as a singlet at δ 1.94 ppm.

Furthermore, the coupling of the fimbrolide and thiazolidine unit was confirmed by the X-ray crystal structure of **190** (Figure **3.11**) which unequivocally proved the structure of the molecule.

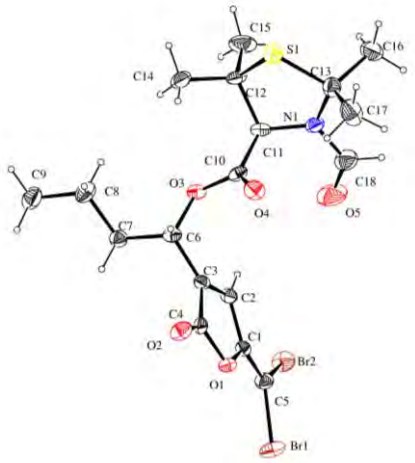

Figure 3.11: ORTEP diagram for **190**.

Ring-opening of the thiazolidine derivative **190** by acid hydrolysis was attempted by reaction with 1 M HCl. The reaction was monitored by TLC, but no reaction occurred even after 72 h. An alternative method for ring-opening utilizing mercuric chloride ($HgCl_2$) and H_2S gas also failed to give the desired product **185** (Scheme **3.30**). The non-reactive nature of **190** toward ring opening is possibly due to the presence of the *N*-acetyl group, which interferes with the ring-opening mechanism.

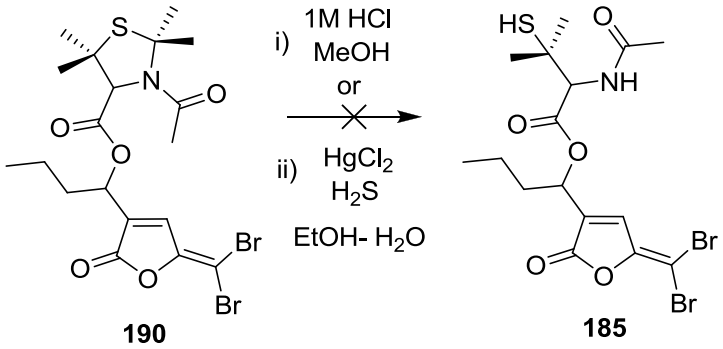

Scheme 3.30: Attempted ring-opening reaction of **190**.

Therefore, attention was directed towards protection of the thiazolidine NH group with an acid-labile functionality. The formamide group was considered to be a good option,

and thus thiazolidine **188** was *N*-protected using formic acid to give product **191**. The coupling of **191** and fimbrolide derivative **156a** was carried out using the same conditions as for **190**, furnishing the fimbrolide thiazolidine ester derivative **192** in 48% yield. The ^{1}H NMR spectrum of **192** was similar to **190** in all aspects, and only varied in the presence of the formyl proton at δ 8.32 and the absence of the acetyl protons at δ 1.94. The proton of the thiazolidine ring appears as singlet at δ 4.80. The product **192** was subsequently reacted with 1 M HCl to bring about the simultaneous deprotection of the *N*-formyl group and thiazolidine ring opening, followed by re-protection with acetic anhydride to furnish the *N*-acetyl derivative. Evaporation of the reaction mixture and purification of the crude product by column chromatography gave the desired product **185** as two diastereoisomers in 42% yield (Scheme **3.31**).

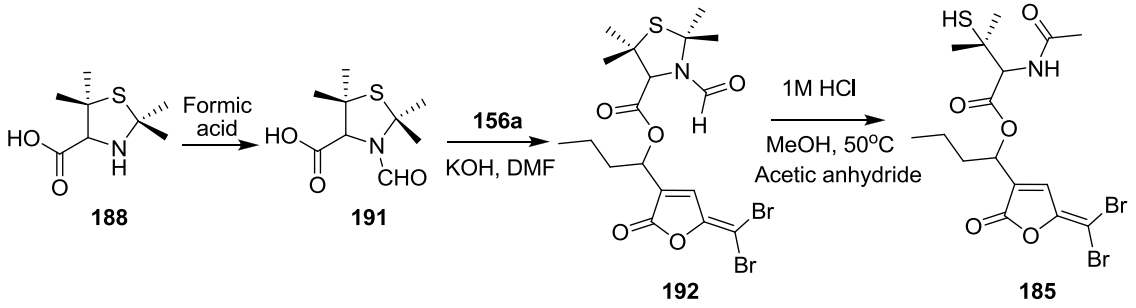

Scheme 3.31: Synthesis of *N*-acetyl-*D*-penicillamine fimbrolide derivative **185**.

The ^{1}H NMR spectrum of **185** indicated the ring-opened structure with the presence of only two methyl protons at δ 1.52 and 1.37 compared to the four methyl groups in the case of **192**. The *N*-acetyl protons appeared as a singlet at δ 2.04, while the NH group appeared as broad doublet at δ 6.43 (J = 8.6 Hz, 1H). In addition, a singlet at δ 2.12 integrating for one proton indicated the presence of the SH functionality. The chiral proton of the *D*-penicillamine unit appeared as a doublet at δ 4.54 (J = 8.7 Hz, 1H). The protons from the fimbrolide region of **185** were similar to those of the starting material **192** (Figure **3.12**).

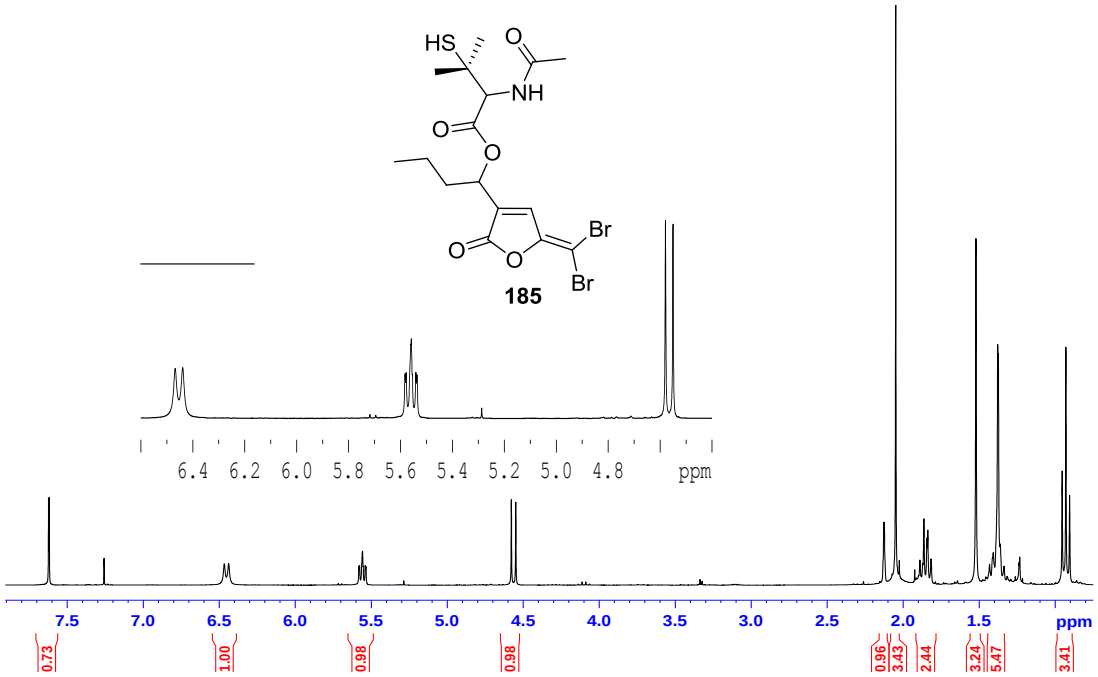

Figure 3.12: ^{1}H NMR spectrum of *D*-penicillamine fimbrolide derivative **185**.

The final step of the synthesis involved the reaction of the thiol group of product **185** with *t*-butyl nitrite. The reaction was carried out in DCM at 0 °C for 30 minute under dark conditions, after which the reaction mixture was evaporated to dryness at r.t. to remove volatile impurities and yield the fimbrolide SNAP derivative **183** as a green viscous product in 81% yield.

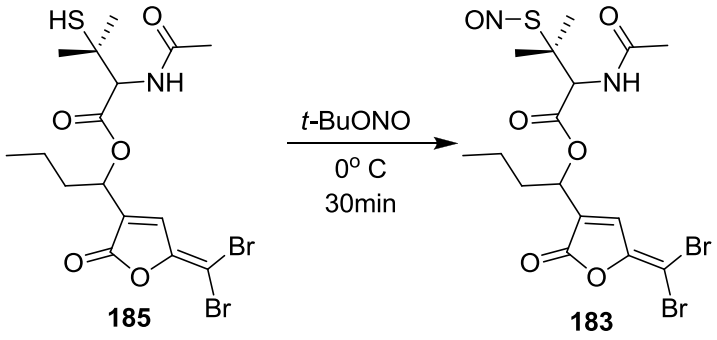

Scheme 3.32: Preparation of fimbrolide S-NO derivative **183**.

The formation of the product was confirmed by ^{1}H NMR spectroscopy data, which indicated the disappearance of the SH peak at δ 2.12. The doublet assigned to the chiral proton of the *D*-penicillamine unit shifted from δ 4.54 to 5.37, while a downfield shift was observed for the two equivalent methyl protons near the S-NO group in the penicillamine system confirming the formation of the desired fimbrolide S-NO derivative.

Unfortunately, it was noticed that the compound was unstable and slowly degraded even at 5 °C which prevented further characterization. This was evident by the brown coloration of the compound upon storage as well as by ^{1}H NMR spectrum which indicated the loss of the characteristic ^{1}H NMR signals of the product.

3.5 Conclusions

A series of fimbrolide-based NO hybrids were synthesized comprising different NO donors such as nitrates, diazeniumdiolates and *S*-nitrosothiols. During the course of synthesis, the unusual conversion of a fimbrolide thioacetate into a thiophene derivative was observed. Furthermore, a new disulphide-bridged fimbrolide derivative was synthesized during the attempted preparation of fimbrolide S-NO derivative. Additionally, a new method for the attachment of SNAP analogues by an ester linkage was developed.

Chapter 4

Dihydropyrrol-2-one-based nitric oxide donors

4.1 Introduction

The structural modification of existing natural products to derive more diverse and potent compounds is a common drug design approach. As described in previous chapters, structural modification of the fimbrolide scaffold has predominantly focused on modifying either the substituents at the α-carbon of the C-3 alkyl chain, the bromination pattern, or the nature of the alkyl chain itself, while conserving the furanone (lactone) scaffold (Figure **4.1**).

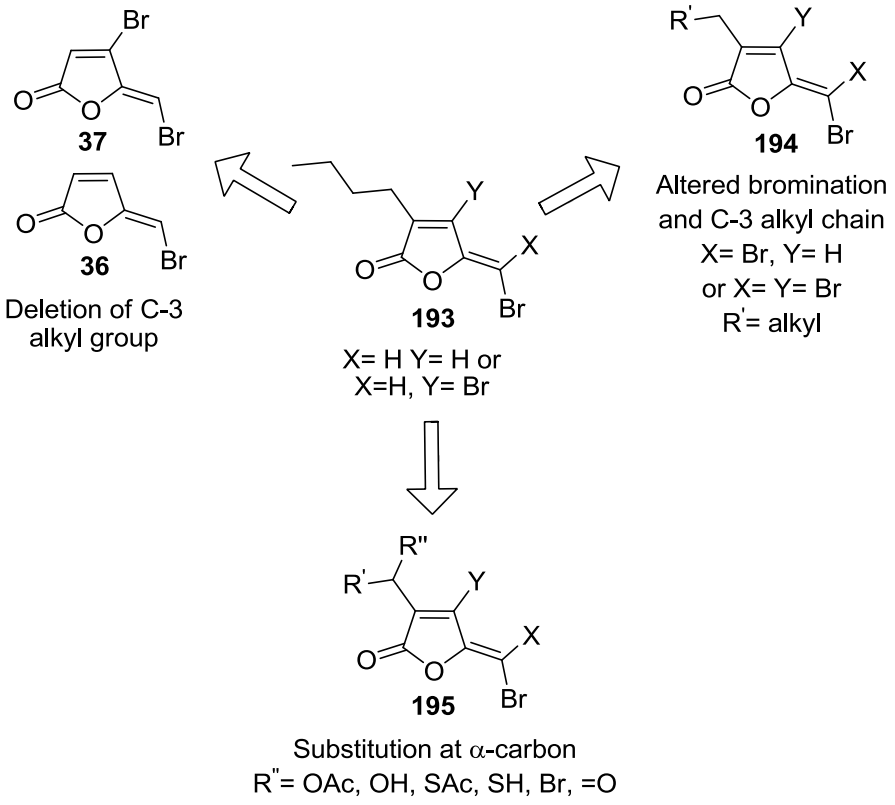

Figure 4.1: Common structural modifications of natural fimbrolides.

Recently, research has been conducted on varying the lactone structural motif, the core _nudeus‘ of the fimbrolides, to generate analogues based on the 1,5-dihydropyrrol-2-one

ring system. The main difference between the two structures is the replacement of the lactone oxygen atom of the heterocyclic ring **196** with the bioisosteric nitrogen atom, thus yielding the pyrrol-2-one (lactam) motif 1**97**. Lactam ring systems would be expected to be hydrolytically more stable compared to the parent fimbrolide, which could be attributed to the resonance stabilization of the five-membered pyrrol-2-one ring system due to the greater availability of the nitrogen lone pair (Figure **4.2**).

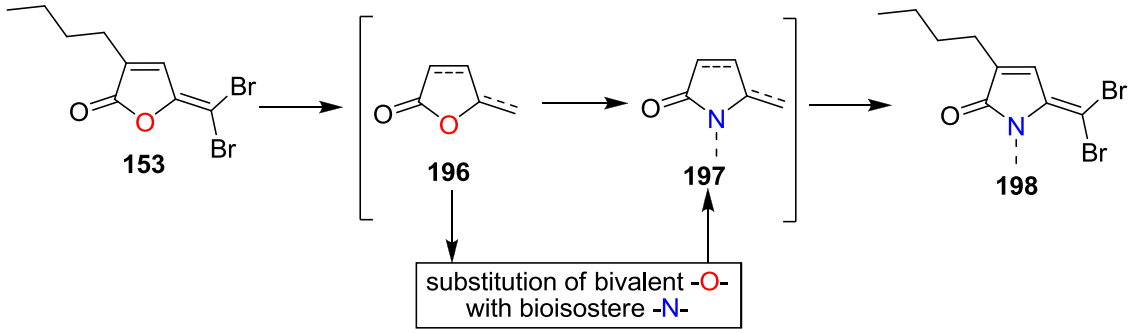

Figure 4.2: Lactone-lactam conversion.

A series of 1,5-dihydropyrrol-2-one-based compounds have been developed in our group, and preliminary biological screening has shown the compounds to be potential QS inhibitors.[107] Furthermore, 1,5-dihydropyrrol-2-ones containing an aryl substituent at C-4, such as 5-methylene-4-phenyl-1,5-dihydropyrrol-2-one (Figure **4.3**), have been synthesized and shown to exhibit excellent QS inhibitory activities. The 1,5-dihydropyrrol-2-ones have also been shown to retain their antimicrobial activities when covalently bound to surfaces, which demonstrates their potential to be developed as novel antimicrobial biomaterials.[233]

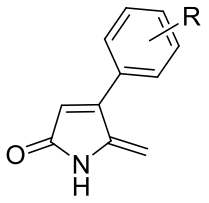

R = H, F, Br

199

Figure 4.3: 4-Aryl-substituted 1,5-dihydropyrrol-2-one derivatives **199**.

The pyrrol-2-one ring system is also a common feature of several important classes of biologically active natural and synthetic molecules. A wide range of natural products with the pyrrol-2-one system have been reported and synthesized, including pulchellalactam **200**, a selective CD45 protein tyrosine phosphate inhibitor for the treatment of autoimmune and chronic anti-inflammatory diseases,[234] γ-lactam PI-091 **201**, a platelet aggregation inhibitor,[235] and the antitumor alkaloid jatropham **202**.[236] Synthetic examples include HIV integrase inhibitors **203**[237] and tetramic acid derivatives **204**, as antimicrobial agent.[238]

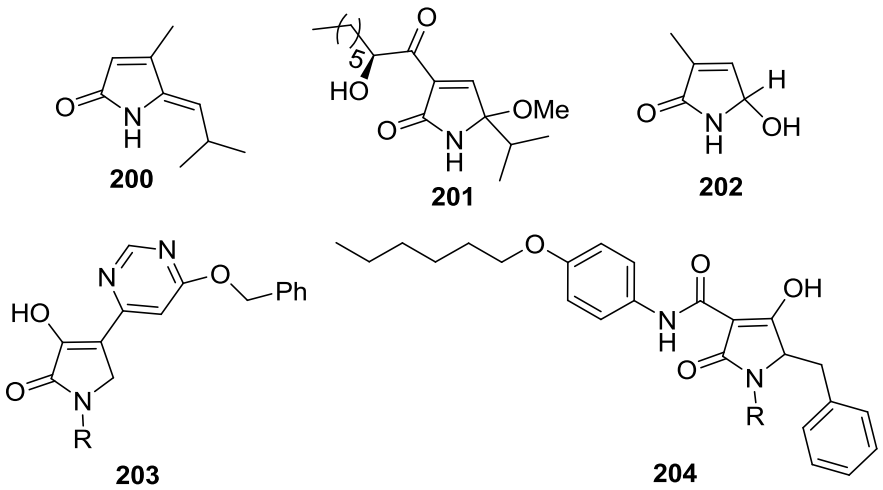

Figure 4.4: Biologically active compounds containing the dihydropyrrol-2-one nucleus.

4.2 Synthesis of dihydropyrrol-2-ones

Various methods for the synthesis of the pyrrol-2-one ring system have been reported in the literature. Figure **4.5** gives an overview of the different synthetic approaches utilized in the synthesis of pyrrol-2-ones.[239]

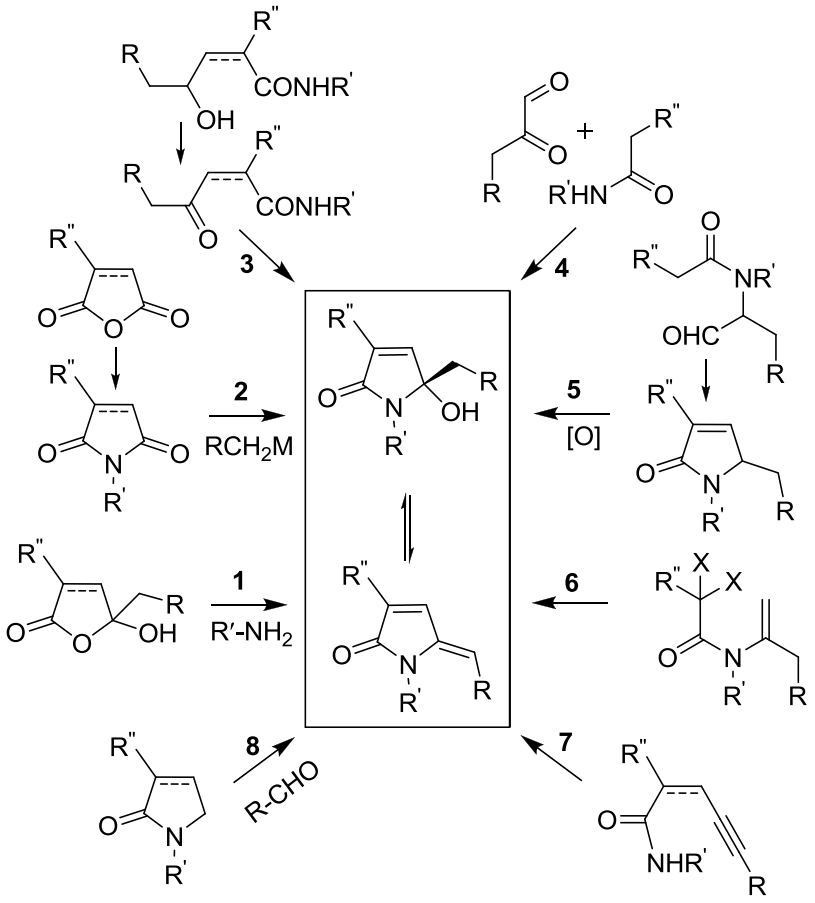

Figure 4.5: Overview of pyrrol-2-one synthetic strategies: (**1**) Direct conversion of lactones into lactams; (**2**) γ-Hydroxylactams from succinimides and maleimides; (**3**) Cyclization of 4-ketoamides into hydroxylactams; (**4**) Condensation of 1,2-diketo compounds with amides; (**5**) Oxidation of 5-alkyl-3-pyrrolin-2-ones; (**6**) Radical cyclization of enamides; (**7**) Intramolecular 5 *exo*-dig addition of amides and alkynes; (**8**) Reaction of 3-pyrrolin-2-ones with aldehydes by condensation and Wittig reactions.[239]

Synthesis of pyrrol-2-ones can be broadly classified into two distinct approaches. The first approach involves the direct conversion of the lactone (furan-2-one) into the corresponding lactam (pyrrol-2-one) ring system *via* either a single step or through an intermediate compound (Strategies **1** and **2**). The second approach includes a variety of different ring-closure cyclization reactions of intermediates possessing a carbonyl-amide or associated amino-based functional groups (Strategies **3** –**7**).

The direct conversion approach employs the structural similarities of the lactone and lactam rings. As previously demonstrated by Shiraki *et al*. in the synthesis of PI-091 **201**, the final step to the target compound can be achieved *via* lactamization of lactone **205** to the corresponding lactam by ammonia (Scheme **4.1**).[235] The lactam motif was reported to be crucial for biological activity.

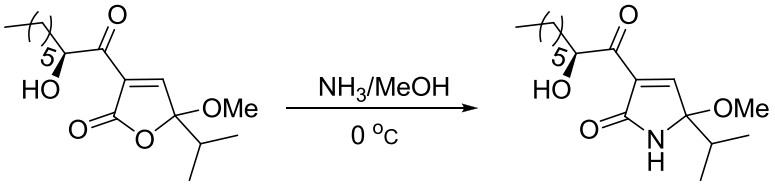

205 **201**

Scheme 4.1: Synthesis of PI-091 **201** *via* direct lactamization.

Similar direct lactone-lactam conversions have been reported by Mase *et al*. in the synthesis of jatropham **202** from citraconic anhydride **206** using ammonium acetate, followed by reduction of the intermediate maleimide **207** to yield the product (Scheme **4.2**).[236]

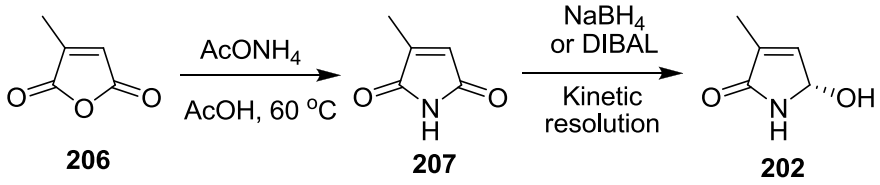

Scheme 4.2: Synthesis of jatropham **13** *via* direct lactamization.

The second approach employs an intramolecular cyclization step to yield the pyrrol-2-one nucleus. In this approach, a terminal amide reacts with an electron-rich double or triple bond, thus forcing ring closure to form the pyrrol-2-one nucleus. Alternatively, a terminal amine or amide reacts with an electron-deficient carbonyl functionality to form the cyclized pyrrol-2-one. These approaches have been demonstrated in the halocyclization of dienamides by iodine monochloride, as well as in the synthesis of Cathepsin B (a protease inhibitor) by the rearrangement and cyclization of alkynyl amidomalonates under basic conditions.[240-241] Moreover, Li *et al.* have utilized the intramolecular cyclization and decarboxylation of glycine acylated Meldrum‘s acid to form the desired dihydropyrrol-2-one scaffold for the synthesis of pulchellalactam **200**.[234]

However, many of the common synthetic methodologies cannot be applied for the synthesis of fimbrolide-like dihydropyrrol-2-one derivatives, due to the presence of multiple bromine atoms in the molecule. A useful synthetic methodology for dihydropyrrol-2-ones bearing the same bromination pattern as observed in fimbrolides has been developed in our group, utilizing the lactone-lactam conversion. In general, the reaction involves the addition of an amine to the fimbrolide derivative **137**, followed by dehydration of the intermediate γ-hydroxylactam **208** to regenerate the C-5 methylene group in the dihydropyrrol-2-one product **209** (Scheme **4.3**).[106]

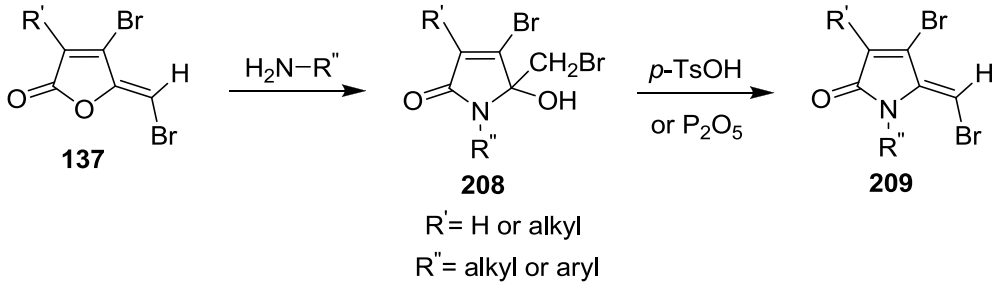

Scheme 4.3: A direct lactone to lactam conversion for the synthesis of dihydropyrrol-2-ones based on fimbrolide derivatives.

4.3 Chapter aims

The dihydropyrrol-2-one scaffold has been represented in a range of biologically active natural and synthetic molecules, including fimbrolide-like antimicrobials, as described above. Thus, the aim of this work was to develop novel bioactive antimicrobial hybrids based on 1,5-dihydropyrrol-2-ones and nitric oxide donors such as nitrates and diazeniumdiolates.

4.4 Synthesis of 1,5-dihydropyrrol-2-one nitrate derivatives

Retrosynthetically, the desired 1,5-dihydropyrrol-2-one nitrate **210** can be synthesized from tribromo derivative **211**. Compound **211** can be obtained from allylic radical bromination of lactam **212**, which in turn can be obtained from the lactone-lactam conversion of fimbrolide analogue **153a** by reaction with amines followed by dehydration (Scheme **4.4**).

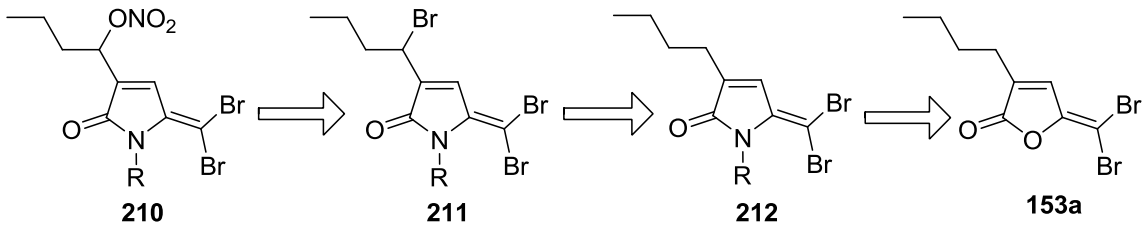

Scheme 4.4: Retrosynthetic synthesis of 1,5-dihydropyrrol-2-one nitrate derivatives **210**.

The required fimbrolides were first synthesized following the synthetic sequence depicted in Scheme 3.4 as described in Chapter 3. The resulting fimbrolides then underwent the lactone-lactam conversion by reaction with an amine as reported previously by our group.

In the first attempt, the model fimbrolide **153a** was reacted with *n*-butylamine **213** under ice-cold conditions to give the γ-hydroxylactam derivative **214** as the major product (Scheme **4.5**).

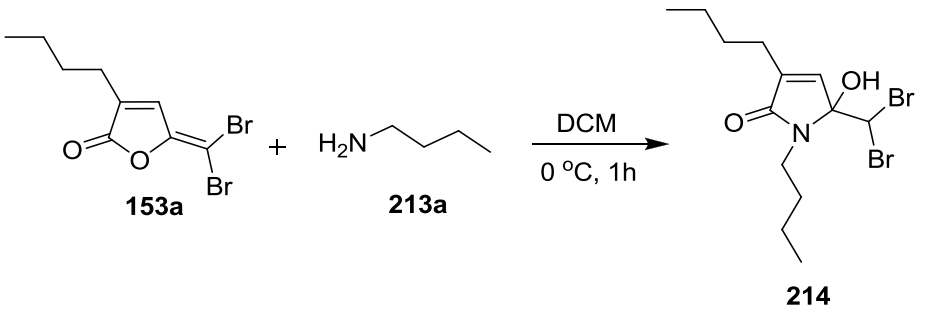

Scheme 4.5: Synthesis of γ-hydroxylactam derivative **214**.

The ^{1}H NMR spectra of the crude product **214** confirmed the insertion of the *N*-butyl moiety, as indicated by the presence of two multiplets at δ 3.02 and 3.37 (each 1H) assigned to the methylene protons adjacent to the nitrogen atom which are diastereotopic due to the presence of the chiral centre at C5. A singlet at δ 5.75 (1H) corresponded to

the newly-formed $CHBr_2$ group, which further confirmed the formation of the intermediate γ-hydroxylactam **214**.

A possible mechanism of this reaction is illustrated in Scheme **4.6**. Nucleophilic addition-elimination of *n*-butylamine on the lactone carbonyl group of the lactone results in the ring-opening to afford the amide intermediate **215**. Subsequent keto-enol tautomerism yields the more stable keto tautomer **216**, which undergoes cyclization into the lactam ring **214** *via* nucleophilic attack of the nitrogen lone pair.

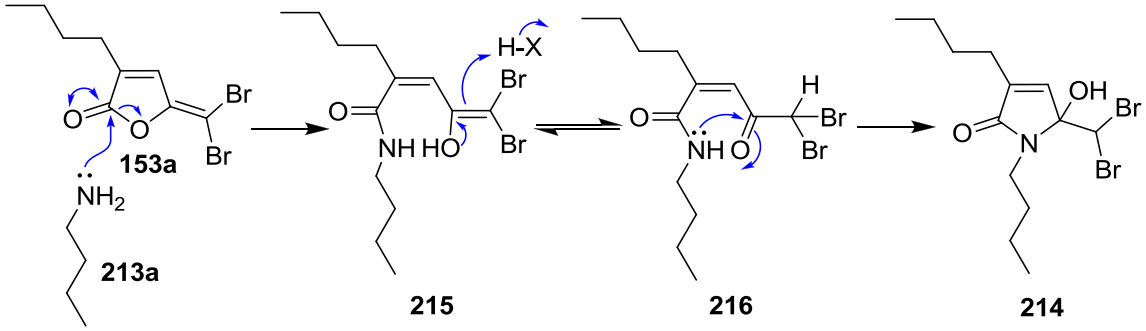

Scheme 4.6: Mechanism of lactone-lactamization reaction.

The γ-hydroxylactam **214** can be subjected to dehydration to regenerate the dibromomethylene group at the C-5 position, giving the desired lactam **212a** bearing the same bromination pattern as the starting fimbrolide. Dehydration of the alcohol **214** was accomplished using *p*-toluenesulfonic acid (*p*-TsOH) as the dehydrating reagent to afford the desired product **212a** (Scheme **4.7**). An additional product **39c** with the loss of bromine atom was also observed.

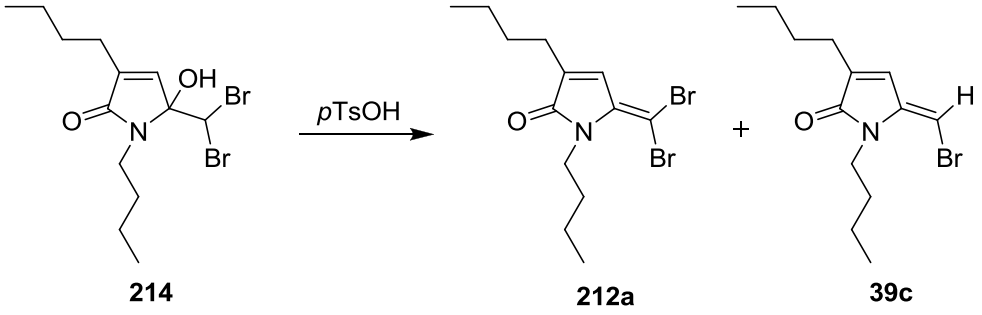

Scheme 4.7: Synthesis of fimbrolide-like 1,5-dihydropyrrol-2-one **212a**.

When phosphorus pentoxide (P_2O_5) was used as the dehydration agent instead of *p*-TsOH, the desired product was obtained in a higher yield with no side products formed.

In the ^{1}H NMR spectrum of the product **212a**, the N-CH_2 protons appeared as a triplet at δ 3.89 (J = 4.23 Hz). The disappearance of the singlet at δ 5.75 corresponding to the $CHBr_2$ group further confirmed the formation of the dehydrated product **212a**.

The next step towards the targeted 1,5-dihydropyrrol-2-one-based nitrates **210** involved allylic bromination at the α-position of the fimbrolide C-3 butyl side chain. This was achieved by free radical allylic halogenation reaction of **212a** using *N*-bromosuccinimide (NBS) as a brominating agent (Scheme **4.8**). The formation of the α-bromo-1,5-dihydropyrrol-2-one derivative **211a** was confirmed by its ^{1}H NMR spectrum, which showed a downfield shift of the α-proton from δ 2.31 to δ 4.79 with a concomitant halving of the integration value upon substitution with the bromine functionality.

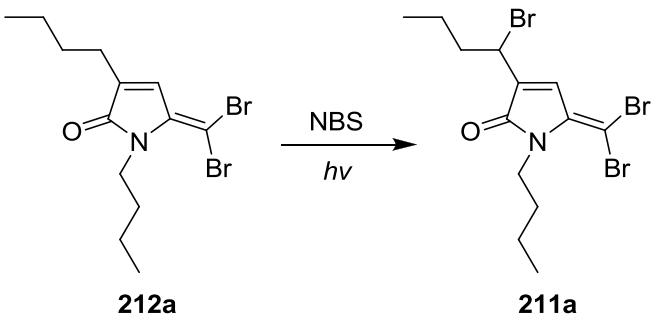

212a **211a**

Scheme 4.8: Allylic bromination of fimbrolide-like 1,5-dihydropyrrol-2-one **212a**.

For the synthesis of the targeted nitrates, the final step involved the nitration of the α-bromo derivative **211a**. The reaction was initially carried out under similar reaction conditions utilized for the nitration of α-bromo fimbrolides **156**, as discussed in Chapter 3. However, treatment of the α-bromo derivative **211a** with silver nitrate in acetonitrile at 70 °C for 18 h resulted in the formation of multiple products, as indicated by TLC analysis. Column chromatography followed by preparative TLC gave the desired product in a low yield of 12%, along with dihydropyrrolone-derived degradation products.

Due to the unexpected formation of multiple side products, the reaction was repeated at a lower temperature of 50 °C, and the progress of the reaction was monitored by ^{1}H NMR spectroscopy. The ^{1}H NMR spectroscopic analysis indicated the complete conversion of the α-bromo derivative **211a** within 5 h, yielding the desired 1,5-dihydropyrrol-2-one nitrate derivative **210a** in 71% yield after column chromatography.

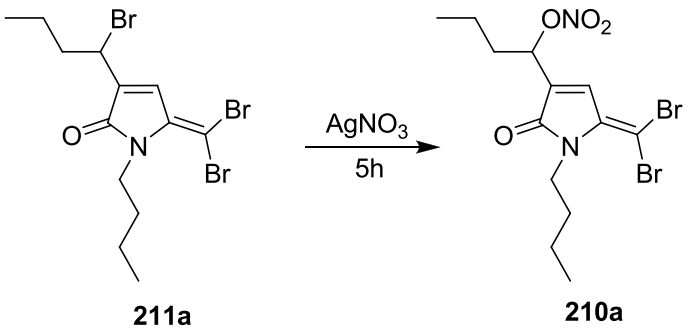

Scheme 4.9: Synthesis of 1,5-dihydropyrrol-2-one nitrate derivative **210a**.

The ^{1}H NMR spectrum of the product **210a** exhibited a distinctive triplet at δ 5.76 (J = 7.26 Hz, 1H) attributed to the proton geminal to the nitrate group, which shifted downfield by 0.98 ppm compared to the bromo derivative **211a**. The H-4 proton appeared as a singlet at δ 7.25, the N-CH_2 group as a doublet of doublet at δ 3.97 (J = 7.56 Hz, 2H), and the remaining aliphatic protons in the alkyl region (δ 1–2 ppm) confirming the formation of the desired nitrate derivative **210a** (Figure 4.6).

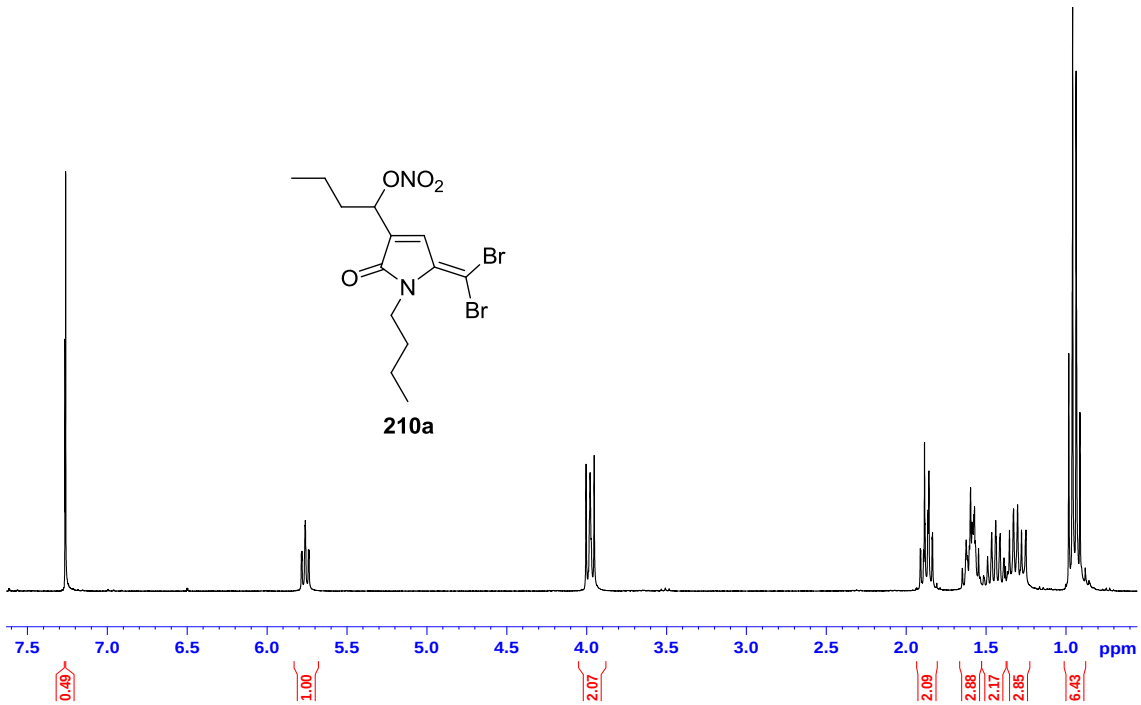

Figure 4.6: ^{1}H NMR spectrum of 1,5-dihydropyrrol-2-ones nitrate derivative **210a**.

Similarly, fimbrolide **153a** was treated with amines **213b–e** under various conditions depending on the reactivity of the amine utilized. Reactive amines such as ammonia and benzylamine required low temperature reaction conditions, while aromatic amines required heating (Table **4.1**). Dehydration of the γ-hydroxylactam afforded the desired 1,5-dihydropyrrol-2-one derivatives **212b–e**. These compounds were further brominated to yield α-bromo derivatives **211b–e**, which were subsequently treated with silver nitrate to give the 1,5-dihydropyrrol-2-one nitrate hybrids **210b–e** (Scheme **4.10**).

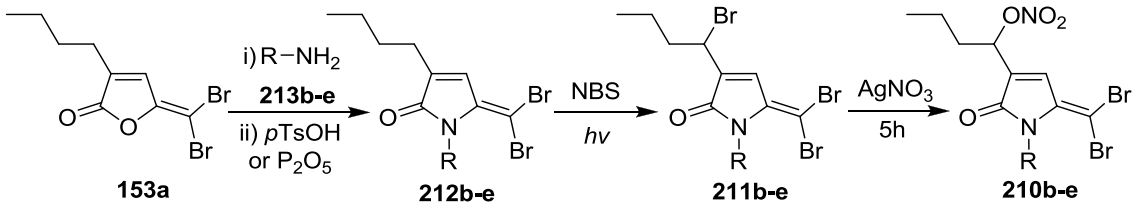

Scheme 4.10: Synthesis of 1,5-dihydropyrrol-2-one nitrate hybrids **210b–e**

Table 4.1: Reaction conditions for preparation of 1,5-dihydropyrrol-2-one **212b-e**

Products	*N*-substitution (R)	Reaction conditions (step i)
212b	H	Ether, –78 °C to r.t., overnight
212c	$C_6H_5CH_2$	DCM, 0 °C to r.t., 2 h
212d	C_6H_5	50 °C (neat), 10 h
212e	4-BrC_6H_4	100 °C (neat), 18 h

The compounds were primarily characterized using NMR spectroscopy and mass spectrometry techniques. The ^{1}H NMR spectra for the products **210b–e** exhibited similar peaks for the C-3 butyl chain and the H-4 proton, as discussed for compound **210a**. As the products differed in their *N*-substitution, they could be easily distinguished by their ^{1}H NMR spectra (Table **4.2**).

Table 4.2: Characteristic ^{1}H NMR values for the 1,5-dihydropyrrol-2-one-nitrates **210b–e**.

Product	*N*-substitution (R)	^{1}H NMR (δ)
210b	H	7.75 ppm (bs)
210c	$C_6H_5CH_2$	5.28 ppm (s, CH_2); 7.04, 7.25 ppm (m, C_6H_5)
210d	C_6H_5	7.22 ppm (m, C_6H_5)
210e	4-BrC_6H_4	7.11, 7.56 ppm (d, C_6H_4)

4.5 Synthesis of 1,5-dihydropyrrol-2-one-based diazeniumdiolate derivatives

A wide range of O^2-arylated diazeniumdiolates have been reported in the literature (Figure **4.6**). The O^2-aryl substitution is generally carried out using nucleophilic aromatic substitution reactions with an aryl halide such as 4-fluoro-1,3-dinitrobenzene.[196,221]

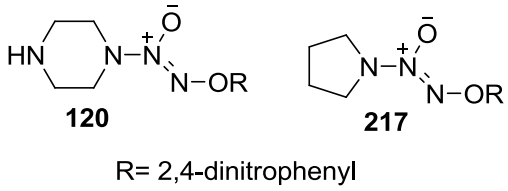

Figure 4.7: Examples of O^2-functionalized diazeniumdiolates.

Thus, it was envisaged that 1,5-dihydropyrrol-2-ones bearing an aryl halide substitution at the lactam nitrogen could be utilized for O^2-substitution reactions with diazeniumdiolates.

For this purpose, the *N*-arylated-1,5-dihydropyrrol-2-one derivative **212f** was obtained *via* lactone-lactam conversion. Heating fimbrolide **153a** with 4-fluoro-3-nitroaniline **213f** gave intermediate γ-hydroxylactam **218**, which underwent dehydration to give the

desired product **212f** in 60% overall yield (Scheme **4.11**). The ^{1}H NMR spectrum of the product confirmed the insertion of the aryl system as indicated by the presence of a triplet at δ 7.36 (J = 9.0), a multiplet at δ 7.54 and a doublet of doublets at δ 7.95 integrating to one proton each for the aromatic protons.

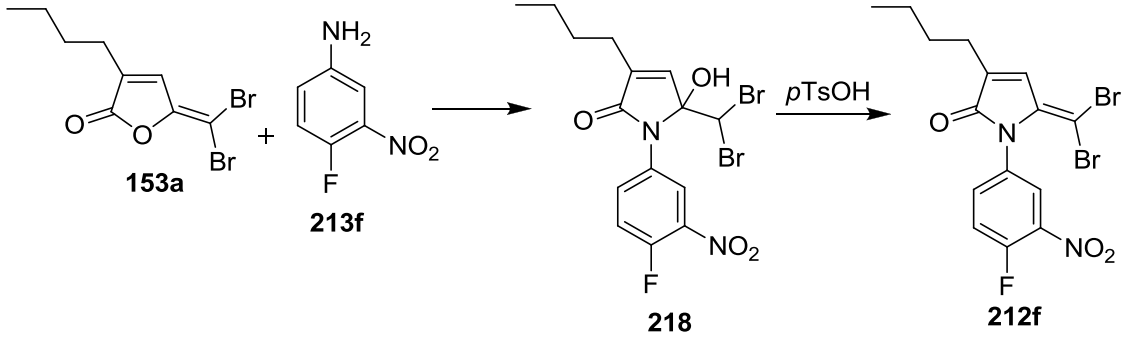

Scheme 4.11: Synthesis of *N*-arylated 1,5-dihydropyrrol-2-one derivative **212f**.

The electron-deficient nature of the aryl system in 1,5-dihydropyrrol-2-one **212f** was then utilized in a nucleophilic aromatic substitution reaction with the O^2-moiety of diazeniumdiolate **170**. The O^2-arylation reaction was initially conducted in acetone in the presence of anhydrous $NaHCO_3$. However, the reaction did not proceed and the starting material 1,5-dihydropyrrol-2-one **212f** was recovered. The reaction was then attempted with different solvents in the presence or absence of a base and for different durations of time, but the reaction yielded either only the starting material or multiple products (Scheme **4.12**). Where multiple products were formed, ^{1}H NMR spectroscopic analysis of the crude reaction mixture indicated that the desired product **219** was not formed, as the peaks corresponding to the diethylamine diazeniumdiolate were absent. The crude reaction mixtures usually included multiple dihydropyrrolone-based degradation products that were difficult to characterize.

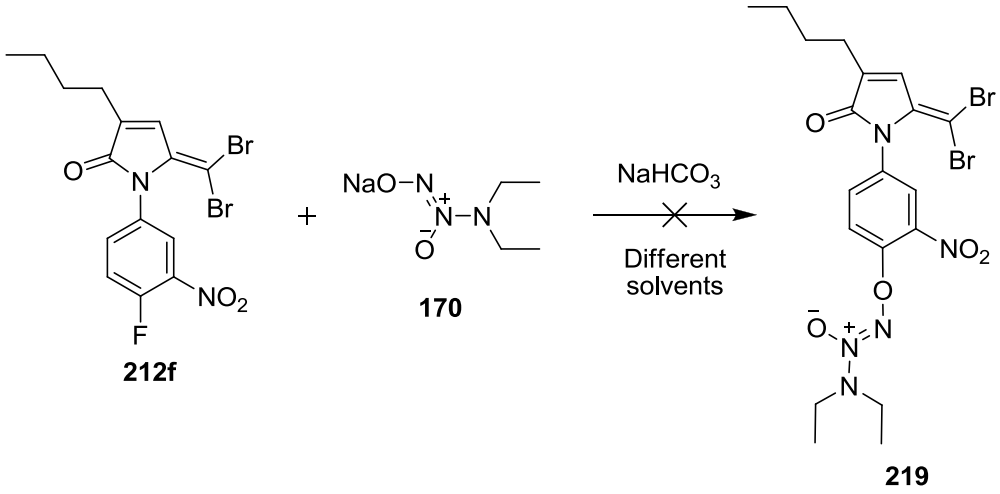

Scheme 4.12: Attempted synthesis of 1,5-dihydropyrrol-2-one diazeniumdiolate derivative **219**.

Entry	Solvents	Time	Conversion result (^{1}H NMR)
1	Acetone	24–72 h	No reaction
2	DMSO	24–72 h	Multiple products
3	THF	24–72 h	Multiple products
4	t-BuOH	72 h	No reaction

The negative outcome of the reactions is tentatively attributed to the low reactivity of the 4-fluoronitrobenzene used. Thus, it was envisaged that the fluoro dinitroaryl system might be more susceptible to nucleophilic aromatic substitution by the O^2-moiety of the diazeniumdiolate. Therefore, the reaction between fimbrolide **153** and 5-fluoro-2,4-dinitroaniline **213g** was carried out under the same reaction conditions as for the synthesis of **218** (Scheme 4.13). However, no reaction was apparent even with prolonged heating and the use of high boiling point solvents such as DMF, and the desired product **220** was not formed. This was possibly due the electron-withdrawing nature of the two nitro groups in **213g**, leading to a loss in nucleophilicity of the aromatic amine. Due to time constrains this part of the work could not be explored further.

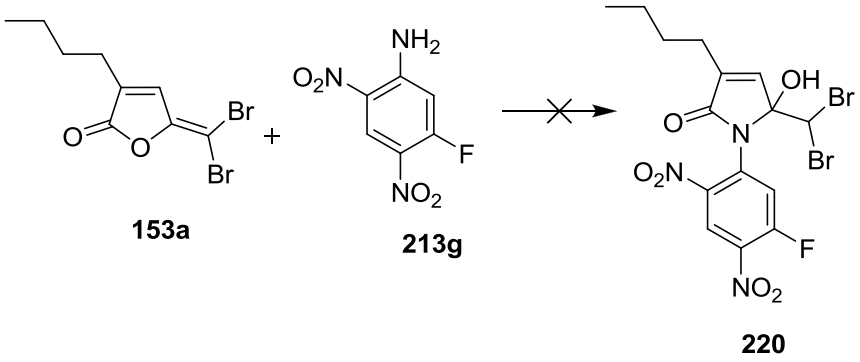

Scheme 4.13: Attempted synthesis of *N*-arylated γ-hydroxylactam **220**.

4.6 Conclusion

A novel series of dihydropyrrolones and their nitrate NO donor hybrids have been synthesized. The attempted synthesis of diazeniumdiolate based dihydropyrrolones proved to be problematic and the desired product could not be isolated.

Chapter 5
Novel indole and high load nitric oxide donors

5.1 Introduction

Nitric oxide (NO), as discussed in Chapter 1, is an essential bioregulatory agent that plays a significant role in many cellular processes and the prevention of pathogen attack. A wide range of NO donors such as nitrates, diazeniumdiolates, *S*-nitrosothiols and sydnonimines have been developed for a broad range of potential applications.[242,243] Nitrates have been used for centuries as a treatment for angina, and their chemistry, pharmacology and toxicology have been well documented. Diazeniumdiolates, particularly *N*-diazeniumdiolates, are a relatively new class of NO donors that offers a controlled release of NO, thus allowing the duration of NO release to be fine-tuned.

However, some of the currently documented nitrates and diazeniumdiolates have some drawbacks as NO donors. Tolerance is an issue with long term usage in the case of the traditional nitrates discussed previously in Chapter 1. To overcome this, aminoalkylnitrate derivatives such as 2-nitrooxyethylammonium nitrate (AEN) have been developed that represent a new class of organic nitrates that do not cause tolerance.[175-177] For the *N*-diazeniumdiolates, a potential drawback is the formation of carcinogenic *N*-nitrosamines *via* the amine by-product formed during the decomposition of *N*-diazeniumdiolate ions to release NO. This potential complication can be avoided by attaching the diazeniumdiolate group to a carbon atom to generate *C*-diazeniumdiolates, but these generally have less desirable NO release profiles compared to the *N*-diazeniumdiolates. Thus, the development of novel *C*-diazeniumdiolates with superior NO-releasing properties but low toxicity profiles could be useful as an antimicrobial strategy. This could be achieved through the use of an organic molecule

with a well-established biological profile that can be conjugated with NO to form the diazeniumdiolate functionality.

In industry, microbial biofilms are a major contributor to microbial induced corrosion (MIC), affecting the pipe systems of various industries from oil and water distribution to food processing. Biofilms can also cause fouling on membrane surfaces found in microfiltration systems for waste water purification. Biofilm-mediated corrosion and fouling can result in billions of dollars of losses in industrial settings. Thus, there is a need for the development of new NO donors with industrial compatibility that can provide sustained release of larger doses of NO to overcome bacterial biofilm formation.

5.2 Chapter aims

The overall aim of the work described in this chapter was to develop novel NO donors based on nitrates and diazeniumdiolates possessing superior pharmacological profiles and fewer drawbacks compared to existing NO donors, for antimicrobial applications. Towards this end, the first specific aim was to explore the synthesis of indole-based diazeniumdiolates, as many indole derivatives show well-established pharmacokinetic and pharmacodynamic properties. The second aim was to combine the different types of NO donors to generate high load NO donors which could be useful for industrial applications such as the prevention of microbial induced corrosion (MIC).

5.3 Indole-based nitric oxide donors

5.3.1 Indole and its biological significance

The indole (**221**) nucleus is one of the most common heterocyclic systems observed in nature. It is found in the human body in the form of the amino acid tryptophan **222** and the neurotransmitter serotonin **223**. It is also an important structural component of a vast

number of complex synthetic molecules and naturally occurring alkaloids that exhibit biological activity with good pharmacodynamic properties.

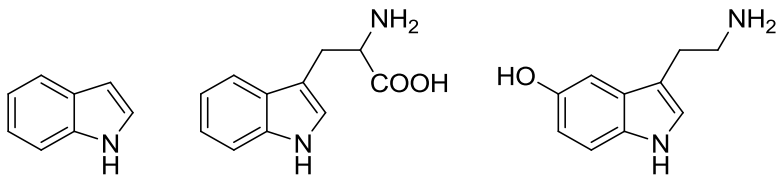

221 **222** **223**

Figure 5.1: Indole and some biologically relevant analogues

The indole motif is widespread in bacterial environments, and is involved in the control of many bacterial phenotypes. In bacteria, the amino acid tryptophan can be hydrolyzed by the enzyme tryptophanase to form indole, pyruvate and ammonia, which are then used as sources of carbon and nitrogen under nutrient-depleted conditions. In *Escherichia coli*, which has a high concentration of extracellular indole, indole plays a regulatory role in biofilm formation by reducing motility through SdiA in a temperature dependent-manner.[244] In addition, 5-hydroxyindole and 7-hydroxyindole have been shown to inhibit biofilm formation through sulfur metabolism and reduction in cell motility.[245] Indole also influences acid resistance, plasmid stability, chemotaxis and attachment to epithelial cells in *E. coli*.[246]

Conversely, other bacteria such as *Pseudomonas aeruginosa* have acquired the ability to degrade indole as a defense mechanism. In *P. aeruginosa,* indole and 7-hydroxyindole (7HI) have been shown to decrease the production of virulence factors, reduce swarming motility, enhance multidrug resistance by inducing eflux pump genes and increase biofilm formation.[246] Indole also has a stimulatory effect on biofilm formation in a variety of other Gram-negative bacteria.[40] Therefore, competition and adaptation

mechanisms involving indole are prevalent in bacteria, and indole can be used as an intra- or interspecies biofilm signal in multispecies consortia.[247]

Indole and its hydroxyl derivatives show potential as non-toxic biofilm inhibitors against *E. coli* as they do not significantly change the specific growth rate of the bacteria even at a concentration of 1000 μM. In addition, indole and 7-hydroxyindole decrease virulence factors in *P. aeruginosa* and they were found to be non-toxic to PAO1 even at 500 μM, thus having potential as anti-virulence agents.[245] Such anti-biofilm and anti-virulence remedies can combat bacterial activity without exerting selection pressure on bacteria to develop resistance.

5.3.2 Reaction of indole with nitric oxide and its oxides

The chemistry of the indole nucleus is enormous, with its electrophilic substitution reactivity patterns being dictated by the substituents attached to the indole ring. A variety of different reactions including formylation, acylation, halogenation, nitration, oxidative dimerization, imine formation and acid-catalyzed addition of aldehydes has been reported for the indole ring, making this a versatile heterocyclic system.[248]

The reaction of indole and its derivatives with NO and its oxidative metabolites is very complex, and is governed by multiple factors. In the literature, the reaction of indole and substituted indoles with NO and its metabolites such as nitrite (NO_2), peroxynitrite and nitrous acid have been reported.[249-252]

Reaction of indole **221** with nitrogen dioxide (NO_2) or nitrous acid (HNO_2) gives dimeric products, which are expected to form *via* an indolyl radical mechanism in the case of compound **224**, or possibly *via* a nitroso derivative for compound **225** (Scheme **5.1**).

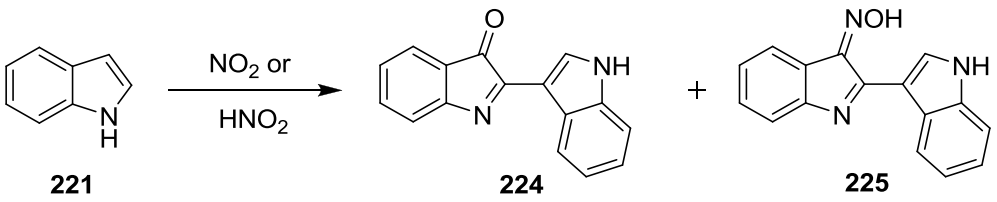

Scheme 5.1: Reactions of indole **221**

2-Phenylindole **226** react with NO, nitrogen dioxide/nitrite (NO_2) or nitrous acid (HNO_2) to give the 3-nitroso derivative **227a**, which tautomerises to the oxime **227b** (Scheme **5.2**).

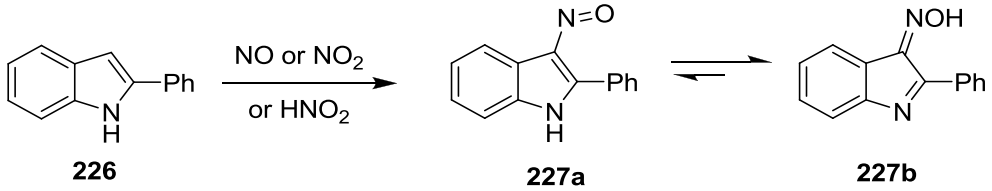

Scheme 5.2: Reactions of 2-phenylindole **226**.

On the other hand, the reaction of *N*-methyl-2-phenylindole **228** with NO, NO_2 or HNO_2 produces a mixture of azo-bis-indole **229**, nitroso **230**, and nitro **231** derivatives (Scheme **5.3**).[249] The azo-bis indole-type products were postulated to be formed *via* a *C*-diazeniumdiolate intermediate, which has not been isolated.

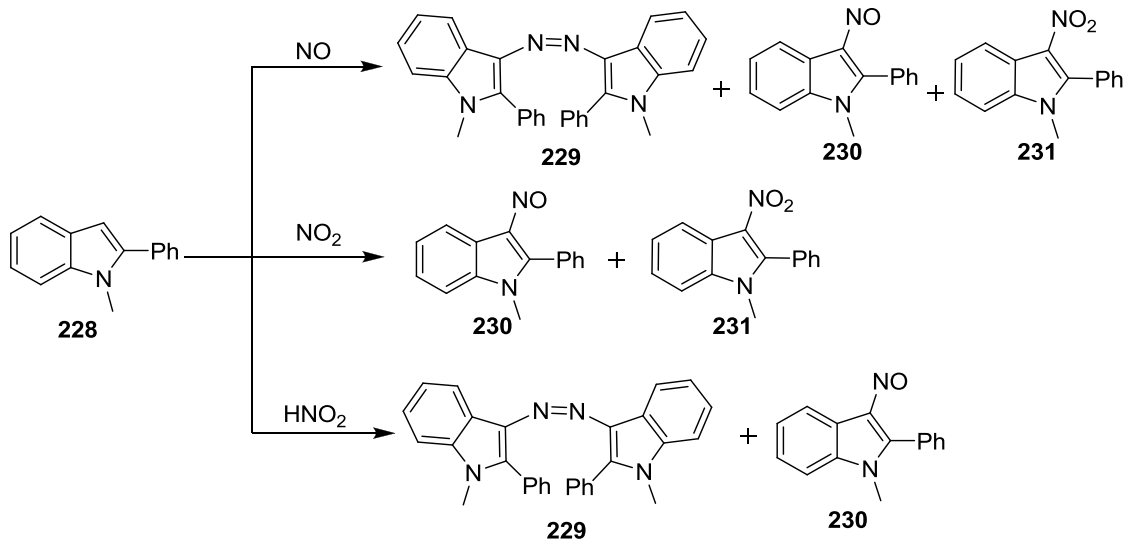

Scheme 5.3: Reactions of *N*-methyl-2-phenyl indole **228**.

3-Substituted indole derivatives such as 3-methylindole **232a** or tryptamine amides **232b-c** react with NO_2 to produce nitro indoles **233-235**, possibly *via* an indolyl radical mechanism (Scheme **5.4**). On the other hand, reaction with HNO_2 produces *N*-nitroso indoles **236** *via* electrophilic attack of the nitrosating agent CH_3COONO formed *in situ* with acetic acid.

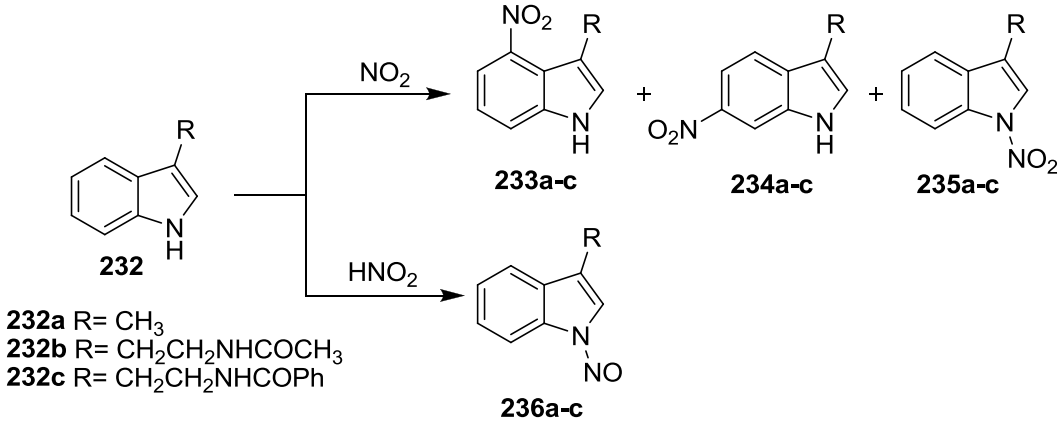

Scheme 5.4: Reactions of 3-substituted indoles **232**.

Although the reaction between indole and NO has not been reported in the literature, indole can be considered to be similar to an enamine system, which has been shown to

react with NO to furnish *C*-diazeniumdiolates. In the case of indole **221**, formation of the C-3 substituted *C*-diazeniumdiolate **237** would be anticipated as the C-3 position is the most reactive site with respect to electrophilic substitution or radical-based reactions. In the presence of a strong base such as sodium methoxide (NaOMe), possible products include *N*-diazeniumdiolate **238** or *N*-nitroso indole **239**, or disubstituted products such as **240** and **241** (Scheme **5.5**). Therefore, it was of interest to investigate if the reaction of indole **221** and NO could furnish any diazeniumdiolate-type products.

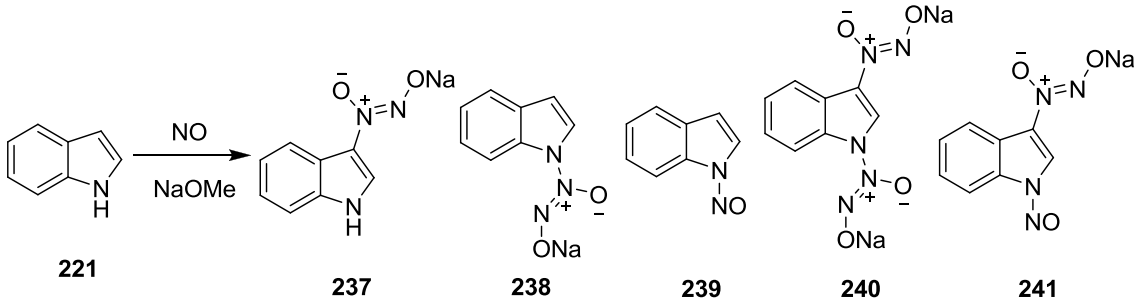

Scheme 5.5: Possible products from the reaction of indole **35** with NO.

To achieve this, indole **221** was dissolved in a mixture of ether and a methanolic solution of sodium methoxide (NaOMe). The solution was transferred to a Parr hydrogenation apparatus, purged with nitrogen and then stirred with NO gas for 48 h at 80 psi. The apparatus was then flushed with nitrogen to discharge any remaining NO, followed by the addition of copious amounts of dry ether. The resulting light yellow precipitate was collected by filtration under vacuum using a nitrogen atmosphere, followed by washing with dry ether. The product obtained was stored at –20 °C.

The product was soluble in water and its structure was elucidated by ^{1}H NMR spectroscopy using a D_2O-NaOD (0.1 M) solution. When compared with the parent indole **221**, the ^{1}H NMR spectrum of the product revealed the absence of the peak at δ 6.4 corresponding to indole H3, indicating that the reaction had occurred at the C-3

position. The spectrum also displayed two triplets at δ 7.12 (J = 7.3 Hz, 1H) and 7.17 (J = 7.5 Hz, 1H) corresponding to H5 and H6, respectively. The H2 proton appeared as a singlet at δ 7.61 ppm, while the H4 and H7 protons appeared as two doublets at δ 7.80 and δ 7.37 (each J = 7.7 Hz, 1H), respectively. Additionally, the presence of the formate ion ($HCOO^-$) was observed, which was presumably formed due to reaction of methoxide ion with NO. Thus, the reaction of indole **221** and NO was repeated using sodium trimethylsilonate [$(CH_3)_3SiONa$] in place of NaOMe to effectively give a single product without the formation of formate as a side product.

In order to confirm whether reaction also occurred at the NH group of indole, a sample of the product was dissolved in d_6-DMSO and analyzed using ^1H NMR spectroscopy. The spectrum revealed a broad singlet at δ 11.28, indicating the presence of the N-H proton of indole. Once it was determined that the reaction had only occurred at C-3, further NMR studies were performed to confirm the formation of a diazeniumdiolate. A long range ^1H-^{15}N HMBC experiment in D_2O-NaOD (0.1 M) revealed the presence of three nitrogen signals at δ 127.2, 300.0 and 427.6, all of which correlated with the indole H2 proton. In addition, the signal at δ 127.2 ppm was assigned to be the indole NH nitrogen due to its correlation with H6 and H7 of the indole nucleus. The nitrogen signals at δ 300.0 and δ 427.6 were thus assigned to the N1 and N2 nitrogen atoms of the diazeniumdiolate group, respectively (Figure **5.2**). The observed correlations confirmed a diazeniumdiolate-type structure **237**, which was further verified through high resolution mass spectrometry (HRMS). The obtained *m/z* value of 222.0250 was consistent with the calculated mass of $C_8H_6N_3Na_2O_2$ (222.0255).

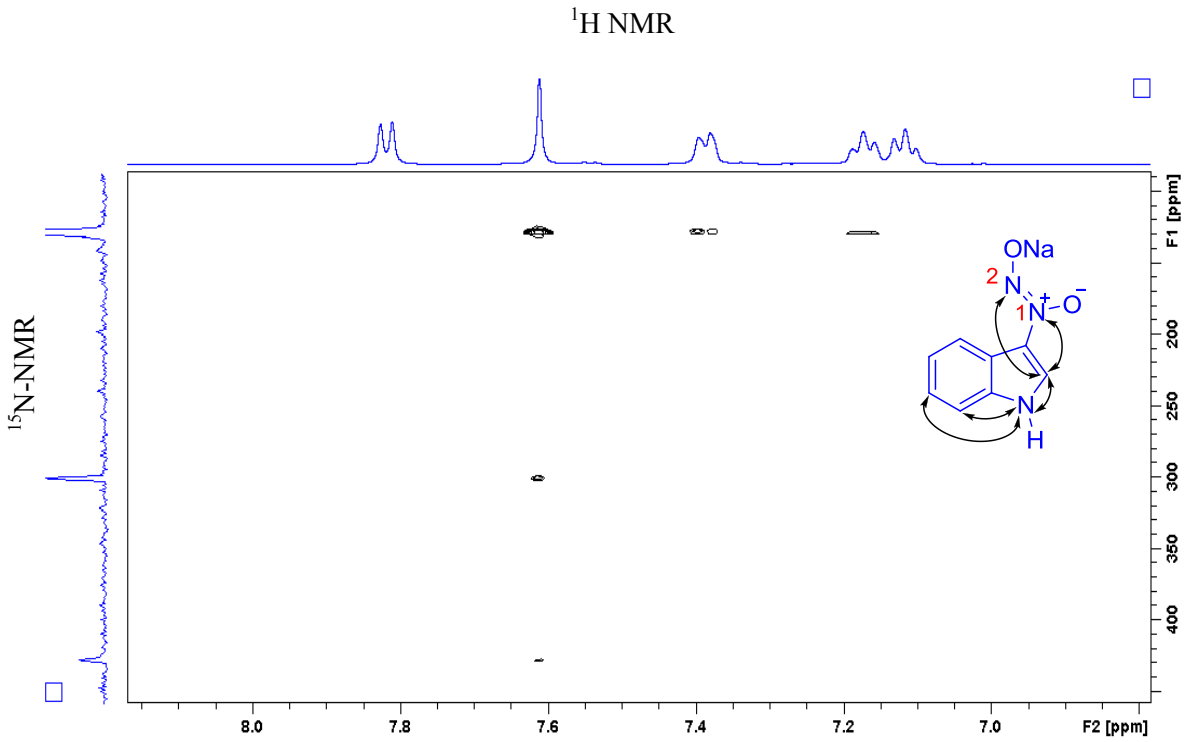

Figure 5.2: ^{1}H-^{15}N HMBC spectrum and the correlations observed for compound **237**.

The scope of the indole *C*-diazeniumdiolate synthesis was further explored with different indole derivatives **242a–d** using the same conditions as for indole **221** (Scheme **5.6**). Interestingly, diazeniumdiolate products **243a–c** were not formed upon reaction of indoles **242a–c** with NO. In the case of **242b**, a small amount of oxime **227b** was observed. In contrast, the reaction of NO with indole **242d**, bearing an electron-donating methoxy group at C5, furnished the desired *C*-diazeniumdiolate derivative **243d** as the major product (Table **5.1**).

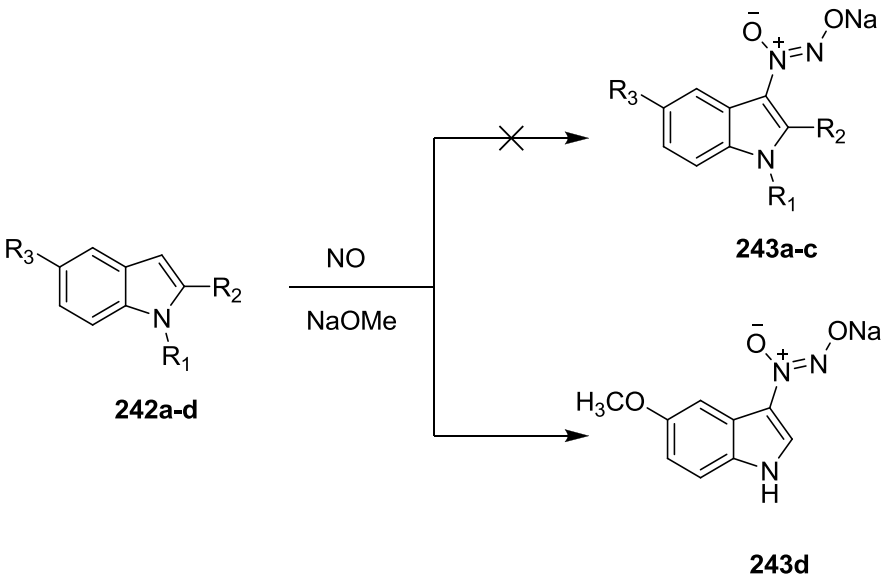

Scheme 5.6: Reaction of indole derivative with NO.

Table 5.1: Results of reaction between indole derivatives and NO

Entry	R_1	R_2	R_3	Result
242a	Me	H	H	Starting material
242b	H	Ph	H	Starting material and **227b**
242c	H	H	Br	Starting material
242d	H	H	OCH_3	*C*-diazeniumdiolate **243d**

The outcomes of these reactions could not be explained by a simple electrophilic substitution reaction mechanism. Thus, it was proposed that the indolyl-type radical intermediate **245** is formed *via* hydrogen radical abstraction by NO at the C-3 position of the indolenine tautomer **244**. The indolyl intermediate **245** could then be attacked by the NO radical and HNO in two steps to form the desired diazeniumdiolate derivative **237** (Scheme **5.7**).[251,253,189] The indolyl free radical mechanism is known to be affected by the substitution at the indole N and C-2 positions and an electron-withdrawing group such as bromine can have a destabilizing effect on the indolyl system, which is consistent with the lack of reaction observed for the indoles **242a–c**. On the other hand,

an electron-donating functionality such as methoxy (OCH_3) should stabilize the indolyl intermediate, facilitating the reaction with NO to afford the *C*-diazeniumdiolate-type product **242d**.

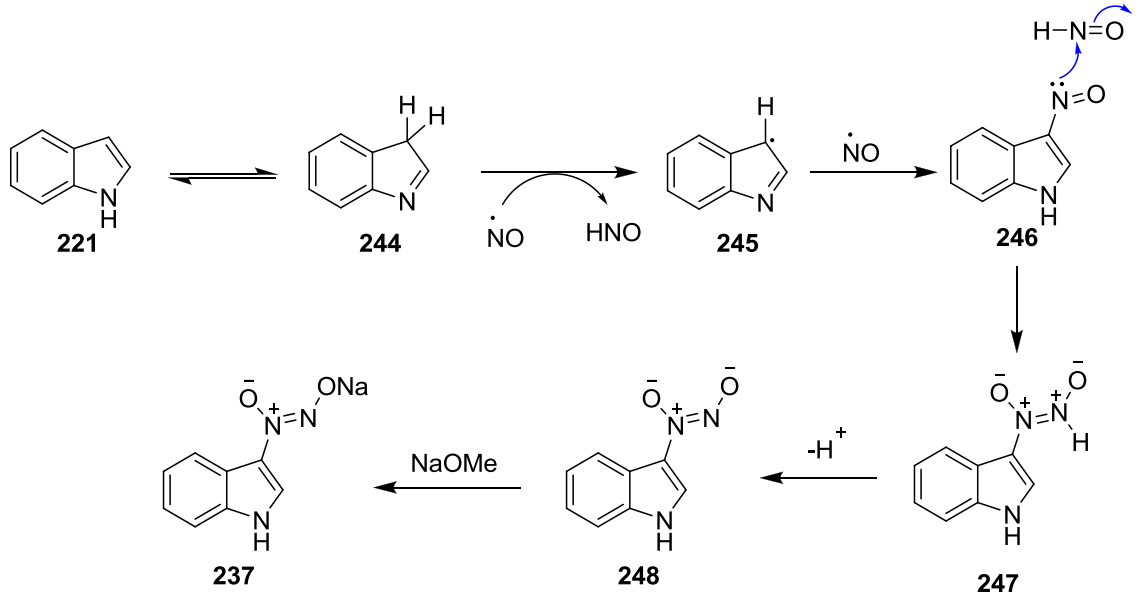

Scheme 5.7: Plausible mechanism of *C*-diazeniumdiolate **237** from indole **221**.

The formation of an indole *N*-diazeniumdiolate was also explored using 3-methylindole **232a**, because it was expected that substitution would occur preferentially at the nitrogen atom when the C-3 position of indole is blocked. 3-Methylindole **232a** was treated with NO at 80 psi for 48 h, but no reaction occurred. Additionally, increasing the pressure to 100 psi for a further 72 h gave the same result. This indicates that the indole NH was not sufficiently reactive towards NO under the conditions employed.

5.3.3 *O*^{2}-substituted indole *C*-diazeniumdiolates

Diazeniumdiolate salts are known to be relatively unstable and prone to degradation with release of NO under normal atmospheric conditions. One way of stabilizing diazeniumdiolates is by terminal oxygen (O^2) derivatization of the compound. Many O^2-

protected diazeniumdiolates have been reported in the literature with enhanced stability or additional functionalities such as enzyme activated or organ-specific NO release.

In order to obtain more stable indole *C*-diazeniumdiolates, O^2-alkylation and arylation reactions were investigated using alkylating agents such as dimethyl sulfate, MOM chloride and benzyl bromide or arylating agents such as fluorodinitrobenzene (F-DNB).

In general, the alkylation reactions were carried out in a solution of indole *C*-diazeniumdiolate **237** in methanol or tetrahydrofuran solvent in the presence of a base such as sodium bicarbonate or potassium carbonate. The desired alkylating agent was then added to the reaction mixture at 0 °C, followed by stirring at r.t. for the stipulated period of time. After completion of the reaction, the compounds were purified by column chromatography to give the desired products **249**–**252** in 36–62% yields (Scheme **5.8**).

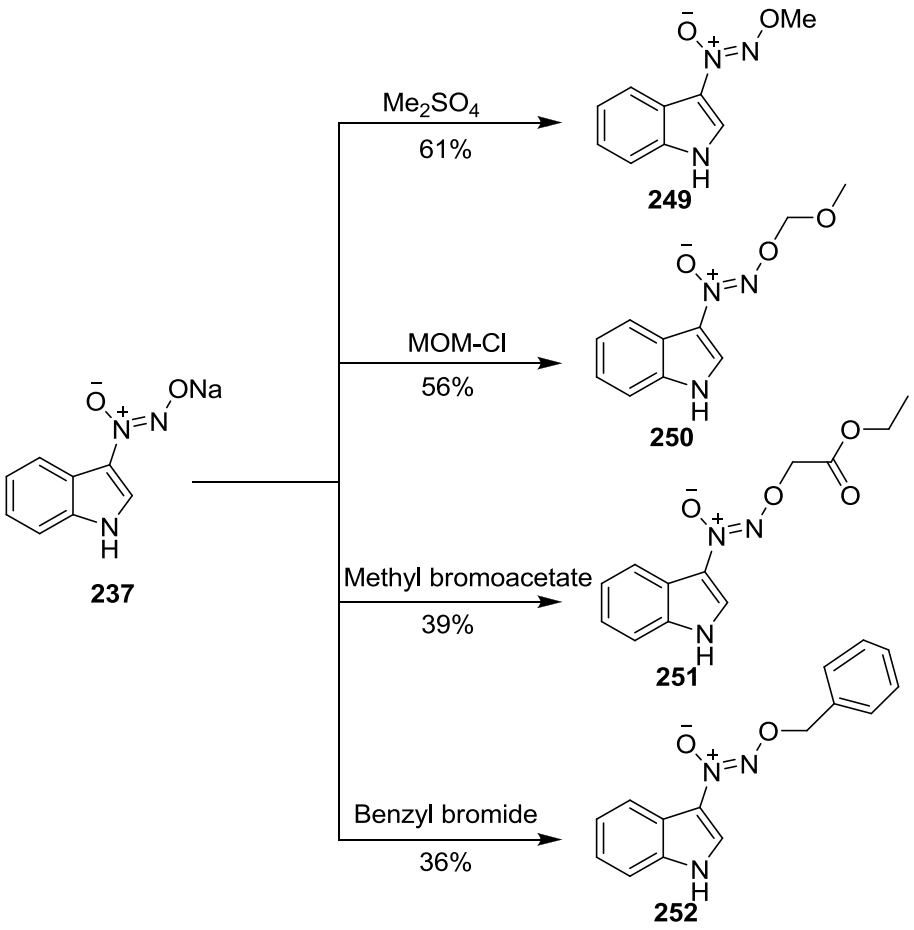

Scheme 5.8: O^2-alkyl derivatives of indole *C*-diazeniumdiolate **237**.

A suitable single crystal was grown from compound **252** for X-ray crystallography which interestingly showed four molecules of **252** in the asymmetric unit in triclinic space group P-1. They form two pairs linked *via* C-H··O extending into two identical double rows.The crystal structure also proved the cisoid stereochemistry for indole diazeniumdiolate **252**.

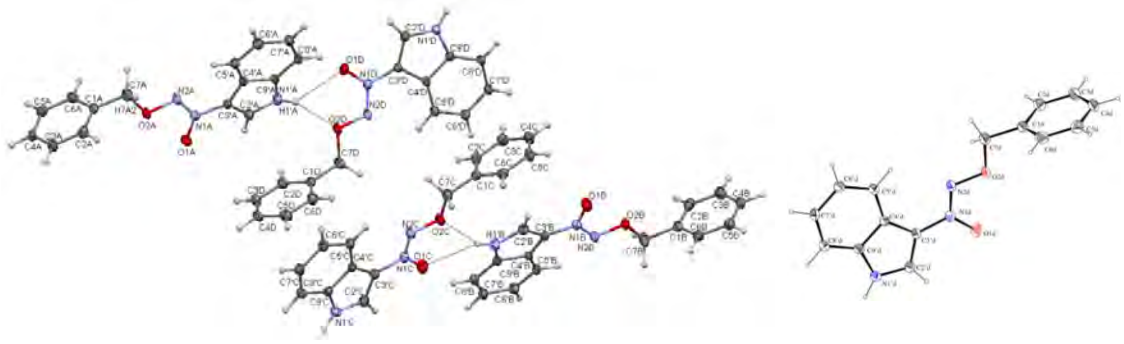

Figure 5.3: Crystal structure and ORTEP diagram of one of the four molecules (molecule D) of **252.**

The O^2-alkylated compounds were characterized primarily through NMR and HRMS to confirm the inclusion of the desired alkylating agent. The signals in the ^{1}H NMR spectra of the products were found to be similar to those in the parent structure **237** in the indole region. Furthermore, the additional peaks for the inserted O^2-alkyl group clearly indicated the formation of the O^2-substituted products **249–252** (Table **5.2**).

Table 5.2: Characteristic ^{1}H NMR values for the O^2-alkyl substitution products **249–252**.

Entry	O^2-alkyl	^{1}H NMR (δ)
249	CH_3	4.29 (s)
250	CH_2OCH_3	5.49 (s, CH_2) , 3.57 (s, CH_3)
251	$CH_2COOC_2H_5$	4.98 (s, CH_2), 4.29 (q, OCH_2), 1.30 (t, CH_3)
252	$CH_2C_6H_5$	4.29 (s, CH_2), 7.41-7.53 (m, C_6H_5)

The arylation reaction of indole *C*-diazeniumdiolate **237** was examined using the arylating agent fluoro-2,4-dinitrobenzene (F-DNB) (Scheme **5.9**). Initially, the reaction was carried out by dissolving compound **237** in 5% aqueous $NaHCO_3$, to which a solution of F-DNB in *t*-butyl alcohol was added at 0 °C. The reaction mixture was brought to r.t. and stirred overnight. After evaporation of the volatile solvents, the reaction mixture was extracted with DCM to yield the crude reaction product. However,

the ^{1}H NMR spectrum of the crude product did not show any peaks correlating with the indole skeleton.

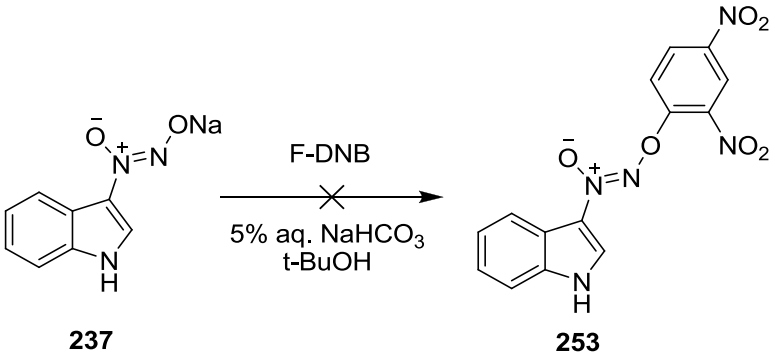

Scheme 5.9: Attempted reaction of indole **237** and F-DNB

Therefore, optimization of the reaction was carried out by varying the solvent and the duration of the reaction time. It was observed that the use of a protic solvent such as H_2O or MeOH resulted in the isolation of aryl compound **254** or **255** as the major product, respectively.

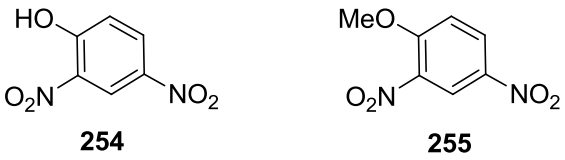

254 **255**

The use of aprotic solvents such as DMSO and THF were also evaluated, but did not led to the formation of the desired product. The outcome of the reaction is possibly due to the low stability and leaving group effect of the dinitrobenzene-substituted product **253**, which could led to spontaneous degradation (Scheme **5.10**).

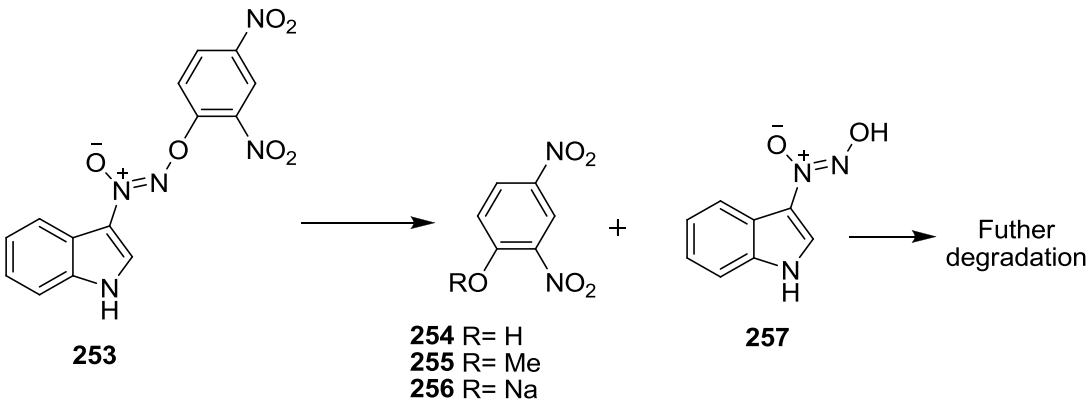

Scheme 5.10: Possible degradation of compound **253.**

5.4 Multiple high load nitric oxide donors

For industrial applications, the ability to generate a sustained release of higher concentrations of NO are highly desirable in order to overcome microbial related corrosion and other biofouling problems. One approach involves combining different NO scaffolds to form a high load NO donor in which the rate of release from each donor site can be metabolically controlled, with an overall high rate of NO release for a longer period.

It was envisaged that in order to generate the high load or mixed NO donors, the core molecule should have multiple reaction sites with controllable reactivity. Cyanuric chloride **258** was thought to be a useful scaffold for this purpose as it contains a triazine ring system with three replaceable chlorine atoms. The ease of replacement of the chlorine atoms in cyanuric chloride to form partial substitution products such as di or mono-chlorotriazines is determined by both the nature of the nucleophilic reagent and the number of substituents attached to the triazine ring. The reactivity of cyanuric chloride itself and of many of its monosubstituted derivatives is approximately equal to that of oxychlorides or acid chlorides, whereas disubstituted cyanuric acid derivatives possess reactivity comparable to the alkyl halides.[254]

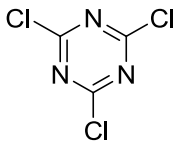

258

Cyanuric chloride is reactive towards different functional groups such as amines, alcohols, phenols and sulfur compounds.[255-257] This has led to the synthesis of a diverse array of 1,3,5-triazine derivatives with widespread applications in pharmaceuticals, textiles, rubber industries, dyestuffs, explosives and surface-active agents. Cyanuric chloride derivatives with pharmaceutical properties include anti-tumor agent **259**,[258] anti-trypanosomal agent **260**,[259] kinase inhibitor **261**[260] and others.[261-262] Cyanuric chloride derivatives have also been developed as insecticides, fungicides, and weed-killers, some of which are commercially used in agricultural applications. In addition, triazine systems based on cyanuric chloride have been utilized for neutron capture therapy,[263] and the synthesis of calixarenes derivatives[264] and macrocyclic receptor molecules.[265]

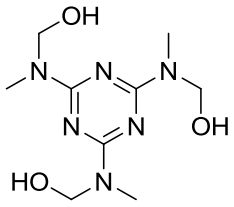

Trimelamol

259

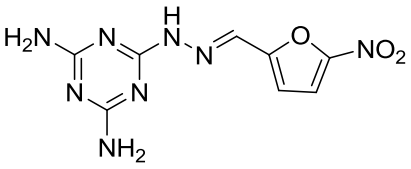

4,6-diamino-2-(5-nitrofurfurylidenehydrazino)-1,3,5-triazines

260

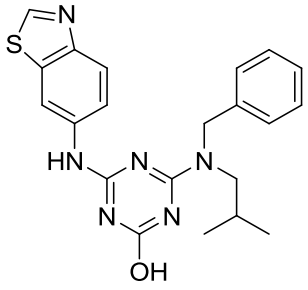

4-(benzothiazol-ylamino)-6-(benzyl-isopropyl-amino)-[1,3,5]triazin-2-ol

261

The diverse applications of cyanuric chloride can be attributed to its unique structure, which allows its three active chlorine atoms to be replaced one by one. From the literature, it is observed that the synthesis of the monosubstitution product **262** requires

only ice-cold or low temperature conditions, whilst substitution of the second chlorine to form product **263** is usually carried out at r.t. or under 45 °C. Finally, the synthesis of the trisubstitution product **264** requires heating at high temperatures (>55 °C) for an extended duration of time (Scheme **5.11**).[266]

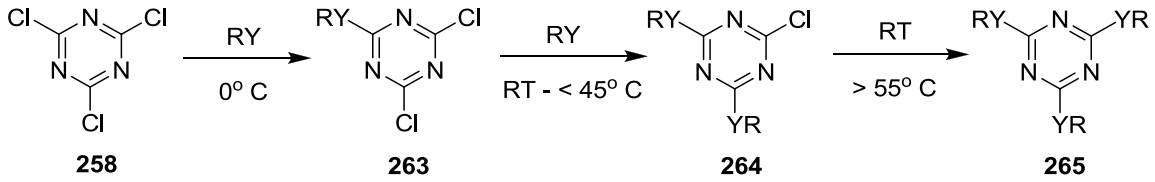

Scheme 5.11: General conditions for the synthesis of cyanuric acid derivatives.

The successive substitution of the chlorine atoms in cyanuric chloride with various functional groups enables a diverse range of substances to be obtained. Thus, it was envisaged that a series of diverse NO donor compounds, including high load and mixed-type NO donors, could be synthesized by controlling the reaction between cyanuric acid and the nucleophilicity of the NO donors (Scheme **5.12**).

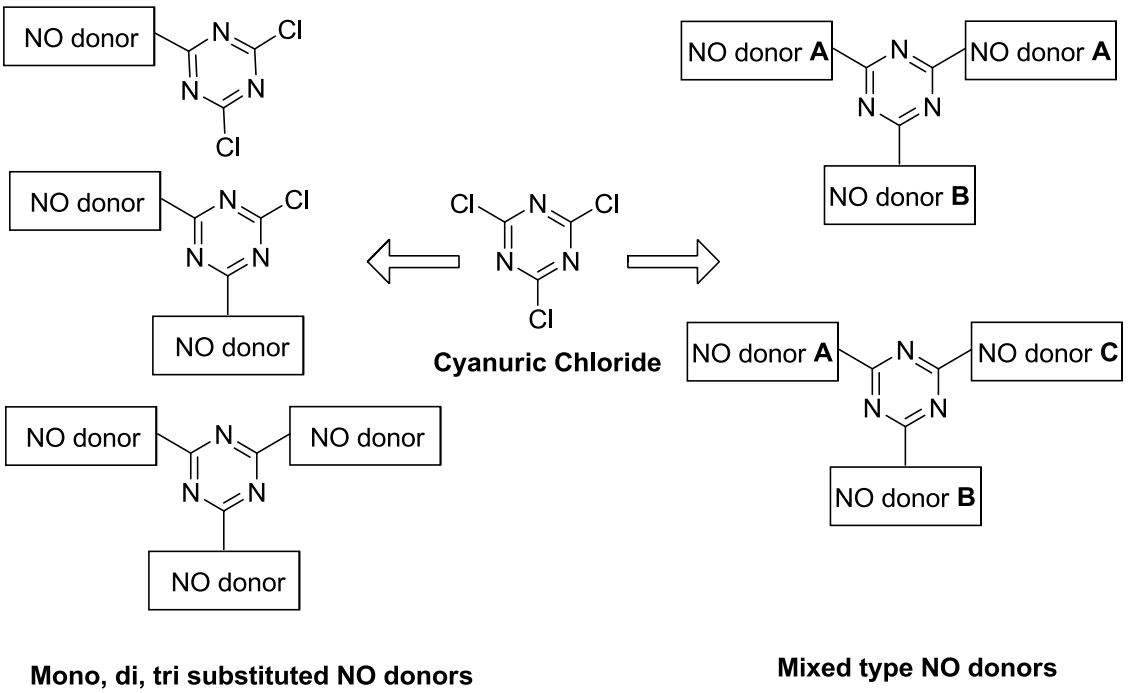

Scheme 5.12: Possible modification of cyanuric acid to generate high load or mixed-type NO donors.

To generate the high load NO donor, different monomeric nitrates and diazeniumdiolates were utilized. Aminoalkyl nitrates and mononitrates were chosen as these nitrates are known to be less prone to tolerance. In the case of the diazeniumdiolates, piperazine-based diazeniumdiolates were used as they provide a feasible site for reaction, and the piperazine motif is also known to have antipathogenic (anti-anthelmintic) effects. The O^2-methoxymethyl (MOM) piperazine diazeniumdiolate was also selected as MOM protected diazeniumdiolate is known to release NO at a slow rate extending over several weeks.

The general procedure for the synthesis of the desired tri-substituted NO donor derivatives involved the addition of the NO derivative to a solution of cyanuric chloride **258** and potassium carbonate in THF or acetone at 0 °C. The temperature of the solution was gradually increased to reflux and the reaction mixture was stirred for 30–40 h. The tri-substituted product was precipitated by the addition of cold water, and the resulting mixture was filtered to remove the salt and unreacted base. The residue was dried to obtain the crude product.

Using the general procedure, compounds **267** and **268** were prepared from nitrates **266** and **47**, respectively (Scheme **5.13**). Compound **267** was readily isolated, but the solubility of compound **268** in water hindered its purification by filtration. Thus, compound **268** was recrystallized from water to remove the salt and unreacted base to obtain the product in pure form.

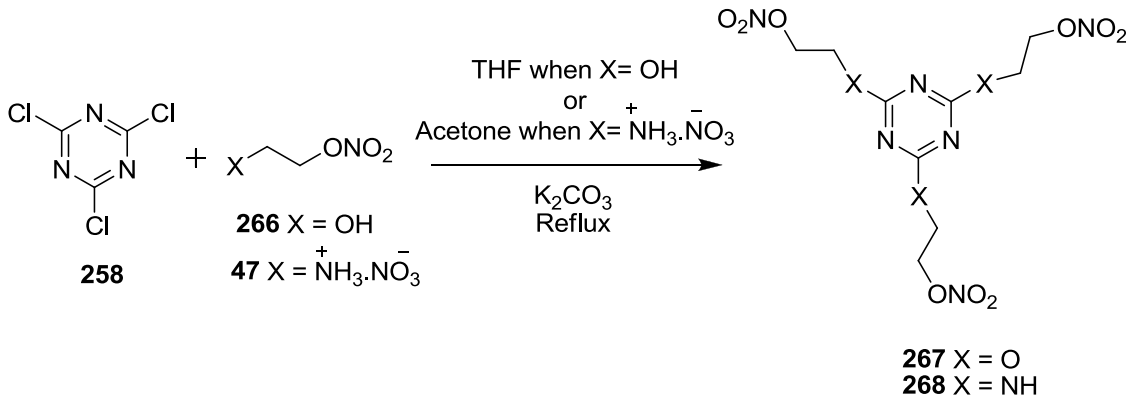

Scheme 5.13: Synthesis of cyanuric acid-based high load nitrate derivatives **267** and **268**.

The formation of products **267** and **268** was confirmed by analysis of their ^{1}H and ^{13}C NMR spectra. For example, the ^{1}H NMR spectrum of **267** revealed peaks at δ 4.91 and 4.68 ppm corresponding to the CH_2 groups of the ethyl nitrates. Due to the symmetrical nature of the molecule, three signals were observed in the carbon spectrum. The formation of the compounds **267** was further confirmed by HRMS showing molecular ion *m/z* values of 397.0575 [M+1] consistent with the molecular formula $C_9H_{12}N_6O_{12}$.

A similar methodology was used for the synthesis of diazeniumdiolate-based high load nitric oxide donors. The di and tri-substituted diazeniumdiolate products **271a** and **271b** required the initial synthesis of diazeniumdiolate **270** which was prepared from the piperazine derivative **114** following a literature procedure (Scheme **5.14**).[220]

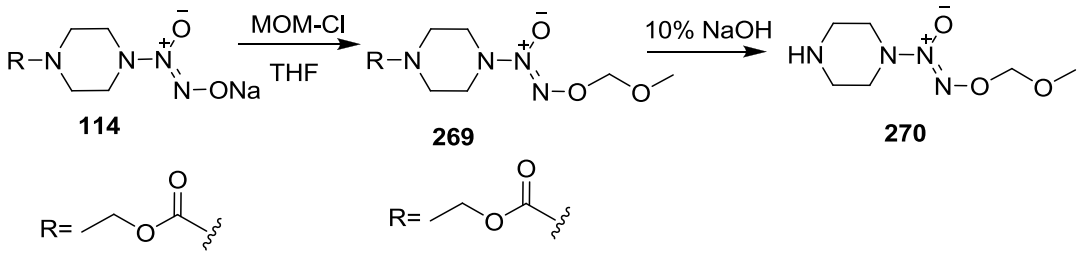

Scheme 5.14: Synthesis of piperazine diazeniumdiolate derivative **270**.

The desired di-substituted product **271a** was then obtained by reacting cyanuric acid **258** and diazeniumdiolate **270** at r.t. for 5 h, while tri-substituted product **271b** could be obtained by heating at reflux for 30 h. After work-up and purification by preparative TLC the desired products **271a** and **271b** were obtained in 38% and 53% yield, respectively (Scheme **5.15**).

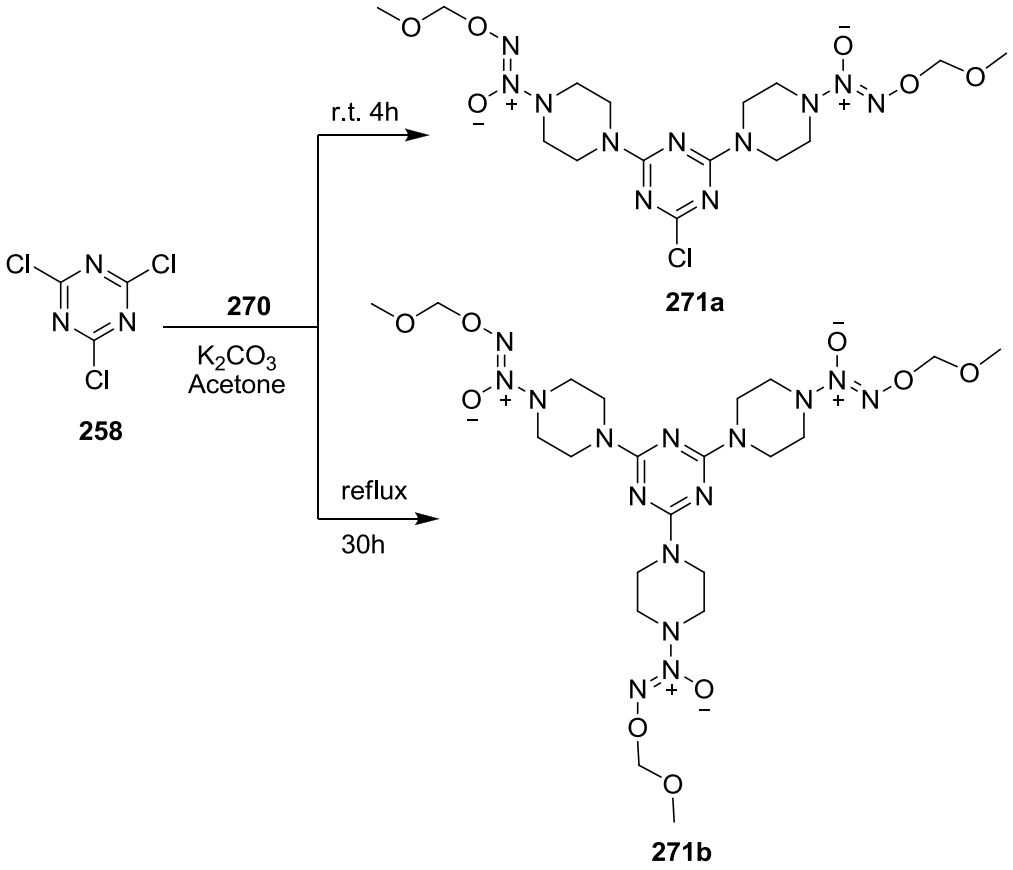

Scheme 5.15: Synthesis of tri-substituted O^2-protected diazeniumdiolate derivatives **271a** and **271b**.

The ^1H NMR spectra of compounds **271** revealed the presence of aliphatic protons corresponding to the piperazine unit and the MOM group, confirming the formation of the desired product (Table **5.3**).

Table 5.3: Characteristic NMR signals for **271a** and **271b**.

Compound	271a		271b	
	^{1}H NMR (δ)	^{13}C NMR (δ)	^{1}H NMR (δ)	^{13}C NMR (δ)
Piperazine moiety	4.07, 3.55	50.6, 42.5	3.98, 3.49	50.7, 42.0
MOM moiety	5.23, 3.54	98.1, 57.1	5.22, 3.48	98.0, 57.1
Cyanuric chloride moiety	-	170.7, 164.2	-	170.0, 164.4

To synthesize O^2-unsubstituted high load diazeniumdiolate derivatives, an alternative approach was employed that introduced the NO donor group in the final step (Scheme **5.16**). Compound **274** was prepared from cyanuric acid **258** and piperazine derivative **113** to form **272** in 86% yield under similar conditions as above. The structure of the intermediate **272** was confirmed by analysis of its ^{1}H NMR spectrum, which showed peaks at δ 3.51 and 3.78 corresponding to the piperazine moiety, as well as peaks at δ 4.15 and 1.28 ppm corresponding to the *N*-carbamate group. HRMS also showed a molecular ion peak at *m/z* 550.3085 [M+1], consistent with the molecular formula of $C_{24}H_{39}N_9O_6$ (549.3023) for **272**. Compound **272** was then deprotected with a solution of 10% ethanolic NaOH to form **273**, followed by reaction with NO in a 1:1 mixture of ether: methanol to afford the desired diazeniumdiolate product **274** in 51% yield.

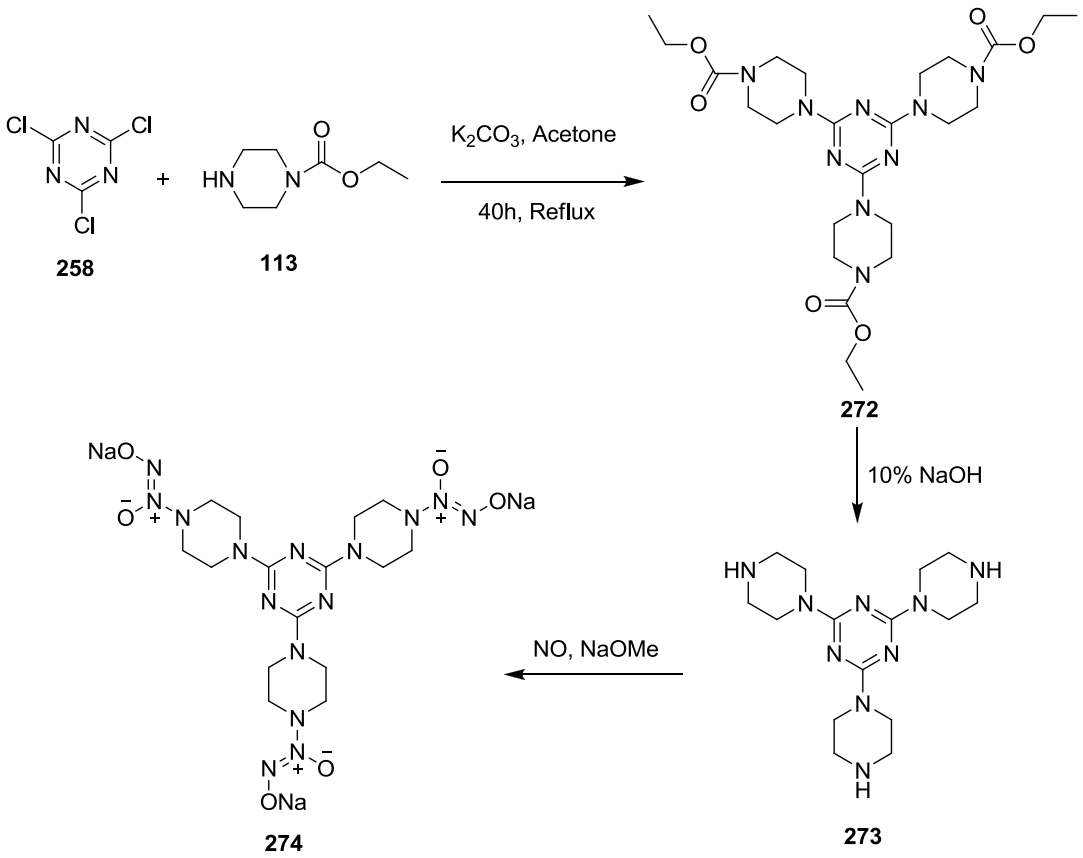

Scheme 5.16: Preparation of tri-substituted diazeniumdiolate derivative **274**.

The ^{1}H NMR spectrum of **274** displayed two triplets at δ 3.71 and 2.85 ppm corresponding to the piperazine group. The product was further confirmed by its HRMS *m/z* value of 602.1625 [M+Na] which was consistent with the calculated value for $C_{15}H_{24}N_{15}Na_3O_6$.

Due to time restriction the synthesis of mixed high load NO donors could not be explored.

5.5 Conclusions

A new series of indole-based *C*-diazeniumdiolates with potential NO-donating properties has been prepared. Harnessing the pharmaceutical properties of the indole scaffold, these molecules could have useful applications as antimicrobial (antivirulence)

and anti-biofilm agents. In addition, the reactivity of indole derivatives towards NO has been explored, and the results suggest an indolyl radical mechanism for the formation of indole *C*-diazeniumdiolates.

In the second part of this chapter, a series of high load uniform NO donors has been synthesized. These dendritic-type NO-donors have potential applications in the field that require the sustained release of a high dose of NO, such as NO-releasing materials or the treatment of industry-related MIC. The chemistry established in this chapter offers potential applications for the synthesis of high load NO-releasing hybrids based on biologically important scaffolds.

Chapter 6

Molecular association via halogen bonding (C-halogen···O) and weak dipolar (C=O···C=O) contacts and their relevance in receptor binding: solid state and computational studies

6.1 Introduction

Non-covalent intermolecular interactions have attracted great interest in diverse fields of chemistry, as they have been found to play important roles in conformational preferences, crystal packing, host-guest complex stabilization, biomolecular structures and chemical reactions. The role of intermolecular interactions in drug design is of great importance as the biological activity of a drug is related to its ability to interact with the desired bio-molecular target. The activity is therefore directly related to the nature and strength of interactions between a drug and its target macromolecule, such as enzymes, other proteins, or DNA and RNA. Understanding the possible interactions between a given molecule and the targeted macromolecule is fundamental for understanding the pharmacological activity, toxicity profile and selectivity of the molecule.

Intermolecular interactions are classified into three categories based on the exponential dependence of electron density (ρb) and interaction length (*R*ij). Hydrogen bonds such as, O-H···O, N-H···O, N-H···Nand N-H···Sare classified as strong hydrogen bonds (*R*ij < 2.3 Å, ρb > 0.08 eÅ-3), or region 1. C-H···Ointeractions reside in the weak hydrogen bond region (2.3 Å < *R*ij < 2.75 Å, 0.07 eÅ-3 > ρb > 0.02 eÅ-3), or region 2. Finally, interactions including C-H···π, C-H···S and π···π (such as O···C, N···N, C···C, O···O, S···S, S···C,S···N and N···C) are among the weakest types of interactions and fall into the van der Waals interaction region (*R*ij > 2.75 Å, ρb < 0.05 eÅ-3), region 3 (Figure **6.1**).[267]

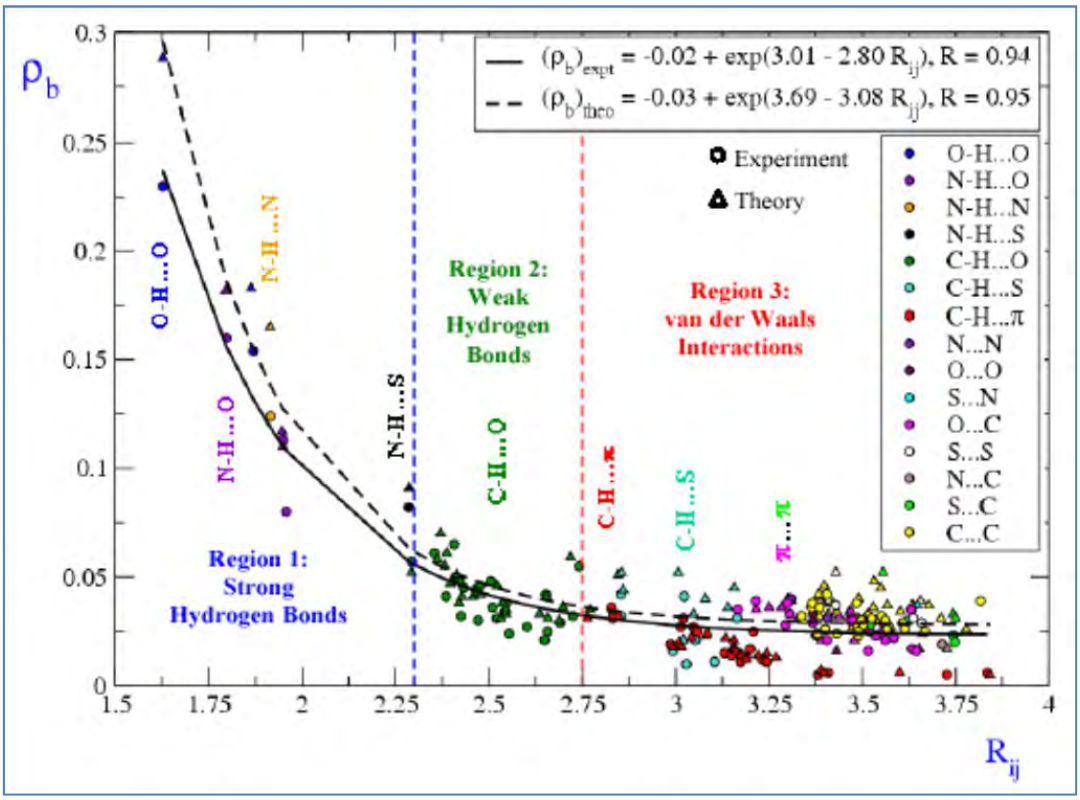

Figure 6.1: Exponential dependence of electron density (ρb) and interaction length (*R*ij) of 15 types of interactions. The circles and triangles represent experimental and theoretical values, respectively, and the solid and dash black lines represent the corresponding fittings. The inset gives the details of the fitting models along with correlation coefficients R and the color code for each type of interactions.[267]

6.2 Non-covalent intermolecular interactions

The nature of the intermolecular non-covalent attractions involved in crystal packing has been increasingly recognized to play a significant role in the solid-state conformation adopted by a molecule, as well as influencing properties such as dissolution, stability and bioavailability of drug substances. A wide range of intermolecular interactions have been reported, ranging from hydrogen bonds to van der Waals interactions.

6.2.1 Strong non-covalent interaction - hydrogen bonding

_Hydrogen bonding‘ is a well-characterized classical example of a strong, specific and highly directional intermolecular interaction. It has emerged as one of the most important factors not only for crystal structures and engineering, but also for the structures of biologic molecules and in supramolecular chemistry. In hydrogen bonds, the donor (D) to acceptor (A) distances are in the range 2.5 to 3.2 Å (e.g. O-H··O, N-H··O, N-H··S and N-H··N) with bond energies ranging from 4–15 Kcal/mol. The interactions involve mainly electrostatic and charge transfer forces, with almost all hydrogen bonds exhibiting bond lengths shorter than the sum of the van der Waals radii of the respective atoms. Hence, the strength of the hydrogen bond lies between a weak covalent bond and van der Waals interaction.[268-269]

6.2.2 Weak non-covalent interactions

Many weak interactions such as π··π, C-H··π, O-H··π and N-H··π interactions are also observed in the crystal structures of small molecules and proteins. Weak intermolecular interactions such as C=O··C=O, C-F··C=O and S=O··C=O (dipole-dipole interactions) have been suggested to play an important role in molecular aggregation and in the binding of drug compounds to the receptor protein molecules. Halogen bonding and carbonyl–carbonyl dipolar contacts are two examples of such weak non-covalent interactions prevalent in biological systems.

6.2.2.1 Halogen bonding

Halogens (Cl, Br, I) exhibit unique properties when it comes to intermolecular interaction as they behave as both halogen bonding donors and hydrogen bonding acceptors due to their anisotropic distribution of electrostatic potential (ESP). Halogens are capable of forming a variety of intermolecular interactions, such as C-H···X(X = F, Cl, Br, I), C-X··π, X···Xand halogen bonding interactions.

A halogen bond can be defined as a short C-X···O-Y interaction between a polarised halogen atom (a Lewis acid) and negatively-charged oxygen, nitrogen or sulfur atom (a Lewis base), where the X···Odistance is less than or equal to the sum of the respective van der Waals radii (3.27 Å for Cl···O, 3.37Å for Br··O, and 3.50 Å for I··O) with geometry consistent with those seen in small organic molecules (C-X··O angle, $\theta_1 \approx$ 165° and the X···O-Y angle, $\theta_2 \approx 120°$) (Figure **6.2**).[270]

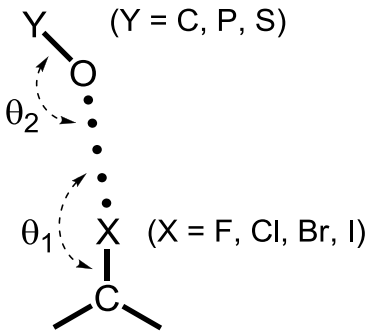

Figure 6.2: Schematic of short halogen (X) interactions to various oxygen containing functional groups (such as carbonyl, carboxylate, phosphate, sulfate).[270]

The halogen bonds are increasingly being reported as vital intermolecular interaction in polymorphic structures, in self-assembled architectures, in the crystalline solid state, in soft matter and in biological systems. Halogen bonding is gaining particular impetus for its implications in drug design, as halogen bonding has been shown to have a significant role in protein-ligand (drug) interactions.[271-273] The diversity of short X··O interactions that are involved in protein-ligand recognition is documented in the literature. For example, the binding of the inhibitor 4,5,6,7-tetra-bromobenzotriazole at the ATP binding site of phospho-CDK2-cyclin involves four short Br··O contacts.[270] Similarly, halogen bonding was observed between aldose reductase and inhibitor IDD 594, which was found to be essential for the selectivity profile of the inhibitor.[274]

Thus, halogen bonding is recognized as an essential intermolecular interaction important for determining the activity and selectivity profiles of drugs, and has been considered to play a key role in the rational drug design process.

6.2.2.2 CO··CO interactions

Carbonyl groups are ubiquitous in many organic and biological systems and their molecular recognition properties, particularly hydrogen bond acceptor abilities, have been studied extensively. However, there is a growing body of literature concerned with non-covalent interactions of the >C(δ+)--O(δ-) dipole that are not mediated by hydrogen. Carbonyl··carbonyl (C=O··C=O) and halogen··carbonyl (C-X···C=O, X = Cl, Br) dipolar interactions are such carbonyl group interactions that are found in the X-ray crystal structures of small molecules and protein–ligand complexes.[275]

The analysis of non-covalent C=O··C=O interactions shows three major dominated motifs, including; a) slightly sheared antiparallel motif, b) the perpendicular motif and c) the sheared parallel motif (Figure **6.3**). These motifs have one or both of the C··O separation distances less than 3.6 Å.[275]

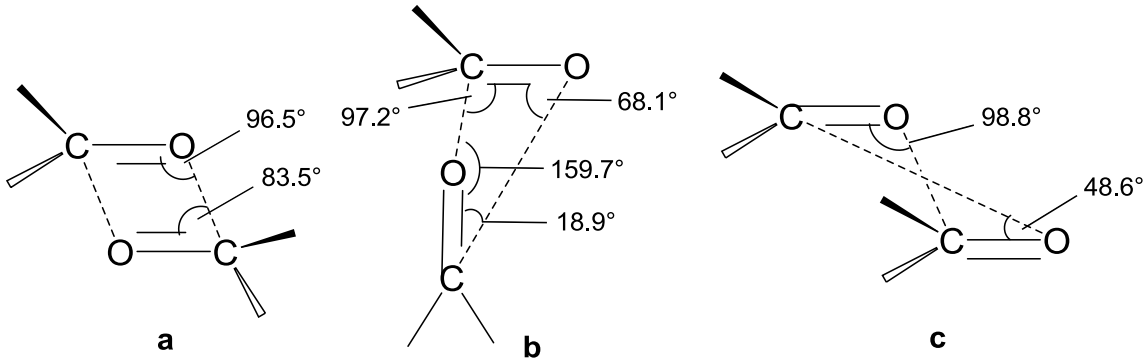

Figure 6.3: Average geometries for the three most common motifs for C=O··C=O interactions: (a) antiparallel motif, (b) perpendicular motif and (c) sheared parallel motif.

The role of C=O··C=O interactions in biological assemblies is increasingly being explored and has been found to be significant in stabilizing the secondary structure of

proteins or protein-ligand complexes. For example, the C=O··C=O interaction influences the conformation of α-helices and antiparallel β-sheets. Similarly, protein-ligand C=O··C=O interactions are seen in a complex of phosphoribosyl pyrophosphatase (PRPP) amidotransferase with 5-oxo-*L*-norleucine ligand (ONL). A short, orthogonal C-Cl··C=O contact has also been shown to contribute to the binding affinity of the antimalarial drug quinacrine to its target, the enzyme histamine *N*-methyltransferase.[276]

Thus, dipolar interactions between a protein and its ligand may substantially contribute to the optimization of both the activity and selectivity of small molecule inhibitors.

6.3 Chapter aims

A range of NO-donating hybrids based on scaffolds such as acylated homoserine lactones and fimbrolides (brominated furanones) have been synthesized during the course of this work for antimicrobial applications. These scaffolds possess characteristic functional groups such as carbonyl, halogen and amino moieties which have the potential to form intermolecular interactions, including dipolar C=O··C=O and C-X···O=C halogen bonding contacts.

The aim of this chapter was to investigate the intermolecular interactions in the novel synthesized molecules using solid state X-ray crystallographic studies and computational docking studies.

6.4 Part A: Solid state X-ray crystallographic studies

Crystals of many of the compounds reported in this thesis were grown suitable for single crystal X-ray analysis. In this part, structures highlighting the molecular association *via*

halogen bonding or dipolar interactions are reported. The organizations of the molecules with these interactions along with their geometrical parameters are discussed below.

6.4.1 Halogen bonding interactions

Example 1:

3-(1-Nitrooxyhexyl)-5-(dibromomethylene)furan-2(5*H*)-one (155c)

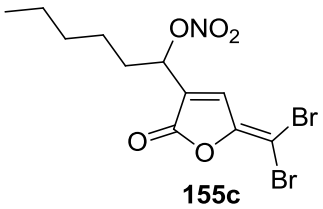

155c

The study of the intermolecular crystal interactions in the compound **155c** revealed three different types of interaction. A C-H···O type hydrogen bonding interaction was observed between two furanone units, involving the C4-H4 and the C2-O1 carbonyl groups (Table **6.1**).

Table 6.1: Geometric parameters for hydrogen bonding

Donor–H···Acceptor	D—H (Å)	H···A (Å)	D···A (Å)	D—H···A (°)
C4–H4···O2	0.95	2.24	3.191(3)	175

The two bromine atoms of the dibromomethylene system were involved in non-covalent halogen bonding and dipolar contacts. Halogen (bromine) bonding was seen between C6-Br1···O1 and C6-Br2···O4, involving the oxygen atoms of the furanone ring and the nitroester group respectively (Figure **6.4**). Geometrical parameters for halogen bonding, C6-Br1···O1 are C6-Br1 = 1.864 Å, Br1···O1 = 3.204 Å, angle C6-Br1···O1 = 141.36° and C6-Br2···O4 are C6-Br2 = 1.870 Å, Br2···O4 = 3.303 Å, angle C6-Br2···O4 = 147.83°. Bromine (Br2) is simultaneously involved in interaction with C2=O2 to form the carbonyl dipolar interaction C6-Br2···C2=O2. Geometrical parameters for C6-Br2···C2=O2: Br2···C2 = 3.462 Å, angle C6-Br2···C2 = 78.71°, angle Br2···C2=O2 = 89.62°

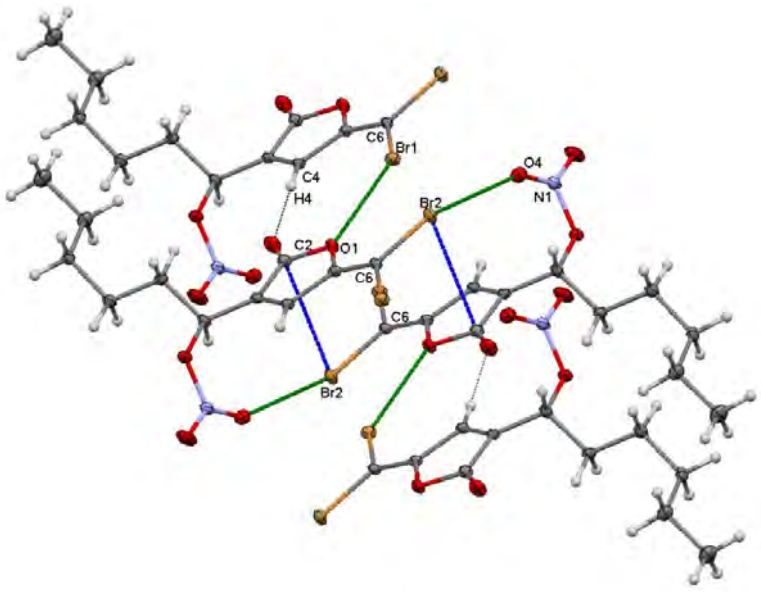

Figure 6.4: Organization of molecule **155c** viewed down the a-axis showing halogen bonded (C-Br···O) dimeric units and dipolar C-Br··C=O contacts.

6.4.2 CO··CO interactions

Example 1:

Methyl 5-formyl-2-propylthiophene-3-carboxylate (165)

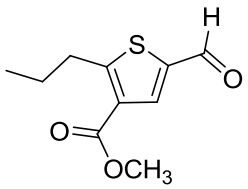

165

Molecules of **165** form infinite planar sheets in the bc plane, making an extensive networks of C-H···O type hydrogen bonding (Figure **6.5**). Each of the carbonyl groups is involved in bifurcated interactions; the oxygen O1 makes contacts with the C11-H11 and C4-H4 protons from the centrosymmetrically related molecule, whereas the methyl group hydrogen atoms C10-H10A (related by translation along b-axis) and C8-H8A (related by centre of symmetry) make short contacts with the carbonyl oxygen O3. The geometrical parameters of the C-H··O hydrogen bonds are given in Table **6.2**.

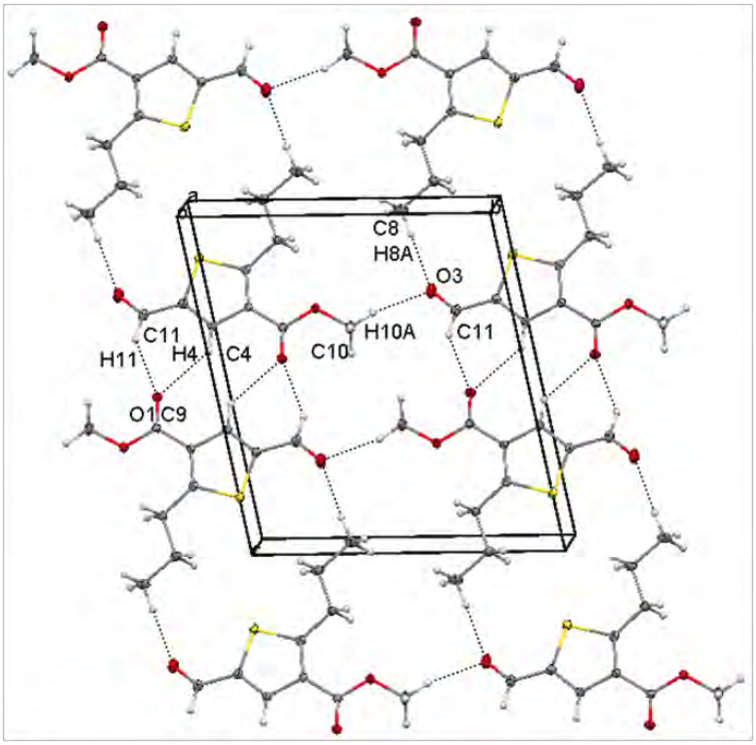

Figure 6.5: Packing of molecule **165** viewed down the a-axis showing the network of C-H···Otype hydrogen bonding, which forms planar sheets along the bc-plane.

Table 6.2: Geometric parameters for hydrogen bonding

Donor–H···Acceptor	D—H (Å)	H···A (Å)	D···A (Å)	D—H···A (°)
C(11)–H(11)··O(1)	0.95	2.62	3.436(3)	144
C(4)–H(4)···O(1)	0.95	2.54	3.340(3)	142
C(8)–H(8A)··O(3)	0.98	2.56	3.506(3)	164
C(10)–H(10A)··O(3)	0.98	2.59	3.535(3)	161

The planar sheets in the bc-plane make dipolar contacts involving carbonyl groups C11=O3 and C9=O1 along the a-axis. A close-up view of these interactions is shown in Figure **6.6**.

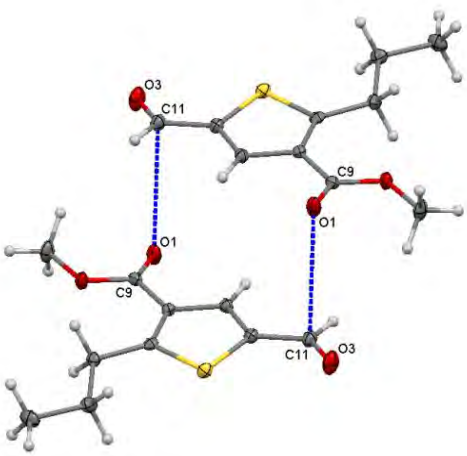

Figure 6.6: Association of molecules **165** *via* dipolar C=O···C=O contacts.

The dipolar contacts are made by two molecules related by a centre of symmetry. The dipolar carbonyl interactions can be classified as sheared but not of the parallel type, with the two carbonyl groups rotated by ≈ 130° with respect to each other. This arrangement of atoms could be attributed to the compromise in optimizing interactions within the C-H···Onetwork along two dimensions and maximizing dipolar interactions along the third. The geometrical parameters of the short contacts C9=O1···C11=O3 are O1···C11 = 3.208 Å, angle C9-O1···C11 = 110.35°and angle O1···C11=O3 = 107.94°.

Example 2:

2-Oxo-2-(2-oxotetrahydrofuran-3-ylamino)ethyl nitrate (95a)

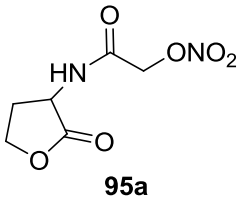

95a

The packing of the compound **95a** along the b-axis shows two molecules connected *via* hydrogen bonding between C3-H3··O3-C6. The hydrogen bonded sub-units are further bridged by intermolecular hydrogen bonding between N1-H1··C2-O2 and the antiparallel C=O···C=O dipolar interaction between two C2-O2 groups (Figure **6.7**).

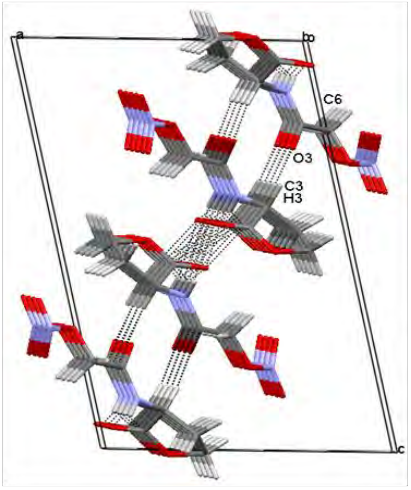

Figure 6.7: Molecular packing of compound **95a** across bc-axis

Compound **95a** formed two major intermolecular interactions in the solid state, which include hydrogen bonding between N1-H1··C2-O2 and the antiparallel carbonyl··carbonyl (C=O···C=O) interaction between two C2-O2 groups (Figure **6.8** and Table **6.3**). The geometric parameters for C2=O2··C2=O2 are O2··C2 = 2.996 Å, angle C2=O2··C2 = 92.17°, angle O2··C2=O2 = 87.83°.

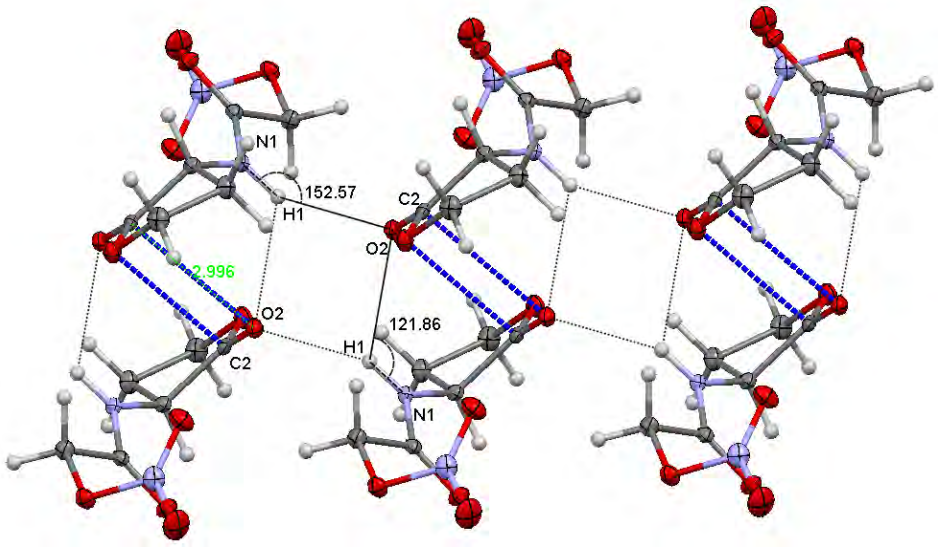

Figure 6.8: Hydrogen bonding and C=O···C=O interactions of compound **95a**

Table 6.3: Hydrogen bonding geometric parameters

Donor–H···Acceptor	D—H (Å)	H···A (Å)	D···A (Å)	D—H···A (°)
N(1)–H(1)···O(2)	0.88	2.18	2.9913(13)	153
N(1)–H(1)···O(2)	0.88	2.42	2.9818(15)	122
C(3)–H(3)···O(3)	1.00	2.57	3.4678(15)	150

Example 3:

2,2-Dimethyl-5-((2-oxotetrahydrofuran-3-ylamino)methylene)-1,3-dioxane-4,6-dione (100)

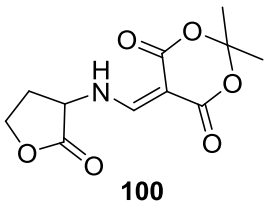

100

Compound **100** contains three carbonyl groups and a hydrogen donor (NH), raising the possibility of different intermolecular interactions. The interaction study revealed two major interactions, which include hydrogen bonding and C=O···C=O interactions, leading to a dimeric unit of the molecule. The geometric parameters for the C10=O6…C10=O6 are O6…C10 = 3.092 Å, angle C10=O6…C10 = 119.62°, angle O6…C10=O6 = 91.96°. Both intermolecular and intramolecular hydrogen bonding was observed between C10-O6 and H1-N1 groups. A weaker C10-O6···H4B-C4 hydrogen bond and a sheared type C=O···C=O interaction between C10-O6···C2-O2 were also observed (Figure **6.9**).

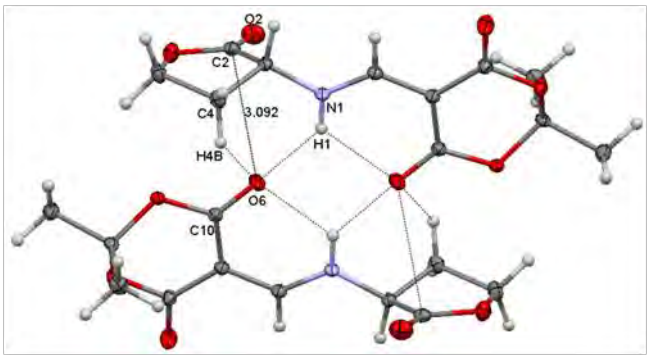

Figure 6.9: Interactions in dimeric unit of compound **100**

The dimeric units of the molecule are further associated with each other *via* two weaker C3-H3··O5 and C5-H5A··O5 hydrogen bonds. With the aid of the weaker hydrogen bonding network, the dimeric units form the packing as illustrated in the Figure **6.10**. The geometric parameter for hydrogen bonding is given in Table **6.4**.

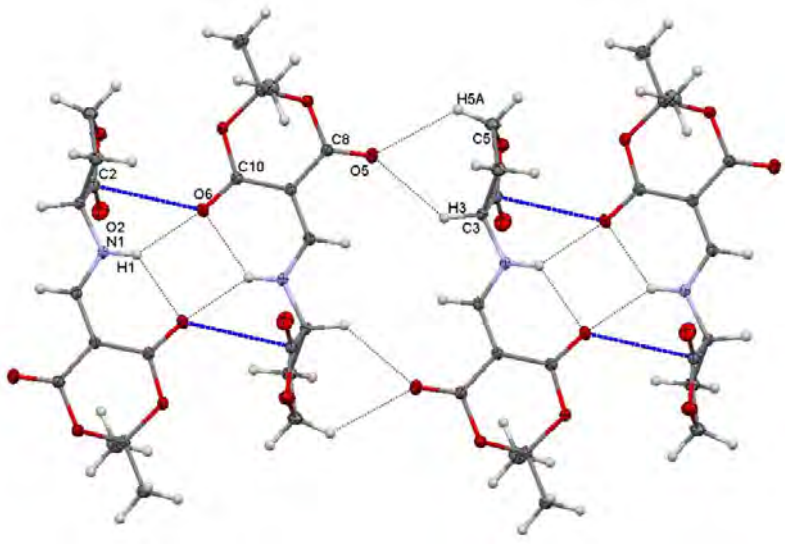

Figure 6.10: Hydrogen bonding and C=O···C=O interactions of compound **100**

Table 6.4: Geometric parameters for hydrogen bonding

Donor–H···Acceptor	D—H (Å)	H···A (Å)	D···A (Å)	D—H···A (°)
N(1)–H(1)···O(6)	0.88	2.15	2.775(2)	128
N(1)–H(1)···O(6)	0.88	2.18	2.901(2)	139
C(3)–H(3)···O(5)	1.00	2.51	3.271(2)	132
C(5)–H(5A)··O(5)	0.99	2.56	3.256(2)	127
C(4)–H(4B)···O(6)	0.99	2.70	3.324(2)	121

6.4.3 Halogen bonding and CO··CO interactions

Example:

3,3-(1,1-Disulfanediylbis(butane-1,1-diyl))bis(5-(dibromomethylene)furan-2(5*H*)-one) (181)

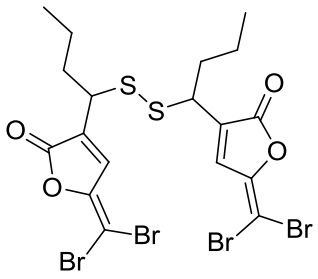

181

The analysis of the crystal structure of **181** reveals the presence of two different types of intermolecular attractions, including halogen bonding and C=O···C=O dipolar contacts. One bromine atom of each bromomethylene group makes halogen bonding contacts with the oxygen atom of the carbonyl group. These doubly „halogen- bonded" bridged chains run almost parallel to the diagonal of the a-c-axis. The geometrical parameters of the contacts are: distance Br···O= 2.90 Å, angle C-Br···O= 165.5°. The lactone carbonyl groups are also involved in C=O···C=O dipolar contacts, which bridge the molecules almost perpendicularly to the direction of the halogen bonding. The two carbonyl groups make short contacts (O···C= 3.09 Å) in an anti-parallel fashion (Figure **6.11**).

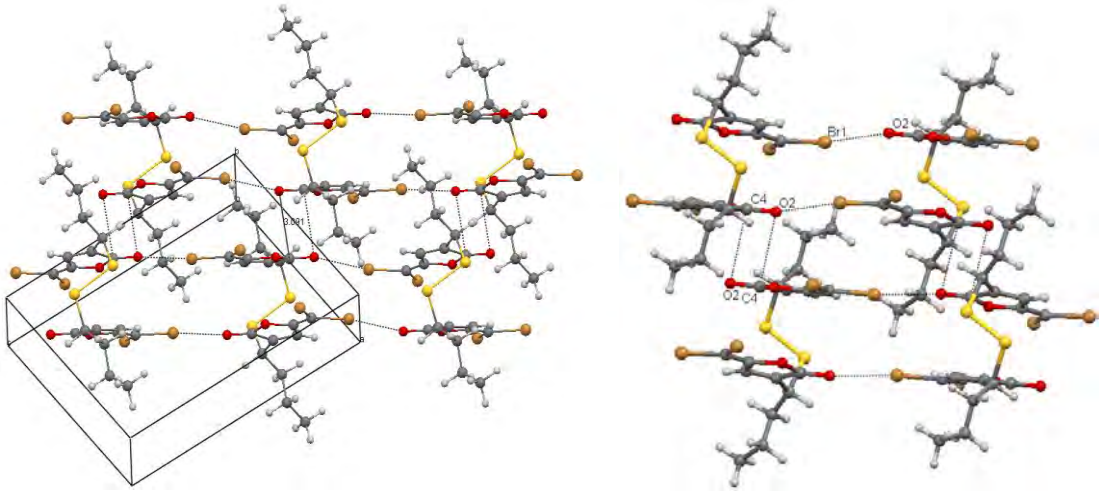

Figure 6.11: a) Halogen bonding and carbonyl-carbonyl dipolar interactions indicated in the unit cell of **181**; **b**) C-Br···O halogen bonded and centrosymmetrically related C=O···C=O dimeric unit of **181**.

6.5 Conclusion

The crystallographic studies clearly indicate that weak interactions such as C-Br··O halogen bonding and C=O···C=O dipolar interactions play an important role, together with hydrogen bonding, in the molecular organisation and packing of crystal structures. Understanding of such crystal packing effects is also gaining impetus in ligand binding studies.[277]

Carbonyl and/or halogen functional groups present in acylated homoserine lactone and fimbrolides have the potential to form weak C=O···C=O dipolar and halogen bonding interactions, which could be utilised in biological recognition events to increase their intermolecular interactions with targeted proteins or DNA. Thus, in addition to their better documented abilities to serve as electron withdrawing substituents or their supposed ‗‗hydrophilic'' properties, carbonyl and halogen groups would contribute to

the design of ligands by providing a framework for the use of these interatomic interaction.[270]

6.6 Part B: Computational protein-ligand docking studies

The majority of the compounds synthesized during the course of this work were based on modification of scaffolds such as acylated homoserine lactone (AHL), fimbrolides and dihydropyrrolones which are known to exhibit quorum sensing inhibitory activities. Thus, the aim of the second part of this chapter was to understand the binding affinity or intermolecular interactions of the novel synthesized molecules with the targeted quorum sensing protein LasR. Using chemoinformatic tools to further understand the molecular binding mechanism would provide important structural information for ligand optimization.

A wide range of chemoinformatic tools for virtual screening are available and can be used to analyze the intermolecular interactions between a protein and a ligand. Virtual screening and structure-based design methodologies are widely used in the pharmaceutical industry, and have contributed to the development of important commercial drugs such as Tamiflu®, Relenza®, Aluviran® and Trusopt®.[278-279] However, one should be cautioned on relying exclusively on computational tools for drug discovery, as the output information obtained from computational platforms depends heavily on the quality of the 3D-protein structures and the algorithms used to calculate the results. Different theories have been developed to generate these computational tools, but they are limited in their accuracy due to limits in both computational resources and knowledge of how ligands and receptors behave *in vivo*. Nevertheless, virtual screening remains a valuable screening tool that can be used to understand protein-ligand interactions.

6.7 Protein-ligand docking

The aim of a docking experiment is to predict the 3D structure (or structures) formed when two or more molecules form an intermolecular complex. It is commonly used to predict the binding conformation of a ligand to its targeted biomolecular receptor. Docking tools for virtual screening have improved significantly in the past decade, with many available theories and methods that are used to construct the docking algorithms. Examples of common docking tools, their approaches to ligand flexibility, and their scoring function used are listed below (Table **6.5**).[280]

Table 6.5: Common docking tools for virtual screening[280]

Method	Ligand flexibility sampling	Scoring function
Dcok	incremental build	force field or contact score
FlexX	incremental build	empirical score
Slide	conformational ensembles	empirical score
Fred (openeye software)	conformational ensembles	Gaussian or empirical score
Gold	genetic algorithm	empirical score
Glide (Schrodinger)	exhaustive search	empirical score
Autodock	genetic algorithm	force field
Ligand fit (Accelrys)	Monte Carlo	empirical score
ICM	Pseudo-Brownian sampling and local minimization	mixed force field and empirical score
QXP	Monte Carlo	force field

For the current work, the Accelrys commercial protein-ligand docking engine *LigandFit* was used. This software is able to analyze the ligand-protein binding conformation and affinity of the synthesized compounds, as well as to dock virtual molecules into the 3D model of the protein target for lead optimization.

For ligand-protein docking, the *LigandFit* docking engine performs two main processes: a) cavity detection to identify any potential binding pockets in the protein; and b) docking of the selected ligand to the site of interest.[281]

The cavity detection step initially employs a space-filling algorithm to identify voids or unoccupied regions in the protein (free points) (Figure **6.12a**). This is followed by the use of an ‗eraser' to etch away ‗outside' points not related to the ‗space pockets', leaving behind possible molecular cavities or binding sites (site points) (Figure **6.12b**).[281]

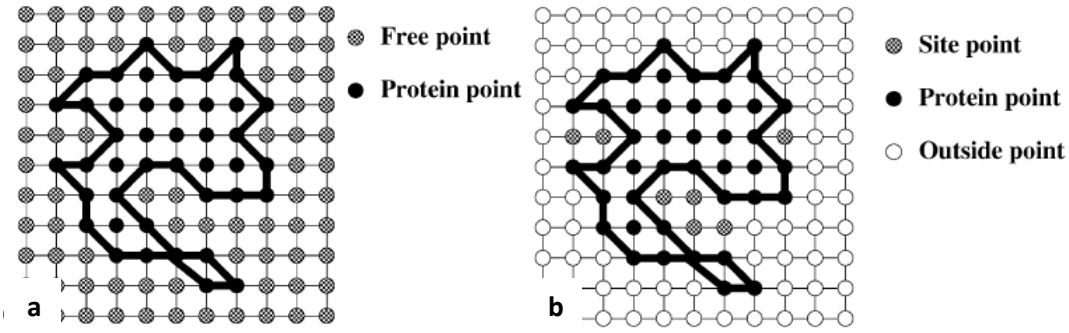

Figure 6.12: A schematic representation of the grid system enclosing the protein a) before, or b) after application of the cavity detection algorithm.[281]

The next part of the screening methodology involves docking of the molecules into the defined binding sites, and evaluating the quality of the ‗fit' through a scoring algorithm. The procedure mainly follows a pre-defined protocol consisting of the following steps: (a) generating different conformations of the ligand with variable torsion angles; (b) ligand shape matching to select the ligand conformation that conforms best to the shape of the pocket site or cavity; and (c) scoring to estimate the binding affinity of the ligand to the protein using a grid-based energy calculation.[281-282]

6.8 Quorum sensing in *Pseudomonas aeruginosa*

The pathogenic Gram-negative bacterium *Pseudomonas aeruginosa* is frequently associated with many chronic bacterial infections in humans. Virulence factor expression of *P. aeruginosa*, including biofilm production, requires the activation of specific genes through a cell-density mediated mechanism of gene expression, termed quorum sensing (QS). In *P. aeruginosa*, two regulatory QS circuits, *rhl* and *las*, are responsible for the production of virulence factors. Each circuit is regulated by their respective signaling molecules, compounds **12** and **19** (Figure **6.13**).[66,41]

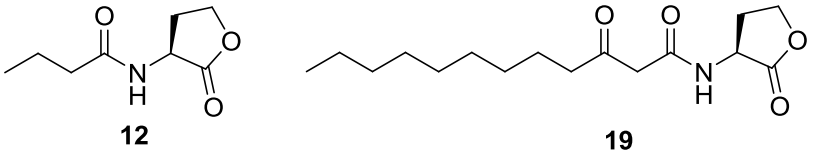

Figure 6.13: Structures of signaling molecules regulating *rhl* and *las* QS circuits in *P. aeruginosa*.

The two circuits complement each other in governing gene expression, with the *las* system directly inducing the expression of *rhl* upon activation. Overall, this hierarchical cascade of event depends largely on the *las* system to coordinate QS-mediated gene expression. The *las*-system encodes two regulatory proteins, LasI and LasR. The former is responsible for the production of the signaling molecule **19**, termed AI1 or 3-oxododecanoyl-HSL (OdDHL). LasR acts as a transcriptional activator, which binds AI1. Upon binding, the LasR-AI1 complex induces dimerization of the tetramer protein leading to transcription of virulence genes.[41]

6.9 The *Pseudomonas aeruginosa* LasR protein

The crystal structure of LasR bound to its signaling molecule was solved by Bottomley *et al* (PDB ID: 2UV0).[283] The resolution data obtained was 1.8 Å, indicating an accurate

representation of the crystal structure. The quality of the structure is highly important in modeling studies, as ambiguities in the crystal structure data can lead to inaccurate model construction in the computational study. The accurately resolved structure of the LasR protein is hence important for this study as it provides visual information regarding the molecular interactions between the LasR protein and its cognate signaling molecule.

6.9.1 Analysis of the LasR-ligand complex

The crystallographic structure of the LasR-ligand complex consists of four protein monomers, each bonded to its signaling molecule, OdDHL **19** (Figure **6.14**). Closer inspection revealed that the LasR crystallographic unit exists as two independent pairs of dimmers, E:G and F:H. The symmetrical protein coordination and the conformation of the ligand exemplify the dimeric arrangement in the unit.[283] The existence of four monomers in the LasR crystallographic unit suggests that all four binding sites must be occupied by ligands for successful folding and dimerization of the tetramers, in order to activate downstream transcription processes.

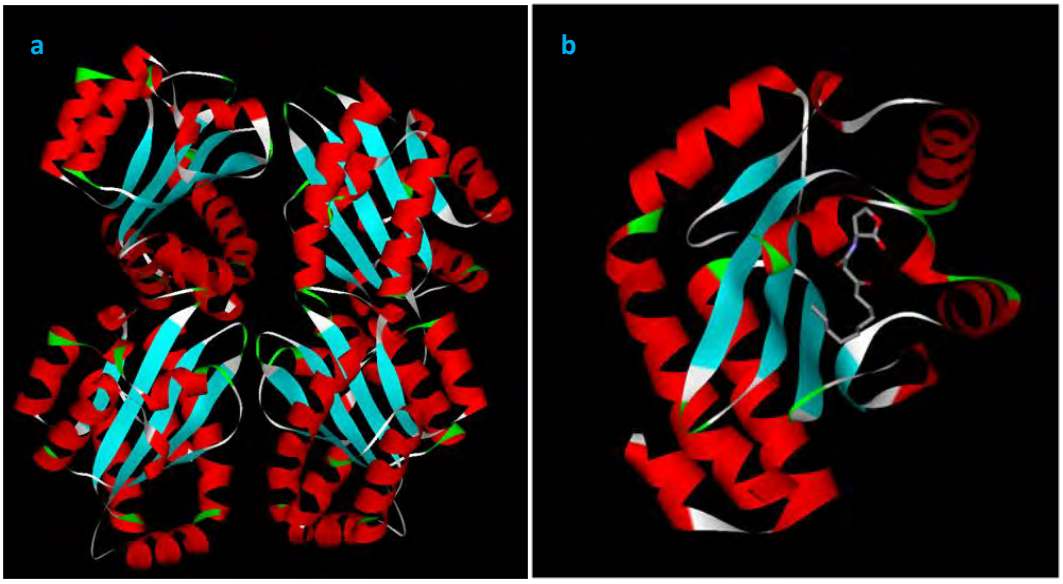

Figure 6.14: a) LasR four protein monomers (E,G, F, H) and b) LasR monomer bound to its signaling molecule.

6.10 Protein-ligand docking protocol

Preparation of the protein: The crystal structure of the quorum sensing protein LasR was retrieved from the protein data bank (PDB) (PDB code, 2UV0, resolution 1.8 Å). The ligand and bound water molecules of crystallization were removed from the binding site. Hydrogen atoms were added to the protein, and the structure was processed using the CHARMm forcefield.

Ligand library preparation: The ligand structures were constructed with the 3D structure generator module, DS Visualizer (Discovery Studio Modeling, Accelrys Software Inc.)

Binding site definition: To define the binding pocket of monomer E of the LasR protein, the LasR autoinducer *N*-(3-oxo-dodecyl)-*L*-homoserine lactone (OdDHL) was used. The binding site of monomer E was defined using an eraser size of 5 Å, which is the optimal size for cavity identification as determined by Venkatachalam *et al*.[281] This

resulted in the identification of the binding site of the ligand with a cavity size of 2051 point units.

Docking process and scoring: The ligands generated were docked into the defined binding site using the default parameters in LigandFit (Discovery Studio Modeling, Accelrys Software Inc.). The docking process resulted in different poses with the relevant docking scores and ligand internal energies as output which was further used for comparison of the different binding poses obtained. After docking, the area within a radius of 5 Å around the ligand was selected for further analysis.

6.11 Validation of protein-ligand docking

The RMSD of all heavy atoms between the ligand (OdDHL) in the protein crystal structure of LasR and the docked OdDHL ligand was 0.19 Å, indicating the reliability of the docking method (Figure **6.15a**).

The binding interactions of the docked ligand to the receptor site show the ligand binding into specific hydrophobic and hydrophilic pockets within the protein. The lactone ‗head' is docked into the hydrophilic pocket and is stabilized by hydrogen bonding to Tyr58, Trp62, Arg63, Asp75 and Ser131, with the aliphatic side chain extending into the hydrophobic pocket bound by Leu36, Gly38, Leu39, Leu40, Tyr47, Val76, Leu125, Gly126 and Ala127 (Figure **6.15b**). These interactions were consistent with the interactions observed between the ligand (OdDHL) and receptor site within the protein crystal structure of LasR (PDB-2UV0).

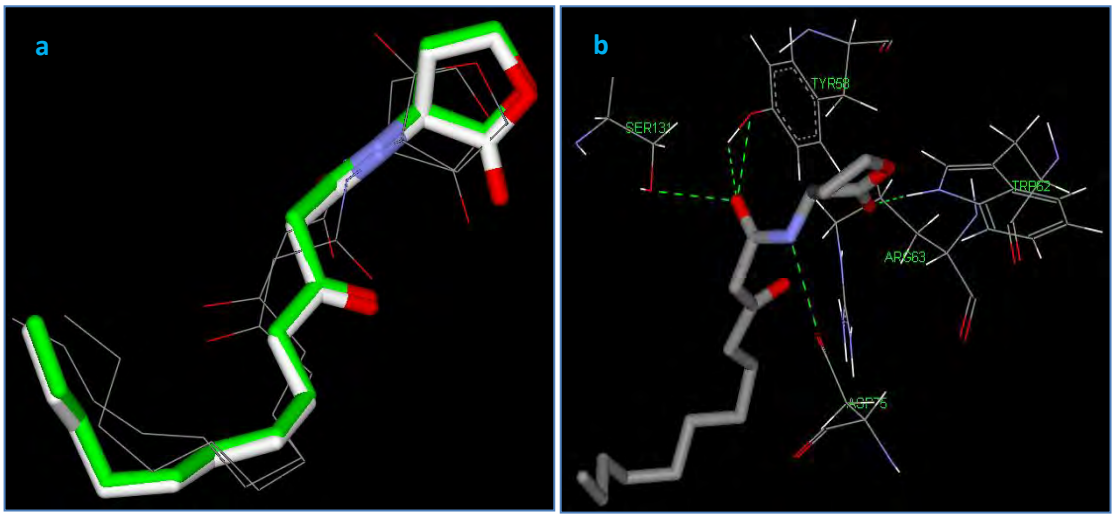

Figure 6.15 a) Superposition of docked ligand poses (green and thin stick model) with reference ligand from crystal structure (white). The RMSD between the best docked ligand poses (green) and the reference ligand (white) was 0.19 Å. b) Representation of LasR:E with the native signaling molecule **28** docked into the receptor site. The atoms of the signaling molecule are displayed as thick lines. The thin lines show different amino acid residues surrounding the binding site. Green dotted lines indicate hydrogen bonding.

6.12 Protein-ligand docking results

Using the docking protocol mentioned above, different classes of QS inhibitor and NO donor hybrids were examined for their ability to bind the receptor protein LasR. Based on the ligand docking experiments, we compared the docking data to the % QS inhibitory activity of the analogues to determine whether a correlation existed between the ligand-binding affinities with the inhibitory activity (activity studies discussed in Chapter 7).

6.12.1 Acylated homoserine lactone (AHL)-based nitric oxide donors

NO-releasing AHL derivatives that mimic the natural QS autoinducers have been synthesized during the course of these studies (Figure **6.16**). Thus, it was important to evaluate the influence of the structural modifications on the binding of the novel AHL derivatives compared to the cognate signaling molecule (OdDHL) in the receptor binding site.

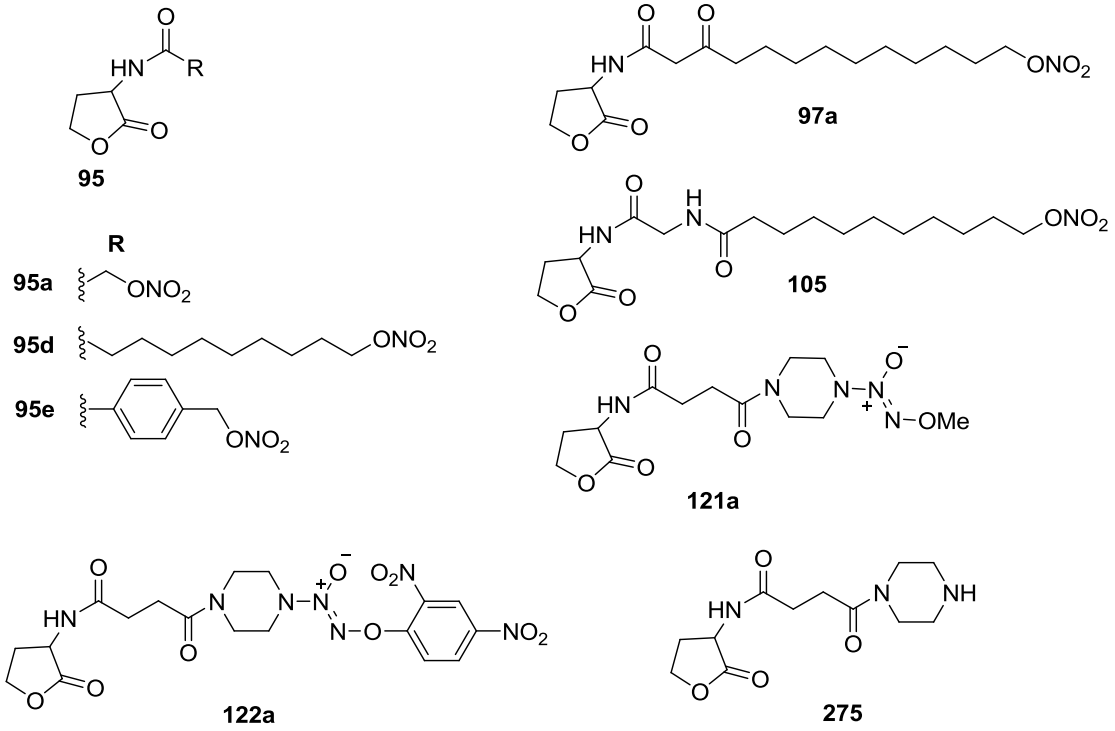

Figure 6.16: Chemical structures of AHL-derivatives used in the study.

The docking protocol ranks the synthesized ligands on the basis of their docking scores and ligand internal energies. Higher docking score values and lower ligand internal energies indicate a stronger ligand binding affinity. The docking results were compared to the *in vitro* quorum sensing inhibitory properties of the compounds (as discussed in Chapter 7) (Table **6.6**).

Table 6.6: Comparison of docking scores and percentage QS inhibitory activities of the AHL NO donor hybrids.

Compound	Docking score	Ligand internal energy (kcal/mole)	% quorum sensing inhibition (at 266 µM)
95a	58.2	–1.4	26.4
95d	72.8	–5.0	70.1
95e	71.0	–1.7	62.2
97a	57.6	–6.7	74.5
105	61.7	–2.6	62.3
121a	72.6	–1.7	43.1
122a	4.5	9.0	57.8
275	66.0	–2.5	Not synthesized
OdDHL (19)	86.4	–4.8	NA

NA-Not antagonist, LasR autoinducer (agonist)

The calculated docking score value is a measure of the predicted binding affinity of the ligand to the receptor. The results show that there is a general correlation between ligand docking score and QS inhibitory activity. This suggests that ligands with stronger binding affinities towards the LasR receptor are better able to exert their QS inhibitory effects, presumably through LasR-mediated QS pathways (Figure **6.17**).

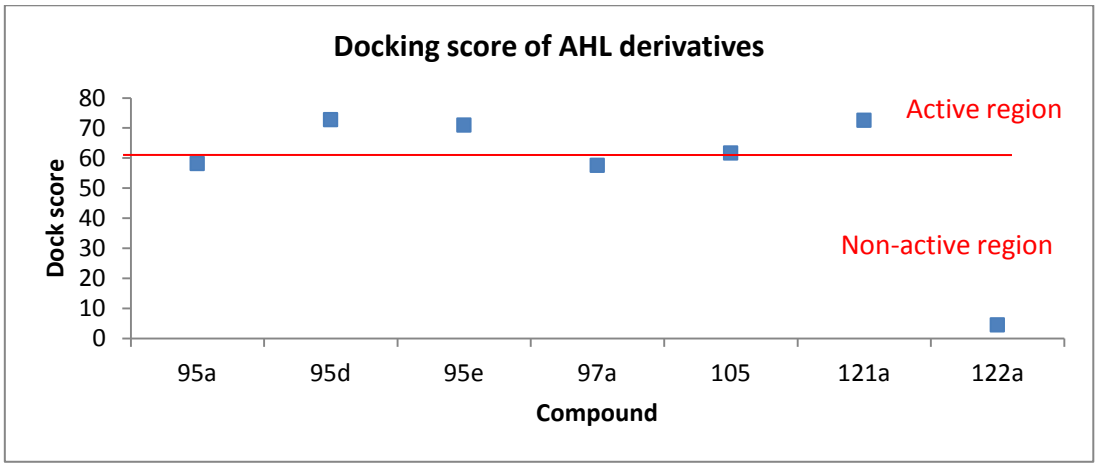

Figure 6.17: Scoring range of active and non-active compounds

However, there are some exceptions to the general correlation. For example, compound **97a** is the most potent QS inhibitor of the series, but had a docking score of only 57.6, which was lower compared to the other active molecules. However, compound **97a** has very low ligand internal energy of –6.7 kcal/mole, which is lower than the ligand internal energy of the autoinducer OdDHL (–4.8 kcal/mole). This means that **97a** has the potential to displace the cognate autoinducer in the binding domain of the protein, which could explain its superior activity in the *in vitro* assay. Thus, this suggests that the different docking outputs can be analyzed together in order to better correlate the docking calculations with the observed *in vitro* activity. Interestingly, **122a** achieved poor values for the docking score and ligand internal energy, and yet exhibited 57% QS inhibition in the biological assay. This could be explained by the fact the **122a** could be metabolized with the release of NO *in vivo*, to form the metabolite **275** which showed a much stronger docking score and ligand internal energy of 66.0 and –2.5 kcal/mole, respectively. Thus, the activity of **122a** could be correlated with its ability to generate high-affinity metabolite **275** *via* NO release.

Further analysis of the docked structures indicates the presence of extensive hydrogen bonding interactions between the synthesized molecules and the ligand binding site.

Compound **95d** had the highest number of intermolecular interactions of the compound studied, with hydrogen bonding to Tyr58, Trp62, Arg63, Asp75 and Ser131. The high number of hydrogen bonding interactions also correlates to the higher dock score and *in vitro* activity of the compound **95d**. Compound **95a** showed hydrogen bonding only with Arg63, which correlates with its low dock score and low *in vitro* activity (Figure **6.18**). In particular, Trp62 and Arg63 were commonly involved in hydrogen bonding with the AHL NO hybrid series.

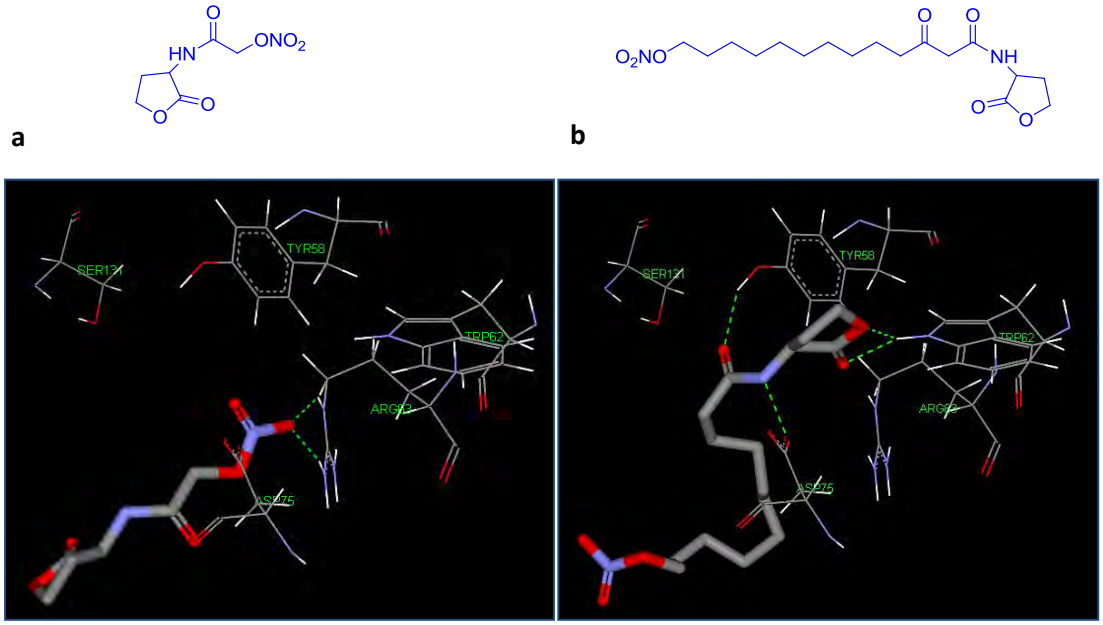

Figure 6.18: Docking poses and hydrogen bonding interactions (green dash) of AHL NO donor hybrids in the LasR protein ligand binding site: a) compound **95a**, b) compound **95d**.

The docking studies highlights the role of alkyl chain length of the compounds in providing a desired orientation in the ligand binding site for optimum hydrogen bonding interaction with the lactone ~~–h~~ead" group. Also bulkier hydrophobic or hydrophilic group as an amide linker gave better dock score compared to a small alkyl group.

6.12.2 Fimbrolide and dihydropyrrolone-based nitric oxide donors

Fimbrolides are a potent class of naturally occurring QS inhibitors. The mechanism of QS inhibition by fimbrolides is still under debate, and may involve different mechanisms as discussed in Chapter 1. One such mechanism is the binding of fimbrolides to the LasR protein, leading to inhibition of bacterial QS functions. Meanwhile, dihydropyrrolone derivatives mimicking the natural fimbrolide have also been studied for their QS inhibitory properties. During the course of this work, series of novel fimbrolide and dihydropyrrolone-based NO hybrids were synthesized (Figure **6.19**). These compounds were docked to the LasR receptor, and the docking results are presented below along with comparison with the QS inhibitory activities of the compounds (discussed in Chapter 7).

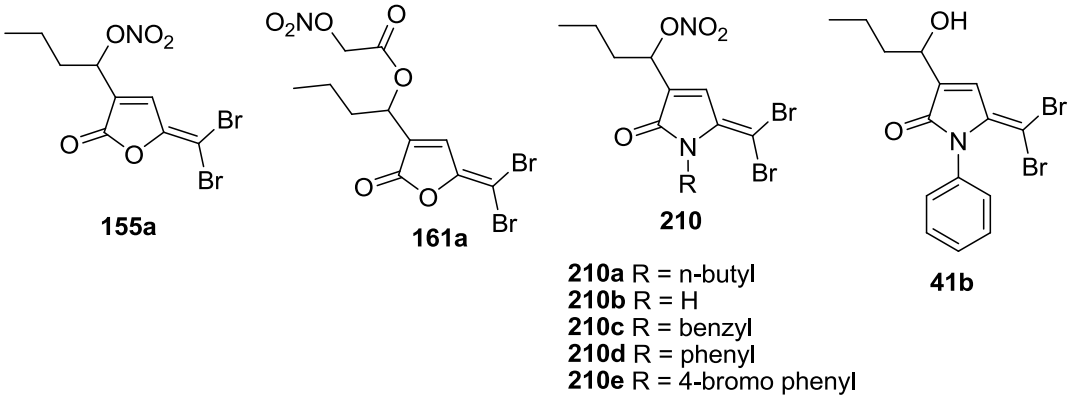

Figure 6.19: Chemical structures of fimbrolide and dihydropyrrolone derivatives used in the study.

The docking scores and ligand internal energies for the fimbrolide and dihydropyrrolone NO hybrids were compared to their *in vitro* percentage quorum sensing inhibitory activities (Table **6.7**).

Table 6.7: Comparison of docking scores and percentage QS inhibitory activities of fimbrolide and dihydropyrrolone NO hybrids.

Compound	Dock score	Ligand internal energy (kcal/mole)	% quorum sensing inhibition
155a	72.6	–2.6	72.3[a]
161a	64.5	–2.8	78.2[a]
210a	72.2	–0.7	29.6[b]
210b	74.6	–2.4	33.4[b]
210c	61.9	0.7	68.9[b]
210d	54.8	1.6	41.0[b]
210e	60.8	–4.6	62.3[b]
OdDHL 18	86.4	–4.8	NA

a-test concentration 88.8 μM, **b**- test concentration 266 μM

The results indicate a weak correlation between the docking and the bioassay studies. The two most active compounds, **155a** and **161a**, had relatively high docking scores of 72.6 and 64.5, respectively, and relatively low ligand internal energy scores of –2.6 and –2.8 kcal/mole, respectively. However, compounds **210a** and **210b** were exceptions to the general trend.

Analysis of the docked structure of the fimbrolide NO hybrid with LasR indicates hydrogen bonding interactions between the ligand and the ligand binding site of the protein. For example, the nitroester group in compound **155a** and furanone ring system in compound **161a** formed hydrogen bonding interactions with Trp62 and Arg63, which were the characteristic amino acid residues involved in hydrogen bonding with the fimbrolide NO hybrids (Figure **6.20**). This similar hydrogen bonding interactions

between compound **155a** and **161a** transpire to the similar *in vitro* activities of these molecules.

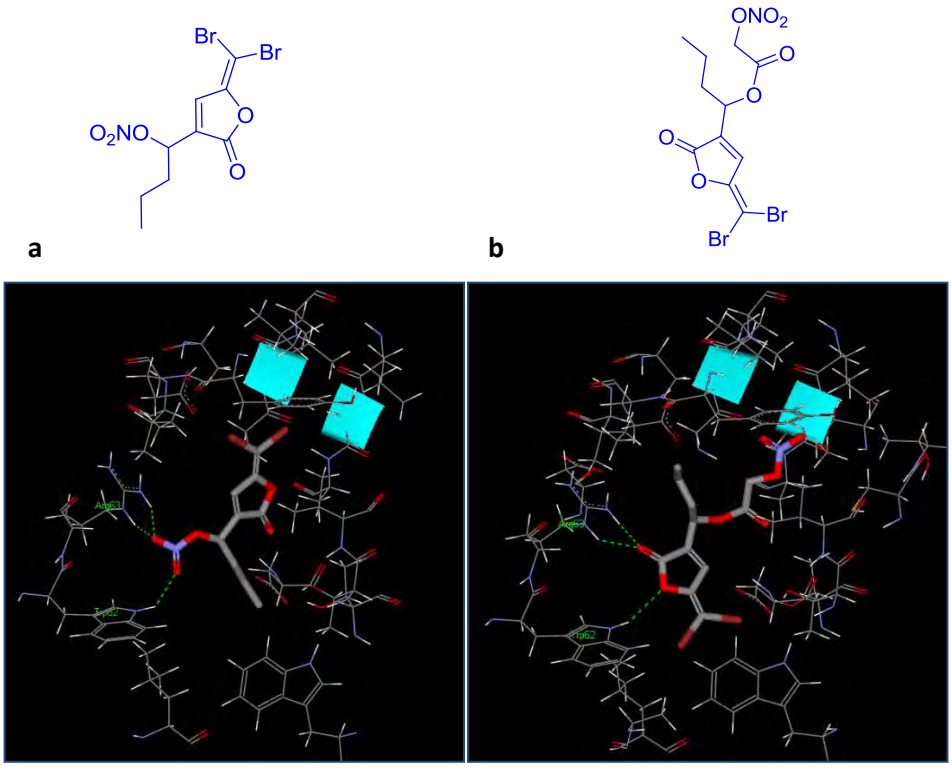

Figure 6.20: Docking poses of fimbrolide NO hybrids in the LasR protein ligand binding site: a) compound **155a** and b) compound **161a**

Similarly, the dihydropyrrolone NO hybrids were predicted to form hydrogen bonding interactions with the LasR ligand binding site. For example, compound **210a** formed hydrogen bonding interactions between the ligand nitroester group and the amino acids Trp62 and Arg63 of the protein. On the other hand, the nitroester group of compound **210c** formed hydrogen bonds only with Arg63 correlating to its low dock score compared to **210a** (Figure **6.21**). Contrary to the dock score the *in vitro* activity of the compound **210c** was higher than compound **210a** highlighting the significance of small alteration in structure and the role of other drug like property such as hydrophilicity in the biological activity of a molecule. Also, in addition to hydrophobic interaction similar

to alkyl chain the benzyl (aromatic) group can be involved in other interactions such as π···πinteractions leading to better *in vitro* activity.

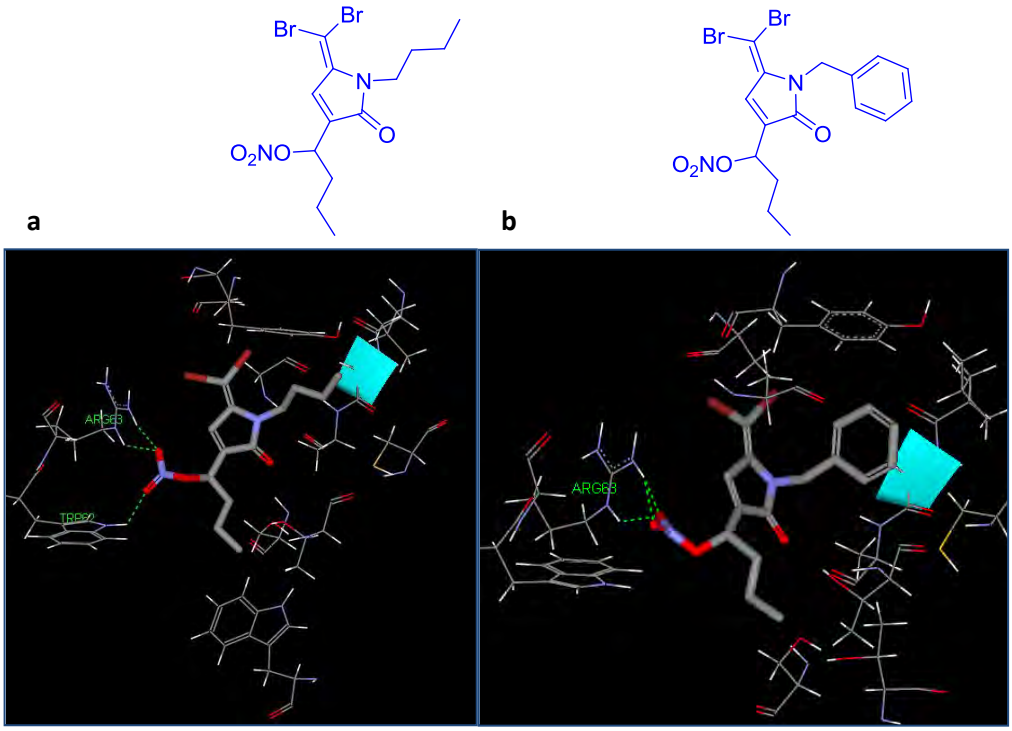

Figure 6.21: Docking poses of dihydropyrrolone NO hybrids in the LasR protein ligand binding site: a) compound **210a** and b) compound **210c**

6.13 Halogen bonding interactions studies

Although fimbrolides displayed similar or even lower binding affinities for the LasR ligand binding domain in the docking studies compared to the AHL and dihydropyrrolone derivatives, they were the most biologically active class of QS inhibitors studied in this work based on the *in vitro* activity. Thus, the unexpected intermolecular interactions observed in the crystal structures of the fimbrolides (described in Part A) could have major implications in the binding of the fimbrolide derivatives to the *Pseudomonas aeruginosa* QS receptor protein LasR. In the absence of an available crystal structure of LasR complexed with a fimbrolide inhibitor, *in silico* molecular docking was used to determine the likelihood of halogen bonding or dipolar

interactions between the fimbrolides and the receptor. Though the docking protocols employed here do not consider halogen bonding or C=O··C=O interactions, the docked poses could be analyzed for the possibility of such interactions. The fimbrolides **155c** and **181** that were crystallized for X-ray studies did not produce any docking score as the docking protocol failed to run during docking studies, indicating the molecule could not be docked to the receptor site. This could be largely due to the size of the ligand being larger than the cavity itself or there exist unfavorable interactions of the compound with the receptor site of the binding cavity. Consequently the model fimbrolide derivatives **156a** and **164** which dock well to the LasR protein autoinducer binding site (LBS) were studied for weak intermolecular interactions.

The docked structures of fimbrolides **156a** and **164** were examined to determine the possibility of halogen bonding and dipolar interactions through assessing the distances between the basic oxygen or carbonyl groups in the LasR-LBS with the bromine or carbonyl groups of the docked compounds, respectively. Interatomic distances around the van der Waals radii for halogen bonding (Br···O) (R_{vdw} = 3.37 Å ≈ 3.4 Å) and for dipolar interactions *d*(C··O) (< 3.6 Å between the two >C=O) were considered based on literature (Figure **6.22** and Table **6.8**).[270,275]

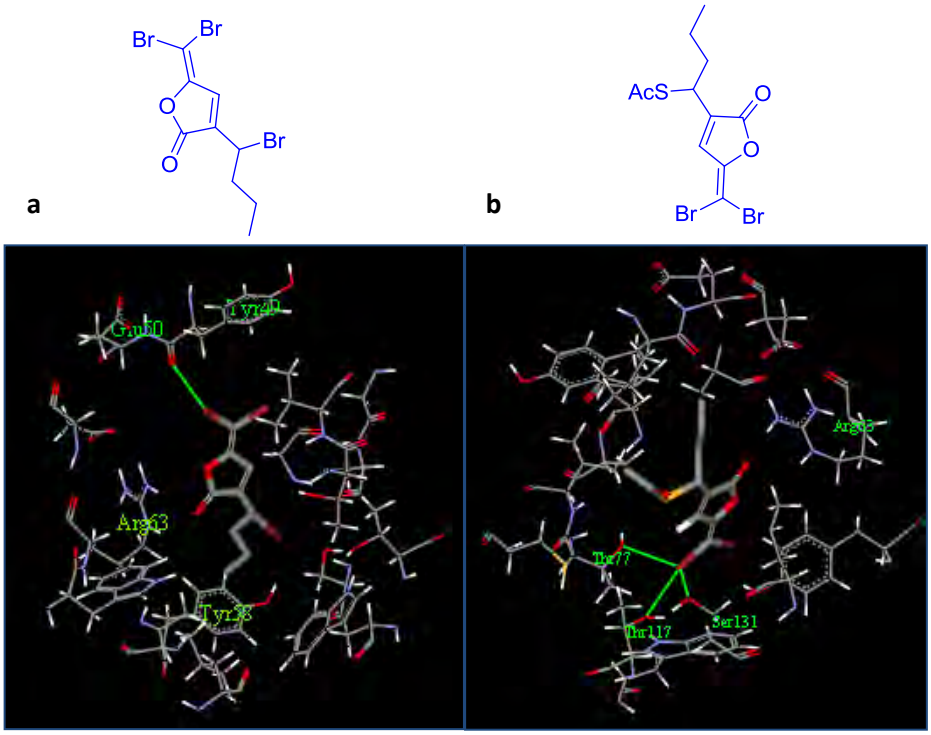

Figure 6.22: Computational models showing distances < 3.5 Å between Br atoms of the ligand and OH or C=O groups of the LasR-LBS for a) compound **156a** and b) compound **164**.

Table 6.8: Summary of (Br···O) distances in the LBS of the docked fimbrolide-LasR complexes.

Protein	**Ligand**	**Halogen**	**Electron donor**	***d*(Br···O) Å**
LasR (PDB ID-2UV0)	**156a**	Br1	Tyr49 (C=O)	2.89
	164	Br2	Thr77 (OH)	2.98
			Thr117 (OH)	3.30
			Ser131 (OH)	3.40

Analysis of docked structures showed that the protein C=O (Tyr49) and OH (Thr77, Thr117, Ser131) moieties were close enough (2.8–3.4 Å) to the bromine atoms of the fimbrolides **156a** and **164** to form halogen bonds. This suggests that halogen bonding could play a role in the interaction between fimbrolides and the QS receptor. However,

no protein carbonyl groups were close enough to the fimbrolide carbonyl group for a dipolar interaction. Further studies, such as obtaining the X-ray crystal structure of a fimbrolide-LasR complex and/or further computational analysis, will be required to elucidate the role of halogen bonding in the binding affinity of the fimbrolide derivatives to the protein receptor.

6.14 Conclusions

The docking studies carried out on the QS inhibitors synthesized in this work with the LasR protein indicate a general correlation between the docking scores of the molecules and their biological efficacies. The molecules were predicted to form hydrogen bonding interactions with the protein through their C=O, NH or nitroester (ONO_2) moieties. For LasR, the most common amino acids in the ligand binding domain involved with hydrogen bonding interactions were Trp62 and Arg63. These docking studies can contribute to understanding the biological activities of the molecules, and the results suggest that the compounds exert their QS inhibitory effects presumably through LasR-mediated QS pathways.

Analysis of the docked fimbrolide-LasR complex revealed the possibility of halogen bonding within the ligand binding domain of the protein, suggesting the significance of the halogen group for the biological activity of the fimbrolides. Obtaining the protein–inhibitor crystal structure and/or further molecular or quantum mechanical studies will be required to understand these weak interactions in greater detail.

In summary, the studies carried out in this chapter indicate that functional groups such as halogens, carbonyl and nitrates are involved in weak intermolecular interactions that play a significant role in the solid state crystal interactions of the molecule. The docking studies show that these functional groups can also be important for protein binding, and

the careful positioning of such functional groups in a molecule can potentially increase the selectivity and potency of the compound. The conclusions drawn from the X-ray crystallographic and docking studies for the QS inhibitors synthesized in this work could be useful for the future design of novel biologically active molecules.

Chapter 7
Biological and chemical evaluation

7.1 Introduction

A wide range of compounds based on quorum sensing (QS) inhibitor scaffolds have been conjugated with nitric oxide (NO) donors during the course of this thesis. It was thus important to understand how these structural changes affect the QS inhibitory activities or the NO-releasing properties of the novel dual action QS-NO hybrids. This chapter describes the biological efficacy studies of the acylated homoserine lactone (AHL), fimbrolide, or dihydropyrrol-2-one-based NO hybrids. Furthermore, the NO-releasing properties of the novel indole-based nitric oxide donors were investigated. The studies are divided into three major sections:

i) The effect of the novel compounds in inhibiting the quorum sensing in Gram-negative bacteria, particularly the AHL-mediated signaling pathways was investigated.

ii) The NO release profiles of synthesized nitric oxide donors and their effect on microbial nitric oxide pathway.

iii) The effect of the selected compounds in controlling biofilm growth or biofilm dispersion.

7.2 Quorum sensing inhibition assay

7.2.1 Assay method

The synthesized compounds were analysed using the QS inhibitory screening system developed by Hentzer *et al*.[67] It uses the QS monitor strain *P. aeruginosa* MH602, which carries a plasmid containing a reporter gene (*gfp* (ASV)) fused to the promoter of the

quorum sensing regulated gene *lasB* from *P. aeruginosa*. The half life of Gfp (ASV) is approximately 110 minutes, allowing online monitoring of changes in gene expression over a time span of a few hours.

When the gene encoding the modified Gfp (ASV) fused to a promoter is positively regulated by quorum sensing (such as the *lasB* promoter), the elevated expression of the quorum sensing-controlled gene will result in an increase in fluorescence. The reporter plasmid is carried in the wild-type strain *P. aeruginosa* PAO1, which produces its own AHLs. The reporter construct, P*lasB::gfp*, is therefore induced in this strain and an increase in Gfp production can be observed during the normal growth of the strain. The addition of a quorum sensing inhibitor to this bioreporter will result in a lowered expression of Gfp (ASV) to an extent that correlates with the efficiency of the inhibitor.

The assay is performed by measuring the Gfp output in fluorescence units in the presence of the inhibitor compounds at various concentrations, and the degree of inhibition is determined by comparison with Gfp expression in control cells in the absence of inhibitor. The final concentration of the inhibitors for this assay ranged from 1000 μM to 1.3 μM, and the plates were incubated in a microtitre plate reader, Wallac Victor^2 (Perkin Elmer). No inhibitor was added to the last row of the plate and hence was used as a control. The measurements were made every 30 min over 15 h for the cell growth (OD600) and the expression of Gfp (fluorescence, excitation 485 nm, emission 535 nm).

In order to compare the relative strength of the inhibitors, the percentage quorum sensing (QS) inhibition values were calculated and compared to the control without inhibitor, at concentrations exhibiting less than 15% growth inhibition on the bacterial host. This latter point is important as it excludes QS inhibitory effects that are due to

inhibition on bacterial growth or viability, and therefore identifies those compounds that have specific QS inhibition activities. The untreated control value was considered as 0% QS inhibition and the percentage inhibition was calculated at the time point of about 8–9 h corresponding to the maximum QS activity in the untreated control. Thus, the potency of a compound as a QS inhibitor is directly correlated with its calculated percentage of QS inhibition.

Initially, the assay was performed on two standard QS inhibitors, (Z)-4-bromo-5-(bromomethylene)-3-butylfuran-2(5H)-one **34a** and (Z)-4-bromo-5-(bromomethylene)-furan-2(5H)-one **37** (comp 30). Compound **34a** is a natural fimbrolide derivative from *Delisea pulchra* which is known to be a potent QS inhibitor.[92] Compound **37** is a synthetic QS inhibitor and is considered as one of the ‗gold standards' for QS inhibition studies.[105]

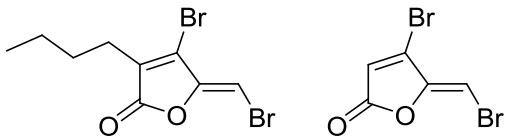

34a **37**

Figure 7.1: Structures of standard QS inhibitors **34a** and **37**.

The data is presented graphically below as the Relative Fluorescence Units (RFU) and OD values observed during the course of the assay (Figure **7.2** and **7.3**). The RFU/OD ratio is also calculated to correct for differences in growth observed at given time points.

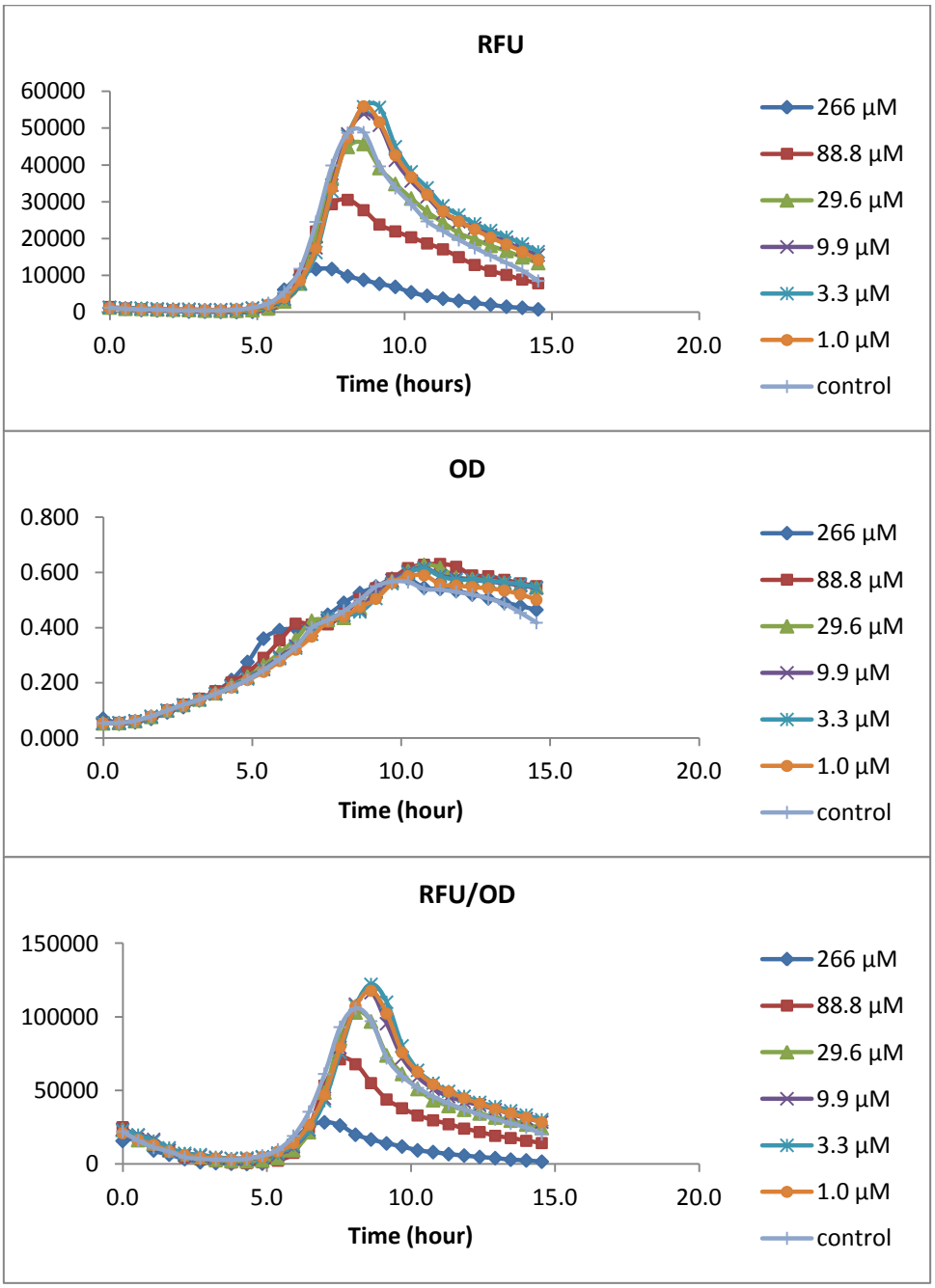

Figure 7.2. Biological screening assay for QS inhibition by known natural fimbrolide **34a**. Upper: Relative Fluorescence Units (RFU), centre: optical density (OD) and lower: RFU/OD as a function of time. The monitor strain *P. aeruginosa* PAO1 harbouring the P*lasB::gfp* (ASV) fusion plasmid was employed.

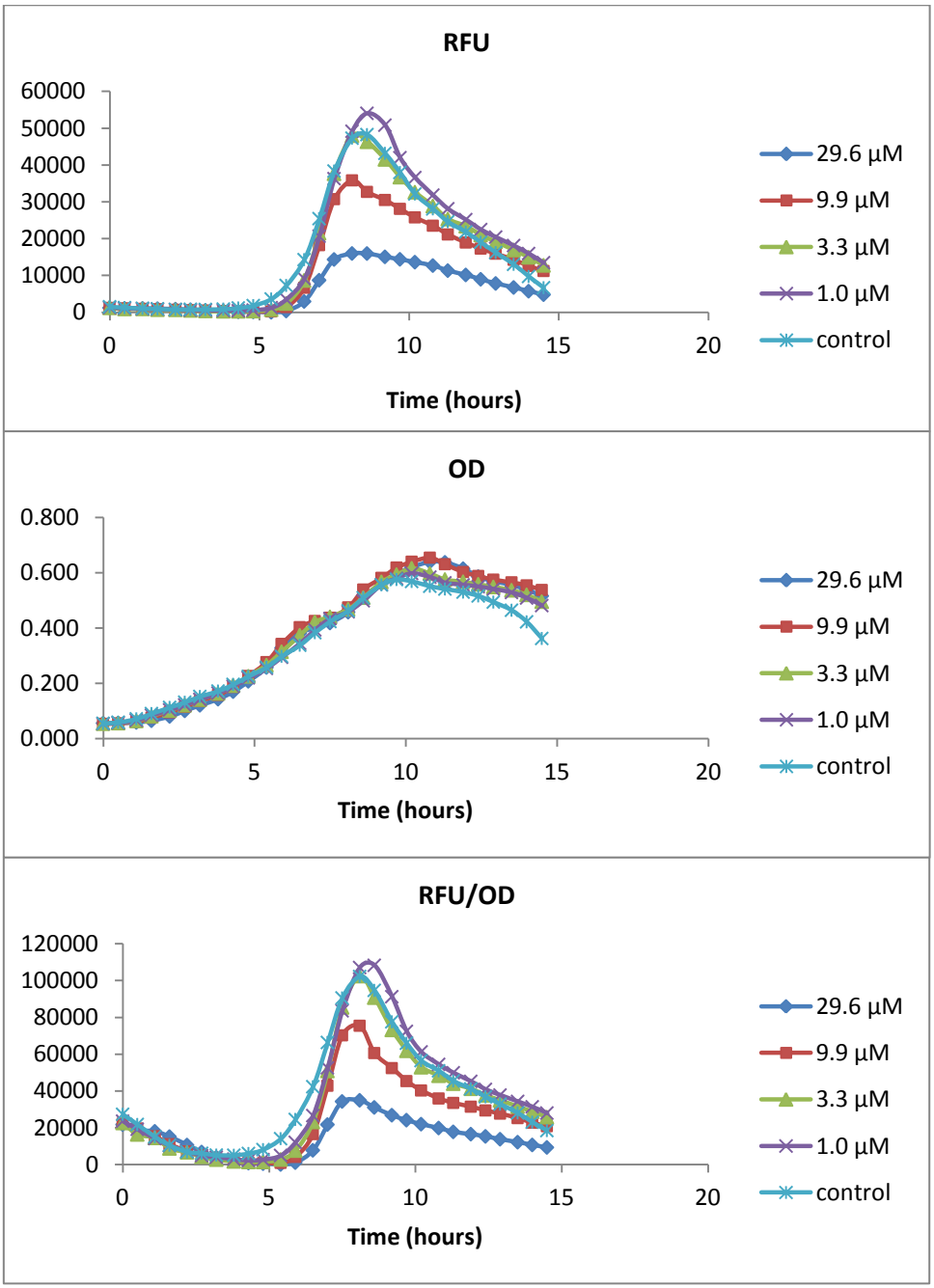

Figure 7.3. Biological screening assay for QS inhibition by known synthetic furanone **37**. Upper: Relative Fluorescence Units (RFU), centre: optical density (OD) and lower: RFU/OD as a function of time. The monitor strain *P. aeruginosa* PAO1 harbouring the P*lasB::gfp* (ASV) fusion plasmid was employed.

The percentage QS inhibition (based on RFU) values of the two compounds at various concentrations measured at the highest QS activity time point (8 h) in control is tabulated in Table 7.1

Table 7.1: Percentage quorum sensing inhibition at different concentration for standard compounds.

Compound	Concentration (µM)					
	266	**88.8**	**29.6**	**9.9**	**3.3**	**1.0**
34a	75.8	39.9	5.9	NA	NA	NA
37	GI	GI	61.9	29.8	3.7	NA

NA- No activity (No reduction in RFU compared to control), **GI**- Growth inhibition of test species MH602 (greater than 15%)

From the results, it is evident that of the two standard compounds, compound **37** has a higher QS inhibition potency. At 29.6 µM, compound **37** inhibited QS activity by 62%, compared to only 6% for compound **34a**. It was also interesting to note that compound **37** was more toxic to the test species with growth inhibition (> 40%) at 88.8 µM, whereas compound **34a** did not affect the growth of the bacterial host even at 266 µM.

7.2.2 Screening results

7.2.2.1 AHL-based nitric oxide donors

The QS inhibitory assay was performed on the following AHL based compounds (Figure **7.4**) and the results of this assay are presented in Table **7.2**. The representative RFU, OD and RFU/OD data for compound **97a** is presented in Figure **7.5**.

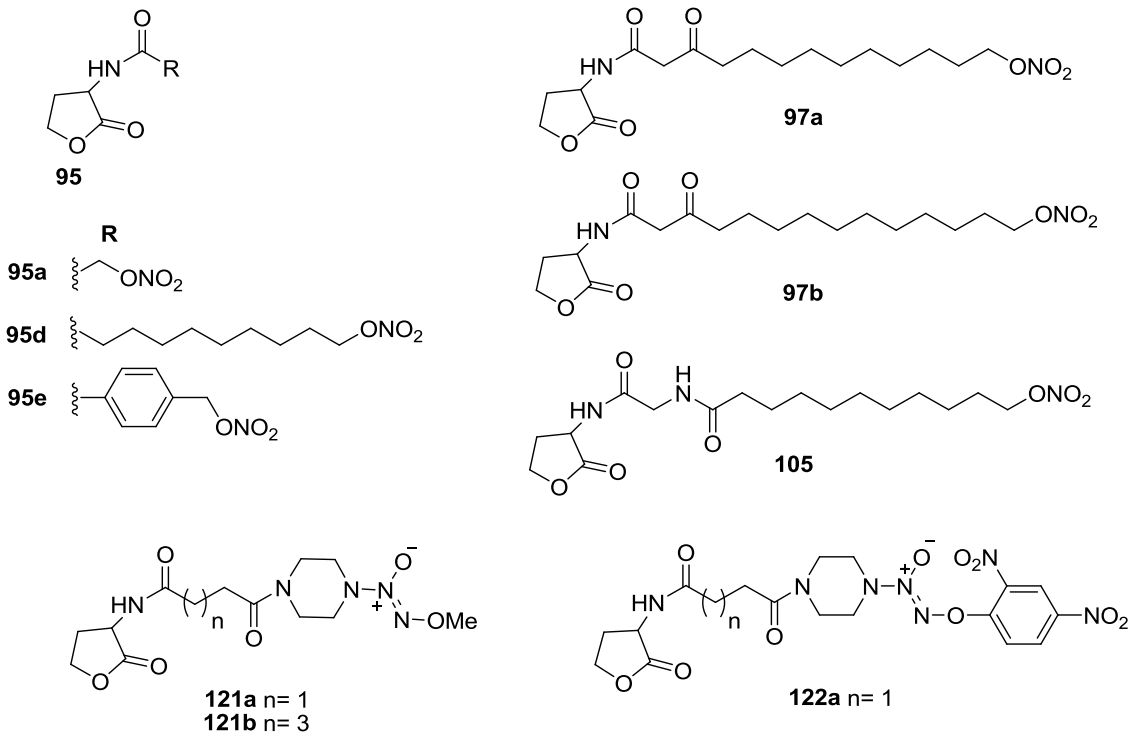

Figure 7.4: AHL-based derivatives screened for QS inhibitory activity.

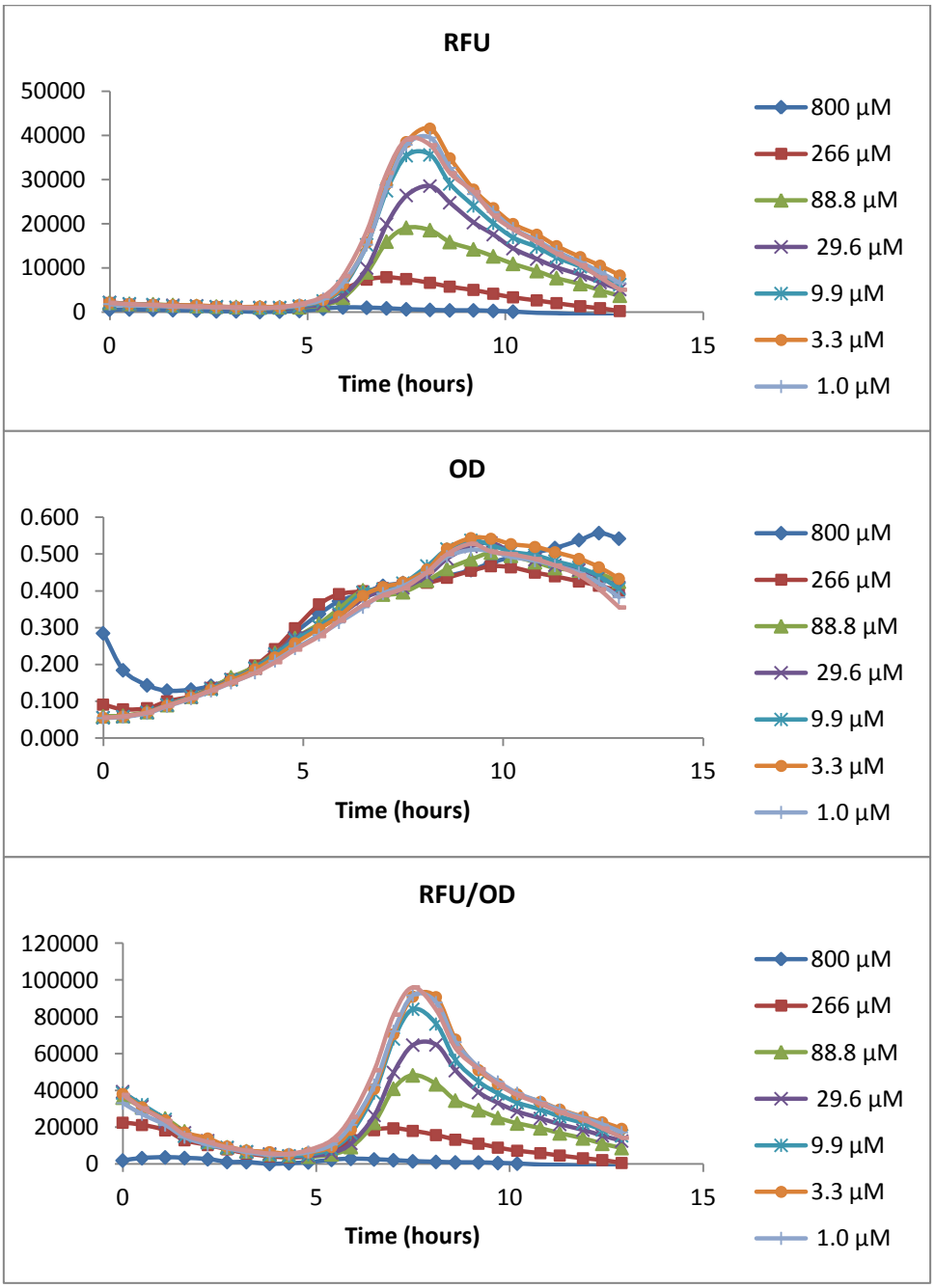

Figure 7.5. Biological screening assay for QS inhibition by AHL derivative **97a**. Upper: Relative Fluorescence Units (RFU), centre: optical density (OD) and lower: RFU/OD as a function of time. The monitor strain *P. aeruginosa* PAO1 harbouring the P*lasB::gfp* (ASV) fusion plasmid was employed.

Table 7.2: Percentage quorum sensing inhibition at different concentrations of AHL derivatives.

Compound	Concentration (µM)					
	266	**88.8**	**29.6**	**9.9**	**3.3**	**1.0**
95a	26.42	5.56	NA	NA	NA	NA
95d	70.07	25.20	NA	NA	NA	NA
95e	62.18	14.16	NA	NA	NA	NA
97a	74.45	47.07	29.90	8.68	1.41	2.86
97b	59.99	20.08	1.08	NA	NA	NA
105	62.26	20.36	4.08	NA	NA	NA
121a	43.07	13.63	2.93	NA	NA	NA
121b	41.66	13.85	2.49	2.07	NA	NA
122a	57.85	25.43	11.77	3.32	0.34	0.41

NA- Not active (No reduction in RFU compared to control)

The comparison of results above indicates that **97a**, highlighted in green, is the most potent AHL derivative in the series, followed by **95d** and **95e**. Significantly, compound **97a** had no effect on growth even at the highest concentration of 800 µM. This result is consistent with the expected outcome as the non NO-substituted AHL backbones of **97a** and **95d** have the greater resemblance to the natural signaling molecule OdDHL **18** recognized by the LasR receptor protein. The activity of **95e** is in accordance with literature studies, which have reported acylated phenyl homoserine lactone derivatives exhibiting potent QS inhibitory activities.[82] Notably, the 3-oxo-AHL analogue **97a** shows better activity in comparison to the non 3-oxo-AHL analogue **95d**. In the case of the diazeniumdiolate AHL derivatives, the bulkier O^2-protected diazeniumdiolate

derivative **122a** displays better QS inhibition compared to the other diazeniumdiolate derivatives.

In summary, the results show that bulkier hydrophobic substitution on the acylated homoserine lactone scaffold is more conducive for inhibitory activity, possibly due to better complementarities with the hydrophobic pocket of the LasR receptor protein, leading to superior inhibition of AHL-mediated QS pathway.

7.2.2.2 Fimbrolide-based nitric oxide donor

The fimbrolide-based NO hybrid derivatives (Figure **7.6**) were screened for biological activity using the same methodology as described above. The results of this assay are presented in Table **7.3** and the representative RFU, OD and RFU/OD data for compound **155a** is presented in Figure **7.7**.

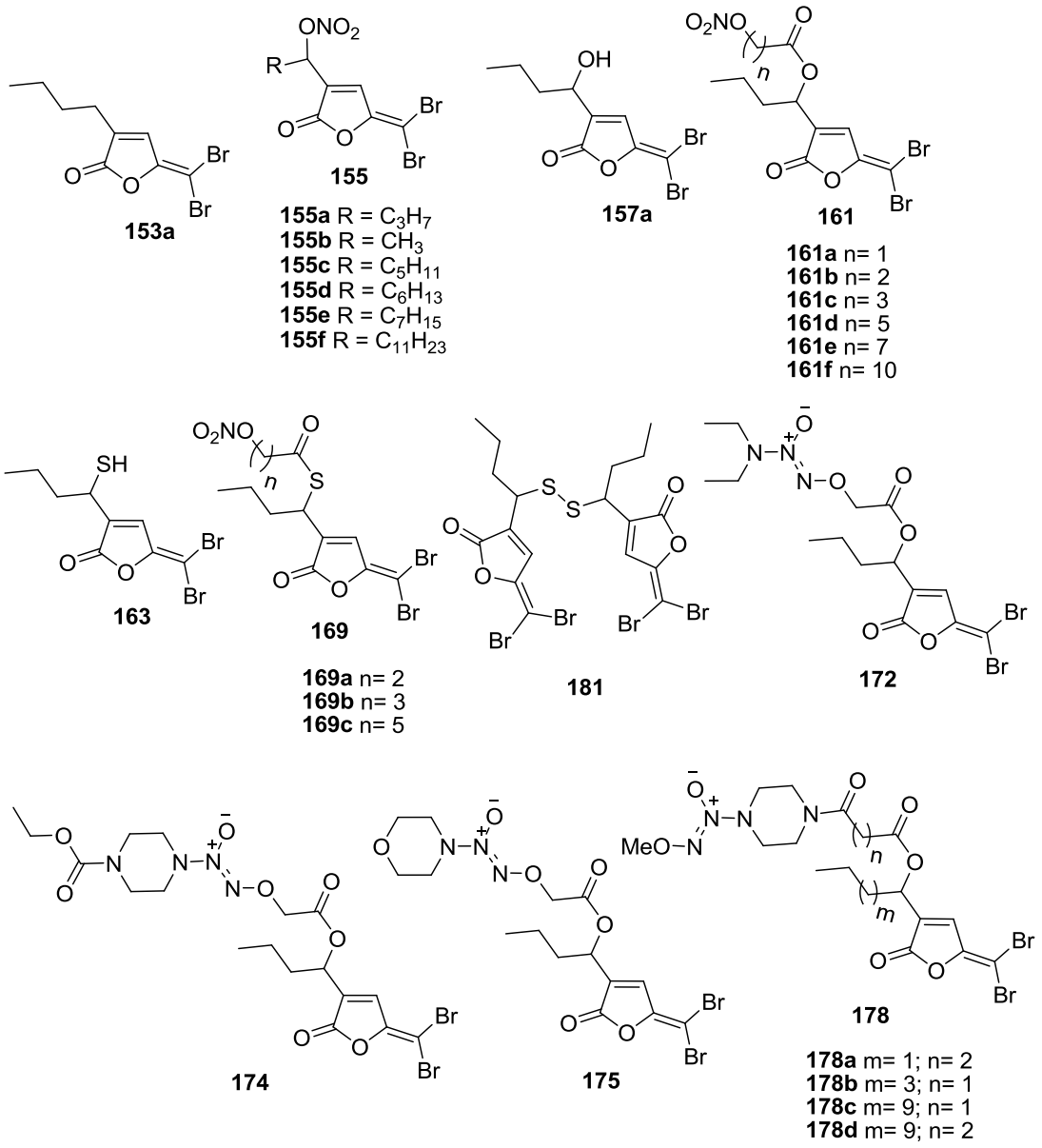

Figure 7.6: Fimbrolide-based derivatives screened for QS inhibitory activity.

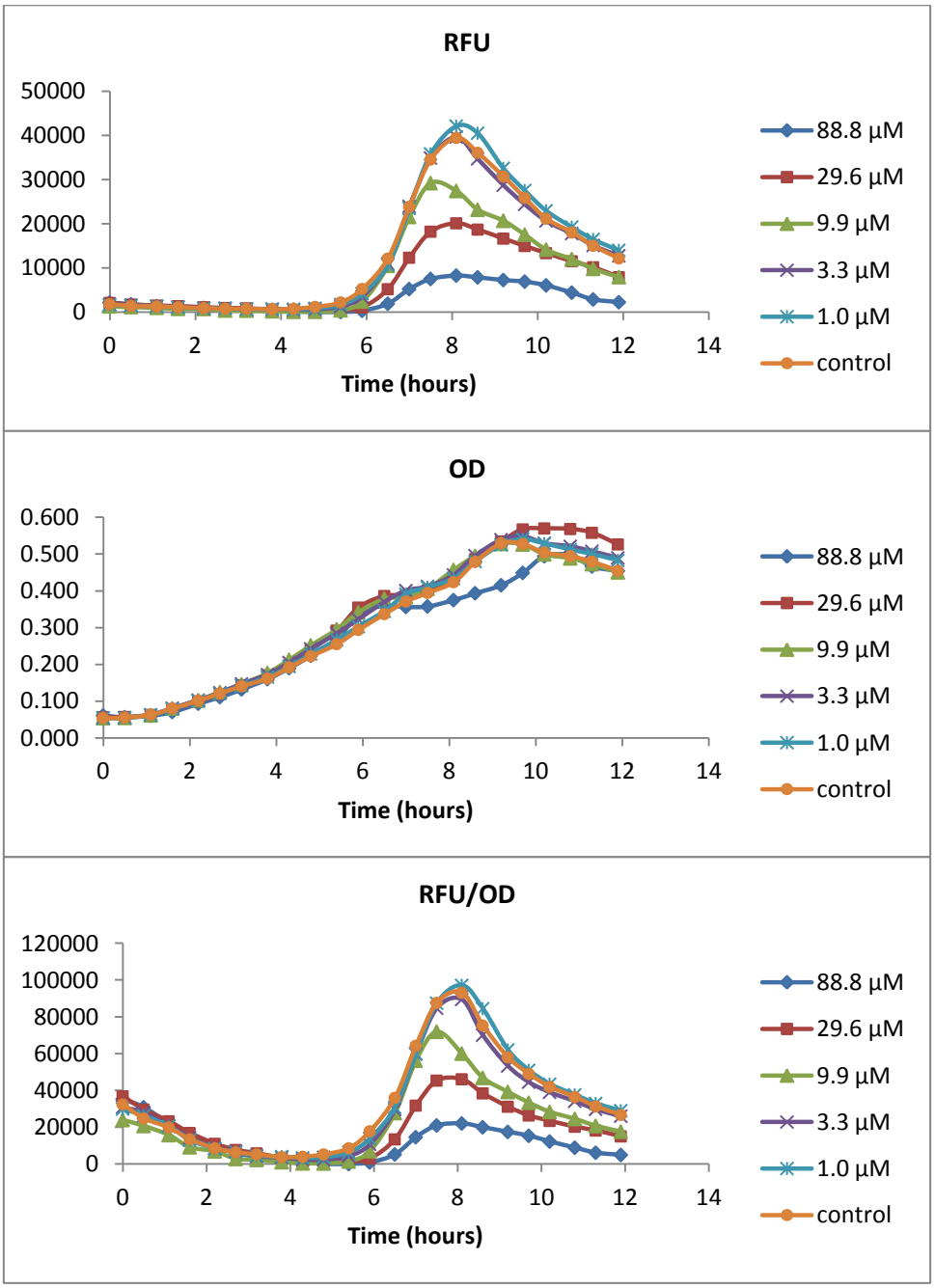

Figure 7.7. Biological screening assay for QS inhibition by fimbrolide derivative **155a**. Upper: Relative Fluorescence Units (RFU), centre: optical density (OD) and lower: RFU/OD as a function of time. The monitor strain *P. aeruginosa* PAO1 harbouring the P*lasB::gfp* (ASV) fusion plasmid was employed.

Table 7.3: Percentage quorum sensing inhibition at different concentrations of the fimbrolide derivatives.

Compound	Concentration (µM)					
	266	**88.8**	**29.6**	**9.9**	**3.3**	**1.0**
153a	72.69	36.31	11.47	NA	NA	NA
155a	GI	72.25	44.80	27.82	NA	NA
155b	GI	GI	26.46	5.46	NA	NA
155c	GI	60.87	39.43	16.27	NA	NA
155d	67.68	34.19	10.33	NA	NA	NA
155e	57.87	17.52	NA	NA	NA	NA
155f	69.84	33.88	0.85	NA	NA	NA
157a	84.67	58.23	32.02	10.63	3.29	0.36
161a	88.98	78.17	57.22	23.65	NA	NA
161b	80.12	60.55	38.40	7.15	NA	NA
161c	55.42	29.01	12.95	6.29	NA	NA
161d	55.44	17.47	4.25	NA	NA	NA
161e	45.73	11.73	NA	NA	NA	NA
161f	56.33	23.72	9.88	3.66	NA	NA
163	50.51	17.85	4.29	1.50	NA	NA
169a	69.71	50.17	30.89	NA	NA	NA
169b	55.94	6.75	NA	NA	NA	NA
169c	51.08	8.50	NA	NA	NA	NA
172	74.45	53.31	25.34	3.12	NA	NA
174	72.71	48.83	25.81	6.57	NA	NA
175	75.38	51.79	18.01	NA	NA	NA
178a	70.69	40.38	15.89	1.26	NA	NA

178b	67.25	47.22	28.33	12.55	3.77	NA
178c	44.57	2.53	NA	NA	NA	NA
178d	44.32	3.58	NA	NA	NA	NA
181	68.57	29.61	7.76	NA	NA	NA

NA- No activity (no reduction in RFU compared to control), **GI**- Growth inhibition of MH602 (greater than 15%)

Fimbrolides are a well known class of marine natural product that are known for potent QS inhibitory activity, and as expected fimbrolide based NO hybrids showed promising results in the biological assay. The most active QS inhibitor in the series was **161a** with 78% QS inhibition at 88.8 μM, followed by **155a** with 72% QS inhibition at 88.8 μM.

Substitution at the C1′-position of the alkyl side chain was observed to have a positive effect on the QS inhibition activity, with the nitroester substituted compound **155a** and the hydroxy- substituted compound **157a** showing higher activity in comparison to compound **153a**. For the series **155,** the increased alkyl carbon chain length at the C3 position led to a decrease in QS inhibition. Furthermore, the growth inhibition effect of the compounds decreased as the alkyl chain length increased. This could be due to the lower molecular weight molecules such as **155b** can interact with multiple targets within the bacterial cell due to its smaller size, leading to toxic effects.

Ester and thioester nitrate derivatives **161a** and **169a** that contain shorter linker regions showed better activity in comparison to the derivatives **161f** and **169c** that contained longer ester/thioester linkers. This is possibly due to steric hindrance of the bulkier ester/thioester linker group, which could limit interaction with the molecular target LasR.

The fimbrolide diazeniumdiolate derivatives **172**, **174** and **175** showed activity of about 50% inhibition at 88.8 µM. The QS inhibition activity was not affected by the type of amine precursor of the attached diazeniumdiolate, indicating that the nature of the diazeniumdiolate group may not be the deciding factor for the activity of compound. For the acid-linked diazeniumdiolate series **178**, the alkyl chain length on the fimbrolide skeleton was an important factor for the QS inhibition activity rather than the piperazine diazeniumdiolate derivative, as the 4 and 6-carbon chain derivatives **178a** and **178b**, respectively, had superior activity compared to the 12-carbon alkyl derivatives **178c** and **178d**.

In general, appending of NO donors to the fimbrolide derivative led to an increase in QS inhibitory activity which was evident from the higher QS inhibitory activity of fimbrolide NO hybrids. Fimbrolide derivatives with shorter alkyl chains and with substitution at the C-α-position (C1′) were the most potent inhibitors. Furthermore, longer alkyl chain lengths result in weaker growth inhibition. Thus, a compromise between QS inhibitory activity and growth inhibition may be maintained by controlling the chain length in order to achieve a desired biological effect. In case of the C-α-substituted derivatives, smaller hydrophobic or hydrophilic substituents resulted in stronger QS inhibition compared to larger hydrophobic or hydrophilic substituents.

7.2.2.3 Dihydropyrrolone-based nitric oxide donors

The dihydropyrrolone-based NO hybrid derivatives and their precursors (Figure **7.8**) were screened for biological activity using the same methodology as described above. The results of this assay are presented in Table **7.4**.

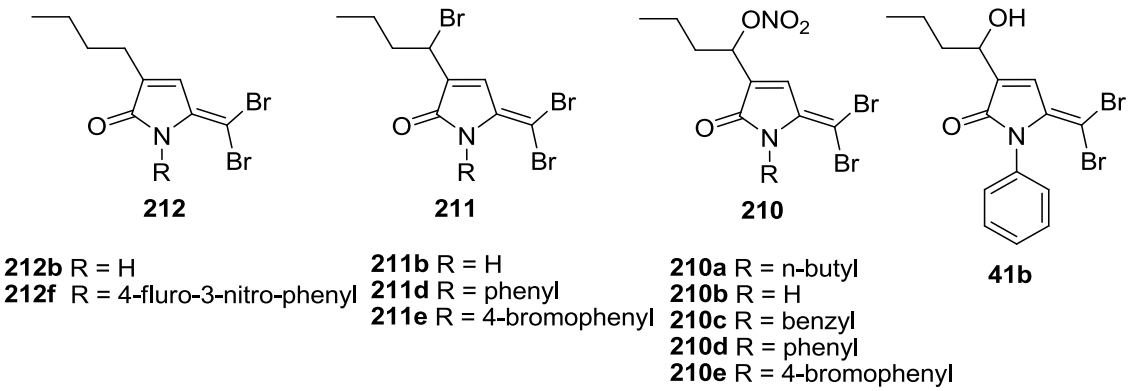

Figure 7.8: Dihydropyrrolone-based derivatives screened for QS inhibitory activity.

Table 7.4: Percentage quorum sensing inhibition at different concentrations of dihydropyrrolones derivatives.

Compound	Concentration (µM)			
	266	**88.8**	**29.6**	**9.9**
212b	41.26	2.00	NA	NA
212f	53.44	16.52	NA	NA
211b	71.58	35.07	15.01	NA
211d	68.60	33.07	10.67	NA
211e	46.87	9.69	NA	NA
210a	29.57	12.65	6.11	NA
210b	33.36	8.67	NA	NA
210c	68.92	29.09	10.56	NA
210d	70.09	27.81	4.76	NA
210e	40.95	9.05	NA	NA
41b	62.32	23.04	13.27	NA

NA- No activity (no reduction in RFU compared to control)

The most active of the dihydropyrrolone derivatives was compound **211b**, highlighted in green, at all concentrations (29.6-266 μM) tested. The C-α-substituted *N*-phenyldihydropyrrolone derivatives exhibited superior activities, with the nitroester substituted derivative **210d** showing the highest activity with 70% QS inhibition at 266 μM. For the dihydropyrrolone derivatives (were R = H), the C-α-bromo derivative **211b** exhibited better activity compared to the C-α-nitroester derivative **210b**. For the nitroester derivatives, *N*-substituted derivatives **210c** (R=Bz) and **210d** (R= Ph) displayed the highest activities, but compound **210b** where (R= H) or the substitution on the phenyl ring (compound **210e**) led to a decrease in activity. None of the tested compounds displayed activity at concentrations of 9.9 μM. Furthermore, no growth inhibition was observed at any of the concentrations tested.

7.3 Nitric oxide release studies

Nitric oxide (NO) is an important signaling compound in mammals, plants, and insects. Recently, NO has been discovered to act as a signaling molecule in bacteria, where it regulates the dispersal of cells from biofilms.[155,157] This discovery has led to the use of NO donors to induce bacterial dispersal. A key challenge with this approach is to deliver the correct amount of NO to the bacteria, since it has been shown that low, non-toxic concentrations of NO induce dispersal, while higher, toxic concentrations of NO favour biofilm growth. The delivery of NO by donor molecules is determined by the release kinetics upon dissolution in aqueous solution, and these kinetics are influenced by the type of NO donor and the nature of the molecules used as NO carriers. Therefore, it is important to determine the NO release properties of these novel donors. A wide range of detection techniques have been developed for nitric oxide. The spectroscopic methods for NO detection include absorbance spectroscopy using the Griess reagent,

fluorescence-based detection involving diaminofluoresceins (DAFs) and chemiluminescence methods that employ the reaction of NO with ozone. Other techniques include electron paramagnetic resonance (EPR) and electrochemical methods using an amperometric NO sensor.[284-286]

The NO detection employed in our laboratory is based on the quantification of nitrite using Griess reagent and an amperometric NO sensor instrument Apollo 4000.

7.3.1 Quantification of nitrate/nitrite by the Griess Reaction

The most common approach for the detection of nitrite is the Griess assay. First developed in 1879, this method has found numerous applications for both nitrate and nitrite analysis. The Griess reagent assay typically relies on the diazotization of a suitable aromatic amine sulfanilamide by acidified nitrite (NO_2^-), followed by a subsequent coupling reaction with *N*-1-naphthylethylenediamine dihydrochloride (NED), producing a highly coloured azo chromophore (Figure **7.9**). The absorption maximum for the azo product is at 540 nm and can be detected using conventional UV-visible absorption spectroscopy, from which the concentration of nitrite can be assessed.[287-288]

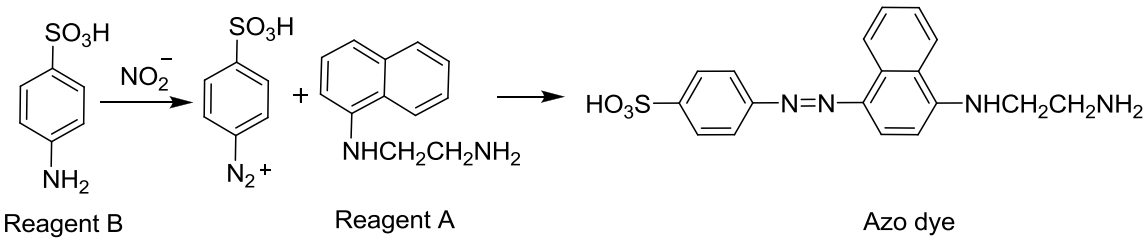

Figure 7.9: The diazotization reaction between nitrite and Griess reagents.

The Griess assay can also be utilized for the measurement of organic nitrate (R-NO_3) after reduction of nitrate to nitrite (NO_2^-). Nitrate can also be converted *via* NO_2^- to NO

which in turn due to its reactive nature converts back to nitrite (NO_2^-) in oxygenated aqueous media as shown below.

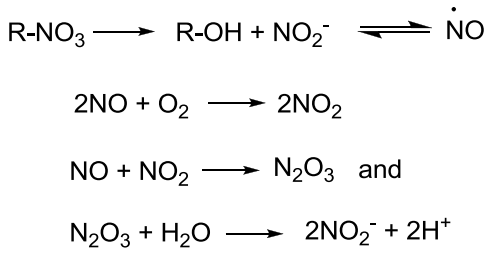

Methods for nitrate reduction to nitrite include treatment with thiols (cysteine) or metal reductants such as cadmium, zinc, and vanadium chlorides. Enzymatic reduction may also be employed using nitrate reductase obtained from bacteria. However, the enzymatic approach requires NADPH (nicotinamide adenine dinucleotide phosphate-oxidase) as a cofactor, and this compound has been shown to interfere with the Griess assay. Organic nitrate can also be reduced to NO using xanthine oxidase in presence of xanthine and cysteine.[288,166]

For preliminary studies, the initial quantitation of NO release was performed for the fimbrolide nitrate derivatives *via* conversion of nitrate to nitrite or NO, followed by detection using the Griess reagent. Different approaches for the reduction were examined, such as the use of cysteine, cadmium, nitrate reductase or xanthine oxidase. The use of xanthine oxidase along with xanthine and cysteine was found to be most suitable for the current work and was thus utilized for the study of the hybrid compounds prepared during the course of this work.

7.3.1.1 Assay procedure

In a 96-well plate, containing a solution of the test compound (7.5 or 15 µl from 5 mM stock solution in 0.1 M phosphate buffer, pH 7.4) was added a freshly prepared solution of L-cysteine (15 µl of a 5 mM solution in 0.1 M phosphate buffer, pH 7.4), xanthine (3

µl of a 1 mM solution in 0.1 M phosphate buffer, pH 7.4) and xanthine oxidase (6 µl of a 2 mg/mL solution in 0.1 M phosphate buffer, pH 7.4). PBS was added to the mixture to a total volume to 150 µl, and the mixture was incubated at 37 °C for 1 h at 180 rpm. The plate was brought to room temperature, an aliquot of the Griess reagent (20 µl), freshly prepared by mixing equal volumes of 1.0% sulfanilamide (reagent B) and 0.1% *N*-naphthylethylenediamine dihydrochloride (reagent A), was added, followed by the addition of 130 µl of 0.1 M phosphate buffer, pH 7.4. After 30 min, the absorbance was measured at 540 nm using a plate reader (Wallac Victor^2, Perkin-Elmer).

Solutions of 0 to 100 µM sodium nitrite were used to prepare a standard curve of nitrite absorbance versus concentration under the same experimental conditions. The concentration of nitric oxide released (quantitated as nitrite ions) was calculated from the standard curve.

7.3.1.2 Nitric oxide quantitation results by Griess Assay

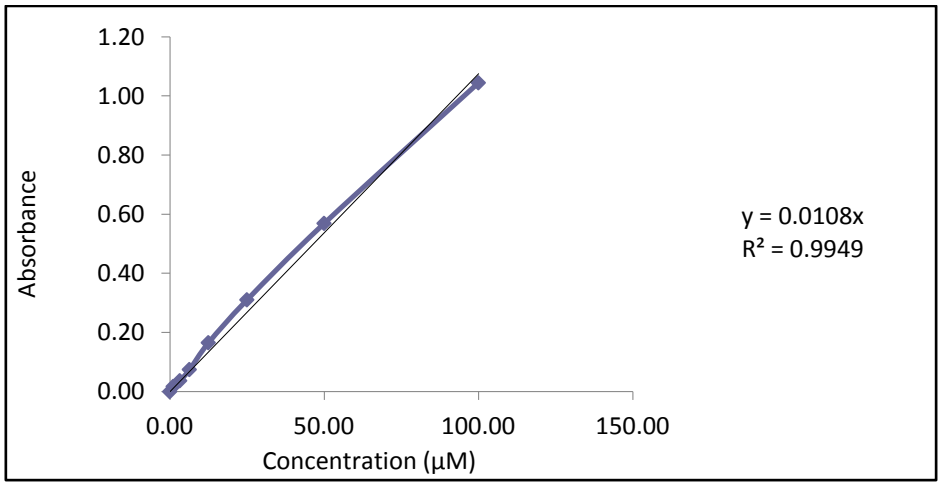

Figure 7.10: Nitrite standard curve obtained using the Griess assay.

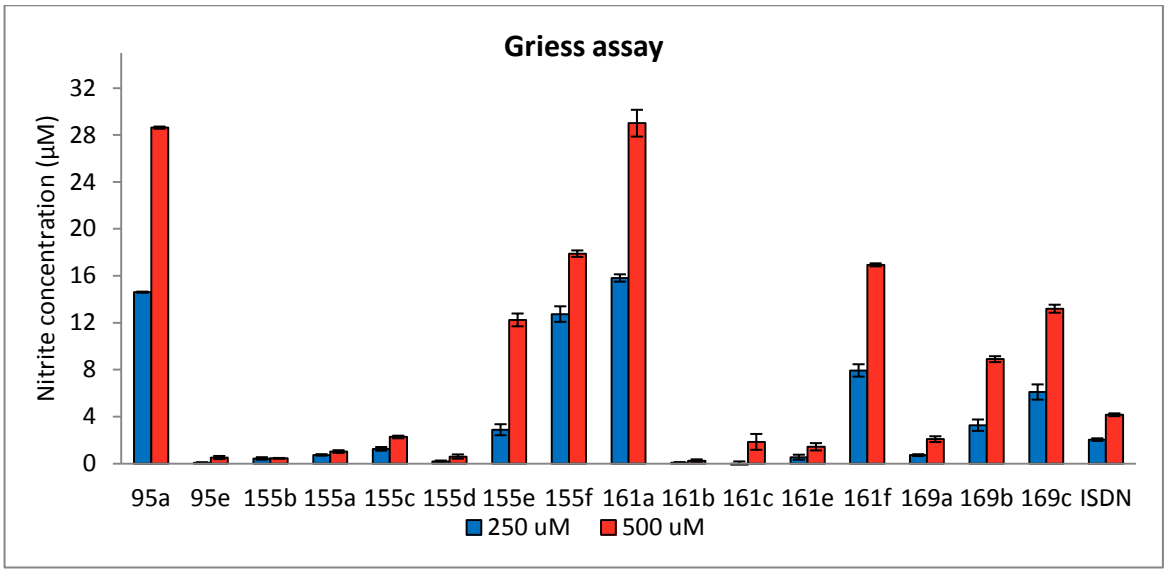

Figure 7.11: Nitrite concentration (µM) obtained for different test compound using the Griess assay.

The standard curve gave a good linear fit between 0 and 120 µM (R^2= 0.995). The Griess assay results indicate that the nitrate derivatives can be converted into NO, and can be quantified as nitrite ions using the Griess reagent. The compounds **95a** and **161a** had the highest nitrite (NO) release of 29.0 µM and 28.6 µM, respectively, at 500 µM of added compound. Compounds **155e**, **155f**, **161f**, **169b** and **169c** also had a better total nitrite release compared to the standard ISDN **43** which has two nitroester (ONO_2) group in the structure, compared to one nitroester group in case of the synthesized derivatives tested.

The NO release properties of fimbrolide diazeniumdiolate derivatives were also examined by incubating the compounds **174** and **178c** in phosphate buffer pH 7.4 for different time periods of 1 h, 2 h, 4 h, 8 h, 16 h, and 24 h and further measuring the NO (nitrite) released by Griess reagent after each time period. The results showed no release of NO from the compounds for the studied time period, indicating the stability of these diazeniumdiolate derivatives which is consistent with the literature results for O^2-

protected diazeniumdiolates. Thus, further studies with different enzymes or blood serum will be required to understand the NO release properties of the stable fimbrolide diazeniumdiolates. The NO releasing properties of high load NO donors could not be evaluated due to time constraint but are expected to behave similarly to the other nitrate and the diazeniumdiolate derivatives tested during the course of the work.

7.3.2 Nitric oxide measurement by Apollo

An Apollo 4000 free radical analyzer (World Precision Instruments (WPI), Sarasota, USA) was used as an alternative technique to measure NO concentrations and is particularly useful for spontaneous NO releasing compounds. An ISO-NOP electrode (2 mm in diameter) was calibrated daily using SNAP and Cu(II) as a catalyst according to the manufacturer‘s instructions. The calibration curve obtained was in the range of 1 to 2 pA for 1 nM NO. For NO release measurements, the electrode was plunged through the hole of a silicone septum of a glass vial containing 10 ml of PBS buffer (pH 7.4) and gently agitated with a magnetic stirrer. Aliquots of the indole diazeniumdiolate derivative IDN-1 in aqueous medium were injected in the solution through the septum and the change in current was monitored. Two set of experiments, one with gentle nitrogen (N_2) purging and another without nitrogen purging was studied. When the NO scavenger PTIO [2-(4-carboxyphenyl)-4,4,5,5-tetramethylimidazoline-1-oxyl-3-oxide] was added to the solution, an immediate drop in the measured current was observed, which confirmed that the change in current was due to the production of NO.

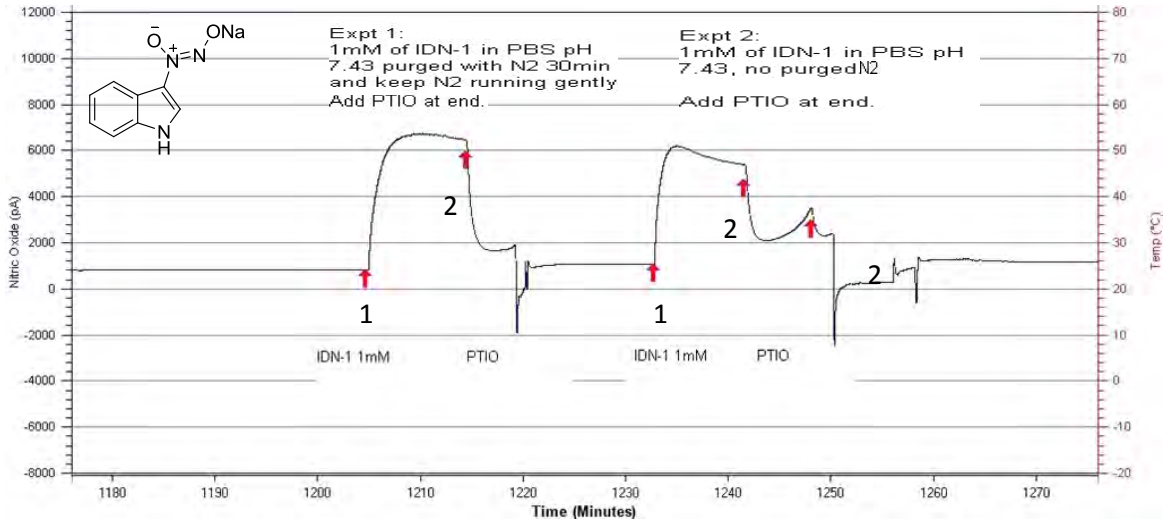

Figure 7.12: NO release study of **237** (IND-1) using Apollo 4000 NO analyzer. The arrow heads **1** and **2** indicates the addition of compound **237** and PTIO respectively for each set of experiment.

The results indicated that the indole diazeniumdiolate derivative **237** (IND-1) can release NO spontaneously in aqueous solution. This is the first-in-class *C*-diazeniumdiolate that spontaneously released NO at concentration of about 2.9 µM and 2.5 µM from experiment 1 and 2 respectively.

Due to time constrains further NO release studies of indole diazeniumdiolate and its derivative could not be explored and will be the subject of future work.

7.4 Effect of nitric oxide on the bacterial *nirS* system

The availability and effects of NO released from donor compounds to *P. aeruginosa* cells was tested using the NSGFP (*P. aeruginosa* P*nirS*::*gfp*) reporter strain.[155] The *nirS* gene is known to be induced in the presence of NO. Planktonic cells of NSGFP were exposed to NO donors at pH 7 for 2 h and the green fluorescence of the cells was measured in a microtitre plate reader (Wallac Victor^2– Perkin Elmer). The level of green fluorescence indicates the degree of transcription of the *nirS* gene, and thus is correlated

with NO availability. The results showed that there was a significant increase in *nirS* expression when cells were exposed to fimbrolide nitrate derivatives **155** and **161** for 2 h, compared to untreated cells.

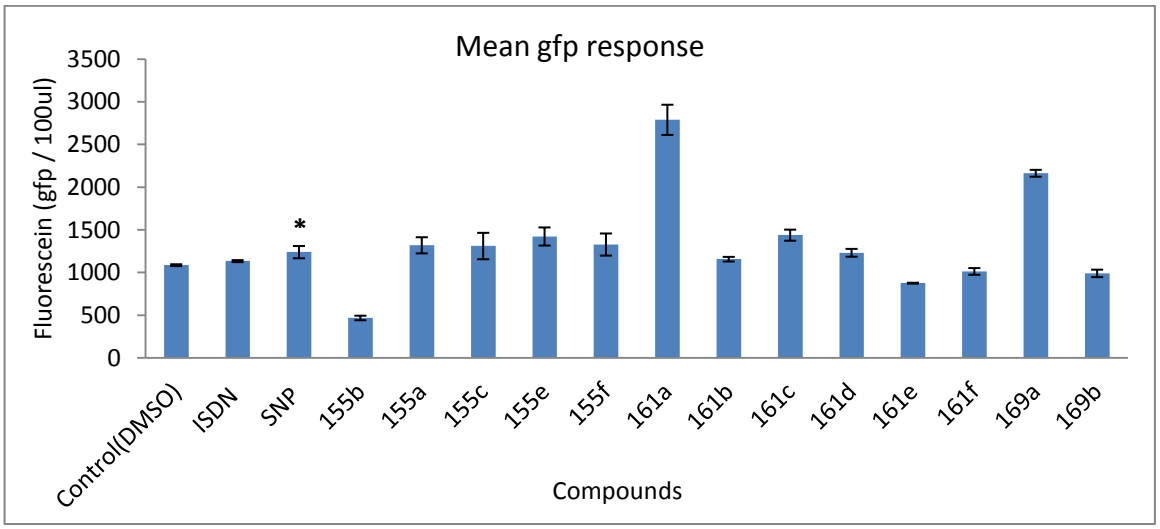

Figure 7.13: Gfp response of novel fimbrolide-NO donors tested at 500 µM on *P. aeruginosa nirS*::*gfp* strain. The error bars represent the standard deviation of triplicate results. ISDN- Isosorbide dinitrate; *sodium nitroprusside (SNP) tested at 150 µM.

The test results indicated that compound **161a** was able to induce the highest expression of *nirS*, with more than a 2.5-fold increase compared to the untreated control. This is consistent with the results of the Griess assay, where **161a** had the highest concentration of nitrite (NO) release. Compound **169a** also exhibited significant activation of the *nirS* system, while the effects of the other derivatives were more modest. Interestingly, compound **155b** showed a negative effect on the Gfp output, which is possibly due to its growth inhibition effect on the test species at the concentration used. Other derivatives tested did not show such inhibitory effect on growth as compound **155b**.

7.5 Studies on biofilm growth and dispersion

One of the key phenotypes of bacteria is the formation of biofilms, which protect the bacteria from stresses such as predation and antibiotics. QS has been shown to regulate biofilm formation and maintenance in *P. aeruginosa*, and the inhibition of QS has been recognized as a strategy to reduce biofilm formation and to increase the sensitivity of biofilms to biocides such as antibiotics. Furthermore, NO has been shown to induce biofilm dispersal, which could potentially make biofilms easier to eradicate. Therefore, the NO-releasing QS inhibitor compounds that were found to be active in the previous studies were tested for their ability to control biofilm formation in *P. aeruginosa*.

7.5.1 Biofilm inhibition assay

Aliquots of 1 mL of overnight cultures of *P. aeruginosa* PAO1 diluted in M9 medium (containing 48 mM Na_2HPO_4, 22 mM KH_2PO_4, 9 mM NaCl, 19 mM NH_4Cl, 2 mM $MgSO_4$, 20mM glucose, 100 µM $CaCl_2$, pH 7.2) to an OD600 of 0.1 were inoculated into 24-well plates (Sarstedt). Compounds were added to the wells to a final concentration of 150 µM from a 30 mM stock solution. Three replicate wells at 150 µM concentration per compound were used. The plates were incubated for 6 h at 37 °C with shaking at 180 rpm. After growth, the planktonic growth was quantified by measurement of the planktonic phase at OD600 using a microtitre plate reader (Wallac-Victor, Perkin-Elmer). For quantification of biofilms in microtitre plates, a method similar to that reported by O'Toole *et al.* was used.[289] Wells containing biofilms were washed twice with phosphate buffered saline (PBS) and stained for 20 min with 1 mL of crystal violet (0.2 %). The wells were washed again three times with PBS, and the remaining crystal violet was dissolved in 1 mL of absolute ethanol. Biofilm formation was quantified by measurement at OD550. [115]

The assay measures the effect of tested compound on biofilm inhibition and planktonic growth. It is important to monitor the growth of planktonic bacteria as inhibition of planktonic bacteria will give a false positive result for biofilm inhibition. Thus an ideal compound for the assay is the one which has biofilm inhibition property with no growth inhibition of the planktonic cells.

Using the method described above different QS-NO hybrid derivatives were studied for their preliminary biofilm inhibition properties. The data obtained for biofilm inhibition (measured as absorbance at OD550) and planktonic cell growth (measured as absorbance at OD600) is plotted in Figure **7.14**

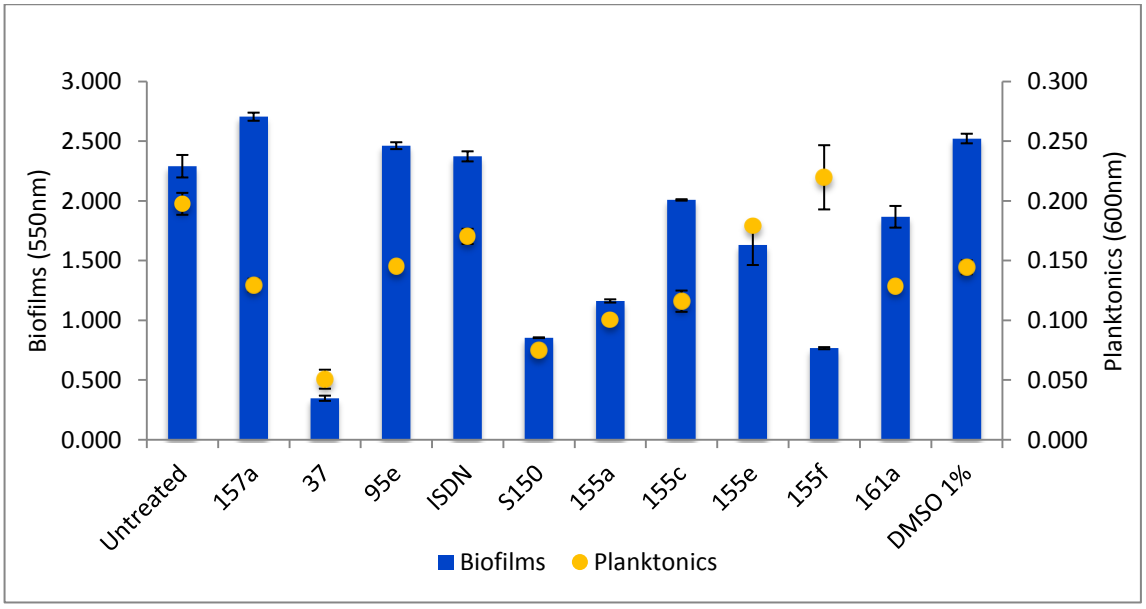

Figure 7.14: Graph showing *P. aeruginosa* biofilm and planktonic growth after treatment with test compounds at 150 µM for 6 h at 180 rpm, 37 °C. Isosorbide dinitrate (ISDN) and Spermine NONOate (S150) were used as standard NO donors.Error bars represent the standard deviation of triplicate results.

From the preliminary biofilm inhibition assay it was evident that some QS-NO hybrid derivatives showed promising biofilm inhibition results and thus these compounds were

further studied at different concentration to see the effect of dose on biofilm inhibition. The results obtained were analyzed and are tabulated below as percentage biofilm inhibition and percentage growth inhibition compared to the control (Table **7.5**).

Table 7.5: *P. aeruginosa* biofilm inhibition (%) and growth inhibition (%) after treatment with test compounds at various concentrations (1, 10, 50 and 150 µM). Spermine NONOate **(**S150) and sodium nitroprusside (SNP) were used as standard NO donors.

Compound	Concentration (µM)	% biofilm inhibition	% growth inhibition
155b	1.0	2.1	21.36
	10.0	39.6	33.25
	50.0	82.5	54.82
155a	1.0	7.9	13.52
	10.0	24.1	27.58
	50.0	64.6	24.80
155f	1.0	8.8	7.98
	10.0	-0.6	23.60
	50.0	19.7	18.70
	150.0	68.7	-16.65
161a	1.0	-5.3	16.79
	10.0	-10.1	31.96
	150.0	7.4	23.52
S150	1.0	-6.3	4.78
	10.0	-13.9	25.81
	50.0	12.9	29.89
	150.0	62.7	62.03
SNP	1.0	21.7	-34.61
	10.0	-11.2	-6.66
	50.0	14.8	-42.13

From the biofilm growth inhibition assays (Figure **7.14** and Table **7.5**), compound **155f** emerged as the promising compound, as it significantly decreased biofilm growth (68% at 150 μM compared to the control) without affecting the growth of the planktonic cells. The biofilms inhibition activity of compound **155f** was also superior to the two standard compounds S150 and SNP tested. Compounds **155a** and **155b** also displayed good inhibitory effects against biofilm formation, but also interfered with the growth of planktonic cells. It is also interesting to note that compound **155a** with a nitroester group has better biofilms inhibition activity compared to non-nitroester containing compound **157a** which has a hydroxyl group. Suprisingly, compound **161a** did not show any significant biofilm inhibition at the concentration studied even though it had shown promising QS inhibition and nitric oxide release activity.

The preliminary biofilm inhibition studies were carried on compounds from the AHL NO hybrid series, fimbrolide-based diazeniumdiolate derivatives, dihydropyrrolone NO hybrids and high load NO donors, but were found to be inactive at the highest concentration (150 μM) tested. Future studies on these compounds are required, particularly at higher concentrations to ascertain their lack of activity in biofilm inhibition. It will also be interesting to test these compounds along with the commercially available antimicrobials to see how they affect the sensitivity of biofilm to antimicrobial treatments.

7.5.2 Biofilm dispersal assay

Biofilm dispersal assay is carried out on established biofilms and is utilized in this work to study the effect of NO on dispersion of established biofilms. This assay is particularly useful for spontaneous NO releasing compound, thus compound **237** (IND-1) which can release NO spontaneously (discussed above) was studied *via* this assay.

The dispersal of *P. aeruginosa* biofilms was assayed by treating biofilms grown for 6 h with NO donors for 10 min. The amount of dispersion was quantified by the crystal violet staining method as described above (Table **7.6**).

Table 7.6: Data from biofilm dispersal studies

Compound	Concentration (µM)	% GI	% BD
237 (IND-1**)**	15.0	8.48	3.58
	100.0	3.69	13.29
	150.0	2.56	17.83
	1000	-32.76	77.09
Proline NONO **52**	1000	-7.17	75.17

GI-growth inhibition, **BD**- Biofilm dispersion

The PAO1 biofilm dispersion assay indicated that compound **237** at 1 mM could induce more than 77 % dispersion of the biofilm within the 10 min, with similar potency to the standard NO donor proline diazeniumdiolate **52**. Importantly, compound **237** did not inhibit the growth of planktonic bacteria, and the increased bacterial population after treatment with compound **237** at 1 mM compared to untreated control suggests that bacteria dispersed from the biofilm are found in the planktonic population. The effect of compound **237** on biofilm dispersion was concentration-dependent.

7.6 Discussion and conclusion

P. aeruginosa is an opportunistic pathogen, and is a major agent of nosocomial infections in immunosuppressed patients. In particular, *P. aeruginosa* uses quorum sensing to control the production of virulence factors and biofilms, which protect bacteria from both the host‘s immune response and antibiotics. This can lead to chronic infections, such as in the lungs of cystic fibrosis patients or wounds of diabetic and burnt

patients, ultimately leading to increased morbidity and/or premature death. Thus, controlling QS related virulence factors and particularly biofilm formation and/or dispersion of biofilms could help in controlling morbidity and mortality from bacterial diseases.

In this chapter, the novel series of quorum sensing and nitric oxide donor hybrids synthesized during the course of this work were shown to have promising activities in quorum sensing inhibition, activation of nitric oxide specific pathways, and biofilm inhibition in *P. aeruginosa*.

The results from the QS inhibition assay indicated that compounds containing relatively small nitric oxide donor groups such as nitroester are more effective QS inhibitors. Fimbrolide derivatives **161a** and **155a** were the most active compounds from this study, with QS inhibition activities comparable to the ‗gold standard' compound **37**. These compounds were 9–10-fold more active than the known natural fimbrolide compound **34a** produced by the red alga *D. pulchra*. The 3-oxo AHL analogues **97a** and the fimbrolide diazeniumdiolate **172**, **174** and **175** also displayed superior activity compared to the natural fimbrolide compound **34a**. In general, substitution of NO donors to the fimbrolide potentiated the QS inhibitor activity.

The nitric oxide release assay and *nirS* specific bioassay indicated that the novel hybrid molecules could release NO and activate the microbial NO pathway, as determined using the *nirS::gfp* reporter strain. Compounds **161a** and **95a** were the most active in terms of NO release, followed by **155f**. In terms of activating the *nirS* pathway, **161a** and **169a** displayed the most promising results.

The biofilm inhibition assay showed that the novel fimbrolide NO hybrid **155f** was the most potent inhibitor of biofilm formation without causing growth inhibition to

planktonic cells, suggesting that the compound exerts its effects through specifically interfering with the QS and/or NO pathways in bacteria.

Thus of the different classes of NO hybrids studied, fimbrolide derivatives were found to be most potent followed by AHLs, whereas in case of NO releasing properties nitrates particularly attached adjacent to an electron withdrawing carbonyl (ester) showed better NO release. Protected diazeniumdiolates derivatives did not show NO release activity and this highlights their stability and need for enzymatic metabolism for NO release. Preliminary NO release and biofilm dispersion studies of indole diazeniumdiolate **237** were promising and future studies of indole-based diazeniumdiolate derivatives and high load NO donors will provide an understanding on the usefulness of these compounds as antibacterial agents.

The biological data demonstrates that the NO-releasing QS inhibitor hybrid molecules synthesized during the course of this work retain both their ability to inhibit QS and to produce NO thereby inducing NO-dependent pathways in bacteria. These results highlight the potential usefulness of compounds with non-toxic modes of action such as quorum sensing inhibition and nitric oxide release as key strategies for the development of future antimicrobial agents that do not exert selective pressure leading to resistance.

Chapter 8
Experimental

8.1 General Information

All reactions requiring anhydrous conditions were performed under an argon atmosphere. Methanol (MeOH), ethanol (EtOH), pentane and ethyl acetate were obtained from commercial sources. Anhydrous dichloromethane (DCM), ether and tetrahydrofuran (THF) were obtained using a PureSolv MD Solvent Purification System. Commercially available reagents were purchased from Fluka, Aldrich, Acros Organics, Alfa Aesar and Lancaster and used without further purification. Nitric oxide gas (99.9%) was purchased from BOC scientific and used without further purification.

Reactions were monitored using thin layer chromatography, performed on Merck DC aluminium plates coated with silica gel GF_{254}. Compounds were detected by short and long wavelength ultraviolet light or using different chemical indicators such as permanganate solutions, iodine vapour, bromocresol green and ninhydrin reagent.

Vacuum column chromatography was carried out using Grace Davison LC60A 6-35 micron silica gel and this method involved the use of vacuum at the base of the column *via* a vacuum pressure line. Preparative thin layer chromatography was carried out on 3×200×200 mm glass plates coated with Merck $60GF_{254}$ silica gel.

NMR spectra were obtained in the designated solvents on a Bruker DPX 300 or a Bruker Avance 400 or a Bruker AVANCE DMX 600 spectrometer as designated. Chemical shifts (δ) are in parts per million and internally referenced relative to the solvent nuclei. ^{1}H NMR spectral data are reported as follows: chemical shift measured in parts per million (ppm) downfield from TMS (δ); multiplicity; observed coupling constant (J) in

Hertz (Hz); proton count; assignment. Multiplicities are assigned as singlet (s), doublet (d), doublet of doublet (dd), doublet of triplet (dt), triplet, (t), quartet (q), quintet (p), doublet of doublet of doublets (ddd), multiplet (m) and broad singlet (bs) where appropriate and the observed coupling constants (*J*) are described in Hertz (Hz). ^{13}C NMR spectra were recorded in the designated solvents and chemical shifts are reported in ppm downfield from TMS and identifiable carbons are given (where possible). ^{1}H-^{15}N HMBC NMR spectra were recorded on a Bruker DPX 300 NMR or a Bruker Avance III 500 NMR.

Melting points were measured using a Mel-Temp melting point apparatus, and are uncorrected. Infrared spectra were recorded on a Perkin Elmer Spotlight 400 FTIR Microscope. Ultraviolet spectra were measured using a Perkin Elmer Lambda 35 UV-Visible Spectrometer in the designated solvents and data reported as wavelength (λ) in nm and adsorption coefficient (ε) in M^{-1} cm^{-1}.

High-resolution mass spectrometry was performed by the Bioanalytical Mass Spectrometry unit, UNSW. Microanalysis was performed on a Carlo Erba Elemental Analyzer EA 1108 at the Campbell Microanalytical Laboratory, University of Otago, New Zealand.

8.2 Experimental Details

2-(Nitrooxy)acetic acid (94a)[290]

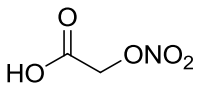

A mixture of 2-bromoacetic acid **93a** (1.00 g, 7.19 mmol) and silver nitrate (1.83 g, 10.8 mmol) in anhydrous acetonitrile (30 mL) was stirred at 70 °C for 18 h. The resulting product was filtered through a column of Celite and silica to remove the silver salt formed. The filtrate was evaporated to dryness and DCM (50 mL) was added. After

standing at room temperature for 2 h the mixture was filtered to remove any leftover silver salt precipitate. The removal of DCM gave the title compound **94a** as a yellow oil (0.74 g, 86%). ^{1}H NMR (300 MHz, $CDCl_3$): δ 4.96 (s, 2H, CH_2), 9.53 (bs, 1H, OH); ^{13}C NMR (75.6 MHz, $CDCl_3$): δ 66.3 (CH_2), 171.6 (C=O).

3-(Nitrooxy)propanoic acid (94b)[290]

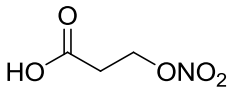

The compound was prepared as described for compound **94a**, using 3-bromopropanoic acid **93b** (1.00 g, 6.53 mmol) and silver nitrate (1.66 g, 9.80 mmol) in acetonitrile (30 mL) at 70 °C for 18 h to yield the title compound **94b** as a yellow oil (0.82 g, 94%). ^{1}H NMR (300 MHz, $CDCl_3$): δ 2.82 (t, J = 6.0 Hz, 2H, CH_2COO), 4.72 (t, J = 6.0 Hz, 2H, CH_2ONO_2), 11.56 (bs, 1H, OH); ^{13}C NMR (75.6 MHz, $CDCl_3$): δ 30.0 (CH_2COO), 66.2 (CH_2ONO_2), 173.9 (C=O).

6-(Nitrooxy)hexanoic acid (94f)[291]

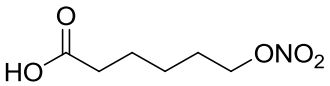

The compound was prepared as described for compound **94a**, using 6-bromohexanoic acid **93f** (2.00 g, 10.2 mmol) and silver nitrate (2.26 g, 13.3 mmol) in acetonitrile (50 mL) at 70 °C for 18 h followed by workup to yield the title compound as a yellow oil (1.68 g, 93%). ^{1}H NMR (300 MHz, $CDCl_3$): δ 1.41-1.49 (m, 2H, CH_2), 1.63-1.75 (m, 4H, 2 × CH_2), 2.36 (t, J = 7.1 Hz, 2H, CH_2COO), 4.43 (t, J = 6.4 Hz, 2H, CH_2ONO_2), 11.72 (bs, 1H, OH); ^{13}C NMR (75.6 MHz, $CDCl_3$): δ 22.3 (CH_2), 23.4 (CH_2), 24.7 (CH_2), 32.0 (CH_2COO), 71.3 (CH_2ONO_2), 178.4 (C=O).

8-(Nitrooxy)octanoic acid (94c)

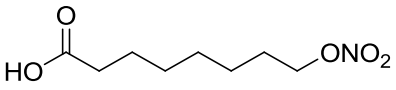

The compound was prepared as described for compound **94a**, using 8-bromooctanoic acid **93c** (0.75 g, 3.36 mmol) and silver nitrate (1.19 g, 7.05 mmol) in acetonitrile (20 mL) to give the desired product **94c** as a yellow oil (0.64 g, 94%). ^{1}H NMR (300 MHz, $CDCl_3$): δ 1.35-1.41 (m, 6H, 3 × CH_2), 1.60-1.72 (m, 4H, 2 × CH_2), 2.34 (t, J = 7.3 Hz, 2H, CH_2COO), 4.42 (t, J = 6.6 Hz, 2H, CH_2ONO_2), 11.37 (bs, 1H, OH).

11-(Nitrooxy)undecanoic acid (94d)

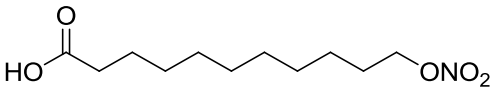

The compound was prepared as described for compound **94a**, by using 11-bromoundecanoic acid **93d** (3.00 g, 11.3 mmol) and silver nitrate (2.40 g, 14.7 mmol) in acetonitrile (60 mL) at 70 °C for 18 h followed by workup to yield the title compound **94d** as a yellow solid (2.68 g, 96%). M.p. 38-40 °C, lit.[292] 40-41 °C; ^{1}H NMR (300 MHz, $CDCl_3$): δ 1.28-1.43 (m, 12H, 6 × CH_2), 1.62-1.73 (m, 4H, 2 × CH_2), 2.34 (t, J = 6.7 Hz, 2H, CH_2COO), 4.43 (t, J = 6.6 Hz, 2H, CH_2ONO_2), 10.23 (bs, 1H, OH); ^{13}C NMR (75.6 MHz, $CDCl_3$): δ 24.5 (CH_2), 25.5 (CH_2), 26.6 (CH_2), 28.9 (CH_2), 29.0 (CH_2), 29.1 (CH_2), 33.99 (CH_2COO), 73.3 (CH_2ONO_2), 180.3 (C=O).

12-(Nitrooxy)dodecanoic acid (94g)

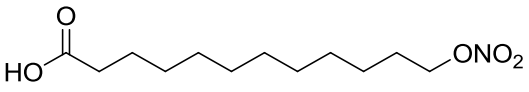

The compound was prepared as described for **94a** using 12-bromododecanoic acid **93g** (2.00 g, 7.16 mmol) and silver nitrate (1.33 g, 7.87 mmol) in acetonitrile (50 mL) to give the desired product **94g** as a yellow oil

(1.77 g, 95%). M.p. 28-30 °C; ^{1}H NMR (300 MHz, $CDCl_3$): δ 1.26-1.39 (m, 14H, 7 × CH_2), 1.58-1.71 (m, 4H, 2 × CH_2), 2.32 (t, J = 7.4 Hz, 2H, CH_2COO), 4.42 (t, J = 6.6 Hz, 2H, CH_2ONO_2), 11.32 (bs, 1H, OH); ^{13}C NMR (75.6 MHz, $CDCl_3$): δ 24.5 (CH_2), 25.5 (CH_2), 26.6 (CH_2), 28.9 (CH_2), 29.0 (CH_2), 29.1 (CH_2), 33.99 (CH_2COO), 73.3 (CH_2ONO_2), 180.3 (C=O).

4-(Nitrooxymethyl)benzoic acid (94e)

The compound was prepared as described for compound **94a**, by using 4-(bromomethyl)benzoic acid **93e** (2.00 g, 9.30 mmol) and silver nitrate (2.05 g, 12.1 mmol) in acetonitrile (50 mL) at 70 °C for 18 h followed by workup to yield the title compound **94e** as a white solid (1.72 g, 94%). M.p. 162-164 °C, lit.[292] 165 °C; ^{1}H NMR (300 MHz, DMSO-d_6): δ 5.63 (CH_2ONO_2), 7.54 (d, J = 9.0 Hz, 2H, H2, H6), 7.95 (d, J = 9.0 Hz, 2H, H3, H5); ^{13}C NMR (75.6 MHz, $CDCl_3$): δ 74.5 (CH_2), 129.3 (ArCH), 129.9 (ArCH), 131.7 (ArC), 137.6 (ArC), 167.2 (C=O).

Sodium 1-(4-Ethoxycarbonylpiperazin-1-yl)diazen-1-ium-1,2-diolate (114)

A solution of 1-ethoxycarbonylpiperazine **113** (5.42 g, 34.0 mmol) in 60 mL of anhydrous ether and methanol (1:1) was placed in a Parr bottle. The solution was treated with sodium methoxide (NaOMe) (2.03 g, 37.0 mmol) and the Parr apparatus was clamped. The apparatus was purged and evacuated with nitrogen (3 ×) followed by charging with 5 atm. nitric oxide (NO) at 25 °C for 48 h. The excess NO was then vented by purging with nitrogen followed by addition of anhydrous ether. The white precipitate was collected by

filtration and washed with cold methanol as well as with copious amounts of anhydrous ether. The product was dried under vacuum to afford the desired title compound **114** as a white solid (3.90 g, 47%). M.p. 184 °C (dec), lit.[220] m.p 184-185 °C; ^{1}H NMR (300 MHz, 0.1 M NaOD in D_2O) δ 1.69 (t, J = 7.1 Hz, 3H, CH_3), 3.02 (m, 4H, 2 × CH_2), 3.59 (m, 4H, 2 × CH_2), 4.05 (q, J = 7.1 Hz, 2H, OCH_2); ^{13}C NMR (75.6 MHz, 0.1M NaOD in D_2O) δ 13.7 (CH_3), 42.5 (CH_2), 44.1 (CH_2), 51.2 (CH_2), 62.7 (CH_2), 156.8 (C=O).

Sodium 1-(4-*tert*-Butoxycarbonylpiperazin-1-yl)diazen-1-ium-1,2-diolate (118)

The title compound reaction was carried out as described for the preparation of **114**. A solution of *tert*-butoxycarbonylpiperazine **117** (5.00 g; 2.68 mmol) and sodium methoxide (1.59 g, 2.95 mmol) in 50 mL of ether and methanol was exposed to nitric oxide to give desired product **118** as a free flowing solid (1.76 g, 24%). M.p. 260 °C, lit.[220] m.p. 262-264 °C; ^{1}H NMR (300 MHz, 0.1 M NaOD in D_2O) δ 1.38 (s, 9 H, 3 × CH_3), 3.01 (m, 4H, 2 × CH_2), 3.56 (m, 4H, 2 × CH_2); ^{13}C NMR (75.6 MHz, 0.1 M NaOD in D_2O) δ 30.44 (CH_3), 45.44 (CH_2), 54.19 (CH_2), 85.05 (C), 159.08 (C=O).

Sodium l-(*N*,*N*-diethylamino)diazen-l-ium-l,2-diolate (170)[190]

N,*N*-Diethylamine (7.00 g, 96.6 mmol) in 60 mL ether: methanol (1:1) and sodium methoxide (6.26 g, 116 mmol) was exposed to NO as described for the preparation of **114** to give the title compound **170** as a white solid (5.60 g, 37%). M.p. 240 °C (dec); ^{1}H NMR (300 MHz, 0.1 M NaOD in D_2O) δ 0.88 (t, J = 7.1 Hz, 3H, CH_3),

2.88 (q, J = 7.1 Hz, 2H, CH_2); ^{13}C NMR (75.6 MHz, 0.1 M NaOD in D_2O) δ 10.7 (CH_3), 48.2 (CH_2).

Sodium 1-(morpholin-1-yl)diazen-1-ium-1,2-diolate (173)

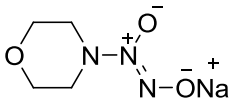

The title compound synthesis was carried out as described for the preparation of **114**. A solution of morpholine (10.0 g; 114.7 mmol) and sodium methoxide (6.82 g, 126.2 mmol) in 120 mL of ether and methanol (1:1) was exposed to nitric oxide to give desired product **173** as a white solid (8.90 g, 45%). M.p. 184-186 °C (dec) ^{1}H NMR (300 MHz, 0.1 M NaOD in D_2O) δ 3.16 (t, J = 4.6 Hz, 4H, 2 × CH_2), 3.90 (t, J =4.8 Hz, 4H, 2 × CH_2); ^{13}C NMR (75.6 MHz, 0.1 M NaOD in D_2O) δ 51.6 (CH_2), 65.6 (CH_2).

***O*^{2}-Methyl-1-(4-ethoxycarbonylpiperazin-1-yl)diazen-1-ium-1,2-diolate (115)**

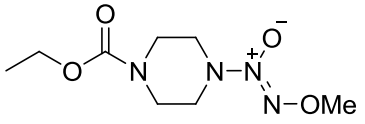

To a solution of diazeniumdiolate **114** (1.63 g, 6.80 mmol) in 30 mL of methanol was added 1.70 g of anhydrous potassium carbonate, and the resulting slurry was cooled in an ice bath. Dimethyl sulfate (0.80 mL, 8.16 mmol) was added dropwise. The reaction mixture was stirred at 0 °C for 1 h and then allowed to warm gradually to room temperature. After an additional hour, the solution was concentrated on a rotary evaporator; the residue was extracted with dichloromethane, washed with water, dried over sodium sulfate, and filtered through a layer of sodium sulfate. The solvent was evaporated under reduced pressure to give the desired product **115** as a light yellow solid (0.84 g, 54%). M.p. 42-44 °C, lit.[220] m.p. 46 °C; ^{1}H NMR (300 MHz, $CDCl_3$) δ 1.26 (t, J = 5.5 Hz, 3H, CH_3),

3.35 (m, 4H, 2 × CH_2), 3.63 (m, 4H, 2 × CH_2), 4.00 (s, 3H, OCH_3), 4.15 (q, J = 5.5 Hz, 2H, OCH_2).

O^2-Methyl 1-(piperazin-1-yl)diazen-1-ium-1,2-diolate (116)[220]

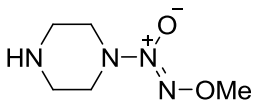

A mixture of diazeniumdioalte **115** (0.65 g) in 20 mL of 10% sodium hydroxide in ethanol, and 1 mL of water was heated at reflux. After 45 min, no starting material remained in the mixture, as assessed from thin-layer chromatography. The solution was allowed to cool to room temperature and evaporated to a viscous residue, which was extracted with dichloromethane, dried over sodium sulfate, filtered, and evaporated to give the title compound **116** as a yellow oil (0.32 g, 71%). ^{1}H NMR (300 MHz, $CDCl_3$) δ 3.02 (m, 4H, 2 × CH_2), 3.36 (m, 4H, 2 × CH_2), 4.00 (s, 3H, OCH_3); ^{13}C NMR (75.6 MHz, $CDCl_3$) δ 44.8 (CH_2), 52.5 (CH_2), 60.9 (CH_2).

O^2-(2,4-Dinitrophenyl)-1-[4-(*tert*-butoxycarbonyl)piperazin-1-yl]diazen-1-ium-1,2-diolate (119)

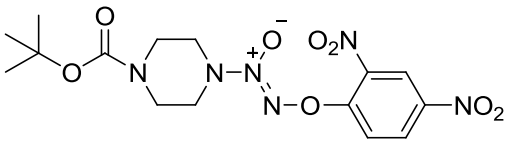

To a solution of sodium 1-[4-(*tert*-butoxycarbonyl)piperazin-1-yl]diazen-1-ium-1,2-diolate **118** (1.00 g, 3.72 mmol) in 5% sodium bicarbonate (15 mL) at 0 °C under a steady stream of nitrogen gas was added 2,4-dinitrofluorobenzene (0.69 g, 3.72) in *tert*-butyl alcohol (10 mL). The reaction was warmed to room temperature and stirred for 24 h. Precipitation occurred at such a rapid rate that stirring was impeded throughout the course of the reaction. The solvent was evaporated off and the residue extracted with dichloromethane. The dichloromethane was removed in *vacuo* and the yellow mixture

was recrystallized in EtOH to give the title compound **119** as yellow crystals (0.41 g, 26%). M.p. 118 °C, lit.[221] m.p. 115-117 °C; ^{1}H NMR (300 MHz, $CDCl_3$) δ 1.41 (s, 9H), 3.53-3.62 (m, 8H), 7.58 (d, J = 9.2 Hz, 1H), 8.37-8.41 (dd, J = 9.2 and 2.7 Hz, 1H), 8.80 (d, J = 2.7 Hz, 1H); ^{13}C NMR (75.6 MHz, CDCl3) δ 28.2 (CH_3), 42.0 (CH_2), 50.5 (CH_2), 80.9 (CH_2), 117.6 (ArH), 122.1 (ArH), 129.0 (ArH), 137.3 (ArC), 142.4 (ArC), 153.7 (ArC), 154.1 (ArC).

O^2-(2,4-Dinitrophenyl) 1-(piperazin-1-yl)diazen-1-ium-1,2-diolate, hydrochloride salt (120)

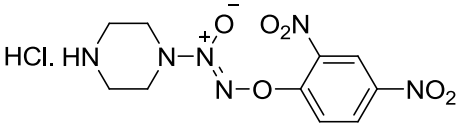

To a solution of diazeniumdiolate **119** (0.35 g) in 22 mL of ethyl acetate was added 1.5 mL of concentrated hydrochloric acid. The resulting yellow solution was stirred at room temperature for 2 h, during which time a white precipitate was evident. The mixture was filtered and washed with ether to yield the title product **120** as a white solid (0.26 g, 98% yield). M.p. 182-184 °C, lit.[221] m.p. 184-185 °C; ^{1}H NMR (300 MHz, DMSO-d_6) δ 3.38 (m, 4H, 2 × CH_2), 3.89 (m, 4H, 2 × CH_2), 7.95 (d, J = 9.3 Hz, 1H, ArH), 8.56-8.60 (dd, J = 9.3 and 2.7 Hz, 1H, ArH), 8.89 (d, J = 2.6 Hz, 1H, ArH), 9.35 (bs, 1H, NH); ^{13}C NMR (75.6 MHz, DMSO-d_6) δ 41.3 (CH_2), 47.3 (CH_2), 118.7 (ArCH), 122.2 (ArCH), 130.1 (ArCH), 137.4 (ArC), 142.8 (ArC), 152.9 (ArC).

O^2-(Methoxymethyl)-1-[(4-ethoxycarbonyl)piperazin-1-yl]diazen-1-ium-1,2-diolate (269)[220]

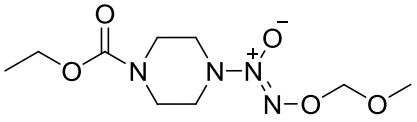

A slurry of diazeniumdiolate **114** (5.00 g, 20.8 mmol)

and 5.00 g of anhydrous sodium carbonate in 100 mL of tetrahydrofuran was stirred under nitrogen at 0 °C. Methyl chloromethyl ether (2.05 mL, 27.1 mmol) was added dropwise through a septum. The resulting mixture was allowed to warm to room temperature and stirred overnight. The reaction mixture was filtered and evaporated to dryness under reduced pressure. The residue was extracted with dichloromethane, dried over sodium sulfate, filtered through a pad of sodium sulfate, and evaporated to give the desired product **269** as an oil (3.47 g, 63%). ^{1}H NMR (300 MHz, $CDCl_3$) δ 1.25 (t, J = 7.1 Hz, 3H, CH_3), 3.42 (t, J = 5.4 Hz, 4H, 2 × CH_2), 3.47 (s, 3H, OCH_3), 3.64 (t, J = 5.4 Hz, 4H, 2 × CH_2), 4.14 (q, J = 7.1 Hz, 2H), 5.20 (s, 2H); ^{13}C NMR (75.6 MHz, $CDCl_3$) δ 14.6 (CH_3), 42.4 (CH_2), 50.9 (CH_2), 57.1 (CH_2), 61.8 (CH_2), 97.9 (CH_2), 155.1 (C=O).

O^{2}-Methoxymethyl-1-(piperazin-1-yl)diazen-1-ium-1,2-diolate (270)[220]

A solution of diazeniumdiolate **269** (3.00 g) in 100 mL of 10% ethanolic sodium hydroxide was heated at reflux for 1 h.

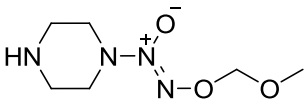

The reaction mixture was cooled to room temperature, and the ethanol was removed on a rotary evaporator. The residue was extracted with dichloromethane, filtered, and extracted with aqueous hydrochloric acid. The aqueous layer was washed with dichloromethane and then made basic with aqueous sodium hydroxide. The product was extracted into dichloromethane, dried over sodium sulfate, and filtered through a pad of sodium sulfate. Evaporation of the solvent gave the title product **270** as a yellow oil (1.2 g, 51%). ^{1}H NMR (300 MHz, $CDCl_3$) δ 3.01 (t, J = 5.1, 4H, 2 × CH_2), 3.41 (t, J = 5.1, 4H, 2 × CH_2), 3.47 (s, 3H, OCH_3), 5.19 (s, 2H, OCH_2); ^{13}C NMR (75.6 MHz, $CDCl_3$) δ 44.8 (CH_2), 52.4 (CH_2), 57.0 (CH_2), 97.7 (CH_2).

2-Oxo-2-(2-oxotetrahydrofuran-3-ylamino)ethyl nitrate (95a)

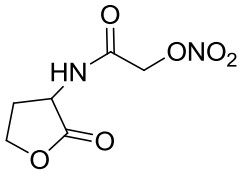

To a stirred solution of L-homoserine lactone hydrobromide **76** (0.36 g, 3.56 mmol) in water (4.00 mL), triethylamine (0.54 mL, 3.92 mmol) was added followed by the addition of acid **94a** (0.64 g, 5.34 mmol) and l-ethyl-3-(3-dimethylaminopropyl)carbodiimide hydrochloride (EDC) (1.09 g, 5.70 mmol). The mixture was stirred at room temperature for 40 h and then evaporated in *vacuo* to dryness. The residue was partitioned between water (20 mL) and ethyl acetate (50 mL) and the organic layer successively washed with 5% sodium bicarbonate ($NaHCO_3$) solution (2 × 20 mL), 1M potassium hydrogen sulfate ($KHSO_4$) solution (2 × 20 mL) and brine. The organic layer was dried over sodium sulfate ($NaSO_4$) and evaporated to dryness to yield the title compound **95a** as a white solid (0.21 g, 54%). M.p. 96-98 °C; ^{1}H NMR (300 MHz, $CDCl_3$) δ 2.16-2.28 (m, 1H, H4a), 2.82-2.91 (m, 1H, H4b), δ 4.27-4.36 (m, 1H, H5a) 4.51 (t, J = 9.1 Hz, 1H, H5b), 4.56-4.65 (m, 1H, H3), 4.95 (s, 2H, CH_2ONO_2), 6.57 (bs, 1H, NH); ^{13}C NMR (75.6 MHz, $CDCl_3$) δ 30.1(CH_2) , 49.1 (CH), 66.1 (CH_2), 69.0 (CH_2), 165.4 (C=O), 174.4 (C=O); IR (neat): ν_{max} 3351, 3000, 2948, 2922, 1764, 1688, 1646, 1546, 1421, 1380, 1288, 1247, 1224, 1195, 1181, 1144, 1046, 1010, 982, 953, 938, 848, 815, 768, 739, 720 cm^{-1}; HRMS (ESI) *m/z* Calcd. for $C_6H_8N_2O_6Na$ $(M + Na)^+$ 227.0280. Found 227.0271.

3-Oxo-3-(2-oxotetrahydrofuran-3-ylamino)propyl nitrate (95b)

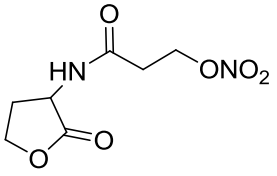

The title compound synthesis was carried out as described for the preparation of compound **95a** using acid **94b** (0.72 g, 5.34 mmol) to give desired product **95b** as an off white solid (0.21 g, 49%). M.p. 74-76 °C; ^{1}H NMR (300 MHz, $CDCl_3$) δ 2.13-2.28 (m, 1H, H4a), 2.67-2.71

(dt, J = 3 and 9, 2H, $COCH_2$), 2.73-2.82 (m, 1H, H4b), 4.25-4.34 (m, 1H, H5a), 4.44-4.51 (dt, J = 9.0, 3.0 Hz, 1H, H5b), 4.56-4.65 (m, 1H, H3), 4.77 (t, J = 6 Hz, 2H, CH_2ONO_2), 6.85 (bd, J = 6 Hz, NH); ^{13}C NMR (75.6 MHz, $CDCl_3$) 29.5 (CH_2), 33.0 (CH_2), 49.1 (CH), 66.1 (CH_2), 68.4 (CH_2), 169.2 (C=O), 175.5 (C=O); IR (neat): ν_{max} 3307, 3098, 2938, 1774, 1649, 1614, 1558, 1456, 1408, 1376, 1355, 1268, 1212, 1170, 1007, 951, 895, 862, 792, 760, 688 cm^{-1}; HRMS (ESI) *m/z* Calcd. for $C_7H_{10}N_2O_6Na$ $(M + Na)^+$ 241.0437. Found 241.0426.

4-Oxo-4-(2-oxotetrahydrofuran-3-ylamino)hexyl nitrate (95c)

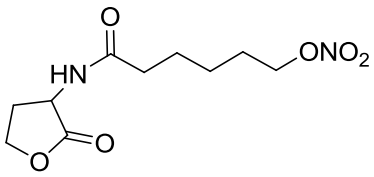

The title compound synthesis was carried out as described for the preparation of compound **95a** using acid **94c** (0.94 g, 5.34 mmol) to give desired product **95c** as an off white solid (0.24 g, 48%). M.p. 50 °C; ^1H NMR (300 MHz, $CDCl_3$) δ 1.42-1.50 (m, 2H, CH_2), 1.62-1.80 (m, 4H, CH_2), 2.06-2.21 (m, 1H, H4a), 2.27 (t, J = 6, 2H, $COCH_2$), 2.79-2.88 (m, 1H, H4b), 4.43-4.50 (m, 3H, CH_2ONO_2 and H5b merge), 4.52-4.59 (m, 1H, H3), 6.06 (bd, J = 3 Hz, NH); ^{13}C NMR (75.6 MHz, $CDCl_3$) δ 24.6 (CH_2), 25.1 (CH_2), 26.4 (CH_2), 30.43 (CH_2), 35.5 (CH_2), 49.2 (CH), 66.0 (CH_2), 72.8 (CH_2), 172.9 (C=O), 175.3 (C=O); IR (neat): ν_{max} 3309, 3074, 2954, 2865, 1775, 1639, 1622, 1543, 1493, 1451, 1382, 1360, 1279, 1225, 1167, 1107, 1014, 998, 976, 947, 899, 865, 759, 700, 684, 657 cm^{-1}; HRMS (ESI) *m/z* Calcd. for $C_{10}H_{16}N_2O_6Na$ $(M + Na)^+$ 283.0906. Found 283.0900.

11-Oxo-11-(2-oxotetrahydrofuran-3-ylamino)undecyl nitrate (95d)

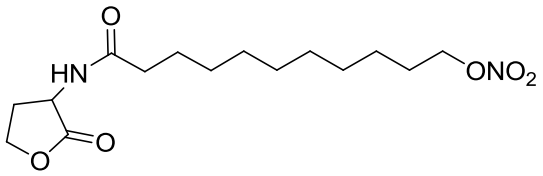

The acid **94d** (0.67 g, 2.67 mmol) was coupled to HSL (0.18 g, 1.78 mmol) using the method described for compound **95a** to give the title compound **95d** as a white solid (0.11 g, 36%). M.p. 62 °C; ^{1}H NMR (300 MHz, $CDCl_3$) δ 1.28-1.43 (m, 12H, 6 × CH_2), 1.58-1.75 (m, 4H, 2 × CH_2), 2.05-2.20 (m, 1H, H4a), 2.24 (t, J = 6.0, 2H, $COCH_2$), 2.80-2.89 (m, 1H, H4b), 4.23-4.32 (m, 1H, H5a), 4.43 (t, J = 6.0 Hz, 2H, CH_2ONO_2), 4.46 (dt, J = 12.0, 3.0 Hz, 1H, H5b), 4.52-4.58 (m, 1H, H3), 6.04 (bs, 1H, NH); ^{13}C NMR (75.6 MHz, $CDCl_3$) δ 25.2 (CH_2), 25.5 (CH_2), 26.6 (CH_2), 28.9 (CH_2), 29.0 (CH_2), 29.12 (CH_2), 29.13 (CH_2), 29.16 (CH_2), 30.5 (CH_2), 36.0 (CH_2), 49.1 (CH), 66.0 (CH_2), 73.3 (CH_2), 173.6 (C=O), 175.4 (C=O); IR (neat): ν_{max} 3317, 3073, 2924, 2852, 1775, 1642, 1622, 1545, 1468, 1381, 1361, 1278, 1225, 1170, 1107, 1012, 999, 946, 865, 803, 758, 722 cm^{-1}; HRMS (ESI) *m/z* Calcd. for $C_{15}H_{26}N_2O_6Na$ $(M + Na)^+$ 353.1689. Found 353.1681; Anal. Calcd. for $C_{15}H_{26}N_2O_6$: C, 54.53; H, 7.93; N, 8.48. Found: C, 54.98; H, 8.15; N, 8.31.

4-(2-Oxotetrahydrofuran-3-ylcarbamoyl)benzyl nitrate (95e)

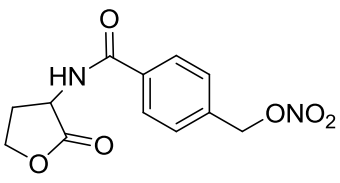

The acid **94e** (0.73 g, 3.71 mmol) was coupled to HSL (0.25 g, 2.47 mmol) using the method described for compound **95a** to give the title compound **95e** as a white solid (0.17 g, 46%). M.p. 152-154 °C; ^{1}H NMR (300 MHz, $CDCl_3$) δ 2.15-2.27 (m, 1H, H4a), 2.87-2.96 (m, 1H, H4b), δ 4.25-4.34 (m, 1H, H5a) 4.50 (dt, J = 9.0, 1.2 Hz, H5b), 4.62-4.70 (m, 1H, H3), 5.40 (s, 2H, CH_2ONO_2), 6.67 (bs, 1H, NH), 7.41 (d, J = 10.2 Hz, 2H, 2 × ArH), 7.82 (d, J = 10.2 Hz, 2H, 2 × ArH); ^{13}C NMR (75.6 MHz, $CDCl_3$) δ 30.1 (CH_2), 49.8

(CH), 66.3 (CH_2), 73.6 (CH_2), 127.7 (ArCH), 128.9 (ArCH), 133.8 (ArC), 136.4 (ArC), 167.0 (C=O), 175.4 (C=O); IR (neat): ν_{max} 3299, 2925, 1775, 1614, 1577, 1533, 1506, 1449, 1384, 1342, 1281, 1221, 1184, 1167, 1115, 1024, 992, 975, 955, 882, 850, 756, 732, 696 cm^{-1}; UV (MeOH): λ_{max} 228 nm (ε 12933 $M^{-1}cm^{-1}$); HRMS (ESI) *m/z* Calcd. for $C_{12}H_{12}N_2O_6Na$ $(M + Na)^+$ 303.0593. Found 303.0587.

11,13-Dioxo-13-(2-oxotetrahydrofuran-3-ylamino)tridecyl nitrate (97a)

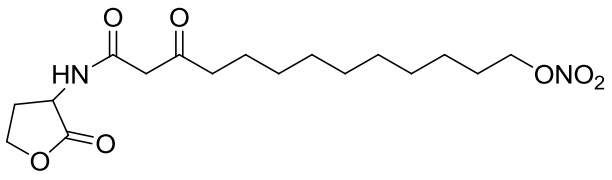

N,N-(dimethylamino)pyridine (DMAP) (0.22 g, 1.96 mmol), *N,N*-dicyclohexylcarbodiimide (DCC) (0.40 g, 1.18 mmol), the acid **94d** (0.40 g, 1.64 mmol) and Meldrum's acid **80** (0.23 g, 1.64 mmol) were dissolved in 20 mL of dichloromethane. The resulting solution was stirred overnight, cooled to r.t. and then filtered to remove *N,N*-dicyclohexyl urea formed in the reaction. The filtrate was concentrated in *vacuo*. The resulting residue was dissolved in DMF (10 mL) and α-amino-γ-butyrolactone hydrobromide **76** (0.30 g, 1.64 mmol) was added. The mixture was stirred at room temperature for 1 h and at 60 °C for an additional 4 h. The resulting solution was diluted with ethyl acetate 50 mL, and washed with saturated sodium carbonate solution, 1 M sodium hydrogen sulfate solution and brine. The organic phase was dried over sodium sulfate, filtered and concentrated in *vacuo*. Further purification by vacuum chromatography using ethyl acetate/ methanol (9.5:0.5) gave the title compound **97a** as a yellow solid (0.32 g, 54%). M.p. 58 °C; ^{1}H NMR (300 MHz, $CDCl_3$) δ 1.28-1.43 (m, 12H, 6 × CH_2), 1.53-1.58 (m, 2H, CH_2), 1.65-1.74 (m, 2H, CH_2), 2.19-2.28 (m, 1H, H4a), 2.49 (t, J = 6.0, 2H, $COCH_2$), 2.66-2.76 (m, 1H, H4b), 3.45 (s, 2H, $COCH_2CO$) 4.21-4.28 (m, 1H, H5a), 4.40 (t, J = 6.0 Hz, 2H,

CH_2ONO_2), 4.45 (dt, *J* = 12.0, 3.0 Hz, 1H, H5b), 4.56-4.62 (m, 1H, H3), 7.65 (bs, 1H, NH); ^{13}C NMR (75.6 MHz, $CDCl_3$) δ 23.2 (CH_2), 25.5 (CH_2), 26.7 (CH_2), 28.9 (CH_2), 29.0 (CH_2), 29.21 (CH_2), 29.25 (CH_2), 29.3 (CH_2), 29.6 (CH_2), 43.7 (CH_2), 48.3 (CH_2), 49.0 (CH), 65.9 (CH_2), 73.4 (CH_2), 166.4 (C=O), 174.9 (C=O), 206.4 (C=O). IR (neat): ν_{max} 3265, 2923, 2853, 1783, 1722, 1647, 1642, 1548, 1467, 1421, 1383, 1348, 1280, 1167, 1033, 999, 976, 866, 721, 702 cm^{-1}; UV (MeOH): λ_{max} 249 nm (ε 12943 $M^{-1}cm^{-1}$); HRMS (ESI) *m/z* Calcd. for $C_{17}H_{29}N_2O_7$ $(M + H)^+$ 373.1975. Found 373.1959.

12,14-Dioxo-14-(2-oxotetrahydrofuran-3-ylamino)tetradecyl nitrate (97b)

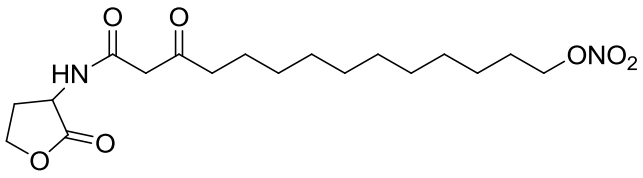

The title compound was synthesized as described for **97a** by reacting acid **94f** (0.42 g, 1.64 mmol) with Meldrum‘s acid **80** followed by HSL **76**, the resulting crude mixture was purified by vacuum chromatography to afford the title product **97b** as a light yellow solid (0.36 g, 57%). M.p. 62 °C; ^1H NMR (300 MHz, CDCl3): 1.25-1.39 (m, 14H, 7 × CH_2), 1.53-1.58 (m, 2H, CH_2), 1.67-1.72 (m, 2H, CH_2), 2.18-2.27 (m, 1H, H4a), 2.51 (t, *J* = 7.3 Hz, 2H, $COCH_2$), 2.67-2.76 (m, 1H, H4b), 3.45 (s, 2H, $COCH_2CO$), 4.21-4.30 (m, 1H, H5a), 4.42 (t, *J* = 6.6 Hz, 2H, CH_2ONO_2), 4.46 (dt, *J* = 9.0, 1.4 Hz, 1H, H5b), 4.53-4.62 (m, 1H, H3), 7.65 (bd, *J* = 6.5 Hz, 1H); ^{13}C NMR (75.6 MHz, $CDCl_3$) δ 23.3 (CH_2), 25.6 (CH_2), 26.7 (CH_2), 28.9 (CH_2), 29.0 (CH_2), 29.30 (CH_2), 29.36 (CH_2), 29.4 (CH_2), 29.7 (CH_2), 43.8 (CH_2), 48.2 (CH_2), 49.0 (CH), 65.9 (CH_2), 73.4 (CH_2), 166.4 (C=O), 174.9 (C=O), 206.5 (C=O). IR (neat): ν_{max} 3290, 2919, 2850, 1776, 1715, 1642, 1625, 1543, 1468, 1418, 1381, 1342, 1278, 1225, 1173, 1016, 1000, 949, 865, 720, 699 cm^{-1};

UV (MeOH): λ_{max} 251 nm (ε 11285 $M^{-1}cm^{-1}$); HRMS (ESI) *m/z* Calcd. for $C_{18}H_{30}N_2O_7Na$ $(M + Na)^+$ 409.1951. Found 409.1931.

11-Oxo-11-(2-oxo-2-(2-oxotetrahydrofuran-3-ylamino)ethylamino)undecyl nitrate (105)

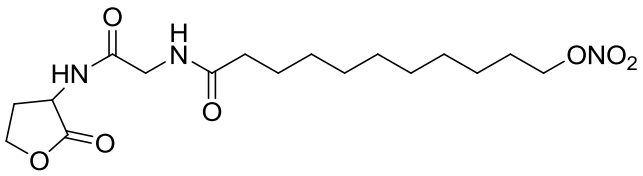

The preparation of the title compound involved the synthesis of 2-amino-*N*-(2-oxotetrahydrofuran-3-yl)acetamide **104** by coupling HSL **76** (0.5 g, 2.73 mmol) with *N*-Boc-glycine **103** (0.57 g, 3.28 mmol) in the presence of EDC (0.783 g, 4.10 mmol) and triethylamine (0.41 mL, 3.07 mmol) in DCM. The mixture was stirred at room temperature for 24h and then evaporated in *vacuo* to dryness. The residue was partitioned between water (20 mL) and ethyl acetate (50 mL) and the organic layer successively washed with 5% sodium bicarbonate ($NaHCO_3$) solution (2 x 20 mL), 1M potassium hydrogen sulfate ($KHSO_4$) solution (1 x 20 mL) and brine. The organic layer was dried over sodium sulfate (Na_2SO_4) and evaporated to dryness to yield the HSL-Boc glycine derivative as a white solid. ^{1}H NMR (300 MHz, $CDCl_3$) δ 1.40 (s, 9H, 3 × CH_3), 2.20-2.28 (m, 1H, H4a), 2.59-2.68 (m, 1H, H4b), 3.81-3.83 (m, 2H, $COCH_2NH$) 4.20-4.29 (m, 1H, H5a) 4.41 (dt, *J* = 8.9, 1.1 Hz, H5b), 4.56-4.64 (m, 1H, H3), 5.59 (bs, 1H, NH), 7.35 (bs, 1H, NH); ^{13}C NMR (75.6 MHz, $CDCl_3$) δ 28.2 (3 × CH_3) , 29.3 (CH_2), 48.8 (CH), 66.0 (CH_2), 156.2 (C=O), 170.6 (C=O), 175.5 (C=O). The product was treated with trifluoroacetic acid (5 mL) to remove the Boc group to give the desired product **104** as yellow oil. ^{1}H NMR (300 MHz, DMSO-d_6) δ 2.13-2.24 (m, 1H, H4a), 2.40-2.46 (m, 1H, H4b), 3.63 (s, 2H, $COCH_2NH$) 4.20-4.28 (m, 1H, H5a) 4.37 (dt, *J* = 1.5 and 8.7 Hz, H5b

), 4.67-4.73 (m, 1H, H3), 8.11 (bs, 1H, NH), 8.94 (bd, J = 7.8, 1H, NH); ^{13}C NMR (75.6 MHz, DMSO-d_6) δ 28.7 (CH_2), 40.5 (CH_2), 48.6 (CH), 65.8 (CH_2), 166.6 (C=O), 175.2 (C=O).

The crude Boc deprotected compound **104** (0.19 g, 0.69 mmol) was then coupled with 11-(nitrooxy)undecanoic acid **94d** (0.17 g, 0.69 mmol) using PyBop (0.36 g, 0.69 mmol) and DIPEA (0.36 mL, 2.09 mmol) in DCM at room temperature for 18h. The reaction mixture was concentrated in *vacuo*, diluted with ethyl acetate (50 mL), and washed with saturated sodium carbonate solution, 1 M sodium hydrogen sulfate solution and brine. The organic phase was dried over sodium sulfate, filtered and concentrated in *vacuo* to give the title compound **105** as an off white solid (0.26 g, 98%). M.p. 76-78 °C; ^{1}H NMR (300 MHz, DMSO-d_6): δ 1.26-1.39 (m, 12H, 6 × CH_2), 1.48-1.52 (m, 2H, CH_2), 1.64-1.78 (m, 2H, CH_2), 2.12 (t, J = 7.3 Hz, 2H, $COCH_2$), 2.16-2.23 (m, 1H, H4a), 2.34-2.43 (m, 1H, H4b), 3.70 (d, J = 5.9 Hz, 2H, $COCH_2NH$), 4.18-4.240 (m, 1H, H5a), 4.35 (dt, J = 1.4 and 9.0 Hz, 1H, H5b), 4.52 (t, J = 6.6 Hz, 2H, CH_2ONO_2), 4.54-4.64 (m, 1H, H3), 8.06 (t, J = 5.8 Hz, NH), 8.33 (d, J = 8.0 Hz, NH); ^{13}C NMR (75.6 MHz, $CDCl_3$) δ 25.3 (CH_2), 26.4 (CH_2), 28.6 (CH_2), 28.9 (CH_2), 29.1 (CH_2), 29.2 (CH_2), 35.6 (CH_2), 42.1 (CH_2), 48.3 (CH), 65.7 (CH_2), 74.3 (CH_2), 169.7 (C=O), 173.0 (C=O), 175.6 (C=O). IR (neat): ν_{max} 3284, 3078, 2922, 2852, 1775, 1661, 1643, 1546, 1465, 1416, 1375, 1353, 1277, 1175, 1017, 1000, 950, 858, 758, 697 cm^{-1}; HRMS (ESI) *m/z* Calcd. for $C_{17}H_{29}N_3O_7Na$ $(M + Na)^+$ 410.1903. Found 410.1881.

4-(Benzyloxy)-4-oxobutanoic acid (111a)

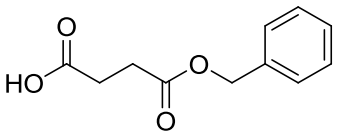

Method A: A mixture of succinic anhydride (5 g, 50.0 mmol), benzyl alcohol (5.69 mL, 55.0 mmol) and catalytic amount DMAP in anhydrous

THF (20 mL) was heated at reflux for 12 h. The solution was made acidic with 1N HCl and THF was evaporated. The residue was taken up in ethyl acetate and washed with 1N HCl. The organic layer was made basic with 5% $NaHCO_3$ and washed with ethyl acetate, and organic layer was discarded. The basic layer was acidified with 1N HCl and extracted with ethyl acetate, dried (Na_2SO_4) and filtered and the solvent was removed under vacuum to provide the title compound **111a** as a white solid (8.63 g, 83 %).

Method B: Succinic anhydride (5 g, 50.0 mmol) was dissolved in anhydrous DCM (40 mL). Benzyl alcohol (5.69 mL, 55.0 mmol), triethylamine (7.50 mL, 55.0 mmol), and a catalytic amount of DMAP were added to this solution. The resulting clear solution was stirred at room temperature for 18h, after which the, all the volatiles were removed under vacuum. The crude residue was taken up in diethyl ether (200 mL) and was extracted with 2N NaOH (2 × 75 mL). The aqueous extracts were carefully acidified to pH 2 with concentrated HCl and then extracted with diethyl ether (2 × 100 mL). The organic layer was dried (Na_2SO_4), filtered and concentrated to give the title acid **111a** as a white solid (8.84 g, 85 %). M.p. 52-54 °C, lit.[293] 56-57 °C; ^{1}H NMR (300 MHz, acetone-d_6): δ 2.68-2.71 (m, 4H, 2 × CH_2), 5.14 (s, 2H, CH_2Ar), 7.34-7.36 (m, 5H, ArH).

6-(Benzyloxy)-6-oxohexanoic acid (111b)

The title compound was synthesized following the 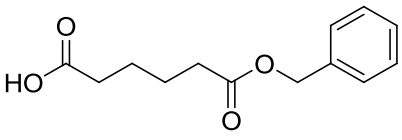

procedure described for compound **111a** using adipic anhydride and benzyl alcohol, the resulting crude mixture was purified by washing to afford the title product **111b** as a white waxy oil (7.45, 81%).^{1}H NMR (300 MHz, $CDCl_3$): δ 1.65-1.70 (m, 4H, 2 × CH_2) 2.32-2.39 (m, 4H, 2 × CH_2), 5.11 (s, 2H, CH_2Ar), 7.31-7.36 (m, 5H, ArH); ^{13}C NMR

(75.6 MHz, $CDCl_3$) δ 24.0 (CH_2), 24.3 (CH_2), 33.1 (CH_2), 33.8 (CH_2), 66.2 (CH_2), 128.2 (ArH), 128.5 (ArH), 173.1 (C=O), 178.7 (C=O).

4-Oxo-4-(2-oxotetrahydrofuran-3-ylamino)butanoic acid (107a)

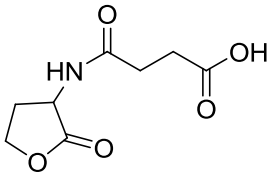

To a stirred solution of L-homoserine lactone hydrobromide **76** (0.5 g, 2.73 mmol) in DCM (10 mL) triethylamine (0.42 mL, 3.00 mmol) was added followed by the addition of acid **111a** (0.62 g, 3.00 mmol) and l-ethyl-3-(3-dimethylaminopropyl)carbodiimide hydrochloride (EDC) (0.78 g, 4.10 mmol). The mixture was stirred at room temperature for 30h and then evaporated in *vacuo* to dryness. The residue was partitioned between water (20 mL) and ethyl acetate (50 mL) and the organic layer successively washed with 5% sodium bicarbonate ($NaHCO_3$) solution (2 x 20 mL), 1M potassium hydrogen sulfate ($KHSO_4$) solution (1 x 20 mL) and brine. The organic layer was dried over sodium sulfate and evaporated to dryness to yield the benzyl protected HSL derivative **112a** as a colorless oil (0.53 g, 66%). ^{1}H NMR (300 MHz, $CDCl_3$): δ 2.05-2.20 (m, 1H, H4a), 2.53-2.58 (m, 2H, CH_2), 2.68-2.73 (m, 3H, CH_2 and H4b), 4.18-4.27 (m, 1H, H5a), 4.40 (dt, J = 9.0, 1.3 Hz, 1H, H5b), 4.49-4.53 (m, 1H, H3), 5.11 (s, 2H, CH_2Ar), 6.68 (bd, J = 6.3 Hz, 1H, NH), 7.32 (m, 5H, ArH). The compound‘s benzyl group was removed by hydrogenation using 10% Pd/C (0.20 g) and H_2 gas at atmospheric pressure in THF at reflux for 30h. The crude reaction mixture was filtered through a column of Celite and silica to remove Pd/C. The filtrate was evaporated to dryness to give the title compound **107a** as a white solid (0.30 g, 84%). M.p. 112-114 °C; ^{1}H NMR (300 MHz, DMSO-d_6): δ 2.07-2.18 (m, 1H, H4a), 2.33-2.51 (m, 5H, 2 × CH_2 and H4b), 4.15-4.24 (m, 1H, H5a), 4.33 (dt, J = 8.7, 1.8 Hz, 1H, H5b), 4.49-4.58 (m, 1H, H3), 6.68 (bd, J = 7.9 Hz, 1H, NH), 12.09 (bs,

COOH); ^{13}C NMR (75.6 MHz, DMSO-d_6) δ 28.7 (CH_2), 29.3 (CH_2), 30.1 (CH_2), 48.3 (CH), 65.7 (CH_2), 171.5 (C=O), 174.1 (C=O), 175.7 (C=O); IR (neat): ν_{max} 3352, 2920, 2519, 1771, 1715, 1611, 1556, 1442, 1427, 1384, 1353, 1277, 1238, 1179, 1131, 1103, 1022, 999, 952, 919, 845, 754, 699, 676 cm^{-1}; HRMS (ESI) *m/z* Calcd. for $C_8H_{11}NO_5Na$ $(M + Na)^+$ 224.0535. Found 224.0524; Anal. Calcd. for $C_8H_{11}NO_5$: C, 47.76; H, 5.51; N, 6.96. Found: C, 47.87; H, 5.49; N, 6.91.

6-Oxo-6-(2-oxotetrahydrofuran-3-ylamino)hexanoic acid (107b)

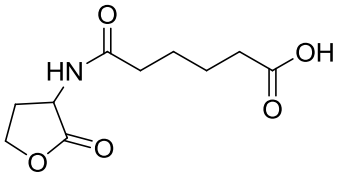

The title compound was synthesized following the procedure for compound **107a** using acid **111b** (0.64 g; 3.00 mmol) first to synthesize protected acid **112b** (0.5 g, 58%). ^{1}H NMR (300 MHz, $CDCl_3$): δ 1.67 (m, 4H, 2 × CH_2), 2.05-2.20 (m, 1H, H4a), 2.23-2.38 (m, 4H, 2 × CH_2), 2.75-2.78 (m, 1H, H4b), 4.18-4.31 (m, 1H, H5a), 4.43 (dt, *J* = 9.0, 1.1 Hz, 1H, H5b), 4.49-4.53 (m, 1H, H3), 5.10 (s, 2H, CH_2Ar), 6.26 (bd, *J* = 5.2 Hz, 1H, NH), 7.32 (m, 5H, ArH). The deprotection of compound **112b** gave the desired product **107b** as a white solid (0.27 g, 78%). M.p. 142-144 °C; ^{1}H NMR (300 MHz, DMSO-d_6): δ 1.48-1.52 (m, 4H, 2 × CH_2), 2.05-2.19 (m, 5H, H4a and 2 × CH_2), 2.33-2.42 (m, 1H, H4b), 4.15-4.23 (m, 1H, H5a), 4.33 (dt, *J* = 8.8, 1.8 Hz, 1H, H5b), 4.47-4.56 (m, 1H, H3), 8.32 (bd, *J* = 7.9 Hz, 1H, NH). ^{13}C NMR (75.6 MHz, DMSO-d_6) δ 24.5 (CH_2), 25.1 (CH_2), 28.7 (CH_2), 33.9 (CH_2), 35.2 (CH_2), 48.2 (CH), 65.6 (CH_2), 172.4 (C=O), 174.8 (C=O), 175.8 (C=O); IR (neat): ν_{max} 3342, 3291, 2955, 2934, 2872, 1763, 1692, 1640, 1536, 1467, 1429, 1407, 1359, 1282, 1251, 1223, 1190, 1171, 1103, 1080, 1015, 999, 945, 920, 803, 734, 716 cm^{-1}; HRMS (ESI) *m/z* Calcd. for

$C_{10}H_{15}NO_5Na$ $(M + Na)^+$ 252.0848. Found 252.0840; Anal. Calcd. for $C_{10}H_{15}NO_5$: C, 52.40; H, 6.60; N, 6.11. Found: C, 52.42; H, 6.73; N, 6.17.

O^2-Methyl-1-(4-(4-oxo-4-(2-oxotetrahydrofuran-3-ylamino)butanoyl)piperazin-1-yl)diazen-1-ium-1,2-diolate (121a)

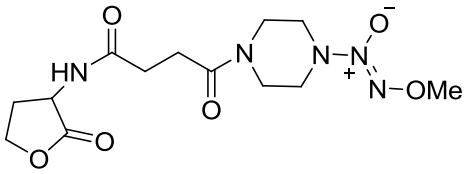

To a solution of acid **107a** (0.15 g, 0.75 mmol) and diazeniumdiolate **116** (0.14 g, 0.90 mmol) in water/acetonitrile (5:1) (6 mL) EDC (0.21g, 1.12 mmol) was added. The reaction mixture was allowed to stir at r.t. for 40 h. The solvent was concentrated under *vacuo*, and extracted with EtOAc (2 × 50 mL). The organic layer was washed with brine (2 × 25 mL), dried over anhydrous Na_2SO_4 and evaporated to give a crude residue. Purification by vacuum chromatography using ethyl acetate/methanol (9.5:0.5) gave the title compound **121a** as a yellow oil (0.11 g, 43%). ^{1}H NMR (300 MHz, $CDCl_3$): δ 2.12-2.26 (m, 1H, H4a), 2.57-2.62 (m, 2H, CH_2), 2.66-2.73 (m, 3H, CH_2 and H4b), 3.36-3.44 (m, 4H, 2 × CH_2), 3.65-3.78 (m, 4H, 2 × CH_2), 4.00 (s, 3H, OCH_3), 4.20-4.29 (m, 1H, H5a), 4.43 (dt, J = 9.0, 1.3 Hz, 1H, H5b), 4.49-4.54 (m, 1H, H3), 6.86 (bd, J = 6.6 Hz, 1H, NH); ^{13}C NMR (75.6 MHz, $CDCl_3$) δ 28.1 (CH_2), 29.8 (CH_2), 30.7 (CH_2), 40.4 (CH_2), 43.9 (CH_2), 49.0 (CH), 51.1 (CH_2), 61.2 (OCH_3), 65.9 (CH_2), 170.3 (C=O), 172.7 (C=O), 175.2 (C=O); IR (neat): ν_{max} 3309, 2919, 2866, 1775, 1637, 1534, 1494, 1442, 1380, 1281, 1213, 1170, 1112, 1028, 946, 914, 813, 727 cm^{-1}; UV (MeOH): λ_{max} 244 nm (ε 5012 $M^{-1}cm^{-1}$); HRMS (ESI) *m/z* Calcd. for $C_{13}H_{21}N_5O_6Na$ $(M + Na)^+$ 366.1390. Found 366.1379.

***O*²-Methyl-1-(4-(4-oxo-4-(2-oxotetrahydrofuran-3-ylamino)hexanoyl)piperazin-1-yl)diazen-1-ium-1,2-diolate (121b)**

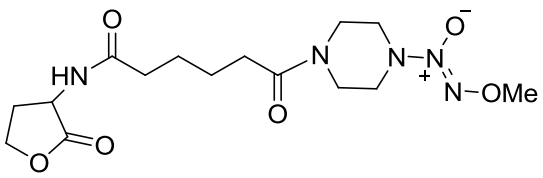

HSL acid **107b** (0.2 g, 0.87 mmol) was coupled with diazeniumdiolate **116** (0.15 g, 0.95 mmol) as described for compound **121a** to give the title compound **121b** as a yellow oil (0.11 g, 35%).^{1}H NMR (300 MHz, $CDCl_3$): δ 2.16-2.21 (m, 1H, H4a), 2.23-2.35 (m, 4H, 2 × CH_2), 2.64-2.73 (m, 1H, H4b), 3.34-3.40 (m, 4H, 2 × CH_2), 3.60-3.77 (m, 4H, 2 × CH_2), 4.00 (s, 3H, OCH_3), 4.20-4.29 (m, 1H, H5a), 4.43 (dt, J = 8.9, 1.4 Hz, 1H, H5b), 4.53-4.62 (m, 1H, H3), 6.94 (bd, J = 6.7 Hz, 1H, NH); ^{13}C NMR (75.6 MHz, $CDCl_3$) δ 24.2 (CH_2), 24.8 (CH_2), 29.7 (CH_2), 32.5 (CH_2), 35.5 (CH_2), 40.1 (CH_2), 43.9 (CH_2), 48.9 (CH), 51.2 (CH_2), 61.2 (OCH_3), 65.9 (CH_2), 171.3 (C=O), 173.3 (C=O), 175.4 (C=O); IR (neat): ν_{max} 3299, 2943, 2869, 2247, 1774, 1629, 1534, 1494, 1439, 1380, 1280, 1218, 1175, 1111, 1064, 1031, 947, 915, 727 cm^{-1}; UV (MeOH): λ_{max} 242 nm (ε 5420 M^{-1}cm^{-1}); HRMS (ESI) *m/z* Calcd. for $C_{15}H_{25}N_5O_6Na$ $(M + Na)^+$ 394.1703. Found 394.1693.

***O*²-(2,4-Dinitrophenyl)-1-(4-(4-oxo-4-(2-oxotetrahydrofuran-3-ylamino)butanoyl)piperazin-1-yl)diazen-1-ium-1,2-diolate (122a)**

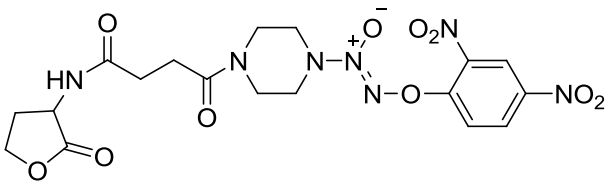

The title compound was synthesized following the procedure for compound **121a** using the HSL acid **107a** (0.1 g; 0.50 mmol) and diazeniumdiolate **120** (0.19 g, 0. 55 mmol) to give desired product **122a** as a yellow solid (0.17 g, 79%). M.p. 112-114 °C; ^{1}H NMR (300 MHz, $CDCl_3$): δ 2.17-2.29 (m, 1H, H4a), 2.63-2.66 (m, 2H, CH_2), 2.69-2.76 (m, 3H, CH_2 and H4b), 3.36-3.87

(m, 8H, 4 × CH_2), 4.22-4.31 (m, 1H, H5a), 4.46 (dt, J = 9.0 and 1.2 Hz, 1H, H5b), 4.49-4.57 (m, 1H, H3), 6.61 (bd, J = 6.5 Hz, 1H, NH), 7.92 (d, J = 9.0 Hz, ArCH), 8.54 (dd, J = 9.0 and 1.2 Hz, ArCH), 8.87 (d, J = 1.2 Hz, ArCH); ^{13}C NMR (75.6 MHz, $CDCl_3$) δ 28.1 (CH_2), 29.8 (CH_2), 30.8 (CH_2), 40.2 (CH_2), 43.8 (CH_2), 49.1 (CH), 50.5 (CH_2), 65.9 (CH_2), 117.8 (ArCH), 122.1 (ArCH), 129.1 (ArCH), 170.3 (C=O), 172.6 (C=O), 175.1 (C=O); IR (neat): ν_{max} 3313, 3053, 2916, 2857, 1780, 1674, 1605, 1527, 1472, 1447, 1343, 1264, 1239, 1209, 1158, 1114, 1068, 1012, 959, 909, 850, 835, 731, 699 cm^{-1}; UV (MeOH): λ_{max} 297 nm (ε 58484 $M^{-1}cm^{-1}$); HRMS (ESI) *m/z* Calcd. for $C_{18}H_{21}N_7O_{10}Na$ $(M + Na)^+$ 518.1248. Found 518.1240.

O^2-(2,4-Dinitrophenyl)-1-(4-(4-oxo-4-(2-oxotetrahydrofuran-3-ylamino)hexanoyl)piperazin-1-yl)diazen-1-ium-1,2-diolate (122b)

The title compound was synthesized following the procedure for compound **121a** using the HSL acid **107b** (0.1 g, 0.43 mmol) and diazeniumdiolate **120** (0.16 g, 0.47 mmol) to give desired product **122b** as a yellow solid (0.16 g, 72%). M.p. 108-110 °C, δ 2.16-2.21 (m, 1H, H4a), 2.25-2.34 (m, 4H, 2 × CH_2), 2.64-2.73 (m, 1H, H4b), 3.57-3.64 (m, 4H, 2 × CH_2), 3.73-3.79 (m, 4H, 2 × CH_2), 4.20-4.29 (m, 1H, H5a), 4.43 (dt, J = 1.4 and 8.9 Hz, 1H, H5b), 4.53-4.62 (m, 1H, H3), 6.94 (bd, J = 6.7 Hz, 1H, NH), 7.68 (d, J = 9.0 Hz, ArCH), 8.47 (dd, J = 9.0 and 1.2 Hz, ArCH), 8.89 (d, J = 1.2 Hz, ArCH); ^{13}C NMR (75.6 MHz, $CDCl_3$) δ 24.2 (CH_2), 24.8 (CH_2), 29.7 (CH_2), 32.5 (CH_2), 35.5 (CH_2), 40.1 (CH_2), 43.9 (CH_2), 48.9 (CH), 51.2 (CH_2), 61.2 (OCH_3), 65.9 (CH_2), 118.3 (ArCH), 122.3 (ArCH), 129.6 (ArCH), 171.3 (C=O), 173.3 (C=O), 175.4 (C=O); IR

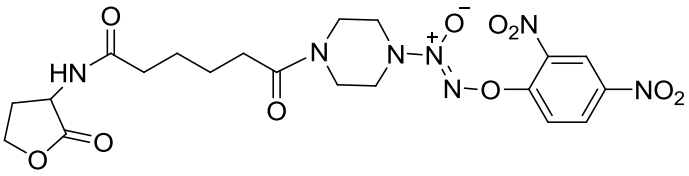

(neat): ν_{max} 3313, 3053, 2916, 2857, 1779, 1664, 1605, 1527, 1472, 1447, 1342, 1264, 1239, 1209, 1158, 1114, 1068, 1012, 959, 909, 848, 832, 731, 667 cm^{-1}; HRMS (ESI) *m/z* Calcd. for $C_{20}H_{25}N_7O_{10}Na$ $(M + Na)^+$ 546.1561. Found 546.1554

3-Acetamido-4,4-dimethylthietan-2-one (124)

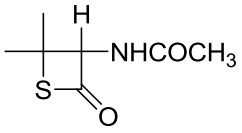

Acetic anhydride was added dropwise to an ice-cooled mixture of D-penicillamine **127** and potassium carbonate and stirred overnight. To the reaction mixture ice-cold water was added and the precipitate filtered to yield the title compound **124** as a white solid. M.p. 164-166 °C; ^{1}H NMR (300 MHz, $CDCl_3$): δ 1.62 (s, 3H, CH_3), 1.84 (s, 3H, CH_3), 2.04 (s, 3H, $NHCOCH_3$), 5.64 (d, J = 8.0 Hz, 1H, CH), 6.46 (bs, 1H, NH); ^{13}C NMR (75.6 MHz, $CDCl_3$) δ 22.5 (CH_3), 26.2 (CH_3), 30.2 (OCH_3), 51.2 (C) 76.3 (CH), 169.5 (C=O), 192.2 (C=O).

2-Acetamido-3-mercapto-3-methyl-N-(2-oxotetrahydrofuran-3-yl)butanamide (128)

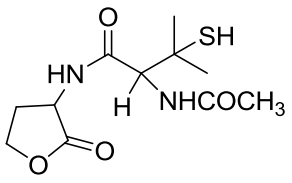

A solution of HSL **76** (0.3 g, 1.64 mmol), triethylamine (0.25 mL, 1.80 mmol) and 3-acetamido-4,4-dimethylthietan-2-one **124** (0.34 g, 1.96 mmol) in dimethylformamide was stirred overnight. The solvent was evaporated to dryness and purified by column chromatography using ethyl acetate/methanol (95:5) as mobile phase to yield the title compound. ^{1}H NMR (300 MHz, $CDCl_3$) δ 2.16-2.28 (m, 1H, H4a), 2.82-2.91 (m, 1H, H4b), δ 4.27-4.36 (m, 1H, H5a) 4.51 (t, J = 9.1 Hz, H5b), 4.56-4.65 (m, 1H, H3), 4.95 (s, 2H, CH_2ONO_2), 6.57 (bs, 1H, NH); ^{13}C NMR (75.6 MHz, $CDCl_3$) δ 30.1(CH_2) , 49.1

(CH), 66.1 (CH_2), 69.0 (CH_2), 165.4 (C=O), 170.2 (C=O), 174.4 (C=O); IR (neat): ν_{max} 3313, 3261, 3083, 2968, 1784, 1635, 1563, 1538, 1462, 1376, 1278, 1171, 1143, 1022, 949, 812, 735, 699 cm^{-1}; HRMS (ESI) *m/z* Calcd. for $C_{11}H_{18}N_2O_4SNa$ $(M + Na)^+$ 297.0885. Found 297.0872.

(*S*)-3-Acetamido-2-methyl-4-oxo-4-(2-oxotetrahydrofuran-3-ylamino)butan-2-yl nitrothioite (129)

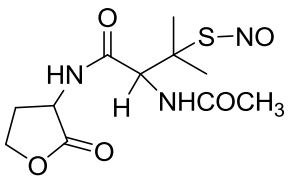

The title compound was obtained by reacting compound **128** (0.02g, 0.072 mmol) with *t*-butyl nitrite (0.02 mL, 0.14 mmol) in chloroform at r.t. for 45 minutes. Evaporation of the solvent yielded the product as yellow green material. ^1H NMR (300 MHz, $CDCl_3$) δ 1.35 (s,)2.00 (s, CH_3), 2.02 (s,CH_3) 2.16-2.24 (m, 1H, H4a), 2.56-2.60 (m, 1H, H4b), δ 4.27-4.36 (m, 1H, H5a) 4.51 (t, J = 9.1 Hz, H5b), 4.56-4.68 (m, 1H, H3), 5.25 (d, H, CH), 6.46 (bs, 1H, NH). ^{13}C NMR (75.6 MHz, $CDCl_3$) δ 30.1(CH_2) , 49.1 (CH), 66.1 (CH_2), 69.0 (CH_2), 165.4 (C=O), 171.1 (C=O), 174.4 (C=O); HRMS (ESI) *m/z* Calcd. for $C_{11}H_{17}N_3O_5SNa$ $(M + Na)^+$ 326.0787. Found 326.0951.

3-(1-Bromobutyl)-5-(dibromomethylene)furan-2(5*H*)-one (156a)

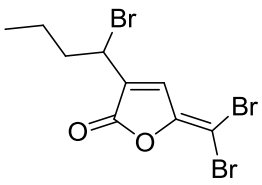

N-bromosuccinimide (NBS) (3.15 g, 17.74 mmol) was added to a solution of 3-butyl-5-(dibromomethylene)-2(5*H*)-furanone **153a** (5 g, 16.13 mmol) and catalytic amount benzoyl peroxide in carbon tetrachloride (CCl_4) (60 mL). The mixture was irradiated with 250W lamp and was refluxed for 18 h. The crude product was filtered through a pad of silica, filtrate

evaporated and purified by vacuum chromatography using dichloromethane/n-hexane to afford the title fimbrolide compound **156a** as a light yellow solid (6.27 g, 100%). M.p. 76 °C; ^{1}H NMR (300 MHz, $CDCl_3$): δ 0.98 (t, J = 7.1 Hz, 3H, CH_3), 1.47 (m, 2H, CH_2), 2.08-2.15 (m, 2H, CH_2), 4.73 (m, 1H, CHBr), 7.55 (s, 1H, CH); ^{13}C NMR (75.6 MHz, $CDCl_3$): δ 13.1 (CH_3), 20.9 (CH_2), 38.6 (CH_2), 42.1 (CHBr), 82.7 (CBr_2), 135.4 (CH), 137.4 (C), 149.1 (C), 165.7 (C=O); IR (neat): ν_{max} 3086, 2964, 2872, 1779, 1612, 1597, 1463, 1376, 1321, 1267, 1185, 1165, 1108, 1061, 1037, 968, 917, 898, 845, 777, 735, 665 cm^{-1}; HRMS (ESI) *m/z* Calcd. for $C_9H_{10}Br_3O_2$ $(M + H)^+$ 386.8231. Found 386.8224

3-(1-Bromoethyl)-5-(dibromomethylene)furan-2(5*H*)-one (156b)

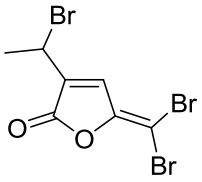

The title compound synthesis was carried out as described for the preparation of compound **156a** using a solution of 3-ethyl-5-(dibromomethylene)-2(5*H*)-furanone **153b** (3.0 g, 10.63 mmol) and NBS (2.27g, 12.76 mmol) in 40 mL carbon tetrachloride to give desired product as an off white solid (3.34 g, 83%). M.p. 110-112 °C; ^{1}H NMR (300 MHz, $CDCl_3$): δ 1.97 (d, J = 6.72 Hz, 3H, CH_3), 4.87 (q, J = 6.72 Hz, 3H, CH_2Br), 7.57 (s, 1H, CH); ^{13}C NMR (75.6 MHz, $CDCl_3$): δ 24.0 (CH_3), 35.9 (CHBr), 82.8 (CBr_2), 134.7 (C=CH), 138.2 (CH), 149.4 ($C=CBr_2$), 166.0 (C=O); IR (neat): ν_{max} 3091, 2920, 1782, 1611, 1595, 1383, 1260, 1170, 1088, 1006, 968, 908, 844, 773, 738 cm^{-1}; HRMS (ESI) *m/z* Calcd. for $C_7H_5Br_3O_2Na$ $(M + Na)^+$ 380.7737. Found 380.7732

3-(1-Bromohexyl)-5-(dibromomethylene)furan-2(5*H*)-one (156c)

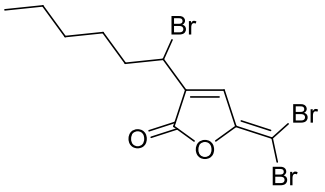

The title compound synthesis was carried out as described for the preparation of compound **156a** using the fimbrolide derivative, 3-hexyl-5-(dibromomethylene)-2(5*H*)-furanone **153c** (2.0 g, 5.91 mmol) and NBS (6.10 mmol) to give the title compound **156c** as an off white solid (2.39 g, 97%). M.p. 76 °C; ^{1}H NMR (300 MHz, $CDCl_3$): δ 0.91 (t, J = 7.1 Hz, 3H, CH_3), 1.29-1.56 (m, 6H, 3 × CH_2), 2.05-2.15 (m, 2H, CH_2), 4.68-4.73 (m, 1H, CHBr), 7.54 (s, 1H, CH); ^{13}C NMR (75.6 MHz, $CDCl_3$): δ 13.9 (CH_3), 22.3 (CH_2), 27.3 (CH_2), 30.8 (CH_2), 36.7 (CH_2), 42.4 (CHBr), 82.6 (CBr_2), 135.7 (CH), 137.4 (C=CH), 149.1 (C=CBr_2), 165.7 (C=O); IR (neat): ν_{max} 3091, 2951, 2857, 1775, 1614, 1597, 1466, 1375, 1269, 1215, 1177, 1115, 1052, 999, 966, 912, 848, 833, 777, 669 cm^{-1}; HRMS (ESI) *m/z* Calcd. for $C_{11}H_{13}Br_3O_2Na$ $(M + Na)^+$ 436.8363. Found 436.8358

3-(1-Bromoheptyl)-5-(dibromomethylene)furan-2(5*H*)-one (156d)

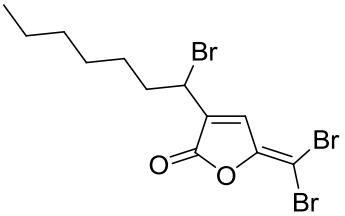

The title compound reaction was carried out as described for the preparation of compound **156a** using a solution of 3-heptyl-5-(dibromomethylene)-2(5*H*)-furanone **153d** (0.80 g, 2.27 mmol) and NBS (0.44 g, 2.49 mmol) in 25 mL carbon tetrachloride to give desired product **156d** as a light yellow solid (0.95 g, 97%). M.p. 76 °C; ^{1}H NMR (300 MHz, $CDCl_3$): δ 0.90 (t, J = 7.1 Hz, 3H, CH_3), 1.26-1.87 (m, 8H, 4 × CH_2), 1.90-1.95 (m, 2H, CH_2), 4.68 (m, 1H, CHBr), 7.53 (s, 1H, CH); ^{13}C NMR (75.6 MHz, $CDCl_3$): δ 14.0 (CH_3), 22.5 (CH_2), 24.8 (CH_2), 31.6 (CH_2), 31.8 (CH_2), 42.3 (CHBr), 83.5 (CBr_2), 135.4 (CH), 137.7 (C=C), 149.1 (C=CBr_2), 165.7 (C=O); IR

(neat): ν_{max} 3092, 2954, 2923, 2855, 1777, 1615, 1596, 1464, 1428, 1377, 1267, 1198, 1177, 1103, 1045, 1007, 967, 913, 848, 832, 774, 670 cm^{-1}; HRMS (ESI) *m/z* Calcd. for $C_{12}H_{15}Br_3O_2Na$ $(M + Na)^+$ 450.8520. Found 450.8521.

3-(1-Bromooctyl)-5-(dibromomethylene)furan-2(5*H*)-one (156e)

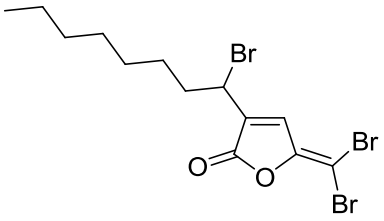

The fimbrolide derivative, 3-octyl-5-(dibromomethylene)-2(5*H*)-furanone **153e** (2.0 g, 5.46 mmol) was brominated using NBS (5.46 mmol) by the method described for compound **156a** to give the title compound **156e** as an off white solid (2.28, 94%). M.p. 76 °C; ^{1}H NMR (300 MHz, $CDCl_3$): δ 0.85 (t, J = 7.0 Hz, 3H, CH_3), 1.27-1.44 (m, 10H, 5 × CH_2), 2.06-2.13 (m, 2H, CH_2), 4.68-4.73 (m, 1H, CHBr), 7.54 (s, 1H, CH); ^{13}C NMR (75.6 MHz, $CDCl_3$): δ 14.0 (CH_3), 22.5 (CH_2), 24.8 (CH_2), 27.6 (CH_2), 28.6 (CH_2), 28.9 (CH_2), 31.6 (CH_2), 36.7 (CH_2), 42.4 (CHBr), 82.6 (CBr_2), 135.3 (CH), 137.4 (C=C), 149.1 ($C=CBr_2$), 165.7 (C=O); IR (neat): ν_{max} 3091, 2921, 2852, 1777, 1699, 1613, 1597, 1464, 1265, 1198, 1177, 1014, 966, 907, 849, 832, 778, 670 cm^{-1}; HRMS (ESI) *m/z* Calcd. for $C_{13}H_{17}Br_3O_2Na$ $(M + Na)^+$ 464.8676. Found 464.8666.

3-(1-Bromododecyl)-5-(dibromomethylene)furan-2(5H)-one (156f)

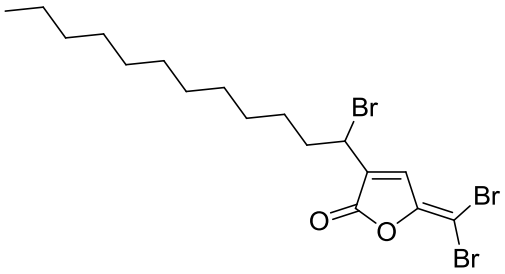

The fimbrolide derivative, 3-dodecyl-5-(dibromomethylene)-2(5*H*)-furanone **153f** (2.0 g, 4.73 mmol) was brominated using NBS (1.01 g, 5.68 mmol) by the method described

for compound **156a** to give the title compound **156f** as an off white solid (2.23 g, 94%). M.p. 52 °C; ^{1}H NMR (300 MHz, $CDCl_3$): δ 0.87 (t, J = 6.9 Hz, 3H, CH_3), 1.26 (m, 18H, 9 × CH_2), 2.08-2.13 (m, 2H, CH_2), 4.71 (m, 1H, CHBr), 7.54 (s, 1H, CH); ^{13}C NMR (75.6 MHz, $CDCl_3$): δ 14.1 (CH_3), 22.6 (CH_2), 27.6 (CH_2), 28.6 (CH_2), 29.3 (CH_2), 29.4 (CH_2), 29.5 (CH_2), 31.9 (CH_2), 36.7 (CH_2), 42.4 (CHBr), 82.6 (CBr_2), 135.3 (CH), 137.4 (C=C), 149.1 (C=CBr_2), 165.7 (C=O); IR (neat): ν_{max} 3091, 2921, 2852, 1777, 1699, 1613, 1597, 1464, 1265, 1198, 1177, 1014, 966, 907, 849, 832, 778, 670 cm^{-1}; HRMS (ESI) *m/z* Calcd. for $C_{17}H_{25}Br_3O_2Na$ $(M + Na)^+$ 520.9302. Found 520.9290.

1-(5-(Dibromomethylene)-2-oxo-2,5-dihydrofuran-3-yl)ethyl nitrate (155b)

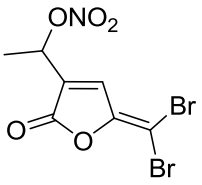

A solution of bromo fimbrolide **156b** (0.50 g, 1.38 mmol) and silver nitrate (0.28 g, 1.66 mmol) in anhydrous acetonitrile (25 mL) was heated at 70 °C for 18h. The crude product was filtered through a column of Celite and silica to remove the silver salt formed. The filtrate was evaporated to dryness and purified by vacuum chromatography using dichloromethane/n-hexane to give the title compound **155b** as a light yellow solid (0.34 g, 72%). M.p. 42-44 °C; ^{1}H NMR (300 MHz, $CDCl_3$): δ 1.63 (d, J = 6.72 Hz, 3H, CH_3), 5.82 (q, J = 6.72 Hz, 3H, CH_2ONO_2), 7.57 (s, 1H, CH); ^{13}C NMR (75.6 MHz, $CDCl_3$): δ 18.0 (CH_3), 73.7 ($CHONO_2$), 83.1 (CBr_2), 134.2 (C=CH), 135.7 (CH), 149.4 (C=CBr_2), 166.0 (C=O); IR (neat): ν_{max} 3090, 2973, 1765, 1614, 1454, 1388, 1327, 1266, 1193, 1124, 1042, 984, 964, 888, 852, 786, 746, 702 cm^{-1}; UV (MeOH): λ_{max} 310 nm (ε 279240 M^{-1}cm^{-1}); HRMS (ESI) *m/z* Calcd. for $C_7H_5Br_2NO_5Na$ $(M + Na)^+$ 367.8391. Found 367.8378; Anal. Calcd. for $C_7H_5Br_2NO_5$: C, 24.52; H, 1.47; N, 4.08. Found: C, 25.16; H, 1.56; N, 3.96.

3-(1-Nitrooxybutyl)-5-(dibromomethylene)-2(5*H*)-furanone (155a)

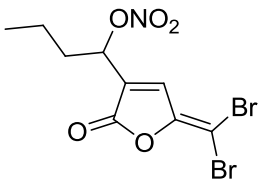

The title compound was synthesized following the procedure for compound **155b** using the bromofimbrolide **156a** (1 g, 2.57 mmol) and silver nitrate (0.65g, 3.85 mmol) to give desired product as a yellow solid (0.76 g, 80%). M.p. 42-44 °C; ^{1}H NMR (300 MHz, $CDCl_3$): δ 0.97 (t, J = 7.1 Hz, 3H, CH_3), 1.46 (m, 2H, CH_2), 1.81-2.05 (m, 2H, CH_2), 5.70 (t, J = 7.1 Hz, 1H, $CHONO_2$), 7.55 (s, 1H, CH); ^{13}C NMR (75.6 MHz, $CDCl_3$): δ 13.4 (CH_3), 18.2 (CH_2), 33.6 (CH_2), 83.5 (CBr_2), 133.6 (C), 135.4 (CH), 149.0 (C), 165.7 (C=O); IR (neat): ν_{max} 3108, 2966, 2875, 1768, 1633, 1607, 1457, 1384, 1321, 1285, 1264, 1180, 1129, 1065, 1034, 1000, 967, 902, 879, 844, 774, 752, 738, 693 cm^{-1}; UV (MeOH): λ_{max} 310 nm (ε 239590 M^{-1}cm^{-1}); HRMS (ESI) *m/z* Calcd. for $C_9H_9Br_2NO_5Na$ $(M + Na)^+$ 391.8745. Found 391.8743; Anal. Calcd. for $C_9H_9Br_2NO_5$: C, 29.14; H, 2.45; N, 3.78. Found: C, 29.48; H, 2.41; N, 3.51.

3-(1-Nitrooxyhexyl)-5-(dibromomethylene)furan-2(5*H*)-one (155c)

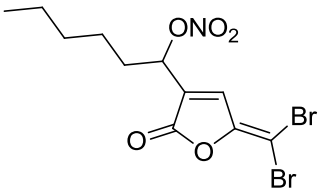

The title compound synthesis was carried out as described for the preparation of compound **155b** using the bromofimbrolide **156c** (0.8g, 2.52 mmol) and silver nitrate (0.64 g, 3.78 mmol) to give the title compound as a white solid (0.58 g, 76%). M.p. 50 °C; ^{1}H NMR (300 MHz, $CDCl_3$): δ 0.93 (t, J = 7.1 Hz, 3H, CH_3), 1.43 (m, 4H, 2 × CH_2), 1.81-2.15 (m, 4H, 2 × CH_2), 5.71 (t, J = 7.1 Hz, 1H, $CHONO_2$), 7.52 (s, 1H, CH); ^{13}C NMR (75.6 MHz, $CDCl_3$): δ 13.9 (CH_3), 22.3 (CH_2), 27.3 (CH_2), 30.8 (CH_2), 36.7 (CH_2), 76.4 ($CHONO_2$), 83.2 (CBr_2), 133.6 (C), 135.4 (CH), 149.0 (C), 165.7 (C=O); IR

(neat): ν_{max} 3095, 2952, 2931, 2862, 1769, 1637, 1449, 1378, 1271, 1203, 1184, 1134, 1047, 1036, 996, 971, 931, 914, 839, 774, 749, 682 cm^{-1}; UV (MeOH): λ_{max} 310 nm (ε 239419 $M^{-1}cm^{-1}$); HRMS (ESI) *m/z* Calcd. for $C_{11}H_{13}Br_2NO_5Na$ $(M + Na)^+$ 419.9058. Found 419.9056.

3-(1-Nitrooxyheptyl)-5-(dibromomethylene)furan-2(5*H*)-one (155d)

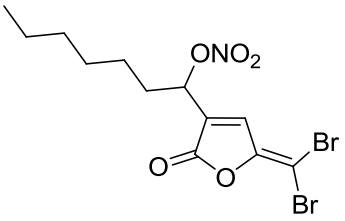

The title compound synthesis was carried out as described for the preparation of compound **155b** using bromofimbrolide **156d** (0.60 g, 1.39 mmol) and silver nitrate (0.30 g, 1.80 mmol) to give the title compound **155d** as a white solid (0.41 g, 71%). M.p. 52 °C; ^{1}H NMR (300 MHz, $CDCl_3$): δ 0.90 (t, J = 7.1 Hz, 3H, CH_3), 1.26-1.87 (m, 8H, 4 × CH_2), 1.90-1.95 (m, 2H, CH_2), 5.68 (t, J = 7.1 Hz, 1H, $CHONO_2$), 7.53 (s, 1H, CH); ^{13}C NMR (75.6 MHz, $CDCl_3$): δ 13.8 (CH_3), 22.3 (CH_2), 24.7 (CH_2), 28.5 (CH_2), 31.2 (CH_2), 31.7 (CH_2), 76.8 ($CHONO_2$), 83.4 (CBr_2), 133.6 (C=C), 135.4 (CH), 148.9 ($C=CBr_2$), 165.6 (C=O); IR (neat): ν_{max} 3093, 2930, 2859, 1767, 1637, 1454, 1378, 1290, 1267, 1195, 1182, 1048, 1030, 1012, 968, 951, 847, 750, 682 cm^{-1}; UV (MeOH): λ_{max} 310 nm (ε 223735 $M^{-1}cm^{-1}$); HRMS (ESI) *m/z* Calcd. for $C_{12}H_{15}Br_2NO_5Na$ $(M + Na)^+$ 433.9215. Found 433.9215.

3-(1-Nitrooxyoctyl)-5-(dibromomethylene)furan-2(5*H*)-one (155e)

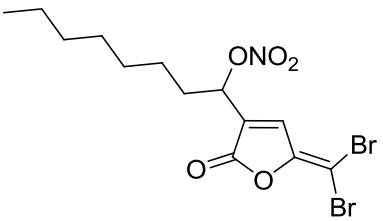

The title compound was synthesized following the procedure for compound **155b** using the bromofimbrolide **156e** (1 g, 2.24 mmol) and silver

nitrate (0.57 g, 3.37 mmol) to give desired product **155e** as a yellow solid (0.70 g, 73%). M.p. 44 °C; ^{1}H NMR (300 MHz, $CDCl_3$): δ 0.88 (t, J = 7.2 Hz, 3H, CH_3), 1.27-1.43 (m, 10H, 5 × CH_2), 1.92-2.15 (m, 2H, CH_2), 5.69 (t, J = 7.1 Hz, 1H, $CHONO_2$), 7.53 (s, 1H, CH); ^{13}C NMR (75.6 MHz, $CDCl_3$): δ 14.0 (CH_3), 22.5 (CH_2), 24.8 (CH_2), 28.9 (CH_2), 31.6 (CH_2), 31.8 (CH_2), 76.9 ($CHONO_2$), 83.5 (CBr_2), 133.7 (C=C), 135.4 (CH), 149.1 ($C=CBr_2$), 165.7 (C=O); IR (neat): ν_{max} 3093, 2957, 2926, 2856, 1766, 1638, 1454, 1379, 1288, 1266, 1194, 1032, 968, 911, 850, 750, 683 cm^{-1}; UV (MeOH): λ_{max} 310 nm (ε 263366 M^{-1}cm^{-1}); HRMS (ESI) *m/z* Calcd. for $C_{13}H_{17}Br_2NO_5Na$ $(M + Na)^+$ 447.9371. Found 447.9369.

3-(1-Nitrooxydodecyl)-5-(dibromomethylene)furan-2(5*H*)-one (155f)

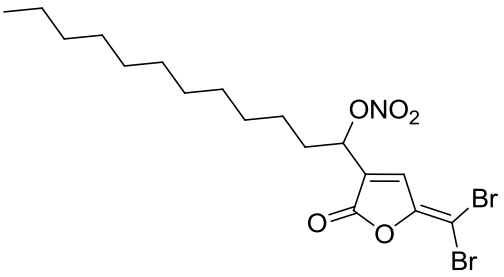

The title compound was synthesized following the procedure for compound **155b** using the bromofimbrolide **156f** (0.30 g, 0.59 mmol) and silver nitrate (0.12 g, 0.71 mmol) to give desired product **155f** as a yellow solid (0.20 g, 71%). M.p. 40 °C; ^{1}H NMR (300 MHz, $CDCl_3$): δ 0.85 (t, J = 6.9 Hz, 3H, CH_3), 1.17-1.43 (m, 18H, 9 × CH_2), 1.87-1.95 (m, 2H, CH_2), 5.68 (t, J = 6.4 Hz, 1H, $CHONO_2$), 7.53 (s, 1H, CH); ^{13}C NMR (75.6 MHz, $CDCl_3$): δ 14.5 (CH_3), 23.0 (CH_2), 25.2 (CH_2), 29.6 (CH_2), 29.7 (CH_2), 29.9 (2C, CH_2), 32.2 (CH_2), 77.3 ($CHONO_2$), 82.5 (CBr_2), 132.7 (C=C), 134.4 (CH), 148.1 ($C=CBr_2$), 164.7 (C=O); IR (neat): ν_{max} 3093, 2922, 2852, 1767, 1636, 1466, 1454, 1378, 1291, 1268, 1187, 1037, 968, 914, 849, 750, 683 cm^{-1}; UV (MeOH): λ_{max} 310 nm (ε 212603 M^{-1}cm^{-1}); HRMS (ESI) *m/z* Calcd. for $C_{17}H_{25}Br_2NO_5Na$ $(M + Na)^+$ 503.9997. Found 503.9986.

3-(1-Hydroxybutyl)-5-(dibromomethylene)furan-2(5*H*)-one (157a)

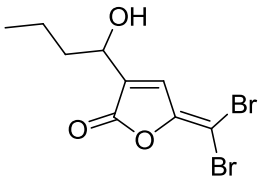

The bromofimbrolide **156a** (7 g, 18.00 mmol) was dissolved in DMSO (10 mL) and few drops of water was added. The mixture was stirred at room temperature for 72 h. To the mixture water (60 mL) was added and extracted with DCM (2 x 20 mL). The organic phase was washed with brine solution (2 x 20 mL), then dried and evaporated. Vacuum chromatography of the residue through silica gel gave the title product **157a** as an off white solid (3.5 g, 59%). M.p. 56 °C; ^{1}H NMR (300 MHz, $CDCl_3$): δ 0.97 (t, J = 7.1 Hz, 3H, CH_3), 1.46-1.52 (m, 2H, CH_2), 1.68-1.81 (m, 2H, CH_2), 2.25 (d, J = 6.1 Hz, 1H, OH) 4.54-4.60 (m, 1H, CHOH), 7.50 (s, 1H, CH); ^{13}C NMR (75.6 MHz, $CDCl_3$): δ 13.7 (CH_3), 18.4 (CH_2), 37.6 (CH_2), 67.0 (CHOH), 81.1 (CBr_2), 134.1 (C), 139.5 (CH), 149.5 (C), 165.7 (C=O); IR (neat): ν_{max} 3262, 3092, 2959, 2931, 2871, 1755, 1606, 1464, 1378, 1340, 1265, 1235, 1180, 1128, 1064, 1019, 962, 950, 917, 889, 802, 784, 745, 682 cm^{-1}; UV (MeOH): λ_{max} 305 nm (ε 207289 M^{-1}cm^{-1}); HRMS (ESI) *m/z* Calcd. for $C_9H_{10}Br_2O_3Na$ $(M + Na)^+$ 346.8894. Found 346.8891

5-(Dibromomethylene)-3-(1-hydroxyhexyl)furan-2(5*H*)-one (157b)

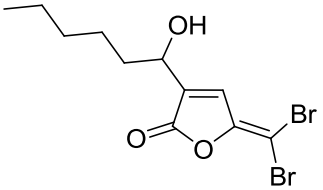

The title compound was synthesized following the procedure for compound **157a** using the bromofimbrolide **156c** (2 g; 4.79 mmol) and DMSO/H_2O to give desired product **157b** as a yellow solid (1.05 g, 62%). M.p. 40 °C; ^{1}H NMR (300 MHz, $CDCl_3$): δ 0.97 (t, J = 7.1 Hz, 3H, CH_3), 1.36-1.48 (m, 4H, 2 × CH_2), 1.63-1.93 (m, 4H, 2 × CH_2), 4.53-4.58 (m, 1H, CHOH), 7.48 (s, 1H, CH); ^{13}C NMR (75.6 MHz, $CDCl_3$): δ 13.9 (CH_3), 22.5 (CH_2), 24.8 (CH_2), 31.4 (CH_2), 35.5 (CH_2), 67.3 (CHOH), 81.1 (CBr_2), 134.1 (C), 139.5 (CH),

149.5 (C), 167.2 (C=O); IR (neat): ν_{max} 3262, 3092, 2959, 2931, 2871, 1755, 1606, 1464, 1378, 1340, 1265, 1235, 1180, 1128, 1064, 1019, 962, 950, 917, 889, 802, 784, 745, 682 cm^{-1}; UV (MeOH): λ_{max} 305 nm (ε 120858 $M^{-1}cm^{-1}$); HRMS (ESI) *m/z* Calcd. for $C_{11}H_{14}Br_2O_3Na$ $(M + Na)^+$ 374.9207. Found 374.9200.

5-(Dibromomethylene)-3-(1-hydroxydodecyl)furan-2(5*H*)-one (157c)

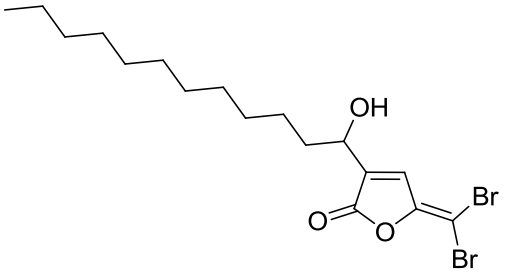

The title compound was synthesized following the procedure for compound **157a** using the bromofimbrolide **156f** (2 g, 4.73 mmol) and DMSO/H_2O to give desired product **157c** as a yellow solid (1.20 g, 58%). M.p. 40 °C; ^1H NMR (300 MHz, $CDCl_3$): δ 0.85 (t, J = 6.9 Hz, 3H, CH_3), 1.17-1.43 (m, 18H, 9 × CH_2), 1.87-1.95 (m, 2H, CH_2), 4.53-4.58 (m, 1H, CHOH), 7.48 (s, 1H, CH); ^{13}C NMR (75.6 MHz, $CDCl_3$): δ 14.1 (CH_3), 22.6 (CH_2), 25.1 (CH_2), 29.2 (CH_2), 29.3 (CH_2), 29.4 (CH_2), 29.5 (CH_2), 29.6 (CH_2), 31.9 (CH_2), 35.6 (CH_2), 67.3 (CH_2OH), 81.0 (CBr_2), 135.0 (CH), 139.5 (C), 149.0 (C), 165.7 (C=O); IR (neat): ν_{max} 3394, 3086, 2917, 2850, 1755, 1617, 1601, 1466, 1377, 1264, 1181, 1044, 965, 911, 845, 778, 720, 708, 681 cm^{-1}; UV (MeOH): λ_{max} 305 nm (ε 114642 $M^{-1}cm^{-1}$); HRMS (ESI) *m/z* Calcd. for $C_{17}H_{26}Br_2O_3Na$ $(M + Na)^+$ 459.0146. Found 459.0136.

1-(5-(Dibromomethylene)-2-oxo-2,5-dihydrofuran-3-yl)butyl 2-bromoacetate (160a)

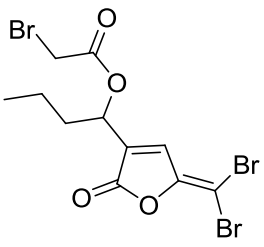

A solution of the 2-bromoacetylbromide (0.08 mL, 0.92 mmol) was slowly added to a stirred solution of hydroxyl fimbrolide **157a** (0.20 g, 0.61 mmol) and dry pyridine (0.99 mL, 1.22 mmol) in anhydrous CH_2Cl_2 (10 mL) at 0 °C under argon. The reaction was allowed to reach room temperature and then stirred for 2.5 h. The mixture was washed with 2 M HCl (3 × 10 mL) and brine (1x 20 mL). The combined organic layers were dried, filtered, and concentrated under reduced pressure. The crude product thus obtained was purified by vacuum chromatography to yield the compound **160a** as a white solid (0.24 g, 87%). M.p. 78 °C; ^{1}H NMR (300 MHz, $CDCl_3$): δ 0.95 (t, J = 7.3 Hz, 3H, CH_3), 1.37-1.54 (m, 2H, CH_2), 1.85-1.92 (q, J = 7.4 Hz, 2H, CH_2), 3.87 (s, 2H, CH_2Br), 5.65 (t, J = 7.1 Hz, 1H, CHOC=O), 7.50 (s, 1H, CH); ^{13}C NMR (75.6 MHz, $CDCl_3$): δ 13.5 (CH_3), 18.2 (CH_2), 25.2 (CH_2), 34.6 (CH_2), 70.2 (CH), 82.3 (CBr_2), 135.0 (C=CH), 135.2 (CH), 149.2 ($C=CBr_2$), 165.9 (C=O), 166.3 (C=O); IR (neat): ν_{max} 3089, 2962, 2872, 1762, 1734, 1608, 1463, 1405, 1381, 1273, 1216, 1186, 1156, 1107, 1033, 966, 917, 885, 842, 770, 683 cm^{-1}; UV (MeOH): λ_{max} 308 nm (ε 261761 M^{-1}cm^{-1}); HRMS (ESI) *m/z* Calcd. for $C_{11}H_{11}Br_3O_4Na$ $(M + Na)^+$ 466.8105. Found 466.8100; Anal. Calcd. for $C_{11}H_{11}Br_3O_4$: C, 29.56; H, 2.48. Found: C, 29.78; H, 2.49.

1-(5-(Dibromomethylene)-2-oxo-2,5-dihydrofuran-3-yl)butyl-4-bromobutanoate (160c)

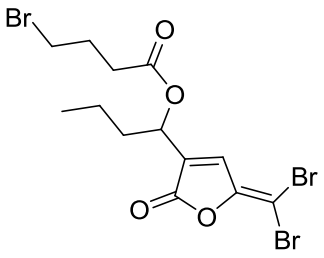

The title compound was synthesized following the procedure for compound **160a** using the 4-bromobutyrylchloride (0.20 g, 0.61 mmol) and hydroxyl fimbrolide **157a** (0.107 mL, 0.92 mmol) to give desired product **160c** as a white solid (0.27 g, 95%). M.p. 76 °C; ^{1}H NMR (300 MHz, $CDCl_3$): δ 0.94 (t, J = 7.3 Hz, 3H, CH_3), 1.32-1.55 (m, 2H, CH_2), 1.81-1.88 (q, J = 7.3 Hz, 2H, CH_2), 2.16-2.23 (p, J = 6.7 Hz, 2H, CH_2), 2.58 (t, J = 7.1, 2H, CH_2C=O), 3.47 (t, J = 6.3 Hz, 2H, CH_2Br), 5.62 (t, J = 7.0 Hz, 1H, CHOC=O), 7.41 (s, 1H, CH); ^{13}C NMR (75.6 MHz, $CDCl_3$): δ 13.6 (CH_3), 18.3 (CH_2), 27.4 (CH_2), 32.2 (CH_2), 32.5 (CH_2), 34.8 (CH_2), 68.5 (CH), 81.8 (CBr_2), 135.0 (CH), 135.9 (C=CH), 149.2 (C=CBr_2), 166.0 (C=O), 171.5 (C=O); IR (neat): ν_{max} 3089, 2961, 2937, 2873, 1759, 1728, 1607, 1436, 1379, 1321, 1285, 1251, 1205, 1185, 1161, 1107, 1060, 1034, 965, 919, 846, 783, 772, 683 cm^{-1}; UV (MeOH): λ_{max} 308 nm (ε 278190 M^{-1}cm^{-1}); HRMS (ESI) *m/z* Calcd. for $C_{13}H_{15}Br_3O_4Na$ $(M + Na)^+$ 494.8414. Found 494.8413; Anal. Calcd. for $C_{13}H_{15}Br_3O_4$: C, 33.29; H, 3.18. Found: C, 33.29; H, 3.17.

1-(5-(Dibromomethylene)-2-oxo-2,5-dihydrofuran-3-yl)butyl 2-(nitrooxy)acetate (161a)

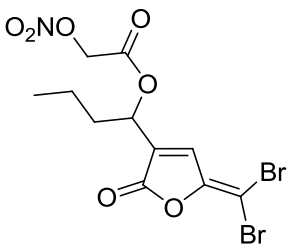

A mixture of the bromoester derivative **160a** (0.20 g, 0.46 mmol) and $AgNO_3$ (0.11 g, 0.69 mmol) in CH_3CN (15 mL) was stirred at 70 °C for 16 h. The mixture was filtered through Celite and concentrated under reduced pressure. The residue was treated with CH_2Cl_2

(50 mL) and H_2O (50 mL). After separation, the aqueous layer was extracted twice with CH_2Cl_2 (50 mL). The combined organic layers were dried, filtered, and concentrated under reduced pressure. The crude product thus obtained was purified by vacuum chromatography with silica gel to yield the title compound **161a** as an off white solid (0.14 g, 72%). M.p. 48-50 °C; ^{1}H NMR (300 MHz, $CDCl_3$): δ 0.95 (t, J = 7.4 Hz, 3H, CH_3), 1.33-1.42 (m, 2H, CH_2), 1.87-1.94 (q, J = 6.9, 2H Hz, CH_2), 4.96 (s, 2H, CH_2ONO_2), 5.73 (t, J = 6.8 Hz, 1H, CHOC=O), 7.44 (s, 1H, CH); ^{13}C NMR (75.6 MHz, $CDCl_3$): δ 13.5 (CH_3), 18.2 (CH_2), 25.2 (CH_2), 68.6 (CH_2), 70.2 (CH), 82.3 (CBr_2), 135.0 (C=CH), 135.2 (CH), 149.2 ($C=CBr_2$), 165.9 (C=O), 166.3 (C=O); IR (neat): ν_{max} 3090, 2970, 2881, 1757, 1652, 1610, 1463, 1409, 1377, 1288, 1205, 1186, 1107, 1063, 1039, 994, 966, 915, 836, 772, 758, 683, 655 cm^{-1}; UV (MeOH): λ_{max} 308 nm (ε 273006 M^{-1}cm^{-1}); HRMS (ESI) *m/z* Calcd. for $C_{11}H_{11}Br_2NO_7Na$ $(M + Na)^+$ 449.8800. Found 449.8792.

1-(5-(Dibromomethylene)-2-oxo-2,5-dihydrofuran-3-yl)butyl 3-(nitrooxy) propanoate (161b)

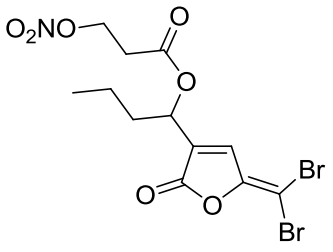

Thionyl chloride ($SOCl_2$) (0.43 mL, 2.22 mmol) and a few drops of dry DMF were added to a solution of the 3-nitrooxypropionic acid **94b** (0.2 g, 5.46 mmol) in anhydrous CH_2Cl_2 (15 mL). The mixture was stirred under argon at room temperature. The stirring was continued for 2 h at room temperature. The solution of the acyl chloride thus obtained was slowly added to a stirred solution of hydroxyfimbrolide (0.25 g, 0.76 mmol) containing dry pyridine (0.12 mL, 1.53 mmol) in dry CH_2Cl_2 (10 mL) kept under argon at 0 °C. The reaction was allowed to reach room temperature and then stirred for

2.5 h. The mixture was washed with 2 M HCl (3 × 10 mL) and the combined organic layer was dried, filtered, and concentrated under reduced pressure. The crude product thus obtained was purified by vacuum chromatography to yield the title compound **161b** as an off white solid (0.24 g, 70%). M.p. 48-50 °C; ^{1}H NMR (300 MHz, $CDCl_3$): δ 0.93 (t, J = 7.3 Hz, 3H, CH_3), 1.32-1.41 (m, 2H, CH_2), 1.81-1.90 (q, J = 7.3 Hz, 2H, CH_2), 2.83 (t, J = 7.1 Hz, 2H, CH_2C=O), 4.61 (t, J = 6.3 Hz, 2H, CH_2ONO_2), 5.62 (t, J = 7.0 Hz, 1H, CHOC=O), 7.43 (s, 1H, CH); ^{13}C NMR (75.6 MHz, $CDCl_3$): δ 13.9 (CH_3), 18.7 (CH_2), 32.5 (CH_2), 35.1 (CH_2), 68.2 (CH_2), 69.7 (CH), 82.6 (CBr_2), 135.6 (C=CH), 135.6 (CH), 149.5 (C=CBr_2), 166.3 (C=O), 168.9 (C=O); IR (neat): ν_{max} 3265, 3086, 2963, 2919, 2850, 1764, 1736, 1640, 1606, 1461, 1434, 1398, 1371, 1280, 1221, 1183, 1109, 1062, 1021, 966, 949, 890, 841, 771, 756, 708, 685 cm^{-1}; UV (MeOH): λ_{max} 307 nm (ε 273879 M^{-1}cm^{-1}); HRMS (ESI) *m/z* Calcd. for $C_{12}H_{13}Br_2NO_7Na$ $(M + Na)^+$ 463.8956. Found 463.8946.

1-(5-(Dibromomethylene)-2-oxo-2,5-dihydrofuran-3-yl)butyl 4-(nitrooxy)butanoate 161c

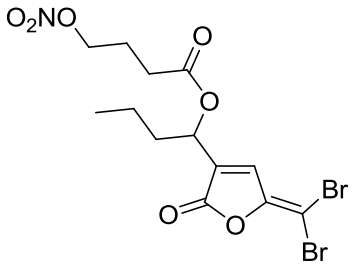

The title compound was synthesized following the procedure for compound **161a** using the 4-bromobutylester derivative **160c** (0.23 g, 0.49 mmol) and silver nitrate (0.12 g, 0.73 mmol) to give desired product **161c** as a white solid (0.16 g, 74 %). M.p. 80 °C; ^{1}H NMR (300 MHz, $CDCl_3$): δ 0.94 (t, J = 7.4 Hz, 3H, CH_3), 1.31-1.40 (m, 2H, CH_2), 1.81-1.89 (q, J = 6.6 Hz, 2H, CH_2), 2.06-2.10 (p, J = 6.3 Hz, 2H, CH_2), 2.52 (t, J = 7.0 Hz, 2H, CH_2C=O), 4.52 (t, J = 6.2 Hz, 2H, CH_2ONO_2), 5.63 (t, J = 6.9 Hz, 1H, CHOC=O), 7.41 (s, 1H, CH); ^{13}C NMR (75.6 MHz, $CDCl_3$): δ 13.6 (CH_3), 18.3 (CH_2),

22.2 (CH_2), 30.1 (CH_2), 34.8 (CH_2), 68.6 (CH), 71.7 (CH_2), 82.0 (CBr_2), 135.2 (CH), 135.5 (C=CH), 149.2 (C=CBr_2), 166.0 (C=O), 171.3 (C=O); IR (neat): ν_{max} 3087, 2967, 2879, 1762, 1723, 1621, 1444, 1389, 1332, 1275, 1249, 1211, 1169, 1107, 1084, 1022, 965, 916, 905, 874, 844, 780, 761, 737, 704, 683 cm^{-1}; UV (MeOH): λ_{max} 308 nm (ε 390578 $M^{-1}cm^{-1}$); HRMS (ESI) *m/z* Calcd. for $C_{13}H_{15}Br_2NO_7Na$ $(M + Na)^+$ 477.9113. Found 477.9114.

1-(5-(Dibromomethylene)-2-oxo-2,5-dihydrofuran-3-yl)butyl 6-(nitrooxy)hexanoate (161d)

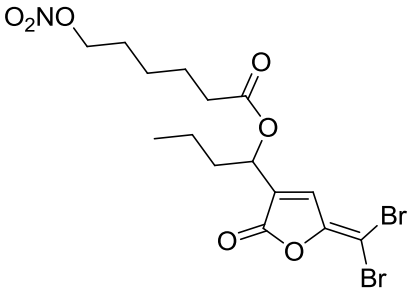

The desired 6-nitrooxyheaxanoylchloride was first synthesized by reacting the desired acid **94f** (0.40 g, 2.25 mmol) with $SOCl_2$ (0.32 mL, 4.51 mmol) followed by reaction with hydroxyfimbrolide (0.3 g, 0.92 mmol) as described for compound **161b** to give the title compound **161d** as an off white solid (0.31 g, 71%). M.p. 34-36 °C; ^{1}H NMR (300 MHz, $CDCl_3$): δ 0.90 (t, J = 7.4 Hz, 3H, CH_3), 1.23-1.46 (m, 4H, 2 × CH_2), 1.65-1.81 (m, 6H, 3 × CH_2), 2.38 (t, J = 7.1 Hz, 2H, CH_2C=O), 4.43 (t, J = 6.7 Hz, 2H, CH_2ONO_2), 5.59 (t, J = 6.0, 1H, CHOC=O), 7.38 (s, 1H, CH); ^{13}C NMR (75.6 MHz, $CDCl_3$): δ 13.5 (CH_3), 18.3 (CH_2), 24.2 (CH_2), 25.1 (CH_2), 26.4 (CH_2), 33.7 (CH_2), 34.8 (CH_2), 68.6 (CH), 72.9 (CH_2), 82.0 (CBr_2), 135.2 (CH), 135.5 (C=CH), 149.2 (C=CBr_2), 166.0 (C=O), 171.3 (C=O); IR (neat): ν_{max} 3101, 2949, 2875, 1764, 1731, 1631, 1464, 1385, 1365, 1275, 1261, 1242, 1167, 1106, 1064, 1027, 962, 913, 872, 842, 758, 733, 702, 687 cm^{-1}; UV (MeOH): λ_{max} 308 nm (ε 310476 $M^{-1}cm^{-1}$); HRMS (ESI) *m/z* Calcd. for $C_{15}H_{19}Br_2NO_7Na$ $(M + Na)^+$ 505.9426. Found 505.9423.

1-(5-(Dibromomethylene)-2-oxo-2,5-dihydrofuran-3-yl)butyl 8-(nitrooxy)octanoate (161e)

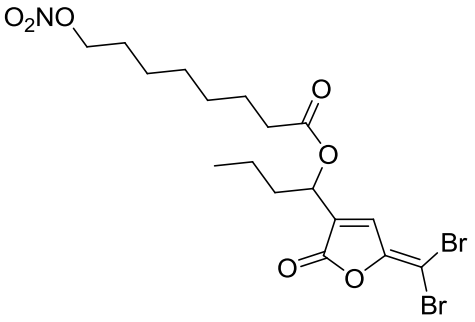

The desired 8-nitrooxyoctanoylchloride was firstly synthesized by reacting acid **94c** (0.34 g, 1.65 mmol) with $SOCl_2$ (0.24 mL, 3.31 mmol) followed by reaction with hydroxyfimbrolide **157a** (0.30 g, 0.92 mmol) as described for compound **161b** to give the title compound **161e** as a low melting off white solid (0.32, 68%). M.p. 34-36 °C; ^{1}H NMR (300 MHz, $CDCl_3$): δ 0.93 (t, J = 7.3, 3H, CH_3), 1.24-1.40 (m, 8H, 4 × CH_2), 1.64-1.70 (m, 4H, 2 × CH_2), 1.79-1.84 (q, J = 7.6 Hz, 2H, CH_2), 2.36 (t, J = 7.1 Hz, 2H, CH_2C=O), 4.43 (t, J = 6.6 Hz, 2H, CH_2ONO_2), 5.59 (t, J = 6.0 Hz, 1H, CHOC=O), 7.38 (s, 1H, CH); ^{13}C NMR (75.6 MHz, $CDCl_3$): δ 14.0 (CH_3), 18.7 (CH_2), 25.1 (CH_2), 25.8 (CH_2), 27.0 (CH_2), 29.1 (CH_2), 29.2 (CH_2), 34.4 (CH_2), 35.2 (CH_2), 68.5 (CH), 73.7 (CH_2), 82.0 (CBr_2), 135.4 (CH), 136.5 (C=CH), 149.6 (C=CBr_2), 166.4 (C=O), 172.9 (C=O); IR (neat): ν_{max} 3092, 2932, 2862, 1766, 1729, 1624, 1459, 1378, 1277, 1215, 1157, 1104, 1065, 1034, 965, 916, 870, 844, 759, 730, 684 cm^{-1}; UV (MeOH): λ_{max} 308 nm (ε 212110 M^{-1}cm^{-1}); HRMS (ESI) *m/z* Calcd. for $C_{17}H_{23}Br_2NO_7Na$ $(M + Na)^+$ 533.9739. Found 533.9736.

1-(5-(Dibromomethylene)-2-oxo-2,5-dihydrofuran-3-yl)butyl-10-(nitrooxy)decanoate (161f)

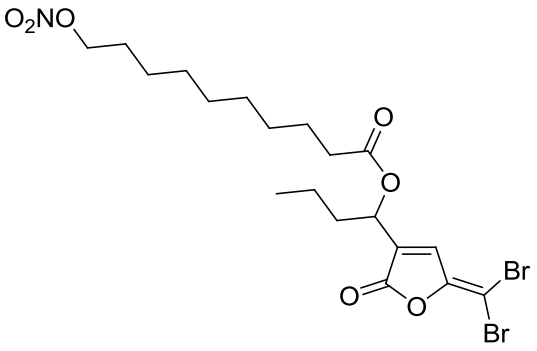

The desired 11-nitrooxydecanoylchloride was firstly synthesized by reacting the acid **94d** (0.31 g, 1.25 mL) with $SOCl_2$ (0.18 mL,

2.50 mmol) followed by reaction with hydroxylfimbrolide **157a** (0.2 g, 0.61 mmol) as described for compound **161b** to give the title compound **161f** as a yellow oil (0.23 g, 69%). M.p. 34-36 °C; ^{1}H NMR (300 MHz, $CDCl_3$): δ 0.93 (t, J = 7.3 Hz, 3H, CH_3), 1.28-1.37 (m, 14H, 7 × CH_2), 1.58-1.73 (m, 4H, 2 × CH_2), 1.79-1.87 (q, J = 7.4 Hz, 2H, CH_2), 2.36 (t, J = 7.5 Hz, 2H, CH_2C=O), 4.43 (t, J = 6.6 Hz, 2H, CH_2ONO_2), 5.60 (t, J = 6.8 Hz, 1H, CHOC=O), 7.38 (s, 1H, CH); ^{13}C NMR (75.6 MHz, $CDCl_3$): δ 13.5 (CH_3), 18.2 (CH_2), 24.7 (CH_2), 25.5 (CH_2), 26.6 (CH_2), 28.9 (CH_2), 29.0 (CH_2), 29.1 (CH_2), 34.0 (CH_2), 34.7 (CH_2), 68.0 (CH), 73.3 (CH_2), 81.4 (CBr_2), 134.8 (CH), 136.1 (C=CH), 149.1 (C=CBr_2), 165.9 (C=O), 172.6 (C=O); IR (neat): ν_{max} 2927, 2855, 1780, 1738, 1623, 1464, 1378, 1275, 1158, 1103, 1062, 1023, 965, 850, 758, 683 cm^{-1}; UV (MeOH): λ_{max} 308 nm (ε 282672 $M^{-1}cm^{-1}$); HRMS (ESI) *m/z* Calcd. for $C_{20}H_{29}Br_2NO_7Na$ $(M + Na)^+$ 576.0208. Found 576.0207.

1-(5-(Dibromomethylene)-2-oxo-2,5-dihydrofuran-3-yl)butyl ethanethioate (164)

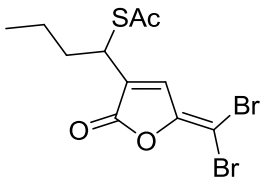

Potassium thioacetate (0.44 g, 3.85 mmol) was added to a solution of bromo fimbrolide **156a** (1g, 2.57 mmol) in acetone (20 mL). The solution was stirred at room temperature for 1h followed by filtration and evaporation of the filtrate under *vacuo*. DCM (50 mL) was added to the crude reaction mixture and residue and the dichloromethane solution washed with water (2 x 10 mL) and brine (1 x 20 mL). The organic layer was dried (Na_2SO_4) and concentrated to give the title compound **164** as a brown oil (0.78 g, 78%). ^{1}H NMR (300 MHz, $CDCl_3$): δ 0.86 (t, J = 7.1 Hz, 3H, CH_3), 1.18-1.33 (m, 2H, CH_2), 1.82-1.91 (m, 2H, CH_2), 2.33 (s, 3H, $COCH_3$), 4.40 (m, 1H, $CHSCOCH_3$), 7.43 (s, 1H, CH); ^{13}C NMR (75.6 MHz, $CDCl_3$): δ 13.4 (CH_3), 20.5 (CH_2), 30.5 (CH), 33.8 (CH_2),

39.2 (CH), 83.5 (CBr_2), 133.6 (C), 135.0 (CH), 149.0 (C), 165.7 (C=O); HRMS (ESI) *m/z* Calcd. for $C_{20}H_{29}Br_2NO_7Na$ $(M + Na)^+$ 576.0208. Found 576.0207.

Methyl 5-formyl-2-propylthiophene-3-carboxylate (165)

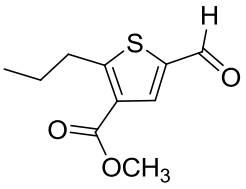

A solution of compound **164** (1.56 g, 4.06 mmol) in 0.8M methanolic hydrochloric acid was stirred under reflux for 18h. The reaction mixture was evaporated to dryness under *vacuo* and dichloromethane was added. The organic layer was washed with water and brine, dried (Na_2SO_4) and concentrated under reduced pressure. The crude product thus obtained was purified by vacuum chromatography with silica gel and dichloromethane/n-hexane as mobile phase to yield the title compound **165** as a light brown solid (0.53 g, 62%). M.p. 28 °C, ^{1}H NMR (300 MHz, $CDCl_3$): δ 1.01 (t, J = 7.1 Hz, 3H, CH_3), 1.71-1.79 (m, 2H, CH_2), 3.25 (t, 2H, CH_2), 3.81 (s, 3H, OCH_3), 8.06 (s, 1H, CH), 9.81 (s, 1H, CH); ^{13}C NMR (75.6 MHz, $CDCl_3$): δ 14.2 (CH_3), 24.8 (CH_2), 32.7 (CH_2), 52.2 (OCH_3), 129.1 (C), 139.1 (CH), 139.5 (C), 163.3 (C), 165.3 (C=O), 182.9 (CHO); IR (neat): ν_{max} 3098, 2956, 2837, 2877, 1780, 1704, 1672, 1537, 1456, 1435, 1403, 1365, 1256, 1208, 1157, 1092, 979, 922, 885, 774, 719, 690 cm^{-1}; UV (MeOH): λ_{max} 229 nm (ε 268862 $M^{-1}cm^{-1}$), 270 nm (ε 116743 $M^{-1}cm^{-1}$), 288 nm (ε 123818 $M^{-1}cm^{-1}$); HRMS (ESI) *m/z* Calcd. for $C_{10}H_{12}O_5S$ $(M + 1)^+$ 213.0585. Found 213.0577.

3-(1-Mercaptobutyl)-5-(dibromomethylene)furan-2(5H)-one (163)

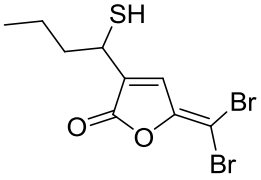

A solution of compound **164** (0.70 g, 1.82 mmol) in 0.3M methanolic hydrochloric acid was stirred at 60 °C for 3h. The reaction mixture was evaporated to dryness under *vacuo*. The residue was dissolved in dichloromethane and the dichloromethane solution washed

with water and brine, then dried (Na_2SO_4) and concentrated under reduced pressure. The crude product thus obtained was purified by vacuum chromatography with silica gel and dichloromethane/n-hexane as mobile phase to yield the title compound **163** as an off white solid (0.30 g, 48%). M.p. 58–60 °C. ^{1}H NMR (300 MHz, $CDCl_3$): δ 0.95 (t, J = 7.3 Hz, 3H, CH_3), 1.44 (m, 2H, CH_2), 1.87 (m, 2H, CH_2), 2.11 (d, J = 7.5 Hz, 1H, SH), 3.71 (q, J = 7.5 Hz, 1H, CHSH), 7.37 (s, 1H, CH) ppm; ^{13}C NMR (75 MHz, $CDCl_3$): δ 13.8, 20.9, 34.7, 38.6, 81.5, 133.5, 140.6, 149.7, 167.3 ppm; IR (KBr): ν_{max} 3091, 2954, 2929, 2869, 1769, 1612, 1595, 1465, 1452, 1267, 1181, 1111, 1037, 993, 966, 898, 846, 771, 740, 669 cm^{-1}; UV (MeOH): λ_{max} 310 nm (ε 205224 M^{-1}cm^{-1}); HRMS (ESI) *m/z* Calcd. for $C_9H_{10}Br_2O_2SNa$ $(M + Na)^+$ 362.8660. Found 362.8636.

1-(5-(Dibromomethylene)-2-oxo-2,5-dihydrofuran-3-yl)butyl-4-bromobutanethioate (168)

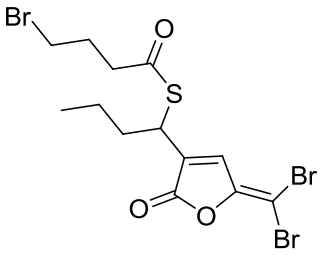

A solution of 4-bromobutryl bromide (0.07 mL, 0.65 mmol) was slowly added to a stirred mixture of fimbrolide **163** (0.15 g, 0.43 mmol) and dry pyridine (0.07 mL, 0.87 mmol) in anhydrous CH_2Cl_2 (10 mL) kept under argon at 0 °C. The reaction was allowed to reach room temperature and then stirred for 2.5 h. The mixture was washed with 2 M HCl (3 × 10 mL) and brine (1 × 20 mL). The combined organic layer was dried, filtered, and concentrated under reduced pressure. The crude product thus obtained was purified by vacuum chromatography to yield the compound **168** as a yellow oil (0.17 g, 81%). ^{1}H NMR (300 MHz, $CDCl_3$): δ 0.91 (t, J = 7.3 Hz, 3H, CH_3), 1.30-1.41 (m, 2H, CH_2), 1.81-1.94 (m, 2H, CH_2), 2.13-2.22 (p, J = 6.6 Hz, 2H, CH_2), 2.70-2.76 (m, 2H, CH_2C=O), 3.41 (t, J = 6.6 Hz, 2H, CH_2Br), 4.40 (t, J = 7.6 Hz, 1H, CHSC=O), 7.41 (s, 1H, CH);

^{13}C NMR (75.6 MHz, $CDCl_3$): δ 13.4 (CH_3), 20.5 (CH_2), 27.9 (CH_2), 32.2 (CH_2), 34.0 (CH_2), 39.0 (CH), 41.9 (CH_2), 81.3 (CBr_2), 134.9 (CH), 136.6 (C=CH), 149.2 ($C=CBr_2$), 166.5 (C=O), 196.5 (C=O); IR (neat): ν_{max} 3099, 2959, 2930, 2871, 1771, 1687, 1613, 1436, 1408, 1268, 1243, 1169, 1025, 965, 850, 779, 714 cm^{-1}; UV (MeOH): λ_{max} 311 nm (ε 301632 $M^{-1}cm^{-1}$); HRMS (ESI) *m/z* Calcd. for $C_{13}H_{15}Br_3O_3SNa$ $(M + Na)^+$ 510.8190. Found 510.8187.

1-(5-(Dibromomethylene)-2-oxo-2,5-dihydrofuran-3-yl)butyl-3-(nitrooxy)propanethioate (169a)

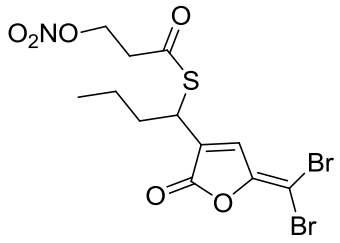

Thionyl chloride ($SOCl_2$) (0.2 mL, 2.22 mmol) and a few drops of dry DMF were added to a solution of the 3-nitrooxypropionic acid **94b** (0.15 mL, 1.11 mmol) in anhydrous CH_2Cl_2 (15 mL), stirred under argon at room temperature. The stirring was continued for 2 h at room temperature. The solution of the acyl chloride thus obtained was slowly added to a stirred solution of thio-fimbrolide **163** (0.15 g, 0.43 mmol) and anhydrous pyridine (0.07 mL, 0.87 mmol) in anhydrous CH_2Cl_2 (20 mL) kept under argon at 0 °C. The reaction was allowed to reach room temperature and then stirred for 2.5 h. The mixture was washed with 2 M HCl (3 × 10 mL). The organic layer was dried, filtered, and concentrated under reduced pressure. The crude product thus obtained was purified by vacuum chromatography to yield the title compound **169a** as a yellow oil (0.12 g, 61%). ^{1}H NMR (300 MHz, $CDCl_3$): δ 0.92 (t, J = 7.3 Hz, 3H, CH_3), 1.31-1.41 (m, 2H, CH_2), 1.82-1.96 (m, 2H, CH_2), 2.94-2.99 (m, 2H, $CH_2C=O$), 4.44 (t, J = 6.3 Hz, 2H, CH_2ONO_2), 4.69-4.74 (m, 1H, CHSC=O), 7.43 (s, 1H, CH); ^{13}C NMR (75.6 MHz, $CDCl_3$): δ 13.4 (CH_3), 20.5 (CH_2), 33.9 (CH_2), 39.4 (CH), 40.6 (CH_2), 67.3 (CH_2), 135.2

(CH), 136.0 (C=CH), 149.1 (C=CBr_2), 166.4 (C=O), 193.5 (C=O); IR (neat): ν_{max} 2961, 2931, 2873, 1770, 1688, 1629, 1463, 1381, 1347, 1278, 1170, 1083, 1025, 964, 877, 847, 779, 755, 693 cm^{-1}; UV (MeOH): λ_{max} 311 nm (ε 321370 $M^{-1}cm^{-1}$); HRMS (ESI) *m/z* Calcd. for $C_{12}H_{13}Br_2NO_6SNa$ $(M + Na)^+$ 479.8728. Found 479.8724.

1-(5-(Dibromomethylene)-2-oxo-2,5-dihydrofuran-3-yl)butyl-4-(nitrooxy)butanethioate (169b)

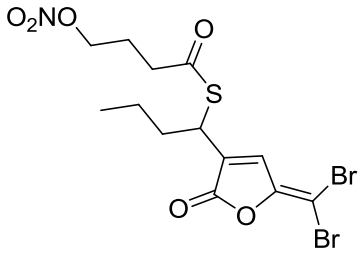

A solution of the bromothioester derivative **168** (0.13 g, 0.26 mmol) and $AgNO_3$ (0.067g, 0.39 mmol) in CH_3CN (15 mL) was stirred at 70 °C for 16 h. The mixture was filtered through Celite and concentrated under reduced pressure. The residue was treated with CH_2Cl_2 (50 mL) and H_2O (50 mL). After separation, the aqueous layer was extracted twice with CH_2Cl_2 (50 mL). The combined organic layer was dried, filtered, and concentrated under reduced pressure. The crude product thus obtained was purified by vacuum chromatography with silica gel to yield the title compound **169b** as a yellow oil (0.091 g, 73%). ^1H NMR (500 MHz, $CDCl_3$): δ 0.96 (t, J = 7.3 Hz, 3H, CH_3), 1.36-1.44 (m, 2H, CH_2), 1.85-2.08 (m, 2H, CH_2), 2.10-2.14 (p, J = 6.7 Hz, 2H, CH_2), 2.68-2.75 (m, 2H, CH_2C=O), 4.45 (t, J = 7.7 Hz, 1H, CHSC=O), 4.50 (t, J = 6.3 Hz, 2H, CH_2ONO_2), 7.45 (s, 1H, CH); ^{13}C NMR (75.6 MHz, $CDCl_3$): δ 13.4 (CH_3), 20.5 (CH_2), 24.8 (CH_2), 34.0 (CH_2), 39.0 (CH), 39.6 (CH_2), 71.5 (CH_2), 81.4 (CBr_2), 135.0 (CH), 136.4 (C=CH), 149.1 (C=CBr_2), 166.5 (C=O), 196.3 (C=O); IR (neat): ν_{max} 2960, 2931, 2873, 1772, 1689, 1625, 1441, 1411, 1381, 1276, 1170, 1097, 1024, 965, 851, 779, 756, 694 cm^{-1}; UV (MeOH): λ_{max} 311 nm (ε 277569 $M^{-1}cm^{-1}$); HRMS (ESI) *m/z* Calcd. for $C_{13}H_{15}Br_2NO_6SNa$ $(M + Na)^+$ 493.8885. Found 493.8878.

1-(5-(Dibromomethylene)-2-oxo-2,5-dihydrofuran-3-yl)butyl-6-(nitrooxy)hexanethioate (169c)

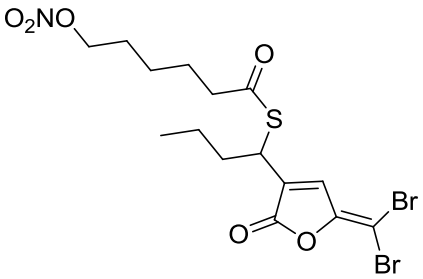

The desired 6-nitrooxyheaxanoylchloride was firstly synthesized by reacting the corresponding acid **94f** (0.15 g, 0.84 mmol) with $SOCl_2$ (0.12 mL, 1.69 mmol) followed by reaction with thiofimbrolide **163** (0.15 g, 0.43 mmol) as described for compound **169a** to give the title compound **169c** as an off white solid (0.14 g, 67%).^{1}H NMR (300 MHz, $CDCl_3$): δ 0.86 (t, J = 7.3 Hz, 3H, CH_3), 1.25-1.41 (m, 4H, 2 × CH_2), 1.58-1.75 (m, 4H, 2 × CH_2), 1.78-1.89 (m, 2H, CH_2), 2.55 (t, J = 7.3 Hz, 2H, CH_2C=O), 4.39 (t, J = 7.9 Hz, 1H, CHSC=O), 4.42 (t, J = 6.6 Hz, 2H, CH_2ONO_2), 7.41 (s, 1H, CH); ^{13}C NMR (75.6 MHz, $CDCl_3$): δ 13.4 (CH_3), 20.5 (CH_2), 24.7 (CH_2), 24.9 (CH_2), 26.4 (CH_2), 34.0 (CH_2), 38.9 (CH), 43.4 (CH_2), 72.8 (CH_2), 81.4 (CBr_2), 134.9 (CH), 136.7 (C=CH), 149.2 (C=CBr_2), 166.5 (C=O), 196.3 (C=O); IR (neat): ν_{max} 2958, 2931, 2871, 1774, 1689, 1621, 1461, 1380, 1276, 1171, 1103, 1024, 965, 851, 779, 756, 696 cm^{-1}; UV (MeOH): λ_{max} 311 nm (ε 320755 M^{-1}cm^{-1}); HRMS (ESI) *m/z* Calcd. for $C_{15}H_{19}Br_2NO_6SNa$ $(M + Na)^+$ 521.9198. Found 521.9193.

(*Z*)-1-(2-(1-(5-(Dibromomethylene)-2-oxo-2,5-dihydrofuran-3-yl)butoxy)-2-oxoethoxy)-3,3-diethyltriaz-1-ene 2-oxide (172)

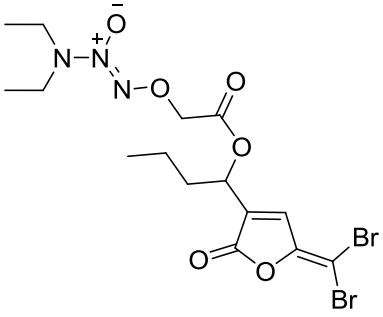

The starting bromoacetyl ester **160a** (0.1 g, 0.22 mmol) was dissolved in DMSO conatining $NaHCO_3$ (0.018 g, 0.22 mmol) and the resulting mixture was stirred at 0 °C. The diazeniumdiolate **170** (0.042 g, 0.26 mmol) was added before the reaction

mixture solidified and the reaction was kept at 0 °C for 20 min. DCM (20 mL) was added and the organic layer was washed with water (2 × 25 mL) and brine (25 mL). The organic layer was dried over Na_2SO_4 and evaporated under *vacuo*. The crude product was purified by silica gel preparative TLC using ethyl acetate/n-hexane (4:6) to yield the desire product **172** as an off white solid (0.051 g, 46%). M.p. 60-62 °C; ^{1}H NMR (300 MHz, $CDCl_3$): δ 0.92 (t, J = 7.4 Hz, 3H, CH_3), 1.10 (t, J = 7.1 Hz, 6H, 2 × CH_3), 1.33-1.42 (m, 2H, CH_2), 1.82-1.90 (m, 2H, CH_2), 3.12 (q, J = 7.1 Hz, 4H, 2 × CH_2), 4.82 (s, 2H, CH_2ON=NO), 5.70 (t, J = 6.8 Hz, 1H, CHOC=O), 7.44 (s, 1H, CH); ^{13}C NMR (75.6 MHz, $CDCl_3$): δ 11.4 (CH_3), 13.4 (CH_3), 18.1 (CH_2), 34.5 (CH_2), 48.6 (CH_2), 68.9 (CH_2), 69.4 (CH), 82.2 (CBr_2), 134.9 (C=CH), 135.3 (CH), 149.0 (C=CBr_2), 165.7 (C=O), 166.8 (C=O); IR (neat): ν_{max} 3108, 2957, 2931, 2875, 1775, 1752, 1604, 1513, 1464, 1450, 1416, 1383, 1282, 1261, 1230, 1204, 1177, 1141, 1098, 1033, 1005, 964, 951, 905, 843, 776, 725, 660 cm^{-1}; UV (MeOH): λ_{max} 307 nm (ε 314073 M^{-1}cm^{-1}); HRMS (ESI) *m/z* Calcd. for $C_{15}H_{21}Br_2N_3O_6Na$ $(M + Na)^+$ 519.9695. Found 519.9692.

(*Z*)-2-(2-(1-(5-(Dibromomethylene)-2-oxo-2,5-dihydrofuran-3-yl)butoxy)-2-oxoethoxy)-1-(4-(ethoxycarbonyl)piperazin-1-yl)diazene oxide (174)

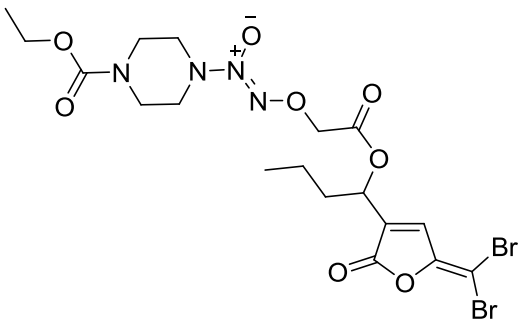

The title compound was synthesized following the procedure described for compound **172** using the 2-bromoacetyl ester derivative **160a** (0.2 g, 0.44 mmol) and piperazine diazeniumdiolate derivative **114** (0.12 g, 0.53 mmol) to give the desired product **174** as a white solid (0.15 g, 58%). M.p. 84-86 °C; ^{1}H NMR (300 MHz, $CDCl_3$): δ 0.93 (t, J = 7.4 Hz, 3H, CH_3), 1.26 (t, J = 7.1 Hz, 3H, CH_3),

1.30-1.38 (m, 2H, CH_2), 1.83-1.91 (m, 2H, CH_2), 3.40 (t, J = 4.9 Hz, 4H, 2 × CH_2), 3.64 (t, J = 4.9 Hz, 4H, 2 × CH_2), 4.13 (q, J = 7.1 Hz, 2H, CH_2), 4.78 (s, 2H, $CH_2ON{=}NO$), 5.69 (t, J = 6.7 Hz, 1H, CHOC=O), 7.43 (s, 1H, CH); ^{13}C NMR (75.6 MHz, $CDCl_3$): δ 13.4 (CH_3), 14.5 (CH_3), 18.1 (CH_2), 34.5 (CH_2), 42.2 (CH_2), 50.8 (CH_2), 61.8 (CH_2), 69.0 (CH_2), 69.3 (CH), 82.3 (CBr_2), 134.8 (C=CH), 135.4 (CH), 149.0 ($C{=}CBr_2$), 154.9 (C=O), 165.7 (C=O), 166.9 (C=O); IR (neat): ν_{max} 3099, 2957, 2932, 2862, 1773, 1697, 1607, 1504, 1473, 1421, 1386, 1283, 1268, 1248, 1215, 1196, 1183, 1135, 1096, 1057, 1041, 1010, 968, 947, 921, 894, 854, 835, 780, 767, 726, 682 cm^{-1}; UV (MeOH): λ_{max} 308 nm (ε 311580 M^{-1}cm^{-1}); HRMS (ESI) *m/z* Calcd. for $C_{18}H_{24}Br_2N_4O_8Na$ $(M + Na)^+$ 604.9859. Found 604.9855.

(Z)-2-(2-(1-(5-(Dibromomethylene)-2-oxo-2,5-dihydrofuran-3-yl)butoxy)-2-oxoethoxy)-1-morpholinodiazene oxide (175)

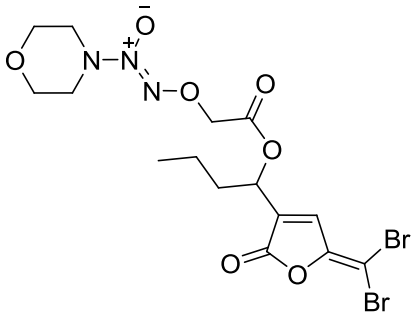

The title compound was synthesized following the procedure described for compound **172** using the 2-bromoacetyl ester derivative **160a** (0.25 g, 0.55 mmol) and morpholine diazeniumdiolate derivative **173** (0.11 g, 0.67 mmol) to give the desired product **175** as a sticky oil (0.11 g, 40%). ^{1}H NMR (300 MHz, $CDCl_3$): δ 0.93 (t, J = 7.4 Hz, 3H, CH_3), 1.27-1.31 (m, 2H, CH_2), 1.77-1.85 (m, 2H, CH_2), 3.42-3.46 (m, 4H, 2 × CH_2), 3.82-3.85 (m, 4H, 2 × CH_2), 4.78 (s, 2H, $CH_2ON{=}NO$), 5.71 (t, J = 6.7 Hz, 1H, CHOC=O), 7.45 (s, 1H, CH); ^{13}C NMR (75.6 MHz, $CDCl_3$): δ 13.5 (CH_3), 18.2 (CH_2), 34.6 (CH_2), 51.4 (CH_2), 65.6 (CH_2), 69.1 (CH_2), 69.4 (CH), 82.4 (CBr_2), 134.9 (C=CH), 135.5 (CH), 149.1 ($C{=}CBr_2$), 165.8 (C=O), 167.0 (C=O); IR (neat): ν_{max} 2962, 2929, 2865, 1767, 1611, 1500, 1456, 1380,

1267, 1228, 1194, 1099, 1064, 1036, 963, 927, 874, 848, 774, 728, 681 cm^{-1}; UV (MeOH): λ_{max} 308 nm (ε 270071 $M^{-1}cm^{-1}$); HRMS (ESI) *m/z* Calcd. for $C_{15}H_{21}Br_2N_3O_7Na$ $(M + Na)^+$ 533.9487 Found 533.9487.

4-(1-(5-(Dibromomethylene)-2-oxo-2,5-dihydrofuran-3-yl)butoxy)-4-oxobutanoic acid (177a)

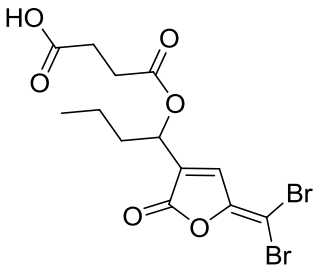

To a solution of succinyl dichloride (0.42 mL, 3.83 mmol) at 0 °C, a solution of hydroxyfimbrolide **157a** (0.5 g, 1.53 mmol) and pyridine (0.36 mL, 4.60 mmol) in DCM was added slowly over a period of 45 min. The reaction mixture was stirred further for 10 min at 0 °C and then at room temperature for 2h. The organic layer was washed with 1M HCl (2 × 20 mL), water (2 × 20 mL) and brine (20 mL). The organic layer was dried, evaporated and the crude product was purified by vacuum chromatography using ethyl acetate/n-hexane (4:6) to give the title compound **177a** as a white solid (0.56 g, 86%). M.p. 130-132 °C; ^1H NMR (300 MHz, $CDCl_3$): δ 0.93 (t, J = 7.3 Hz, 3H, CH_3), 1.33-1.41 (m, 2H, CH_2), 1.81-1.89 (m, 2H, CH_2), 2.68-2.73 (m, 4H, 2 × CH_2C=O), 5.61 (t, J = 6.7 Hz, 1H, CHOC=O), 7.42 (s, 1H, CH); ^{13}C NMR (75.6 MHz, $CDCl_3$): δ 13.5 (CH_3), 18.2 (CH_2), 28.6 (CH_2), 28.7 (CH_2), 34.6 (CH_2), 68.9 (CH), 81.8 (CBr_2), 135.1 (CH), 135.7 (C=CH), 149.2 (C=CBr_2), 166.0 (C=O), 171.1 (C=O), 177.2 (C=O); IR (neat): ν_{max} 3095, 2974, 1768, 1731, 1712, 1409, 1234, 1204, 1169, 1035, 968, 905, 843, 771, 678 cm^{-1}; UV (MeOH): λ_{max} 307 nm (ε 217372 $M^{-1}cm^{-1}$); HRMS (ESI) *m/z* Calcd. for $C_{13}H_{14}Br_2O_6Na$ $(M + Na)^+$ 446.9055. Found 446.9051; Anal. Calcd. for $C_{13}H_{14}Br_2O_6$: C, 36.65; H, 3.31. Found: C, 36.90; H, 3.28.

3-(1-(5-(Dibromomethylene)-2-oxo-2,5-dihydrofuran-3-yl)hexyloxy)-3-oxopropanoic acid (177b)

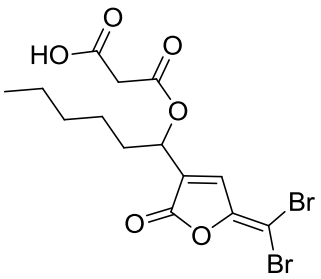

The desired compound was synthesized using malonyl dichloride (0.35 mL, 3.53 mmol), hydroxyfimbrolide **157b** (0.5 g, 1.41 mmol) and pyridine (0.34 mL, 4.23 mmol) as described for the compound **177a** to yield the title compound **177b** as an off white solid (0.46 g, 75%). M.p. 74-76 °C; ^{1}H NMR (300 MHz, $CDCl_3$): δ 0.88 (t, J = 7.3 Hz, 3H, CH_3), 1.30-1.34 (m, 6H, 3 × CH_2), 1.84-1.95 (m, 2H, CH_2), 3.52 (d, 2H, CH_2), 5.61-5.66 (m, 1H, CHOC=O), 7.55 (s, 1H, CH); ^{13}C NMR (75.6 MHz, $CDCl_3$): δ 13.8 (CH_3), 22.2 (CH_2), 24.4 (CH_2), 31.1 (CH_2), 32.4 (CH_2), 40.7 (CH_2), 70.2 (CH), 81.8 (CBr_2), 135.0 (C=CH), 135.3 (CH), 149.1 ($C=CBr_2$), 165.1 (C=O), 165.9 (C=O), 171.2 (C=O); IR (neat): ν_{max} 3104, 2955, 2926, 2859, 1750, 1698, 1609, 1550, 1467, 1421, 1405, 1335, 1264, 1208, 1184, 1147, 1066, 1042, 1027, 988, 967, 892, 857, 844, 775, 751, 725, 686, 670 cm^{-1}; UV (MeOH): λ_{max} 306 nm (ε 266715 M^{-1}cm^{-1}); HRMS (ESI) *m/z* Calcd. for $C_{14}H_{16}Br_2O_6Na$ $(M + Na)^+$ 460.9211. Found 460.9212; Anal. Calcd. for $C_{14}H_{16}Br_2O_6$: C, 38.21; H, 3.66. Found: C, 38.40; H, 3.55.

3-(1-(5-(Dibromomethylene)-2-oxo-2,5-dihydrofuran-3-yl)dodecyloxy)-3-oxopropanoic acid (177c)

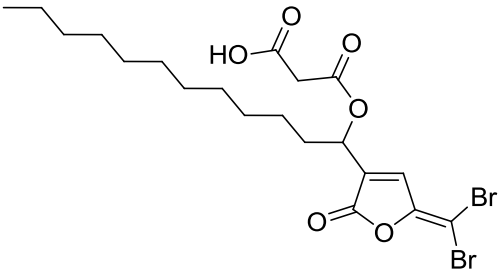

The desired compound was synthesized using malonyl dichloride (0.40 g, 2.85 mmol), hydroxyfimbrolide **157c** (0.5 g, 1.14 mmol) and pyridine (0.27 mL, 3.42 mmol) as described for the compound **177a** to yield the title compound as an off white solid (0.47 g, 79%). M.p. 46-48 °C; ^{1}H NMR (300 MHz,

$CDCl_3$): δ 0.88 (t, J = 7.3 Hz, 3H, CH_3), 1.23-1.30 (m, 18H, 9 × CH_2), 1.84-1.89 (m, 2H, CH_2), 3.45 (d, 2H, CH_2), 5.61-5.66 (m, 1H, CHOC=O), 7.55 (s, 1H, CH); ^{13}C NMR (75.6 MHz, $CDCl_3$): δ 14.1 (CH_3), 22.6 (CH_2), 24.9 (CH_2), 29.0 (CH_2), 29.3 (CH_2), 29.5 (CH_2), 29.6 (CH_2), 31.9 (CH_2), 32.5 (CH_2), 40.8 (CH_2), 70.3 (CH), 77. 2 (CH), 82.2 (CBr_2), 135.1 (C=CH), 135.5 (CH), 149.2 (C=CBr_2), 165.3 (C=O), 166.0 (C=O), 171.1 (C=O); IR (neat): ν_{max} 3092, 2919, 2850, 1759, 1699, 1608, 1466, 1423, 1334, 1266, 1236, 1208, 1183, 1152, 1068, 1040, 1026, 989, 966, 892, 850, 774, 750, 723, 684, 670 cm^{-1}; UV (MeOH): λ_{max} 307 nm (ε 290145 $M^{-1}cm^{-1}$); HRMS (ESI) *m/z* Calcd. for $C_{20}H_{28}Br_2O_6Na$ $(M + Na)^+$ 545.0150. Found 545.0146; Anal. Calcd. for $C_{20}H_{28}Br_2O_6$: C, 45.82; H, 5.38. Found: C, 45.52; H, 5.30.

4-(1-(5-(Dibromomethylene)-2-oxo-2,5-dihydrofuran-3-yl)dodecyloxy)-4-oxobutanoic acid (177d)

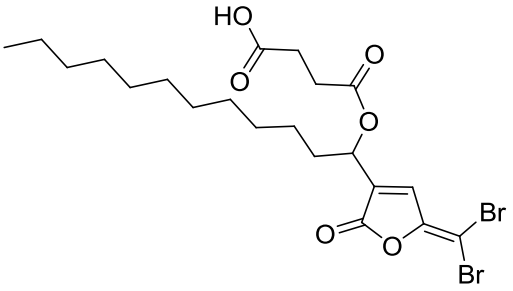

The desired compound was synthesized using succinyl dichloride (0.31 mL, 2.85 mmol), hydroxyfimbrolide **157c** (0.5 g, 1.14 mmol) and pyridine (0.27 mL, 3.42 mmol) as described for the compound **177a** to yield the title compound **177d** as an off white solid (0.50 g, 83%). M.p. 58-60 °C; ^{1}H NMR (300 MHz, $CDCl_3$): δ 0.88 (t, J = 6.9 Hz, 3H, CH_3), 1.23-1.30 (m, 18H, 9 × CH_2), 1.83-1.88 (m, 2H, CH_2), 2.69-2.73 (m, 4H, 2 × CH_2), 5.59 (t, J = 5.3 Hz, 1H, CHOC=O), 7.55 (s, 1H, CH); ^{13}C NMR (75.6 MHz, $CDCl_3$): δ 14.1 (CH_3), 22.6 (CH_2), 24.9 (CH_2), 28.5 (CH_2), 28.7 (CH_2), 29.1 (CH_2), 29.3 (CH_2), 29.5 (CH_2), 29.6 (CH_2), 31.9 (CH_2), 32.6 (CH_2), 69.2 (CH), 77. 2 (CH), 81.7 (CBr_2), 135.1 (CH), 135.7 (C=CH), 149.2 (C=CBr_2), 166.0 (C=O), 171.1 (C=O), 176.3 (C=O); IR (neat): ν_{max} 3086, 2924, 2852, 1759, 1740,

1709, 1608, 1466, 1441, 1417, 1370, 1322, 1279, 1262, 1162, 1086, 1045, 1020, 965, 913, 847, 800, 774, 720, 684 cm^{-1}; UV (MeOH): λ_{max} 307 nm (ε 223431 $M^{-1}cm^{-1}$); HRMS (ESI) *m/z* Calcd. for $C_{21}H_{30}Br_2O_6Na$ $(M + Na)^+$ 559.0307. Found 559.0304; Anal. Calcd. for $C_{20}H_{28}Br_2O_6$: C, 46.86; H, 5.62. Found: C, 47.12; H, 5.48.

(Z)-1-(4-(4-(1-(5-(Dibromomethylene)-2-oxo-2,5-dihydrofuran-3-yl)butoxy)-4-oxobutanoyl)piperazin-1-yl)-2-methoxydiazene oxide (178a)

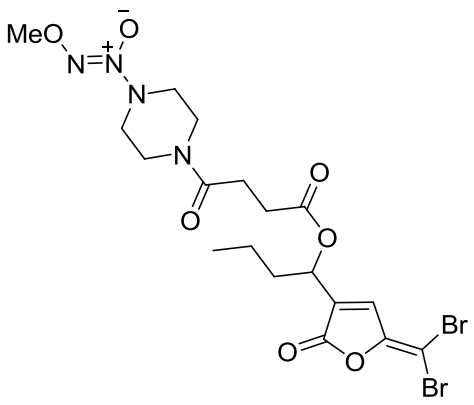

To the solution of fimbrolide mono acid **177a** (0.2 g, 0.47 mmol) and piperazine diazeniumdiolate **116** (0.09 g, 0.56 mmol) in DCM was added EDC (0.13 g, 0.70 mmol) and the mixture was stirred for 7h at room temperature. The organic layer was successively washed with water (2 × 20 mL), brine, dried over sodium sulfate and evaporated to dryness followed by vacuum chromatography using ethyl acetate/n-hexane (50:50) to yield the title compound **178a** as sticky brown oil (0.15 g, 57%). ^{1}H NMR (300 MHz, $CDCl_3$): δ 0.92 (t, J = 7.4 Hz, 3H, CH_3), 1.36-1.41 (m, 2H, CH_2), 1.78-1.85 (m, 2H, CH_2), 2.60-2.75 (m, 4H, 2 × CH_2C=O), 3.35-3.43 (m, 4H, 2 × CH_2), 3.65 (t, J = 5.2 Hz, 2H, CH_2), 3.76 (t, J = 5.2 Hz, 2H, CH_2), 4.00 (s, 3H, OCH_3), 5.61 (m, 1H, CHOC=O), 7.61 (s, 1H, CH); ^{13}C NMR (75.6 MHz, $CDCl_3$): δ 13.6 (CH_3), 18.3 (CH_2), 27.9 (CH_2), 29.0 (CH_2), 29.6 (CH_2), 34.6 (CH_2), 40.3 (CH_2), 43.7 (CH_2), 51.0 (CH_2), 51.2 (CH_2), 61.2 (OCH_3), 69.0 (CH), 81.3 (CBr_2), 135.3 (CH), 135.9 (C=CH), 149.5 ($C=CBr_2$), 166.2 (C=O), 169.5 (C=O), 172.0 (C=O); IR (neat): ν_{max} 2961, 2933, 2871, 1769, 1736, 1645, 1496, 1440, 1371, 1281, 1214, 1156, 1109, 1066, 1030, 965, 912, 847, 774, 725,

683 cm^{-1}; UV (MeOH): λ_{max} 307 nm (ε 174472 $M^{-1}cm^{-1}$); HRMS (ESI) *m/z* Calcd. for $C_{18}H_{24}Br_2N_4O_7Na$ $(M + Na)^+$ 588.9909. Found 588.9911.

(*Z*)-1-(4-(3-(1-(5-(Dibromomethylene)-2-oxo-2,5-dihydrofuran-3-yl)hexyloxy)-3-oxopropanoyl)piperazin-1-yl)-2-methoxydiazene oxide (178b)

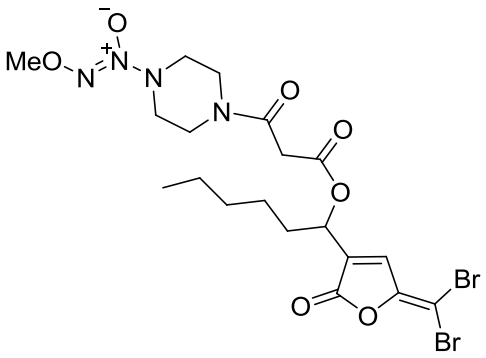

The title compound was synthesized following the procedure described for compound **178a** using the mono acid fimbrolide derivative **177b** (0.2 g, 0.454 mmol), piperazine diazeniumdiolate derivative **116** (0.08 g, 0.496 mmol) and EDC (0.11 g, 0.59 mmol) to give desired product **178b** as a yellow sticky oil (0.21 g, 79%). ^1H NMR (300 MHz, $CDCl_3$): δ 0.88 (t, J = 7.3 Hz, 3H, CH_3), 1.28-1.33 (m, 6H, 3 × CH_2), 1.85-1.89 (m, 2H, CH_2), 3.40-3.48 (m, 4H, 2 × CH_2), 3.53 (d, J = 2.8 Hz, 2H, CH_2), 3.63 (t, J = 5.4 Hz, 2H, CH_2), 3.82 (t, J = 5.7 Hz, 2H, CH_2), 4.02 (s, OCH_3), 5.58-5.62 (m, 1H, CHOC=O), 7.62 (s, 1H, CH); ^{13}C NMR (75.6 MHz, $CDCl_3$): δ 13.9 (CH_3), 22.3 (CH_2), 24.6 (CH_2), 31.2 (CH_2), 32.5 (CH_2), 40.5 (CH_2), 40.79 (CH_2), 44.88 (CH_2), 51.03 (CH_2), 61.2 (OCH_3), 69.9 (CH), 82.2 (CBr_2), 135.0 (C=CH), 135.7 (CH), 149.2 ($C=CBr_2$), 164.0 (C=O), 166.1 (C=O), 166.3 (C=O); IR (neat): ν_{max} 2930, 2860, 1769, 1744, 1648, 1497, 1442, 1380, 1316, 1266, 1213, 1150, 1111, 1069, 1035, 1003, 962, 914, 848, 776, 728, 684 cm^{-1}; UV (MeOH): λ_{max} 308 nm (ε 218887 $M^{-1}cm^{-1}$); HRMS (ESI) *m/z* Calcd. for $C_{18}H_{24}Br_2N_4O_7Na$ $(M + Na)^+$ 603.0066. Found 603.0059.

(*Z*)-1-(4-(3-(1-(5-(Dibromomethylene)-2-oxo-2,5-dihydrofuran-3-yl)dodecyloxy)-3-oxopropanoyl)piperazin-1-yl)-2-methoxydiazene oxide (178c)

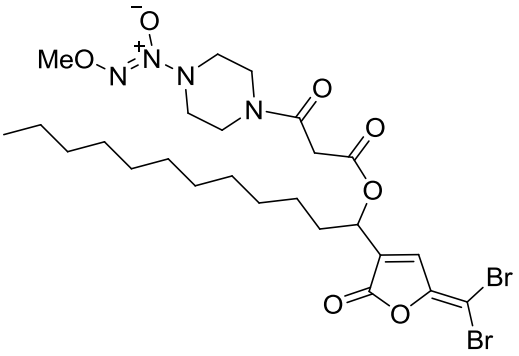

The desired compound was synthesized using mono acid fimbrolide **177c** (0.2 g, 0.37 mmol), piperazine diazeniumdiolate derivative **116** (0.07 g, 0.44 mmol) and EDC (0.10 g, 0.55 mmol) as described for the compound **178a** to yield the title compound **178c** as a white solid (0.20 g, 80%). ^{1}H NMR (300 MHz, $CDCl_3$): δ 0.86 (t, J = 7.3 Hz, 3H, CH_3), 1.23-1.30 (m, 18H, 9 × CH_2), 1.84-1.89 (m, 2H, CH_2), 3.39-3.46 (m, 4H, CH_2), 3.52 (d, J = 2.8 Hz, 2H, CH_2), 3.62 (t, J = 5.4 Hz, 2H, CH_2), 3.81 (t, J = 5.4 Hz, 2H, CH_2), 4.01 (s, 3H, OCH_3), 5.57-5.62 (m, 1H, CHOC=O), 7.62 (s, 1H, CH); ^{13}C NMR (75.6 MHz, $CDCl_3$): δ 14.1 (CH_3), 22.6 (CH_2), 24.9 (CH_2), 29.1 (CH_2), 29.3 (CH_2), 29.4 (CH_2), 29.5 (CH_2), 29.6 (CH_2), 31.9 (CH_2), 32.5 (CH_2), 40.4 (CH_2), 40.7 (CH_2), 44.8 (CH_2), 51.0 (CH_2), 61.2 (OCH_3), 69.9 (CH), 82.2 (CBr_2), 135.0 (C=CH), 135.7 (CH), 149.2 ($C=CBr_2$), 164.0 (C=O), 166.1 (C=O), 166.3 (C=O); IR (neat): ν_{max} 2923, 2853, 1773, 1748, 1650, 1498, 1442, 1316, 1266, 1212, 1150, 1111, 1069, 1035, 1005, 962, 848, 774, 729, 684 cm^{-1}; UV (MeOH): λ_{max} 308 nm (ε 279253 $M^{-1}cm^{-1}$); HRMS (ESI) *m/z* Calcd. for $C_{18}H_{24}Br_2N_4O_7Na$ $(M + Na)^+$ 687.1005. Found 687.1003.

(*Z*)-1-(4-(4-(1-(5-(Dibromomethylene)-2-oxo-2,5-dihydrofuran-3-yl)dodecyloxy)-4-oxobutanoyl)piperazin-1-yl)-2-methoxydiazene oxide (178d)

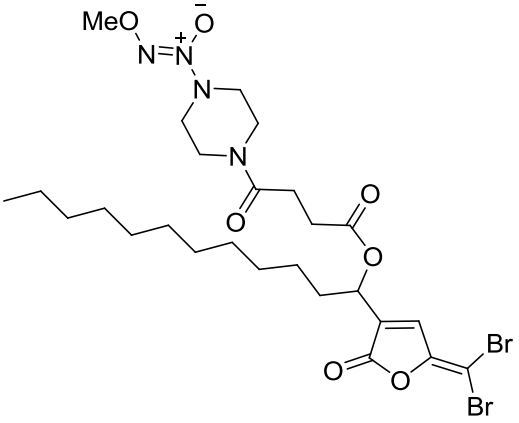

The title compound was synthesized following the procedure described for compound **178a** using the mono acid fimbrolide derivative **177c** (0.2 g; 0.38 mmol), piperazine diazeniumdiolate derivative **116** (0.08 g, 0.45 mmol) and EDC (0.11 g, 0.57 mmol) to give desired product **178d** as a yellow sticky oil (0.18 g, 71%). ^{1}H NMR (300 MHz, $CDCl_3$): δ 0.86 (t, J = 6.9 Hz, 3H, CH_3), 1.23-1.28 (m, 18H, 9 × CH_2), 1.81-1.87 (m, 2H, CH_2), 2.60-2.76 (m, 4H, 2 × CH_2), 3.35-3.44 (m, 4H, CH_2), 3.65 (t, J = 5.2 Hz, 2H, CH_2), 3.78 (t, J = 5.1 Hz, 2H, CH_2), 4.01 (s, 3H, OCH_3), 5.49-5.54 (t, J = 5.3 Hz, 1H, CHOC=O), 7.61 (s, 1H, CH); ^{13}C NMR (75.6 MHz, $CDCl_3$): δ 14.1 (CH_3), 22.6 (CH_2), 24.9 (CH_2), 27.9 (CH_2), 29.1 (CH_2), 29.3 (CH_2), 29.4 (CH_2), 29.5 (CH_2), 29.6 (CH_2), 31.9 (CH_2), 32.6 (CH_2), 40.3 (CH_2), 43.7 (CH_2), 51.0 (CH_2), 51.1 (CH_2), 61.2 (OCH_3), 69.2 (CH), 77. 2 (CH), 81.3 (CBr_2), 135.3 (CH), 135.8 (C=CH), 149.5 ($C=CBr_2$), 166.2 (C=O), 169.5 (C=O), 172.1 (C=O); IR (neat): ν_{max} 2923, 2853, 1774, 1738, 1648, 1498, 1440, 1372, 1281, 1214, 1155, 1112, 1068, 1031, 1004, 967, 848, 775, 730, 683 cm^{-1}; UV (MeOH): λ_{max} 307 nm (ε 295837 M^{-1}cm^{-1}); HRMS (ESI) *m/z* Calcd. for $C_{18}H_{24}Br_2N_4O_7Na$ $(M + Na)^+$ 701.1161. Found 701.1163.

3,3'-(1,1'-Disulfanediylbis(butane-1,1-diyl))bis(5-(dibromomethylene)furan-2(5H)-one) (181)

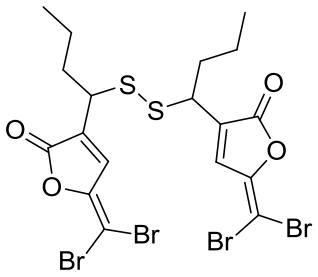

To a solution of thiofimbrolide **163** (0.11 g, 0.32 mmol) in DCM (15 mL) was added *t*-butyl nitrite (0.04 mL, 0.48 mmol) and the solution was stirred for 1h at room temperature. The crude reaction mixture was evaporated to dryness under *vacuo* and the crude product was purified by vacuum chromatography to yield the title compound **181** as a brown solid (0.06 g, 61%). M.p. 112–114°C. ^{1}H NMR (300 MHz, $CDCl_3$): δ 0.91 (6H, t, J = 7.3 Hz, 2 x CH_3), 1.35 (4H, m, 2 x CH_2), 1.85 (4H, q, J = 7.5 Hz 2 x CH_2), 3.53 (2H, t, J = 7.5 Hz, 2 x CHS), 7.32 (2H, s) ppm; ^{13}C NMR (75 MHz, $CDCl_3$): δ 13.9, 21.1, 35.1, 46.7, 82.2, 135.2, 135.8, 149.8, 167.4 ppm; IR (KBr): ν_{max} 3099, 2959, 2929, 2871, 1777, 1612, 1267, 1171, 1031, 966, 851, 779 cm^{-1}; HRMS (ESI) *m/z* Calcd. for $C_{18}H_{18}Br_4O_4S_2Na$ $(M + Na)^+$ 700.7272. Found 700.7283.

2,2,5,5-Tetramethylthiazolidine-4-carboxylic acid (188)

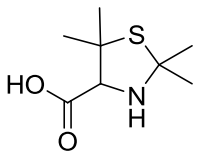

A solution of D-penicillamine **182** (3.7 g, 24.79 mmol) was dissolved in acetone (30 mL) containing few beads of molecular sieves and the mixture refluxed for 4h followed by stirring at room temperature for 16h. The reaction mixture was filtered to remove the molecular sieves and the precipitate rinsed with acetone and methanol. The filtrate was evaporated under *vacuo* to yield the title compound **188** as an off white solid (4.7 g, 100%). M.p. 160-162 °C; ^{1}H NMR (300 MHz, acetone-d_6): δ 1.24 (s, 3H, CH_3), 1.49 (s, 3H, CH_3), 1.60 (s, 6H, 2 × CH_3), 3.86 (s, 1H, CH); ^{13}C NMR (75.6 MHz, acetone-d_6): δ 27.9 (CH_3), 29.0 (CH_3), 31.7 (CH_3), 33.6 (CH_3), 61.3 (>C-S), 72.9 (>C-S), 73.3 (CH), 170.7 (C=O); IR (neat): ν_{max} 3261, 2968,

2452, 1710, 1573, 1456, 1372, 1328, 1241, 1194, 1109, 1020, 998, 923, 842, 819, 753, 651 cm^{-1}; HRMS (ESI) *m/z* Calcd. for $C_8H_{16}NO_2S_2$ $(M + H)^+$ 190.0902. Found 190.0891.

3-Acetyl-2,2,5,5-tetramethylthiazolidine-4-carboxylic acid (189)

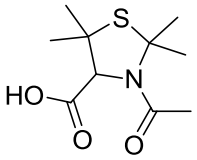

Compound **188** (2.4 g, 12.68 mmol) was added to a solution of acetic anhydride (7 mL) at 0 °C and slowly brought to room temperature and stirred for 18h. Ice was added to the reaction mixture and the resulting precipitate was filtered and washed with cold water to give the title compound **189** as a white solid (1.9 g, 66%). M.p. 176-178 °C; ^1H NMR (300 MHz, $CDCl_3$): δ 1.47 (s, 3H, CH_3), 1.72 (s, 3H, CH_3), 1.94 (s, 3H, CH_3), 1.96 (s, 3H, CH_3), 2.23 (s, 3H, $COCH_3$), 4.46 (s, 1H, CH), 10.10 (bs, 1H, COOH); ^{13}C NMR (75.6 MHz, acetone-d_6): δ 25.7 (CH_3), 25.9 (CH_3), 28.7 (CH_3), 32.5 (CH_3), 34.2 (CH_3), 49.8 (>C-S), 74.7 (>C-S), 77.0 (CH), 170.4 (C=O), 173.4 (C=O); IR (neat): ν_{max} 3351, 2972, 2576, 1692, 1612, 1537, 1456, 1373, 1248, 1181, 1124, 956, 731, 651 cm^{-1}; HRMS (ESI) *m/z* Calcd. for $C_{10}H_{17}NO_3SNa$ $(M + Na)^+$ 254.0827. Found 256.0608.

1-(5-(Dibromomethylene)-2-oxo-2,5-dihydrofuran-3-yl)butyl 3-acetyl-2,2,5,5-tetramethylthiazolidine-4-carboxylate (190)

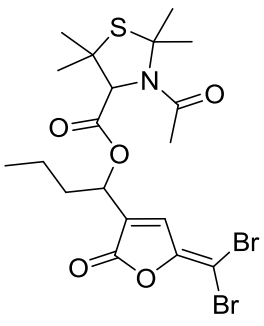

To a solution of bromofimbrolide **156a** (2 g, 5.16 mmol) and powdered potassium hydroxide (0.40 g, 7.23 mmol) in DMF (7 mL), was added thiazolidine acid derivative **189** (1.5 g, 6.71 mmol) and the mixture stirred for 72h at room temperature. Water

was added to the reaction mixture and the resulting mixture was extracted with DCM. The organic layer was further washed with water, brine and evaporated to dryness. The crude product was purified by vacuum chromatography using DCM/n-hexane to yield two diasteromeric products **190** (total yield-1.56 g, 56%). **Isomer 1**: M.p. 150-152 °C; ^{1}H NMR (300 MHz, $CDCl_3$): δ 0.93 (t, J = 7.4 Hz, 3H, CH_3), 1.34 (s, 3H, CH_3), 1.37-1.41 (m, 2H, CH_2), 1.72 (s, 3H, CH_3), 1.84-1.87 (m, 2H, CH_2), 1.99 (s, 2H, CH_3), 4.45 (s, 1H, CH), 5.60-5.65 (m, 1H, CHOC=O), 7.80 (s, 1H, CH), 8.34 (s, 1H, CHO); ^{13}C NMR (75.6 MHz, $CDCl_3$): δ 13.9 (CH_3), 18.9 (CH_2), 25.7 (CH_3), 25.9 (CH_3), 28.5 (CH_3), 32.6 (CH_3), 34.3 (CH_3), 35.2 (CH_2), 50.1 (>C-S), 70.6 (CH), 74.6 (>C-S), 77.2 (CH), 83.0 (CBr_2), 135.7 (C), 136.4 (CH), 149.6 (C), 166.2 (C=O), 169.3 (C=O), 170.0 (C=O); IR (neat): ν_{max} 3094, 2963, 2930, 2873, 1764, 1756, 1672, 1442, 1378, 1332, 1264, 1234, 1163, 1136, 1104, 1031, 964, 921, 846, 778, 737, 693 cm^{-1}. **Isomer 2**: M.p. 108-110 °C; ^{1}H NMR (300 MHz, $CDCl_3$): δ 0.95 (t, J = 7.4 Hz, 3H, CH_3), 1.37-1.50 (m, 2H, CH_2), 1.40 (s, 3H, CH_3), 1.66 (s, 3H, CH_3), 1.86-1.88 (m, 2H, CH_2), 1.98 (s, 3H, CH_3), 4.43 (s, 1H, CH), 5.68-5.73 (m, 1H, CHOC=O), 7.40 (s, 1H, CH); ^{13}C NMR (75.6 MHz, $CDCl_3$): δ 13.3 (CH_3), 18.5 (CH_2), 25.2 (CH_3), 33.3 (CH_3), 33.7 (CH_3), 34.2 (CH_2), 34.5 (CH_3), 50.2 (>C-S), 70.3 (>C-S), 70.5 (CH), 72.4 (CH), 81.8 (CBr_2), 135.3 (C), 135.5 (CH), 149.0 (C), 160.2 (CHO), 167.1 (C=O), 168.3(C=O); IR (neat): ν_{max} 3095, 2964, 2936, 2873, 1766, 1750, 1673, 1641, 1463, 1373, 1332, 1266, 1173, 1066, 1032, 966, 888, 848, 776, 737, 680 cm^{-1}. HRMS (ESI) *m/z* Calcd. for $C_{19}H_{26}Br_2NO_5S$ $(M + H)^+$ 537.9898. Found 537.9890

3-Formyl-2,2,5,5-tetramethylthiazolidine-4-carboxylic acid (191)

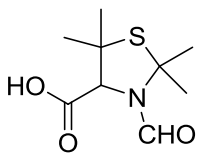

Acetic anhydride (10 mL, 15.84 mmol) was added dropwise over a

period of 30 min to a stirring solution of formic acid (25 mL, 15.84 mmol) containing thiazolidine derivative **188** (3 g, 15.84 mmol) and sodium formate (1.18 g, 17.43 mmol) at 0 °C. The reaction mixture was further stirred at 0 °C for 1h, followed by room temperature for 6h. At the end of this period, ice water was added and the resulting precipitate collected by filtration to give the title compound **191** as a white solid (2.1 g, 63%). M.p. 178 °C; ^{1}H NMR (300 MHz, $CDCl_3$): δ 1.50 (s, 3H, CH_3), 1.65 (s, 3H, CH_3), 1.93 (s, 6H, 2 × CH_3), 4.53 (s, 1H, CH), 8.36 (s, 1H, CHO); ^{13}C NMR (75.6 MHz, acetone-d_6): δ 25.9 (CH_3), 32.9 (CH_3), 33.7 (CH_3), 34.5 (CH_3), 50.2 (>C-S), 70.2 (>C-S), 72.0 (CH), 161.4 (C=O), 170.2 (C=O); IR (neat): ν_{max} 2976, 2944, 2507, 1738, 1613, 1466, 1364, 1318, 1194, 1163, 1137, 1109, 953, 917, 733, 717, 691 cm^{-1}; HRMS (ESI) *m/z* Calcd. for $C_9H_{15}NO_3SNa$ $(M + Na)^+$ 240.0607. Found 240.0659.

1-(5-(Dibromomethylene)-2-oxo-2,5-dihydrofuran-3-yl)butyl 3-formyl-2,2,5,5-tetramethylthiazolidine-4-carboxylate (192)

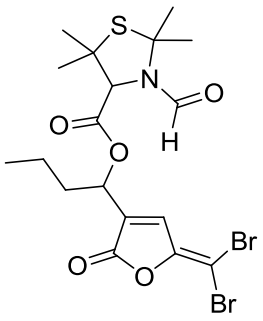

To a solution of bromofimbrolide **156a** (2 g, 5.14 mmol) and powdered potassium hydroxide (0.4 g, 7.19 mmol) in DMF (7 mL), was added thiazolidine acid derivative **191** (1.3 g, 6.68 mmol) and stirred for 72h at room temperature. Water was added to the reaction mixture and the resulting mixture was extracted with DCM. The organic layer was further washed with water, brine and evaporated to dryness. The crude product was purified by vacuum chromatography using ethyl acetate/n-hexane to yield two diasteromeric products **192**. **Isomer 1** (0.74 g, 27%): M.p. 134-136 °C; ^{1}H NMR (300 MHz, $CDCl_3$): δ 0.95 (t, J = 7.4 Hz, 3H, CH_3), 1.37-1.43 (m, 2H, CH_2), 1.46 (s, 3H, CH_3), 1.69 (s, 3H, CH_3), 1.81-1.88 (m, 2H, CH_2), 1.93 (s, 2H, CH_3), 4.81 (s, 1H, CH),

5.54-5.58 (m, 1H, CHOC=O), 7.80 (s, 1H, CH), 8.34 (s, 1H, CHO); ^{13}C NMR (75.6 MHz, $CDCl_3$): δ 13.4 (CH_3), 18.5 (CH_2), 25.7 (CH_3), 33.0 (CH_3), 33.5 (CH_3), 34.3 (CH_2), 34.5 (CH_3), 50.1 (>C-S), 70.3 (>C-S), 70.5 (CH), 72.4 (CH), 81.8 (CBr_2), 135.3 (C), 135.5 (CH), 149.0 (C), 160.2 (CHO), 166.1 (C=O), 168.3(C=O); IR (neat): ν_{max} 2960, 2928, 1768, 1748, 1671, 1462, 1372, 1325, 1177, 1136, 1113, 1062, 1026, 964, 881, 842, 772, 680 cm^{-1}; HRMS (ESI) *m/z* Calcd. for $C_{18}H_{24}Br_2NO_5S$ $(M + H)^+$ 523.9742. Found 523.9730. **Isomer 2** (0.52 g, 19%): M.p. 98 °C; ^{1}H NMR (300 MHz, $CDCl_3$): δ 0.92 (t, J = 7.4 Hz, 3H, CH_3), 1.37-1.50 (m, 2H, CH_2), 1.40 (s, 3H, CH_3), 1.66 (s, 3H, CH_3), 1.86-1.88 (m, 2H, CH_2), 1.93 (s, 3H, CH_3), 4.73 (s, 1H, CH), 5.58-5.63 (m, 1H, CHOC=O), 7.57 (s, 1H, CH), 8.38 (s, 1H, CHO); ^{13}C NMR (75.6 MHz, $CDCl_3$): δ 13.4 (CH_3), 18.5 (CH_2), 25.7 (CH_3), 33.0 (CH_3), 33.5 (CH_3), 34.3 (CH_2), 34.5 (CH_3), 50.1 (>C-S), 70.3 (>C-S), 70.5 (CH), 72.4 (CH), 81.8 (CBr_2), 135.3 (C), 135.5 (CH), 149.0 (C), 160.2 (CHO), 166.1 (C=O), 168.3(C=O); IR (neat): ν_{max} 3096, 2967, 2934, 2872, 1767, 1749, 1669, 1468, 1386, 1370, 1326, 1267, 1175, 1142, 1118, 1058, 1026, 965, 915, 890, 844, 774, 735, 714 cm^{-1}; HRMS (ESI) *m/z* Calcd. for $C_{18}H_{24}Br_2NO_5S$ $(M + H)^+$ 523.9742. Found 523.9728.

1-(5-(Dibromomethylene)-2-oxo-2,5-dihydrofuran-3-yl)butyl-2-acetamido-3-mercapto-3-methylbutanoate (185)

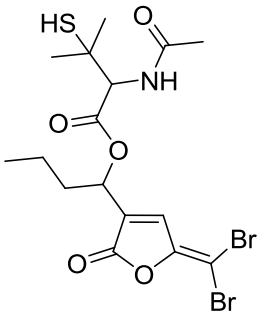

The thiazolidine fimbrolide derivative **192** (0.4 g, 0.81 mmol) was dissolved in a mixture of 1M methanolic hydrochloric acid (1.5 mL) and methanol (2 mL) by gentle warming. The reaction mixture was kept at 50 °C for 18h and the solvent evaporated to dryness. Aqueous sodium bicarbonate solution (7 mL, 0.81 mmol) was added to the

residue and the reaction mixture was cooled in an ice bath. Acetic anhydride (2 mL) was added dropwise to the mixture followed by stirring for 18h at room temperature. The reaction mixture was concentrated to dryness and the residue purified by vacuum chromatography using ethyl acetate/n-hexane to give title compound **185** as an off white solid (0.16 g, 42%). M.p. 134-136 °C; ^{1}H NMR (300 MHz, $CDCl_3$): δ 0.93 (t, J = 7.4 Hz, 3H, CH_3), 1.31-1.43 (m, 2H, CH_2), 1.37 (s, 3H, CH_3), 1.52 (s, 3H, CH_3), 1.81-1.89 (m, 2H, CH_2), 2.04 (s, 3H, $COCH_3$), 2.12 (s, 1H, SH), 4.54 (d, J = 8.7 Hz, 1H, CH), 5.53-5.58 (m, 1H, CHOC=O), 6.43 (bd, J = 8.6 Hz, 1H, NH) 7.61 (s, 1H, CH); ^{13}C NMR (75.6 MHz, $CDCl_3$): δ 13.5 (CH_3), 18.4 (CH_2), 23.0 (CH_3), 29.3 (CH_3), 31.3 (CH_3), 34.7 (CH_2), 45.6 (>C-SH), 60.7 (CH), 70.1 (CH), 82.1 (CBr_2), 135.2 (C), 135.6 (CH), 149.3 (C), 166.1 (C=O), 170.1 (C=O), 170.3(C=O); IR (neat): ν_{max} 2964, 2919, 2857, 1769, 1748, 1667, 1463, 1372, 1325, 1262, 1175, 1136, 1113, 1062, 1026, 964, 912, 849, 772, 755, 714 cm^{-1}; HRMS (ESI) *m/z* Calcd. for $C_{16}H_{21}Br_2NO_5SNa$ $(M + Na)^+$ 519.9405. Found 519.9412.

1-(5-(Dibromomethylene)-2-oxo-2,5-dihydrofuran-3-yl)butyl-2-acetamido-3-methyl-3-(nitrosothio)butanoate (183)

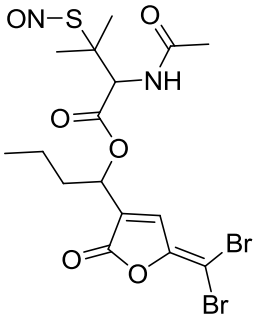

To a solution of fimbrolide **185** (1.0 mmol) in DCM (15 mL) was added *t*-butyl nitrite (2.0 mmol) and the solution was stirred at 0 °C for 20 min. The crude reaction mixture was evaporated to dryness under *vacuo* and the residue purified by vacuum chromatography to yield the title compound **183** as green sticky oil. ^{1}H NMR (400 MHz, $CDCl_3$): δ 0.89 (t, J = 7.4 Hz, 3H, CH_3), 1.31-1.37 (m, 2H, CH_2), 1.78-1.84 (m, 2H, CH_2), 1.97 (s, 3H, CH_3), 2.02 (s, 3H, CH_3), 2.07 (s, 3H, $COCH_3$), 5.35 (d, J =9.0 Hz,

1H, CH), 5.53 (t, *J* = 6.0 Hz, 1H, CHOC=O), 6.41 (bd, *J* = 8.1 Hz, 1H, NH) 7.51 (s, 1H, CH). Due to the instability of the *S*-Nitrosothiol compound it could not be fully characterized.

1,3-Dibutyl-5-(dibromomethylene)-1H-pyrrol-2(5H)-one (212a)

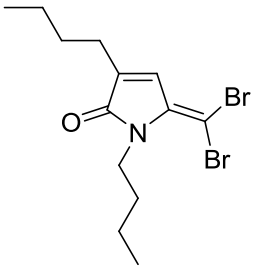

A solution of 3-butyl-5-(dibromomethylene)furan-2(5*H*)-one **153a** (1.00 g, 3.22 mmol) in DCM (20 mL) was stirred in an ice bath at 0 °C followed by dropwise addition of *n*-butylamine **213a** (0.70 g, 9.68 mmol) in DCM (2 mL). The mixture was allowed to stir for 1 h at 0 °C and, then the mixture was successively washed with HCl (2M, 10 mL), water (10 mL) and brine solution (10 mL). The organic phase was separated, dried (Na_2SO_4) and the solvent evaporated in *vacuo*. A mixture of the residual oil and *p*-TsOH (0.02 g, 0.11 mmol) in toluene (10 mL) was refluxed for 1 h. The solvent was evaporated in *vacuo* and the residue purified by silica gel chromatography (2:1 dichloromethane/light petroleum) to afford the title compound **212a** as a yellow oil (0.66 g, 56%). ^{1}H NMR (300 MHz, $CDCl_3$): δ 0.92 (m, 6H, 2 x CH_3), 1.25-1.43 (m, 4H, 2 x CH_2), 1.51-1.63 (m, 4H, 2 x CH_2), 2.28-2.33 (m, 2H, CH_2), 3.96 (t, *J* = 7.6 Hz, 2H, CH_2), 6.99 (s, 1H, CH); ^{13}C NMR (75.6 MHz, $CDCl_3$): δ 14.2 (2 x CH_3), 20.2 (CH_2), 22.8 (CH_2), 25.5 (CH_2), 30.0 (CH_2), 32.5 (CH_2), 41.1 (CH_2), 73.9 (C), 132.2 (CH), 139.2 (C), 141.0 (C), 172.3 (C=O); IR (neat): ν_{max} 2957, 2871, 1701, 1586, 1455, 1361, 1194, 1168, 1134, 1047, 829; UV (CH_3OH): λ_{max} 205.0 nm (9270 $M^{-1}cm^{-1}$), 284.0 nm (20630 $M^{-1}cm^{-1}$).

3-Butyl-5-(dibromomethylene)-1H-pyrrol-2(5H)-one (212b)

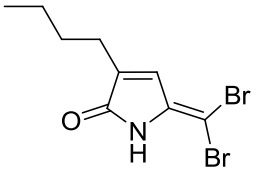

A solution of 3-butyl-5-(dibromomethylene)furan-2(5*H*)-one **153a** (1.00 g, 3.22 mmol) in ether (30 mL) was stirred in a dry-ice bath at -78 °C followed by slow bubbling of ammonia gas for approximately 15 min. The stirred mixture was slowly brought to room temperature and allowed to react for 18 h. The crude reaction mixture was successively washed with water (20 mL), HCl (2M, 20 mL) and brine solution (20 mL). The organic phase was separated, dried (Na_2SO_4) and the solvent evaporated in *vacuo*. The residual solid and *p*-TsOH (0.02 g, 0.11 mmol) in toluene (10 mL) was refluxed for 1 h. The solvent was evaporated in *vacuo* and the residue purified by silica gel chromatography (2:1 ethyl acetate/n-hexane) to afford the title compound **212b** as a white solid (0.66 g, 36%). M.p. 104-106 °C ^{1}H NMR (300 MHz, DMSO-d_6): δ 0.86 (t, J = 7.2, 3H, CH_3), 1.24-1.31 (m, 2H, CH_2), 1.44-1.49 (m, 2H, CH_2), 2.15-2.26 (m, 2H, CH_2), 6.95 (s, 1H, CH), 10.37 (bs, 1H, NH); ^{13}C NMR (75.6 MHz, DMSO-d_6): δ 14.0 (CH_3), 22.1 (CH_2), 24.9 (CH_2), 29.6 (CH_2), 74.6 (C), 129.6 (CH), 141.6 (C), 141.7 (C), 171.6 (C=O); IR (neat): ν_{max} 3142, 3093, 3034, 2946, 2925, 2869, 2762, 1705, 1618, 1465, 1431, 1386, 1314, 1298, 1201, 1131, 1097, 1005, 929, 862, 845, 793, 743, 712 cm^{-1}; UV (MeOH): λ_{max} 311 nm (ε 130984 M^{-1}cm^{-1}); HRMS (ESI) *m/z* Calcd. for $C_9H_{11}Br_2NONa$ $(M + Na)^+$ 329.9105. Found 329.9096.

1-Benzyl-3-butyl-5-(dibromomethylene)-1H-pyrrol-2(5H)-one (212c)

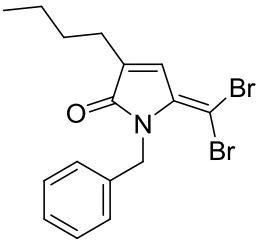

A solution of 3-butyl-5-(dibromomethylene)furan-2(5*H*)-one **153a** (1.03 g, 3.32 mmol) in DCM (20 mL) was stirred in an ice bath at 0 °C followed by dropwise addition of benzylamine (0.98

g, 9.1 mmol) in DCM (2 mL). The stirred mixture was brought to room temperature and allowed to react for 2 h and then successively washed with water (10 mL), HCl (2M, 10 mL) and brine solution (10 mL). The organic phase was separated, dried (Na_2SO_4) and the solvent evaporated in *vacuo*. A mixture of the residual solid and *p*-TsOH (0.02 g, 0.11 mmol) in toluene (10 mL) was refluxed for 2 h. The solvent was evaporated in *vacuo* and the residue purified by silica gel chromatography (2:1 dichloromethane/light petroleum) to afford the title compound **212c** as a yellow solid (0.78 g, 60%). M.p. 112-114 °C; ^{1}H NMR (300 MHz, $CDCl_3$): δ 0.98 (t, J = 7.2 Hz, 3H, CH_3), 1.30-1.47 (m, 2H, CH_2), 1.51-1.58 (m, 2H, CH_2), 2.28-2.34 (m, 2H, CH_2), 5.18 (s, 2H, NCH_2), 6.98-7.22 (m, 6H, CH and Haryl); ^{13}C NMR (75.6 MHz, $CDCl_3$): δ 14.7 (CH_3), 22.8 (CH_2), 25.7 (CH_2), 30.0 (CH_2), 44.6 (NCH_2), 75.1 (C), 126.4 (2 x ArCH), 127.4 (ArCH), 128.9 (2 x ArCH), 132.7 (CH), 138.2 (C), 139.2 (C), 140.8 (C), 172.5 (C=O); IR (KBr disc): ν_{max} 2953, 1706, 1626, 1494, 1435, 1352, 1268, 1235, 1094, 747, 721; UV (CH_3OH): λ_{max} 206.0 nm (10970 $M^{-1}cm^{-1}$), 283.0 nm (16200 $M^{-1}cm^{-1}$).

3-Butyl-5-(dibromomethylene)-1-phenyl-1H-pyrrol-2(5H)-one (212d)

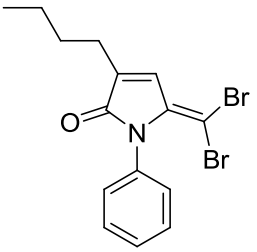

A mixture of 3-butyl-5-(dibromomethylene)furan-2(5*H*)-one **153a** (1 g, 3.22 mmol) and aniline (0.94 g, 0.96 mmol) was refluxed for 3 h. The residue was dissolve in DCM (30 mL) and successively washed with water (20 mL), HCl (2M, 20 mL) and brine solution (20 mL). The organic phase was separated, dried (Na_2SO_4) and the solvent evaporated *in vacuo*. The residual solid was purified by flash chromatography (dichloromethane). A mixture of the residual solid and *p*-TsOH (0.02 g, 0.11 mmol) in toluene (10 mL) was refluxed for 1 h. The solvent was evaporated in *vacuo* and the residue purified by silica

gel chromatography (dichloromethane) to afford the title compound **212d** as a yellow solid (0.53 g, 43%). M.p. 48 °C; ^{1}H NMR (300 MHz, $CDCl_3$): δ 0.95 (t, J = 7.2, 3H, CH_3), 1.37-1.45 (m, 2H, CH_2), 1.58-1.64 (m, 2H, CH_2), 2.35-2.40 (m, 2H, CH_2), 7.16-7.37 (m, 6H, CH and ArH); ^{13}C NMR (75.6 MHz, $CDCl_3$): δ 13.7 (CH_3), 22.3 (CH_2), 25.2 (CH_2), 29.5 (CH_2), 76.1 (C), 128.3 (ArCH), 128.8 (2 x ArCH), 129.3 (2 x ArCH), 132.0 (CH), 135.0 (C), 138.9 (C), 140.2 (C), 171.7 (C=O); IR (neat): ν_{max} 3107, 3047, 2962, 2919, 2853, 1692, 1592, 1498, 1460, 1356, 1186, 1172, 1124, 1083, 1067, 1038, 857, 833, 797, 778, 755, 740, 687 cm^{-1}; UV (MeOH): λ_{max} 308.0 nm (72090 M^{-1}cm^{-1}). HRMS (ESI) *m/z* Calcd. for $C_{15}H_{16}Br_2NO$ $(M + H)^+$ 383.9599. Found 383.9590.

1-(4-Bromophenyl)-3-butyl-5-(dibromomethylene)-1H-pyrrol-2(5H)-one (212e)

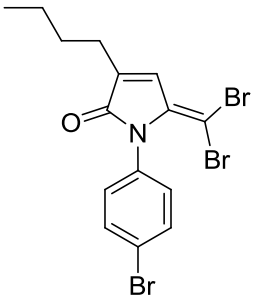

A mixture of 3-butyl-5-(dibromomethylene)furan-2(5*H*)-one **153a** (1.00 g, 3.22 mmol) and 4-bromoaniline (1.6 g, 0.96 mmol) were heated at 80 °C for 18h without any solvent. The residue was redissolve in DCM (15 mL) and successively washed with water (10 mL), HCl (2M, 10 mL) and saturated NaCl solution (10 mL). The organic phase was separated, dried (Na_2SO_4) and the solvent evaporated in *vacuo*. The residual solid was purified by flash chromatography (dichloromethane). A mixture of the residual solid and P_2O_5 (0.02 g, 0.11 mmol) in toluene (10 mL) was refluxed for 1 h. The solvent was evaporated in *vacuo* and the residue purified by silica gel chromatography (dichloromethane/n-hexane) to afford the title compound **212e** as an off white solid (0.95 g, 64%). M.p. 88 °C; ^{1}H NMR (300 MHz, $CDCl_3$): δ 0.95 (t, J =7.4, 3H, CH_3), 1.37-1.44 (m, 2H, CH_2), 1.57-1.63 (m, 2H, CH_2), 2.34-2.40 (m, 2H, CH_2), 7.09-7.12 (m,

2H, ArH), 7.17 (s, 1H, CH), 7.53-7.56 (m, 2H, ArH); ^{13}C NMR (75.6 MHz, $CDCl_3$): δ 13.7 (CH_3), 22.3 (CH_2), 25.2 (CH_2), 29.5 (CH_2), 53.3 (C), 122.3 (ArC), 130.8 (2 x ArH), 132.0 (2 x ArH), 132.3 (CH), 134.1 (C), 138.8 (C), 139.9 (C), 171.4 (C=O); IR (neat): ν_{max} 3091, 2955, 2930, 2863, 1698, 1585, 1485, 1464, 1397, 1360, 1196, 1123, 1091, 1066, 1010, 935, 864, 838, 825, 737, 716, 658 cm^{-1}; UV (MeOH): λ_{max} 308 nm (ε 84538 $M^{-1}cm^{-1}$); HRMS (ESI) *m/z* Calcd. for $C_{15}H_{14}Br_3NONa$ $(M + Na)^+$ 483.8523. Found 483.8508.

3-(1-Bromobutyl)-1-butyl-5-(dibromomethylene)-1H-pyrrol-2(5H)-one 211a

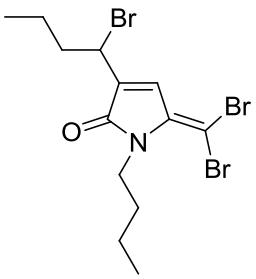

N-Bromosuccinimide (0.22 g, 1.24 mmol) was added to a solution of 1,3-dibutyl-5-(dibromomethylene)-1H-pyrrol-2(5H)-one **212a** (0.412 g, 1.12 mmol) and benzoyl peroxide (0.03 g) in carbon tetrachloride (CCl_4) (30 mL). The mixture was irradiated with 250W lamp and was refluxed for 24 h. The crude product was filtered through a pad of silica, evaporated and purified by vacuum chromatography using dichloromethane/n-hexane to afford the title fimbrolide compound **211a** as a yellow oil (0.4 g, 79%).^{1}H NMR (300 MHz, $CDCl_3$): δ 0.92 (m, 6H, 2 x CH_3), 1.24-1.63 (m, 8H, 4 x CH_2), 1.99-2.12 (m, 2H, CH_2), 3.97 (t, J = 7.6 Hz, 2H, CH_2), 4.76-4.81 (m, 2H, CH_2), 7.28 (s, 1H, CH); ^{13}C NMR (75.6 MHz, $CDCl_3$): δ 13.1 (CH_3), 13.6 (CH_3), 19.7 (CH_2), 20.9 (CH_2), 32.0 (CH_2), 32.0 (CH_2), 38.8 (CH_2), 40.8 (CH_2), 43.4 (CH), 73.9 (C), 133.3 (CH), 138.0 (C), 139.9 (C), 169.0 (C=O); IR (neat): ν_{max} 3094, 2953, 2931, 2871, 1688, 1605, 1581, 1464, 1454, 1440, 1378, 1337, 1254, 1194, 1169, 1132, 1052, 1009, 864, 833, 776, 743, 732, 669; UV (CH_3OH): λ_{max} 280 nm (ε 53916 $M^{-1}cm^{-1}$); 325 nm (ε 57589 $M^{-1}cm^{-1}$); HRMS (ESI) *m/z* Calcd. for $C_{13}H_{18}Br_3NONa$ $(M + Na)^+$ 463.8836. Found 463.8824.

3-(1-Bromobutyl)-5-(dibromomethylene)-1H-pyrrol-2(5H)-one 211b

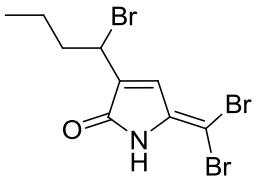

The title compound was prepared as described for the compound **211a**. A solution of 3-butyl-5-(dibromomethylene)-1H-pyrrol-2(5H)-one **212b** (0.32 g; 1.03 mmol), benzoyl peroxide (0.03 g) and NBS (0.20 g, 1.13 mmol) in 15 mL carbon tetrachloride was reacted to give desired product **211b** as a light yellow solid (0.34 g, 85%). M.p. 108 °C; ^{1}H NMR (300 MHz, $CDCl_3$): δ 0.96 (t, J = 7.3, 3H, CH_3), 1.40-1.60 (m, 2H, CH_2), 1.85-1.93 (m, 2H, CH_2), 5.72-5.77 (m, 1H, CH), 7.12 (s, 1H, CH), 7.95 (bs, 1H, NH); ^{13}C NMR (75.6 MHz, $CDCl_3$): δ 13.6 (CH_3), 18.3 (CH_2), 34.1 (CH_2), 77.4 (CH), 79.7 (C), 130.4 (CH), 137.6 (C), 139.5 (C), 168.0 (C=O); IR (neat): ν_{max} 3091, 2961, 2931, 2870, 1698, 1613, 1583, 1492, 1454, 1373, 1195, 1174, 1136, 1086, 1040, 1006, 892, 869, 833, 782, 738, 692 cm^{-1}; UV (MeOH): λ_{max} 323 nm (ε 92630 M^{-1}cm^{-1}); HRMS (ESI) *m/z* Calcd. for $C_9H_{10}Br_3NONa$ $(M + Na)^+$ 407.8210. Found 407.8205.

1-Benzyl-3-(1-bromobutyl)-5-(dibromomethylene)-1H-pyrrol-2(5H)-one 211c

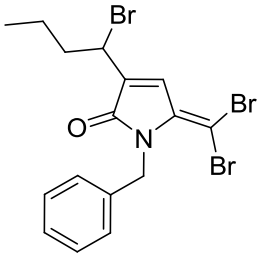

The title compound was prepared as described for the compound **211a**. The fimbrolide derivative, 1-benzyl-3-butyl-5-(dibromomethylene)-1H-pyrrol-2(5H)-one **212c** (0.4 g, 1.00 mmol) was brominated using NBS (0.21 g, 1.20 mmol) in presence of benzoyl peroxide (0.04 g) to give the title compound **211c** as an off white solid (0.48 g, 100%). M.p.76 °C; ^{1}H NMR (300 MHz, $CDCl_3$): δ 0.98 (t, J = 7.3 Hz, 3H, CH_3), 1.32-1.59 (m, 2H, CH_2), 2.00-2.11 (m, 2H, CH_2), 4.77-4.82 (m, 1H, CHBr), 5.21 (s, 2H, NCH_2), 6.98-7.24 (m, 5H, ArH), 7.32 (s, 1H, CH); ^{13}C NMR (75.6 MHz, $CDCl_3$): δ 13.2 (CH_3), 21.0 (CH_2), 38.9 (CH_2), 43.5 (CHBr), 44.4 (NCH_2), 78.3 (C),

125.9 (2 x ArCH), 127.1 (ArCH), 128.6 (2 x ArCH), 133.8 (CH), 137.3 (C), 138.1 (C), 139.7 (C), 169.3 (C=O); IR (neat): ν_{max} 3376, 2955, 2933, 2871, 1688, 1604, 1581, 1493, 1450, 1431, 1369, 1347, 1328, 1291, 1190, 1166, 1144, 1085, 1072, 1025, 956, 920, 887, 856, 826, 778, 743, 709, 695, 660; UV (CH_3OH): λ_{max} 325 nm (ε 49141 $M^{-1}cm^{-1}$); HRMS (ESI) *m/z* Calcd. for $C_{16}H_{16}Br_3NONa$ $(M + Na)^+$ 497.8680. Found 497.8668.

3-(1-Bromobutyl)-5-(dibromomethylene)-1-phenyl-1H-pyrrol-2(5H)-one (211d)

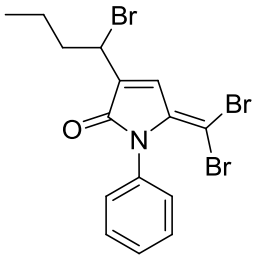

The title compound was prepared as described for the compound **211a**. A solution of 3-butyl-5-(dibromomethylene)-1-phenyl-1H-pyrrol-2(5H)-one **212d** (0.3 g; 0.77 mmol), benzoyl peroxide (0.03 g) and NBS (0.15 g, 0.85 mmol) in 15 mL carbon tetrachloride was reacted to give desired product **211d** as a light brown solid (0.47 g, 80%). M.p. 52-54 °C; ^1H NMR (300 MHz, $CDCl_3$): δ 1.00 (t, J = 7.3, 3H, CH_3), 1.46-1.70 (m, 2H, CH_2), 2.10-2.20 (m, 2H, CH_2), 4.85-4.90 (m, 1H, CH_2), 7.21-7.41 (m, 5H, ArH), 7.49 (s, 1H, CH); ^{13}C NMR (75.6 MHz, $CDCl_3$): δ 13.2 (CH_3), 21.0 (CH_2), 39.0 (CH_2), 43.5 (CH_2Br), 79.7 (CBr_2), 128.7 (ArCH), 129.0 (2 x ArCH), 129.4 (2 x ArCH), 133.8 (CH), 134.5 (C), 138.2 (C), 139.6 (C), 168.8 (C=O); IR (neat): ν_{max} 3388, 3092, 2962, 2930, 2869, 1698, 1583, 1491, 1454, 1371, 1193, 1169, 1135, 1085, 1040, 887, 832, 782, 763, 740, 691, 661 cm^{-1}; UV (MeOH): λ_{max} 325 nm (ε 78315 $M^{-1}cm^{-1}$); HRMS (ESI) *m/z* Calcd. for $C_{15}H_{15}Br_3NO$ $(M + H)^+$ 461.8704. Found 461.8695.

3-(1-Bromobutyl)-1-(4-bromophenyl)-5-(dibromomethylene)-1H-pyrrol-2(5H)-one (211e)

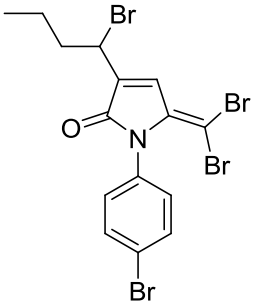

The title compound was prepared as described for the compound **211a**. The fimbrolide derivative, 1-(4-bromophenyl)-3-butyl-5-(dibromomethylene)-1H-pyrrol-2(5H)-one **212e** (0.50 g, 1.07 mmol) was brominated using NBS (0.23 g, 1.29 mmol) and benzoyl peroxide (0.03 g) to give the title compound **211e** as an off white solid (0.57 g, 97%). M.p. 88 °C; ^{1}H NMR (300 MHz, $CDCl_3$): δ 0.98 (t, J = 7.4, 3H, CH_3), 1.46-1.65 (m, 2H, CH_2), 2.07-2.18 (m, 2H, CH_2), 4.81-4.86 (m, 1H, CHBr), 7.09-7.15 (m, 2H, ArH), 7.47 (s, 1H, CH), 7.55-7.58 (m, 2H, ArH); ^{13}C NMR (75.6 MHz, $CDCl_3$): δ 13.2 (CH_3), 21.0 (CH_2), 39.0 (CH_2), 43.2 (CH), 79.9 (C), 122.7 (ArC), 130.9 (ArH), 132.2 (ArH), 133.6 (C), 133.9 (2 × ArH), 138.2 (C), 139.3 (C), 168.6 (C=O); IR (neat): ν_{max} 3093, 2964, 2868, 1698, 1606, 1580, 1486, 1462, 1375, 1255, 1189, 1131, 1089, 1070, 1012, 938, 898, 867, 835, 824, 776, 744, 714, 687, 667 cm^{-1}; UV (MeOH): λ_{max} 321 nm (ε 89517 M^{-1}cm^{-1}); HRMS (ESI) *m/z* Calcd. for $C_{15}H_{13}Br_4NONa$ $(M + Na)^+$ 561.7628. Found 561.7613.

1-(1-Butyl-5-(dibromomethylene)-2-oxo-2,5-dihydro-1H-pyrrol-3-yl)butyl nitrate (210a)

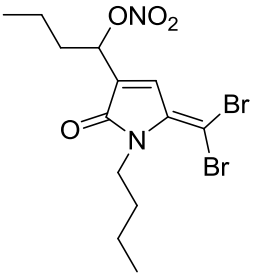

A solution of bromo-derivative **211a** (0.5 g, 1.12 mmol) and silver nitrate (0.22 g, 1.35 mmol) in anhydrous acetonitrile (20 mL) was heated at 50 °C for 5h. The crude product was filtered through a pad of Celite and silica to remove the silver salt formed. The filtrate was evaporated to dryness and the residue purified by vacuum chromatography

using dichloromethane/n-hexane to give the title compound **210a** as a light yellow solid (0.34 g, 71%). M.p. 36-38 °C; ^{1}H NMR (300 MHz, $CDCl_3$): δ 0.93 (m, 6H, 2 x CH_3), 1.22-1.61 (m, 8H, 4 x CH_2), 1.99-2.16 (m, 2H, CH_2), 3.98 (t, J = 7.6 Hz, 2H, CH_2), 4.72-4.81 (m, 2H, CH_2), 7.2 (s, 1H, CH); ^{13}C NMR (75.6 MHz, $CDCl_3$): δ 13.6 (CH_3), 13.7 (CH_3), 18.3 (CH_2), 19.7 (CH_2), 32.1 (CH_2), 34.2 (CH_2), 40.9 (CH_2), 77.5 (CH), 73.9 (C), 133.1 (CH), 134.4 (C), 139.9 (C), 169.1 (C=O); IR (neat): ν_{max} 3153, 2957, 2930, 2871, 1684, 1633, 1581, 1465, 1453, 1437, 1353, 1334, 1296, 1272, 1196, 1144, 1103, 1046, 967, 915, 873, 833, 771, 746, 691, 677; UV (CH_3OH): λ_{max} 281 nm (ε 53936 $M^{-1}cm^{-1}$); 331 nm (ε 66072 $M^{-1}cm^{-1}$); HRMS (ESI) *m/z* Calcd. for $C_{13}H_{18}Br_2N_2O_4Na$ $(M + Na)^+$ 446.9531. Found 446.9521.

1-(5-(Dibromomethylene)-2-oxo-2,5-dihydro-1H-pyrrol-3-yl)butyl nitrate (210b)

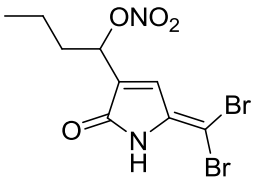

The title compound was synthesized following the procedure for compound **210a** using the bromo-derivative **211b** (0.13 g; 0.35 mmol) and silver nitrate (0.75 g, 0.43 mmol) to give desired product **210b** as a yellow solid (0.09 g, 78%). M.p. 90-92 °C; ^{1}H NMR (300 MHz, $CDCl_3$): δ 0.96 (t, J = 7.2, 3H, CH_3), 1.39-1.64 (m, 2H, CH_2), 2.01-2.17 (m, 2H, CH_2), 4.75-4.80 (m, 1H, CH), 7.14 (s, 1H, CH), 7.75 (bs, 1H, NH). ^{13}C NMR (75.6 MHz, $CDCl_3$): δ 14.0 (CH_3), 22.1 (CH_2), 24.9 (CH_2), 29.6 (CH_2), 74.6 (C), 129.6 (CH), 141.6 (C), 141.7 (C), 171.6 (C=O); IR (neat): ν_{max} 3116, 3040, 2966, 2931, 2872, 1692, 1651, 1625, 1464, 1455, 1379, 1327, 1298, 1273, 1201, 1160, 1114, 1102, 1051, 1019, 966, 881, 871, 833, 775, 751, 700, 669 cm^{-1}; UV (MeOH): λ_{max} 322 nm (ε 99037 $M^{-1}cm^{-1}$); HRMS (ESI) *m/z* Calcd. for $C_9H_{10}Br_2N_2O_4Na$ $(M + Na)^+$ 390.8905. Found 390.8896.

1-(1-Benzyl-5-(dibromomethylene)-2-oxo-2,5-dihydro-1H-pyrrol-3-yl)butyl nitrate (210c)

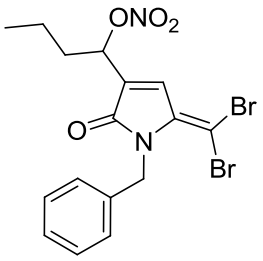

The title compound was synthesized following the procedure for compound **210a** using the bromo-derivative **211c** (0.3 g, 0.62 mmol) and silver nitrate (0.13 g, 0.81 mmol) to give the title compound **210c** as a yellow solid (0.20 g, 69%). M.p. 76 °C; ^{1}H NMR (300 MHz, $CDCl_3$): δ 0.98 (t, J = 7.1 Hz, 3H, CH_3), 1.43-1.53 (m, 2H, CH_2), 1.89-1.97 (m, 2H, CH_2), 5.28 (s, 2H, NCH_2), 5.81-6.86 (m, 1H, $CHONO_2$), 7.04-7.07 (m, 2H, ArH), 7.25-7.35 (m, 3H, ArH), 7.37 (s, 1H, CH); ^{13}C NMR (75.6 MHz, $CDCl_3$): δ 13.6 (CH_3), 18.4 (CH_2), 34.3 (CH_2), 44.4 (NCH_2), 77.5 (CH), 79.2 (C), 125.9 (2 x ArCH), 127.2 (ArCH), 128.7 (2 x ArCH), 133.5 (CH), 134.4 (C), 137.2 (C), 139.6 (C), 169.4 (C=O); IR (neat): ν_{max} 2962, 2929, 1687, 1633, 1585, 1496, 1454, 1434, 1382, 1332, 1319, 1294, 1266, 1191, 1153, 1133, 1107, 1074, 993, 946, 923, 884, 863, 831, 754, 738, 701, 693, 677; UV (CH_3OH): λ_{max} 281 nm (ε 49297 $M^{-1}cm^{-1}$); 327 nm (ε 62742 $M^{-1}cm^{-1}$); HRMS (ESI) *m/z* Calcd. for $C_{16}H_{16}Br_2N_2O_4Na$ $(M + Na)^+$ 480.9375. Found 480.9366.

1-(5-(Dibromomethylene)-2-oxo-1-phenyl-2,5-dihydro-1H-pyrrol-3-yl)butyl nitrate (210d)

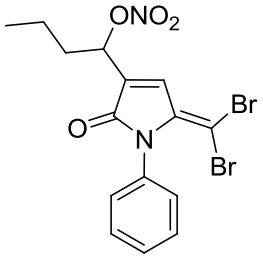

The title compound was synthesized following the procedure for compound **210a** using the bromo-derivative **211d** (0.22 g; 0.47 mmol) and silver nitrate (0.10 g, 0.61 mmol) to give desired product **210d** as a light brown solid (0.15 g, 72 %). ^{1}H NMR (300 MHz, $CDCl_3$): δ 0.97 (t, J = 7.2, 3H, CH_3), 1.43-1.54 (m, 2H, CH_2), 1.89-1.97 (m, 2H,

CH_2), 5.80-5.85 (m, 2H, CH_2ONO_2), 7.22-7.44 (m, 6H, CH and ArH); ^{13}C NMR (75.6 MHz, $CDCl_3$): δ 13.6 (CH_3), 18.4 (CH_2), 34.2 (CH_2), 77.6 (CH_2), 80.6 (C), 128.8 (ArCH), 129.0 (ArCH), 129.1 (ArCH), 129.3 (ArCH), 129.4 (ArCH), 133.3 (CH), 134.2 (C), 134.4 (C), 139.4 (C), 168.9 (C=O); IR (neat): ν_{max} 2959, 2918, 2849, 1708, 1634, 1595, 1497, 1455, 1368, 1270, 1192, 1096, 1071, 963, 887, 753, 740, 694 cm^{-1}; HRMS (ESI) *m/z* Calcd. for $C_{15}H_{14}Br_2N_2O_4Na$ $(M + Na)^+$ 466.9218. Found 466.9205.

1-(1-(4-Bromophenyl)-5-(dibromomethylene)-2-oxo-2,5-dihydro-1H-pyrrol-3-yl)butyl nitrate (210e)

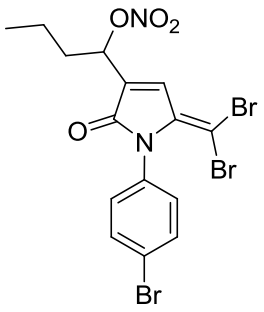

The title compound was synthesized following the procedure for compound **210a** using the bromo-derivative **211e** (0.30 g, 0.55 mmol) and silver nitrate (0.12 g, 0.71 mmol) to give the title compound **210e** as a white solid (0.18 g, 74%). M.p. 88 °C; ^1H NMR (300 MHz, $CDCl_3$): δ 0.98 (t, J = 7.4, 3H, CH_3), 1.43-1.54 (m, 2H, CH_2), 1.89-1.97 (m, 2H, CH_2), 5.78-5.83 (m, 1H, CHBr), 7.11-7.13 (m, 2H, ArH), 7.43 (s, 1H, CH), 7.56-7.59 (m, 2H, ArH); ^{13}C NMR (75.6 MHz, $CDCl_3$): δ 13.6 (CH_3), 18.4 (CH_2), 34.2 (CH_2), 77.4 (CH), 80.9 (C), 122.9 (ArC), 130.9 (2 × ArH), 132.1 (2 × ArH), 133.6 (CH), 134.5 (C), 139.2 (C), 168.6 (C=O); IR (neat): ν_{max} 3121, 2962, 1695, 1625, 1583, 1485, 1464, 1359, 1296, 1270, 1192, 1169, 1097, 1068, 1011, 953, 882, 860, 841, 823, 772, 754, 716, 675, 655 cm^{-1}; UV (MeOH): λ_{max} 325 nm (ε 85764 $M^{-1}cm^{-1}$); HRMS (ESI) *m/z* Calcd. for $C_{15}H_{13}Br_3N_2O_4Na$ $(M + Na)^+$ 544.8323. Found 544.8310.

3-Butyl-5-(dibromomethylene)-1-(4-fluoro-3-nitrophenyl)-1H-pyrrol-2(5H)-one (212f)

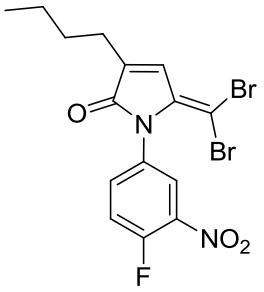

A mixture of 3-butyl-5-(dibromomethylene)furan-2(5*H*)-one **153a** (1 g, 3.22 mmol) and 3-nitro-4-fluoro-aniline (2.01 g, 12.9 mmol) was heated at 50 °C for 10h. The residue was dissolved in DCM (50 mL) and successively washed with water (20 mL), HCl (2M, 20 mL) and saturated NaCl solution (20 mL). The organic phase was separated, dried (Na_2SO_4) and the solvent evaporated in *vacuo*. The residual solid was purified by flash chromatography (dichloromethane). A mixture of the residual solid and *p*-TsOH (0.02 g, 0.11 mmol) in toluene (10 mL) was refluxed for 1 h. The solvent was evaporated in *vacuo* and the residue purified by silica gel chromatography (dichloromethane) to afford the title compound **212f** as a yellow solid (0.86 g, 59%). M.p. 100-102 °C; ^{1}H NMR (300 MHz, $CDCl_3$): δ 0.94 (t, J = 7.2, 3H, CH_3), 1.34-1.47 (m, 2H, CH_2), 1.55 (m, 2H, CH_2), 2.34 (m, 2H, CH_2), 7.22 (s, CH), 7.36 (t, J = 9.0, 1H, ArH), 7.49-7.54 (m, 1H, ArH), 7.95 (dd, J = 2.4 and 6.5, ArH); ^{13}C NMR (75.6 MHz, $CDCl_3$): δ 13.7 (CH_3), 22.3 (CH_2), 25.2 (CH_2), 29.4 (CH2), 76.2 (C), 118.6 (ArH), 126.7 (ArH), 132.9 (CH), 136.2 (ArH), 138.8 (C), 139.5 (C), 153.1 (C), 156.6 (C), 171.6 (C=O); IR (neat): ν_{max} 3094, 2954, 2930, 2870, 1705, 1614, 1591, 1537, 1494, 1465, 1375, 1346, 1262, 1240, 1191, 1133, 1115, 1094, 1043, 939, 853, 838, 815, 792, 744, 700, 658 cm^{-1}; UV (MeOH): λ_{max} 246 nm (ε 63549 M^{-1}cm^{-1}); 309 nm (ε 79706 M^{-1}cm^{-1});

Sodium 1-(1*H*-indol-3-yl)-diazen-1-ium-1,2-diolate (237)

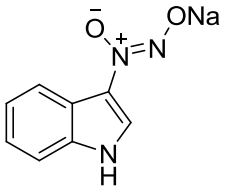

A solution of indole **221** (4.00 g, 34.14 mmol) in anhydrous ether and methanol (1:1) was placed in a Parr bottle. The solution was treated with sodium methoxide (NaOMe) (3.68 g, 68.28 mmol) and the Parr apparatus was clamped. The apparatus was purged with nitrogen and evacuated (3x) followed by charging with 5 atm. nitric oxide (NO) at 25 °C for 72h. The excess NO was vented by purging with nitrogen followed by addition of anhydrous ether. The resulting precipitate was collected by filtration and washed with copious amounts of anhydrous ether. The product was dried under vacuum to afford the desired title compound **237** as a yellow solid (3.91 g, 57%). M.p. 220 °C (dec); ^{1}H NMR (300 MHz, DMSO-d_6): δ 7.05 (t, J = , 1H, H5), 7.14 (t, J = , 1H, H6), 7.38 (d, J = 7.3, 1H, H7), 7.56 (s, 1H, H2), 8.00 (d, J = 7.3, 1H, H4), 11.28 (bs, 1H, NH); ^{13}C NMR (75.6 MHz, DMSO-d_6): δ 112.2 (C7), 116.1 (C4), 119.3 (C3), 119.9 (C5), 121.8 (C6), 122.1 (C2), 125.1 (C3a), 135.8 (C7a); IR (neat): ν_{max} 3403, 3144, 2831, 1594, 1454, 1437, 1354, 1329, 1302, 1252, 1229, 1159, 1112, 1098, 995, 892, 851, 820, 766, 740; UV (10 mM aqueous NaOH): λ_{max} 273 nm (ε 20924 $M^{-1}cm^{-1}$), 299 nm (ε 22367 $M^{-1}cm^{-1}$); HRMS (ESI) *m/z* Calcd. for $C_8H_6N_3Na_2O_2$ $(M + Na)^+$ 222.0255. Found 222.0248.

Sodium 1-(5-methoxy-1*H*-indol-3-yl)-diazen-1-ium-1,2-diolate (243d)

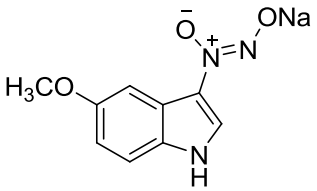

The desired compound was prepared from 5-methoxyindole (3.00 g, 20.38 mmol), NaOMe (2.20 g, 40.76 mmol), and nitric oxide as described for compound **237** to give the title compound **243d** as a yellow solid (3.4 g, 72%). M.p. 180 °C (dec) ; ^{1}H NMR (300 MHz, 0.1M NaOD in D_2O): δ 3.80 (s, 3H, OCH_3), 6.88 (m, 1H, H6), 7.36 (m, 2H, H4 and H7),

7.62 (s, 1H, H2); ^{13}C NMR (75.6 MHz, 0.1M NaOD in D_2O): δ 57.3 (OCH_3), 103.2 (C4), 114.4 (C7), 114.7 (C6), 120.5 (C3), 120.6 (C2), 123.1 (C3a), 131.8 (C7a), 155.4 (C5); IR (neat): ν_{max} 3330, 3119, 2831, 2702, 1579, 1435, 1359, 1300, 1280, 1252, 1222, 1143, 1023, 1008, 919, 899, 879, 854, 799, 767; UV (10 mM aqueous NaOH): λ_{max} 273 nm (ε 27499 $M^{-1}cm^{-1}$), 299 nm (ε 21770 $M^{-1}cm^{-1}$); HRMS (ESI) *m/z* Calcd. for $C_9H_8N_3Na_2O_3$ $(M + Na)^+$ 252.0361. Found 252.0354.

(*Z*)-1-(1*H*-Indol-3-yl)-2-methoxydiazene oxide (249)

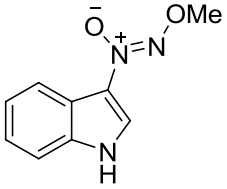

To a solution of diazeniumdiolate **237** (1.00 g, 5.02 mmol) in 30 mL of methanol at 0 °C under argon was added 1 g of anhydrous potassium carbonate, and the resulting slurry was cooled in an ice bath. Dimethyl sulfate (0.52 mL, 5.50 mmol) was added dropwise and the reaction mixture was allowed to warm gradually to room temperature. After an additional two hour, the solution was concentrated on a rotary evaporator, the residue was extracted with dichloromethane, washed with water, dried over sodium sulfate, and filtered through a pad of sodium sulfate. The solvent was evaporated under reduced pressure and the residue chromatographed on silica gel. Elution with ethyl acetate/n-hexane (1:1) gave the title compound **249** as a light brown crystalline solid (0.58 g, 61%). M.p. 216-218 °C (dec); ^{1}H NMR (300 MHz, $CDCl_3$): δ 4.29 (OCH_3), 7.27-7.34 (m, 2H, H5 and H6), 7.41-7.46 (m, 1H, H7), 7.97 (d, J = 3.3 Hz, 1H, H2), 8.06-8.09 (m, 1H, H4), 8.86 (bs, 1H, NH); ^{13}C NMR (75.6 MHz, $CDCl_3$): δ 61.6 (OCH_3), 112.0 (C7), 118.4 (C3), 120.7 (C4), 121.8 (C5), 122.3 (C6), 123.9 (C2), 125.1 (C3a), 135.8 (C7a); IR (neat): ν_{max} 3187, 2946, 2834, 1641, 1586, 1530, 1466, 1440, 1400, 1369, 1330, 1273, 1239, 1211, 1198, 1128, 1061, 1007, 937, 882, 839, 774, 731, 659; UV (MeOH): λ_{max} 253 nm (ε 72648 M^-

$^{1}cm^{-1}$), 318 nm (ε 65001 $M^{-1}cm^{-1}$); HRMS (ESI) *m/z* Calcd. for $C_9H_9N_3O_2Na$ $(M + Na)^+$ 214.0592. Found 214.0584.

(*Z*)-1-(1*H*-Indol-3-yl)-2-(methoxymethoxy)diazene oxide (250)

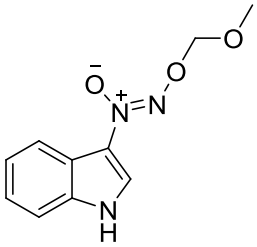

To the solution of indole diazeniumdiolate **237** (0.50 g, 2.51 mmol) in THF (10 mL) at 0 °C under argon was added chloromethyl methyl ether (0.2 mL, 2.51 mmol). The reaction mixture was brought to room temperature and stirred for 16h. The solution was concentrated on a rotary evaporator and the residue was extracted with dichloromethane. The organic layer was washed with water, dried over sodium sulfate, and filtered through a pad of sodium sulfate. The solvent was evaporated under reduced pressure and the residue was purified by silica gel vacuum chromatography. Elution with ethyl acetate/n-hexane (1:1) gave the title compound **250** as a brown crystalline solid (0.31 g, 56%). M.p. 116 °C (dec); ^{1}H NMR (300 MHz, $CDCl_3$): δ 3.57 (s, 3H, OCH_3), 5.49 (s, 2H, OCH_2), 7.28-7.33 (m, 2H, H5 and H6), 7.43-7.46 (m, 1H, H7), 8.00 (d, J = 3.0 Hz, 1H, H2), 8.09-8.11 (m, 1H, H4), 9.13 (bs, 1H, NH); ^{13}C NMR (75.6 MHz, $CDCl_3$): δ 57.3 (OCH_3), 98.4 (OCH_2), 112.0 (C7), 118.5 (C3), 120.7 (C4), 122.2 (C5), 122.4 (C6), 123.9 (C3a), 124.0 (C2), 135.8 (C7a); IR (neat): ν_{max} 3218, 2992, 2943, 1587, 1526, 1445, 1404, 1367, 1330, 1273, 1237, 1208, 1158, 1107, 1054, 998, 947, 920, 837, 729, 670; UV (MeOH): λ_{max} 251 nm (ε 72619 $M^{-1}cm^{-1}$), 318 nm (ε 61447 $M^{-1}cm^{-1}$); HRMS (ESI) *m/z* Calcd. for $C_{10}H_{11}N_3O_3Na$ $(M + Na)^+$ 244.0698. Found 244.0690.

(*Z*)-2-(2-Ethoxy-2-oxoethoxy)-1-(1H-indol-3-yl)diazene oxide (251)

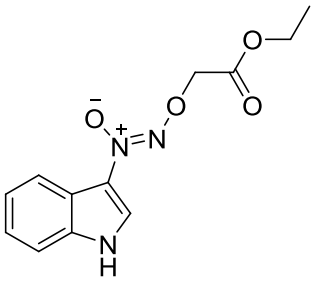

The indole diazeniumdiolate derivative **237** (0.50 g, 2.51 mmol), was alkylated using ethyl-2-bromoacetate (0.28 mL, 2.51 mmol) by the method described for compound **250** to give the title compound **251** as a brown solid (0.25 g, 39%). M.p. 134-136 °C (dec); ^{1}H NMR (300 MHz, $CDCl_3$): δ 1.30 (t, J = 7.1, 3H, CH_3), 4.29 (q, J = 7.1, 2H, OCH_3), 4.98 (s, 2H, $OCH_2C{=}O$), 7.24-7.29 (m, 2H, H5 and H6), 7.41-7.44 (m, 1H, H7), 7.94-7.96 (m, 2H, H2 and H4), 9.02 (bs, 1H, NH); ^{13}C NMR (75.6 MHz, $CDCl_3$): δ 14.1 (CH_3), 61.7 (OCH_2), 69.9 ($OCH_2C{=}O$), 112.1 (C7), 118.4 (C3), 120.5 (C4), 122.4 (C5 and C6), 123.3 (C3a), 123.9 (C2), 135.0 (C7a), 168.1 (C=O); IR (neat): ν_{max} 3247, 3167, 2999, 2935, 1758, 1587, 1537, 1446, 1436, 1421, 1382, 1325, 1246, 1226, 1214, 1153, 1086, 1054, 1023, 1015, 949, 848, 773, 750, 723, 669; UV (MeOH): λ_{max} 251 nm (ε 84612 $M^{-1}cm^{-1}$), 320 nm (ε 71450 $M^{-1}cm^{-1}$); HRMS (ESI) *m/z* Calcd. for $C_{12}H_{13}N_3O_4Na$ $(M + Na)^+$ 286.0804. Found 286.0795.

(*Z*)-2-(Benzyloxy)-1-(1H-indol-3-yl)diazene oxide (252)

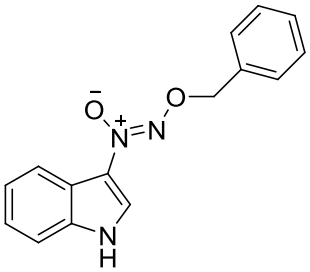

The indole diazeniumdiolate derivative **237** (0.5 g, 2.51 mmol), was alkylated using benzyl bromide (0.33 mL, 2.76 mmol) by the method described for compound **250** to give the title compound **252** as a brown solid (0.24 g, 36%). M.p. 174-176 °C (dec); ^{1}H NMR (300 MHz, $CDCl_3$): δ 4.29 (OCH_3), 7.27-7.34 (m, 2H, H5 and H6), 7.36-7.41 (m, 4H, H7, 3 × ArH), 7.49-7.53 (m, 2H, 2 × ArH), 7.90-7.94 (m, 2H, H2 and H4), 8.65 (bs, 1H, NH); ^{13}C NMR (75.6 MHz, $CDCl_3$): δ 111.8 (C7), 118.4 (C3), 120.7 (C4), 121.7 (C5), 122.3 (C6), 123.9 (C2), 125.1 (C3a), 128.6 (ArH), 128.7

(ArH), 128.8 (ArH), 135.8 (C7a); IR (neat): ν_{max} 3298, 3132, 2956, 1732, 1675, 1587, 1529, 1451, 1416, 1372, 1343, 1328, 1245, 1205, 1194, 1094, 1065, 1032, 981, 835, 771, 750, 696; UV (MeOH): λ_{max} 254 nm (ε 68676 $M^{-1}cm^{-1}$), 319 nm (ε 61251 $M^{-1}cm^{-1}$); HRMS (ESI) *m/z* Calcd. for $C_{15}H_{14}N_3O_2$ $(M + H)^+$ 268.1086. Found 268.1075.

2-Hydroxyethyl nitrate (266)

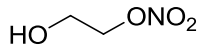

A mixture of 2-bromoethanol (1.13 mL (2.0 g), 16.00 mmol) and silver nitrate (2.9 g, 17.60 mmol) in acetonitrile (20 mL) was stirred at 70 °C for 18h. The resulting product was concentrated under *vacuo* and DCM (50 mL) was added to the residue. The organic layer was filtered through a pad of Celite and silica to remove the silver salt formed. The filtrate was evaporated to dryness to give the title compound **266** as a yellow oil (1. 59 g, 93%). ^{1}H NMR (300 MHz, $CDCl_3$): δ 3.87-3.91 (m, 2H, CH_2OH), 4.55-4.58 (m, 2H, CH_2ONO_2), 7.77 (bs, 1H, OH); ^{13}C NMR (75.6 MHz, $CDCl_3$): δ 58.8 (CH_2COO), 74.2 (CH_2ONO_2).

2-Aminoethyl nitrate (47)

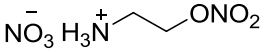

To a solution of nitric acid (70%) (7.2 mL, 163 mmol) and concentrated sulfuric acid (8.9 mL, 163 mmol) at 0 °C was added a small amount of urea (few grains) and ethanolamine (4.9 mL, 81.9 mmol) dropwise. The reaction was stirred at 0 °C for 1h followed by room temperature for 2h. The crude reaction mixture was evaporated to dryness under high vacuum to remove the unreacted acid to give a sticky white compound. Acetone was added to the crude product to get the title compound **47** as a white solid (7.0 g, 51%). M.p. 258-260 °C; ^{1}H NMR (300 MHz, DMSO-d_6): δ 3.01 (q, *J*

= 4.1, 2H, CH_2NH_3), 3.94 (t, J = 3.8, 2H, CH_2ONO_2), 7.77 (bs, 3H, NH_3); ^{13}C NMR (75.6 MHz, DMSO-d_6): δ 39.5 (CH_2NH_3), 66.9 (CH_2ONO_2).

2,2',2''-(1,3,5-Triazine-2,4,6-triyl)tris(oxy)tris(ethane-2,1-diyl) trinitrate (267)

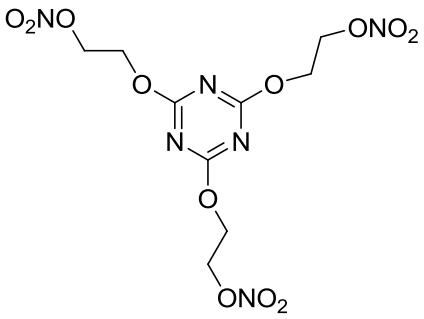

The nitrate derivative **266** (0.69 g, 6.50 mmol) was added to a solution of cynauric chloride **258** (0.4 g, 2.76 mmol) and potassium carbonate (0.92 g, 6.72 mmol) in THF and the mixture was stirred at reflux for 24h. Ice water was added to the reaction mixture and the resulting precipitate was filtered under vacuum. The precipitate was further washed with water and dried to yield the title compound **267** as an off white solid (0.59 g, 69%). M.p. 128-130 °C; ^1H NMR (300 MHz, $CDCl_3$): δ 4.67-4.70 (m, 2H, CH_2O), 4.89-4.91 (m, 2H, CH_2ONO_2); ^{13}C NMR (75.6 MHz, $CDCl_3$): δ 64.4 (CH_2), 71.7 (CH_2), 172.7 (ArC); IR (neat): ν_{max} 2904, 1752, 1629, 1575, 1458, 1416, 1382, 1340, 1282, 1243, 1156, 1108, 1017, 902, 844, 860, 808, 753, 709, 670; HRMS (ESI) *m/z* Calcd. for $C_9H_{13}N_6O_{12}$ $(M + H)^+$ 397.0591. Found 397.0575.

2,2',2''-(1,3,5-Triazine-2,4,6-triyl)tris(azanediyl)tris(ethane-2,1-diyl) trinitrate (268)

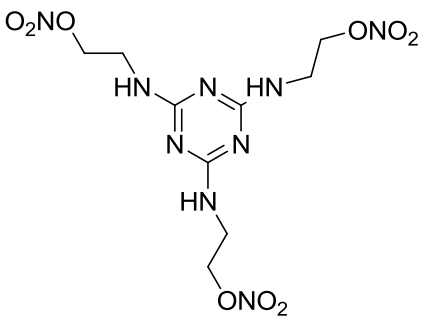

2-aminoethyl nitrate **47** (1.7 g, 16.26 mmol) was added to a solution of cynauric chloride **258** (1 g, 5.42 mmol) and potassium carbonate (4.49 g, 32.5 mmol) in acetone and the reaction mixture was stirred at reflux for 40h. The precipitate was filtered under vacuum and recrystallised from water/MeOH to yield the title compound **268** as a white solid (1.34 g, 63%). M.p. 204-206 °C; ^{1}H NMR (300 MHz, DMSO-d_6): δ 3.38-3.43 (m, 2H, CH_2NH_3), 3.78-3.87 (m, 2H, CH_2ONO_2), 7.79 (bs, 1H, NH); ^{13}C NMR (75.6 MHz, DMSO-d_6): δ 40.5 (CH_2NH), 64.2 (CH_2ONO_2), 165.7 (ArC); IR (neat): ν_{max} 3254, 2959, 1631, 1575, 1417, 1382, 1341, 1274, 1244, 1157, 1109, 1070, 1017, 903, 861, 847, 808, 754, 672; HRMS (ESI) *m/z* Calcd. for $C_9H_{15}N_9O_9K$ $(M + K)^+$ 432.0630. Found 432.0635.

(1Z,1'Z)-1,1'-(4,4'-(6-Chloro-1,3,5-triazine-2,4-diyl)bis(piperazine-4,1-diyl))bis(2-(methoxymethoxy)diazene oxide) (271a)

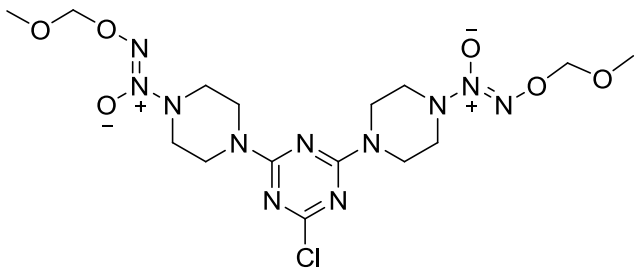

Piperazine diazeniumdiolate derivative **270** (0.10 g, 0.54 mmol) was added to a mixture of cynauric chloride **258** (0.05 g, 0.27 mmol) and potassium carbonate (0.07 g, 0.56 mmol) in acetone and stirred at r.t. for 4h. The crude reaction mixture was extracted with ethyl acetate and purified by preparative TLC to yield the title compound **271a** as an off white solid (0.05 g, 41%). M.p. 110-112 °C; ^{1}H NMR (300 MHz, $CDCl_3$) δ 3.49 (s, 3H), 3.55 (t, J = 5.3, 4H, 2 × CH_2), 4.07 (t, J =

5.1, 4H, 2 × CH_2), 5.23 (s, 2H); ^{13}C NMR (75.6 MHz, $CDCl_3$) δ 42.5 (2 × CH_2), 50.6 (2 × CH_2), 57.0 (CH_3), 98.1 (OCH_2), 164.2 (ArC), 170.7 (ArC); IR (neat): ν_{max} 2924, 1740, 1578, 1557, 1500, 1472, 1450, 1423, 1345, 1325, 1273, 1230, 1164, 1146, 1104, 1066, 1008, 991, 927, 843, 788, 734, 697, 675; UV (MeOH): λ_{max} 237 nm (ε 170795 $M^{-1}cm^{-1}$); HRMS (ESI) *m/z* Calcd. for $C_{15}H_{26}ClN_{11}O_6Na$ $(M + Na)^+$ 514.1654. Found 514.1635.

(1Z,1'Z,1''Z)-1,1',1''-(4,4',4''-(1,3,5-Triazine-2,4,6-triyl)tris(piperazine-4,1-diyl))tris(2-(methoxymethoxy)diazene oxide) (271b)

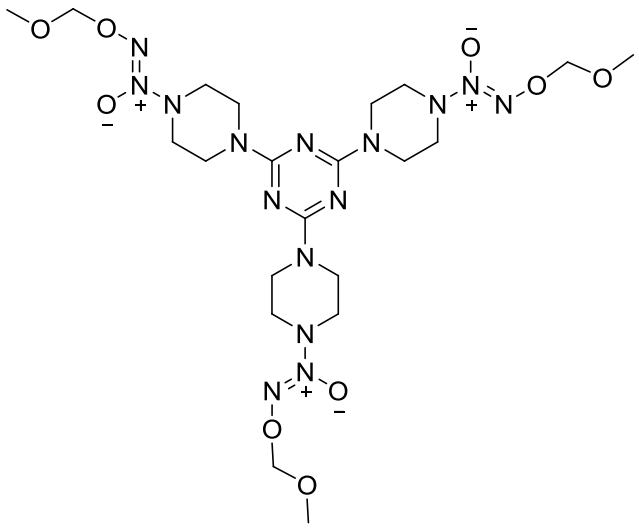

Piperazine diazeniumdiolate derivative **270** (0.31 g, 1.62 mmol) was added to a mixture of cynauric chloride **258** (0.1 g, 0.54 mmol) and potassium carbonate (0.23 g, 1.68 mmol) in acetone (15 mL) and stirred for 40h at reflux. The crude reaction mixture was extracted with ethyl acetate and purified by preparative TLC to yield the title compound **271b** as an off white solid (0.16 g, 46%). M.p. 98 °C; ^{1}H NMR (300 MHz, $CDCl_3$) δ 3.48-3.51 (m, 4H, 2 × CH_2), 3.49 (s, 3H), 3.98 (bs, 4H, 2 × CH_2), 5.22 (s, 2H); ^{13}C NMR (75.6 MHz, $CDCl_3$) δ 42.0 (2 × CH_2), 50.7 (CH_2), 51.0 (CH_2), 57.1 (OCH_3), 98.0 (OCH_2), 164.4 (ArC), 170.0 (ArC); IR (neat): ν_{max} 2920, 1697, 1563, 1489, 1441, 1386, 1367, 1308, 1260, 1216, 1160, 1098, 1015, 1000, 991, 927, 838, 795, 731, 698; UV (MeOH): λ_{max} 227 nm (ε 387372 $M^{-1}cm^{-1}$); HRMS (ESI) *m/z* Calcd. for $C_{21}H_{39}N_{15}O_9Na$ $(M + Na)^+$ 668.2953. Found 668.2922.

Triethyl 4,4',4''-(1,3,5-triazine-2,4,6-triyl)tripiperazine-1-carboxylate (272)

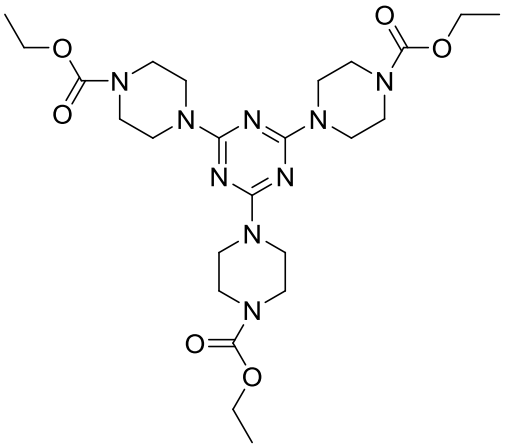

Piperazine derivative **113** (2.5 g, 16.2 mmol) was added to a solution of cynauric chloride **258** (1 g, 5.42 mmol) and potassium carbonate (2.2 g, 16.26 mmol) in acetone (50 mL) and the mixture was stirred for 40 h at reflux. Ice water was added to the reaction mixture and the precipitate was filtered under vacuum. The precipitate was further washed with water and dried to yield the title compound **272** as a white solid (2.5 g, 86%). M.p. 194 °C; ^{1}H NMR (300 MHz, $CDCl_3$) δ 1.27 (t, J = 7.1, 3H), 3.46-3.49 (m, 4H), 3.72-3.75 (m, 4H), 4.15 (q, J = 7.1, 2 H); ^{13}C NMR (75.6 MHz, $CDCl_3$) δ 14.6 (CH_3), 42.9 (CH_2), 43.6 (CH_2), 61.5 (OCH_2), 155.6 (C=O), 165.3 (ArC); IR (neat): ν_{max} 2986, 2912, 2852, 1694, 1540, 1484, 1424, 1381, 1355, 1272, 1249, 1205, 1177, 1109, 1069, 991, 877, 826, 804, 765, 733, 659; UV (MeOH): λ_{max} 230 nm (ε 16079 $M^{-1}cm^{-1}$); HRMS (ESI) *m/z* Calcd. for $C_{24}H_{40}N_9O_9$ $(M + H)^+$ 550.3102. Found 550.3085.

2,4,6-Tri(piperazin-1-yl)-1,3,5-triazine (273)

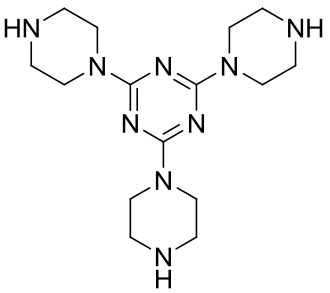

A solution of triazine derivative **272** (0.70 g) in alcoholic sodium hydroxide (10%, 50 mL) and 1 mL of water was heated at reflux. After 2 h, no starting material remained in the mixture, as assessed from qualitative thin-layer chromatography. The solution was allowed to cool to room temperature and evaporated to a viscous oily residue, which was extracted with

dichloromethane. The dichloromethane solution was dried over sodium sulfate, filtered, and evaporated to give the title compound **273** as an off white solid (0.35 g, 83%). M.p. 220-222 °C; ^{1}H NMR (300 MHz, $CDCl_3$) δ 2.85 (t, J = 5.1, 4H), 3.72 (t, J = 5.1, 4H); ^{13}C NMR (75.6 MHz, $CDCl_3$) δ 44.3 (2 × CH_2), 46.0 (2 × CH_2), 165.3 (ArC); IR (neat): ν_{max} 3268, 2913, 2849, 1520, 1480, 1424, 1364, 1291, 1238, 1191, 1172, 1125, 1053, 1006, 900, 872, 803, 735; HRMS (ESI) *m/z* Calcd. for $C_{15}H_{28}N_9$ $(M + H)^+$ 334.2468. Found 334.2455.

Trisodium-1-(4,4',4''-(1,3,5-triazine-2,4,6-triyl)tripiperazine-1-yl)trisdiazen-1-ium-1,2-diolate (274)

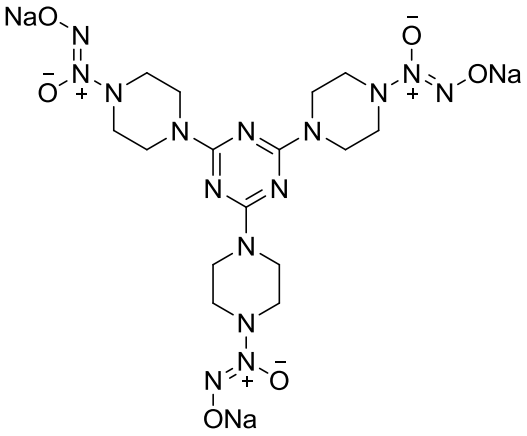

A solution of triazine derivative **273** (0.85 g, 2.55 mmol) in 60 mL of anhydrous ether and methanol (3:7, v/v) was placed in a Parr bottle. The solution was treated with sodium methoxide (NaOMe) (0.41 g, 7.64 mmol) and the Parr apparatus was clamped. The apparatus was purged with nitrogen and evacuated (3 ×) followed by charging with 5 atm. nitric oxide (NO) at 25 °C for 48h. The excess NO was then vented by purging with nitrogen followed by addition of anhydrous ether (50 mL). The resulting precipitate was collected by filtration and washed with cold methanol as well as with copious amounts of anhydrous ether. The product was dried under vacuum to afford the desired title compound **274** as an off white solid (0.71 g, 51%). M.p. 158-160 °C; ^{1}H NMR (300 MHz, $CDCl_3$) δ 2.85 (t, J = 5.1, 4H), 3.72 (t, J = 5.1, 4H); ^{13}C NMR (75.6 MHz, $CDCl_3$) δ 44.3 (2 × CH_2), 49.4 (2 ×

CH_2), 165.3 (ArC); IR (neat): ν_{max} 3351, 2790, 2703, 1583, 1411, 1363, 1300, 1050, 998, 927, 880, 827, 804, 767; UV (10 mM aqueous NaOH): λ_{max} ; HRMS (ESI) *m/z* Calcd. for $C_{15}H_{24}N_{15}O_6Na_3$ $(M + H)^+$ 579.1727. Found 579.1755.

References

1. Falagas, M. E.; Karveli, E. A. *Clin. Infect. Dis.* 2006, *43*, 630-633.
2. Jones, K. E.; Patel, N. G.; Levy, M. A.; Storeygard, A.; Balk, D.; Gittleman, J. L.; Daszak, P. *Nature (London)* 2008, *451*, 990-994.
3. WHO. WHO press: France, 2011.
4. Gollogly, L.; World Health Statistics-2009; World Health Organisation, 2009.
5. Andersson, D. I.; Hughes, D. *Nat. Rev. Microbiol.* 2010, *8*, 260-271.
6. Habich, D.; Nussbaum, F.; Brands, M.; Hinzen, B.; Weigand, S. *Angew. Chem. Int. Ed.* 2006, *45*, 5072 - 5129.
7. Demain, A. L. *Med. Res. Rev.* 2009, *29*, 821-842.
8. Neu, H. C. *Science* 1992, *257*, 1064-1072.
9. McManus, M. *Am. J. Health Syst. Pharm.* 1997, *54*, 1420-1433.
10. Edwards, J. R.; Park, J. T. *J. Bacteriol.* 1969, *99*, 459-462.
11. Georgopapadakou, N. H.; Smith, S. A.; Sykes, R. B. *Antimicrob. Agents Chemother.* 1982, *21*, 950-956.
12. Park, J. T.; Strominger, J. L. *Science* 1957, *125*, 99-101.
13. Caron, W. P.; Mousa, S. A. *Infect. Drug Resist.* 2010, *3*, 25-33.
14. Gold, H. S.; Moellering, R. C. *N. Engl. J. Med.* 1996, *335*, 1445-1453.
15. Clatworthy, A. E.; Pierson, E.; Hung, D. T. *Nat. Chem. Biol.* 2007, *3*, 541-548.
16. Costerton, W.; Veeh, R.; Shirtliff, M.; Pasmore, M.; Post, C.; Ehrlich, G. *J. Clin. Invest.* 2003, *112*, 1466-1477.
17. Lewis, K. *Antimicrob. Agents Chemother.* 2001, *45*, 999-1007.

18. Davies, D. G.; Parsek, M. R.; Pearson, J. P.; Iglewski, B. H.; Costerton, J. W.; Greenberg, E. P. *Science* 1998, *280*, 295-299.

19. Costerton, J. W.; Lewandowski, Z.; Caldwell, D. E.; Korber, D. R.; Lappin-Scott, H. M. *Annu. Rev. Microbiol.* 1995, *49*, 711-745.

20. Pasmore, M.; Costerton, J. W. *J. Ind. Microbiol. Biotechnol.* 2003, *30*, 407-413.

21. Stoodley, P.; Sauer, K.; Davies, D. G.; Costerton, J. W. *Annu. Rev. Microbiol.* 2002, *56*, 187-209.

22. Brooun, A.; Liu, S.; Lewis, K. *Antimicrob. Agents Chemother.* 2000, *44*, 640-646.

23. Cerca, N.; Jefferson, K. K.; Oliveira, R.; Pier, G. B.; Azeredo, J. *Infect. Immun.* 2006, *74*, 4849-4855.

24. Reid, G. *Int. J. Antimicrob. Agents* 1999, *11*, 223-226.

25. Costerton, J. W.; Stewart, P. S.; Greenberg, E. P. *Science* 1999, *284*, 1317-1322.

26. Davies, D. *Nat. Rev. Drug. Discov.* 2003, *2*, 114-122.

27. Evans, D. J.; Brown, M. R.; Allison, D. G.; Gilbert, P. *J. Antimicrob. Chemother.* 1990, *25*, 585-591.

28. Donlan, R. M.; Costerton, J. W. *Clin. Microbiol. Rev.* 2002, *15*, 167-193.

29. Boles, B. R.; Thoendel, M.; Singh, P. K. *Proc. Natl. Acad. Sci. U.S.A* 2004, *101*, 16630–16635.

30. Hall-Stoodley, L.; Hu, F. Z.; Gieseke, A.; Nistico, L.; Nguyen, D.; Hayes, J.; Forbes, M.; Greenberg, D. P.; Dice, B.; Burrows, A.; Wackym, P. A.; Stoodley, P.; Post, J. C.; Ehrlich, G. D.; Kerschner, J. E. *J. Am. Med. Assoc.* 2006, *296*, 202-211.

31. Post, J. C. *Laryngoscope* 2001, *111*, 2083-2094.

32. Hall-Stoodley, L.; Costerton, J. W.; Stoodley, P. *Nat. Rev. Microbiol.* 2004, *2*, 95-108.

33. Singh, P. K.; Schaefer, A. L.; Parsek, M. R.; Moninger, T. O.; Welsh, M. J.; Greenberg, E. P. *Nature* 2000, *407*, 762-764.

34. Scheie, A. A.; Petersen, F. C. *Crit. Rev. Oral Biol. Med.* 2004, *15*, 4-12.

35. Khardori, N.; Yassien, M. *J. Ind. Microbiol. Biotechnol.* 1995, *15*, 141-147.

36. Coetser, S. E.; Cloete, T. E. *Crit. Rev. Microbiol.* 2005, *31*, 213-232.

37. Neria-Gonzalez, I.; Wang, E. T.; Ramirez, F.; Romero, J. M.; Hernandez-Rodriguez, C. *Anaerobe* 2006, *12*, 122-133.

38. Piriou, P.; Dukan, S.; Levi, Y.; Jarrige, P. A. *Water Sci. Technol.* 1997, *35*, 283-287.

39. Skjevrak, I.; Lund, V.; Ormerod, K.; Due, A.; Herikstad, H. *Water Sci. Technol.* 2004, *49*, 211-217.

40. Karatan, E.; Watnick, P. *Microbiol. Mol. Biol. Rev.* 2009, *73*, 310-347.

41. Miller, M. B.; Bassler, B. L. *Annu. Rev. Microbiol.* 2001, *55*, 165-199.

42. Parsek, M. R.; Greenberg, E. P. *Proc. Natl. Acad. Sci. U.S.A* 2000, *97*, 8789-8793.

43. Zumft, W. G. *Arch. Microbiol.* 1993, *160*, 253-264.

44. Barraud, N., Ph.D. Thesis;The University of New South Wales, 2007.

45. Webb, J. S.; Thompson, L. S.; James, S.; Charlton, T.; Tolker-Nielsen, T.; Koch, B.; Givskov, M.; Kjelleberg, S. *J. Bacteriol.* 2003, *185*, 4585-4592.

46. Weiss, B. *J. Bacteriol.* 2006, *188*, 829-833.

47. Harshey, R. M.; Matsuyama, T. *Proc. Natl. Acad. Sci. U.S.A.* 1994, *91*, 8631-8635.

48. Winans, S. C.; Bassler, B. L. *J. Bacteriol.* 2002, *184*, 873-883.

49. Lyon, G. J.; Muir, T. W. *Chem. Biol.* 2003, *10*, 1007-1021.

50. Nealson, K. H.; Platt, T.; Hastings, J. W. *J. Bacteriol.* 1970, *104*, 313-322.

51. Fuqua, W. C.; Winans, S. C.; Greenberg, E. P. *J. Bacteriol.* 1994, *176*, 269-275.

52. Drenkard, E.; Ausubel, F. M. *Nature* 2002, *416*, 740 - 743.

53. Taga, M. E.; Bassler, B. L. *Proc. Natl. Acad. Sci U.S.A.* 2003, *100*, 14549-14554.

54. Henke, J. M.; Bassler, B. L. *Trends Cell Biol.* 2004, *14*, 648-656.

55. Camilli, A.; Bassler, B. L. *Science* 2006, *311*, 1113-1116.

56. Bassler, B. L. *Curr. Opin. Microbiol.* 1999, *2*, 582-587.

57. Waters, C. M.; Bassler, B. L. *Annu. Rev. Cell Dev. Biol.* 2005, *21*, 319-46.

58. Byrd, C. M.; Bentley, W. E. *Cell Res.* 2009, *19*, 1229-1230.

59. Xavier, K. B.; Bassler, B. L. *Curr. Opin. Microbiol.* 2003, *6*, 191-197.

60. Fuqua, C.; Parsek, M. R.; Greenberg, E. P. *Annu. Rev. Genet.* 2001, *35*, 439-468.

61. Fuqua, C.; Winans, S. C.; Greenberg, E. P. *Annu. Rev. Microbiol.* 1996, *50*, 727-51.

62. Kievit, T. R. d.; Iglewski, B. H. *Infect. Immun.* 2000, *68*, 4839-4849.

63. Schaefer, A. L.; Greenberg, E. P.; Oliver, C. M.; Oda, Y.; Huang, J. J.; Bittan-Banin, G.; Peres, C. M.; Schmidt, S.; Juhaszova, K.; Sufrin, J. R.; Harwood, C. S. *Nature* 2008, *454*.

64. Dobretsov, S.; Teplitski, M.; Paul, V. *Biofouling* 2009, *25*, 413-427.

65. Raffa, R. B.; Iannuzzo, J. R.; Levine, D. R.; Saeid, K. K.; Schwartz, R. C.; Sucic, N. T.; Terleckyj, O. D.; Young, J. M. *J. Pharmacol. Exp. Ther.* 2005, *312*, 417-423.

66. Passador, L.; Cook, J. M.; Gambello, M. J.; Rust, L.; Iglewski, B. H. *Science* 1993, *260*, 1127-1130.

67. Hentzer, M.; Riedel, K.; Rasmussen, T. B.; Heydorn, A.; Andersen, J. B.; Parsek, M. R.; Rice, S. A.; Eberl, L.; Molin, S.; Høiby, N.; Kjelleberg, S.; Givskov, M. *Microbiology* 2002, *148*.

68. Smith, R. S.; Iglewski, B. H. *Curr. Opin. Microbiol.* 2003, *6*, 56-60.

69. Atkinson, S.; Throup, J. P.; Stewart, G. S. A. B.; Williams, P. *Mol. Microbiol.* 1999, *33*, 1267-1277.

70. Rasko, D. A.; Sperandio, V. *Nat. Rev. Drug Discovery* 2010, *9*, 117-128.

71. Kaufmann, G. F.; Park, J.; Janda, K. D. *Expert Opin. Biol. Ther.* 2008, *8*, 719-724.

72. Lowery, C. A.; Salzameda, N. T.; Sawada, D.; Kaufmann, G. F.; Janda, K. D. *J. Med. Chem.* 2010, *53*, 7467-7489.

73. Galloway, W. R. J. D.; Hodgkinson, J. T.; Bowden, S. D.; Welch, M.; Spring, D. R. *Chem. Rev.* 2011, *111*, 28-67.

74. Ni, N.; Li, M.; Wang, J.; Wang, B. *Med. Res. Rev.* 2009, *29*, 65-124.

75. Eberhard, A.; Widrig, C. A.; McBath, P.; Schineller, J. B. *Arch. Microbiol.* 1986, *146*, 35-40.

76. Schaefer, A. L.; Hanzelka, B. L.; Eberhard, A.; Greenberg, E. P. *J. Bacteriol.* 1996, *178*, 2897-2901.

77. Reverchon, S.; Chantegrel, B.; Deshayes, C.; Doutheau, A.; Cotte-Pattat, N. *Bioorg. Med. Chem. Lett.* 2002, *12*, 1153-1157.

78. Passador, L.; Tucker, K. D.; Guertin, K. R.; Journet, M. P.; Kende, A. S.; Iglewski, B. H. *J. Bacteriol.* 1996, *178*, 5995-6000.

79. Smith, K. M.; Bu, Y.; Suga, H. *Chem. Biol.* 2003, *10*, 81-89.

80. Suga, H.; Smith, K. M. *Curr. Opin. Chem. Biol.* 2003, *7*, 586-591.

81. Castang, S.; Chantegrel, B.; Deshayes, C.; Dolmazon, R.; Gouet, P.; Haser, R.; Reverchon, S.; Nasser, W.; Hugouvieux-Cotte-Pattat, N.; Doutheau, A. *Bioorg. Med. Chem. Lett.* 2004, *14*, 5145-5149.

82. Geske, G. D.; O'Neill, J. C.; Blackwell, H. E. *ACS Chem. Biol.* 2007, *2*, 315-320.

83. Newman, D. J.; Cragg, G. M. *J. Nat. Prod.* 2004, *67*, 1216-1238.

84. Newman, D. J.; Cragg, G. M. *J. Nat. Prod.* 2012, *75*, 311−335.

85. McConnell, O. J.; Fenical, W. *Phytochemistry* 1980, *19*, 233-247.

86. Haefner, B. *Drug Discov. Today* 2003, *8*, 536-544.

87. Pawlik, J. R. *Chem. Rev.* 1993, *93*, 1911-1922.

88. Gram, L.; Nys, R. d.; Maximilien, R.; Givskov, M.; P, S.; S., K. *Appl. Environ. Microbiol.* 1996, *62*, 4284-4287.

89. de Nys, R.; Givskov, M.; Kumar, N.; Kjelleberg, S.; Steinberg, P. D., Eds. *In Antifouling compounds*; Springer-Verlag: Berlin, Heidelberg, 2006; Vol. 42.

90. de Nys, R.; Wright, A. D.; Konig, G. M.; Sticher, O. *Tetrahedron* 1993, *49*, 11213-11220.

91. Manefield, M.; Nys, R. d.; Kumar, N.; Read, R.; Givskov, M.; Steinberg, P.; Kjelleberg, S. *Microbiology* 1999, *145*, 283-291.

92. Rasmussen, T. B.; Manefield, M.; Andersen, J. B.; Eberl, L.; Anthoni, U.; Christophersen, C.; Steinberg, P.; Kjelleberg, S.; Givskov, M. *Microbiology* 2000, *146*, 3237-3244.

93. Kazlauskas, R.; Murphy, P. T.; R.J.Quinn; Wells, R. J. *Tetrahedron Lett.* 1977, *1*, 37-40.

94. Pettus, J. A.; Wing, R. M.; Sims, J. J. *Tetrahedron Lett.* 1977, *1*, 41-44.

95. de Nys, R.; Coll, J. C.; Bowden, B. F. *Aust. J. Chem.* 1992, *45*, 1625-1632.

96. Rice, S. A.; McDougald, D.; Kumar, N.; Kjelleberg, S. *Curr. Opin. Invest. Drugs* 2005, *6*, 178-184.

97. Manefield, M.; Welch, M.; Givskov, M.; Salmond, G. P. C.; Kjelleberg, S. a. *FEMS Microbiology Lett.* 2001, *205*, 131-138.

98. Manefield, M.; Rasmussen, T. B.; Henzter, M.; Andersen, J. B.; Steinberg, P.; Kjelleberg, S.; Givskov, M. *Microbiology* 2002, *148*, 1119-1127.

99. Defoirdt, T.; Miyamoto, C. M.; Wood, T. K.; Meighen, E. A.; Sorgeloos, P.; Verstraete, W.; Bossier, P. *EnViron. Microbiol.* 2007, *9*, 2486.

100. Ren, D.; Sims, J. J.; Wood, T. K. *Environ. Microbiol.* 2001, *3*, 731-736.

101. de March, P.; Font, J.; Gracia, A.; Qingying, Z. *J. Org. Chem.* 1995, *60*, 1814-1822.

102. Iskander, G.; Zhang, R.; Chan, D. S.-H.; Black, D. S.; Alamgir, M.; Kumar, N. *Tetrahedron Lett.* 2009, *50*, 4613-4615.

103. Zhang, R.; Chan, D.; Jessica, S.; Iskander, G.; Black, D. S.; Kumar, N. *ARKIVOC* 2009, *V*, 102-115.

104. Janssens, J. C. A.; Steenackers, H.; Robijns, S.; Gellens, E.; Levin, J.; Zhao, H.; Hermans, K.; Coster, D. D.; Verhoeven, T. L.; Marchal, K.; Vanderleyden, J.; Vos, D. E. D.; Keersmaecker, S. C. J. D. *Applied and Environmental Microbiology* 2008, *74*, 6639-6648.

105. Hentzer, M.; Wu, H.; Andersen, J. B.; Riedel, K.; B.Rasmussen, T.; Bagge, N.; Kumar, N.; A.Schembri, M.; Song, Z.; Kristoffersen, P.; Manefield, M.;

W.Costerton, J.; Molin, S.; Eberl, L.; Steinberg, P.; Kjelleberg, S.; Hùiby, N.; Givskov, M. *The EMBO Journal* 2003, *22*, 3803-3815.

106. Goh, W. K.; Iskander, G.; Black, D. S.; Kumar, N. *Tetrahedron Lett.* 2007, *48*, 2287-2290.

107. Goh, W. K. Ph.D. Thesis, School of chemistry, University of New South Wales, 2008.

108. Culotta, E.; Koshland, D. E. *Science* 1992, *258*, 1862-1863.

109. Sergio, H.; Sapna, C.; Benjamin, B. *Int. J. Oncol.* 2008, *33*, 909-927.

110. Murad, F. *Angew. Chem. Int. Ed.* 1999, *38*, 1856-1868.

111. Gorren, A. C. F.; Mayer, B. *Biochim. Biophys. Acta* 2007, *1770*, 432-445.

112. Crane, B. R.; Arvai, A. S.; Ghosh, D. K.; Wu, C.; Getzoff, E. D.; Stuehr, D. J.; Tainer, J. A. *Science* 1998, *279*, 2121-2126.

113. Groves, J. T.; Wang, C. C.-Y. *Curr. Opin. Chem. Biol.* 2000, *4*, 687-695.

114. Brown, G. C. *Science* 2003, *299*, 838-839.

115. Alderton, W. K.; Cooper, C. E.; Knowles, R. G. *Biochem. J.* 2001, *357*, 593-615.

116. Pfeiffer, S.; Mayer, B.; Hemmens, B. *Angew. Chem. Int. Ed.* 1999, *38*, 1714 -1731.

117. Eiserich, J. P.; Patel, R. P.; O'Donnell, V. B. *Molec. Aspects Med.* 1998, *19*, 221-357.

118. Stamler, J. S.; Singel, D. J.; Loscalzo, J. *Science* 1992, *258*, 1898-1902.

119. Wink, D. A.; Kasprzak, K. S.; Maragos, C. M.; Elespuru, R. K.; Misra, M.; Dunams, T. M.; Cebula, T. A.; Koch, W. H.; Andrews, A. W.; Allen, J. S.; Keefer, L. K. *Science* 1991, *254*, 1001-1003.

120. Davis, K. L.; Martin, E.; Turko, I. V.; Murad, F. *Annu Rev Pharmacol Toxicol* 2001, *41*, 203-236.

121. Coleman, J. W. *Int. Immunopharmacol.* 2001, *1* 1397-1406.

122. Ignarro, L. J. *Angew. Chem. Int. Ed.* 1999, *38*, 1882 -1892.

123. Bruckdorfer, R. *Mol.Aspects Med.* 2005, *26*, 3-31.

124. Handy, D. E.; Loscalzo, J. *Arterioscler. Thromb. Vasc. Biol.* 2006, *26*, 1207-1214.

125. Galla, H.-J. *Angew. Chem. Int. Ed.* 1993, *32*, 378-380.

126. Dawson, V. L.; Dawson, T. M. *J. Chem. Neuroanatomy* 1996, *10*, 179-190.

127. Bonthius, D. J.; Luong, T.; Bonthius, N. E.; Hostager, B. S.; Karacay, B. *Neuropharmacology* 2009, *56*, 716-731.

128. Zumft, W. G. *J. Mol. Microbiol. Biotechnol.* 2002, *4*, 277-286.

129. Cruz-Ramos, H.; Crack, J.; Wu, G.; Hughes, M. N.; Scott, C.; Thomson, A. J.; Green, J.; Poole, R. K. *EMBO J.* 2002, *21*, 3235-3244.

130. Korner, H.; Sofia, H. J.; Zumft, W. G. *FEMS Microbiol. Rev.* 2003, *27*, 559-592.

131. Rinaldo, S.; Giardina, G.; Brunori, M.; Cutruzzolà, F. *Biochem. Soc. Trans.* 2006, *34*, 185-187.

132. Zumft, W. G. *J. Mol. Microbiol. Biotechnol.* 2002, *4*, 277-286.

133. Arai, H.; Igarashi, Y.; Kodama, T. *FEBS Lett.* 1995, *371*, 73-76.

134. Arai, H.; Kodama, T.; Igarashi, Y. *Mol. Microbiol.* 1997, *25*, 1141-1148.

135. Yoon, S. S.; Karabulut, A. C.; Lipscomb, J. D.; Hennigan, R. F.; Lymar, S. V.; Groce, S. L. *EMBO J.* 2007, *26*, 3662-3672.

136. Giardina, G.; Rinaldo, S.; Johnson, K. A.; Matteo, A. D.; Brunori, M.; Cutruzzolà, F. *J. Mol. Biol.* 2008, *378*, 1002-1015.

137. Ye, R. W.; Averill, B. A.; Tiedje, J. M. *Appl. Environ. Microbiol.* 1994, *60*, 1053-1058.

138. Moura, I.; Moura, J. J. G. *Curr. Opin. Chem. Biol.* 2001, *5*, 168-175.

139. D'Autréaux, B.; Touati, D.; Bersch, B.; Latour, J. M.; Michaud-Soret, I. *Proc. Natl. Acad. Sci. U. S. A.* 2002, *99*, 16619-16624.

140. Moore, C. M.; Nakano, M. M.; Wang, T.; Ye, R. W.; Helmann, J. D. *J. Bacteriol.* 2004, *186*, 4655-4664.

141. Firoved, A. M.; Wood, S. R.; Ornatowski, W.; Deretic, V.; Timmins, G. S. *J. Bacteriol.* 2004, *186*, 4046-4050.

142. Ochsner, U. A.; Wilderman, P. J.; Vasil, A. I.; Vasil, M. L. *Mol. Microbiol.* 2002, *45*, 1277-1287.

143. Toyofuku, M.; Nomura, N.; Fujii, T.; Takaya, N.; Maseda, H.; Sawada, I.; Nakajima, T.; Uchiyama, H. *J. Bacteriol.* 2007, *189*, 4969-4972.

144. Toyofuku, M.; Nomura, N.; Kuno, E.; Tashiro, Y.; Nakajima, T.; Uchiyama, H. *J. Bacteriol.* 2008, *190*, 7947-7956.

145. Hentzer, M.; Eberl, L.; Givskov, M. *Biofilms* 2005, *2*, 37-61.

146. Sauer, K.; Cullen, M. C.; Rickard, A. H.; Zeef, L. A.; Davies, D. G.; Gilbert, P. *J. Bacteriol.* 2004, *186*, 7312-7326.

147. Wagner, V. E.; Bushnell, D.; Passador, L.; Brooks, A. I.; Iglewski, B. H. *J. Bacteriol.* 2003, *185*, 2080-2095.

148. Hassett, D. J.; Cuppoletti, J.; Trapnell, B.; Lymar, S. V.; Rowe, J. J.; Yoon, S. S.; Hilliard, G. M.; Parvatiyar, K.; Kamani, M. C.; Wozniak, D. J.; Hwang, S. H.; McDermott, T. R.; Ochsner, U. A. *Adv. Drug. Deliv. Rev.* 2002, *54*, 1425-1443.

149. Schuster, M.; Lostroh, C. P.; Ogi, T.; Greenberg, E. P. *J. Bacteriol.* 2003, *185*, 2066-2079.

150. Burgner, D.; Rockett, K.; Kwiatkowski, D. *Arch. Dis. Child* 1999, *81*, 185-188.

151. Nathan, C. F.; Hibbs-Jr, J. B. *Curr. Opin. Immunol.* 1991, *3*, 65-70.

152. Fang, F. C. *J. Clin. Invest.* 1997, *99*, 2818-2825.

153. Spiro, S. *Cell Host Microbe* 2011, *10*, 1-2.

154. Richardson, A. R.; Payne, E. C.; Younger, N.; Karlinsey, J. E.; Thomas, V. C.; Becker, L. A.; Navarre, W. W.; Castor, M. E.; Libby, S. J.; Fang, F. C. *Cell Host Microbe* 2011, *10*, 33-43.

155. Barraud, N.; Hassett, D. J.; Hwang, S. H.; Rice, S. A.; Kjelleberg, S.; Webb, J. S. *J. Bacteriol.* 2006, *188*, 7344-7353.

156. Barraud, N.; Schleheck, D.; Klebensberger, J.; Webb, J. S.; Hassett, D. J.; Rice, S. A.; Kjelleberg, S. *J. Bacteriol.* 2009, doi:10.1128/JB.00975-09.

157. Barraud, N.; Storey, M. V.; Moore, Z. P.; Webb, J. S.; Rice, S. A.; Kjelleberg, S. *Microb. Biotechnol.* 2009, *2*, 370-378.

158. Megson, I. L.; Webb, D. J. *Expert Opin. Investig. Drugs* 2002, *11*, 587-601.

159. Scatena, R.; Bottoni, P.; Martorana, G. E.; Giardina, B. *Expert Opin. Investig. Drugs* 2005, *14*, 835-846.

160. Wang, P. G.; Xian, M.; Tang, X.; Wu, X.; Wen, Z.; Cai, T.; Janczuk, A. J. *Chem. Rev.* 2002, *102*, 1091-1134.

161. Keefer, L. K.; Flippen-Anderson, J. L.; George, C.; Shanklin, A. P.; Dunams, T. M.; Christodoulou, D.; Saavedra, J. E.; Sagan, E. S.; Bohle, D. S. *Nitric oxide: Biol. Chem.* 2001, *5*, 377-394.

162. Rang, H. P.; Dale, M. M.; Ritter, J. M.; Flower, R. J. *Rang & Dale's Pharmacology*, 6 ed.; Churchill Livingstone, 2007.

163. Murad, F. *N. Engl. J. Med.* 2006, *355*, 2003-2011.

164. Thatcher, G. R. J.; Nicolescu, A. C.; Bennett, B. M.; Toader, V. *Free Radical Biol. Med.* 2004, *37*, 1122-1143.

165. Needleman, P.; F. Edmund Hunter, J. *Mol. Pharmacol.* 1965, *1*, 77-86.

166. Li, H.; Cui, H.; Liu, X.; Zweier, J. L. *J. Biol. Chem.* 2005, *280*, 16594-16600.

167. Mayer, B. *Angew. Chem. Int. Ed.* 2003, *42*, 388-391.

168. Ignarro, L. J. *Angew. Chem. Int. Ed.* 1999, *38*, 1882 - 1892.

169. Needleman, P.; Johnson, E. M. *J. Pharmacol. Exp. Ther.* 1973, *184*, 709.

170. Sydow, K.; Daiber, A.; Oelze, M.; Chen, Z.; August, M.; Wendt, M. *J. Clin. Invest* 2004, *113*, 482-489.

171. Munzel, T.; Sayegh, H.; Freeman, B. A.; Tarpey, M. M.; Harrison, D. G. *J. Clin. Invest.* 1995, *95*, 187-194.

172. Munzel, T.; Daiber, A.; Mulsch, A. *Circ. Res.* 2005, *97*, 618-628.

173. Ishihara, S.; Saito, F.; Ohhata, Y.; Kanai, M.; Mizuno, H.; Fujisawa, M.; Yorikane, R.; Koike, H. *Bioorg. Med. Chem. Lett.* 2003, *13*, 1527-1530.

174. Koenig, A.; Lange, K.; Konter, J.; Daiber, A.; Stalleicken, D.; Glusa, E.; Lehmann, J. *J. Cardiovasc. Pharmacol.* 2007, *50*, 68-74.

175. Koenig, A.; Roegler, C.; Lange, K.; Daiber, A.; Glusa, E.; Lehmann, J. *Bioorg. Med. Chem. Lett.* 2007, *17*, 5881-5885.

176. Schuhmacher, S.; Schulz, E.; Oelze, M.; König, A.; Roegler, C.; Lange, K.; Sydow, L.; Kawamoto, T.; Wenzel, P.; Münzel, T.; Lehmann, J.; Daiber, A. *Br. J. Pharmacol.* 2009, doi:10.1111/j.1476-5381.2009.00303.x.

177. Roegler, C.; König, A.; Glusa, E.; Lehmann, J. *J Cardiovasc Pharmacol* 2010, *56*, 484-490.

178. Hrabie, J. A.; Keefer, L. K. *Chem. Rev.* 2002, *102*, 1135-1154.

179. Konter, J.; A., G. E.-D. A.; Abuo-Rahma; El-Emam, A.; Lehmann, J. *Eur. J. Org. Chem.* 2007, 616-624.

180. Keefer, L. K. *Annu. Rev. Pharmacol. Toxicol.* 2003, *43*, 585-607.

181. Hrabie, J. A.; Klose, J. R.; Wink, D. A.; Keefer, L. K. *J. Org. Chem.* 1993, *58*, 1472-1476.

182. Saavedra, J. E.; Southan, G. J.; Davies, K. M.; Lundell, A.; Markou, C.; Hanson, S. R.; Adrie, C.; Hurford, W. E.; Zapol, W. M.; Keefer, L. K. *J. Med. Chem.* 1996, *39*, 4361-4365.

183. Rao, W.; Smith, D. J. *Chem. Pharm. Bull.* 1998, *46*, 1846-1847.

184. Hrabie, J. A.; Arnold, E. V.; Citro, M. L.; George, C.; Keefer, L. K. *J. Org. Chem.* 2000, *65*, 5745-5751.

185. Hrabie, J. A.; Citro, M. L.; Chmurny, G. N.; Keefer, L. K. *J. Org. Chem.* 2005, *70*, 7647-7653.

186. Arulsamy, N.; Bohle, D. S. *J. Org. Chem.* 2006, *71*, 572-581.

187. Arnold, E. V.; Citro, M. L.; Saavedra, E. A.; Davies, K. M.; Keefer, L. K.; Hrabie, J. A. *Nitric oxide* 2002, *7*, 103-108.

188. Davies, K. M.; Wink, D. A.; Saavedra, J. E.; Keefer, L. K. *J. Am. Chem. Soc.* 2001, *123*, 5473-5481.

189. Dutton, A. S.; Fukuto, J. M.; Houk, K. N. *Inorg. Chem.* 2004, *43*, 1039-1045.

190. Drago, R. S.; Paulik, F. E. *J. Am. Chem. Soc.* 1960, *82*, 96-98.

191. Drago, R. S.; Karstetter, B. R. *J. Am. Chem. Soc.* 1961, *83*, 1819-1822.

192. Longhi, R.; Ragsdale, R. O.; Drago, R. S. *Inorg. Chem.* 1962, *1*, 768-770.

193. Arnold, E. V.; Citro, M. L.; Keefer, L. K.; Hrabie, J. A. *Org. Lett.* 2002, *4*, 1323-1325.

194. Saavedra, J. E.; Dunams, T. M.; Flippen-Anderson, J. L.; Keefer, L. K. *J. Org. Chem.* 1992, *57*, 6134-6138.

195. Saavedra, J. E.; Shami, P. J.; Wang, L. Y.; Davies, K. M.; Booth, M. N.; Citro, M. L.; Keefer, L. K. *J. Med. Chem.* 2000, *43*, 261-269.

196. Saavedra, J. E.; Srinivasan, A.; Bonifant, C. L.; Chu, J.; Shanklin, A. P.; Flippen-Anderson, J. L.; Rice, W. G.; Turpin, J. A.; Davies, K. M.; Keefer, L. K. *J. Org. Chem.* 2001, *66*, 3090-3098.

197. Singh, S. P.; Wishnok, J. S.; Keshive, M.; Deen, W. M.; Tannenbaum, S. R. *Proc. Natl. Acad. Sci. USA* 1996, *93*, 14428-14433.

198. Williams, D. L. H. *Acc. Chem. Res.* 1999, *32*, 869-876.

199. Al-Sa'doni, H.; Ferro, A. *Clin. Sci.* 2000, *98*, 507-520.

200. Roy, B.; d'Hardemare, A. d. M.; Fontecave, M. *J. Org. Chem.* 1994, *59*, 7019-7026.

201. Spivey, A. C.; Colley, J.; Sprigens, L.; Hancock, S. M.; Cameron, D. S.; Chigboh, K. I.; Veitch, G.; Frampton, C. S.; Adams, H. *Org. Biomol. Chem.* 2005, *3*, 1942-1952.

202. Al-Sa'doni, H. H.; Khan, I. Y.; Poston, L.; Fisher, I.; Ferro, A. *Nitric Oxide: Biol. Chem.* 2000, *4*, 550-560.

203. Field, L.; Dilts, R. V.; Ravichandran, R.; Lenhert, P. G.; Carnahan, G. E. *J.C.S. Chem.Comm* 1978, 249-250.

204. Megson, I. L.; Morton, S.; Greig, I. R.; Mazzei, F. A.; Field, R. A.; Butler, A. R.; Caron, G.; Gasco, A.; Fruttero, R.; Webb, D. J. *Br. J. Pharmacol.* 1999, *126*, 639-648.

205. Letts, G.; Loscalzo, J. *J. Am. Soc. Nephrol.* 2007, *18*, 2863-2869.

206. Rigas, B.; Williams, J. L. *Nitric Oxide* 2008, *19*, 199-204.

207. Tang, X.; Cai, T.; Wang, P. G. *Bioorg. Med. Chem. Lett.* 2003, *13*, 1687-1690.

208. Konter, J.; Möllmann, U.; Lehmann, J. *Bioorg. Med. Chem.* 2008, *16*, 8294-8300.

209. Bertinaria, M.; Galli, U.; Sorba, G.; Fruttero, R.; Gasco, A.; Brenciaglia, M. I.; Scaltrito, M. M.; Dubini, F. *Drug Dev. Res.* 2003, *60*, 225-239.

210. Geske, G. D.; O'Neill, J. C.; Miller, D. M.; Mattmann, M. E.; Blackwell, H. E. *J. Am. Chem. Soc.* 2007, *129*, 13613-13625.

211. Chhabra, S. R.; Stead, P.; Bainton, N. J.; Salmond, G. P. C.; Stewart, G. S. A. B.; Williams, P.; Bycroft, B. W. *J. Antibiot.* 1993, *46*, 441-454.

212. Chhabra, S. R.; Harty, C.; Hooi, D. S. W.; Daykin, M.; Williams, P.; Telford, G.; Pritchard, D. I.; Bycroft, B. W. *J. Med. Chem.* 2003, *46*, 97-104.

213. Amara, N.; Mashiach, R.; Amar, D.; Krief, P.; Spieser, S. A. H.; Bottomley, M. J.; Aharoni, A.; Meijler, M. M. *J. Am. Chem. Soc.* 2009, *131*, 10610-10619.

214. Horikawa, M.; Tateda, K.; Tuzuki, E.; Ishii, Y.; Ueda, C.; Takabatake, T.; Miyairi, S.; Yamaguchi, K.; Ishiguro, M. *Bioorg. Med. Chem. Lett.* 2006, *16*, 2130-2133.

215. Dubinsky, L.; Jarosz, L. M.; Amara, N.; Krief, P.; Kravchenko, V. V.; Krom, B. P.; Meijler, M. M. *Chem. Commun.* 2009, 7378-7380.

216. Oliver, C. M.; Schaefer, A. L.; Greenberg, E. P.; Sufrin, J. R. *J. Med. Chem.* 2009, *52*, 1569-1575.

217. Praneenararat, T.; Geske, G. D.; Blackwell, H. E. *Org. Lett.* 2009, *11*, 4600-4603.

218. Ballard, T. E.; Richards, J. J.; Wolfe, A. L.; Melander, C. *Chem. Eur. J.* 2008, *14*, 10745 - 10761.

219. Sharma, S. K.; Miller, M. J.; Payne, S. M. *J. Med. Chem.* 1989, *32*, 357-367.

220. Saavedra, J. E.; Booth, M. N.; Hrabie, J. A.; Davies, K. M.; Keefer, L. K. *J. Org. Chem.* 1999, *64*, 5124-5131.

221. Shami, P. J.; Saavedra, J. E.; Bonifant, C. L.; Chu, J.; Udupi, V.; Malaviya, S.; Carr, B. I.; Kar, S.; Wang, M.; Jia, L.; Ji, X.; Keefer, L. K. *J. Med. Chem.* 2006, *49*, 4356-4366.

222. Moynihan, H. A.; Roberts, S. M. *J. Chem. Soc. Perkin Trans. I* 1994, 797-805.

223. Soulere, L.; Sturm, J.-C.; Nunez-Vergara, L. J.; Hoffmann, P.; Perie, J. *Tetrahedron* 2001, *57*, 7173-7180.

224. Kubanek, J.; Jensen, P. R.; Keifer, P. A.; Sullards, M. C.; Collins, D. O.; Fenical, W. *Proc. Natl, Acad. Sci. U. S. A.* 2003, *100*, 6916-6921.

225. Vervoort, H. C.; Richards-Gross, S. E.; Fenical, W. *J. Org. Chem.* 1997, *62*, 1486-1490.

226. Bhosale, S. H.; Nagle, V. L.; Jagtap, T. G. *Mar. Biotechnol. (NY)* 2002, *4*, 111-118.

227. Pawlik, J. R. *Chem. Rev.* 1993, *93*, 1911-1922.

228. Edreva, A.; Velikova, V.; Tsonev, T.; Dagnon, S.; Gurel, A.; Aktas, L.; Gesheva, E. *Gen. Appl. Plant Physiol.* 2008, *34*, 67-78.

229. Beechan, C. M.; Sims, J. J. *Tetrahedron Lett.* 1979, *19*, 1649-1652.

230. Caine, D.; Ukachukwu, V. C. *J. Org. Chem.* 1985, *50*, 2195-2198.

231. Font, J.; Gracia, A.; de March, P. *Tetrahedron Lett.* 1990, *38*, 5517-5520.

232. Manny, A. J.; Kjelleberg, S.; Kumar, N.; de Nys, R.; Read, R. W.; Steinberg, P. *Tetrahedron* 1997, *46*, 15813-15826.

233. Ho, K. K. K.; Cole, N.; Chen, R.; Willcox, M. D. P.; Rice, S. A.; Kumar, N. *Biofouling* 2010, *26*, 913-921.

234. Li, W. R.; Lin, S. T.; Hsu, N. M.; Chern, M. S. *J. Org. Chem.* 2002, *67*, 4702-4706.

235. Shiraki, R.; Sumino, A.; Tadano, K.; Ogawa, S. *J. Org. Chem.* 1996, *61*, 2845-2852.

236. Mase, N.; Nishi, T.; Takamori, Y.; Yoda, H.; Takabe, K. *Tetrahedron: Asymmetry* 1999, *10*, 4469-4471.

237. Kawasuji, T.; Fuji, M.; Yoshinaga, T.; Sato, A.; Fujiwara, T.; Kiyama, R. *Bioorg. Med. Chem. Lett.* 2007, *15*, 5487-5492.

238. Peukert, S.; Sun, Y.; Zhang, R.; Hurley, B.; Sabio, M.; Shen, X.; Gray, C.; Dzink-Fox, J.; Tao, J.; Cebula, R.; Wattanasin, S. *Bioorg. Med. Chem. Lett.* 2008, *18*, 1840-1844.

239. Nay, B.; Riache, N.; Evanno, L. *Nat. Prod. Rep.* 2009, *26*, 1044-1062.

240. Cherry, K.; Thibonnet, J.; Duchene, A.; Parrain, J. L.; Abarbri, M. *Tetrahedron Lett.* 2004, *45*, 2063-2066.

241. Nagao, Y.; Sano, S.; Morimoto, K.; Kakegawa, H.; Takatani, T.; Shiro, M.; Katunuma, N. *Tetrahedron Lett.* 2000, *41*, 2419-2424.

242. Scatena, R.; Bottoni, P.; Pontoglio, A.; Giardina, B. *Curr. Med. Chem.* 2010, *17*, 61-73.

243. Low, S. Y. *Mol. Aspects Med.* 2005, *26*, 97-138.

244. Lee, J.; Jayaraman, A.; Wood, T. K. *BMC Microbiology* 2007, *7*.

245. Lee, J.; Bansal, T.; Jayaraman, A.; Bentley, W. E.; Wood, T. K. *Appl. Environ. Microbiol.* 2007, *73*, 4100–4109.

246. Lee, J.; Attila, C.; Cirillo, S. L. G.; Cirillo, J. D.; Wood, T. K. *Microb. Biotechnol.* 2009, *2*, 75-90.

247. Lee, J.; Maeda, T.; Hong, S. H.; Wood, T. K. *Appl. Environ. Microbiol.* 2009, *75*, 1703–1716.

248. Clementi, S.; Linda, P.; Marino, G. *J.C.S. Chem. Comm.* 1972, 427-428.

249. Astolfi, P.; Greci, L. *Nitric Oxide* 2003, *8*, 202-205.

250. Suzuki, T.; Mower, H. F.; Friesen, M. D.; Gilibert, I.; Sawa, T.; ohshima, H. *Free Radical Biol. Med.* 2004, *37*, 671 - 681.

251. Astolfi, P.; Panagiotaki, M.; Rizzoli, C.; Greci, L. *Org. Biomol. Chem.* 2006, *4*, 3282-3290.

252. Peyrot, F.; Fernandez, B. O.; Bryan, N. S.; Feelisch, M.; Ducrocq, C. *Chem. Res. Toxicol.* 2006, *19*, 58-67.

253. Hartung, J. *Chem. Rev.* 2009, *109*, 4500-4517.

254. Mur, V. I. *Russ. Chem. Rev.* 1964, *33*, 92.

255. Thurston, J. T.; Dudley, J. R.; Kaiser, D. W.; Hechenbleikner, I.; Schaefer, F. C.; Holm-Hansen, D. *J. Am. Chem. Soc.* 1951, *73*, 2981-2983.

256. Dudley, J. R.; Thurston, J. T.; Schaefer, F. C.; Holm-Hansen, D.; Hull, C. J.; Adams, P. *J. Am. Chem. Soc.* 1951, *73*, 2986-2990.

257. Schaefer, F. C.; Thurston, J. T.; Dudley, J. R. *J. Am. Chem. Soc.* 1951, *73*, 2990-2992.

258. Jarman, M.; Coley, H. M.; Judson, I. R.; Thornton, T. J.; Wilman, D. E. V.; Abel, G.; Rutty, C. J. *J. Med. Chem.* 1993, *36*, 4195-4200.

259. Baliani, A.; Bueno, G. J.; Stewart, M. L.; Yardley, V.; Brun, R.; Barrett, M. P.; Gilbert, I. H. *J. Med. Chem.* 2005, *48*, 5570-5579.

260. Baindur, N.; Chadha, N.; Brandt, B. M.; Asgari, D.; Patch, R. J.; Schalk-HiHi, C.; Carver, T. E.; Petrounia, I. P.; Baumann, C. A.; Ott, H.; Manthey, C.; Springer, B. A.; Player, M. R. *J. Med. Chem.* 2005, *48*, 1717-1720.

261. Rodriguez, A. L.; Tamrazi, A.; Collins, M. L.; Katzenellenbogen, J. A. *J. Med. Chem.* 2004, *47*, 600-611.

262. Lozano, V.; Aguado, L.; Hoorelbeke, B.; Renders, M.; Camarasa, M.-J.; Schols, D.; Balzarini, J.; San-Felix, A.; Perez-Perez, M.-J. *J. Med. Chem.* 2011, *54*, 5335-5348.

263. Ronchi, S.; Prosperi, D.; Compostella, F.; Panza, L. *Synlett* 2004, *6*, 1007-1010.

264. Yang, X.; Lowe, C. R. *Tet. Lett.* 2003, *44*, 1359-1362.

265. Löwik, D. W. P. M.; Lowe, C. R. *Eur. J. Org. Chem.* 2001, 2825-2839.

266. Gustafson, G. R.; Baldino, C. M.; O'Donnell, M.-M. E.; Sheldon, A.; Tarsa, R. J.; Verni, C. J.; Coffen, D. L. *Tetrahedron* 1998, *54*, 4051-4065.

267. Munshi, P.; Row, T. N. G. *Crystallogr. Rev.* 2005, *11*, 199.

268. Desiraju, G. R., Ed. *Crystal Engineering: The Design of Organic Solids*; Elsevier: Amsterdam, 1989.

269. Etter, M. C. *Acc. Chem. Res.* 1990, *23*, 120.

270. Auffinger, P.; Hays, F. A.; Westhof, E.; Ho, P. S. *Proced. Natl. Acad. Sci.* 2004, *101*, 16789-16794.

271. Lu, Y.; Shi, T.; Wang, Y.; Yang, H.; Yan, X.; Luo, X.; Jiang, H.; Zhu, W. *J. Med. Chem.* 2009, *52*, 2854-2862.

272. Voth, A. R.; Khuu, P.; Oishi, K.; Ho, P. S. *Nat. Chem.* 2009, *1*

273. Fourmigué, M. *Curr. Opin. Solid State Mater. Sci.* 2009, *13*, 36-45.

274. Howard, E. I.; Sanishvili, R.; Cachau, R. E.; Mitschler, A.; Chevrier, B.; Barth, P.; Lamour, V.; Zandt, M. V.; Sibley, E.; Bon, C.; Moras, D.; Schneider, T. R.; Joachimiak, A.; Podjarny, A. *PROTEINS: Structure, Function, and Bioinformatics* 2004, *55*, 792–804.

275. Allen, F. H.; Baalham, C. A.; Lommerse, J. P. M.; Raithby, P. R. *Acta Cryst.* 1998, *B54*, 320-329.

276. Paulini, R.; Muller, K.; Diederich, F. *Angew Chem Int Ed* 2005, *44*, 1788-1805.

277. Bergner, A.; Gunther, J.; Hendlich, M.; Klebe, G.; Verdonk, M. *Biopolymers (Nucleic Acid Sciences)* 2002, *61*, 99-110.

278. Congreve, M.; Murray, C. W.; Blundell, T. L. *Drug Discov. Today* 2005, *10*, 895-907.

279. Thiel, K. A. *Nature Biotechnol.* 2004, *22*, 513-519.

280. Gasteiger, J.; Engel, T., Eds. *Chemoinformatics: A textbook*; Wiley-VCH Verlag GmbH & Co. KGaA: Germany, 2003.

281. Venkatachalam, C. M.; Jiang, X.; Oldfield, T.; Waldman, M. *J. Mol. Graphics Modell.* 2003, *21*, 289-307.

282. Montes, M.; Miteva, M. A.; Villoutreix, B. O. *Proteins: Struct., Funct., Bioinf.* 2007, *68*, 712-725.

283. Bottomley, M. J.; Muraglia, E.; Bazzo, R.; Carfı, A. *J. Biol. Chem.* 2007, *282*, 13592–13600.

284. Miles, A. M.; Wink, D. A.; Cook, J. C.; Grisham, M. B. *Methods Enzymol.* 1996, *268*, 105-120.

285. Yang, Y.; Seidlits, S. K.; Adams, M. M.; Lynch, V. M.; Schmidt, C. E.; Anslyn, E. V.; Shear, J. B. *J. Am. Chem. Soc.* 2010, *132*, 13114-13116.

286. Hetrick, E. M.; Schoenfisch, M. H. *Annu. Rev. Anal. Chem.* 2009, *2*, 409-433.

287. Moorcroft, M. J.; Davis, J.; Compton, R. G. *Talanta* 2001 *54*, 785-803.

288. Giustarini, D.; Rossi, R.; Milzani, A.; Dalle-Donne, I. *Methods Enzymol.* 2008, *440*, 361-380.

289. O'Toole, G. A.; Kolter, R. *Mol. Microbiol.* 1998, *28*, 449-461.

290. McCallum, K. S.; Emmons, W. D. *J. Org. Chem.* 1956, *21*, 367-368.

291. Piermatti, O.; Fringuelli, F.; Pochini, L.; Indiveri, C.; Palmerini, C. A. *Bioorg. Med. Chem.* 2008, *16*, 1444-1451.

292. Endres, S.; Hacker, A.; Noack, E.; Kojda, G.; Lehmann, J. *Eur. J. Med. Chem.* 1999, *34*, 895−901.

293. Sharma, S. K.; Miller, M. J.; Payne, S. M. *J. Med. Chem.* 1989, *32*, 357-367.

Appendix

Crystal Structure Data

Introduction

The X-ray crystallography data shown in the appendix were obtained by Mohan Bhadbhade at the University of New South Wales, Sydney, Australia.

Structure determination

Reflexion data were measured with an Enraf-Nonius CAD-4 diffractometer in $\theta/2\theta$ scan mode using nickel filtered copper radiation (γ 1.5418Å). Reflexions with $I>3\sigma(I)$ were considered observed. The structures were determined by direct phasing and Fourier methods. Hydrogen atoms were included in calculated position s and were assigned thermal parameters equal to those of the atom to which they were bonded. Positional and anisitropic thermal parameters for the noNHydrogen atoms were refined using full matrix least squares. Reflexion weights used were $1/\sigma^2(F_o)$, with $\sigma(F_o)$ being derived from $\sigma(I_o) = [\sigma^2(I_o) + (0.04I_o)^2]^{1/2}$. The weighted residual is defined as $R_w = (\Sigma w\Delta^2/\Sigma wF_o^2)^{1/2}$. Atomic scattering factors and anomalous dispersion parameters were from International Tables for X-ray crystallography[1]. Structure solutions were performed by SIR92[2] and refinements used RAELS[3]. ORTEP-II[4] running on a Macintosh was used for the structural diagrams.

1. Ibers, J.A. and Hamilton, W.C., (Eds) International Tables for X-Ray Crystallography Vol. 4 , Kynoch Press, Birmingham, 1974.
2. Altomare, A., Burla, M.C., Camalli, M., Cascarano, G., Giacovazzo, C., Guagliardi, A., Polidori, G., J. Appl. Cryst., 1994, 27, 435.
3. Rae, A.D., RAELS. A comprehensive Constrained Least Squares Refinement Program, University of New South Wales, 1989.
4. Johnson, C.K.,'ORTEP-II', Oak Ridge National Laboratory, Tennessee, U.S.A., 1976.

1. 2-Oxo-2-(2-oxotetrahydrofuran-3-ylamino)ethyl nitrate (95a)

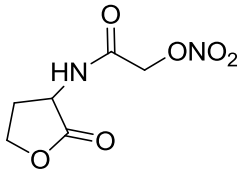

Table 1. Experimental details

	Compound 95a
Crystal data	
Chemical formula	$C_6H_8N_2O_6$
M_r	204.14
Crystal system, space group	Monoclinic, $P2_1/n$
Temperature (K)	152
a, b, c (Å)	10.0324 (6), 5.2469 (2), 16.1420 (9)
b (°)	101.826 (3)
V (Å^3)	831.66 (8)
Z	4
Radiation type	Mo Ka
m (mm^{-1})	0.15
Crystal size (mm)	0.47 × 0.27 × 0.08
Data collection	
Diffractometer	Bruker kappa APEXII CCD Diffractometer
Absorption correction	Multi-scan *SADABS* (Bruker, 2001)
T_{min}, T_{max}	0.934, 0.988
No. of measured, independent and observed [$I > 2s(I)$] reflections	6746, 1812, 1552
R_{int}	0.032
Refinement	
$R[F^2 > 2s(F^2)]$, $wR(F^2)$, S	0.032, 0.089, 1.04
No. of reflections	1812
No. of parameters	127
No. of restraints	0
H-atom treatment	H-atom parameters constrained
$D\rho_{max}$, $D\rho_{min}$ (e Å^{-3})	0.27, -0.24

Computer programs: *APEX2* (Bruker, 2007), *SHELXS-97* (Sheldrick, 2008), *SHELXL-97* (Sheldrick, 2008), *SHELXTL-Plus* (Sheldrick, 2008).

Table 2. Selected geometric parameters (Å, º)

O1—C2	1.3362 (15)	C2—C3	1.5171 (17)
O1—C5	1.4634 (17)	C3—C4	1.5223 (17)
O2—C2	1.2065 (16)	C3—H3	1.0000
O3—C6	1.2210 (15)	C4—C5	1.5226 (19)
O4—N2	1.4037 (15)	C4—H4B	0.9900
O4—C7	1.4400 (15)	C4—H4A	0.9900
O5—N2	1.2017 (16)	C5—H5B	0.9900
O6—N2	1.2005 (15)	C5—H5A	0.9900
N1—C6	1.3363 (16)	C6—C7	1.5244 (17)
N1—C3	1.4388 (15)	C7—H7B	0.9900
N1—H1	0.8800	C7—H7A	0.9900
C2—O1—C5	109.89 (10)	C5—C4—H4B	111.5
N2—O4—C7	112.50 (9)	C3—C4—H4A	111.5
C6—N1—C3	121.31 (10)	C5—C4—H4A	111.5
C6—N1—H1	119.3	H4B—C4—H4A	109.3
C3—N1—H1	119.3	O1—C5—C4	105.00 (10)
O6—N2—O5	129.31 (13)	O1—C5—H5B	110.7
O6—N2—O4	112.44 (11)	C4—C5—H5B	110.7
O5—N2—O4	118.25 (11)	O1—C5—H5A	110.7
O2—C2—O1	122.41 (12)	C4—C5—H5A	110.7
O2—C2—C3	127.51 (11)	H5B—C5—H5A	108.8
O1—C2—C3	110.08 (10)	O3—C6—N1	124.92 (11)
N1—C3—C2	112.01 (10)	O3—C6—C7	121.16 (11)
N1—C3—C4	116.74 (10)	N1—C6—C7	113.91 (10)
C2—C3—C4	102.41 (10)	O4—C7—C6	109.72 (10)
N1—C3—H3	108.4	O4—C7—H7B	109.7
C2—C3—H3	108.4	C6—C7—H7B	109.7
C4—C3—H3	108.4	O4—C7—H7A	109.7
C3—C4—C5	101.36 (10)	C6—C7—H7A	109.7
C3—C4—H4B	111.5	H7B—C7—H7A	108.2
C7—O4—N2—O6	170.32 (11)	N1—C3—C4—C5	-153.99 (11)
C7—O4—N2—O5	-10.48 (16)	C2—C3—C4—C5	-31.27 (12)
C5—O1—C2—O2	179.63 (11)	C2—O1—C5—C4	-19.87 (14)
C5—O1—C2—C3	-1.07 (13)	C3—C4—C5—O1	31.65 (13)

C6—N1—C3—C2	98.81 (13)	C3—N1—C6—O3	2.77 (19)
C6—N1—C3—C4	-143.60 (12)	C3—N1—C6—C7	-177.92 (10)
O2—C2—C3—N1	-33.54 (17)	N2—O4—C7—C6	-65.25 (13)
O1—C2—C3—N1	147.21 (10)	O3—C6—C7—O4	-11.01 (16)
O2—C2—C3—C4	-159.40 (12)	N1—C6—C7—O4	169.65 (10)
O1—C2—C3—C4	21.34 (13)		

2. 2,2-dimethyl-5-((2-oxotetrahydrofuran-3-ylamino)methylene)-1,3-dioxane-4,6-dione (100)

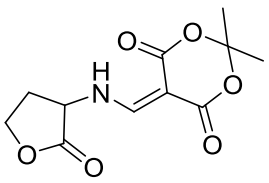

Table 3. Experimental details

	Compound 100
Crystal data	
Chemical formula	$C_{11}H_{13}NO_6$
M_r	255.22
Crystal system, space group	Triclinic, $P\bar{1}$
Temperature (K)	151
a, *b*, *c* (Å)	5.5616 (2), 8.7867 (3), 12.5620 (4)
a, b, g (°)	72.734 (2), 84.564 (2), 88.461 (2)
V (Å^3)	583.58 (3)
Z	2
Radiation type	Mo *K*a
m (mm^{-1})	0.12
Crystal size (mm)	0.34 × 0.23 × 0.11
Data collection	
Diffractometer	Bruker kappa APEXII CCD Diffractometer
Absorption correction	Multi-scan *SADABS* (Bruker, 2001)
T_{min}, T_{max}	0.961, 0.987
No. of measured, independent and observed [$I > 2s(I)$] reflections	7750, 2043, 1881

R_{int}	0.025
Refinement	
$R[F^2 > 2s(F^2)]$, $wR(F^2)$, S	0.030, 0.076, 1.06
No. of reflections	2043
No. of parameters	165
No. of restraints	0
H-atom treatment	H-atom parameters constrained
$D\rho_{max}$, $D\rho_{min}$ (e Å^{-3})	0.25, -0.19

Computer programs: *APEX2* (Bruker, 2007), *SHELXS-97* (Sheldrick, 2008), *SHELXL-97* (Sheldrick, 2008), *SHELXTL-Plus* (Sheldrick, 2008).

Table 4. Selected geometric parameters (Å, º)

O1—C2	1.3444 (15)	C4—H4B	0.9900
O1—C5	1.4485 (16)	C4—H4A	0.9900
O2—C2	1.1974 (16)	C5—H5B	0.9900
O3—C8	1.3729 (15)	C5—H5A	0.9900
O3—C9	1.4309 (14)	C6—C7	1.3879 (17)
O4—C10	1.3650 (15)	C6—H6	0.9500
O4—C9	1.4389 (14)	C7—C10	1.4315 (17)
O5—C8	1.2098 (15)	C7—C8	1.4440 (17)
O6—C10	1.2170 (15)	C9—C11	1.5049 (17)
N1—C6	1.3066 (16)	C9—C12	1.5053 (18)
N1—C3	1.4452 (15)	C11—H11B	0.9800
N1—H1	0.8800	C11—H11C	0.9800
C2—C3	1.5199 (18)	C11—H11A	0.9800
C3—C4	1.5186 (17)	C12—H12C	0.9800
C3—H3	1.0000	C12—H12B	0.9800
C4—C5	1.5177 (18)	C12—H12A	0.9800
C2—O1—C5	110.13 (9)	C7—C6—H6	116.7
C8—O3—C9	118.18 (9)	C6—C7—C10	121.70 (11)
C10—O4—C9	117.27 (9)	C6—C7—C8	117.38 (11)
C6—N1—C3	123.14 (10)	C10—C7—C8	120.90 (11)
C6—N1—H1	118.4	O5—C8—O3	117.35 (11)
C3—N1—H1	118.4	O5—C8—C7	127.03 (12)

O2—C2—O1	122.28 (12)	O3—C8—C7	115.57 (10)
O2—C2—C3	128.11 (12)	O3—C9—O4	110.63 (9)
O1—C2—C3	109.60 (10)	O3—C9—C11	105.85 (10)
N1—C3—C4	116.11 (10)	O4—C9—C11	105.98 (10)
N1—C3—C2	111.53 (10)	O3—C9—C12	110.72 (10)
C4—C3—C2	102.99 (10)	O4—C9—C12	110.03 (10)
N1—C3—H3	108.6	C11—C9—C12	113.47 (11)
C4—C3—H3	108.6	O6—C10—O4	117.30 (11)
C2—C3—H3	108.6	O6—C10—C7	125.44 (11)
C5—C4—C3	101.69 (10)	O4—C10—C7	117.23 (10)
C5—C4—H4B	111.4	C9—C11—H11B	109.5
C3—C4—H4B	111.4	C9—C11—H11C	109.5
C5—C4—H4A	111.4	H11B—C11—H11C	109.5
C3—C4—H4A	111.4	C9—C11—H11A	109.5
H4B—C4—H4A	109.3	H11B—C11—H11A	109.5
O1—C5—C4	106.20 (9)	H11C—C11—H11A	109.5
O1—C5—H5B	110.5	C9—C12—H12C	109.5
C4—C5—H5B	110.5	C9—C12—H12B	109.5
O1—C5—H5A	110.5	H12C—C12—H12B	109.5
C4—C5—H5A	110.5	C9—C12—H12A	109.5
H5B—C5—H5A	108.7	H12C—C12—H12A	109.5
N1—C6—C7	126.64 (11)	H12B—C12—H12A	109.5
N1—C6—H6	116.7		
C5—O1—C2—O2	178.34 (12)	C6—C7—C8—O5	7.5 (2)
C5—O1—C2—C3	-2.20 (13)	C10—C7—C8—O5	-170.66 (13)
C6—N1—C3—C4	-122.94 (13)	C6—C7—C8—O3	-175.26 (11)
C6—N1—C3—C2	119.52 (12)	C10—C7—C8—O3	6.60 (18)
O2—C2—C3—N1	-34.92 (17)	C8—O3—C9—O4	-49.56 (14)
O1—C2—C3—N1	145.67 (10)	C8—O3—C9—C11	-163.93 (11)
O2—C2—C3—C4	-160.12 (13)	C8—O3—C9—C12	72.70 (13)
O1—C2—C3—C4	20.46 (13)	C10—O4—C9—O3	48.32 (13)
N1—C3—C4—C5	-151.03 (10)	C10—O4—C9—C11	162.61 (10)
C2—C3—C4—C5	-28.86 (12)	C10—O4—C9—C12	-74.34 (13)
C2—O1—C5—C4	-17.23 (14)	C9—O4—C10—O6	160.83 (11)
C3—C4—C5—O1	28.70 (13)	C9—O4—C10—C7	-21.14 (16)
C3—N1—C6—C7	-173.91 (12)	C6—C7—C10—O6	-7.6 (2)

N1—C6—C7—C10	-0.9 (2)	C8—C7—C10—O6	170.51 (13)
N1—C6—C7—C8	-179.01 (12)	C6—C7—C10—O4	174.60 (11)
C9—O3—C8—O5	-159.59 (12)	C8—C7—C10—O4	-7.34 (18)
C9—O3—C8—C7	22.87 16)		

3. 3-(1-Nitrooxyhexyl)-5-(dibromomethylene)furan-2(5*H*)-one (155c)

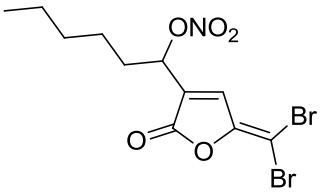

Table 5. Experimental details

	Compound 155c
Crystal data	
Chemical formula	$C_{11}H_{13}Br_2NO_5$
M_r	399.04
Crystal system, space group	Triclinic, $P\bar{1}$
Temperature (K)	150
a, b, c (Å)	6.4900 (2), 7.5676 (3), 15.8199 (6)
α, β, γ (°)	90.215 (2), 97.553 (1), 115.007 (1)
V (Å^3)	696.50 (4)
Z	2
Radiation type	Mo $K\alpha$
μ (mm^{-1})	5.83
Crystal size (mm)	0.27 × 0.21 × 0.10
Data collection	
Diffractometer	Bruker kappa APEXII CCD Diffractometer
Absorption correction	Multi-scan *SADABS* (Bruker, 2001)
T_{min}, T_{max}	0.306, 0.582
No. of measured, independent and observed [$I > 2\sigma(I)$] reflections	9276, 2412, 2235
R_{int}	0.048
Refinement	
$R[F^2 > 2\sigma(F^2)]$, $wR(F^2)$, S	0.020, 0.054, 1.08
No. of reflections	2412
No. of parameters	173

No. of restraints	0
H-atom treatment	H-atom parameters constrained
$\Delta\rangle_{max}$, $\Delta\rangle_{min}$ (e Å^{-3})	0.35, -0.37

Computer programs: *APEX2* (Bruker, 2007), *SHELXS-97* (Sheldrick, 2008), *SHELXL-97* (Sheldrick, 2008), *SHELXTL-Plus* (Sheldrick, 2008).

Table 6. Selected geometric parameters (Å, º)

Br1—C6	1.8645 (19)	C7—H7	1.0000
Br2—C6	1.8706 (19)	C8—C9	1.521 (3)
O1—C5	1.383 (2)	C8—H8B	0.9900
O1—C2	1.390 (2)	C8—H8A	0.9900
O2—C2	1.186 (2)	C9—C10	1.529 (3)
O3—N1	1.411 (2)	C9—H9A	0.9900
O3—C7	1.458 (2)	C9—H9B	0.9900
O4—N1	1.204 (2)	C10—C11	1.513 (3)
O5—N1	1.199 (2)	C10—H10A	0.9900
C2—C3	1.476 (3)	C10—H10B	0.9900
C3—C4	1.331 (3)	C11—C12	1.521 (3)
C3—C7	1.496 (3)	C11—H11A	0.9900
C4—C5	1.450 (3)	C11—H11B	0.9900
C4—H4	0.9500	C12—H12A	0.9800
C5—C6	1.328 (3)	C12—H12B	0.9800
C7—C8	1.516 (3)	C12—H12C	0.9800
C5—O1—C2	107.92 (15)	C9—C8—H8B	108.9
N1—O3—C7	115.00 (16)	C7—C8—H8A	108.9
O5—N1—O4	129.81 (19)	C9—C8—H8A	108.9
O5—N1—O3	112.22 (19)	H8B—C8—H8A	107.7
O4—N1—O3	117.97 (16)	C8—C9—C10	112.97 (17)
O2—C2—O1	121.30 (18)	C8—C9—H9A	109.0
O2—C2—C3	131.46 (19)	C10—C9—H9A	109.0
O1—C2—C3	107.23 (17)	C8—C9—H9B	109.0
C4—C3—C2	108.04 (17)	C10—C9—H9B	109.0
C4—C3—C7	132.12 (18)	H9A—C9—H9B	107.8
C2—C3—C7	119.83 (17)	C11—C10—C9	114.22 (19)

C3—C4—C5	108.23 (17)	C11—C10—H10A	108.7
C3—C4—H4	125.9	C9—C10—H10A	108.7
C5—C4—H4	125.9	C11—C10—H10B	108.7
C6—C5—O1	120.49 (17)	C9—C10—H10B	108.7
C6—C5—C4	130.95 (18)	H10A—C10—H10B	107.6
O1—C5—C4	108.56 (16)	C10—C11—C12	112.8 (2)
C5—C6—Br1	120.92 (15)	C10—C11—H11A	109.0
C5—C6—Br2	121.40 (15)	C12—C11—H11A	109.0
Br1—C6—Br2	117.68 (10)	C10—C11—H11B	109.0
O3—C7—C3	110.55 (16)	C12—C11—H11B	109.0
O3—C7—C8	105.51 (17)	H11A—C11—H11B	107.8
C3—C7—C8	113.31 (16)	C11—C12—H12A	109.5
O3—C7—H7	109.1	C11—C12—H12B	109.5
C3—C7—H7	109.1	H12A—C12—H12B	109.5
C8—C7—H7	109.1	C11—C12—H12C	109.5
C7—C8—C9	113.32 (17)	H12A—C12—H12C	109.5
C7—C8—H8B	108.9	H12B—C12—H12C	109.5

4. Methyl 5-formyl-2-propylthiophene-3-carboxylate (165)

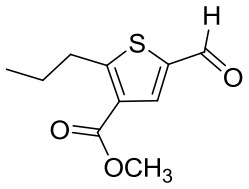

Table 7. Experimental details

	Compound 165
Crystal data	
Chemical formula	$C_{10}H_{12}O_3S$
M_r	212.26
Crystal system, space group	Triclinic, $P\bar{1}$
Temperature (K)	150
a, *b*, *c* (Å)	3.9700 (4), 10.8689 (11), 12.1299 (12)
a, b, g (°)	78.463 (4), 89.643 (4), 85.444 (4)
V (Å^3)	511.18 (9)
Z	2

Radiation type	Mo *K*a
m (mm^{-1})	0.29
Crystal size (mm)	0.26 × 0.07 × 0.05
Data collection	
Diffractometer	Bruker kappa APEXII CCD Diffractometer
Absorption correction	Multi-scan *SADABS* (Bruker, 2001)
T_{min}, T_{max}	0.928, 0.987
No. of measured, independent and observed [$I > 2s(I)$] reflections	7181, 1788, 1347
R_{int}	0.049
Refinement	
$R[F^2 > 2s(F^2)]$, $wR(F^2)$, S	0.037, 0.093, 1.05
No. of reflections	1788
No. of parameters	129
No. of restraints	0
H-atom treatment	H-atom parameters constrained
$D\rho_{max}$, $D\rho_{min}$ (e $Å^{-3}$)	0.33, -0.27

Computer programs: *APEX2* (Bruker, 2007), *SHELXS-97* (Sheldrick, 2008), *SHELXL-97* (Sheldrick, 2008), *SHELXTL-Plus* (Sheldrick, 2008).

Table 8. Selected geometric parameters (Å, º)

S1—C2	1.718 (2)	C6—C7	1.519 (3)
S1—C5	1.721 (2)	C6—H6B	0.9900
O1—C9	1.206 (3)	C6—H6A	0.9900
O2—C9	1.341 (3)	C7—C8	1.519 (3)
O2—C10	1.444 (3)	C7—H7A	0.9900
O3—C11	1.213 (3)	C7—H7B	0.9900
C2—C3	1.385 (3)	C8—H8C	0.9800
C2—C6	1.504 (3)	C8—H8A	0.9800
C3—C4	1.419 (3)	C8—H8B	0.9800
C3—C9	1.474 (3)	C10—H10B	0.9800
C4—C5	1.359 (3)	C10—H10A	0.9800
C4—H4	0.9500	C10—H10C	0.9800
C5—C11	1.455 (3)	C11—H11	0.9500

C2—S1—C5	92.19 (10)	C8—C7—H7A	109.2
C9—O2—C10	115.47 (17)	C6—C7—H7B	109.2
C3—C2—C6	129.7 (2)	C8—C7—H7B	109.2
C3—C2—S1	110.69 (16)	H7A—C7—H7B	107.9
C6—C2—S1	119.59 (16)	C7—C8—H8C	109.5
C2—C3—C4	112.72 (19)	C7—C8—H8A	109.5
C2—C3—C9	127.8 (2)	H8C—C8—H8A	109.5
C4—C3—C9	119.45 (19)	C7—C8—H8B	109.5
C5—C4—C3	112.6 (2)	H8C—C8—H8B	109.5
C5—C4—H4	123.7	H8A—C8—H8B	109.5
C3—C4—H4	123.7	O1—C9—O2	123.0 (2)
C4—C5—C11	126.1 (2)	O1—C9—C3	123.7 (2)
C4—C5—S1	111.77 (17)	O2—C9—C3	113.25 (18)
C11—C5—S1	122.08 (17)	O2—C10—H10B	109.5
C2—C6—C7	115.56 (18)	O2—C10—H10A	109.5
C2—C6—H6B	108.4	H10B—C10—H10A	109.5
C7—C6—H6B	108.4	O2—C10—H10C	109.5
C2—C6—H6A	108.4	H10B—C10—H10C	109.5
C7—C6—H6A	108.4	H10A—C10—H10C	109.5
H6B—C6—H6A	107.5	O3—C11—C5	124.8 (2)
C6—C7—C8	112.15 (19)	O3—C11—H11	117.6
C6—C7—H7A	109.2	C5—C11—H11	117.6
C5—S1—C2—C3	-0.52 (18)	C3—C2—C6—C7	-171.1 (2)
C5—S1—C2—C6	-179.94 (18)	S1—C2—C6—C7	8.2 (3)
C6—C2—C3—C4	179.5 (2)	C2—C6—C7—C8	179.2 (2)
S1—C2—C3—C4	0.1 (2)	C10—O2—C9—O1	-0.4 (3)
C6—C2—C3—C9	-0.7 (4)	C10—O2—C9—C3	179.60 (19)
S1—C2—C3—C9	179.99 (19)	C2—C3—C9—O1	172.2 (2)
C2—C3—C4—C5	0.5 (3)	C4—C3—C9—O1	-7.9 (3)
C9—C3—C4—C5	-179.4 (2)	C2—C3—C9—O2	-7.8 (3)
C3—C4—C5—C11	177.9 (2)	C4—C3—C9—O2	172.10 (19)
C3—C4—C5—S1	-0.9 (3)	C4—C5—C11—O3	-173.8 (2)
C2—S1—C5—C4	0.81 (19)	S1—C5—C11—O3	4.9 (4)
C2—S1—C5—C11	-178.0 (2)		

5. 1-(5-(Dibromomethylene)-2-oxo-2,5-dihydrofuran-3-yl)butyl-3-acetyl-2,2,5,5-tetramethylthiazolidine-4-carboxylate (190)

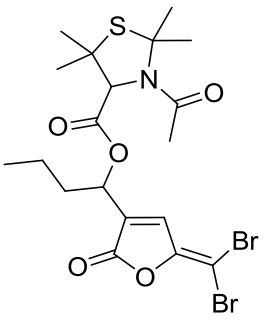

Table 9. Experimental details

	Compound 190
Crystal data	
Chemical formula	$C_{18}H_{23}Br_2NO_5S$
M_r	525.25
Crystal system, space group	Monoclinic, $P2_1$
Temperature (K)	150
a, b, c (Å)	10.1728 (6), 9.3448 (5), 11.3945 (6)
b (°)	99.681 (2)
V (Å^3)	1067.77 (10)
Z	2
Radiation type	Mo Ka
m (mm^{-1})	3.92
Crystal size (mm)	0.36 × 0.23 × 0.13
Data collection	
Diffractometer	Bruker kappa APEXII CCD Diffractometer
Absorption correction	Multi-scan *SADABS* (Bruker, 2001)
T_{min}, T_{max}	0.336, 0.634
No. of measured, independent and observed [$I > 2s(I)$] reflections	7895, 3617, 3162
R_{int}	0.037
Refinement	
$R[F^2 > 2s(F^2)]$, $wR(F^2)$, S	0.029, 0.062, 0.90
No. of reflections	3617
No. of parameters	249
No. of restraints	1
H-atom treatment	H-atom parameters constrained

$D\rho_{max}$, $D\rho_{min}$ (e Å^{-3})	0.35, -0.29
Absolute structure	Flack H D (1983), Acta Cryst. A39, 876-881
Flack parameter	0.021 (7)

Computer programs: *APEX2* (Bruker, 2007), *SHELXS-97* (Sheldrick, 2008), *SHELXL-97* (Sheldrick, 2008), *SHELXTL-Plus* (Sheldrick, 2008).

Table 10. Selected geometric parameters (Å, º)

Br1—C5	1.871 (4)	C8—H8A	0.9900
Br2—C5	1.867 (4)	C8—H8B	0.9900
S1—C13	1.821 (4)	C9—H9A	0.9800
S1—C12	1.823 (4)	C9—H9B	0.9800
O1—C4	1.388 (4)	C9—H9C	0.9800
O1—C1	1.388 (4)	C10—C11	1.525 (5)
O2—C4	1.194 (4)	C11—C12	1.541 (5)
O3—C10	1.345 (5)	C11—H11	1.0000
O3—C6	1.461 (4)	C12—C15	1.518 (6)
O4—C10	1.199 (5)	C12—C14	1.526 (5)
O5—C18	1.214 (6)	C13—C17	1.522 (6)
N1—C18	1.348 (5)	C13—C16	1.527 (5)
N1—C11	1.456 (5)	C14—H14A	0.9800
N1—C13	1.490 (5)	C14—H14B	0.9800
C1—C5	1.328 (5)	C14—H14C	0.9800
C1—C2	1.441 (5)	C15—H15A	0.9800
C2—C3	1.341 (5)	C15—H15B	0.9800
C2—H2	0.9500	C15—H15C	0.9800
C3—C4	1.461 (5)	C16—H16A	0.9800
C3—C6	1.491 (5)	C16—H16B	0.9800
C6—C7	1.519 (5)	C16—H16C	0.9800
C6—H6	1.0000	C17—H17A	0.9800
C7—C8	1.526 (5)	C17—H17B	0.9800
C7—H7A	0.9900	C17—H17C	0.9800
C7—H7B	0.9900	C18—H18	0.9500
C8—C9	1.510 (6)		
C13—S1—C12	96.06 (18)	O3—C10—C11	110.0 (3)
C4—O1—C1	107.7 (3)	N1—C11—C10	110.5 (3)
C10—O3—C6	115.1 (3)	N1—C11—C12	106.8 (3)

C18—N1—C11	117.8 (3)	C10—C11—C12	114.5 (3)
C18—N1—C13	122.6 (4)	N1—C11—H11	108.3
C11—N1—C13	118.7 (3)	C10—C11—H11	108.3
C5—C1—O1	120.0 (3)	C12—C11—H11	108.3
C5—C1—C2	131.5 (3)	C15—C12—C14	111.0 (4)
O1—C1—C2	108.3 (3)	C15—C12—C11	108.4 (3)
C3—C2—C1	108.3 (3)	C14—C12—C11	114.5 (3)
C3—C2—H2	125.9	C15—C12—S1	111.6 (3)
C1—C2—H2	125.9	C14—C12—S1	107.5 (3)
C2—C3—C4	107.9 (3)	C11—C12—S1	103.7 (3)
C2—C3—C6	129.9 (3)	N1—C13—C17	112.2 (4)
C4—C3—C6	122.0 (3)	N1—C13—C16	111.4 (3)
O2—C4—O1	121.0 (3)	C17—C13—C16	110.4 (4)
O2—C4—C3	131.4 (3)	N1—C13—S1	102.9 (2)
O1—C4—C3	107.6 (3)	C17—C13—S1	108.1 (3)
C1—C5—Br2	122.0 (3)	C16—C13—S1	111.7 (3)
C1—C5—Br1	121.0 (3)	C12—C14—H14A	109.5
Br2—C5—Br1	116.89 (19)	C12—C14—H14B	109.5
O3—C6—C3	109.8 (3)	H14A—C14—H14B	109.5
O3—C6—C7	107.2 (3)	C12—C14—H14C	109.5
C3—C6—C7	111.7 (3)	H14A—C14—H14C	109.5
O3—C6—H6	109.4	H14B—C14—H14C	109.5
C3—C6—H6	109.4	C12—C15—H15A	109.5
C7—C6—H6	109.4	C12—C15—H15B	109.5
C6—C7—C8	114.3 (3)	H15A—C15—H15B	109.5
C6—C7—H7A	108.7	C12—C15—H15C	109.5
C8—C7—H7A	108.7	H15A—C15—H15C	109.5
C6—C7—H7B	108.7	H15B—C15—H15C	109.5
C8—C7—H7B	108.7	C13—C16—H16A	109.5
H7A—C7—H7B	107.6	C13—C16—H16B	109.5
C9—C8—C7	112.7 (3)	H16A—C16—H16B	109.5
C9—C8—H8A	109.0	C13—C16—H16C	109.5
C7—C8—H8A	109.0	H16A—C16—H16C	109.5
C9—C8—H8B	109.0	H16B—C16—H16C	109.5
C7—C8—H8B	109.0	C13—C17—H17A	109.5
H8A—C8—H8B	107.8	C13—C17—H17B	109.5
C8—C9—H9A	109.5	H17A—C17—H17B	109.5

C8—C9—H9B	109.5	C13—C17—H17C	109.5
H9A—C9—H9B	109.5	H17A—C17—H17C	109.5
C8—C9—H9C	109.5	H17B—C17—H17C	109.5
H9A—C9—H9C	109.5	O5—C18—N1	123.8 (4)
H9B—C9—H9C	109.5	O5—C18—H18	118.1
O4—C10—O3	124.4 (3)	N1—C18—H18	118.1
O4—C10—C11	125.6 (4)		
C4—O1—C1—C5	-171.6 (3)	C13—N1—C11—C10	-96.9 (4)
C4—O1—C1—C2	4.2 (4)	C18—N1—C11—C12	-162.1 (3)
C5—C1—C2—C3	170.3 (4)	C13—N1—C11—C12	28.2 (4)
O1—C1—C2—C3	-4.9 (4)	O4—C10—C11—N1	25.8 (5)
C1—C2—C3—C4	3.5 (4)	O3—C10—C11—N1	-153.8 (3)
C1—C2—C3—C6	-170.4 (4)	O4—C10—C11—C12	-94.8 (5)
C1—O1—C4—O2	176.9 (3)	O3—C10—C11—C12	85.6 (4)
C1—O1—C4—C3	-2.1 (4)	N1—C11—C12—C15	83.8 (4)
C2—C3—C4—O2	-179.8 (4)	C10—C11—C12—C15	-153.5 (3)
C6—C3—C4—O2	-5.4 (6)	N1—C11—C12—C14	-151.6 (3)
C2—C3—C4—O1	-0.9 (4)	C10—C11—C12—C14	-29.0 (5)
C6—C3—C4—O1	173.5 (3)	N1—C11—C12—S1	-34.8 (3)
O1—C1—C5—Br2	177.3 (2)	C10—C11—C12—S1	87.8 (3)
C2—C1—C5—Br2	2.6 (6)	C13—S1—C12—C15	-87.7 (3)
O1—C1—C5—Br1	0.7 (5)	C13—S1—C12—C14	150.4 (3)
C2—C1—C5—Br1	-173.9 (3)	C13—S1—C12—C11	28.7 (3)
C10—O3—C6—C3	-77.4 (4)	C18—N1—C13—C17	-59.7 (5)
C10—O3—C6—C7	161.2 (3)	C11—N1—C13—C17	109.5 (4)
C2—C3—C6—O3	-33.1 (5)	C18—N1—C13—C16	64.6 (5)
C4—C3—C6—O3	153.8 (3)	C11—N1—C13—C16	-126.3 (4)
C2—C3—C6—C7	85.6 (5)	C18—N1—C13—S1	-175.6 (3)
C4—C3—C6—C7	-87.5 (4)	C11—N1—C13—S1	-6.5 (4)
O3—C6—C7—C8	-62.0 (4)	C12—S1—C13—N1	-13.9 (3)
C3—C6—C7—C8	177.8 (3)	C12—S1—C13—C17	-132.7 (3)
C6—C7—C8—C9	-177.6 (3)	C12—S1—C13—C16	105.7 (3)
C6—O3—C10—O4	-0.8 (5)	C11—N1—C18—O5	1.4 (6)
C6—O3—C10—C11	178.9 (3)	C13—N1—C18—O5	170.6 (4)
C18—N1—C11—C10	72.8 (4)		

6. (Z)-2-(Benzyloxy)-1-(1H-indol-3-yl)diazene oxide (252)

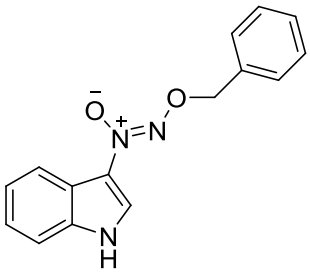

Table 11. Experimental details

	Compound 252
Crystal data	
Chemical formula	$C_{15}H_{13}N_3O_2$
M_r	267.28
Crystal system, space group	Triclinic, $P\bar{1}$
Temperature (K)	160
a, b, c (Å)	13.1597 (8), 14.3792 (8), 14.5523 (8)
α, β, γ (°)	84.576 (2), 75.042 (2), 80.089 (2)
V (Å^3)	2617.0 (3)
Z	8
Radiation type	Mo $K\alpha$
μ (mm^{-1})	0.09
Crystal size (mm)	0.22 × 0.15 × 0.06
Data collection	
Diffractometer	Bruker kappa APEXII CCD Diffractometer
Absorption correction	Multi-scan *SADABS* (Bruker, 2001)
T_{min}, T_{max}	0.980, 0.994
No. of measured, independent and observed [$I > 2\sigma(I)$] reflections	36246, 9167, 6033
R_{int}	0.046
Refinement	
$R[F^2 > 2\sigma(F^2)]$, $wR(F^2)$, S	0.042, 0.105, 1.01
No. of reflections	9167
No. of parameters	721
No. of restraints	0
H-atom treatment	H-atom parameters constrained
$\Delta\rangle_{max}$, $\Delta\rangle_{min}$ (e Å^{-3})	0.17, -0.28

Computer programs: *APEX2* (Bruker, 2007), *SHELXS-97* (Sheldrick, 2008), *SHELXL-97*

(Sheldrick, 2008), *SHELXTL-Plus* (Sheldrick, 2008).

Table 12. Selected geometric parameters (Å, º)

O1A—N1A	1.2652 (17)	O1C—N1C	1.2638 (18)
O2A—N2A	1.3832 (18)	O2C—N2C	1.3805 (18)
O2A—C7A	1.457 (2)	O2C—C7C	1.452 (2)
N1A—N2A	1.286 (2)	N1C—N2C	1.2847 (19)
N1A—C3'A	1.424 (2)	N1C—C3'C	1.422 (2)
N1'A—C2'A	1.356 (2)	N1'C—C2'C	1.353 (2)
N1'A—C9'A	1.380 (2)	N1'C—C9'C	1.380 (2)
N1'A—H1'A	0.8800	N1'C—H1'C	0.8800
C2'A—C3'A	1.358 (2)	C2'C—C3'C	1.362 (2)
C2'A—H2'A	0.9500	C2'C—H2'C	0.9500
C3'A—C4'A	1.439 (2)	C3'C—C4'C	1.432 (2)
C4'A—C5'A	1.399 (2)	C4'C—C5'C	1.406 (2)
C4'A—C9'A	1.412 (2)	C4'C—C9'C	1.407 (2)
C5'A—C6'A	1.376 (2)	C5'C—C6'C	1.375 (2)
C5'A—H5'A	0.9500	C5'C—H5'C	0.9500
C6'A—C7'A	1.399 (3)	C6'C—C7'C	1.396 (2)
C6'A—H6'A	0.9500	C6'C—H6'C	0.9500
C7'A—C8'A	1.367 (3)	C7'C—C8'C	1.375 (3)
C7'A—H7'A	0.9500	C7'C—H7'C	0.9500
C8'A—C9'A	1.389 (2)	C8'C—C9'C	1.389 (2)
C8'A—H8'A	0.9500	C8'C—H8'C	0.9500
C1A—C6A	1.388 (3)	C1C—C6C	1.382 (3)
C1A—C2A	1.388 (3)	C1C—C2C	1.393 (3)
C1A—C7A	1.495 (3)	C1C—C7C	1.491 (2)
C2A—C3A	1.374 (3)	C2C—C3C	1.373 (3)
C2A—H2A	0.9500	C2C—H2C	0.9500
C3A—C4A	1.377 (3)	C3C—C4C	1.374 (3)
C3A—H3A	0.9500	C3C—H3C	0.9500
C4A—C5A	1.376 (3)	C4C—C5C	1.380 (3)
C4A—H4A	0.9500	C4C—H4C	0.9500
C5A—C6A	1.378 (3)	C5C—C6C	1.382 (3)
C5A—H5A	0.9500	C5C—H5C	0.9500
C6A—H6A	0.9500	C6C—H6C	0.9500
C7A—H7A1	0.9900	C7C—H7C1	0.9900

C7A—H7A2	0.9900	C7C—H7C2	0.9900
O1B—N1B	1.2698 (17)	O1D—N1D	1.2699 (18)
O2B—N2B	1.3872 (18)	O2D—N2D	1.3862 (17)
O2B—C7B	1.449 (2)	O2D—C7D	1.460 (2)
N1B—N2B	1.279 (2)	N1D—N2D	1.2858 (19)
N1B—C3'B	1.423 (2)	N1D—C3'D	1.421 (2)
N1'B—C2'B	1.352 (2)	N1'D—C2'D	1.353 (2)
N1'B—C9'B	1.376 (2)	N1'D—C9'D	1.384 (2)
N1'B—H1'B	0.8800	N1'D—H1'D	0.8800
C2'B—C3'B	1.365 (2)	C2'D—C3'D	1.364 (2)
C2'B—H2'B	0.9500	C2'D—H2'D	0.9500
C3'B—C4'B	1.430 (2)	C3'D—C4'D	1.432 (2)
C4'B—C5'B	1.404 (2)	C4'D—C5'D	1.401 (2)
C4'B—C9'B	1.410 (2)	C4'D—C9'D	1.407 (2)
C5'B—C6'B	1.373 (2)	C5'D—C6'D	1.372 (2)
C5'B—H5'B	0.9500	C5'D—H5'D	0.9500
C6'B—C7'B	1.401 (2)	C6'D—C7'D	1.393 (2)
C6'B—H6'B	0.9500	C6'D—H6'D	0.9500
C7'B—C8'B	1.374 (3)	C7'D—C8'D	1.375 (2)
C7'B—H7'B	0.9500	C7'D—H7'D	0.9500
C8'B—C9'B	1.393 (2)	C8'D—C9'D	1.389 (2)
C8'B—H8'B	0.9500	C8'D—H8'D	0.9500
C1B—C6B	1.386 (3)	C1D—C6D	1.384 (3)
C1B—C2B	1.387 (3)	C1D—C2D	1.384 (3)
C1B—C7B	1.495 (3)	C1D—C7D	1.495 (3)
C2B—C3B	1.375 (3)	C2D—C3D	1.377 (3)
C2B—H2B	0.9500	C2D—H2D	0.9500
C3B—C4B	1.377 (3)	C3D—C4D	1.376 (3)
C3B—H3B	0.9500	C3D—H3D	0.9500
C4B—C5B	1.376 (3)	C4D—C5D	1.376 (3)
C4B—H4B	0.9500	C4D—H4D	0.9500
C5B—C6B	1.379 (3)	C5D—C6D	1.377 (3)
C5B—H5B	0.9500	C5D—H5D	0.9500
C6B—H6B	0.9500	C6D—H6D	0.9500
C7B—H7B1	0.9900	C7D—H7D1	0.9900
C7B—H7B2	0.9900	C7D—H7D2	0.9900

N2A—O2A—C7A	106.47 (12)	N2C—O2C—C7C	106.00 (13)
O1A—N1A—N2A	125.30 (15)	O1C—N1C—N2C	125.57 (15)
O1A—N1A—C3'A	119.90 (14)	O1C—N1C—C3'C	120.63 (15)
N2A—N1A—C3'A	114.79 (14)	N2C—N1C—C3'C	113.79 (14)
N1A—N2A—O2A	108.38 (13)	N1C—N2C—O2C	108.36 (14)
C2'A—N1'A—C9'A	109.45 (15)	C2'C—N1'C—C9'C	109.53 (15)
C2'A—N1'A—H1'A	125.3	C2'C—N1'C—H1'C	125.2
C9'A—N1'A—H1'A	125.3	C9'C—N1'C—H1'C	125.2
N1'A—C2'A—C3'A	108.92 (16)	N1'C—C2'C—C3'C	108.59 (16)
N1'A—C2'A—H2'A	125.5	N1'C—C2'C—H2'C	125.7
C3'A—C2'A—H2'A	125.5	C3'C—C2'C—H2'C	125.7
C2'A—C3'A—N1A	123.48 (16)	C2'C—C3'C—N1C	123.54 (16)
C2'A—C3'A—C4'A	108.81 (15)	C2'C—C3'C—C4'C	108.89 (16)
N1A—C3'A—C4'A	127.69 (16)	N1C—C3'C—C4'C	127.52 (16)
C5'A—C4'A—C9'A	119.17 (16)	C5'C—C4'C—C9'C	119.08 (16)
C5'A—C4'A—C3'A	136.23 (16)	C5'C—C4'C—C3'C	136.14 (16)
C9'A—C4'A—C3'A	104.57 (15)	C9'C—C4'C—C3'C	104.78 (15)
C6'A—C5'A—C4'A	118.10 (17)	C6'C—C5'C—C4'C	118.13 (17)
C6'A—C5'A—H5'A	120.9	C6'C—C5'C—H5'C	120.9
C4'A—C5'A—H5'A	120.9	C4'C—C5'C—H5'C	120.9
C5'A—C6'A—C7'A	121.77 (18)	C5'C—C6'C—C7'C	121.83 (17)
C5'A—C6'A—H6'A	119.1	C5'C—C6'C—H6'C	119.1
C7'A—C6'A—H6'A	119.1	C7'C—C6'C—H6'C	119.1
C8'A—C7'A—C6'A	121.27 (17)	C8'C—C7'C—C6'C	121.21 (18)
C8'A—C7'A—H7'A	119.4	C8'C—C7'C—H7'C	119.4
C6'A—C7'A—H7'A	119.4	C6'C—C7'C—H7'C	119.4
C7'A—C8'A—C9'A	117.56 (17)	C7'C—C8'C—C9'C	117.39 (17)
C7'A—C8'A—H8'A	121.2	C7'C—C8'C—H8'C	121.3
C9'A—C8'A—H8'A	121.2	C9'C—C8'C—H8'C	121.3
N1'A—C9'A—C8'A	129.66 (16)	N1'C—C9'C—C8'C	129.43 (16)
N1'A—C9'A—C4'A	108.25 (15)	N1'C—C9'C—C4'C	108.22 (15)
C8'A—C9'A—C4'A	122.09 (16)	C8'C—C9'C—C4'C	122.35 (16)
C6A—C1A—C2A	118.42 (17)	C6C—C1C—C2C	118.87 (17)
C6A—C1A—C7A	120.78 (18)	C6C—C1C—C7C	120.34 (17)
C2A—C1A—C7A	120.79 (19)	C2C—C1C—C7C	120.77 (17)
C3A—C2A—C1A	120.67 (18)	C3C—C2C—C1C	120.20 (18)
C3A—C2A—H2A	119.7	C3C—C2C—H2C	119.9

C1A—C2A—H2A	119.7	C1C—C2C—H2C	119.9
C2A—C3A—C4A	120.14 (18)	C2C—C3C—C4C	120.68 (19)
C2A—C3A—H3A	119.9	C2C—C3C—H3C	119.7
C4A—C3A—H3A	119.9	C4C—C3C—H3C	119.7
C5A—C4A—C3A	120.10 (18)	C3C—C4C—C5C	119.66 (18)
C5A—C4A—H4A	120.0	C3C—C4C—H4C	120.2
C3A—C4A—H4A	120.0	C5C—C4C—H4C	120.2
C4A—C5A—C6A	119.75 (18)	C4C—C5C—C6C	120.03 (19)
C4A—C5A—H5A	120.1	C4C—C5C—H5C	120.0
C6A—C5A—H5A	120.1	C6C—C5C—H5C	120.0
C5A—C6A—C1A	120.90 (18)	C5C—C6C—C1C	120.56 (18)
C5A—C6A—H6A	119.5	C5C—C6C—H6C	119.7
C1A—C6A—H6A	119.5	C1C—C6C—H6C	119.7
O2A—C7A—C1A	107.44 (14)	O2C—C7C—C1C	107.72 (14)
O2A—C7A—H7A1	110.2	O2C—C7C—H7C1	110.2
C1A—C7A—H7A1	110.2	C1C—C7C—H7C1	110.2
O2A—C7A—H7A2	110.2	O2C—C7C—H7C2	110.2
C1A—C7A—H7A2	110.2	C1C—C7C—H7C2	110.2
H7A1—C7A—H7A2	108.5	H7C1—C7C—H7C2	108.5
N2B—O2B—C7B	105.99 (12)	N2D—O2D—C7D	105.19 (12)
O1B—N1B—N2B	125.11 (15)	O1D—N1D—N2D	125.36 (14)
O1B—N1B—C3'B	120.17 (15)	O1D—N1D—C3'D	120.80 (14)
N2B—N1B—C3'B	114.72 (14)	N2D—N1D—C3'D	113.82 (14)
N1B—N2B—O2B	108.54 (13)	N1D—N2D—O2D	109.06 (13)
C2'B—N1'B—C9'B	109.76 (15)	C2'D—N1'D—C9'D	109.48 (14)
C2'B—N1'B—H1'B	125.1	C2'D—N1'D—H1'D	125.3
C9'B—N1'B—H1'B	125.1	C9'D—N1'D—H1'D	125.3
N1'B—C2'B—C3'B	108.42 (16)	N1'D—C2'D—C3'D	108.70 (15)
N1'B—C2'B—H2'B	125.8	N1'D—C2'D—H2'D	125.7
C3'B—C2'B—H2'B	125.8	C3'D—C2'D—H2'D	125.7
C2'B—C3'B—N1B	123.28 (16)	C2'D—C3'D—N1D	124.16 (16)
C2'B—C3'B—C4'B	108.92 (16)	C2'D—C3'D—C4'D	108.76 (15)
N1B—C3'B—C4'B	127.79 (16)	N1D—C3'D—C4'D	126.92 (15)
C5'B—C4'B—C9'B	118.80 (16)	C5'D—C4'D—C9'D	118.86 (16)
C5'B—C4'B—C3'B	136.50 (16)	C5'D—C4'D—C3'D	136.16 (16)
C9'B—C4'B—C3'B	104.70 (15)	C9'D—C4'D—C3'D	104.97 (14)
C6'B—C5'B—C4'B	118.60 (16)	C6'D—C5'D—C4'D	118.64 (16)

C6'B—C5'B—H5'B	120.7	C6'D—C5'D—H5'D	120.7
C4'B—C5'B—H5'B	120.7	C4'D—C5'D—H5'D	120.7
C5'B—C6'B—C7'B	121.62 (17)	C5'D—C6'D—C7'D	121.54 (17)
C5'B—C6'B—H6'B	119.2	C5'D—C6'D—H6'D	119.2
C7'B—C6'B—H6'B	119.2	C7'D—C6'D—H6'D	119.2
C8'B—C7'B—C6'B	121.19 (17)	C8'D—C7'D—C6'D	121.37 (17)
C8'B—C7'B—H7'B	119.4	C8'D—C7'D—H7'D	119.3
C6'B—C7'B—H7'B	119.4	C6'D—C7'D—H7'D	119.3
C7'B—C8'B—C9'B	117.43 (17)	C7'D—C8'D—C9'D	117.28 (16)
C7'B—C8'B—H8'B	121.3	C7'D—C8'D—H8'D	121.4
C9'B—C8'B—H8'B	121.3	C9'D—C8'D—H8'D	121.4
N1'B—C9'B—C8'B	129.48 (16)	N1'D—C9'D—C8'D	129.62 (16)
N1'B—C9'B—C4'B	108.20 (15)	N1'D—C9'D—C4'D	108.08 (15)
C8'B—C9'B—C4'B	122.31 (16)	C8'D—C9'D—C4'D	122.30 (16)
C6B—C1B—C2B	118.81 (17)	C6D—C1D—C2D	118.66 (18)
C6B—C1B—C7B	120.68 (19)	C6D—C1D—C7D	120.77 (19)
C2B—C1B—C7B	120.48 (19)	C2D—C1D—C7D	120.57 (19)
C3B—C2B—C1B	120.45 (19)	C3D—C2D—C1D	120.56 (19)
C3B—C2B—H2B	119.8	C3D—C2D—H2D	119.7
C1B—C2B—H2B	119.8	C1D—C2D—H2D	119.7
C2B—C3B—C4B	120.22 (19)	C4D—C3D—C2D	120.01 (19)
C2B—C3B—H3B	119.9	C4D—C3D—H3D	120.0
C4B—C3B—H3B	119.9	C2D—C3D—H3D	120.0
C5B—C4B—C3B	120.02 (18)	C5D—C4D—C3D	120.16 (18)
C5B—C4B—H4B	120.0	C5D—C4D—H4D	119.9
C3B—C4B—H4B	120.0	C3D—C4D—H4D	119.9
C4B—C5B—C6B	119.85 (19)	C4D—C5D—C6D	119.65 (19)
C4B—C5B—H5B	120.1	C4D—C5D—H5D	120.2
C6B—C5B—H5B	120.1	C6D—C5D—H5D	120.2
C5B—C6B—C1B	120.65 (18)	C5D—C6D—C1D	120.94 (19)
C5B—C6B—H6B	119.7	C5D—C6D—H6D	119.5
C1B—C6B—H6B	119.7	C1D—C6D—H6D	119.5
O2B—C7B—C1B	108.50 (15)	O2D—C7D—C1D	107.33 (14)
O2B—C7B—H7B1	110.0	O2D—C7D—H7D1	110.2
C1B—C7B—H7B1	110.0	C1D—C7D—H7D1	110.2
O2B—C7B—H7B2	110.0	O2D—C7D—H7D2	110.2
C1B—C7B—H7B2	110.0	C1D—C7D—H7D2	110.2

H7B1—C7B—H7B2	108.4	H7D1—C7D—H7D2	108.5
O1A—N1A—N2A—O2A	1.0 (2)	O1C—N1C—N2C—O2C	-0.6 (2)
C3'A—N1A—N2A—O2A	-178.33 (13)	C3'C—N1C—N2C—O2C	178.23 (13)
C7A—O2A—N2A—N1A	178.99 (15)	C7C—O2C—N2C—N1C	-174.46 (14)
C9'A—N1'A—C2'A—C3'A	0.6 (2)	C9'C—N1'C—C2'C—C3'C	-0.4 (2)
N1'A—C2'A—C3'A—N1A	-179.64 (15)	N1'C—C2'C—C3'C—N1C	177.81 (15)
N1'A—C2'A—C3'A—C4'A	-0.8 (2)	N1'C—C2'C—C3'C—C4'C	0.3 (2)
O1A—N1A—C3'A—C2'A	11.2 (3)	O1C—N1C—C3'C—C2'C	1.1 (3)
N2A—N1A—C3'A—C2'A	-169.36 (17)	N2C—N1C—C3'C—C2'C	-177.76 (17)
O1A—N1A—C3'A—C4'A	-167.33 (16)	O1C—N1C—C3'C—C4'C	178.17 (16)
N2A—N1A—C3'A—C4'A	12.1 (2)	N2C—N1C—C3'C—C4'C	-0.7 (2)
C2'A—C3'A—C4'A—C5'A	-177.3 (2)	C2'C—C3'C—C4'C—C5'C	178.9 (2)
N1A—C3'A—C4'A—C5'A	1.5 (3)	N1C—C3'C—C4'C—C5'C	1.4 (3)
C2'A—C3'A—C4'A—C9'A	0.71 (19)	C2'C—C3'C—C4'C—C9'C	-0.03 (19)
N1A—C3'A—C4'A—C9'A	179.44 (16)	N1C—C3'C—C4'C—C9'C	-177.45 (16)
C9'A—C4'A—C5'A—C6'A	1.4 (3)	C9'C—C4'C—C5'C—C6'C	-0.9 (2)
C3'A—C4'A—C5'A—C6'A	179.16 (19)	C3'C—C4'C—C5'C—C6'C	-179.65 (19)
C4'A—C5'A—C6'A—C7'A	0.0 (3)	C4'C—C5'C—C6'C—C7'C	0.5 (3)
C5'A—C6'A—C7'A—C8'A	-1.3 (3)	C5'C—C6'C—C7'C—C8'C	0.4 (3)
C6'A—C7'A—C8'A—C9'A	1.1 (3)	C6'C—C7'C—C8'C—C9'C	-0.8 (3)
C2'A—N1'A—C9'A—C8'A	179.52 (18)	C2'C—N1'C—C9'C—C8'C	-179.40 (18)
C2'A—N1'A—C9'A—C4'A	-0.17 (19)	C2'C—N1'C—C9'C—C4'C	0.38 (19)
C7'A—C8'A—C9'A—N1'A	-179.26 (18)	C7'C—C8'C—C9'C—N1'C	-179.86 (17)
C7'A—C8'A—C9'A—C4'A	0.4 (3)	C7'C—C8'C—C9'C—C4'C	0.4 (3)
C5'A—C4'A—C9'A—N1'A	178.06 (15)	C5'C—C4'C—C9'C—N1'C	-179.33 (15)
C3'A—C4'A—C9'A—N1'A	-0.33 (18)	C3'C—C4'C—C9'C—N1'C	-0.21 (18)
C5'A—C4'A—C9'A—C8'A	-1.7 (3)	C5'C—C4'C—C9'C—C8'C	0.5 (3)
C3'A—C4'A—C9'A—C8'A	179.96 (16)	C3'C—C4'C—C9'C—C8'C	179.59 (16)
C6A—C1A—C2A—C3A	1.1 (3)	C6C—C1C—C2C—C3C	-0.5 (3)
C7A—C1A—C2A—C3A	-177.93 (18)	C7C—C1C—C2C—C3C	178.14 (17)
C1A—C2A—C3A—C4A	0.4 (3)	C1C—C2C—C3C—C4C	0.2 (3)
C2A—C3A—C4A—C5A	-1.6 (3)	C2C—C3C—C4C—C5C	0.3 (3)
C3A—C4A—C5A—C6A	1.2 (3)	C3C—C4C—C5C—C6C	-0.4 (3)
C4A—C5A—C6A—C1A	0.3 (3)	C4C—C5C—C6C—C1C	0.0 (3)
C2A—C1A—C6A—C5A	-1.5 (3)	C2C—C1C—C6C—C5C	0.4 (3)
C7A—C1A—C6A—C5A	177.57 (17)	C7C—C1C—C6C—C5C	-178.24 (17)

N2A—O2A—C7A—C1A	176.34 (15)	N2C—O2C—C7C—C1C	-170.40 (14)
C6A—C1A—C7A—O2A	-82.1 (2)	C6C—C1C—C7C—O2C	-124.60 (18)
C2A—C1A—C7A—O2A	96.9 (2)	C2C—C1C—C7C—O2C	56.8 (2)
O1B—N1B—N2B—O2B	-0.3 (2)	O1D—N1D—N2D—O2D	-1.2 (2)
C3'B—N1B—N2B—O2B	-179.59 (13)	C3'D—N1D—N2D—O2D	177.05 (13)
C7B—O2B—N2B—N1B	176.72 (15)	C7D—O2D—N2D—N1D	-179.28 (15)
C9'B—N1'B—C2'B—C3'B	-0.3 (2)	C9'D—N1'D—C2'D—C3'D	0.6 (2)
N1'B—C2'B—C3'B—N1B	-178.32 (15)	N1'D—C2'D—C3'D—N1D	175.51 (15)
N1'B—C2'B—C3'B—C4'B	0.8 (2)	N1'D—C2'D—C3'D—C4'D	-0.1 (2)
O1B—N1B—C3'B—C2'B	-7.5 (3)	O1D—N1D—C3'D—C2'D	5.2 (3)
N2B—N1B—C3'B—C2'B	171.79 (17)	N2D—N1D—C3'D—C2'D	-173.15 (17)
O1B—N1B—C3'B—C4'B	173.49 (16)	O1D—N1D—C3'D—C4'D	179.98 (16)
N2B—N1B—C3'B—C4'B	-7.2 (2)	N2D—N1D—C3'D—C4'D	1.6 (2)
C2'B—C3'B—C4'B—C5'B	178.5 (2)	C2'D—C3'D—C4'D—C5'D	-179.2 (2)
N1B—C3'B—C4'B—C5'B	-2.4 (3)	N1D—C3'D—C4'D—C5'D	5.4 (3)
C2'B—C3'B—C4'B—C9'B	-0.99 (19)	C2'D—C3'D—C4'D—C9'D	-0.49 (19)
N1B—C3'B—C4'B—C9'B	178.09 (16)	N1D—C3'D—C4'D—C9'D	-175.91 (16)
C9'B—C4'B—C5'B—C6'B	-2.0 (2)	C9'D—C4'D—C5'D—C6'D	-0.2 (3)
C3'B—C4'B—C5'B—C6'B	178.49 (19)	C3'D—C4'D—C5'D—C6'D	178.31 (19)
C4'B—C5'B—C6'B—C7'B	0.2 (3)	C4'D—C5'D—C6'D—C7'D	-0.2 (3)
C5'B—C6'B—C7'B—C8'B	1.5 (3)	C5'D—C6'D—C7'D—C8'D	0.7 (3)
C6'B—C7'B—C8'B—C9'B	-1.2 (3)	C6'D—C7'D—C8'D—C9'D	-0.8 (3)
C2'B—N1'B—C9'B—C8'B	178.36 (18)	C2'D—N1'D—C9'D—C8'D	178.67 (17)
C2'B—N1'B—C9'B—C4'B	-0.3 (2)	C2'D—N1'D—C9'D—C4'D	-0.93 (19)
C7'B—C8'B—C9'B—N1'B	-179.28 (18)	C7'D—C8'D—C9'D—N1'D	-179.21 (17)
C7'B—C8'B—C9'B—C4'B	-0.7 (3)	C7'D—C8'D—C9'D—C4'D	0.3 (3)
C5'B—C4'B—C9'B—N1'B	-178.83 (15)	C5'D—C4'D—C9'D—N1'D	179.80 (15)
C3'B—C4'B—C9'B—N1'B	0.80 (18)	C3'D—C4'D—C9'D—N1'D	0.85 (18)
C5'B—C4'B—C9'B—C8'B	2.4 (3)	C5'D—C4'D—C9'D—C8'D	0.2 (2)
C3'B—C4'B—C9'B—C8'B	-178.01 (16)	C3'D—C4'D—C9'D—C8'D	-178.79 (16)
C6B—C1B—C2B—C3B	0.2 (3)	C6D—C1D—C2D—C3D	1.0 (3)
C7B—C1B—C2B—C3B	-178.08 (17)	C7D—C1D—C2D—C3D	-179.28 (17)
C1B—C2B—C3B—C4B	-0.3 (3)	C1D—C2D—C3D—C4D	-0.2 (3)
C2B—C3B—C4B—C5B	0.1 (3)	C2D—C3D—C4D—C5D	-0.8 (3)
C3B—C4B—C5B—C6B	0.1 (3)	C3D—C4D—C5D—C6D	0.9 (3)
C4B—C5B—C6B—C1B	-0.2 (3)	C4D—C5D—C6D—C1D	-0.1 (3)
C2B—C1B—C6B—C5B	0.0 (3)	C2D—C1D—C6D—C5D	-0.9 (3)

C7B—C1B—C6B—C5B	178.27 (17)	C7D—C1D—C6D—C5D	179.42 (17)
N2B—O2B—C7B—C1B	178.57 (16)	N2D—O2D—C7D—C1D	167.08 (16)
C6B—C1B—C7B—O2B	72.7 (2)	C6D—C1D—C7D—O2D	-89.0 (2)
C2B—C1B—C7B—O2B	-109.1 (2)	C2D—C1D—C7D—O2D	91.2 (2)